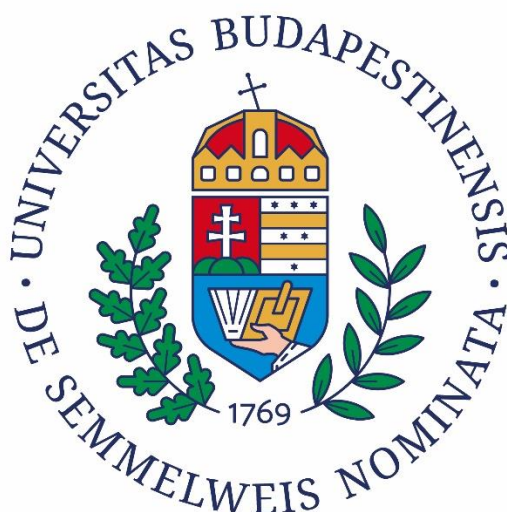MTA DOKTORI ÉRTEKEZÉS

AZ AT1 ANGIOTENZIN RECEPTOR MŰKÖDÉSÉBEN SZEREPET JÁTSZÓ MECHANIZMUSOK VIZSGÁLATA

Dr. Balla András

SEMMELWEIS EGYETEM
ÁLTALÁNOS ORVOSTUDOMÁNYI KAR
ÉLETTANI INTÉZET

BUDAPEST
2023

TARTALOMJEGYZÉK

1. A KITŰZÖTT KUTATÁSI FELADAT RÖVID ÖSSZEFOGLALÁSA, BEVEZETÉS

1.1 Irodalmi háttér és a kutatás előzményei

Az angiotenzin II (AngII) a hormonoknak abba a csoportjába tartozik, mely az inozitol lipidek metabolizmusának megváltoztatásán keresztül fejtik ki hatásaikat. Az MTA Doktori Értekezésben ismertetett kutatómunkámban a foszfoinozitidekkel és a szintézisükben fontos egyik enzim, a foszfatidilinozitol (PtdIns) 4-kinázzal, valamint az 1-es típusú angiotenzin receptorral (AT1-receptor) foglalkoztam. A kutatásaim során kiemelten foglalkoztam az AT1-receptor stimulusa során bekövetkező celluláris foszfoinozitid szintek változásával, valamint ezek szintéziséért felelős lipid kinázokkal, illetve a plazmamembrán PtdIns 4,5-biszfoszfát szerepének felderítésével a receptor működésében. Ennek megfelelően az eredmények részletes ismertetése előtt szeretném röviden áttekinteni a kísérletek megértéséhez szükséges témákat, beleértve a foszfoinozitidek és a szintézisükért felelős enzimek szerepét a sejtekben, illetve a G-fehérjéhez kapcsolt receptorok (GFKR), különös tekintettel az AT1-receptor működését.

1.1.1 A foszfoinozitidek és a szintézisükben fontos lipid kinázok

A foszfoinozitidek olyan glicerofoszfolipid molekulák, melyek a foszfatidilinozitol lipid molekula eltérően foszforilált származékai. Az eukarióta sejtekben található inozitol tartalmú foszfolipidek a sejtek teljes foszfolipid tartalmának csak 2-8%-át alkotják, mégis központi szerepet játszanak a különféle hormonok, növekedési faktorok és neurotranszmitterek jelátviteli folyamataiban. Az inozitol tartalmú foszfolipidek hozzávetőlegesen 5-10%-a foszforilált az inozitolgyűrű egy vagy több pontján az emlős sejtekben. A foszfatidilinozitol (PtdIns) anyagcsere a figyelem középpontjában áll a jelátvitelben játszott szerepének felismerése óta. A PtdIns 4,5-biszfoszfátot [PtdIns(4,5)P_2], a sejtet érő extracelluláris hatásokra a foszfoinozitid-specifikus foszfolipáz C (PLC) hidrolizálja és ezzel két másodlagos hírvivőt hoz létre, az inozitol 1,4,5-triszfoszfátot [Ins(1,4,5)P_3] és a diacilglicerint (DAG). Az Ins(1,4,5)P_3 kalciumot szabadít fel az intracelluláris raktárakból, ezáltal sokféle kalciumfüggő folyamatot aktivál. A DAG a protein kináz C-t (PKC) stimulálja, mely széles specificitású szerin/treonin protein kináz. A PtdIns poláris és hidrofób részből áll, a poláris részén elhelyezkedő inozitolgyűrűben öt szabad hidroxil csoport van, melyek potenciálisan mind foszforilálódhatnak (1. ábra). A sejtekben jól ismert a PtdIns(4)P, PtdIns(4,5)P_2, PtdIns(3)P, PtdIns(5)P, PtdIns(3,4)P_2, PtdIns(3,5)P_2 és a PtdIns(3,4,5)P_3 jelenléte. A foszfoinozitidek a lipid természetüknél fogva a sejtek membránjaiban helyezkednek el és igen szerteágazó

szereppel bírnak, tulajdonképp nehéz találunk olyan sejtfolyamatot, amelyet a foszfoinozitidek nem szabályozhatnak. A foszfoinozitidek metabolizmusa igen szigorúan szabályozott mechanizmus, mely különböző lipid kinázok és foszfatázok részvételével jön létre. A foszfoinozitidek bioszintézisének legfontosabb első lépését a különböző foszfatidilinozitol (PtdIns) 4-kináz izoformák katalizálják. A képződött PtdIns 4-foszfátot PtdIns 4-foszfát 5-kináz tovább foszforilálja PtdIns(4,5)P_2-vé, amely másodlagos hírvivők prekurzora. A sejteket ért egyes stimulusok során, pl. az AT1-receptor fiziológiás stimulusa után a PtdIns(4,5)P_2 koncentrációja erősen lecsökken, de hamar újraképződik, ami bioszintézisének szabályozottságára utal. Ebben fontos tényező a PtdIns 4-kináz működése, amely a PtdIns(4,5)P_2 képződéséhez vezető foszforilációs folyamatban az első elkötelező lépést katalizálja.

1. ábra: A foszfoinozitidek metabolizmusa. A foszfoinozidek az inozitolgyűrű különböző helyein foszforilálódhatnak. A DAG és az Ins(1,4,5)P_3 képződéséhez vezető klasszikus útvonal kék és rózsaszín háttérrel jelölt. Az I-es típusú PtdIns 3-kináz termékei narancs, a III-as típusú PtdIns 3-kináz termékei zöld háttérrel jelöltek. A piros nyíl jelöli a PtdIns 4-kinázok által katalizált lépést. (Balla A *et al*.: Trends in Cell Biology, 2006).

A PtdIns 4-kináz (EC 2.7.1.67.) a PtdIns inozitolgyűrűjét D-4 helyzetben foszforilálja az ATP γ-foszfátjával. A PtdIns 4-kináz család négy izoformát tartalmaz, melyek két csoportba oszthatók. Korai enzimológiai munkák az adenozin-gátlás és a nem-ionos detergensek iránti érzékenység alapján három csoportba osztották a foszfatidilinozitol kinázokat. Ezen osztályozás szerint az I-es típusú foszfatidilinozitol kináz a PtdIns 3-kinázok lettek, míg az addig ismert két PtdIns 4-kináz izoformát II-es és III-as típusúnak nevezték el (1. táblázat).

	PtdIns4KII	**PtdIns4KIIIα**	**PtdIns4KIIIβ**
Más elnevezés	PI4KII; PI4K55; II-es típusú PI 4-kináz	PI4KA, PIK4ca; PI4K230; PI 4-kináz alfa	PI4KB, PIK4cb; PI4K92; PI 4-kináz beta
Látszólagos mol.t.	55-56 kDa	210 kDa	110 kDa
Számított mol.t.	54 kDa	230 kDa	92 kDa
Wortmannin	érzéketlen	IC_{50}: 50-300 nM	IC_{50}: 50-300 nM
LY-294002	érzéketlen	IC_{50}: 50-100 μM	IC_{50}: 100 μM
K_i (adenozin)	10-70 μM	1,5 mM	0,85 mM

1. táblázat: A foszfatidilinozitol kinázok enzimológiai jellemzése

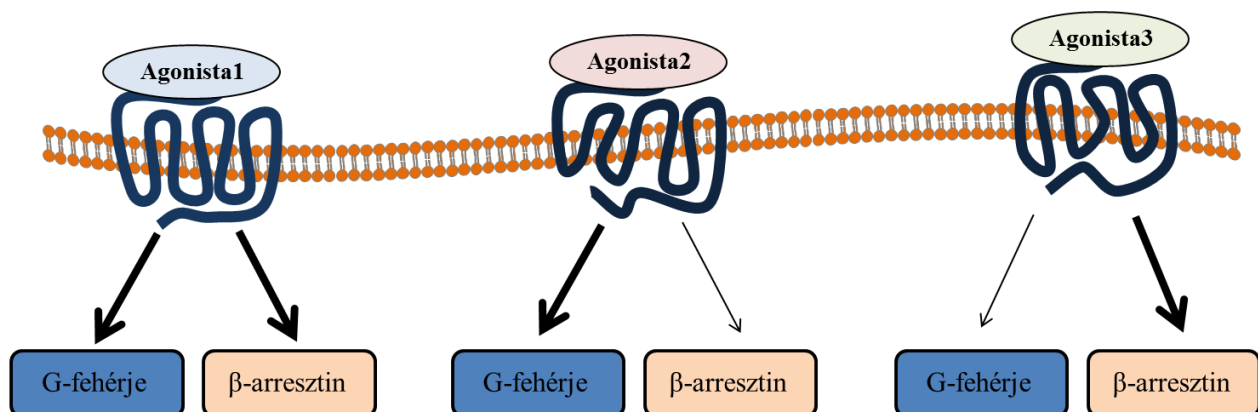1.1.2 G-fehérjéhez kapcsolt receptorok (GFKR)

A G-fehérjéhez kapcsolt receptorok (GFKR) alkotják a plazmamembrán-receptorok legnagyobb csoportját, melyek az extracelluláris (hormonok, neurotranszmitterek), illetve a külső térből érkező (fény, szagok, ízek) jelek közvetítésében vesznek részt. Jelentőségüket jelzi, hogy a kódolt fehérjék kb. 3%-a GFKR, és a használatban lévő gyógyszerek többsége ezen receptorok működését befolyásolja. Szerkezeti felépítésükre jellemző, hogy 7 transzmembrán doménnel rendelkeznek, amino-terminális végük a plazmamembrán sejten kívüli felszínén, míg karboxi-terminális végük a citoszólikus felszínen található. Ezen típusú receptorok a ligandumaik kötését követően úgynevezett heterotrimer G-fehérjéket aktiválnak, majd ennek következtében az adott receptorra jellemző sejten belüli jelpályák indulnak be, melyek kiváltják a sejtválaszt. A különböző típusú GFKR-ok eltérő heterotrimer G-fehérjét kötnek, mely alapjául szolgál a specifikus sejtválasznak, és legtöbbször a Gα alegység típusa alapján csoportosítjuk

receptorokat. Agonista kötés hatására a receptor konformáció változáson megy keresztül, mely szükséges az intracelluláris jeltovábbítás elindításához. Nyugalmi állapotban a heterotrimer G-fehérjék három alegységből (α, βγ) állnak, az α-alegység GDP kötött állapotban van. Az agonista stimulációt követően a heterotrimer G-fehérje az aktivált receptorhoz kötődik, majd az α-alegység a GDP-t GTP-re cseréli, miközben a G-fehérje eltávolodik a receptortól. Az értekezésem központjában lévő AT1 angiotenzin receptor a legfőbb hatásait a $G\alpha_{q/11}$-hez kapcsolva fejti ki, mely a foszfolipáz Cβ (PLCβ) aktiválásán keresztül a plazmamembrán PtdIns(4,5)P_2 hasítását és következményes kalcium jelet vált ki. A GFKR-ok ligandum kötése következtében nemcsak sejten belüli szignalizáció, hanem egyéb szabályozási mechanizmusok is aktiválódnak. Többek közt a GFKR-ok agonista stimulus hatására G-fehérje kapcsolt receptor kinázok (GRK) által foszforilálódnak, mely elindítja a receptorok β-arresztin kötését és deszenzitizációját. A kötődött arresztin fehérjék scaffold (váz) fehérjeként elindítják azon folyamatokat, melyek a receptor internalizációjához (sejt belsejébe helyeződés) vezetnek. Az arresztin fehérjék nemcsak a receptorok internalizációjában játszhatnak szerepet, de újabb jelátviteli mechanizmusok szervezésében is hozzájárulhatnak (2. ábra).
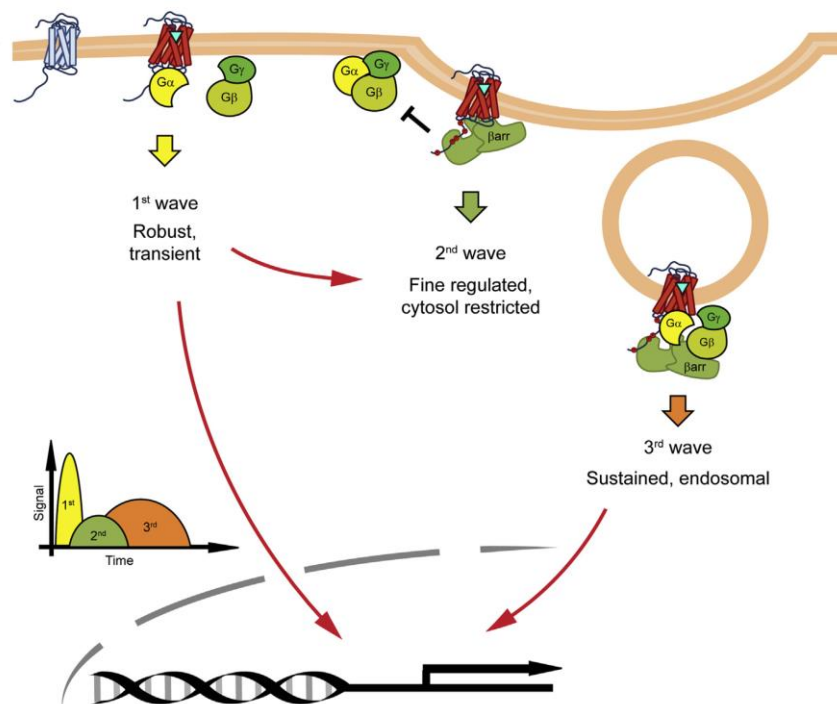
2. ábra. A GFKR-ok jelátviteli sémája. Agonista kötésére létrejövő receptor aktiváció komplex jelátviteli mechanizmusokat és sejtválaszokat indíthat el G-fehérje-függő, illetve β–arresztin mediált módon is (Tóth AD, Turu G, Hunyady L, Balla A.: Best Pract Res Clin Endocrinol Metab. 2018).

A klasszikus receptorteória szerint a receptorok a működésük során bimodális kapcsolóként működnek, két alternatív konformációs állapot, egy aktív és egy inaktív konformációt vehetnek fel: az agonista ligandum kötődése a receptor aktív konformációjának felvételét okozza, míg a receptor nyugalmi állapotában, vagy antagonista ligandum kötésének hatására inaktív konformációt vesz fel. Az elmúlt évek eredményei alapján a különböző ligandumok eltérő receptor konformációkat indukálnak vagy stabilizálnak. Az is egyértelművé vált, hogy egy adott GFKR-nak nem csak több aktív konformációja létezhet, hanem aktivációjakor többféle jelátviteli folyamat is létrejöhet, melyet egyes agonisták szelektíven befolyásolhatják (ezt a jelenséget nevezzük jelátvitel-szelektív agonizmusnak). A más-más receptorkonformációkhoz köthető, eltérő jelátviteli utak és receptorszabályozási útvonalak szelektív, útvonal-specifikus ligandumok által befolyásolhatók. Lehetséges, például a receptor internalizációját szelektíven, G-fehérje-aktiválás nélkül elindítani, így a receptor működését leállítani. Ennek ellenkezője is megvalósítható: szelektív ligandum alkalmazásával internalizáció és deszenzitizáció nélkül G-fehérje aktiválást létrehozni, így kisszámú sejtfelszíni receptorral is nagy sejtválaszt lehet elérni (3. ábra).

3. ábra. A G-fehérje kapcsolt receptorok jelátvitel szelektív agonizmusa. A GFKR-ok klasszikus jelátviteli útvonalaikat G-fehérjéken keresztül aktiválják, azonban a β-arresztin fehérje kötésével további, G-fehérjétől független jelpályákat is képesek működésbe hozni. Az Agonista1 a klasszikus agonistát jelképezi, mely azonos mértékben segítik elő mindkét fehérje kötését, és jelpályáik elindulását. Az Agonista2, a G-fehérje jelátvitelt szelektíven aktiváló ligandumokra utal, melyek kötődése a receptort G-fehérje kötést és aktivációt preferáló konformációban stabilizálja. A β-arresztin jelátvitel irányába elfogult ligandumok esetén a G-fehérje jelpályák helyett a receptor elsősorban β-arresztin függő mechanizmusokat indít el (Agonsita3).

1.1.3 Az 1-es típusú angiotenzin receptor (AT1-receptor)

Az angiotenzin II (AngII) egy oktapeptid hormon (Asp-Arg-Val-Tyr-Ile-His-Pro-Phe), amely a renin-angiotenzin rendszer fő effektor hormonja. Az AngII központi szerepet játszik a vérkeringés és a só-vízháztartás szabályozásában. Az AngII a célsejtek felszínén található specifikus GFKR-hoz, az AT1-receptorhoz (AT1R) kötődik. Az aktiválódást követő jelátviteli folyamatok egyrészt azonnali válaszokat hoznak létre (pl. aldoszteron szekréció, vazokonstrikció, szomjúságérzet), másrészt hosszabb távon sejtproliferációs, differenciálódási és apoptotikus folyamatokat szabályoznak. Az AT1R agonista kötésre bekövetkező aktivációja $G_{q/11}$-fehérjén keresztül intracelluláris Ca^{2+}-jel kialakulásához és PKC aktiválódásához vezet, illetve képes mitogén aktivált protein kináz (MAP kináz, MAPK)-kaszkád MAP kináz kaszkádok aktiválására is (4. ábra).
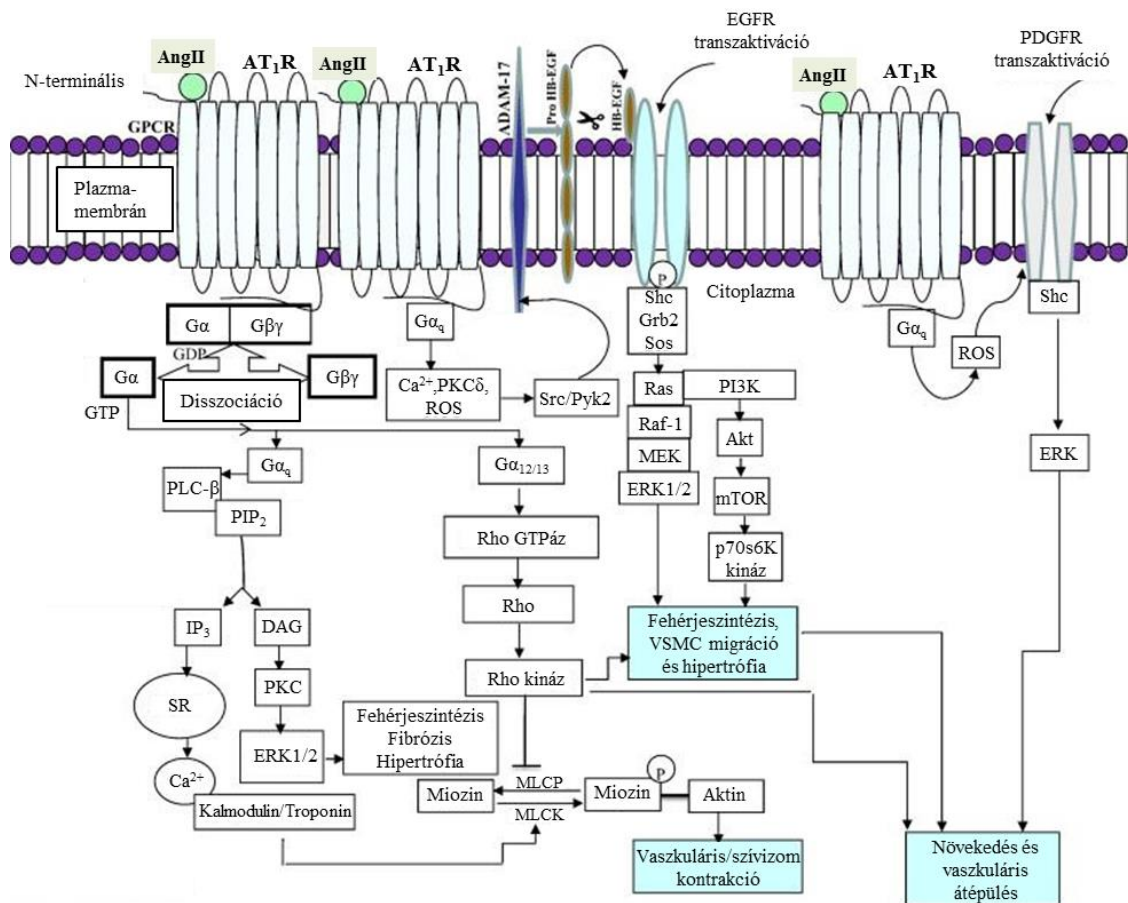
4. ábra. Az AT1-receptor G-fehérjék által közvetített jelátviteli útvonalai, illetve az AT1- receptor tirozin kinázok transzaktivációja. Az aktivált AT1R elsősorban G_q fehérjét aktivál, melynek hatására a PLCβ enzim a foszfatidilinozitol-4,5-biszfoszfát (PIP₂) inozitol-1,4,5-triszfoszfátra (IP₃) és daicilglicerinre (DAG) hasítja. Az IP₃ Ca-jelet indukál. A G_q jelátvitel többek között PKC, Src és prolingazdag tirozin kináz2 (Pyk2) tirozin kinázok aktivitását fokozzák, valamint reaktív oxigén származékok (ROS) termelődését okozhatják. Az ADAM-17 metalloproteáz aktivitásán keresztül pro heparin kötő epidermális növekedési faktorból (proHB-EGF) HB-EGF keletkezik, mely képes az epidermális növekedési faktor receptort (EGFR) transzaktiválni. Az EGFR a a Ras kis G-fehérje/Raf-1/mitogén aktivált protein kináz kináz (MEK)/extracelluláris szignál-regulált kináz1/2 (ERK1/2) kaszkádot

indíthatja el, illetve aktiválódhat a PI3K/Akt/mTor/ p70s6k kináz jelpálya is. A G_q mediált ROS képződés a trombocita eredetű növekedési faktor receptort (PDGFR) is képes transzaktiválni, mely vaszkuláris átépüléshez vezethet. A $G_{12/13}$ fehérjék közvetítésével az AT1R a Rho kis G-fehérje közvetítésével gátolni képes a miozin könnyű lánc foszfatázt (MLCP), mely elnyújtott vaszkuláris kontrakcióhoz és hipertrófiához vezet (Balakumar *et al.* Cellular signalling, 26 (2014) 2147-2160, alapján módosítva).

Az AT1-receptornak a hagyományos G-fehérjén keresztül létrejövő jelátviteli útvonala mellett több alternatív jelátviteli útvonalát is leírták, többek között intracelluláris tirozin-kinázok, JAK/STAT útvonal és Akt/PKB aktiválását, valamint a Rho, Ras és Rac aktivitásának szabályozását.

Az AT1-receptor MAPK-kaszkád DAG/PKC úton történő aktiválásával is eredményez növekedési faktor-szerű hatásokat, ám ezen útvonal önmagában valószínűleg nem lenne elég az AngII által hosszútávon kiváltott proliferációt, hipertrófiát és migrációt okozó sejtválaszaihoz. Ezen jelenségek hátterében döntő szerepet játszik az EGFR transzaktivációja, mely során egy mátrix-metalloproteáz (MMP) a pro-Hb-EGF (pro-heparin kötő epidermális növekedési faktor) fehérjét aktív, szolubilis Hb-EGF-fé hasítja, mely az EGFR-hez kötődve MAPK-ok aktiválódását okozza a sejtekben.

Az AT1-receptor aktiválása számos jelátviteli utat indít el a sejt belsejében, amelyek különféle rövid- és hosszú távú biológiai hatásokat eredményeznek az AngII fiziológiás célsejtjeiben. A vaszkuláris simaizomsejtekben (VSMC), amely az AngII egyik legfőbb célsejtje, a receptor stimulus legismertebb rövid távú hatása a simaizomsejtek összehúzódása, és ezen keresztül az artériás vérnyomás emelkedése. A hosszú távú hatások különböző génexpressziós változásokon keresztül nyilvánulnak meg, melyek az AngII káros hatásaiért is felelősek. Ezek közül a legjelentősebb a különböző szív- és érrendszeri betegségek, például a magas vérnyomás, az érfal remodelling, az érelmeszesedés, a szív hipertrófia, a szívizom fibrózis és a szívelégtelenség kialakulása. A renin-angiotenzin rendszer működésének befolyásolásával, az angiotenzin konvertáló enzim gátlókkal és az AT1-receptort blokkoló vegyületekkel kedvező eredményeket értek el a magas vérnyomás és más keringési betegségek kezelésében.

Az aktivált AT1R kapcsolódik a β-arresztin fehérjékkel, melyek jelátviteli folyamatok szervezésében (pl. MAP kináz kaszkád második hullámának aktiválása) is részt vesznek. Az aktivált AT1R szorosan kötődik a β-arresztin molekulához és kapcsolódásuk a recetor internalizácója közben is megmarad. Napjainkra elfogadott, hogy a β-arresztin fehérjék felelősek az AT1R G-fehérje független jelátviteli mechanizmusaiért. Úgy tekinthetünk ezen β-arresztin közvetített mechanizmusokra, mint a jelátviteli események második hullámára (2.

ábra). Ezek akár alternatív folyamatokat eredményezhetnek, úgymint a G-fehérje függő módon aktivált MAP kinázok sejtmag fehérjéket módosítanak, míg a G-fehérje függetlenül aktivált MAP kinázok citoplazmában elhelyezkedő fehérjéket képesek foszforilálni.

Az AT1R jelátvitel-szelektív aktivációja során a különböző ligandumok eltérő aktív konformációban stabilizálhatják a receptort, mely így eltérő mértékben képes aktiválni a különböző jelátviteli útvonalakat. Számos jelátvitel-szelektív AngII analóg AT1R agonista ismert, melyek által aktivált AT1R nem képes G-fehérjét kötni, azonban β-arresztin-kötése, ezáltal pedig a G-fehérje-független jelátvitele továbbra is megmarad, mely klinikailag igen előnyös hatáskombinációt eredményezhet (5.ábra).
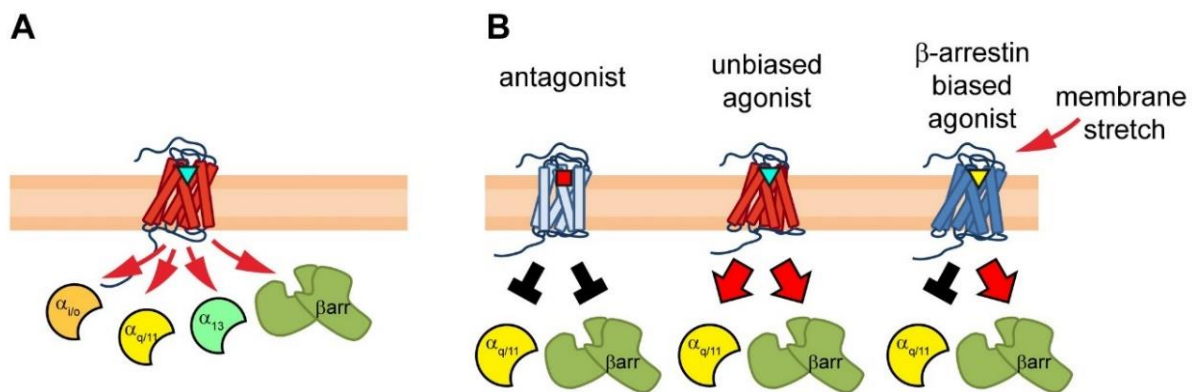
5. ábra. Az AT1-receptor effektor mechanizmusai. (A) A receptor számos effektor fehérjével léphet kapcsolatba. (B) Eltérő természetű ligandumok kötődése vagy a plazmamembrán mechanikai változása eltérő receptor konformációs változást indukálhat (Tóth AD, Turu G, Hunyady L, Balla A.: Best Pract Res Clin Endocrinol Metab. 2018).

1.2 Célkitűzések

1. A PtdIns 4-kinázok különböző izoformáinak tanulmányozása biokémiai és molekuláris biológiai módszerekkel abból a célból, hogy jobban megismerjük működésüket és a sejtekben betöltött szerepüket.

2. Egy új PtdIns 4-kináz izoforma klónozása és alapvető tulajdonságainak meghatározása.

3. A sejtben található különböző PtdIns 4-kinázok szerepének megértéséhez szükséges eszköztár létrehozása (mutagenezis és szelektív inhibitorok azonosítása).

4. Az AT1-receptor jelátvitelében alapvető hormon-szenzitív foszfoinozitidek szintéziséért felelős PtdIns 4-kináz izoforma azonosítása.

5. Kis G-fehérje aktiválódás vizsgálata az AT1-receptor stimuláció hatására, illetve az ehhez szükséges molekuláris biológiai és metodikai háttér létrehozása.

6. Az AT1-receptor deszenzitizációjának és mozgásának tanulmányozása agonista stimulus hatására.

7. Az AT1R internalizációjának vizsgálata jelátvitel szelektív aktivációt követően.

8. Terápiásan potenciálisan használni kívánt ligandumok által, jelátvitel-szelektív módon aktivált AT1R-ok sejten belüli hosszabb távú sorsának vizsgálata és összevetése a fiziológiás ligandum által kiváltott receptor-sorssal.

9. A plazmamembrán PtdIns$(4,5)P_2$ és a foszfatidilinozitol 4-kinázok szerepének vizsgálata az AT1R internalizációjában.

10. Az AngII által indukált génexpressziós változások vizsgálata, valamint a változásokért felelős jelátviteli útvonal feltérképezése vaszkuláris simaizomsejtekben.

2. A KÍSÉRLETEK RÖVID LEÍRÁSA, MÓDSZEREK

2.1. PtdIns 4-kináz aktivitás mérése

A PtdIns 4-kináz aktivitás mérése során a [γ-32P]ATP-ből a PtdIns-ba beépülő radioaktív foszfát mennyiségét határoztuk meg. A képződő PtdIns 4-foszfát savas közegben történő kloroform-metanolos extrakcióval választható el a be nem épült ATP-től és a foszfoproteinektől. A PtdIns-be beépült radioaktív foszfát mennyiségét folyadékszcintillációs spektrométerrel mértük. A terméket néhány kísérleti felállásban vékonyréteg kromatográfiával azonosítottuk, illetve esetenként rekombináns I-es típusú PtdIns 5-kináz segítségével tovább foszforiláltattuk.

2.2 SDS-poliakrilamid gélelektroforézis és western blot kísérletek

Különböző fehérjék méret szerinti elválasztásához SDS-poliakrilamid gélelektroforézist használtunk. A fehérjemintákhoz vagy a sejtekhez SDS-mintapuffert adtunk és az így kapott mintákat általában 100 °C-on forraltuk (5 perc). A vizsgálni kívánt fehérje nagyságától függően 4%-16%-os SDS poliakrilamid gélt használtunk, minigél rendszerre vittük fel a mintákat, egyenként 20-50 μg mennyiségben. A mintafelvitelkor arra törekedtünk, hogy az egyes mintákból azonos mennyiségű fehérjét vigyünk fel a gél vályúiba, így a kapott jelintenzitások (pl. western blot, autoradiográfia) mennyiségi összehasonlításra is lehetőséget adtak. A futtatott minták fehérjéinek molekulasúlyát standardok segítségével határoztuk meg. Az SDS-PAGE befejezése után a gélben elválasztott fehérjéket vagy membránra transzferáltuk vagy a gélben megfestettük. Western blot kísérletek esetén az elválasztott fehérjéket polivinilidén-fluorid membránokra átblottoltuk. A különböző primer antitestek tulajdonságaitól függően az inkubálás körülményei, időtartam, hígítások eltérhettek egymástól. Általában 1 órás blokkolást követően a membránokat 1 órán keresztül szobahőmérsékleten vagy 16 óráig 4 °C-on elsődleges antitestekkel, majd pedig HRP-vel konjugáltatott megfelelő másodlagos antitestekkel inkubáltuk 1 órát szobahőmérsékleten. Az antitesteket felerősített kemilumineszcencia módszerrel tettük láthatóvá.

2.3 Bioszenzorok és egyéb DNS konstruktok létrehozása

Az AT1R és a különböző PtdIns 4-kinázok funkcióinak vizsgálata céljából fúziós és mutáns fehérjéket állítottunk elő standard molekuláris biológiai módszerekkel. A létrehozott konstrukciókat, illetve a mutagenezist tartalmazó cDNS-eket restrikciós emésztéssel

11

azonosítottuk, majd a szekvenciákat DNS-szekvenálással ellenőriztük. A DNS-konstruktokat eukarióta sejtben fehérjekifejeződés létrehozására alkalmas plazmidokba építettük be. A vizsgálni kívánt fehérjéket a sejtkultúrában fenntartott eukarióta sejtvonalakban fejeztük ki. Az immortalizált sejtek tranziens transzfekciója a megfelelő cDNS-t tartalmazó plazmiddal és transzfekciós reagens segítségével történt. A transzfektálást követően a sejtek 24 órán belül kifejezik a vizsgálni kívánt fehérjéket.

A kis G-fehérje aktiválódás méréséhez olyan konstruktokat terveztünk és készítettünk, melyek tartalmazták a kis G-fehérje aktiválódáshoz szükséges komponenseket. A Ras aktiválódás méréséhez használt (RasBRET) szondában a sárga fluoreszcens fehérjéhez (YFP) kötöttük a Ras-t, mely kapcsolódik egy Ras-kötő doménhez (Raf-1 RBD), ettől C-terminálisan helyezkedik el a renilla luciferáz és egy kompartment-specifikus irányító domén. Bioszenzoraink működését az irodalomban elfogadott módon validáltuk. A szondákból számos verziót készítettünk és a legjobban működő konstruktokat használtuk tovább, majd a különböző kis G-fehérjék aktiválódásának vizsgálatára készített és optimalizált szondáknak különböző intracelluláris kompartmentekhez targetált verzióit is elkészítettük. Ennek érdekében a szondák N-, vagy C-terminális végéhez fúzionáltunk különböző targetáló szekvenciákat, melyek az expresszálódó szondát a megfelelő intracelluláris kompartmenthez irányítják. A targetált bioszenzorok sejten belüli helyzetét konfokális mikroszkóppal ellenőriztük.

Számos, membrán mikrodoméneket jelző fluoreszcens bioszenzort készítettünk és BRET mérésekkel élő sejtekben követtük nyomon a receptor eloszlásának változását *Renilla* luciferázzal jelölt receptor, illetve YFP-vel jelölt membrán-bioszenzorok segítségével. Az AT1R vezikuláris transzportjának vizsgálataihoz YFP-vel jelölt Rab4, Rab5, Rab7 és Rab11 konstrukciókat készítettünk a munkacsoportunk által már korábban is használt zöld fluoreszcens fehérjét (eGFP) tartalmazó konstrukciókból, a GFP-t kódoló szakasz YFP-re cserélésével. A PLCδ1 enzim foszfatidilinozitol 4,5-biszfoszfátot (PtdIns(4,5)P$_2$) kötő pleckstrin homológia doménjének (PH domén)-szuper Renilla luciferáz konstrukció készítésénél pedig a PLCδ1-PH-YFP plazmid eYFP-t kódoló régiója került kicserélésre a szuper *Renilla* luciferáz (Sluc) szekvenciájára.

2.4 PtdIns4KIIβ klónozása

A különböző humán és egyéb fajok genom szekvenciáit tartalmazó adatbázisok (pl. I.M.A.G.E. Consortium EST adatbázis) megjelenését követően a cDNS-ek klónozása egyszerűbbé vált. Szekvencia homológia alapján megvásárolt EST klónból azonosítottunk egy új PtdIns 4-kináz izoformát (PtdIns4KIIβ, az újabb nómenklatúra szerint PI4K2B). A kódoló

szekvenciát szubklónoztuk különböző expressziós vektorokba, illetve *in vitro* transzlációs assay-ben meghatároztuk az átíródó izoforma molekulatömegét. Egy cDNS könyvtár felhasználásával egy rövidebb variánst is izoláltunk.

2.5 Sejtkultúra és transzfekció

Kísérleteinkhez általában kétféle humán embrionális vesesejtet (HEK293, illetve HEK293T) vagy COS7 (majomvese sejtvonal) alkalmaztunk. A sejteket 100 IU/ml penicillint, 100 μg/ml streptomycint és 10 % hőinaktivált FBS-t tartalmazó Dulbecco által módosított médiumban (DMEM) tartottuk fenn. A tenyésztés 37°C-on, 5% CO_2 és 95% levegő keverékét tartalmazó termosztátban történt. A sejtek transzfekciójához jellemzően Lipofectamin 2000 (fehérjék overexpressziójához) vagy Oligofectamine (siRNS-sel történő fehérje kifejeződés csökkentéséhez) reagenseket használtunk.

A BRET kísérletekhez a sejteket 10 cm-es edényekben tenyésztettük, majd a transzfekció előtt tripszinezéssel felszedtük, és Lipofectamine-2000 reagenssel, Opti-MEM médiumban tranziensen transzfektáltuk. A BRET vizsgálatok előtt 24-48 órával a donor, illetve az akceptor fehérjéket tartalmazó plazmidokkal transzfektáljuk 96-lyukú, poli-L-lizinnel kezelt edényekben a sejteket. Egyes kísérletekben a BRET mérést 6 órás szérum-megvonást követően végeztük.

A génexpressziós vizsgálatinkhoz patkányból származó vaszkuláris simaizom sejttenyészeteket használtunk. Fiatal hím Wistar (170-250g testtömegű) patkányok aorta thoracalisát kipreparáltuk, majd az érszakaszokat módosított Krebs-Ringer oldatban (120 mM NaCl; 4,7 mM KCl; 1,8 mM $CaCl_2$; 0,7mM $MgSO_4$; 10 mM glükóz; 10 mM Na-HEPES; pH 7,4) tartottuk, róluk az oldalágakat, valamint a tunica adventiciát eltávolítottuk. Az így előkészített aorta szakaszt ezek után körülbelül egy milliméteres darabokra vágtuk, kollagenázzal emésztettük 25 percen át 37°C hőmérsékleten. Az aorta gyűrűket FBS-t tartalmazó DMEM-be helyeztük. A preparálást követő harmadik napon sejtek jelennek meg az aorta darabok körül, ekkor a szövet darabokat eltávolítottuk. A teljes konfluencia elérése után a sejteket sejttenyésztő flaskákra vittük át (1. passzálás). Kísérleteinket a harmadik passzálásban lévő sejteken végeztük.

2.6 Rekombináns fehérjék előállítása, *in vitro* transzláció

Számos kérdés megválaszolásához szükség volt fehérjék (pl. különböző PtdIns 4-kináz izoformák, illetve különböző mutáns fehérjék) rekombináns fehérjeként való előállítása is.

Ehhez a fehérjéket kódoló szekvenciákat pET23b bakteriális expressziós vektorba klónoztuk át. A kapott DNS konstruktokkal *E. Coli* baktériumokat (BL21-es törzs) transzformáltunk, melyeket 100 ml médiumban 37 °C-on növesztettünk A600=0,6 értékig. A fehérjeexpressziót 16 °C-on 6 órán keresztül 30 µM izopropil-1-tio-β-galaktopiranoziddal (IPTG) indukáltuk. A baktériumokat lízis pufferben ultrahanggal feltártuk, majd a 10.000 *g*-s (30 perc 4 °C) fugálás után kapott felülúszót glutation-agaróz gyöngyökkel. Mosást követően a gyöngyökhöz kötődött rekombináns fehérjét PreScission vagy TEV proteázos emésztéssel nyertük ki. A fehérjék tisztaságát SDS poliakrilamid gélbe történő futtatást követően Coomassie-Blue festéssel láthatóvá tettük, illetve mennyiségüket fehérje koncentráció méréssel, albumin standardok felhasználásával állapítottuk meg.

Néhány kísérletben a vizsgálni kívánt kinázokat in vitro transzlációs segítségével vizsgáltuk TnT-kapcsolt retikulocita lizátum és [^{35}S]metionin felhasználásával. A képződött fehérjéket SDS-poliakrilamid gélelektroforézist követő autoradiográfiával analizáltuk.

2.7 Sejtpermeabilizációs kísérletek

A különböző PtdIns 4-kináz izoformák endogén lipid szubsztrát specificitásának meghatározásához permeabilizációs kísérletet végeztünk. COS-7 sejteket a PtdIns 4-kinázok expressziós plazmidjaival transzfektáltuk, majd 24 órát követően permeabilizációs médiummal (110 mM KCl, 10 mM NaCl, 5 mM MgCl$_2$, 20 mM Hepes, pH 7,4, 2 mM EGTA, 0,05% BSA, 15 µg/ml digitonin, 0,3 mM ATP, 12,5 µCi/ml [γ-32P]ATP) inkubáltuk 37 °C-on 10 percig. A reakciót 5%-os perklórsavval állítottuk le, majd az inozitol lipideket vékonyréteg kromatográfiával választottuk el, a radioaktivitást pedig PhosphorImager-rel határoztuk meg.

2.8 Citoplazmatikus Ca^{2+} mérés sejtszuszpenzión

A HEK293 sejteket enyhe tripszines kezeléssel mobilizáltuk és Fura-2/AM tartalmú médiumban 45 percig szobahőmérsékleten sötétben inkubáltuk. A mérés előtt a sejteket lecentrifugáltuk és Fura-2/AM mentes médiumban reszuszpendáltuk, majd PTI Deltascan spectrofluorometer segítségével 340, illetve 380 nm-en történő excitációt követően 505 nm-en detektáltunk emissziót. Az emittált fénysugarak intenzitásának hányadosából következtettünk a minta intracelluláris Ca^{2+} koncentrációjára.

2.9 Immuncitokémia és konfokális mikroszkópia

Az immunflureszcens festésekhez a sejteket üveg fedőlemezen tenyésztettük. A sejtek fixálást szobahőmérsékleten végeztük 10 percen át, 2%-os vagy 4%-os paraformaldehid oldattal. A fixálást háromszori PBS-ben történő mosás követte. Ezután a mintákat 0,1%-os Triton-X vagy 0,2%-os saponin oldattal kezeltük, majd 1%-os BSA vagy 10% FBS tartalmú PBS oldatban blokkoltuk, majd PBS-es mosást követően 1 óráig az elsődleges antitesttel inkubáltuk. PBS-es mosást követően a mintákat a fluoreszcensen jelölt másodlagos antitesttel inkubáltuk. Végezetül az üveglemezeket mounting médiummal rögzítettük a tárgylemezekre.

A konfokális mikroszkópos vizsgálatokhoz ZEISS LSM410, LSM510, illetve egy LSM710 pásztázó lézer konfokális rendszert használtunk. GFP-vel jelölt AT1R-t stabilan kifejező HEK293 sejteket különböző ligandumokkal stimuláltuk, majd a receptor lokalizációját Zeiss LSM710 konfokális lézer mikroszkóp segítségével követtük nyomon. A GFP fluorofort 488 nm hullámhosszú argon lézerrel gerjesztettük. A konfokális felvételek elemzését ZEN, illetve MetaMorph szoftverek segítségével végeztük el.

2.10 Immunprecipitációs kísérletek

Az immunprecipitációs kísérletekhez a sejteket a vizsgálni kívánt fehérjéket kódoló plazmidokkal transzfektáltuk. 48 óra múlva a sejteket lízis pufferben (50 mM Tris/HCl, pH 7,4, 150 mM NaCl, 1 mM EDTA, 1% Nonidet P-40, 0,25% Na-deoxilát, 1 mM dithiothreitol, 1 mM 4-(2-aminoetil)benzenesulfonil-fluorid, 10 µg/ml leupeptin, 10 µg/ml aprotinin) lizáltuk, majd centrifugálással (14000 g, 15 perc) előállított felülúszóhoz mértünk a fehérjére (vagy ahhoz kapcsolt epitópra) specifikus antitestet. A mintákat legalább két óráig kevertettük 4°C hőmérsékleten. Az antitesteket protein G-agaróz gyöngyökkel kötöttük meg, majd a kötődött fehérjéket western blot módszerrel vagy kináz aktivitás méréssel analizáltuk.

2.11 Biolumineszcencia és fluoreszcencia rezonancia energiatranszfer módszer

A rezonancia energiatranszfer módszerek, úgymint a BRET (biolumineszcencia rezonancia energiatranszfer) módszer lehetőséget teremtett arra, hogy fehérjék közötti kapcsolatokat jobban feltérképezzük, illetve akár egy polipeptidláncon belül a különböző hatásokra bekövetkező konformáció változásokat monitorozzuk. A BRET módszer két fehérje vagy fehérjerészlet közötti molekuláris közelség mérését teszi lehetővé nagy érzékenységgel, mivel a mérés során nincs szükség excitáló fény használatára. A BRET mérés során egy sejtpermeábilis szubsztrát (coelenterazin) hatására a vizsgált fehérjéhez kapcsolt *Renilla*

luciferáz (lumineszcens 'energiadonor') fotonokat emittál, mely két vizsgált fehérje (úgynevezett „intermolekuláris" szondák), vagy ugyanazon fehérje különböző részei („intramolekuláris" szondák) molekuláris szintű (<100 Å) közelsége esetén energiatranszfert képes kiváltani, mely a YFP vagy mVenus ('energiaakceptor') fényemisszióját hozza létre. A BRET módszer előnye, hogy a jelátvitelben szereplő fehérjék interakcióit élő sejtekben vizsgálhatjuk, ezáltal lehetőségünk van valós időben követni a jelátvitelben részt vevő komplexek konformációs változásait, valamint a résztvevő molekulák mozgásának időbeni és térbeni dinamizmusát. A mérések előtt a sejteken lévő 10% FBS tartalmú DMEM médiumot módosított Krebs-Ringer oldatra cseréltük. A BRET méréseket a *Renilla* luciferáz szubsztrátjának, a coelenterazin *h*-nak (5 µM) hozzáadását követően kezdtük meg Berthold Mithras LB 940, illetve Varioskan Flash többcsatornás lemezolvasó készülékekkel 37 °C-on. Az energiaakceptor, illetve az energiadonor emissziós maximumain, 485 és 530 nm-es hullámhosszokon detektáltunk fényintenzitásokat melyek hányadosát, BRET hányadosnak vagy BRET jelnek nevezzük. A molekuláris közelség létrejöttét a hányados emelkedése jelzi, míg a távolság növekedésével a hányados csökken. A vizsgálataink során homogén sejtszuszpenzió osztásával létrehozott kísérleti mintákon végzünk önkontrollos kísérleteket. Az adatokat esetenként úgy ábrázoltuk, hogy az ingerelt sejtek értékeiből kivontuk a kontroll, csak vívőanyagot kapott sejteken mért értékeket, illetve a stimulálás előtti átlagértékeket.

FRET (fluoreszcencia rezonancia energiatranszfer) mérés esetén cián fluoreszcens fehérje (CFP) és YFP fúziós fehérjék közötti lokalizációs változásokat követtük. COS-7 sejteket 10-cm-es szövettenyésztő edényeken növesztettük és transzfektáltuk, majd a mérés előtt a sejteket enyhe tripszines kezeléssel szuszpendáltuk, és spectrofluorometer segítségével 425 nm-en történő excitációt követően 525 és 475 nm-en detektáltunk emissziót. Az 525/475 emittált fénysugarak intenzitásának hányadosából következtettünk a fehérjék lokalizációjának megváltozására a citoszól és a membrán között.

2.12 RNS izolálás sejttenyészetből, cDNS készítés és qPCR

Az RNS preparálását megelőzően a megfelelő kísérletekben a stimulust a médium eltávolításával és ezt követő kétszeri hideg 1x PBS-ben történő mosással szüntettük meg, majd az RNeasy Mini Kit (QIAGEN) segítségével a teljes RNS mennyiséget izoláltuk a sejtekből. Az RNS koncentrációkat NanoDrop ND-1000 típusú spektrofotométerrel mértük. A cDNS készítés során 1µg RNS-ből indultunk ki, a reverz transzkripcióhoz a Thermo Fisher Scientific által gyártott termékeket használtuk. A reakcióelegy összeállítása után a cDNS szintézis PCR készülékben történt. A real-time vagy valós idejű, másnéven kvantitatív PCR (qPCR) a

klasszikus PCR reakció, valamint a fluoreszcens fotometria ötvözésén alapuló módszer. Méréseinkhez LightCycler480 (Roche) készüléket használtunk, a fotokémiai reakcióhoz pedig SYBR-Green fluoreszcens reportert alkalmaztunk. A folyamat során a készülék a mintákat tartalmazó műanyag lemezt ciklikusan hevíti fel, majd hűti le, a ciklusok során pedig detektáltuk a megnövekvő DNS mennyiségből adódó fluoreszcens jel növekedését, a mért fluoreszcens jel arányos a keletkező duplaszálú DNS molekulák mennyiségével a reakció során. A valós idejű PCR az alkalmazott protokolltól függően abszolút- és relatív mennyiségek meghatározására is képes. Az AngII-indukált génexpressziós változások meghatározásához relatív kvantifikációt alkalmaztunk, tehát a keresett gének expresszióját egy referencia gén expressziójához viszonyítottuk. Méréseinkben erre a célra a glicerinaldehid-3-foszfát dehidrogenáz (*Gapdh*) gént használtuk.

## 2.13 Adatok elemzése, statisztikai analízis

Az adatok elemzéséhez és az ábrák készítéséhez a GraphPad Prism valamint a Sigmaplot programokat használtuk. Az egyes kísérletekben legalább két párhuzamos mérést végeztünk. Statisztikai módszerként egy-, illetve kétszempontos varianciaanalízist (ANOVA), majd Bonferroni, vagy Tukey post hoc tesztet alkalmaztunk, illetve néhány esetben többszörös lineáris regresszió alkalmazására került sor. A csoportok közti különbségeket akkor tekintettük szignifikánsnak, ha a szignifikancia szintje kisebb, mint 0,05.

3. A TUDOMÁNYOS EREDMÉNYEK ÖSSZEFOGLALÁSA

## 3.1 PtdIns 4-kináz izoformák azonosítása és jellemzése

3.1.1 A II-es típusú PtdIns 4-kinázok vizsgálata

Munkánk során a PtdIns 4-kinázok különböző izoformáit kívántuk tanulmányozni, hogy jobban megismerjük működésüket és a sejtekben betöltött szerepüket. Annak ellenére, hogy a II-es típusú PtdIns 4-kinázt homogenitásig tisztították és enzimológiailag sokkal jobban jellemezték, mint a más típusú formákat, a II-es típusú formát nem sikerült sokáig klónozni. Kutatómunkám során sikerült elsőként klónozni a II-es típusú PtdIns 4-kináz β izoformáját (újabb nómenklatúra szerint PI4K2B). Ezen izoformát az elsőként klónozott II-es típusú PtdIns 4-kinázzal, a PtdIns4KIIα-val, való homológiája alapján azonosítottuk az NCBI adatbázisában (NCBI: 8922869). Az azonosított transzkript 3468 bp méretű volt, amely egy 1503 bázispárból álló nyitott leolvasási keretet (open reading frame, ORF) tartalmaz (6. ábra, A panel). A PtdIns4KIIα és a PtdIns4KIIβ szekvenciáinak összehasonlítása alapján a C-terminálisan elhelyezkedő katalitikus domén nagymértékű homológiát mutatnak, viszont az N-terminális régiók között kisebb mértékű a hasonlóság (6. ábra, B panel).
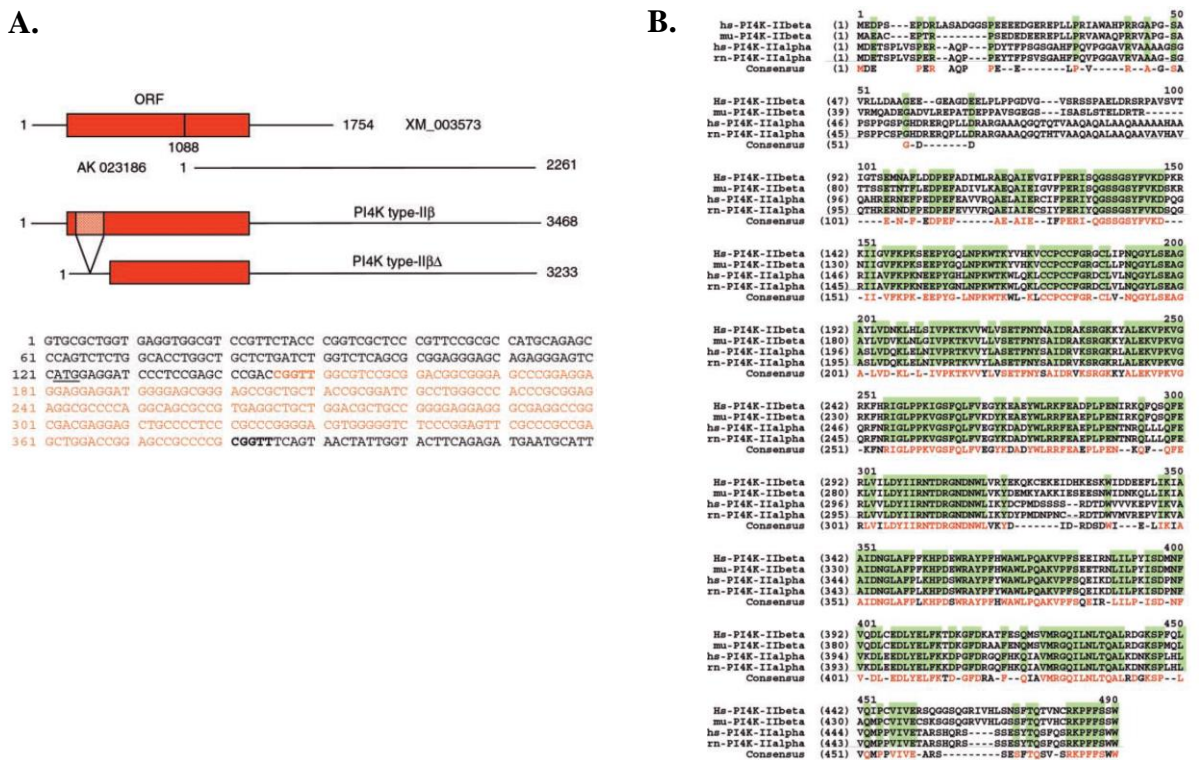

6. ábra. A PtdIns4KIIβ cDNS-ének szerkezete és a II-es típusú PtdIns 4-kinázok szekvenciáinak összehasonlítása. (A) Az AL527283 EST klón tartalmazta a PtdIns4KIIβ kódoló szakaszokat, melyben egy 1503 bp-os ORF található. Marathon-Ready cDNS könyvtár PCR-ezésével egy N-terminális trunkált formát is izoláltunk (IIβΔ). (B) A PtdIns4KIIβ és a PtdIns4KIIα polipeptid-lánc szekvenciájának összehasonlítása (Balla A, *et al.*: J Biol Chem. 2002).

Az izoformák biokémiai és enzimológiai jellemzéséhez a II-es típusú PtdIns 4-kinázok kódoló szekvenciáit pcDNA3.1 expressziós plazmidokba illesztettük. *In vitro* transzlációs kísérletek alapján mind a PtdIns4KIIα, mind a PtdIns4KIIβ mérete ~54 kDa-nak bizonyult (7. ábra, A panel). Ez megfelelt a korai munkákban becsült értéknek, amelyekben a homogenitásig tisztított fehérje molekulatömege ~ 55-56 kDa volt. Kimutattuk, hogy a két izoforma hasonló érzékenységet mutat különböző vegyületek iránt, a wormannin (a PtdIns 3-kinázok és a III-as típusú PtdIns 4-kinázok hatékony gátlószere) nem gátolta aktivitásukat, a nem-ionos detergensek iránti érzékenységük hasonlónak bizonyult, illetve adenozin hatékonyan gátolta aktivitásukat (7. ábra, B panel). A II-es típusú PtdIns 4-kinázok kevésbé bizonyultak érzékenyek fenil-arzén(III)-oxid (PAO) iránt, mely leginkább a PtdIns 4-kináz IIIα izoformát gátolta (7. ábra, C panel).
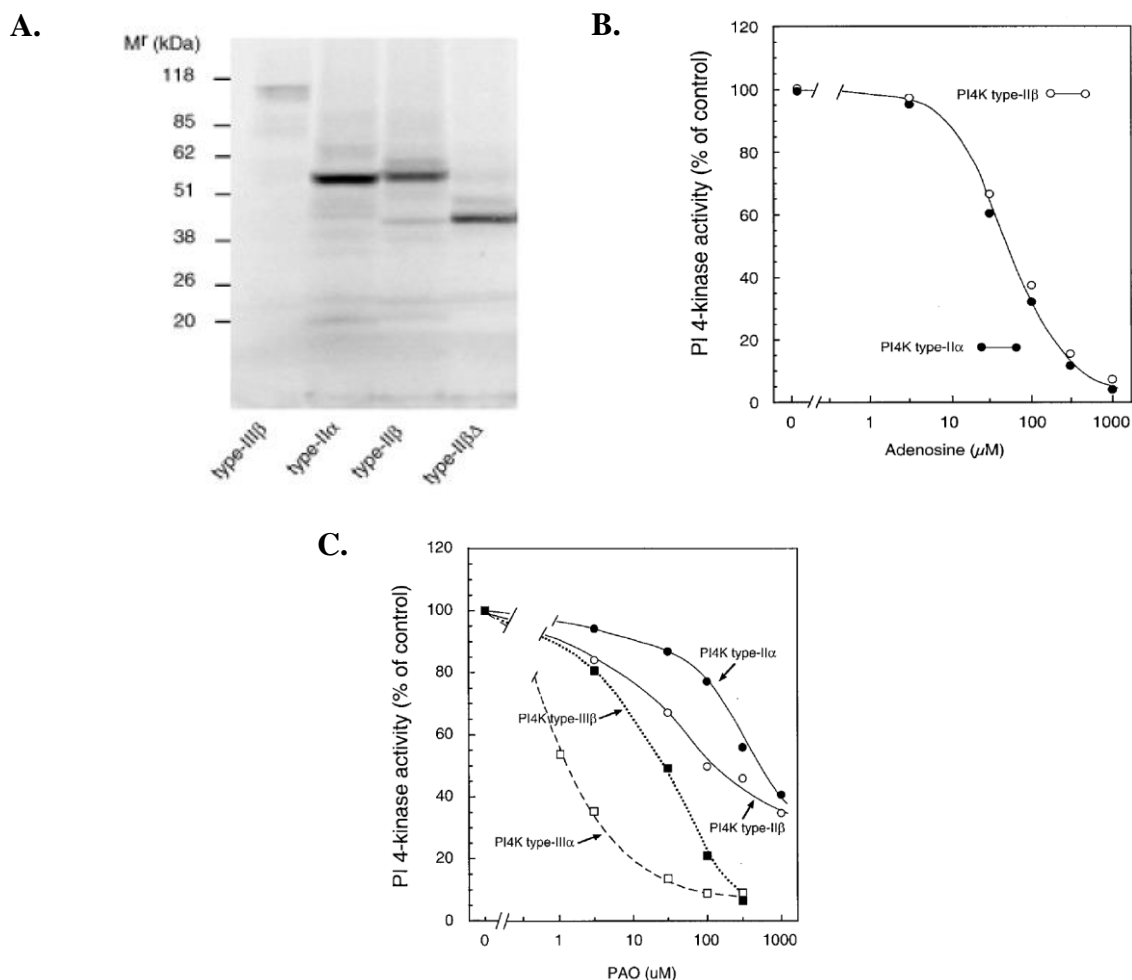
7. ábra. PtdIns 4-kináz (PI4K) izoformák alapvető biokémiai tulajdonságainak meghatározása. (A) PtdIns 4-kinázok *in vitro* transzlációja. A PtdIns4KIIIβ, a PtdIns4KIIα, a PtdIns4KIIβ, illetve a PtdIns4KIIβ egy variánsának cDNS-ét tartalmazó expressziós vektorjainak és nyúl retikulocita transzlációs rendszer felhasználásával vizsgáltuk az izoformák expresszióját. Expresszált PI 4-kináz izoformák tulajdonságainak jellemzése során kimutattuk, hogy a II-es típusú formák adenozin (B) és PAO (C) érzékenysége nagyon hasonló (Balla A, *et al.*: J Biol Chem. 2002).

19

A II-es típusú PtdIns 4-kinázokat COS-7 sejtekben is expresszáltattuk és permeabilizált sejtekkel végzett kísérleteinkben kimutattuk, hogy mindkét izoforma csak PtdIns-t képes endogén szubsztrátként használni, illetve azt, hogy a PtdIns4KIIβ izoforma enzimaktivitása kisebb, mint a PtdIns4KIIα-é (8. ábra, A és B panel). Az enzimaktivitásokban tapasztalható különbségeket az expresszált enzimek immunprecipitációs tisztítását követő enzimaktivitás mérésekben is igazoltuk (8. ábra, C panel). Az immunprecipitációval tisztított enzim-preparátumokkal is alátámasztottuk, hogy az általunk azonosított PtdIns4KIIβ a PtdIns-ból csak PtdIns(4)P-ot képes szintetizálni, melyet az I-es típusú PtdIns 5-kináz szubsztrátként használhat fel PtdIns(4,5)P_2 képzéséhez (8. ábra, D panel).
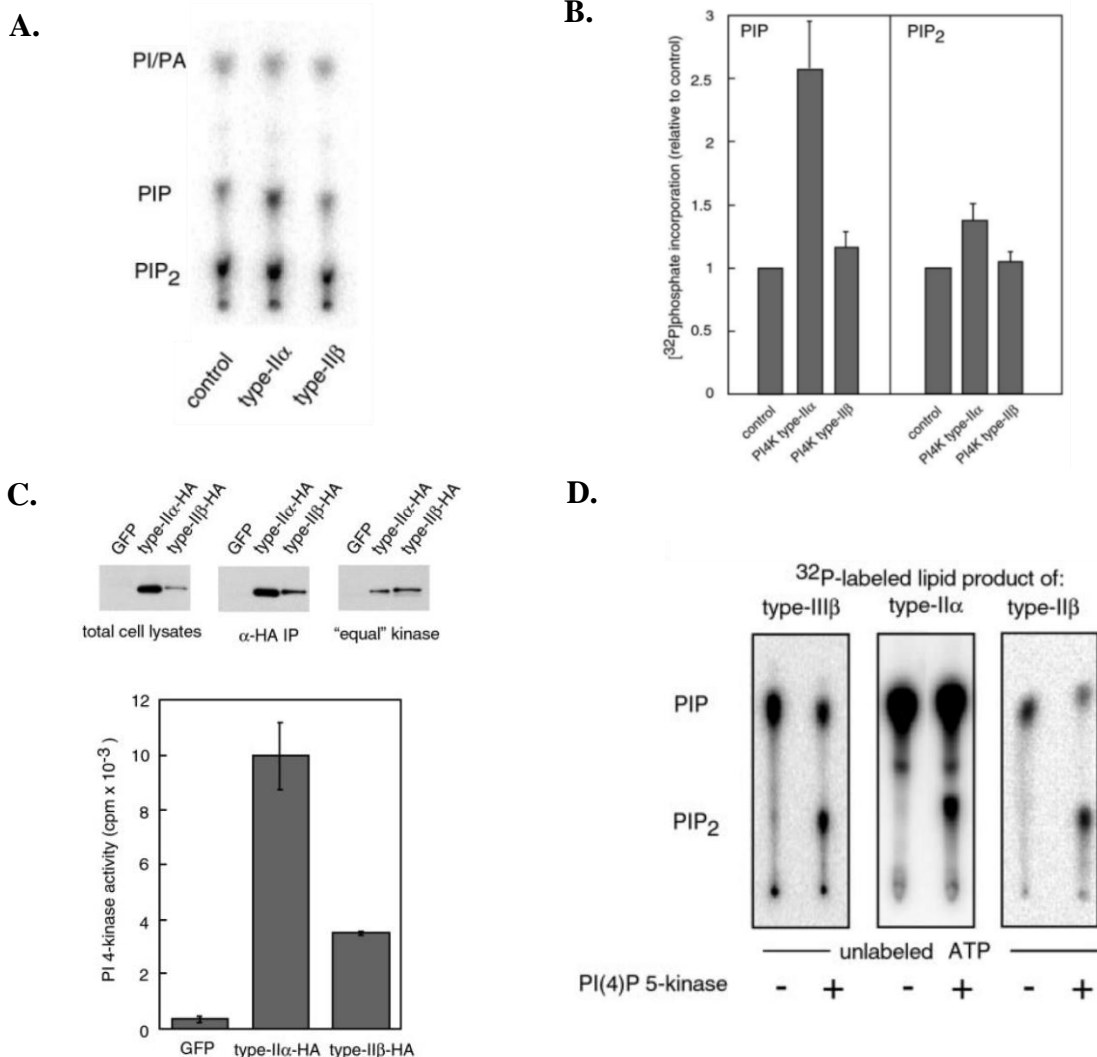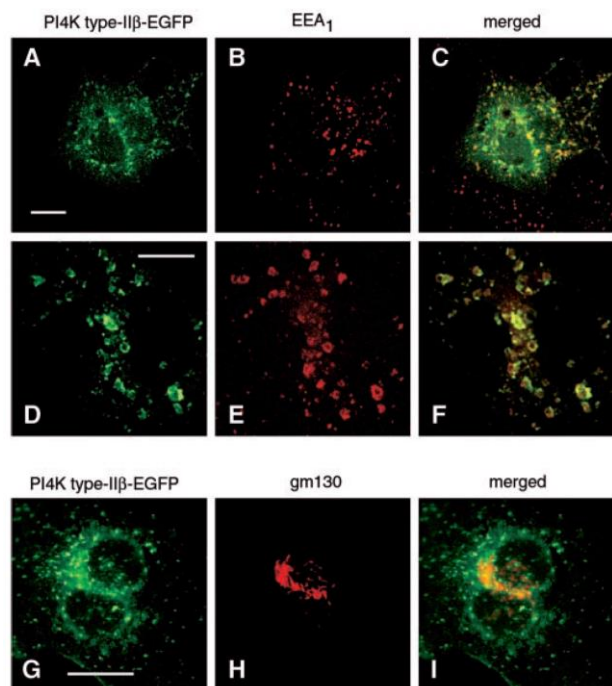

8. ábra. A II-es típusú PtdIns 4-kinázok (PI4K) aktivitásának vizsgálata. COS-7 sejteket a különböző izoformák expressziós vektorjaival transzfektáltuk, majd a különböző, radioaktívan jelölt foszfoinozitideket vékonyréteg kromatográfiával azonosítottuk (A), illetve a foszfolipidekbe beépült radioaktivitás erősségét PhosphorImager segítségével határoztuk meg (B). COS-7 sejtekből a II-es típusú PtdIns 4-kinázok HA-tag fúziós fehérjéit immunprecipitáltuk, majd a tisztított enzimek kináz aktivitását (C) és a képződött lipideket vékonyréteg kromatográfiával analizáltuk (D) (Balla A, *et al.*: J Biol Chem. 2002).

Megvizsgáltuk a II-es típusú PtdIns 4-kinázok elhelyezkedését a sejtekben, mert a rendelkezésre álló adatok alapján csak az volt ismert, hogy membránhoz kapcsolva helyezkedhetnek el. COS-7, illetve HEK293 sejtekben is expresszáltattuk a HA-tag, illetve GFP-fúziós PtdIns 4-kinázokat. Konfokális mikroszkópiával végzett meghatározásaink alapján meglepő módon mindkét II-es típusú PtdIns 4-kináz főleg az intracelluláris membránokban lokalizálódik és csak kis mennyiség található a plazmamembránon (9. ábra). Immuncitokémiai vizsgálatokat végeztünk, hogy pontosan megállapítsuk melyik intracelluláris kompartmentekben lokalizálódnak a II-es típusú PtdIns 4-kinázok. Eredményeink alapján mindkét forma szoros kolokalizációt mutat a korai endoszóma (EEA1) markerrel, illetve a PtdIns4KIIβ izoforma a gm130 Golgi markerrel is mutat egy kismértékű kolokalizációt (9. ábra, B panel, „G-I").
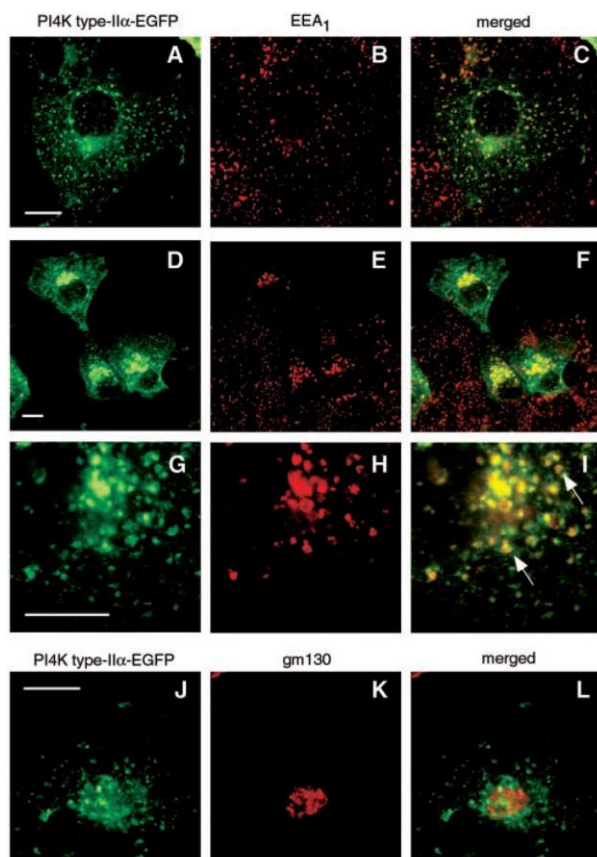
A.   **B.**

9. ábra. A II-es típusú PtdIns 4-kinázok lokalizációjának vizsgálata. GFP-vel fúzionáltatott PtdIns4KIIα (A) vagy PtdIns4KIIβ (B) expresszáló COS-7 sejteket fixáltuk és permeabilizációt követően különböző sejtorganellum markerekkel (piros) immunfestettük. Konfokális mikroszkópos felvételeket készítettünk, a lépték: 10 μm (Balla A, *et al*.: J Biol Chem. 2002).

21

Kimutattuk, hogy mindkét II-es típusú PtdIns 4-kináz megtalálható receptorok endocitótikus útvonalaiban, illetve az AT1-receptort stabilan expresszáló élő HEK293 sejtekben az AngII stimulus hatására a II-es típusú PtdIns 4-kináz lokalizációja nem változik meg számottevően és hogy ugyanabban a kompartmentben található, amelyikben az endocitózisra került receptor is (10. ábra).
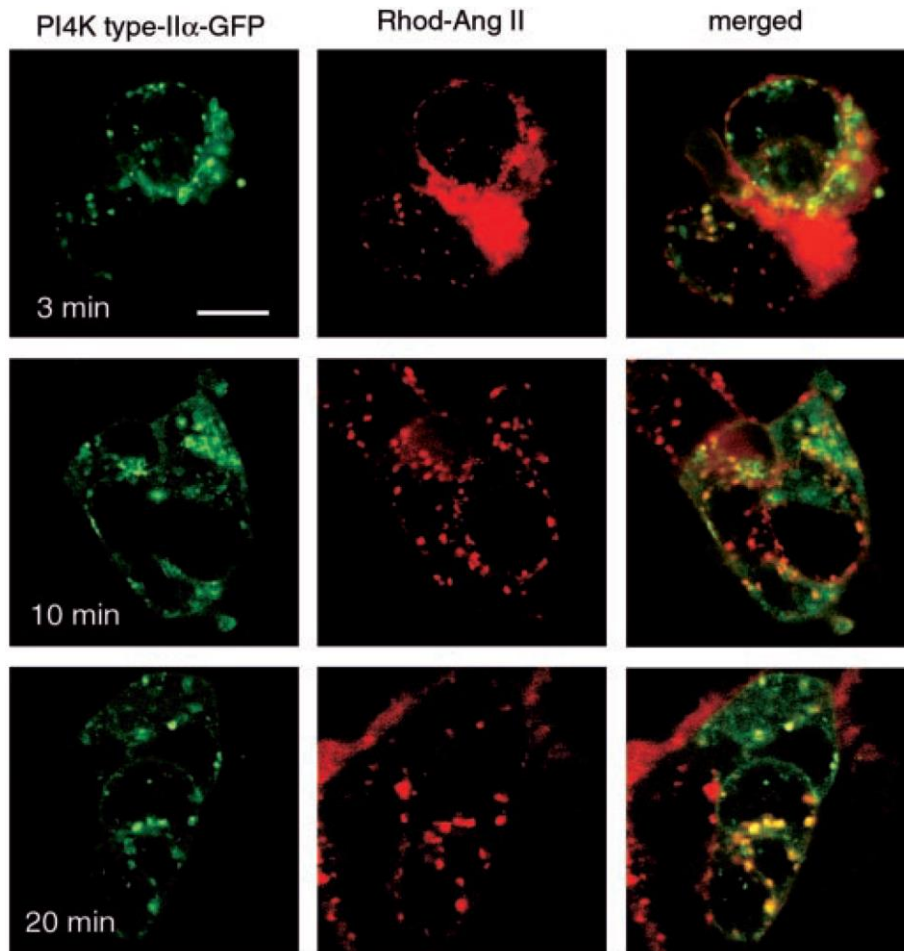

10. ábra. A II-es típusú PtdIns 4-kináz kolokalizál az internalizált AT1 angiotenzin receptorral. AT1-receptort expresszáló HEK293 sejteket GFP-vel fúzionáltatott II-es típusú PtdIns 4-kinázzal (PI4K) transzfektáltuk. 24 óra múlva a sejteket rodamin (piros) jelölt AngII-vel inkubáltuk, és a jelzett időpontokban konfokális mikroszkópos felvételeket készítettünk. (Balla A, *et al.*: J Biol Chem. 2002).

3.1.2 A III-as típusú PtdIns 4-kinázok vizsgálata

A korai foszfatidilinozitol kináz kutatások arra irányultak, hogy vizsgálják, milyen szerepe van ezen enzimeknek az agonista-szenzitív, plazmamembránban található PtdIns(4,5)P_2-pool fenntartásában és ezáltal a DAG és Ins(1,4,5)P_3 képződésében. Az alábbiakban ismertetésre kerülő kísérleteinkben a III-as típusú PtdIns 4-kinázok különböző izoformáit kívántuk tanulmányozni, hogy megértsük, mely izoforma lehet a felelős az agonista-

szenzitív PtdIns(4,5)P_2-pool fenntartásában, illetve a sejteket ért stimulusok során a jelátviteli folyamatok során hasított foszfoinozitidek reszintéziséért. Előzetes munkák alapján annyit lehetett tudni, hogy ezen foszfoinozitidek képzéséért valamelyik wortmannin-érzékeny (III-as típusú PtdIns 4-kinázok) izoforma felelhet. Csalódást keltő eredmény volt, hogy sem az endogén (11. ábra), sem a sejtekben expresszáltatott III-as típusú PtdIns 4-kinázok nem mutattak számottevő plazmamembrán lokalizációt (12. ábra), ezért másféle megközelítéssel próbáltuk a kérdést megközelíteni.
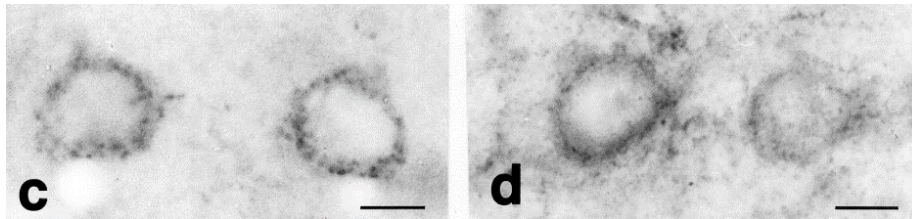
11. ábra. A PtdIns4KIIIα és a PtdIns4KIIIβ immunlokalizációjának összehasonlítása patkány agyban. Fénymikroszkópos felvételek patkányok agykéreg lamina IV. rétegéből anti-PtdIns4KIIIα (c) és IIIβ (d) immunreakcióról. A lépték 10 μm. (Balla A, *et al*.: Exp. Brain Res. 2000).
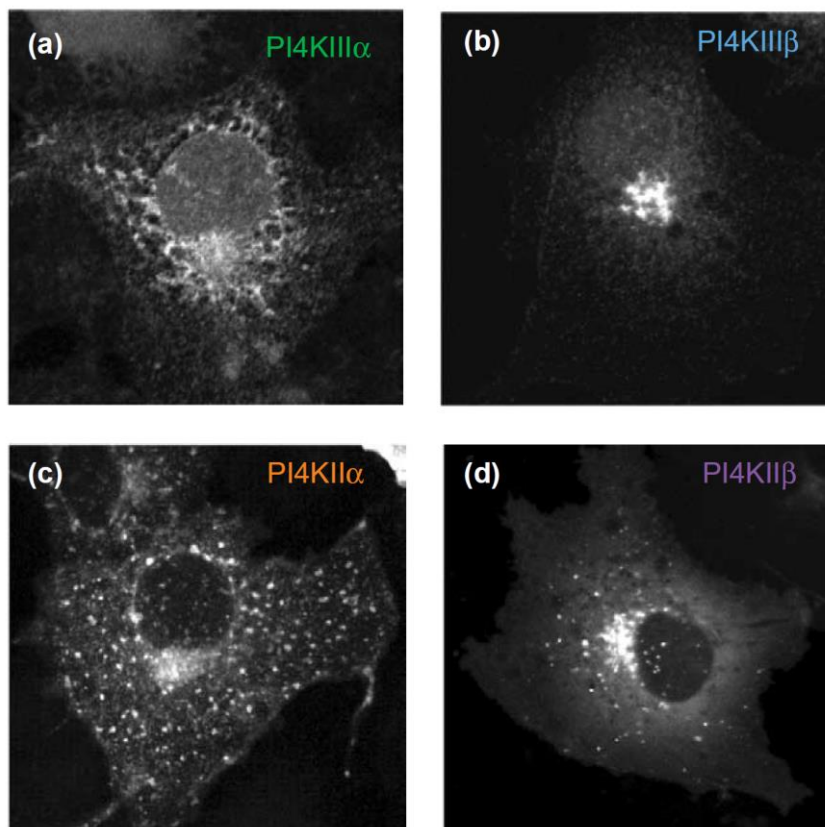
12. ábra. A különböző PtdIns 4-kináz (PI4K) izoformák elhelyezkedése a sejtekben. (a-d) COS7 sejtek különböző PtdIns4-kináz expressziós vektorokkal transzfektáltuk, majd 24 óra múlva detektáltuk az expresszálódó izoformák elhelyezkedését konfokális mikroszkóppal (Balla A *et al*.: Trends in Cell Biology, 2006).

A foszfoinozitidek a lipid természetüknél fogva a sejtek membránjaiban helyezkednek el, és fontos szereppel bírnak a sejtorganellumok membránjának a megjelölésében is, mintegy felcímkézik azokat a specifikus felismerő domének számára. A PH domének nagyon sok fehérjében előfordulnak, amelyek elősegítik ezen fehérjék kötődését a membránok foszforilált foszfoinozitidjeihez. Ezen mechanizmus szerepet játszik a PH domént tartalmazó fehérjék sejten belüli lokalizációjának szabályozásában, és ezáltal a foszfoinozitidek fontos regulátorai a fehérjék mozgásának és funkcióinak is. Bizonyos foszfoinozitidek szintjének megváltozása egy adott sejtkompartmentben a fehérjék membránhoz kötődésének dinamikus megváltozását okozhatják, amely jelenthet az adott membránhoz kihorganyzódást, de eltávolodást is. A kísérleteinkben elsősorban olyan PH doméneket használtunk, amelyek vagy a PtdIns(4)P, vagy a PtdIns(4,5)P_2 foszfoinozitideket ismernek fel. Kísérletekben a különböző stimulusok, gátlószerek, illetve fehérjeszintek változtatásának hatását térképeztük fel az eltérő foszfoinozitid specificitású PH domének elhelyezkedésére élő sejtekben. A munkáink során sikerült a sejtmembrán PtdIns(4)P szintjének változtatására alkalmas rendszert kidolgozni és jellemezni.

Irodalmi adatok alapján a FAPP1 (Four-phosphate-adaptor protein 1) és az OSBP (Oxysterol-binding protein) fehérjék PH doménjei PtdIns(4)P specifikusak élesztő sejtekben. Kísérleteinkben ezen PH doméneket GFP-vel fúzionáltattuk, majd megvizsgáltuk a lokalizációjukat COS-7 sejtekben (13. ábra).
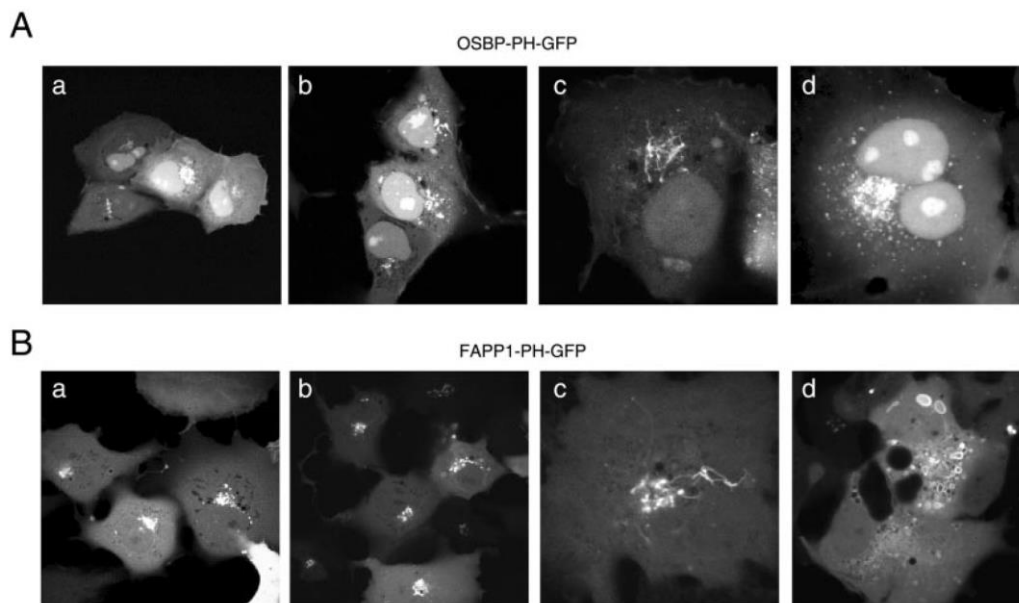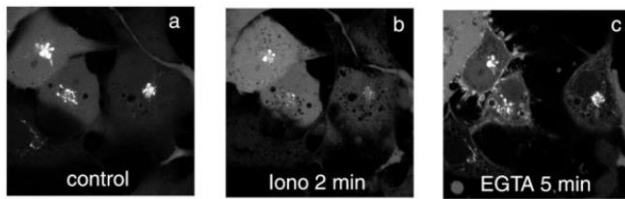

13. ábra. Az OSBP-PH-GFP és a FAPP1-PH-GFP fúziós fehérjék elhelyezkedése COS-7 sejtekben.
A sejtekben a PtdIns(4)P-t felismerő OSBP-PH-GFP (A), illetve FAPP1-PH-GFP (B) konstruktokat expresszáltattuk, majd a fehérjék lokalizációját konfokális mikroszkóppal vizsgáltuk élő sejtekben (Balla A *et al*.: Mol Biol Cell. 2005).

A mikroszkópos felvételek alapján az OSBP-PH-GFP és a FAPP1-PH-GFP is a sejtek különböző kompertmentjeihez lokalizálódhat, az expresszió mértékétől függően heterogenitást mutatnak, de elsősorban a Golgihoz asszociálódva fordulnak elő (13. ábra). A fúziós fehérjék lokalizációja a PH domének steady state eloszlását tükrözik, amely a membránokban található foszfoinozitidek mellett egyéb tényezőktől, pl. fehérje-fehérje kölcsönhatásoktól is függhetnek. Megvizsgáltuk, hogy a foszfoinoziditek szintjének gyors változtatása milyen módon változtatja meg a vizsgált PH domének eloszlását. A foszfolipáz C aktiválás hatására a különböző inozitol lipidek szintjének gyors változása következik be, amely a foszfoinozitid specifikus PH domének eloszlását megváltoztathatja a sejtekben. A kísérleteinkben 10 µM ionomycin kezelés hatására bekövetkező PLC aktiválódás hatására megfigyeltük, hogy mind a FAPP1-PH (14. ábra, A panel), mind az OSBP-PH doménje (14. ábra, B panel) a membránokból a citoszólba jut. A Ca^{2+}-jel és így a PLC aktiválódás megszüntetése EGTA vagy BAPTA kezeléssel a membránokban a foszfolipidek gyors reszintézisét teszi lehetővé, és ilyenkor a PtdIns(4)P specifikus FAPP1-PH-GFP (14. ábra, A panel, c), illetve az OSBP-PH-GFP (14. ábra, B panel, c-d) is részben a plazmamembránhoz kötődik. Kimutattuk, hogy a plazmamembránban nem jelenik meg PtdIns(4)P specifikus PH domén, ha a COS-7 sejteket 10 µM wortmannin inhibitorral előkezeltük (14. ábra, B panel, g-h). Ezen eredmény valamelyik III-as típusú PtdIns 4-kináz szerepére utal a plazmamembrán PtdIns(4)P reszintézisében.

A plazmamembránban történő, a foszfolipid reszintézist követő PH domén transzlokációt fluoreszcencia rezonancia energiatranszfer (FRET) mérésekben kvantifikáltuk. A sejtek stimulusa nélkül a PtdIns(4)P-t felismerő OSBP-PH-GFP és a PtdIns(4,5)P_2-t felismerő PLCδ1-PH-RFP szondák eltérő kompartmentben helyezkednek el, így köztük az energiatranszfer mértéke kismértékű. Az ionomycin (iono) hatására bekövetkező foszfoinozitid lebomlást, majd az ezt követő foszfolipid reszintézist az OSBP-PH-GFP és a PLCδ1-PH-RFP transzlokációjának követésével vizsgáltuk és kimutattuk, hogy a stimulust követő reszintézis során az OSBP-PH-GFP is megjelenik a PLCδ1-PH-RFP közelében a plazmamembránban, így köztük nagy FRET jel mérhető ezen időpontokban (15. ábra, B panel, kék görbe). Demonstráltuk, hogy 10 µM wortmannin (wm) előkezelés nagymértékben gátolta a vizsgált PH domének megjelenését a plazmamembránban (15. ábra, B panel, piros görbe).

A.

B.

after Wm (10 µM) treatment
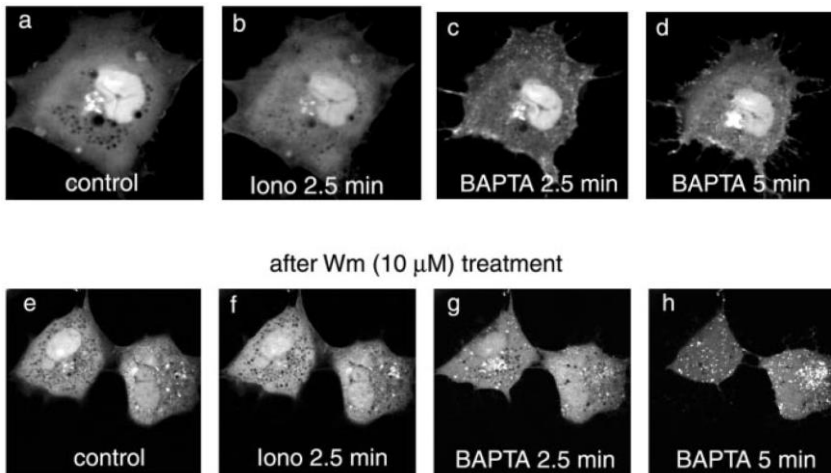
14. ábra. PtdIns(4)P specifikus PH domének transzlokációja. COS7 sejtekben PtdIns(4)P-t felismerő FAPP1-PH-GFP (A) vagy OSBP-PH-GFP (B) szondákat expresszáltattunk, majd ionomycinnel (iono) indukált Ca^{2+}-jel generálása után a GFP fúziós fehérjék transzlokációját vizsgáltuk konfokális mikroszkóp segítségével (Balla A *et al*.: Mol Biol Cell. 2005).
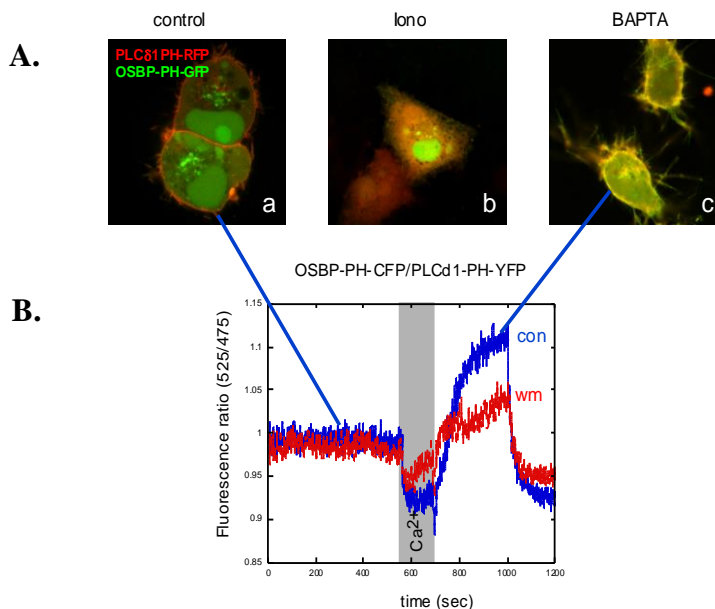
15. ábra. A plazmamembrán PtdIns(4)P szintéziséért egy wortmannin-szenzitív PtdIns 4-kináz felel. COS7 sejtekben PtdIns(4)P-t felismerő OSBP-PH-GFP (zöld), illetve a PtdIns(4,5)P_2-t felismerő PLCδ1-PH-RFP (piros) szondákat expresszáltattunk. (A) Konfokális mikroszkópos felvételen látható, hogy a PtdIns(4)P és PtdIns(4,5)P_2 reszintézis során ezen foszfoinozitideket felismerő PH domének a plazmamembrán lipid pool-okat jelölik. (B) 10 µM wortmannin (wm) kezelés hatását FRET mérésben kvantifikáltuk (Balla A *et al*.: Mol Biol Cell. 2005).

26

További kísérleteinkben különböző gátlószerekkel és géncsendesítéses módszerekkel vizsgáltuk, hogy a plazmamembrán PtdIns(4)P szintézisében melyik wortmannin-érzékeny PtdIns 4-kináz játszik kulcsszerepet. A kísérleteinkben a különböző PtdIns 4-kinázok (PI4K) izoformák lecsendesítése siRNS technikával történt, a specificitást és a hatékonyságot western-blot módszerrel igazoltuk, kontrollként β-aktin (actin) immunfestést alkalmaztunk (16. ábra, A panel). Ezek után a COS7 sejtekben PtdIns(4)P-t felismerő FAPP1-PH-GFP szondát expresszáltattuk, majd ionomycinnel (iono) indukált Ca^{2+}-jel generálása után a szonda transzlokációját vizsgáltuk (16. ábra, B panel). A PtdIns 4-kináz IIIα genetikai lecsendesítése (16. ábra, B panel, „D"), illetve 10 μM fenil-arzén(III)-oxid (PAO) (16. ábra, B panel, „E"), mely csak a PtdIns 4-kináz IIIα izoformát gátolja (7. ábra, C panel, illetve 18. ábra, A panel) plazmamembrán PtdIns(4)P-reszinézisét meggátolta. Eredményeink alapján megállapítottuk, hogy a plazmamembrán PtdIns(4)P készlet szintéziséért a PtdIns 4-kináz IIIα izoformája a felelős.

A.

B.
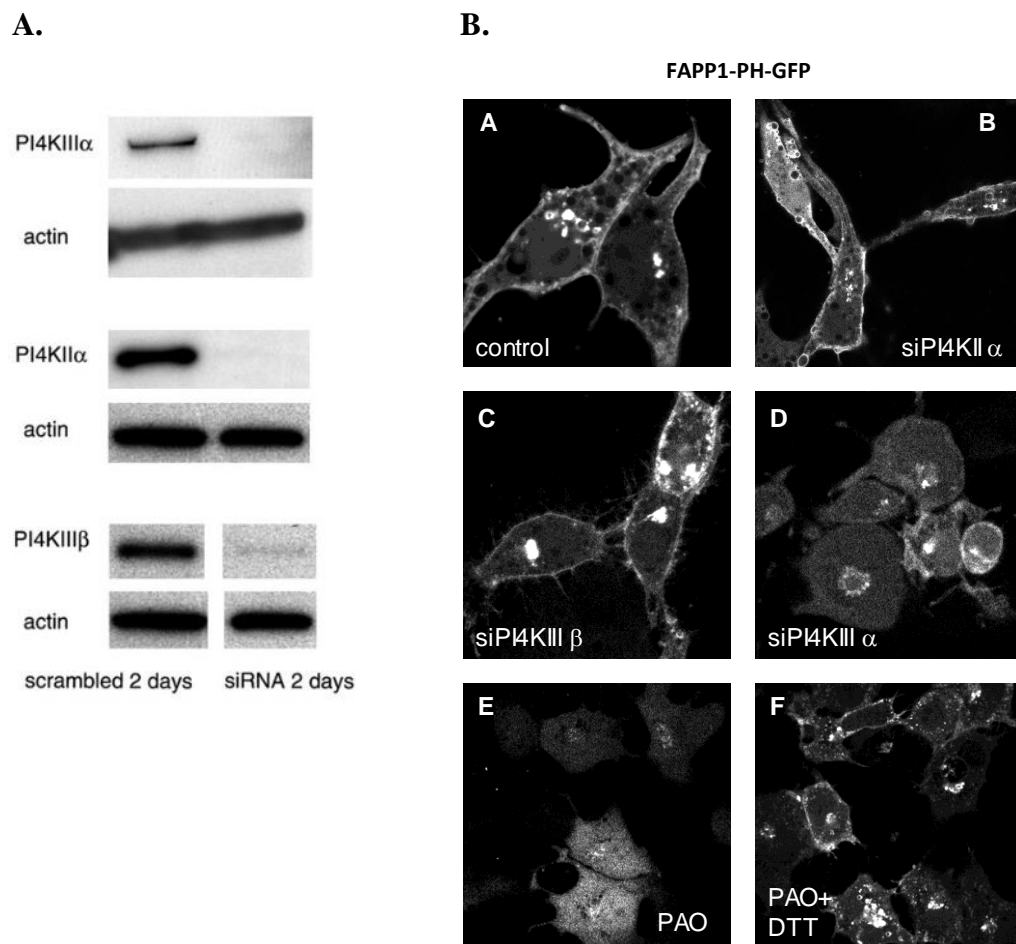
16. ábra. A plazmamembrán PtdIns(4)P szintéziséért a PtdIns 4-kináz IIIα izoformája felel. (A) A különböző PtdIns4K (PI4K) izoformák lecsendesítése siRNS technikával. (B) COS7 sejtekben PtdIns(4)P-t felismerő FAPP1-PH-GFP szondát expresszáltattunk, majd ionomycinnel (iono) indukált Ca^{2+}-jel generálása után a szonda transzlokációját vizsgáltuk (Balla A *et al.*: Mol Biol Cell. 2005).

További kísérleteinkben különböző kináz mutánsok (pl. wortmannin inszenzitív III-as típusú PtdIns 4-kinázok) létrehozásával, valamint gátlószeres- és enzimológiai vizsgálatok eredményeképp sikerült olyan körülményeket létrehoznunk, amelyek segítségével a PtdIns 4-kináz IIIα és a PtdIns 4-kináz IIIβ működését szelektíven gátolhattuk kísérleteinkben. Molekuláris modellezéssel, mutagenezissel és rekombináns fehérjék segítségével meghatároztuk, hogy a PtdIns 4-kináz IIIβ wortmannin érzékenységében mely aminosavak vehetnek részt, illetve sikerült egy wortmanninra kismértékben érzékeny mutánst (Y583M) előállítani (17. ábra, A panel). A PtdIns4KIIIβ-Y583-at stabilan expresszáló, illetve II-es típusú PtdIns 4-kinázokat nem tartalmazó (siRNS technikával) COS-7 sejtek felhasználásával igazoltuk, hogy valóban a PtdIns4KIIIβ szabályozza a Golgi PtdIns(4)*P*–függő szfingomielin-ceramid átalakulást.
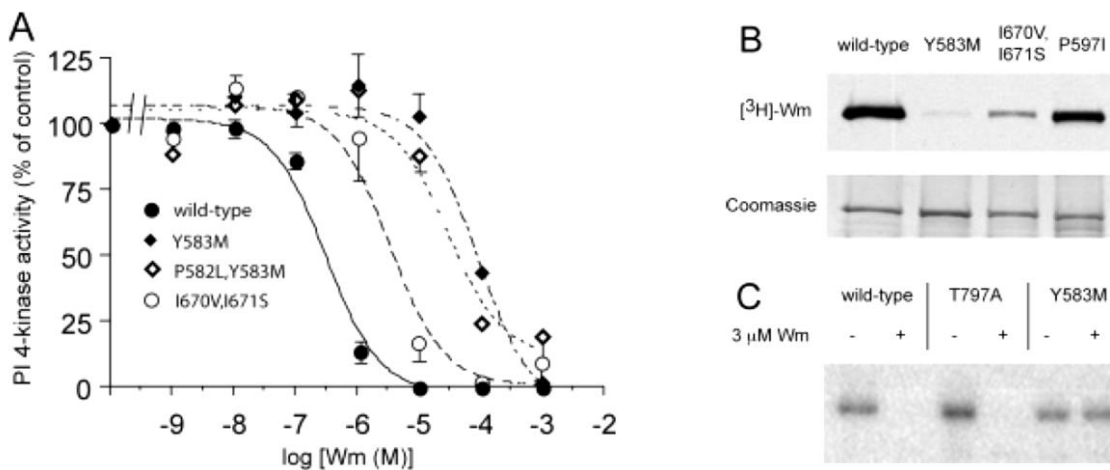
17. ábra. Vad típusú és mutáns PtdIns 4-kináz IIIβ rekombináns fehérjék biokémiai jellemzése. A különböző rekombináns PtdIns 4-kináz fehérjéket *E. Coli* baktériumokban (BL21-es törzs) termeltettük, majd nagy tisztaságban izoláltuk az enzimeket. Vizsgáltuk a fehérjék wortmannin (Wm) gátolhatóságát (A) és kötését (B), valamint az autofoszforilációs képességüket 3 μM Wm jelenlétében (C) (Balla A *et al*.: Biochemistry. 2008).

Mutagenezissel és rekombináns fehérjék segítségével azt is sikerült meghatároznunk, hogy mely aminosavak játszanak fontos szerepet a PtdIns 4-kináz IIIα nagyobb PAO érzékenységében a többi izoformához képest. Térben egymáshoz közel elhelyezkedő két cisztein aminosav közül az egyik módosítása (C1843S) jelentősen csökkentette a PtdIns4KIIIα gátolhatóságát PAO-val (18. ábra, A panel). A további kísérleteinkben szerettünk volna olyan gátlószert is azonosítani, amely masszívan eltérő hatékonysággal gátolja a wortmannin-szenzitív III-as típusú PtdIns 4-kinázokat. Sikerült egy olyan gátlószert találnunk (PIK93),

amely a IIIβ formát sokkal jobban képes gátolni és mára fontos vegyülete a PtdIns4KIIIβ kutatásoknak (18. ábra, B panel).

A.

B.
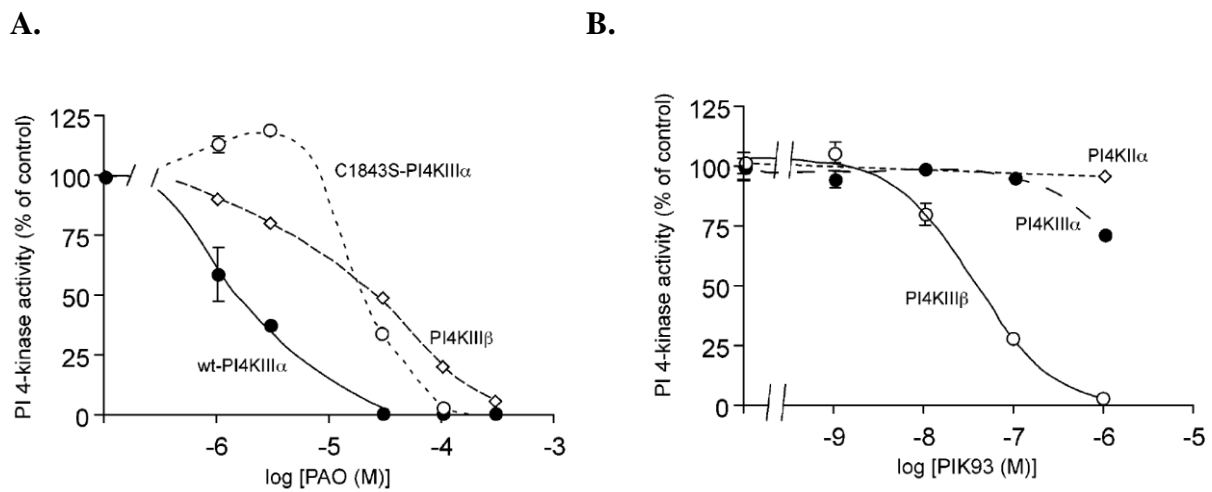
18. ábra. A PtdIns 4-kinázok eltérő gátlószer érzékenysége. A különböző PtdIns 4-kináz izoformákat *E. Coli* baktériumokban (BL21-es törzs) termeltettük, majd nagy tisztaságban izoláltuk az enzimeket. Vizsgáltuk a PtdIns 4-kinázok (A) PAO, illetve (B) PIK93 szenzitivitását enzim aktivitásmérésekben (Balla A *et al*.: Biochemistry. 2008).

Előzetes munkáink során létrehozott eszköztár (specifikus gátlószerek, siRNS technikák stb.) segítségével megkíséreltük megválaszolni azt, hogy melyik PtdIns 4-kináz felelős az úgynevezett hormon-szenzitív foszdoinozitidek szintéziséért a plazmamembránban, amelyek az agonista-indukált foszfolipáz C aktiválódás hatására létrejövő Ca^{2+}-jel generálásában vesz részt. Az $Ins(1,4,5)P_3$ keletkezésekor hidrolizált $PtdIns(4,5)P_2$ gyorsan reszintetizálódik egy reakciósorozatban, amelynek első elkötelező lépést katalizálja egy PtdIns 4-kináz. Kimutattuk, hogy az AT1-receptor ingerlése AngII-vel egy PAO-ra érzékeny, de PIK93-mal nem gátolható PtdIns 4-kináz által szabályozott foszfoinozitid készlet segítségével okoz $Ins(1,4,5)P_3$- és Ca^{2+}-jelet (19. ábra). A specifikus gátlószerek segítségével azt is demonstráltuk, hogy a hormon stimulusra elhasználódott foszfoinozitidek, a $PtdIns(4)P$ és a $PtdIns(4,5)P_2$ reszintézisét jelentősen lecsökkentette a csak PtdIns 4-kináz IIIα gátlását okozó PAO koncentráció, ellenben a PtdIns 4-kináz IIIβ-re specifikus PIK93 gátlószer nem csökkentette ezen foszfoinozitidek reszintézisét (20. ábra).
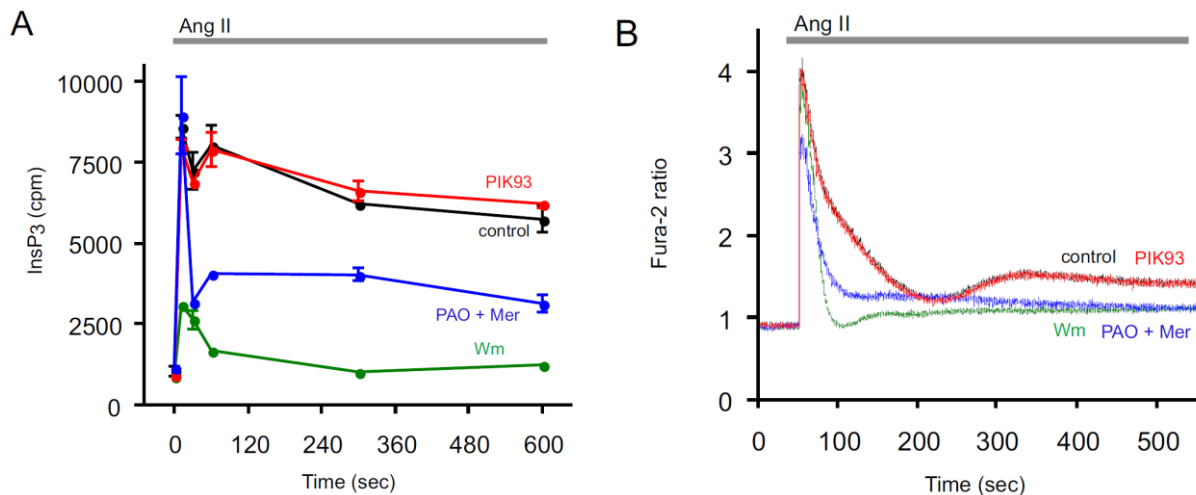
19. ábra. PtdIns 4-kináz inhibitorok hatása az AT1-receptor stimulációjára bekövetkező Ins(1,4,5)P₃- és Ca²⁺-jelre. (A) Az AT1-receptort stabilan expresszáló HEK293 sejtekhez a megjelölt időben történő 100 nM AngII stimulus előtt 24 órával radioaktívan jelölt *myo*-inozitollal kezeltük. A hormon stimulus után a jelölt Ins(1,4,5)P_3-at HPLC-vel azonosítottuk. (B) Az AT1-receptort stabilan expresszáló HEK293 sejteket 100 nM AngII-vel stimuláltuk és a Ca²⁺-jelet Fura-2/AM segítségével határoztuk meg. Mindkét mérési sorozatban az AngII stimulus előtt a sejteket 10 percig előkezeltük vagy vehikulummal (control) vagy 10 µM PAO-val (Mer: 1 mM β-merkaptoetanollal, ami a PAO aspecifikus mellékhatásait csökkenti) vagy 250 nM PIK93-mal, vagy 10 µM wortmanninnal (wm) (Balla A *et al.*: Mol Biol Cell. 2008).
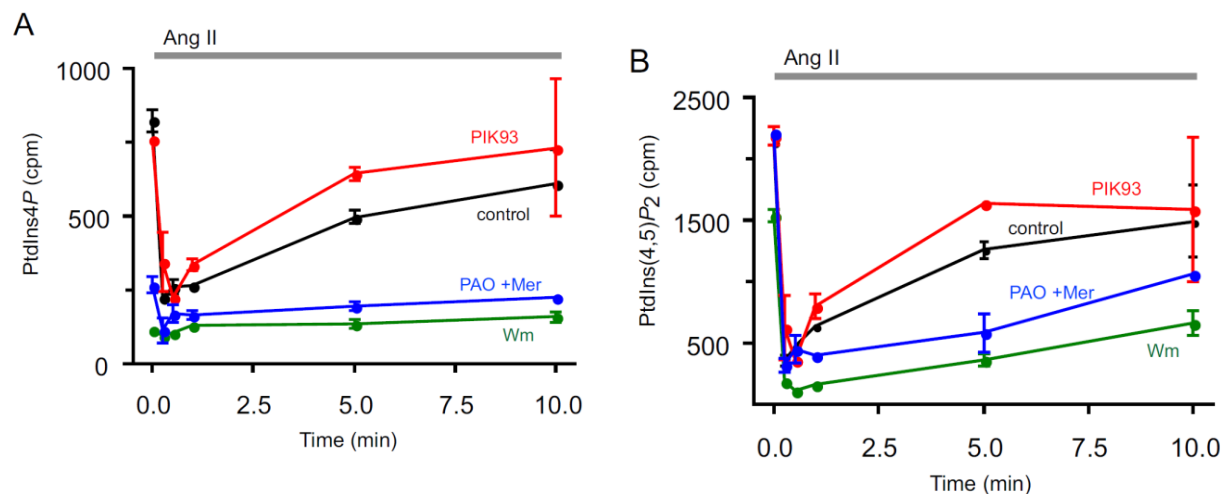
20. ábra. PtdIns 4-kináz inhibitorok hatása az AT1-receptor stimulációjára bekövetkező foszfoinozitid szintekre. AT1-receptort stabilan expresszáló HEK293 sejtekhez a megjelölt időben történő 100 nM AngII stimulus előtt 3 órával radioaktívan jelölt foszfáttal kezeltük. Az AngII stimulus előtt a sejteket 10 percig előkezeltük vagy vehikulummal (control) vagy 10 µM PAO-val (Mer: 1 mM β-merkaptoetanollal, ami a PAO aspecifikus mellékhatásait csökkenti) vagy 250 nM PIK93-mal, vagy 10 µM wortmanninnal (wm). A hormon stimulus után a sejtek foszfoinozitidjeit vékonyréteg kromatográfiával azonosítottuk. (A) PtdIns(4)P és (B) PtdIns(4,5)P_2 mennyiségét PhosphorImager segítségével kvantifikáltuk (Balla A *et al.*: Mol Biol Cell. 2008).

Eredményeinket élő sejtes kísérletekkel is alátámasztottuk. AT1-receptort stabilan expresszáló HEK293 sejtekben a PtdIns(4,5)P_2-t felismerő PLCδ1-PH domén CFP-vel és YFP-vel fuzionáltatott változatait is expresszáltattuk, majd ezen szondák közötti FRET-jel követésével határoztuk meg a plazmamembrán PtdIns(4,5)P_2 szintjének változásait hormon stimulus (AngII) vagy ionomycin kezelés hatására. A 21. ábra alapján a PtdIns(4,5)P_2 reszintézisét csak a PtdIns 4-kináz IIIα gátlását okozó PAO koncentráció akadályozta meg, ellenben a PtdIns 4-kináz IIIβ-re specifikus PIK93 gátlószer nem befolyásolta ezt a folyamatot.
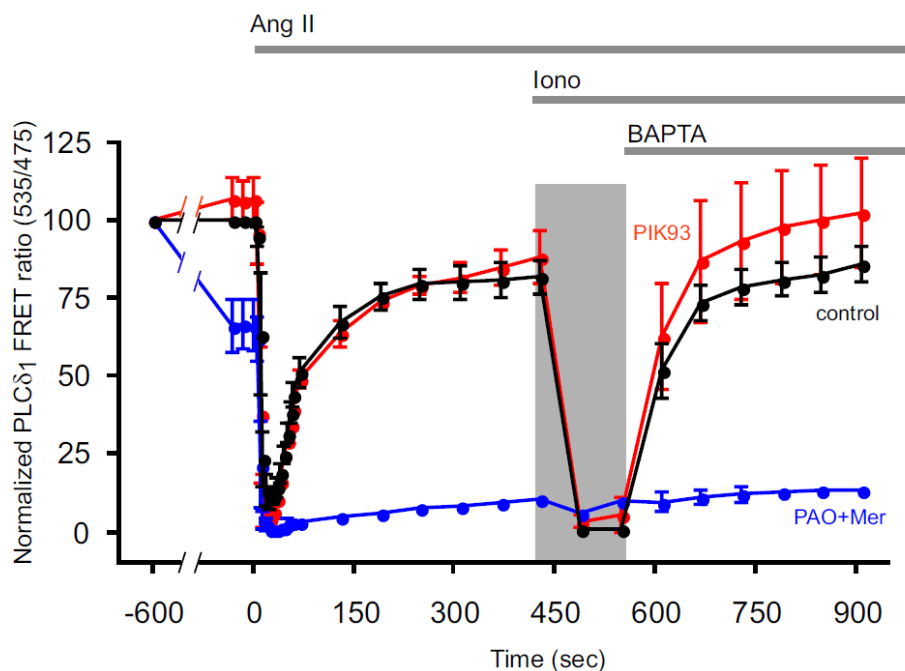
21. ábra. Ca^{2+}-jelet okozó stimulusok hatására bekövetkező PLCδ1-PH domén eloszlásának vizsgálata, illetve a PtdIns 4-kináz inhibitorok hatása. AT1-receptort stabilan expresszáló HEK293 sejtekhez a megjelölt időben ingereltük 100 nM AngII-vel, vagy 10 µM ionomycinnel (Iono). A PLCδ1-PH domének eloszlásának változását FRET segítségével kvantifikáltuk (Balla A *et al*.: Mol Biol Cell. 2008).

Előző munkánkban kimutattuk, hogy az OSBP-PH és a FAPP1-PH domén bizonyos speciális körülmények között képes nemcsak a Golgi, hanem a plazmamembrán PtdIns(4)P készletet megjelölni. Szerettünk volna egy optimálisabb szondát létrehozni a plazmamembrán PtdIns(4)P szintjének monitorozásához élő sejtes kísérletekben. Sikerült egy élesztőben található OSH2 fehérje PH doménjének felhasználásával egy olyan konstruktot készíteni (GFP-OSH2-PH2x), amely felismeri a plazmamembrán PtdIns(4)P-jét, de nem kötődik a Golgiban található PtdIns(4)P-hoz (22. ábra). A GFP-OSH2-PH2x, valamint a PLCδ1-PH-mRFP

szondák segítségével élő sejtben demonstráltuk az AngII stimulus hatására bekövetkező gyors foszfoinozitid szint változásokat (22. ábra).
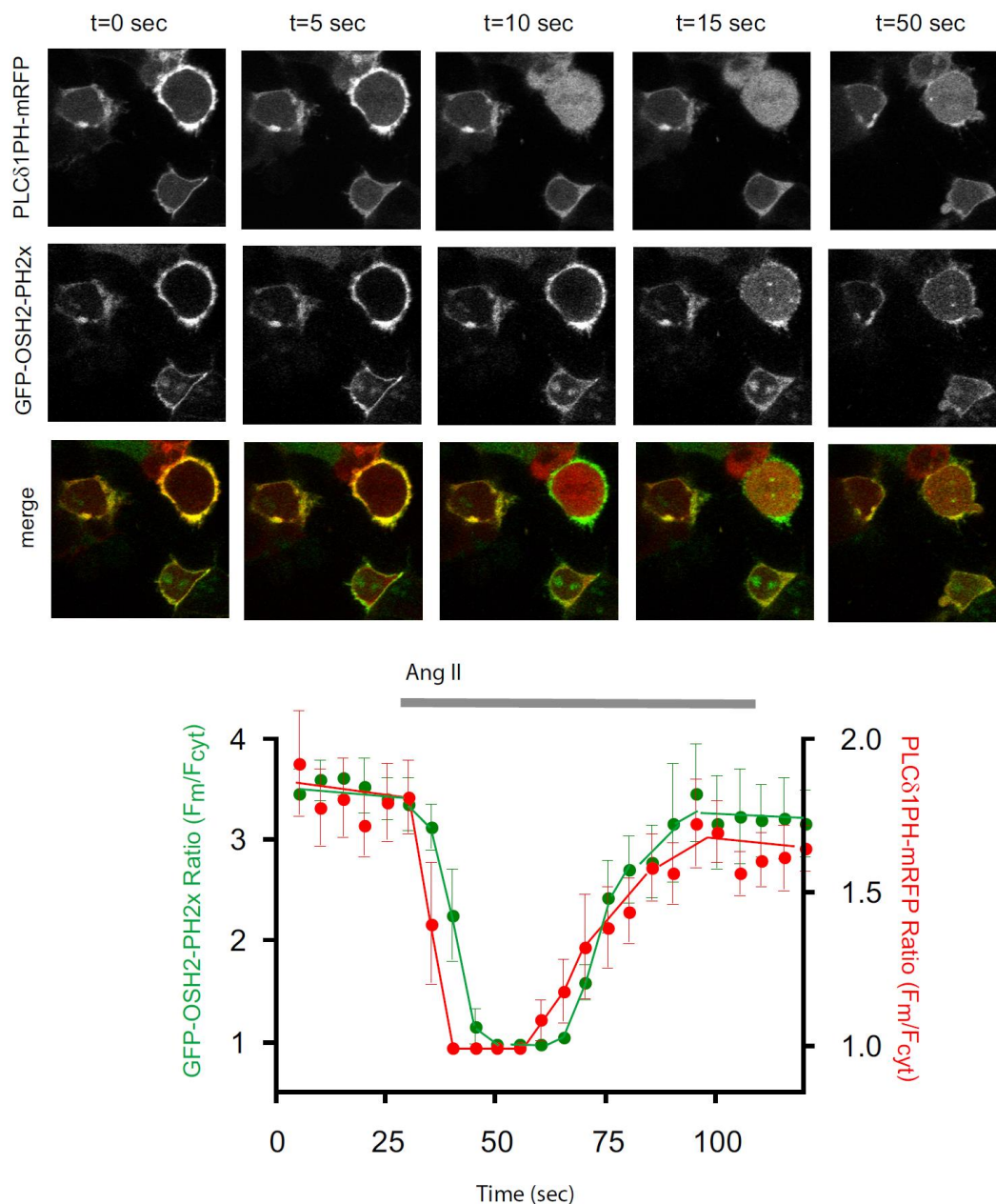
22. ábra. AngII stimulus hatására bekövetkező foszfoinozitid szintek monitorozása GFP-OSH2-PH2x és PLCδ1-PH-mRFP szondákkal. AT1-receptort stabilan expresszáló HEK293 sejteket GFP-OSH2-PH2x (zöld) és PLCδ1-PH-mRFP (piros) plazmidokkal transzfektáltuk, majd 24 óra múlva a megjelölt időben ingereltük 100 nM AngII-vel. A szondák eloszlásának változását a membrán/citoszól fluoreszcencia intenzitások segítségével kvantifikáltuk (Balla A *et al*.: Mol Biol Cell. 2008).

A GFP-OSH2-PH2x eloszlásának nyomon követésével is igazoltuk, hogy a plazmamembrán PtdIns(4)P-ért a PtdIns 4-kináz IIIα a felelős. Kimutattuk, hogy a PAO

gátlószer használata gátolta a GFP-OSH2-PH2x relokalizációját 100 nM AngII stimulust követően, hasonlóan a PtdIns 4-kináz III izoformákra nem specifikus wortmannin által kifejtett hatáshoz (23. ábra). Ezzel ellentétben, a PtdIns 4-kináz IIIβ specifikus PIK93 gátlószer nem gátolta a foszfoinozitidek reszintézisét a plazmamembránban (23. ábra, A panel).
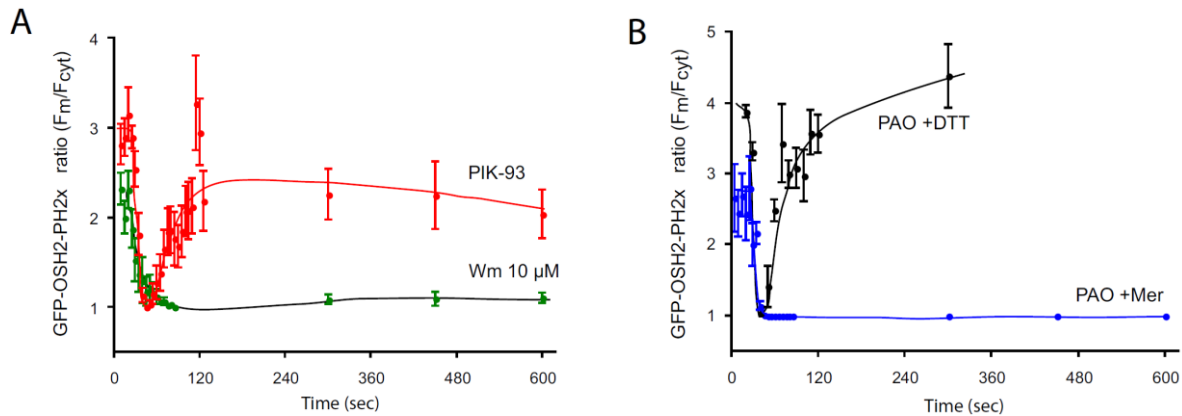
23. ábra. PtdIns 4-kináz inhibitorok hatása az AngII stimulus indukált GFP-OSH2-PH2x plazmamembrán lokalizációs változásaira. AT1-receptort stabilan expresszáló HEK293 sejteket GFP-OSH2-PH2x plazmiddal transzfektáltuk 24 óráig. A sejteket 10 percig előkezeltük 250 nM PIK-93 (A panel, piros görbe) vagy 10 µM wortmannin (A panel, fekete görbe) vagy 10 µM PAO (B panel fekete görbe: 1 mM DTT-vel, ami , kék görbe 1 mM β-merkaptoetanollal) gátlószerrel, majd ingereltük 100 nM AngII-vel. A GFP-OSH2-PH2x fúziós fehérje eloszlásának változását a membrán/citoszól fluoreszcencia intenzitások segítségével kvantifikáltuk, miután az élő sejtekről konfokális mikroszkópos felvételeket készítettünk (Balla A *et al*.: Mol Biol Cell. 2008).

A PtdIns 4-kináz inhibitorokkal kapott eredmények a PtdIns 4-kináz IIIα kulcsszerepére mutatott a hormon-szenzitív foszfoinozitid készletek képzéséért a plazmamembránban. A gátlószeres kísérleteinket a PtdIns 4-kinázok expressziójának siRNS-sel történő, specifikus csökkentésével végzett kísérleteinkben is megerősítettük. A hormon-szenzitív PtdIns(4,5)P_2 készletért felelős forma szerepének megerősítése céljából az AT1-receptort stabilan expresszáló HEK293 sejteket három napig kezeltünk PtdIns 4-kináz izoforma specifikus siRNS-sel, a csendesítés hatékonyságát pedig western blot módszerrel ellenőriztük (24. ábra, A panel). Az siRNS kezelés után a sejteket radioaktívan jelölt foszfáttal kezeltük 3 óráig, és majd a foszfolipidek szintjét vékonyréteg kromatográfiával azonosítottuk és PhosphorImager segítségével kvantifikáltuk (24. ábra, B panel). Az siRNS kezelések valamennyi sejt elvesztését eredményezték, ezért a PtdIns(4)P és a PtdIns(4,5)P_2 értékeket a foszfatidilinozitol/foszfatidsav (PtdIns/PtdA) értékek figyelembevételével számoltuk. A radioaktívan jelölt HEK-AT1-receptor sejteket 10 percig 100 nM AngII-vel vagy fiziológiás sóoldattal (control) stimuláltuk

és demonstráltuk, hogy csak a PtdIns 4-kináz IIIα depléciója okozott szignifikáns csökkenést az agonista stimulust követően a PtdIns(4,5)P_2 reszintézisében (24. ábra, C panel).

A.

B.

C.
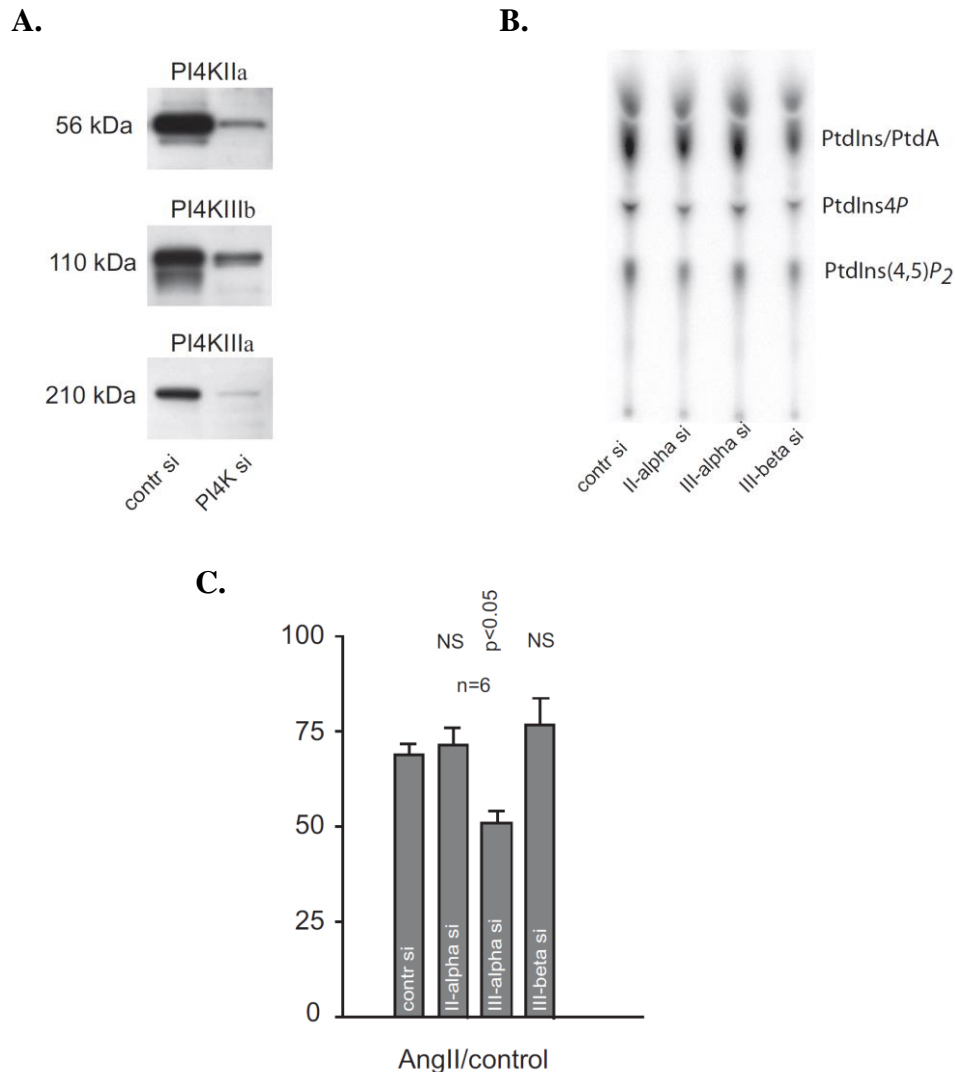
24. ábra. PtdIns 4-kináz izoformák csendesítésének hatása az AT1-receptor stimulációjára követő PtdIns(4,5)P_2 szintre. (A) AT1-receptort stabilan expresszáló HEK293 sejtek PtdIns 4-kináz izoforma specifikus siRNS kezelésének ellenőrzése western blot módszerrel. (B) A sejteket radioaktívan jelölt foszfáttal kezeltük, majd a sejtek foszfoinozitidjeit vékonyréteg kromatográfiával azonosítottuk. (C) A jelölt sejteket 10 percig 100 nM AngII-vel stimuláltuk, majd a sejtek foszfoinozitidjeit vékonyréteg kromatográfiával azonosítottuk és a PtdIns(4,5)P_2 mennyiségét PhosphorImager segítségével kvantifikáltuk (Balla A *et al*.: Mol Biol Cell. 2008).

Röviden összefoglalva, a 3.1. fejezetben leírt munkánk alpján sikerült tisztázni, hogy az AT1-receptor jelátvitelében kitüntetett, ún. hormon-szenzitív PtdIns(4,5)P_2 képzéséért a PtdIns 4-kináz IIIα felelős, míg a PtdIns 4-kináz IIIβ a Golgiban található PtdIns(4)P-ért felel.

3.2 Kis G-fehérje aktiválódás vizsgálata az AT1-receptor stimuláció hatására

Az AT1R a heterotrimer G-fehérjéken kívül kis G-fehérjék (pl. Ras, Rho, Rac) aktiválásán keresztül is szabályoz egyes sejtfunkciókat, mint pl. a génexpressziót, aktin citoszkeletont, vezikuláris transzportot és a mikrotubulus szerveződést. Ezen folyamatok pontosabb megértése alapvető a kardiovaszkuláris remodelling, endothel diszfunkció és egyéb patológiás történések vizsgálatában. A kis G-fehérjék közös jellemvonása a kis molekulasúlyuk, amelyről nevüket is kapták. Ezen fehérjék aktiválódása GTP kötésén keresztül jön létre, ezen állapotban képes más fehérjék állapotát megváltoztatni és így a sejtműködést befolyásolni, míg az inaktiválódás kulcsa a GTP-GDP átalakulás. Kis G-fehérje aktiválódás mérésére az irodalomban már leírtak olyan szondákat, melyek alkalmasak a kis G-fehérjék sejten belüli aktiválódási állapotuk, illetve az ebben bekövetkező változások meghatározására fluoreszcens mikroszkóppal FRET alapú mérésekben, mikroszkópos felvételeken, kép-analizáló szoftverek segítségével. A munkánk során olyan bioszenzorokat hoztunk létre, melyek segítségével BRET módszerrel élő sejtekben lehet nyomon követni e jelátviteli mechanizmust. A szondákat HEK293 epitél sejtekben expresszáltuk és működésüket epidermális növekedési faktor (EGF), vagy AngII stimulus hatására vizsgáltuk. Ezen kísérleti felállásban a kis G-fehérje aktiválódás hatására BRET-jel növekedését kapjuk, hiszen a szondákban nyugalmi helyzetben egymáshoz viszonylag távol van az akceptor a donortól (RBD nem kötődik a kis G-fehérjéhez), de aktiválódás során az RBD kötődik a kis G-fehérjéhez, így a polipeptidlánc két vége közelebb kerül egymáshoz, nagyobb energiatranszfer lesz (a BRET-jel nő). A Ras kis G-fehérje aktiválódás méréséhez használt intramolekuláris RasBRET-tK szondában a YFP-hez kötöttük a Ras-t, mely egy flexibilis linkeren keresztül kapcsolódik egy Ras-kötő doménhez (RBD), ezen RBD-hez pedig C-terminálisan helyezkedik el a renilla luciferáz és egy CAAX domén (plazmamembránba targetál, a K-Ras fehérjéből származik). A sejteket 24 órával a vizsgálatok előtt a szondákat tartalmazó plazmidokkal transzfektáltuk 96-lyukú, poli-L-lizinnel kezelt edényekben és az adherens sejteken végeztük a BRET mérést 6 órás szérum-megvonást követően. A 25. ábra A paneljén látható, hogy a kiindulási pontnak használt FRET szonda elrendezésének megfelelő intramolekuláris RasBRET-tK BRET szonda milyen választ mutat agonista stimulus hatására. Az intramolekuláris RasBRET szonda többféle, a plazmamembrán targetált variánsát is elkészítettük és a legjobb verziónak a fúziós fehérje N-terminálisára helyezett mirisztoilálás és palmitoilálás (MP) konszenzus szekvenciát tartalmazó szonda bizonyult (25. ábra, B panel).

Ezek után elhatároztuk, hogy megpróbálkozunk szondáink intermolekuláris verzióinak elkészítésével, mely konstruktoknál az adott kis G-fehérje, illetve annak GTP-kötött „aktív"

formáját felismerő specifikus domén külön polipeptidláncban található. Az intermolekuláris MP-RasBRET szonda mutatta a legnagyobb mértékű BRET-jel emelkedést agonista stimulus hatására élő sejtes kísérleteinkben (25. ábra, C panel).
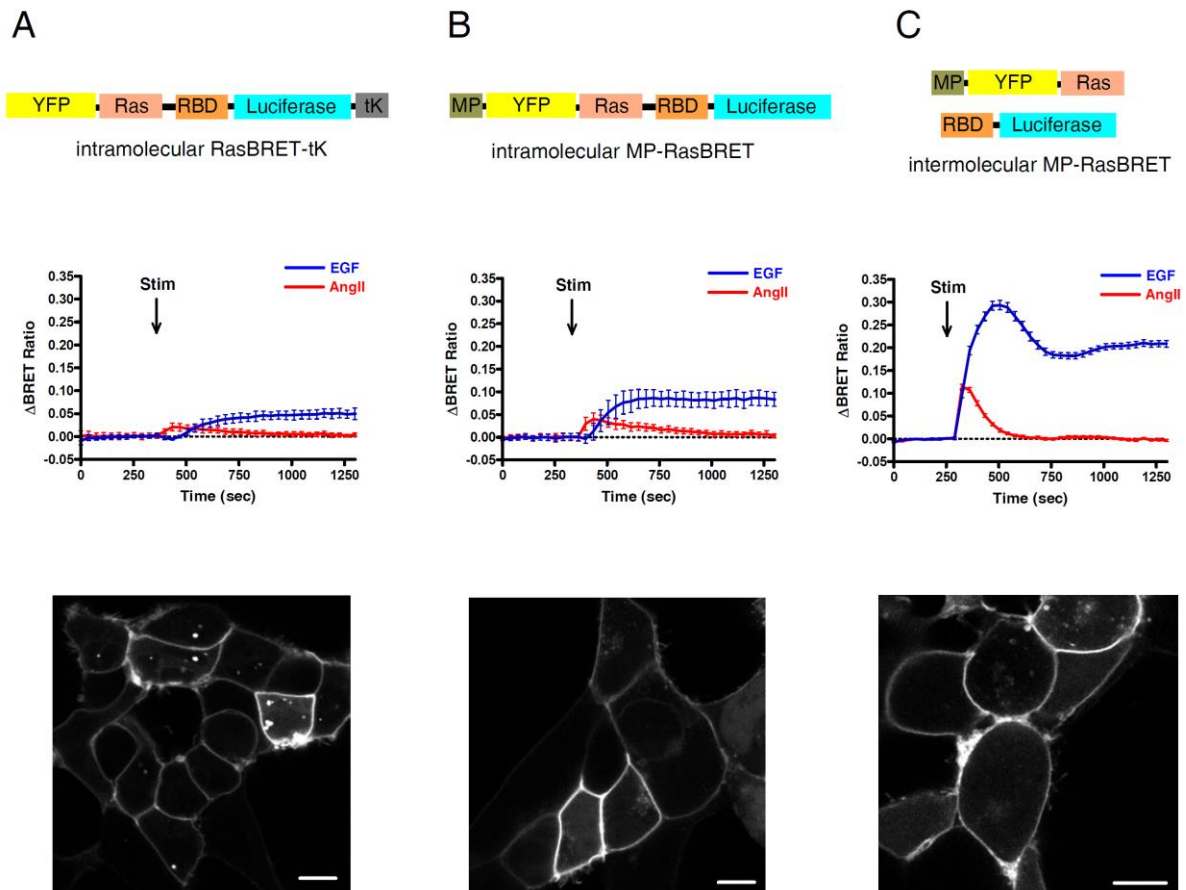
25. ábra. BRET-jelek változása különböző RasBRET szondákkal AngII vagy EGF stimulus hatására HEK293 sejtekben. (A) Az intramolekuláris RasBRET-tk, (B) az intramolekuláris MP-RasBRET és (C) az intermolekuláris MP-RasBRET szondák vázlatos felépítése (felső sor), BRET-jelek változása stimulus (50 ng/ml EGF, kék görbék vagy 100 nM AngII, piros görbék) hatására HEK293 sejtekben (középső sor), illetve sejten belüli eloszlásuk (alsó sor). Az EGF-receptort a sejt endogénen tartalmazza, míg az angiotenzin receptort tranziensen transzfektáltuk HEK293 sejtekben. Az EGF válszoknál kisebb AngII válaszok magyarázata lehet, hogy az AT1-receptor nem található meg minden sejten, mivel a transzfekciós hatékonyság ~ 50%-os HEK293 sejtekben. A targetáló szekvenciák a plazmamembránba irányítják a BRET szondát, amelyet konfkális mikroszkóppal ellenőriztünk. A lépték 10 μm. (Balla A *et al.*: J Biol Chem. 2011).

A Ras aktiválódását mérő szondáknak elkészítettük két mutáns verzióját is, hogy megvizsgáljuk a bioszenzoraink hozzávetőleges dinamikai tartományát (kis G-fehérjék stabilan expresszálódó GDP-kötött „inaktív", vagy GTP-kötött „aktív" formái), mivel az aktív formák expresszálásával maximális BRET jelet detektálhatunk, míg a GDP-kötött mutánsok a mérhető

BRET-jel minimálisra csökkentik. Az intermolekuláris MP-RasBRET szonda egy bazális BRET-jelet ad nyugalmi állapotban lévő sejtekben, míg a G12V RasBET ("aktív" forma) szonda expresszálása ezt a BRET-jelet jelentősen tovább növeli, illetve az S17N RasBRET ("inaktív" forma) expresszálása ezt a bazális jelet minimumra csökkenti (26. ábra). A RasBRET szonda működésének validálásán túl ezen eredmény azt is mutatja, hogy mekkora az a dinamikai tartomány, amelyben a különböző stimulusok hatására bekövetkező változásokat mérhetjük.
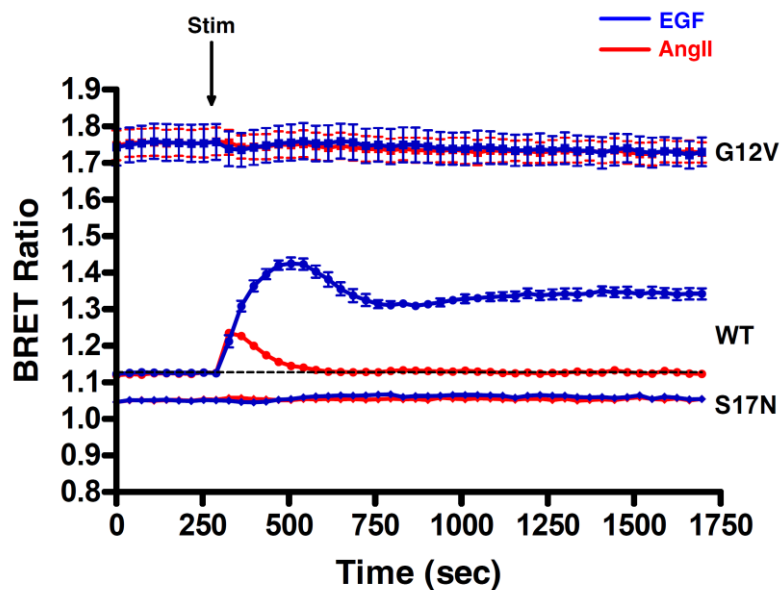
26. ábra. A BRET-jel változása és a BRET-alapú Ras aktiválódás mérésének validálása intermolekuláris MP-RasBRET variánsok használatával. A BRET-jelek változása stimulus (50 ng/ml EGF vagy 100 nM AngII) hatására HEK293 sejtekben vad típusú (WT), "aktív" G12V és "inaktív" S17N MP-RasBRET szondapárok esetében. A HEK293 sejteket a különböző MP-RasBRET szondapárokkal plazmidjaival transzfektáltuk, majd 24 óra múlva 50 ng/ml EGF-fel (kék görbék) vagy 100 nM AngII-vel (piros görbék) stimuláltuk a sejteket a jelzett időpontban (Balla A *et al*.: J Biol Chem. 2011).

A beállított módszer felhasználásával megvizsgáltuk a Ras kis G-fehérje aktiválódást a sejtek különböző kompartmentjeiben növekedési faktorok és hormonok hatására élő sejtekben. A sejtek belsejébe targetált szondák esetében a transz-Golgi-hoz (TGN), illetve az endoplazmatikus retikulumhoz (Sac1) targetált konstrukt mutatott Ras aktiválódást, az endoszómákon (FYVE) nem tudtunk Ras aktiválódást kimutatni agonista ingerlést követően. Különböző AT1R konstruktok koexpressziójával (vad típus és internalizációra képtelen mutáns) megállapítottuk, hogy Golgin (TGN) és endoplazmatikus retikulumon (Sac1) kapott

aktiválódás a plazmamembránnal áll kapcsolatban, és nem az internalizált AT1-receptorok okozzák a kis G-fehérje aktiválódást (27. ábra).
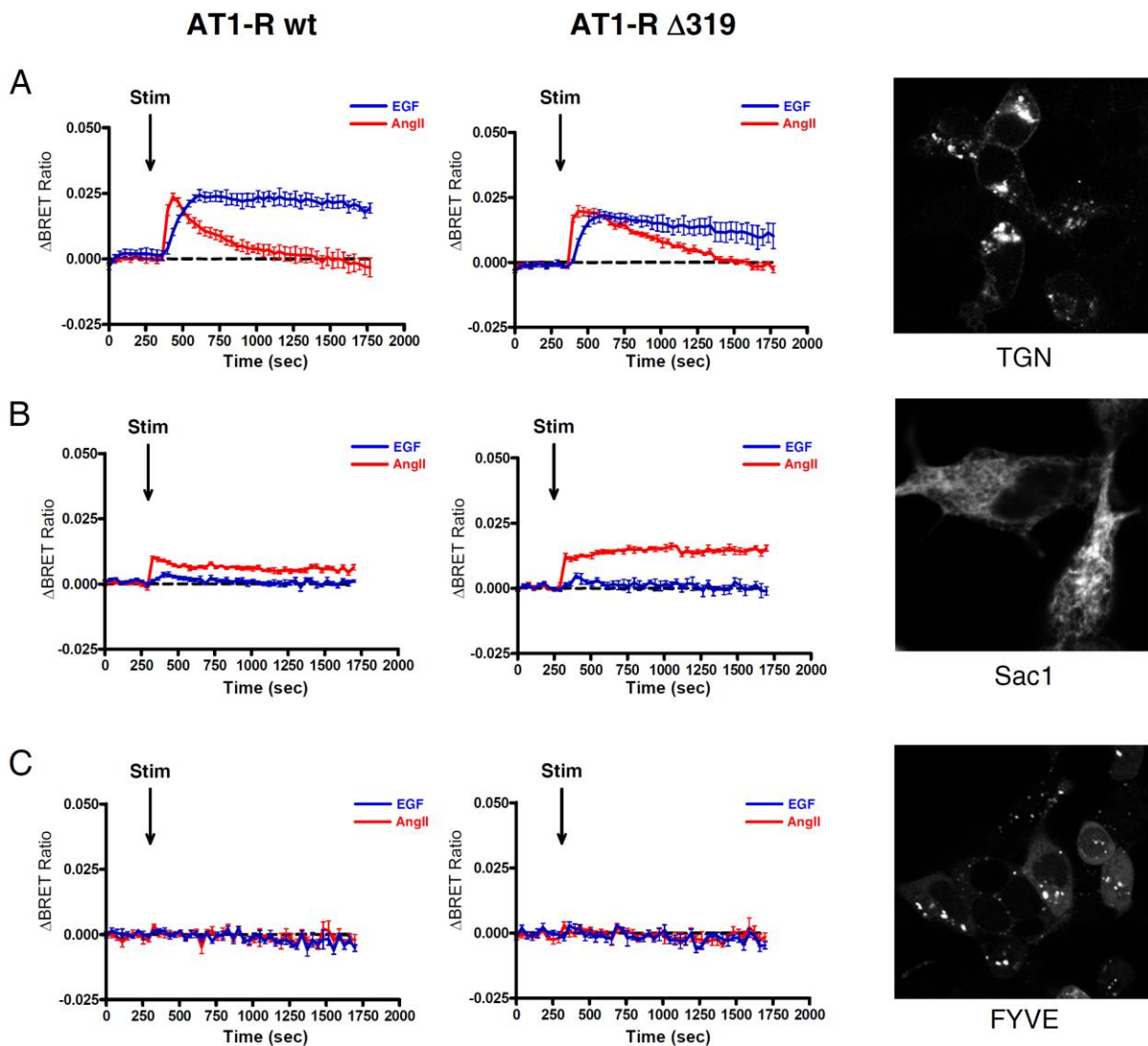
27. ábra. Ras aktiválódás detektálása AngII vagy EGF stimulus hatására HEK293 sejtek különböző intracelluláris organellumaiban. Vad típus AT1-receptort (AT1R wt, első oszlop) vagy internalizációra képtelen AT1-receptort (AT1R Δ319, középső oszlop) koexpresszáló HEK293 sejteket intermolekuláris RasBRET szondapárok plazmidjaival transzfektáltuk. A sejteket 24 óra múlva 50 ng/ml EGF-fel (kék görbék) vagy 100 nM AngII-vel (piros görbék) stimuláltuk a jelzett időpontban. Konfokális mikroszkóppal ellenőriztük, hogy a különböző intracelluláris kompartmentekbe irányított szondák lokalizációja megfelelt az előzetesen vártaknak (utolsó oszlop) (Balla A *et al.*: J Biol Chem. 2011).

A különböző AT1R konstruktok használatával nemcsak azt tudtuk állapítani, hogy a kapott intracelluláris aktiválódás a plazmamembrán eredetű, vagy az internalizálódott receptorok működése hatására jön-e létre (27. ábra), hanem azt is demonstráltuk, hogy a Ras aktiválódás $G_{q/11}$-fehérje aktiváláson keresztül történik. A DRY/AAY mutációt tartalmazó

AT1-receptor mutáns, mely heterotrimer $G_{q/11}$-fehérjét aktiválni képtelen, használatával megállapítottuk, hogy mind plazmamembrán eredetű, mind az intracelluláris Ras aktiválódás G-fehérje függő jelpályákon keresztül jön létre AngII hatására HEK293 sejtekben (28. ábra). Ezen eredményünket [Sar^1,Ile^4,Ile^8]-AngII (SII-AngII) agonista használatával is megerősítettük, mivel ezen agonista az AT1R-hoz kötődve nem aktiválják a $G_{q/11}$ fehérjét.
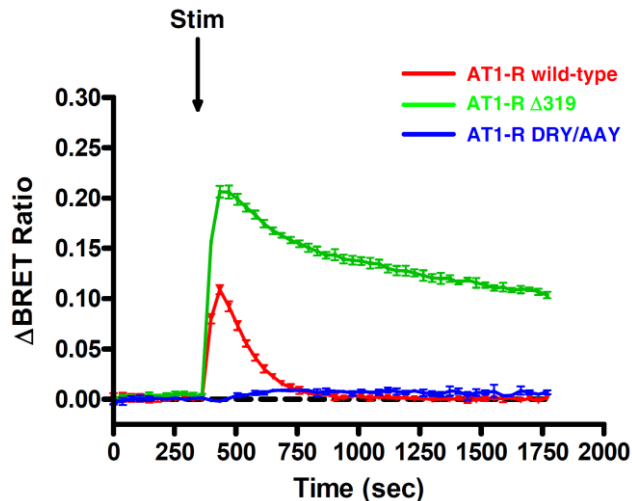
28. ábra. Intermolekuláris BRET szonda vad típusú és mutáns AT1-receptorok ingerlését követően HEK293 sejtekben. Vad típus AT1-receptort (piros) vagy internalizációra képtelen (AT1R Δ319, zöld) vagy G_q-fehérjét aktiválni képtelen (AT1R DRY/AAY, kék) AT1-receptort és intermolekuláris BRET szondapárt koexpresszáltattunk HEK293 sejtekben. A sejteket 24 óra múlva 100 nM AngII-vel ingereltük a jelzett időpontban (Balla A *et al*.: J Biol Chem. 2011).

A szondák targetálása tette lehetővé a különböző plazmamembrán mikrodomének és intracelluláris membránok Ras aktivációjának vizsgálatát, a mutáns receptorok a létrejött aktiváció mechanizmusára vonatkozóan szolgáltattak információt. Adataink alapján a plazmamembránban létrejövő Ras aktiváció mértéke az internalizálódó és deszenzitizálódó receptorok miatt gyorsan csökken élő sejtekben, azonban ha az internalizáció folyamatát AT1R Δ319 mutáns receptorral felfüggesztjük, megnövekedett és hosszan fenntartott Ras aktivációt tapasztalhatunk. EGF-receptor kináz inhibitor (10 µM AG1478) alkalmazásával kimutattuk, hogy az AngII hatására bekövetkező Ras kis G-fehérje aktiválódás nem a hagyományos útvonalon történő, ún. EGF-receptor transzaktiváció eredménye a plazmamembránban (29. ábra). Ez az eredmény az AngII és EGF stimulus okozta Ras aktiválódás kinetikájának különbözőségéből is sejthető volt (25. ábra).

Eredményeink szerint ezen bioszenszorok alkalmasak növekedési faktorok, hormonok szignalizációjának vizsgálatára, illetve különböző vegyületek ezen szignalizációs jelpályákra

történő farmakológiai hatásának tesztelésére élő sejtekben, valamint a szondák targetálásával különböző intracelluláris kompartmentekben vizsgálhatjuk kis G-fehérje jelpályák működését és különböző farmakonok hatását specifikus sejtkompartmentekben.

AG1478
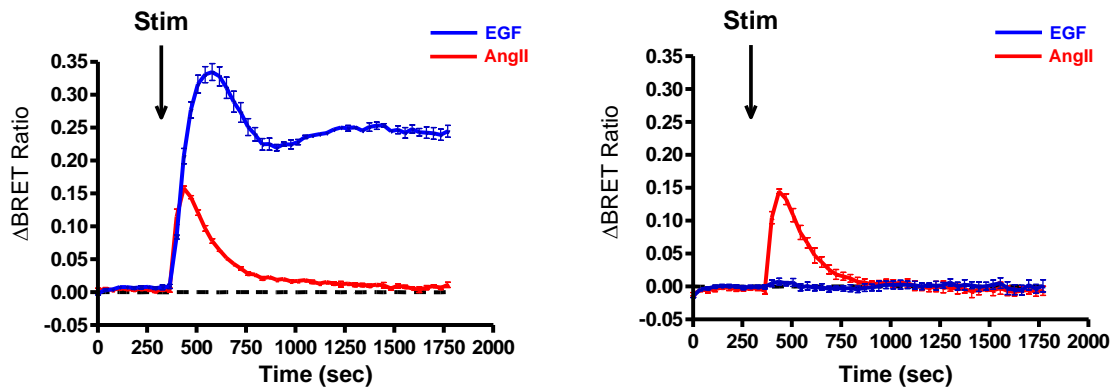
29. ábra. Ras aktiválódás mechanizmusa EGFR transzaktivációtól független folyamat HEK293 sejtekben. BRET-jelek változása stimulus (50 ng/ml EGF vagy 100 nM AngII) hatására HEK293 sejtekben. Az EGF-receptort a sejt endogénen tartalmazza, míg az angiotenzin receptort tranziensen transzfektáltuk HEK293 sejtekben. 10 µM AG1478 (EGFR inhibitor) nem befolyásolta az AngII-indukált Ras aktiválódást (Balla A *et al*.: J Biol Chem. 2011).

3.3 Az aktiválódott AT1R által elindított jelátvitel vizsgálata

Kísérletes munkánk során az AT1R működését szerettük volna nyomon követni, azonban nem csak az endogén ligand AngII, hanem funkcionálisan szelektív aktiváció hatására is (receptor mutánsok vagy speciális ligandumok segítségével). Ehhez a BRET technikát alkalmaztuk, melynek előnye, hogy nagy érzékenységgel képes a fehérjék közötti specifikus kapcsolatok valós idejű detektálására élő sejtekben.

Ellenőriztük, hogy a BRET mérésekhez szükséges *Renilla* luciferáz (Rluc) jelölés befolyásolja-e a receptorok működését, a vad típusú AT1R-Rluc, valamint DRY/AAY AT1R-Rluc funkcionális hatásai megegyeznek-e a jelöletlen receptorokról korábban leírtakkal. Ennek érdekében kontroll kísérleteket végeztünk, melyekben az AT1R jelátvitelének két fontos elemét vizsgáltuk meg. A citoplazmatikus Ca^{2+} méréssel a G_q-fehérje aktivációját, western blot módszerrel pedig az ERK1/2 MAPK aktiválásának mértékét határoztuk meg HEK293 sejteken. A 30. ábrán látható, hogy az AT1R-Rluc esetén, a jelöletlen receptornál leírtakhoz hasonlóan, az AngII stimulus hatására Ca^{2+} szint emelkedés jött létre a citoplazmában. A jelátvitel szelektív agonista SII-AngII általi ingerlés esetén, nem alakult ki Ca^{2+} jel a jelölt AT1R-on keresztül,

40

mely alátámasztja, hogy ezen ligandum hatására nem jön létre G_q-fehérje aktiváció (30. ábra, A panel). A DRY/AAY AT1R-Rluc aktivációja a jelöletlen DRY/AAY AT1-receptorról nem hozott létre jelentős G_q-fehérje aktivációt sem AngII, sem pedig SII-AngII hozzáadásának hatására (30. ábra, B panel). Az ERK1/2 aktivációjának vizsgálatakor mind az AT1R-Rluc, mind pedig a DRY/AAY AT1R-Rluc képes volt ERK1/2 foszforilációt kiváltani AngII, illetve SII-AngII kezelés hatására (30. ábra, C panel) Ezen kontroll kísérletek alapján tehát megállapítottuk, hogy az Rluc jelölt AT1R-ok, a jelöletlen receptorokkal megegyező módon funkcionálnak, és alkalmasak BRET-alapú funkcionális kísérletek végzésére.

Calcium measurement

ERK-1/2 assay
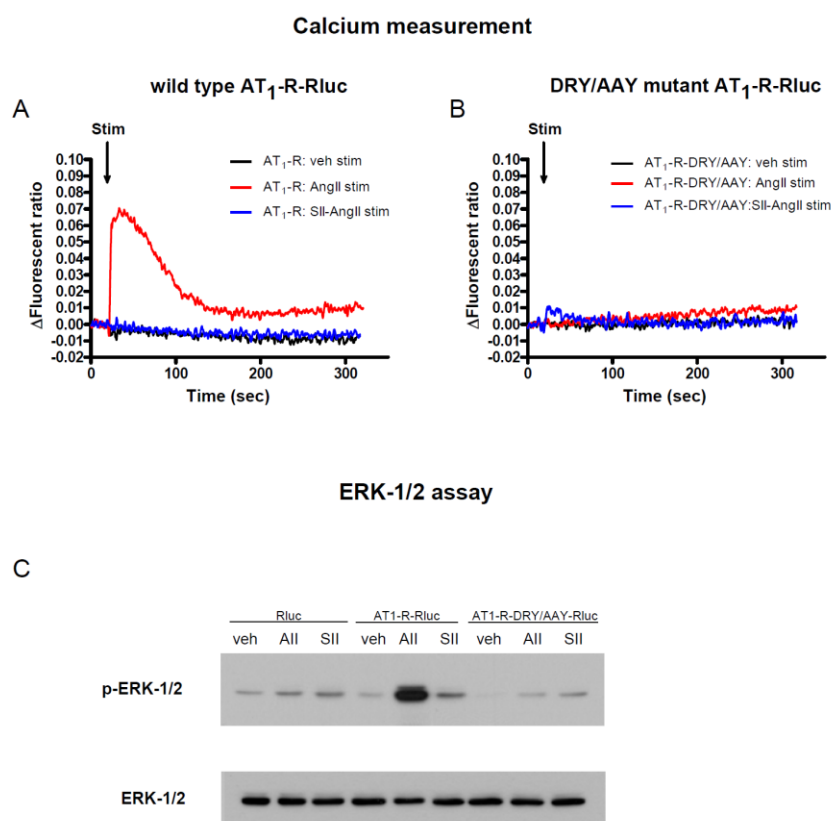
30. ábra Renilla-luciferázzal jelölt vad típusú és DRY/AAY mutáns AT1R-ok funkcionális vizsgálata. (A-C) AT1R-Rluc, DRY/AAY AT1R-Rluc, illetve (C) Rluc plazmidokkal transzfektáltunk HEK293 sejteket 24 órával a kísérletek előtt. (A és B) A citoplazmatikus Ca^{2+} mérések során a jelzett időpontban 100 nM AngII-t (piros görbék), 10 μM SII-AngII-t (kék görbék) vagy vivőanyagot (fekete görbék) adtunk a sejtekhez. (C) A foszforilált ERK1/2 (p-ERK1/2) és a teljes ERK1/2 fehérjék mennyiségének kimutatása western blottal Rluc-ot, vad típusú AT1R-Rluc-ot, vagy DRY/AAY AT1R Rluc-ot kifejező HEK293 sejtekben, 5 perces AngII (100nM), illetve SII-AngII (10 μM) kezelést követően. (Szakadáti G, Tóth AD, Oláh I, Erdélyi LS, Balla T, Várnai P, Hunyady L, Balla A.: Mol Pharmacol. 2015).

Az AT1-receptor stimuláció hatására $G_{q/11}$ fehérjék közvetítésével PLCβ aktiválódás történik. A PLCβ bontja a plazmamembránban található $PtdIns(4,5)P_2$-t mely másodlagos hírvivők ($Ins(1,4,5)P_3$ és DAG) képződését eredményezi. A $PtdIns(4,5)P_2$ szint változás

méréséhez AT1-receptor Rluc-cal fúzionáltatott variánsát és PLCδ1-PH-YFP plazmidokat transzfektáltunk HEK293 sejtekben. A PLCδ1-PH doménje specifikusan kötődik a PtdIns(4,5)P_2 molekulákhoz, így nyugalmi állapotban mind az energiadonor receptor-Rluc, mind az energiaakceptor PLCδ1-PH-YFP a plazmamembránban helyezkedik el, mely egy viszonylag nagy energiatranszfert tesz lehetővé a két szonda között (intermolekuláris BRET mérés). Demonstráltuk, hogy 100 nM AngII stimulus hatására megtörténik a PLCβ aktiválás következtében a PtdIns(4,5)P_2 hasítása, mely a PLCδ1-PH fehérjék gyors áthelyeződését eredményezi a citoszólba. Míg a plazmamembránban a szondák egy síkban elhelyezkedve relatíve közel helyezkedtek el egymáshoz, addig sejtplazmába áthelyeződött szondák molekuláris közelsége és ezáltal a BRET hányados értéke lecsökken. A PtdIns(4,5)P_2 hasítása után rövid idővel elkezdődik a PtdIns(4,5)P_2 reszintézise, amely a PLCδ1-PH-YFP plazmamembránba történő visszahelyeződéséhez vezet és ebből kifolyólag a BRET hányados emelkedését okozza rövid időn belül (31. ábra, F panel, magenta görbe). A BRET-jel ezután újra csökken, mivel az aktiválódott receptorok eltávolódnak a plazmamembrántól a receptor-mediált endocitózisuk miatt.

3.4 Receptor deszenzitizáció kimutatása

Az AT1-receptor aktiválódását követően rövid idővel elindulnak a deszenzitizációs mechanizmusok is. Ahhoz, hogy az agonista indukált AT1-receptor interakcióját más fehérjékkel jellemezzük a receptort *Renilla* luciferázzal, míg az interakciós fehérjét YFP-vel jelöltük, majd a fúziós fehérjéket HEK293 sejekben fejeztük ki és intermolekuláris BRET méréseket végeztünk, hasonlóan a 3.3 fejezetben leírtakhoz. Az AT1-receptor stimulálása után bekövetkező deszenzitizációja másodperceken-perceken belül megtörténik, és ezt a GRK-ok által végzett foszforiláció okozza, majd a β-arresztin fehérje kötődnek a receptorhoz (31. ábra, A panel, magenta görbe). A β-arresztin a foszorilált receptort szétkapcsolja a G fehérjétől és beindítja az endocitózist, amely a Rab5 endoszóma fehérje és a receptor közötti BRET-jel emelkedését eredményezi élő sejtes méréseinkben (31. ábra, B panel, magenta görbe), ezen mechanizmus részletesebben kifejtésre kerül a 3.5 fejezetben. A HEK293 sejtekben a 2-es típusú GRK izoforma (GRK2) felelős az AT1-receptor agonista indukált foszforilációjáért és az ezt követő β-arresztin2 kötés elősegítéséért. Az AT1-receptor-Rluc és a GRK2-YFP konstruktokat kifejező sejteket 100nM AngII-vel stimuláltuk, amelyet BRET hányados hirtelen emelkedése követett utalva a rövid idő alatt bekövetkező AT1-receptor és GRK2 közötti kapcsolódásra (31. ábra, G panel). A BRET mérés időbeni felbontása azt is lehetővé teszi, hogy kimutassuk a különböző folyamatok sorrendiségét és sikeresen demonstráltuk, hogy az AT1-

receptor agonista indukált GRK kötése megelőzi a β-arresztin kötését a receptorhoz (31. ábra, H panel).
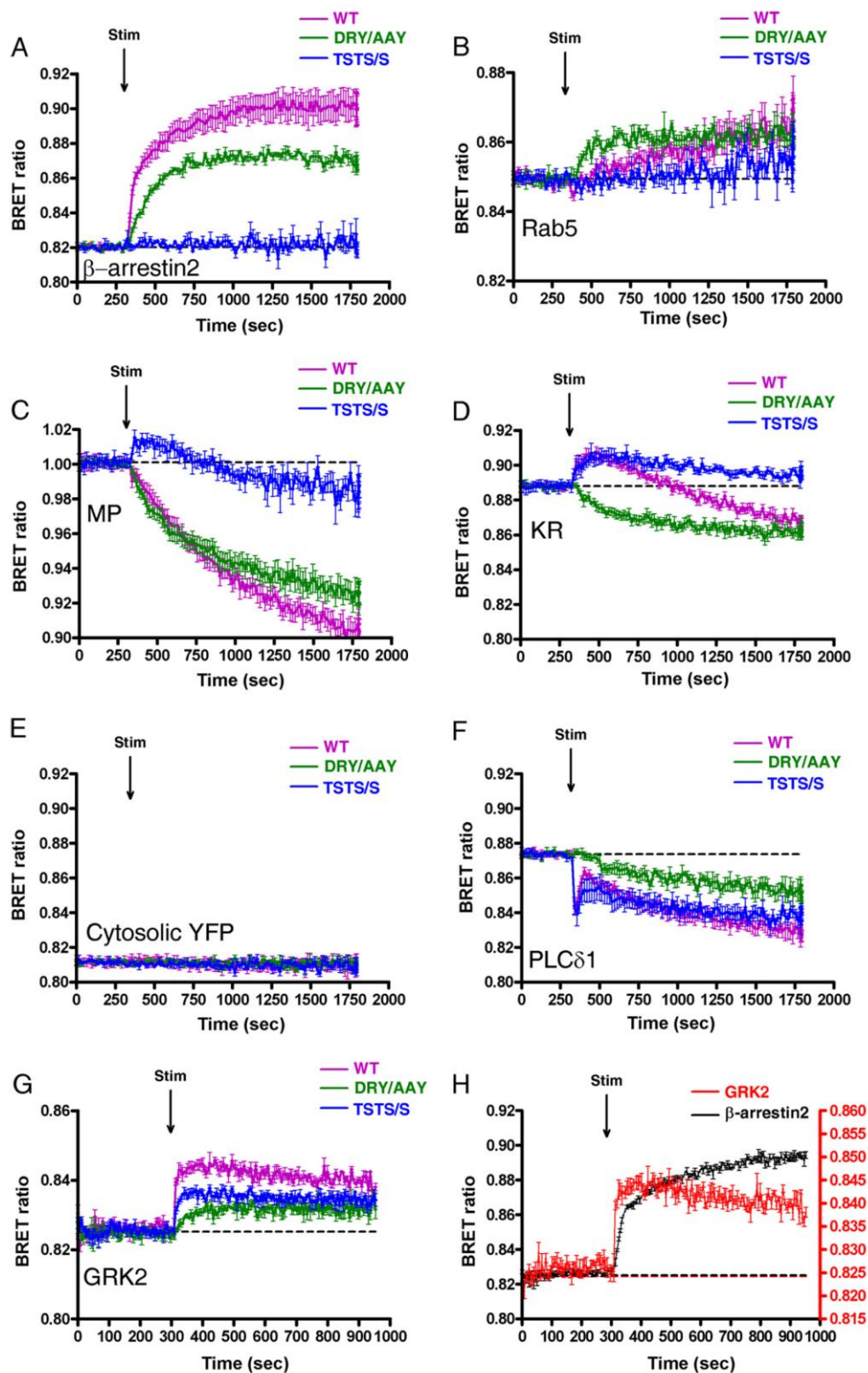
31. ábra. BRET-jel változása az AT1-receptor és YFP-vel jelölt fehérjék között AngII stimuláció után. HEK293 sejteket transzfektáltunk 24 órával a mérés előtt vad típusú (WT) vagy a jelzett mutáns AT1R-Rluc, illetve YFP-fúziós fehérjék plazmidjaival. A jelzett időpontban 100 nM AngII vagy vehikulum

(szaggatott vonal) hozzáadásával stimuláltuk a sejteket. A BRET hányados emelkedése a molekuláris közelség létrejöttére utal az AT1R és a jelzett YFP-fúziós fehérjék között. A BRET görbék legalább három független kísérlet eredményei. Átlag ± SEM értékeket ábrázoltunk (Balla A *et al.*: J Biol Chem. 2012).

A különböző AT1-receptor ligandumokkal indukált receptor-β-arresztin2-kötések vizsgálatakor ugyanakkor azt találtuk, hogy jelátvitel-szelektív aktivációt SI-AngII, SII-AngII, TRV120023 vagy TRV120027 ligandumokkal kiváltva kisebb mértékű a β-arresztin2-kötés erőssége, az AngII által kiváltotthoz képest. Hasonlóan kisebb mértékű β-arresztin2-kötést tapasztaltunk AngIV alkalmazása esetén is. Dózis-hatás görbék készítésével meggyőződtünk arról, hogy a tapasztalt eltérések, nem a szubmaximális ligandum koncentrációknak köszönhetők, hanem a ligandumok affinitásával van összefüggésben (32. ábra).
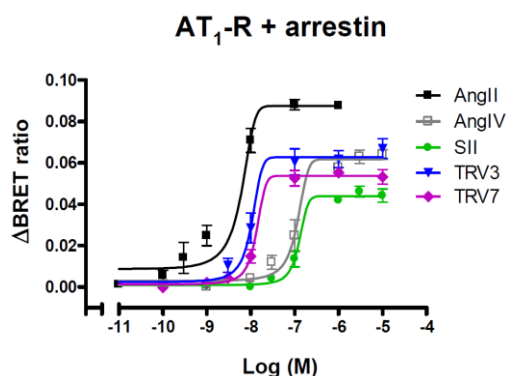
32. ábra Az AT1R stimulus indukált β-arresztin2-kötődés dózis-hatás görbéi. Dózis-hatás görbék, melyek a β-arresztin2-YFP AT1R-Rluc molekulához való kötődését mutatja HEK293 sejtekben különböző ligandokkal stimulált körülmények között. A legalább három független kísérletből származó adatokat átlag ± SEM formában ábrázoltuk. (Szakadáti G, Tóth AD, Oláh I, Erdélyi LS, Balla T, Várnai P, Hunyady L, Balla A.: Mol Pharmacol. 2015).

3.5 Az AT1-receptor lokalizációjának megváltozása agonista hatására

Megvizsgáltuk, hogy vajon az AT1R aktiválódása során megváltoztatja-e a receptor lokalizációját a plazmamembrán különböző mikrodoménjeiben, mielőtt receptor-mediált endocitózis következtében internalizációra kerül. Az AT1-receptor-luciferáz és a különböző lipid "tutajok" megjelölésére használt konstruktok segítségével BRET mérésekkel követtük a receptor eloszlásának változását hormon-stimulus hatására.

Eredményeink szerint a mirisztoil és palmitoil (MyrPalmYFP), illetve a két plamitoil csoporttal kihorganyzott fehérjék (PalmPalmYFP) nyugvó sejtekben jelentős BRET interakciót mutattak az AT1-receptorral, mely AngII hatására csökkent, ami arra utal, hogy a receptor AngII hatására a koleszterol- és szfingolipid-gazdag lipid mikrodoménekből más

kompartmentekbe helyeződik át. Ezt az áthelyeződést igazoltuk olyan plazmamembrán bioszenzor segítségével (K-Ras fehérje CAAX doménjét tartalmazza, KR-YFP), mely a plazma membrán rendezetlen („disordered" vagy „non-raft") mikrodoménjében helyezkedik el, mivel a KR-YFP és AT1-R-luciferáz jelentősen emelkedett BRET interakciót mutatnak AngII hatására a receptor internalizációja előtti időpontokban (31. ábra, C és D panel, magenta görbék). További kísérleteinkben az AT1R konzervált AAY szekvenciájának DRY mutációjával kimutattuk, hogy ezen mozgás a különböző plazmamembrán mikrodomének között G-fehérjétől nem független folyamat HEK293 sejtekben (31. ábra, C és D panel, zöld görbék), mely eredményeket jelátvitel szelektív agonisták felhasználásával is megerősítettünk (33. ábra, B panel, zöld és kék görbék).
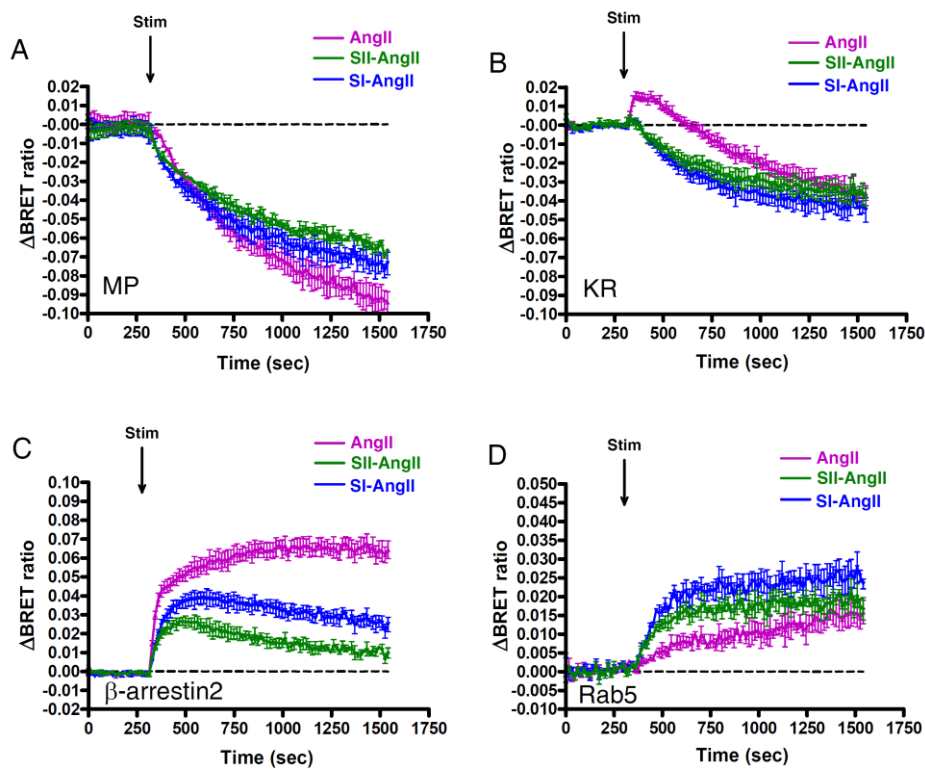
33. ábra. BRET-jel változása az AT1-receptor és YFP-vel jelölt fehérjék között AngII stimuláció után. HEK293 sejteket transzfektáltunk 24 órával a mérés előtt AT1R-Rluc, illetve YFP-fúziós fehérjék plazmidjaival. A jelzett időpontban 100 nM AngII (magenta görbék), 100 nM SI-AngII (kék görbék), 10 µM SII-AngII vagy vehikulum (szaggatott vonal) hozzáadásával stimuláltuk a sejteket. A BRET görbék legalább három független kísérlet eredményei. Átlag ± SEM értékeket ábrázoltunk (Balla A *et al*.: J Biol Chem. 2012).

3.6 Az AT1-receptor internalizációjának vizsgálata

A GFKR-okra jellemző, hogy aktiválódást követően foszforilálódnak, deszenzitizálódnak, majd pedig internalizálódnak a sejt belsejébe. A lefűződött vezikulából

először kialakul a korai endoszóma, melyből a receptor vagy a lizoszómális lebontás irányába, vagy pedig reciklizáló endoszómák segítségével a plazmamembrán felé folytathatja tovább az útját. A sejtek egy adott ligandum iránti válaszkészségét alapvetően a plazmamembránban található ligandum-specifikus receptorok számától függ, melyet az oda kihelyeződő (bioszintézis vagy recirkuláció miatt), illetve az onnan endocitózissal eltávolított receptorok dinamikus egyensúlya határoz meg. Az arresztin állványfehérje kötődése az AT1-receptorhoz nemcsak leállítja a G-fehérjén keresztüli jelátvitelt, hanem egyúttal az endocitózis felé irányítja a receptort. Ezáltal az AT1-receptor a deszenzitizációt követően a sejt belsejébe kerül, így a receptorszám a sejt felszínén hosszabb távon lecsökken. A receptor internalizációja többféle módon is történhet, dinamin-függő (kaveolák által, vagy klatrin-függő módon), vagy dinamintól független mechanizmussal. A receptor plazmamembránról való eltűnését demonstráltuk olyan intermolekuláris BRET mérésben, ahol az energiadonor az AT1-receptor-Rluc, míg az energiaakceptor egy plazmamembrán marker-YFP fúziós fehérje. Alapállapotban a receptor a sejtfelszínen helyezkedik el, így a plazmamembrán marker-YFP fúziós fehérjevel nagy energiatranszfert ad. Stimulációt követően a receptor internalizálódik, így távolabb kerül a plazmamembrán markertől és a BRET hányados lecsökken (31. ábra, C panel). Az internalizálódott receptor a sejten belül endomembránokba kerül, melyet egy endoszómában elhelyezkedő Rab5-YFP szondával demonstráltuk (31. ábra, B panel, illetve 33. ábra D panel). Az internalizációs kísérletekben úgynevezett nem-specifikus BRET kölcsönhatást mértünk, a BRET jelváltozások az azonos membránba (kompartmentbe) kerülő molekulák közelségével, illetve ennek a közelségnek a megszűnésével magyarázhatók. Kimutattuk, hogy AngII ingerlés hatására a vad típusú AT1R-hoz képest gyorsabban jelent meg a G-fehérje kötésére képtelen DRY/AAY jelátvitel-szelektív mutáns AT1R a Rab5-tartalmú korai endoszómákban (34. ábra, D panel, illetve 31. ábra, B panel, zöld görbe). β-arresztin jelátvitelre szelektív AngII analóg, úgymint SI-AngII, SII-AngII, TRV120023, vagy TRV120027 ligandumok hatására is az AT1R gyorsabb korai endoszómákban való megjelenését tapasztaltuk összevetve az AngII ingerléssel (34. ábra). Konfokális mikroszkópiával is bizonyítottuk, hogy a jelátvitel-szelektíven aktivált AT1R korai internalizációja felgyorsult (35. ábra). A vizsgált jelátvitel-szelektív ligandumokhoz hasonlóan alacsonyabb affinitással rendelkező angiotenzin IV (AngIV), mely mind a G-fehérje-függő, mind pedig a G-fehérje-független jelpályákat képes aktiválni, az AngII-nél látottakhoz hasonló internalizációs kinetikát eredményezett (34. ábra, C panel).
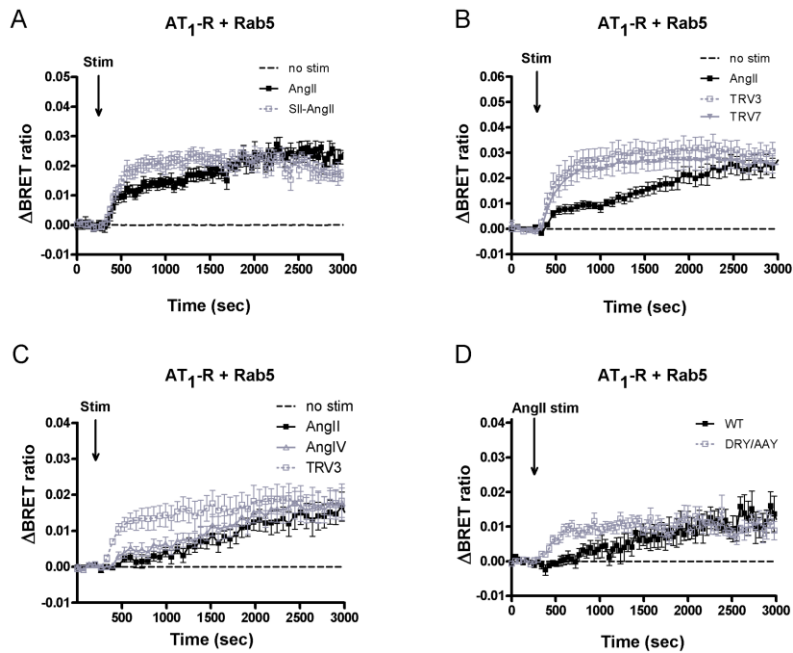
34. ábra. BRET-jel változása az AT1-receptor és YFP-vel jelölt fehérjék között AngII stimuláció után. HEK293 sejteket transzfektáltunk 24 órával a mérés előtt vad típusú WT-AT1R-Rluc (A-D panel) vagy DRY/AAY AT1R-Rluc (D panel), illetve Rab5-YFP plazmidjaival. A jelzett időpontban 100 nM AngII, 10 µM SII-AngII, 10 µM TRV120023 (TRV3), 1 µM TRV120027 (TRV7), 10 µM AngIV vagy vehikulum (szaggatott vonal) hozzáadásával stimuláltuk a sejteket. A BRET görbék legalább három független kísérlet eredményei. Átlag ± SEM értékeket ábrázoltunk (Szakadáti G, Tóth AD, Oláh I, Erdélyi LS, Balla T, Várnai P, Hunyady L, Balla A.: Mol Pharmacol. 2015).
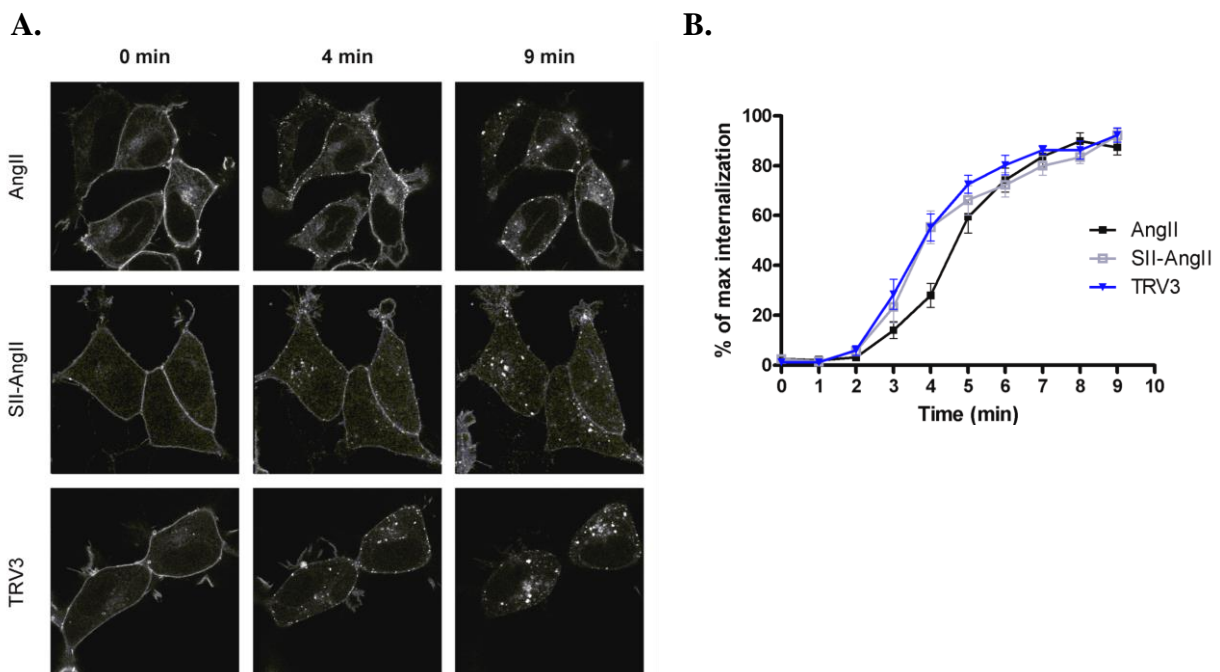

35 ábra. Az AT1-receptor internalizációja gyorsabb jelátvitel-szelektív agonisták hatására. (A) AT1R-GFP-t stabilan kifejező HEK293 sejtekről készült reprezentatív konfokális lézer mikroszkóp felvételek az AT1R sejten belüli eloszlásáról. A felvételek 100 nM AngII (felső sor felvételei), 10 µM SII (középső

47

sor felvételei) vagy 1 µM TRV3 (alsó sor felvételei) hozzáadása előtt közvetlenül (0 perc), illetve a hozzáadást követően 4 és 9 perccel készültek. A GFP fluoreszcencia mérése Zeiss LSM 710 konfokális lézer mikroszkóppal történt. (B) Az AT1R-GFP internalizációjának kvantifikálása MetaMorph szoftver morfometriai elemzésével készült. A plazmamembrántól egyértelműen elkülöníthető AT1R-GFP tartalmú vezikulák arányát ábrázoltuk a maximális internalizáció, illetve az idő függvényében. Az internalizáció maximumának az egyes kísérletek egyes kondicióiban egy időben mérhető legmagasabb vezikulaszámot tekintettük. Az ábrán 7 független kísérlet átlaga ± SEM értékei láthatók. (Szakadáti G, Tóth AD, Oláh I, Erdélyi LS, Balla T, Várnai P, Hunyady L, Balla A.: Mol Pharmacol. 2015).

3.7 A PtdIns 4-kinázok és a PtdIns(4,5)P_2 szerepének vizsgálata a receptor működésében

Az alábbi kísérleteinkben demonstráltuk, hogy a plazmamembránban található PtdIns(4,5)P_2 foszfoinozitid esszenciális szereppel bír az AT1-receptor endocitózisának szabályozásában. A PtdIns(4,5)P_2 eltávolítása a plazmamembránról az agonista indukált internalizációt megakadályozza; bár a receptor bekerül a klatrin-burkos vezikulákba, de azok lefűződése nem történik meg. Igazoltuk, hogy a β-arresztin jelátvitelre szelektív ligandumjaink (SI-AngI, SII-AngII, TRV120023 és TRV120027), valóban nem hoznak létre G-fehérje aktivációt és így PtdIns(4,5)P_2 bontást (36.ábra). Alacsony koncentrációjú wortmanninnal gátolva a foszfatidilinozitol 3-kinázokat nem tapasztaltunk változást a korai internalizációban. Ezzel szemben nagyobb dózisú wortmanninnal, így a már foszfatidilinozitol 4-kinázok gátlásával az AngII, illetve AngIV stimulációra létrejövő internalizáció teljesen gátlódott, míg a TRV3-ra létrejövő internalizáció nem változott. A PtdIns4KIIIα izoforma gátlásával (A1 szelektív inhibitorral) teljesen megszűnt az AT1R korai endoszómákban való megjelenése AngII, AngIV hatására, azonban TRV3 ingerlésnél nem tapasztaltunk változást. Ezzel ellentétben a PtdIns4KIIIβ gátlása a PIK93 inhibitorral nem okozott változást a receptor internalizációs viselkedésében (37. ábra).

A PtdIns(4,5)P_2 szintézisét követően a PtdIns(4,5)P_2 bontásának szerepét is megvizsgáltuk. Domináns negatív GRK2 konstrukció kifejeztetésével meggátoltuk az AngII-re létrejövő G$_q$-fehérje aktivációt és így a PtdIns(4,5)P_2 bontást, melynek hatására az AngII-re létrejövő korai internalizáció felgyorsult, míg TRV120023 alkalmazásakor nem változott. Eredményeinket kiterjesztve, más GFKR hatására létrejövő PtdIns(4,5)P_2 bontás szerepét is elemeztük. Az α1-adrenerg receptor előzetes ingerlésének hatására az AT1R korai internalizációja lelassult, mind AngII, mind pedig TRV120023 hatására.
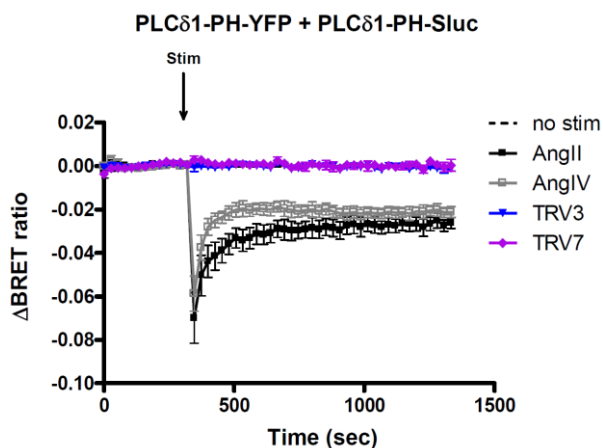
36. ábra. A PtdIns(4,5)P₂ szint változása AT1R stimulusát követően HEK293 sejtekben. PLCδ1-PH-Rluc és PLCδ1-PH-YFP plazmidokat transzfektáltunk AT1-receptort tartalmazó HEK293 sejtekben. A stimulus előtt mind a PLCδ1-PH-Rluc, mind a PLCδ1-PH-YFP a plazmamembránban helyezkedik el, mely egy viszonylag nagy energiatranszfert tesz lehetővé a két szonda között (intermolekuláris BRET mérés). A G_q-fehérje aktiválást okozó agonisták (AngII, fekete görbe, illetve AngIV, szürke görbe) indukálta PtdIns(4,5)P_2 hasítása után rövid idővel elkezdődik a PtdIns(4,5)P_2 reszintézise, amely a PLCδ1-PH-Rluc és -YFP plazmamembránba történő visszahelyeződéséhez vezet és ebből kifolyólag a BRET hányados emelkedését okozza. Az ábrákon három független kísérlet, triplikátumokban mért eredményei láthatók, átlag ± SEM érték formátumban. (Szakadáti G, Tóth AD, Oláh I, Erdélyi LS, Balla T, Várnai P, Hunyady L, Balla A.: Mol Pharmacol. 2015).

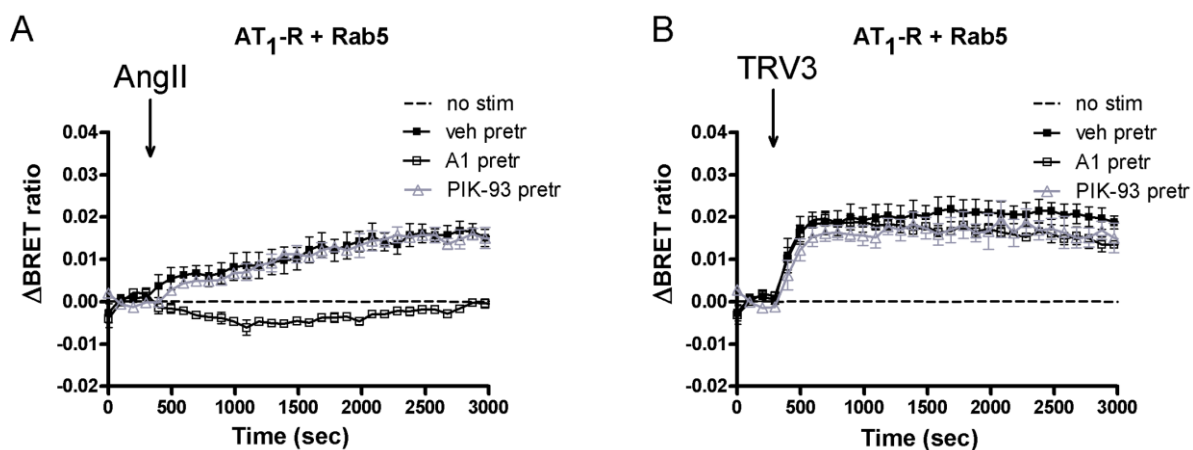**37. ábra. PtdIns 4-kináz gátlószereinek hatása AT1-receptor internalizációjára.** Különböző agonisták által aktivált AT1R internalizációját BRET mérésben követtük nyomon HEK293 sejteken, 24 órával az AT1R-Rluc és YFP-Rab5 transzfekció után. A mérés előtt a sejteket 10 percig előkezeltük médiummal („veh pretr"), PtdIns4KIIIα specifikus gátlószerként 10 nM A1-el vagy a PtdIns4KIIIβ izoformát specifikusan gátló PIK-93-al, 250 nM-os koncentrációban. A jelzett időpontokban vehikulumot (A és B panelek, szaggatott vonal), 100 nM AngII-t (A panel) vagy 1 μM TRV3-at (B panel) adtunk a sejtekhez. Az ábrákon három független kísérlet, triplikátumokban mért eredményei láthatók, átlag ± SEM érték formátumban (Szakadáti G, Tóth AD, Oláh I, Erdélyi LS, Balla T, Várnai P, Hunyady L, Balla A.: Mol Pharmacol. 2015).

### 3.8 Az AT1R sejten belüli sorsának nyomon követése

A Rab5 korai endoszómákon kívül vizsgáltuk a stimulált receptor megjelenését a Rab4 tartalmú korai reciklizáló endoszómákban, a Rab7 tartalmú késői endoszómákban és lizoszómákban, valamint a Rab11 tartalmú késői reciklizáló endoszómákban is. Mindegyik vizsgált kompartmentben korábban jelent meg az AT1R a jelátvitel szelektív aktivációt követően, mint az AngII ingerlés hatására. A Rab7 tartalmú lizoszómákban kevéssé, míg a Rab11 tartalmúakban az AngII-nél tapasztaltakhoz képest gyorsabban és nagyobb mértékben jelent meg a receptor mind a jelátvitel-szelektív aktivációt követően, mind pedig az AngIV hatására. Kimutattuk, hogy a receptor késői intracelluláris sorsát nem befolyásolja a Ca^{2+}-jel hiánya. Ezzel szemben a különböző β-arresztin asszociációs kinetikának és erősségnek alapvető fontossága lehet a receptor későbbi sorsának meghatározásában, mely megnyilvánulhat a receptor eltérő sebességű reszenzitizációjában és recirkulációjában is a sejt felszínére. Eredményeink alapján elmondhatjuk, hogy a jelátvitel-szelektív aktiváció fontos szerepet játszhat a receptor hosszú távú sorsában, valamint az externalizáció/internalizáció egyensúlyában. Ezen folyamatok megváltoztatják a sejtfelszínen lévő receptorszámot, melynek befolyásolása szelektív ligandumokkal klinikailag fontos lehet.

3.9 Az AT1R génexpresszóra kifejtett hatásának vizsgálata

Az AT1-receptor aktiválása számos jelátviteli utat indít el az AngII fiziológiás célsejtjeiben, amelyek különféle rövid- és hosszú távú biológiai hatásokat eredményeznek. A vaszkuláris simaizomsejtekben (VSMC) az AngII legismertebb rövid távú hatása a simaizomsejtek összehúzódása, és ezen keresztül az artériás vérnyomás szabályozása. Az AngII azonban hosszú távon is befolyásolja a célszöveteit, melyek leginkább a gének expressziójának változtatásán keresztül nyilvánulnak meg. Ezen hatások számos, a kardiovaszkuláris rendszert érintő betegségek (pl. hipertenzió, érfal-gyulladás és vaszkuláris remodelling) pathomechanizmusában is fontos szerepet tölthetnek be. A vaszkuláris remodelling során az érfal szerkezete megváltozik, melynek fontos lépései közé tartozik a simaizomsejtek proliferációja, hipertrófiája és fibrózisa, valamint az extracelluláris mátrix megváltozása. Ezen változások létrejöttében az AT1R kulcsfontosságú szerepet tölt be, melyre bizonyítékot ad a renin-angiotenzin rendszer gátlószereinek kiemelkedő jelentősége és eredményessége a klinikumban, az AT1-receptor specifikus gátlószerei klinikai kísérletekben szingnifikánsan csökkentették a vaszkuláris remodelling mértékét. A folyamat molekuláris hátterében szerepet játszik különböző MAPK jelpályák aktivációja, károsító reaktív oxigén gyökök (ROS) képződése, valamint az EGF-receptor transzaktivációja. A MAP kinázok a sejtekben rendkívül

fontos effektorok, a sejt alapvető működéseire vannak hatással, elsősorban a sejt növekedésére és proliferációjára, illetve a sejtciklusra. A MAPK-ok működését és aktivált állapotuk hosszát számos fehérje befolyásolja és szabályozza. A MAPK-foszfatázok (MKP), a kettős specifitású foszfatázok (DUSP) családjába tartoznak, melyek szubsztrátjaikat egyrészt egy tirozinon, másodrészt egy szerinen vagy treoninon defoszforilálják, az aktivált MAPK-ok esetében az inaktiváló defoszforilációjukat a T-X-Y motívumon végzik. Egy DUSP izoformának jellemzően egynél több szubszrátja is lehet és szabályozásuk történhet expressziós és poszttranszlációs szinten is. A DUSP-ok egy érdekes tulajdonsága, hogy nemcsak a foszforilált szubsztrátjukat képesek megkötni, illetve defoszforiláció után nem feltétlenül eresztik el a szubsztrát MAPK-t, hanem ki is horgonyozhatják azt. Ezért a MAPK-k szabályozása nem egyszerű ki-bekapcsoló mechanizmusokra épül, úgy tűnik, hogy a DUSP izoformák képesek a MAPK szignálok erősségét, idejét és térbeliségét is komplex módon szabályozni.

A kutatócsoportunk Affymetrix gén-chip módszer alkalmazásával vizsgálta az AngII hatására létrejövő génexpressziós változásokat érfal simaizomsejtekben. A mérések során megállapítottuk, hogy a sejteken végzett 2 órás Ang II stimuláció hatására körülbelül 100 gén expressziójában állt be változás. Részletesebben három DUSP izoforma expressziós változásait vizsgáltuk, a kiválasztott izoformák a DUSP enzimek 3 alcsaládjának egy-egy képviselői. A DUSP5 egy sejtmagban lokalizálódó MAPK foszfatáz, amely főleg a tirozin-kináz receptorokról kiinduló MAP kináz kaszkád szabályozásában vesz részt; a DUSP6 egy citoplazmában található MAPK foszfatáz, amely jellemzően ERK1/2 kinázt defoszforilál; a DUSP10 pedig egy sejtmagban és a citoplazmában is jelenlévő forma, melynek célmolekulái közé tartozik a JNK, p38 és az ERK1/2 MAPK is. Génexpressziós méréseinkben meghatároztuk a változások időkinetikáját és megállapítottuk, hogy a DUSP5 és DUSP10 génexpressziója az AngII stimulus után 2 órával adja a maximális mértéket, melyet egy gyors csökkenés követ (38. ábra, A és C panel). A DUSP6 mRNS expressziója is a stimulust követő második órában éri el a legmagasabb szintet, de az expressziója hosszabb ideig magas szinn marad AngII ingerlést követően (38. ábra, B panel). Megvizsgáltuk a génexpressziós változásokhoz vezető jelátviteli útvonalak szerepét is érfal simaizomsejtekben különböző gátlószerek segítségével. Megállapítottuk, hogy a vizsgált DUSP génexpressziós változások esetén a 100 nM AngII kezelés csak az AT1-receptoron keresztül fejti ki hatását, az AT2-receptor nem játszik szerepet, hiszen 10 µM candesatran (specifikus AT1R blokkoló) előkezelés teljesen megakadályozta az AngII által kiváltott válaszokat (39. ábra).
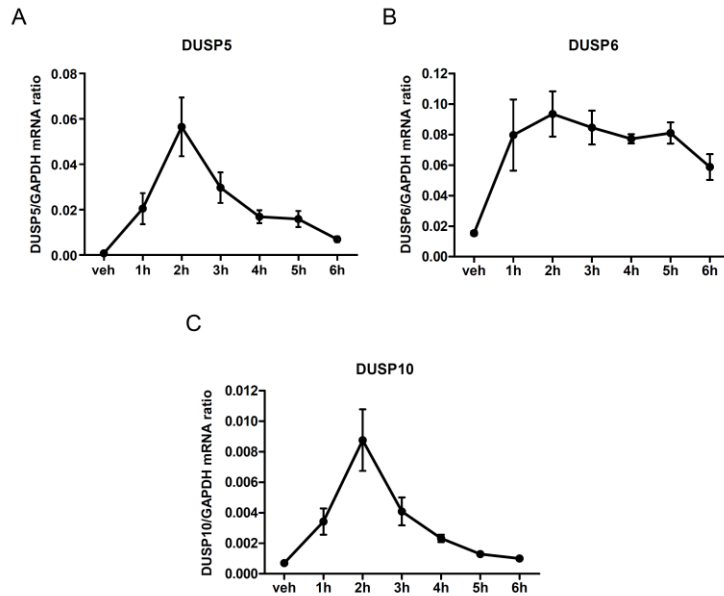
38. ábra. Az AngII által okozott DUSP génexpressziós változások időkinetikája. Primer vaszkuláris simaizomsejteket 100 nM AngII-vel stimuláltuk különböző időpontokig. (A) DUSP5, (B) DUSP6 és (C) DUSP10 mRNS szintjeit qPCR kísérletekben határoztuk meg. A függőleges tengelyeken a *GAPDH* referenciagénhez viszonyított génexpresszió fokozódás mértéke látható. Az ábrákon 5-6 független kísérlet eredményei láthatók (Gém JB, Kovács KB, Szalai L, Szakadáti G, Porkoláb E, Szalai B, Turu G, Tóth AD, Szekeres M, Hunyady L, Balla A.: Cells. 2021).
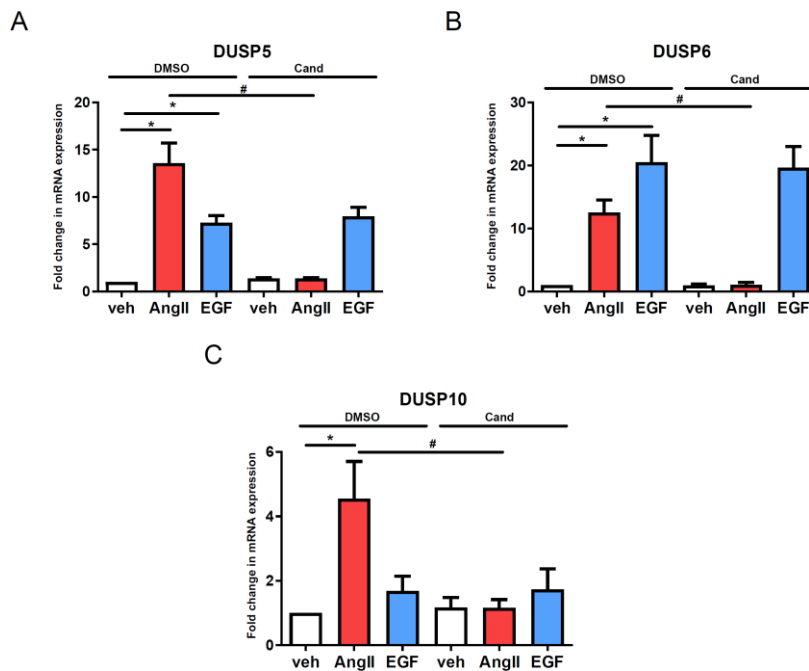
39. ábra. Az AngII által okozott DUSP génexpressziós változások időkinetikája. Primer vaszkuláris simaizomsejteket 30 percig előkezeltük 10 μM candesatran („Cand") vagy DMSO-val, majd ezt követően 2 óráig kezeltük a sejteket 100 nM AngII-vel (piros oszlopok), 50 ng/ml EGF-fel (kék oszlopok) vagy vehikulummal (fehér oszlopok). (A) DUSP5, (B) DUSP6 és (C) DUSP10 mRNS szintjeit qPCR kísérletekben határoztuk meg. A függőleges tengelyeken a GAPDH referenciagénhez viszonyított génexpresszió fokozódás mértéke látható. Az ábrákon négy független kísérlet eredményei láthatók (Gém JB, Kovács KB, Szalai L, Szakadáti G, Porkoláb E, Szalai B, Turu G, Tóth AD, Szekeres M, Hunyady L, Balla A.: Cells. 2021).

Az EGFR transzaktivációját vaszkuláris simaizomsejtekben az EGFR farmakológiai gátlása segítségével vizsgálják az irodalomban, viszont saját kísérleteink alapján az irodalomban alkalmazott EGFR inhibitoros koncentrációk egyéb tirozin kinázokat is gátolhatnak a sejtekben. Kísérleteinkben az EGFR kifejeződését shRNS módszerrel, lentivirális rendszer segítségével csökkentettük. Kísérleteinkhez két EGFR-re specifikus shRNS pLKO-puro plazmidot készítettünk és helper plazmidok segítségével lentivírusokat készítettünk. Az shEGFR#1 és az shEGFR#2 vírusok hatékonyságát qPCR és western blot módszerrel ellenőriztük (40. ábra).

A. **B.**
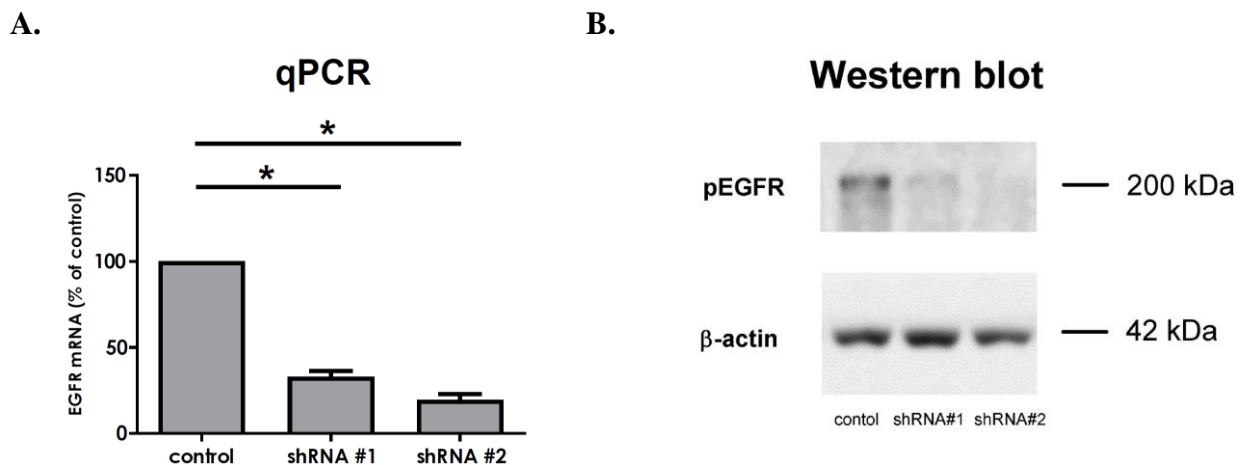
40. ábra. Az EGFR szintjének változása az shEGFR#1 és shEGFR#2 vírusokkal infektált sejtekben a kontroll vírusokkal fertőzött sejtekben mérhető szinthez viszonyítva. Az AngII által okozott DUSP génexpressziós változások időkinetikája. (A) qPCR és (B) western blot módszerrel ellenőriztük az EGFR szintet 48 órás vírus infekciót követően (Gém JB, Kovács KB, Szalai L, Szakadáti G, Porkoláb E, Szalai B, Turu G, Tóth AD, Szekeres M, Hunyady L, Balla A.: Cells. 2021).

Megvizsgáltuk néhány DUSP gén AngII stimulus általi expressziós változásait, olyan körülmények között, hogy az EGFR expresszióját jelentősen lecsökkentettük shEGFR vírusokkal. Eredményeink alapján kijelenthetjük, hogy az AngII stimulusára bekövetkező DUSP génexpressziós változások döntően nem EGF-receptor transzaktiváción keresztül történnek érfal simaizomsejtekben (41. ábra). Az adataink jelentős különbségeket tártak fel a vizsgált gének AngII stimulusra történő expressziójában az AG1478 EGFR inhibitorral kezelt, valamint az shEGFR#2-vel infektált sejtek között. A különbségek feltételezéseink szerint nem csupán a gátlási módszerek különbségeiből adódnak. Feltételezzük, hogy az AT1-receptor EGFR transzaktivációjában más, nem receptor tirozin-kinázok is részt vesznek.
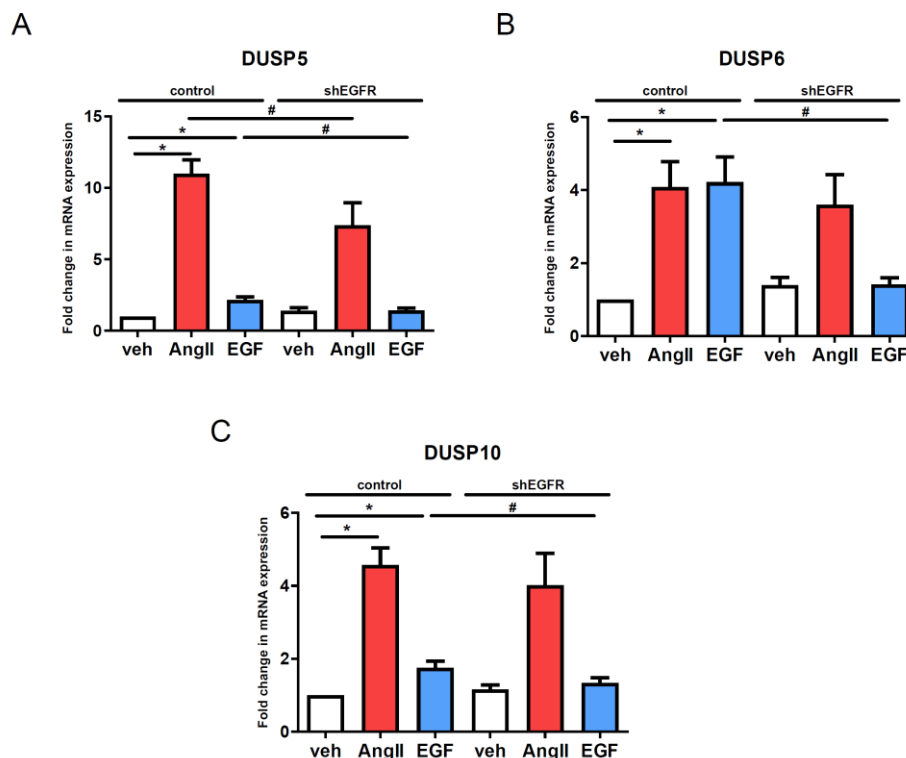
41. ábra. EGFR csendesítésének hatása az AngII vagy EGFR által indukált génexpressziós változásokra VSMC sejtekben. Primer vaszkuláris simaizomsejteket kontrol („control") vagy EGFR specifikus („shEGFR") shEGFR#2 lentivírusokkal kezeltük 48 óráig, majd 2 óráig kezeltük azokat 100 nM AngII-vel (piros oszlopok), 50 ng/ml EGF-fel (kék oszlopok) vagy vehikulummal (fehér oszlopok). (A) DUSP5, (B) DUSP6 és (C) DUSP10 mRNS szintjeit qPCR kísérletekben határoztuk meg. A függőleges tengelyeken a *GAPDH* referenciagénhez viszonyított génexpresszió fokozódás mértéke látható. Az ábrákon négy független kísérlet eredményei láthatók (Gém JB, Kovács KB, Szalai L, Szakadáti G, Porkoláb E, Szalai B, Turu G, Tóth AD, Szekeres M, Hunyady L, <u>Balla A.</u>: Cells. 2021).

Megvizsgáltunk egy másik, az AngII hatására jelentős génexpresszió fokozódást mutató fehérje, a koleszterin-25-hidroxiláz (CH25H) szerepét érfal simaizomsejtekben. Az oxiszterolok, mint például a CH25H enzim terméke, a 25-hidroxikoleszterin (25-HC), elősegíthetik kardiovaszkuláris elváltozások kialakulását. A 25-HC) a lipid metabolizmus és az immunválaszok szabályozásában vesz részt, mindemellett károsíthatja a vaszkuláris simaizomsejteket is. Azonban nem volt ismert kapcsolat a 25-HC termelődése, és az AngII sejtélettani hatásai között VSMC-ben, ezért célunk volt az AngII CH25H expresszióra gyakorolt hatásának feltárása. Megállapítottuk, hogy a koleszterin 25-hidroxiláz mRNS expressziója az AngII stimulus után 1 órával a legmagasabb, illetve kimutattuk, hogy a vaszkuláris simaizomsejtek az angiotenzin II hatására 25-hidroxikoleszterint termelnek, mely a sejtekből kijutva az atherosclerosis kialakulásában szerepet játszó gyulladásos folyamatokat segítheti elő (42. ábra). További kísérleteink adatai alapján az AngII stimulusa AT1R és $G_{q/11}$-

fehérje aktiválásán keresztül fejti ki a szignifikáns *Ch25h* génexpressziót fokozó hatását (43. ábra, A panel), illetve kimutattuk, hogy a p38 MAPK jelpálya kiemelt szerepet játszik a *Ch25h* génexpressziót szabályozásában (43. ábra, B panel).
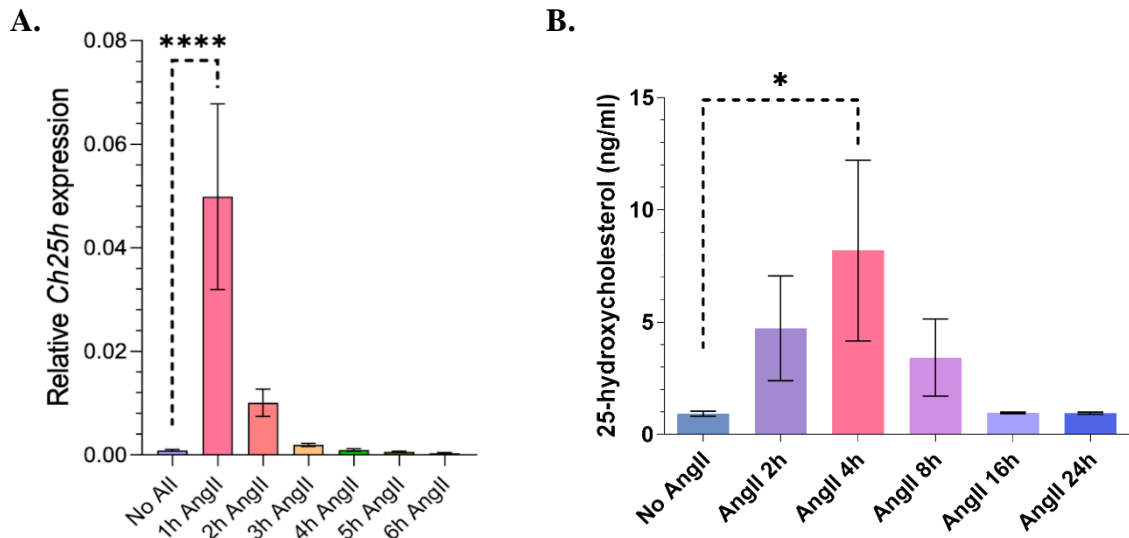
42. ábra. Az AngII stimulus hatása Ch25h kifejeződésére VSMC sejtekben. (A) Primer vaszkuláris simaizomsejteket 100 nM AngII-vel stimuláltuk és a *Ch25h* génexpresszió változását mértük qPCR módszerrel. A *Ch25h* mRNS szinteket a *GAPDH* referenciagénhez viszonyítva ábrázoltuk. Átlag ± SEM, n =5 független kísérlet. Többszörös lineáris regresszió, ****: p < 0.0001. (B) A simaizomsejteket 1 µM AngII-vel stimuláltuk 2, 4, 8, 16, 24 órán át, vagy nem stimuláltuk őket. A sejtek felülúszóját a stimulust követően begyűjtöttük, majd LC-MS/MS méréssel meghatároztuk a minták 25-HC tartalmát és koncentrációját. Átlag ± SEM, n =3 független kísérlet. Többszörös lineáris regresszió, * p<0,05 (Kovács KB, Szalai L, Szabó P, Gém JB, Barsi S, Szalai B, Perey-Simon B, Turu G, Tóth AD, Várnai P, Hunyady L, Balla A.: Int J Mol Sci, 2023).
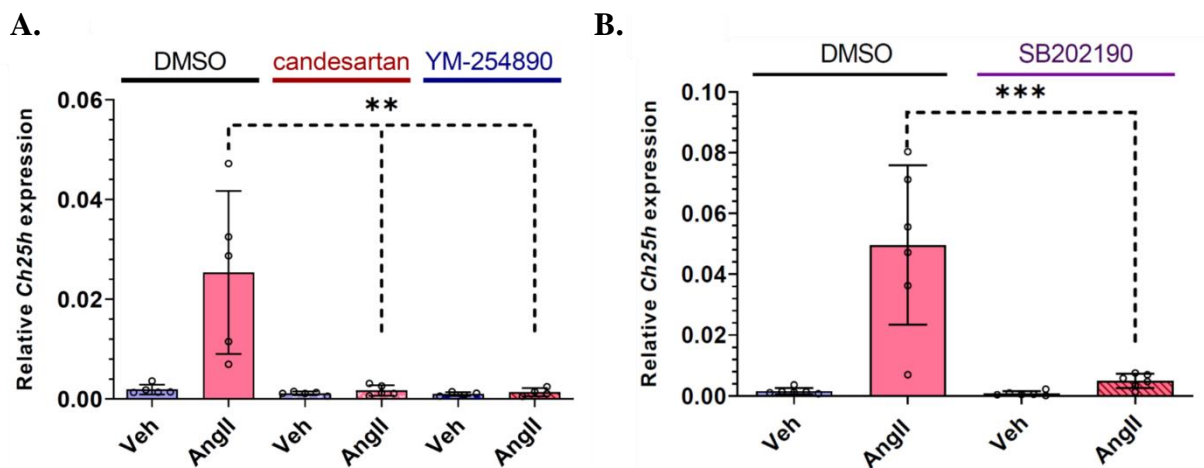
43. ábra. Az AngII stimulus hatása Ch25h kifejeződésére VSMC sejtekben. (A) Primer vaszkuláris simaizomsejteket 30 percig előkezeltük 10 µM candesatran (AT1R blokkoló) vagy 1 µM YM-254890 (G_q inhibitor) vagy 50 µM SB202190 (p38 MAPK inhibitor) vegyületekkel vagy DMSO-val, majd ezt követően 1 óráig kezeltük a sejteket 100 nM AngII-vel (rózsazín oszlopok), majd a *Ch25h* génexpresszió változását mértük qPCR módszerrel. (Kovács KB, Szalai L, Szabó P, Gém JB, Barsi S, Szalai B, Perey-Simon B, Turu G, Tóth AD, Várnai P, Hunyady L, Balla A.: Int J Mol Sci, 2023).

3.10 Az eredmények gyakorlati jelentősége

Az értekezésemben olyan kísérleteket mutattam be, melyekben számos módszer felhasználásával követni tudtuk az AT1-receptor stimulusát követő aktiválódást, különböző regulációs lépéseket, foszfoinoizitidek szintjében bekövetkező változásokat, illetve receptor-mediált endocitózist élő HEK293 sejtekben, illetve a receptor stimulusára bekövetkező hosszú távú hatásokat érfal simaizomsejtekben. Példáinkban az AT1-receptor sejtválaszait demonstráltuk, de egyéb plazmamembránban elhelyezkedő receptor vizsgálata is ugyanilyen módon megvalósítható. A különböző bioszenzorok, illetve a molekuláris közelséget érzékenyen kimutató BRET módszer alkalmas a GFKR-ok aktivációjának, jelátviteli mechanizmusainak, endocitózisának, illetve különböző vegyületek ezen sejtválaszokra történő farmakológiai hatásának tanulmányozására élő sejtekben. Az eredmények gyakorlati hasznosítása szempontjából az is lényeges, hogy a jelátviteli folyamatok nyomon követésére kifejlesztett rezonancia energiatranszferen alapuló módszerek továbbfejleszthetőek nagy számú vegyület hatásának „high-throughput" vizsgálatára. Klinikai szempontból is releváns génexpressziós kísérleti adataink segíthetnek megérteni az AngII által kiváltott hosszú távú, káros hatások patomechanizmusait és felfedhetik az AT1-receptor működésének új aspektusait. Eredményeink hozzájárulhatnak a magasvérnyomás és más keringési betegségek terápiájában fontos célpontot jelentő AT1R működésének jobb megértéséhez. Tekintettel a renin-angiotenzin rendszer gátlásának terápiás jelentőségére az elvégzett munka eredményei támpontul szolgálnak az AT1R blokkolók és az angiotenzin konvertáló enzim gátlók hatásainak és mellékhatásainak jobb megértéséhez. A munkáink eredményeképp több összefoglaló közleményt közöltünk, melyekben az eredményeink gyakorlati vonatkozásait, illetve a klinikummal való kapcsolatát is igyekeztünk feltárni.

4. AZ ÉRTEKEZÉS LEGFONTOSABB ÚJ MEGÁLLAPÍTÁSAI

1. Kimutattuk, hogy a II-es típusú PtdIns 4-kinázok az endoszómákkal asszociálódnak és megklónoztuk a II-es típusú PtdIns 4-kinázok egyik izofomáját (PtdIns4KIIβ).

2. Bebizonyítottuk, hogy a PtdIns4KIIIα enzim szerepet játszik a plazmamembrán a PtdIns(4)P szintézisében.

3. Kimutattuk, hogy a PtdIns4KIIIα enzim felelős a plazmamembránban az AngII hormon-szenzitív PtdIns(4)P és PtdIns(4,5)P_2 pool képződéséért és fenntartásáért.

4. BRET módszer felhasználásával feltérképeztük az AT1-receptor stimulusát követő aktiválódást, regulációs lépéseket, illetve receptor-mediált endocitózist élő HEK293 sejtekben. Kimutattuk, hogy az angiotenzin receptor megoszlása az aktivációt követően a plazmamembrán különböző mikrodoménjei között megváltozik az internalizációt megelőzően. Adataink alapján ez a mozgás a receptor G-fehérje aktivációjának az eredménye.

5. Kimutattuk az AT1-receptor szelektív aktiválásának következményeit különböző ligandumokkal. Jellemeztük az eltéréseket a receptor β-arresztin2 kötésében, a kalcium jel generálásban és internalizációs képességében a receptor G-fehérje független aktiválódását követően.

6. A Ras kis G-fehérje aktiválódás mérésére létrehozott BRET bioszenszorok alkalmasak növekedési faktorok, hormonok (pl. AngII) szignalizációjának vizsgálatára, illetve különböző vegyületek ezen szignalizációs jelpályákra történő farmakológiai hatásának tesztelésére élő sejtekben, valamint a szondák targetálásával különböző intracelluláris kompartmentekben demonstráltuk kis G-fehérje jelpályák működését. Jellemeztük a Ras kis G-fehérje aktiválódást az AT1R stimulusát követően, illetve kimutattuk, hogy HEK293 sejtekben ez a folyamat nem az EGF-receptor transzaktiváció következménye.

7. Kimutattuk, hogy az AT1-receptor internalizációja lényegesen korábbi időpontban megtörténik, ha a receptor stimulálása G-fehérje független módon történik. Eredményeink alapján a jelátvitel-szelektív agonisták által okozott gyors korai internalizáció nem az eltérő endocitotikus útvonalakon keresztül jön létre, valamint sem az eltérő β-arresztin kötés erősség, sem pedig a Ca^{2+} jel hiánya nem játszik szerepet a folyamatban.

8. Vizsgáltuk a plazmamembrán PtdIns(4,5)P_2 szerepét az AT1R teljes agonista és funkcionálisan szelektív agonista indukált internalizációjában. A G-fehérje aktiváció

következtében létrejövő PtdIns(4,5)P_2 bontás, majd pedig reszintézis meghatározó az AngII által kiváltott lassabb internalizációban.

9. Bebizonyítottuk, hogy a PtdIns 4-kináz IIIα esszenciális szereppel bír az AT1-receptor endocitózisának szabályozásában.

10. Kimutattuk, hogy az AngII-stimulus hatására számos DUSP izoforma expressziója megemelkedik érfal simaizomsejtekben és bizonyítottuk, hogy ezen változások döntően nem EGF-receptor transzaktiváción keresztül történnek érfal simaizomsejtekben.

11. Kimutattuk, hogy a koleszterin 25-hidroxiláz enzim expressziója jelentősen fokozódik vaszkuláris simaizomsejtekben az angiotenzin II hatására, illetve a stimulus hatására a sejtek 25-hidroxikoleszterint termelnek, mely az atherosclerosis kialakulásában szerepet játszó gyulladásos folyamatokat segítheti elő.

5. A RÖVIDÍTÉSEK JEGYZÉKE

25-HC	25-hidroxikoleszterin
AngII	Angiotenzin II
AT1-receptor	1-es típusú angiotenzin receptor
AT1R	AT1-receptor
BRET	Biolumineszcencia rezonancia energiatranszfer
CH25H	Koleszterin-25-hidroxiláz
CFP	cián fluoreszcens fehérje
DAG	Diacilglicerin
DMEM	Dulbecco által módosított médium
DUSP	Kettős specificitású foszfatáz (dual specificity phosphatase)
EGF	Epidermális eredetű növekedési faktor (epidermal growth factor)
EGFR	EGF-receptor
ERK1/2	Extracelluláris szignál regulált kináz 1 és 2
GAPDH	Glicerinaldehid-3-foszfát dehidrogenáz
GFKR	G-fehérjéhez kapcsolt receptor
GFP	Zöld fluoreszcens fehérje
GRK	G-fehérje kapcsolt receptor kináz
Hb-EGF	Heparin kötő epidermális növekekedés fakor
$Ins(1,4,5)P_3$	Inozitol 1,4,5-triszfoszfát
IPTG	Izopropil-1-tio-β-galaktopiranozid
MAPK	Mitogén aktivált protein kináz
MEK	Mitogén aktivált protein kináz kináz
MLCP	Miozin könnyű lánc foszfatáz
MMP	Mátrix-metalloproteáz
PAO	Fenil-arzén(III)-oxid
PBS	Phosphate-buffered saline
PDGFR	Trombocita eredetű növekedési faktor receptor
PH domén	plekstrin homológia domén (pleckstrin homology domain)
PI4K	Foszfatidilinozitol 4-kináz
PKC	Protein kináz C
PLC	Foszfolipáz C
PtdIns	Foszfatidilinozitol; 1-(3-sn-foszfatidil)-D-mio-inozitol
PtdIns4K	Foszfatidilinozitol 4-kináz
$PtdIns(4)P$	Foszfatidilinozitol 4-foszfát
$PtdIns(4,5)P_2$	1-(3-sn-foszfatidil)-D-mio-inozitol 4,5-biszfoszfát
ROS	Reaktív oxigén származékok
SDS	Nátrium-dodecil szulfát
Slus	Szuper *Renilla* luciferáz
VSMC	Vaszkuláris simaizomsejt
WM	Wortmannin
YFP	Sárga fluoreszcens fehérje

6. KÖZLEMÉNYEK

a) A doktori értekezés alapjául szolgáló saját eredeti közlemények

1. **Balla, A.**, Vereb, G., Gulkan, H., Gehrmann, T., Gergely, P., Heilmeyer, L. M. G., & Antal, M. (2000). Immunohistochemical localisation of two phosphatidylinositol 4-kinase isoforms, P14K230 and P14K92, in the central nervous system of rats. Experimental Brain Research, 134, 279-88. **IF: 2,137**

2. **Balla, A.**, Tuymetova, G., Barshishat, M., Geiszt, M., & Balla, T. (2002). Characterization of type II phosphatidylinositol 4-kinase isoforms reveals association of the enzymes with endosomal vesicular compartments. Journal of Biological Chemistry, 277, 20041-50. **IF: 6,696**

3. **Balla, A.**, Tuymetova, G., Tsiomenko, A., Varnai, P., & Balla, T. (2005). A plasma membrane pool of phosphatidylinositol 4-phosphate is generated by phosphatidylinositol 4-kinase type-III alpha: Studies with the PH domains of the oxysterol binding protein and FAPP1. Molecular Biology of the Cell, 16, 1282-95. **IF: 6,52**

4. **Balla, A.**, Kim, Y. J., Varnai, P., Szentpetery, Z., Knight, Z., Shokat, K. M., & Balla, T. (2008). Maintenance of hormone-sensitive phosphoinositide pools in the plasma membrane requires phosphatidylinositol 4-kinase IIIalpha. Mol Biol Cell, 19, 711-21. **IF: 5,558**

5. **Balla, A.**, Tuymetova, G., Toth, B., Szentpetery, Z., Zhao, X., Knight, Z. A., Shokat, K., Steinbach, P. J., & Balla, T. (2008). Design of drug-resistant alleles of type-III phosphatidylinositol 4-kinases using mutagenesis and molecular modeling. Biochemistry, 47, 1599-607. **IF: 3,379**

6. **Balla, A.**, Erdelyi, L. S., Soltesz-Katona, E., Balla, T., Varnai, P., & Hunyady, L. (2011). Demonstration of angiotensin II-induced Ras activation in the trans-Golgi network and endoplasmic reticulum using bioluminescence resonance energy transfer-based biosensors. J Biol Chem, 286, 5319-27. **IF: 4,773**

7. **Balla, A.**, Toth, D. J., Soltesz-Katona, E., Szakadati, G., Erdelyi, L. S., Varnai, P., & Hunyady, L. (2012). Mapping of the localization of type 1 angiotensin receptor in membrane microdomains using bioluminescence resonance energy transfer-based sensors. J Biol Chem, 287, 9090-9. **IF: 4,651**

8. Szakadati, G., Toth, A. D., Olah, I, Erdelyi, L. S., Balla, T., Varnai, P., Hunyady, L., & **Balla, A.** (2015). Investigation of the fate of type I angiotensin receptor after biased activation. Mol Pharmacol, 87, 972-81. **IF: 3,931**

9.   Gém, J. B., Kovács, K. B., Szalai, L., Szakadáti, G., Porkoláb, E., Szalai, B., Turu, G., Tóth, A.D., Szekeres, M., Hunyady, L., & **Balla A**. (2021). Characterization of type 1 angiotensin II receptor activation induced dual-specificity MAPK phosphatase gene expression changes in rat vascular smooth muscle cells. Cells 10 : 12 Paper: 3538, 22. **IF: 7,666**

10.   Kovács KB, Szalai L, Szabó P, Gém JB, Barsi S, Szalai B, Perey-Simon B, Turu G, Tóth AD, Várnai P, Hunyady L, & **Balla A.** **(2023)** An Unexpected Enzyme in Vascular Smooth Muscle Cells: Angiotensin II Upregulates Cholesterol-25-Hydroxylase Gene Expression. Int J Mol Sci. 24(4):3968. doi: 10.3390. **IF: 6.208**

b) az értekezéshez kapcsolódó összefoglaló közlemények

11.   **Balla, A.**, & Balla, T. (2006). Phosphatidylinositol 4-kinases: old enzymes with emerging functions. Trends Cell Biol, 16, 351-61. **IF: 12,429**

12.   Toth, A. D., Turu, G., Hunyady, L., & **Balla, A.** (2018). Novel mechanisms of G-protein-coupled receptors functions: AT1 angiotensin receptor acts as a signaling hub and focal point of receptor cross-talk. Best Pract Res Clin Endocrinol Metab, 32, 69-82. **IF: 3,808**

c) az értekezésben nem tárgyalt közlemények

13.   Gehrmann, T., Gulkan, H., Suer, S., Herberg, F. W., **Balla, A.**, Vereb, G., Mayr, G. W., & Heilmeyer, L. M. G. (1999). Functional expression and characterisation of a new human phosphatidylinositol 4-kinase PI4K230. Biochimica Et Biophysica Acta-Molecular and Cell Biology of Lipids, 1437, 341-56. **IF: 2,59**

14.   Pelyvas, I. F., Toth, Z. G., Vereb, G., **Balla, A.**, Kovacs, E., Gorzsas, A., Sztaricskai, F., & Gergely, P. (2001). Synthesis of new cyclitol compounds that influence the activity of phosphatidylinositol 4-kinase isoform, PI4K230. Journal of Medicinal Chemistry, 44, 627-32. **IF: 4,139**

15.   Vereb, G., **Balla, A.**, Gergely, P., Wymann, M. P., Gulkan, H., Suer, S., & Heilmeyer, L. M. G. (2001). The ATP-binding site of brain phosphatidylinositol 4-kinase PI4K230 as revealed by 5 '-p-fluorosulfonylbenzoyladenosine. International Journal of Biochemistry & Cell Biology, 33, 249-59. **IF: 3,258**

16.   Zhao, X., Varnai, P., Tuymetova, G., **Balla, A.,** Toth, Z E ; Oker-Blom, C., Roder, J., Jeromin, A., & Balla, T. (2001). Interaction of neuronal calcium sensor-1 (NCS-1) with phosphatidylinositol 4-kinase beta stimulates lipid kinase activity and affects membrane

trafficking in COS-7 cells. Journal of Biological Chemistry, 276(43): p. 40183-40189. **IF: 7,258**

17.   **Balla, A.,** Toth, B., Timar, G., Bak, J., & Krajcsi, P. (2001) Molecular targets for pharmacological cytoprotection. Biochem Pharmacol, 61(7): p. 769-77. **IF: 3,34**

18.   Bondeva, T., **Balla, A.,** Varnai, P., & Balla, T. (2002). Structural determinants of Ras-Raf interaction analyzed in live cells. Mol Biol Cell, 13, 2323-33. **IF: 7,599**

19.   Denes, L., Jednakovits, A., Hargitai, J., Penzes, Z., **Balla, A.,** Talosi, L., Krajcsi, P., & Csermely, P. (2002) Pharmacologically activated migration of aortic endothelial cells is mediated through p38 SAPK. British Journal of Pharmacology, 136(4): p. 597-603. **IF: 3,45**

20.   Lee, S. B., Varnai, P., **Balla, A.,** Jalink, K., Rhee, S. G., & Balla, T. (2004) The pleckstrin homology domain of phosphoinositide-specific phospholipase C delta(4) is not a critical determinant of the membrane localization of the enzyme. Journal of Biological Chemistry, 279(23): p. 24362-24371. **IF: 6,355**

21.   Lin, X ; Varnai, P ; Csordas, G ; **Balla, A** ; Nagai, T ; Miyawaki, A ; Balla, T ; & Hajnoczky, G. (2005) Control of calcium signal propagation to the mitochondria by inositol 1,4,5-trisphosphate-binding proteins. Journal of Biological Chemistry, 280(13): p. 12820-12832. **IF: 5,854**

22.   Varnai, P ; **Balla, A** ; Hunyady, L ; & Balla, T. (2005) Targeted expression of the inositol 1,4,5-triphosphate receptor (IP3R) ligand-binding domain releases Ca2+ via endogenous IP3R channels. Proc Natl Acad Sci U S A, 102(22): p. 7859-64. IF: 10,231

23.   Kakuk, A., Friedlander, E., Vereb, G., Jr., Kasa, A., **Balla, A.,** Balla, T., Heilmeyer, L. M., Jr., Gergely, P., & Vereb, G. (2006). Nucleolar localization of phosphatidylinositol 4-kinase PI4K230 in various mammalian cells. Cytometry A, 69, 1174-83. **IF: 3,293**

24.   Knight, Z. A., Gonzalez, B., Feldman, M. E., Zunder, E. R., Goldenberg, D. D., Williams, O., Loewith, R., Stokoe, D., **Balla, A.,** Toth, B., Balla, T., Weiss, W. A., Williams, R. L., & Shokat, K. M. (2006). A pharmacological map of the PI3-K family defines a role for p110 alpha in insulin signaling. Cell, 125, 733-47. **IF: 29,194**

25.   Toth, B., **Balla, A.,** Ma, H., Knight, Z. A., Shokat, K. M., & Balla, T. (2006). Phosphatidylinositol 4-kinase IIIbeta regulates the transport of ceramide between the endoplasmic reticulum and Golgi. J Biol Chem, 281, 36369-77. **IF: 5,808**

26.   Knight, Z. A., Feldman, M. E., **Balla, A.,** Balla, T., & Shokat, K. M. (2007). A membrane capture assay for lipid kinase activity. Nat Protoc, 2, 2459-66. **IF: 1,671**

27.   Lukacs, V., Thyagarajan, B., Varnai, P., **Balla, A.,** Balla, T., & Rohacs, T. (2007) Dual regulation of TRPV1 by phosphoinositides. J Neurosci, 27(26): p. 7070-80. **IF: 7,49**

28. Szentpetery, Z., **Balla, A.**, Kim, Y. J., Lemmon, M. A., & Balla, T. (2009). Live cell imaging with protein domains capable of recognizing phosphatidylinositol 4,5-bisphosphate; a comparative study. BMC Cell Biology, 10:67. **IF: 2,654**

29. Szekeres, M., Nadasy, G. L., Turu, G., Soltesz-Katona, E., Toth, Z. E., **Balla, A.**, Catt, K. J., & Hunyady, L. (2012). Angiotensin II Induces Vascular Endocannabinoid Release, Which Attenuates Its Vasoconstrictor Effect via CB1 Cannabinoid Receptors. J Biol Chem, 287, 31540-50. **IF: 4,651**

30. Toth, D. J., Toth, J. T., Gulyas, G., **Balla, A.**, Balla, T., Hunyady, L., & Varnai, P. (2012). Acute depletion of plasma membrane phosphatidylinositol 4,5-bisphosphate impairs specific steps in endocytosis of the G-protein-coupled receptor. J Cell Sci, 125, 2185-97. **IF: 5,877**

31. Erdelyi, L. S., **Balla, A.**, Patocs, A., Toth, M., Varnai, P., & Hunyady, L. (2014) Altered agonist sensitivity of a mutant v2 receptor suggests a novel therapeutic strategy for nephrogenic diabetes insipidus. Mol Endocrinol, 28(5): p. 634-43. **IF: 4,022**

32. Erdélyi, L. S., Mann, W. A., Morris-Rosendahl, D. J., Groß, U., Nagel, M., Várnai, P., **Balla, A.**, & Hunyady, L. (2015) Mutation in the V2 vasopressin receptor gene, AVPR2, causes nephrogenic syndrome of inappropriate diuresis. Kidney Int, 88(5): p. 1070-8. IF: 8,564

33. Tóth, J. T., Gulyás, G., Tóth, D. J., **Balla, A.**, Hammond, G. R.V., Hunyady, L., Balla, T., & Várnai, P. (2016) BRET-monitoring of the dynamic changes of inositol lipid pools in living cells reveals a PKC-dependent PtdIns4P increase upon EGF and M3 receptor activation. Biochim Biophys Acta, 1861(3): p. 177-87. **IF: 5,162**

34. Gulyas, G., Radvanszki, G., Matuska, R., **Balla, A.**, Hunyady, L., Balla, T., & Varnai, P. (2017) Plasma membrane phosphatidylinositol 4-phosphate and 4,5-bisphosphate determine the distribution and function of K-Ras4B but not H-Ras proteins. J Biol Chem, 292(46): p. 18862-18877. **IF: 4,01**

35. Toth, A. D., Prokop, S., Gyombolai, P., Varnai, P., **Balla, A.**, Gurevich, V. V., Hunyady, L., & Turu, G. (2018). Heterologous phosphorylation-induced formation of a stability lock permits regulation of inactive receptors by beta-arrestins. J Biol Chem, 293, 876-92. **IF: 4,106**

36. Turu, G., **Balla, A.**, & Hunyady, L. (2019). The Role of beta-Arrestin Proteins in Organization of Signaling and Regulation of the AT1 Angiotensin Receptor. Front Endocrinol (Lausanne), 10, 519. **IF: 3,644**

37. Turu, G., Soltész-Katona, E., Tóth, A.D., Juhász, C., Cserző, M., Misák, Á., **Balla, A.**, Caron, M.G., Hunyady, L. (2021). Biased Coupling to β-Arrestin of Two Common Variants of the CB2 Cannabinoid Receptor. Front Endocrinol (Lausanne). 12:714561. **IF: 6,055**

38.   Tóth, A.D., Garger, D., Prokop, S., Soltész-Katona, E., Várnai, P., **Balla, A.**, Turu, G., Hunyady, L. (2021). A general method for quantifying ligand binding to unmodified receptors using Gaussia luciferase. J Biol Chem. 296:100366. **IF: 5,485**

39.   Szalai, L., Sziráki, A., Erdélyi, L. S., Kovács, K. B., Tóth, M., Tóth, A. D., Turu, G., Bonnet, D., Mouillac, B., Hunyady, L., & **Balla, A.** (2022). Functional rescue of a nephrogenic diabetes insipidus causing mutation in the V2 vasopressin receptor by specific antagonist and agonist pharmacochaperones. Front. Pharmacol. 13:811836. doi: 10.3389/fphar.2022.811836. **IF: 5,988**

40.   Erdélyi, L. S., Hunyady, L., & **Balla, A.** (2023). V2 vasopressin receptor mutations: future personalized therapy based on individual molecular biology. Front. Endocrinol. 14:1173601. doi.org/10.3389/fendo.2023.1173601. **IF: 6,055**

7. TUDOMÁNYMETRIAI ADATOK ÉS EGYÉB KÖZLEMÉNYEK

Idegen nyelvű közlemények tudománymetriai adatai (2023. 05. 24. MTMT adatok alapján)

Tudományos folyóiratcikkek száma: 40

Összesített impakt faktor: 229

Összes idézettség: 3034

Független idézettség: 2600

Hirsch index: 25

Tudományos közlemények	Száma		Hivatkozások[1]	
	Összesen	Részletezve	Független	Összes
I. Tudományos folyóiratcikk[2]	40			
teljes cikk[2], nemzetközi folyóiratban		39	2597	3029
teljes cikk, hazai idegen nyelvű folyóiratban		0	0	0
teljes cikk, hazai magyar nyelvű folyóiratban		1	0	0
teljes cikk, rövid közlemény		0	0	0
II. Könyvek	0			
a) Szakkönyv, tankönyv, szerzőként	0			
Szakkönyv, kézikönyv idegen nyelvű		0	0	0
Szakkönyv, kézikönyv magyar nyelvű		0	0	0
Felsőoktatási tankönyv		0	0	0
b) Szakkönyv szerkesztőként	0			
Szakkönyv, kézikönyv, idegen nyelvű		0		
Szakkönyv, kézikönyv, magyar nyelvű		0		
Felsőoktatási tankönyv		0		
III. Könyvfejezet, szaktanulmány	1			
Könyvfejezet idegen nyelvű		1	3	4
Könyvfejezet magyar nyelvű		0	0	0
Felsőoktatási tankönyvfejezet		0	0	0
IV. Konferenciaközlemények[3]	1		0	0
Tudományos és oktatási közlemények összesen (I-IV.)	42		2600	3033
V. Egyéb tudományos	1			
Egyéb tudományos művek, ide értve a nem teljes folyóiratcikkeket és a nem ismert lektoráltságú folyóiratokban megjelent teljes folyóiratcikkeket is		0	0	0
Szerkesztőségi levelezés, hozzászólások, válaszok		1	0	1
VI. Absztrakt	1		0	0
Összesített impakt faktor	229,008			
Idézettség száma[1]			2600	3034
Hirsch index[1]	25			

Magyar nyelvű közlemények jegyzéke

1. Balla, András; Erdélyi, László Sándor; Hunyady, László: „G-fehérjéhez kapcsolt receptorok aktivációs modelljeinek elemzése. Magyar Tudomány 173.évf. k.sz. 68-74 (2012)

2. Hunyady, László; Erdélyi, László Sándor; Balla, András: A V2 vazopresszinreceptor betegséget okozó mutációi. Magyar Belorvosi Archivum 69 : 2-3 pp. 69-75. (2016)

Könyvek, könyvfejezetek jegyzéke

1. Genetics of Endocrine Diseases and Syndromes (Springer 2019; Editors: Peter Igaz and Attila Patócs): „Nephrogenic Diabetes Insipidus" c. fejezet

2. Ezerarcú fehérjék (Semmelweis Kiadó és Multimédia Stúdió 2018; Szerkesztők: Buday László, Nyitray László, Perczel András): „G-fehérjéhez kapcsolt receptorok működésének tanulmányozása biolumineszcencia rezonancia energiatranszfer módszerrel" c. fejezet

8. KÖSZÖNETNYILVÁNÍTÁS

9. A DOKTORI ÉRTEKEZÉS ALAPJÁUL SZOLGÁLÓ SAJÁT EREDETI ÉS ÖSSZEFOGLALÓ KÖZLEMÉNYEK

RESEARCH ARTICLE

András Balla · György Vereb · Hülya Gülkan
Thor Gehrmann · Pál Gergely
Ludwig M.G. Heilmeyer Jr · Miklós Antal

Immunohistochemical localisation of two phosphatidylinositol 4-kinase isoforms, PI4K230 and PI4K92, in the central nervous system of rats

Abstract The distribution and cellular localisation of the phosphatidylinositol 4-kinase isoforms, PI4K230 and PI4K92, that are believed to play important roles in the intracellular signalling mechanisms were studied in the rat brain (cortex, cerebellum, hippocampus and spinal cord) using immunocytochemistry with light and electron microscopy. PI4K230 was detected with a specific antibody purified by affinity chromatography from the egg yolk of chicken immunised with a 33-kDa fragment of bovine PI4K230, comprising amino acids 873–1175 of the native protein. PI4K92 was immunostained with a commercially available antibody raised in rabbit against amino acid residues 410–537 of human PI4K92. At the light microscopic level, the immunostaining of PI4K230 and PI4K92 showed a very similar distribution throughout the neurons and appeared as dense punctate labelling in the cytoplasm of perikarya and stem dendrites of various neurons. In addition to neurons, a strongly stained cell population was observed in the molecular layer of the cerebellar cortex that resembled Bergmann glia cells. Electron microscopy of neurons in the ventral horn of the spinal cord showed dense granular immunoprecipitates for both PI4K230 and PI4K92, mostly associated with the outer membrane of mitochondria and membranes of the rough endoplasmic reticulum. In addition, immunostaining of PI4K92 was also frequently found on the outer surface of cisterns and vesicles of Golgi complexes, whereas PI4K230 immunoreactivity was colocalised with some multivesicular bodies. Neither nuclear localisation nor a regular attachment to the cell membrane of these enzymes were observed. Our findings indicate that PI4K230 and PI4K92 are not involved directly in the ligand-stimulated turnover of phosphoinositides at the plasma membrane of neurons. However, they may provide regulatory phosphoinositides for intracellular vesicular traffic being associated with various organelles.

Key words Phosphoinositide signalling ·
Immunocytochemistry · Ultrastructural localisation

A. Balla · G. Vereb (✉) · P. Gergely
Department of Medical Chemistry,
Faculty of Medicine, University of Debrecen,
Bem-tér 18/B, 4026 Debrecen, Hungary
e-mail: vgyorgy@jaguar.dote.hu
Tel.: +36-52-412345, Fax: +36-52-412566

H. Gülkan · T. Gehrmann · L.M.G. Heilmeyer Jr
Institute of Physiological Chemistry, Ruhr University,
Bochum, Germany

M. Antal
Department of Anatomy, Histology and Embryology,
Faculty of Medicine, University of Debrecen, Hungary

Introduction

Polyphosphoinositides play important roles in the intracellular signal transduction in response to a variety of hormones, neurotransmitters and growth factors (Berridge 1984; Divecha and Irvine 1995). In the classic signalling pathway, phosphatidylinositol 4-kinase (PI4K) catalyses the first committed step that leads to the phosphorylation of plasma membrane-bound phosphatidylinositol (PtdIns) at the D4 position of the inositol ring. Phosphatidylinositol 4-phosphate (PtdIns(4)P) can be further phosphorylated by PtdIns 4P 5-kinase to yield PtdIns(4,5)P_2, the precursor of the second messengers inositol(1,4,5)P_3 and diacylglycerol. PtdIns(4)P and PtdIns(4,5)P_2 are also substrates of phosphoinositide 3-kinase, giving rise to a wide variety of lipid messengers (for review see Carpenter and Cantley 1996). Polyphosphoinositides are formed not only in the plasma membranes but also in the cell nucleus (Boronenkov et al. 1998; D'Santos et al. 1998) and intracellular membranes like the sarcoplasmic reticulum, endoplasmic reticulum, Golgi complexes, lysosomal membranes and secretory vesicles (for review see Gehrman and Heilmeyer 1998). Some of them, like PtdIns(4,5)P_2 regulate the actin-modifying effect of various actin-binding proteins, thereby modulating structural changes in the actin cytoskeleton (Hinchliffe et al. 1998; Toker 1998). Phosphoinositides are also involved in the control of intracellular vesicular traffic (Schu et al. 1993; De Camilli et al. 1996; Martin 1997; Odorizzi et al. 1998).

280

Since the precursor for the most polyphosphoinositides is PtdIns(4)P (Martin 1998), PI4K is essential for these processes.

Many phosphatidylinositol kinases have been purified, characterised and cloned (Gehrmann and Heilmeyer 1998; Rao et al. 1998). PI4Ks with known amino acid sequences belong to two subfamilies, best represented by PI4K92 and PI4K230. A third form, PI4K55, has not yet been cloned. PI4K55 is associated with plasma membranes of several cells (for review see Gehrmann and Heilmeyer 1998), liver microsomes (Olsson et al. 1995), chromaffin granules (Husebye et al. 1990; Wiedemann et al. 1996) and lysosomes (Arneson et al. 1999). Soluble PI4K92 and PI4K230 were detected in the adrenal cortex (Downing et al. 1996). Most membrane-associated PI4Ks have not been differentiated on a molecular basis till now. In transfected cells, antibodies detected overexpressed PI4K92 and PI4K230 associated with the Golgi apparatus and/or endoplasmic reticulum (Nakagawa et al. 1996a,b; Wong et al. 1997).

The high level of mRNA for PI4K92 (Nakagawa et al. 1996b; Balla et al. 1997) and PI4K230 (Nakagawa et al. 1996a; Balla et al. 1997; Gehrmann et al. 1999) in the brain is in accordance with earlier observations that indicate the preferential occurrence of these enzymes in nervous tissue (Carpenter and Cantley 1990). More recent findings suggest that PI4Ks are involved in neuron-specific functions such as neurotransmitter release (Wiedemann et al. 1996, 1998; Khvotchev and Sudhof 1998) and endocytosis of some acetylcholine receptors (Sorensen et al. 1998). Additionally, PI4Ks take part in the regulation of ion channels (Zeng et al. 1994; Baukrowitz et al. 1998; Shyng and Nichols 1998; Kim and Bang 1999; Zhainazarov and Ache 1999). While PI4Ks have been isolated predominantly from the brain, their intracellular localisation and function in nerve cells are still unknown. In the present paper we provide data on the cellular and subcellular localisation of endogenous native lipid kinases, PI4K92 and PI4K230, in the central nervous system of rats.

Materials and methods

Materials

Anti-rabbit immunoglobulin peroxidase conjugate, anti-chicken immunoglobulin peroxidase conjugate and Tween 20 were from Sigma, Phenyl-Sepharose from Pharmacia and biotinylated anti-rabbit immunoglobulin, biotinylated anti-chicken immunoglobulin, normal goat serum and avidin-biotinylated horseradish peroxidase complex (ABC) system were from Vector Laboratories. Polyclonal antibodies against PI4K92 raised in rabbit against the polypeptide comprising amino acids 410–537 of PI4K92 (Meyers and Cantley 1997) were from Upstate Biotechnology (anti-PtdIns 4-K 110β). Enhanced chemiluminescence (ECL) reagents were from Amersham and Pierce. All other chemicals used were obtained from Sigma or Reanal (Budapest).

Preparation of antibodies against PI4K230

Monospecific antibodies to the N-terminal part of bovine PI4K230 comprising amino acids 873–1175 (Balla et al. 1997) were prepared and affinity purified from chicken egg yolk as described by Gehrmann et al. (1999). Protein concentration of the purified preparation was 50 μg/ml. For control experiments, chicken IgY was purified from egg yolk of non-immunised chickens on Phenyl-Sepharose according to Hassl and Aspöck (1988), obtaining a protein concentration of 6.4 mg/ml. Treatment of the experimental animals was carried out according to established protocols consistent with the "Principles of Laboratory Animal Care" (NIH publication number 86–23, revised 1985) and following the recommendations of the Hungarian Law on Animal Protection.

Sodium dodecyl sulphate-polyacrylamide gel electrophoresis (SDS-PAGE) and western blotting

SDS-PAGE was performed according to Laemmli (1970) using a mini-slab gel apparatus (Bio-Rad). The separated proteins were then electrophoretically transferred onto a polyvinylidene fluoride (PVDF) membrane (Immobilon-P; Millipore). After electrotransfer, the unspecific binding sites of the PVDF membrane were blocked with 5% (w/v) skimmed milk in 10 mM potassium phosphate, 120 mM NaCl, 2.7 mM KCl, pH 7.4 (phosphate-buffered saline) containing 0.1% (v/v) Tween 20 for 1 h at room temperature. The PVDF membranes were incubated with the primary antibody either at 4°C overnight or at room temperature for 1 h and then with secondary antibody at room temperature for 1 h. Usually, the secondary antibodies were labelled with peroxidase. ABC system was used when the secondary antibodies were labelled with biotin. Immuno-reactive proteins were detected using an ECL kit and recorded using Fuji medical X-ray or ECL Hyperfilm (Amersham).
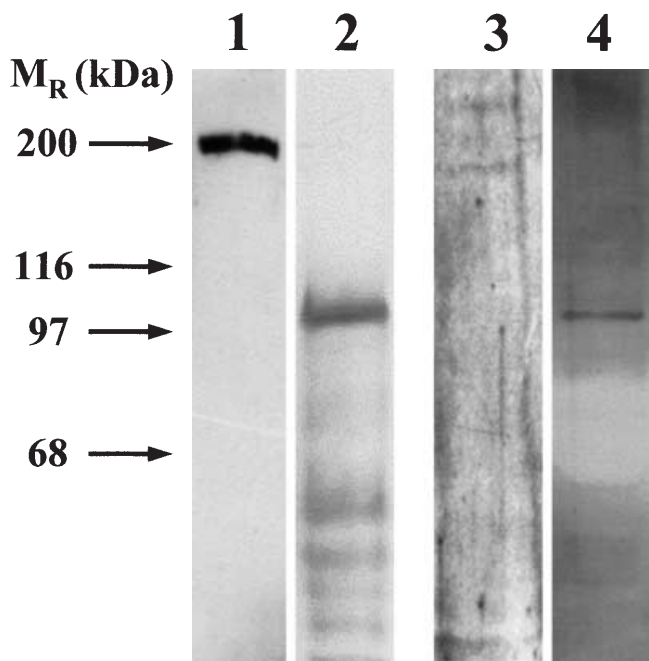
Fig. 1 Isoenzyme specificity of antibodies and detection of phosphatidylinositol 4-kinase isoforms, PI4K230 and PI4K92, in bovine brain preparation and rat brain homogenate using immunoblots. Samples from bovine brain preparation were separated by sodium dodecyl sulphate-polyacrylamide gel electrophoresis and immunoblotted with anti-PI4K230 (*lane 1*) or anti-PI4K92 (*lane 2*). Rat brain homogenates were immunoblotted also with either anti-PI4K230 (*lane 3*) or anti-PI4K92 (*lane 4*). *Arrows* represent the molecular mass standard
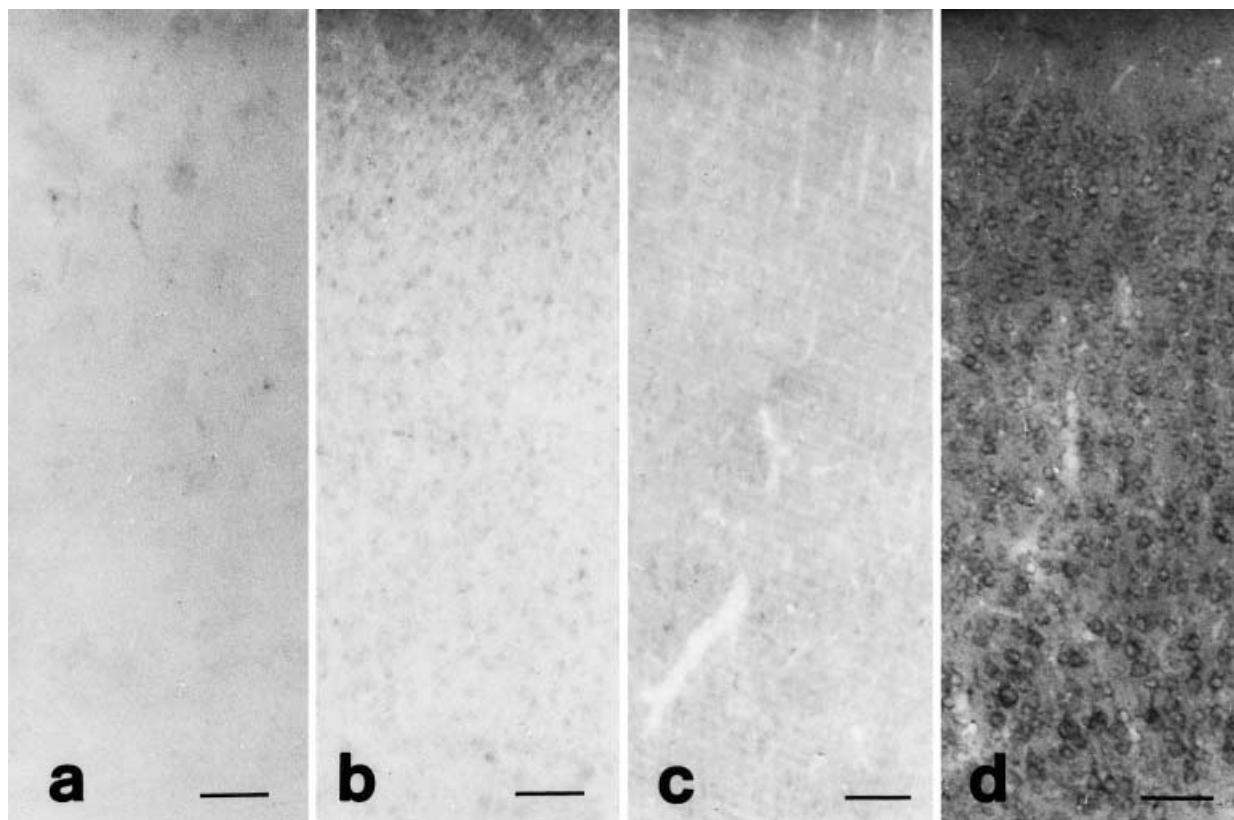
Fig. 2a–d Specificity of immunohistochemical detection of PI4K230. Photomicrographs from sections of the cerebral cortex of rats: **a** The primary antibodies were replaced with normal goat serum. **b** The primary antibodies were replaced with non-specific chicken IgY. **c** The primary antibodies against PI4K230 were adsorbed by PI4K230 preparation. **d** Section treated with anti-PI4K230 as the primary antibody. *Bars* 50 μm

immunoreactive band of about 100 kDa. The 190-kDa band could be the result of a splice alternative or of proteolysis. A PI4K species with similar molecular weight was stained with the anti-PI4K230 in extracts of CHO cells as well (Wong et al. 1997). The biotin-labelled secondary antibodies and the ABC system used in immunocytochemistry were also tested and yielded western blots identical to those presented (data not shown).

Purification of PI4K230 from bovine brain

PI4K230 was prepared from the grey matter of bovine brain as described previously (Gehrmann et al. 1996). The solubilised membrane fraction after the first hydroxylapatite chromatography was used for western blot analysis and a highly purified preparation (3000 U/mg protein) was used for adsorbing the specific antibodies against PI4K230 in control immunostainings. Protein concentration was determined according to Bradford (1976) with bovine serum albumin as a standard.

Specificity of the detection of PI4K92 and PI4K230
with antibodies using immunoblots

Since the different PI4Ks have partially similar sequences (Gehrmann and Heilmeyer 1998), it is important to verify that the antibodies against the PI4K230 and PI4K92 react only with the appropriate enzyme species without any crossreaction. The specificity of anti-PI4K230 and anti-PI4K92 was tested by western blotting either a solubilised bovine brain preparation enriched in PI4K230 and PI4K92 or rat brain homogenate. Western blot analysis of solubilised bovine brain preparation showed a single band of ca 200 kDa with the anti-PI4K230 corresponding to the purified PI4K230 (Fig. 1 *lane 1*), while anti-PI4K92 reacted specifically with a ca 100-kDa protein (Fig. 1 *lane 2*). We also tested the specificity of anti-PI4K230 and anti-PI4K92 western blotting rat brain homogenate. The anti-PI4K230 (Fig. 1 *lane 3*) revealed two faintly stained bands (190 kDa and 230 kDa), while the anti-PI4K92 (Fig. 1 *lane 4*) reacted with a single

Immunocytochemistry

Wistar rats were deeply anaesthetised with chloral hydrate (35 mg/kg i.p.) and perfused through the heart first with Tyrode's solution, followed by a fixative containing 4% paraformaldehyde or 4% paraformaldehyde and 0.1% glutaraldehyde in 0.1 M phosphate buffer pH 7.4 (PB). At higher concentrations of glutaraldehyde the immunoreactivity was lost. The brain and the spinal cord were removed and fixed in the same fixative for 1–3 h. Blocks of the cerebral cortex, hippocampus, cerebellum and the lumbar segments of the spinal cord were dissected and immersed sequentially into 10 and 20% sucrose dissolved in 0.1 M PB until they sank. Tissue blocks were frozen in liquid nitrogen and sectioned at 60 μm on a vibratome. Following extensive washes in 0.1 M PB, the free-floating sections were first incubated with the antibody against PI4K230 (dilution 1:100 or 1:200) or PI4K92 (dilution 1:100 or 1:200) for 2 days. After several washes they were transferred into biotinylated goat anti-chicken (1:200) or biotinylated goat anti-rabbit immunoglobulin (1:200) solution for 5–6 h. Thereafter, they were treated with a solution of ABC (1:100), and the immunoreaction was completed with a diaminobenzidine (Sigma) chromogen reaction. All incubation steps were performed under continuous gentle agitation and in the presence of normal goat serum (dilution 1:100) in 50 mM TRIS-HCl, 150 mM NaCl, pH 7.4. Immunostained sections were mounted on chrome alum–gelatine-coated slides, air dried, dehydrated in ethanol, cleared in xylene and mounted with DePex neutral medium.

For electron microscopy, sections were treated with 1% OsO_4 for 45 min after the chromogen reaction, dehydrated and embed-

282

ded into Durcupan ACM resin (Fluka). Ultrathin sections were collected onto Formvar-coated grids and counterstained with lead citrate and examined with a Jeol 1010 electron microscope.

Specificity of the immunohistochemical detection of PI4K230

Consecutive sections of the cerebral cortex were treated as described above with the following modifications: in negative controls the primary antibodies were replaced with normal goat serum (dilution 1:100; Fig. 2a), with non-specific chicken IgY purified from egg yolk on Phenyl-Sepharose (dilution 1:10; Fig. 2b) or with specific antibodies adsorbed with highly purified bovine brain PI4K230 preparation (1 µg enzyme protein per ml antibody preparation diluted to 1:100; Fig. 2c). Under these conditions, no specific peroxidase reaction was observed. In the positive control (Fig. 2d), the use of specific antisera against PI4K230 (dilution 1:200) yielded a clearly distinguishable immunostaining.

Results

Distribution of PI4K230 immunoreactivity in the rat brain

In the cerebellum, the most prominent immunostaining was observed in the molecular layer of the cerebellar cortex (Fig. 3a). The intense staining was mainly due to a large number of immunoreactive filaments that were oriented perpendicular to the outer surface and traversed

Fig. 3a–c PI4K230-immunoreactive structures in the cerebellum of rats. Photomicrographs from rat cerebellum show: (**a**) strong immunoreactivity in the molecular layer of the cerebellar cortex, (**b**) immunoreactive neurons in a cerebellar nucleus and (**c**) immunoreactive cell bodies and processes in the molecular layer of the cerebellar cortex. *Pc* layer of Purkinje cells, *Mol* molecular layer, *Gran* granular layer. *Bars* 50 µm (**a**); 10 µm (**b,c**)

the entire thickness of the molecular layer (Fig. 3c). The immunostained filaments showed a triangular enlargement at their inner end at or just above the level of the Purkinje cells. In some cases, the triangular enlargement was completed into a circular ring that surrounded an unstained central spheroid area that made the immunoreactive structure similar to the cell body and process of Bergmann glia cells (Fig. 3a). In addition to the strong immunoreactivity of the molecular layer, some neurons in the cerebellar nuclei showed a punctate labelling in their cytoplasm (Fig. 3b). No further analysis of the cerebellar nuclei has been performed.

A large number of immunoreactive neurons were revealed in all layers of the cerebral cortex (Fig. 4a). The immunoreactivity appeared as a dense granular staining in the cytoplasm of the soma and stem dendrites (Fig. 4c,d,g).

Principal cells were heavily stained in the hippocampus (Fig. 4b). Similar to the cerebral cortex, the labelling appeared as a granular staining and was confined to the cytoplasm of somata and stem dendrites of the pyramidal cells. Neurons in the stratum oriens, stratum radiatum and lacunosum-moleculare were stained only occasionally.

At the level of the lumbar spinal cord, immunoreactive neurons with cytoplasmic granular staining were revealed both in the dorsal and ventral horns. In addition to neurons in lamina VII (Fig. 4f), some motoneurons were also labelled in the lateral motor column (Fig. 4e).

To associate the granular staining with specific cytoplasmic organelles, an ultrastructural study has been done on immunostained neurons in the ventral horn of the spinal cord. Most of the electron-dense immunoprecipitates with diameters varying in the range of
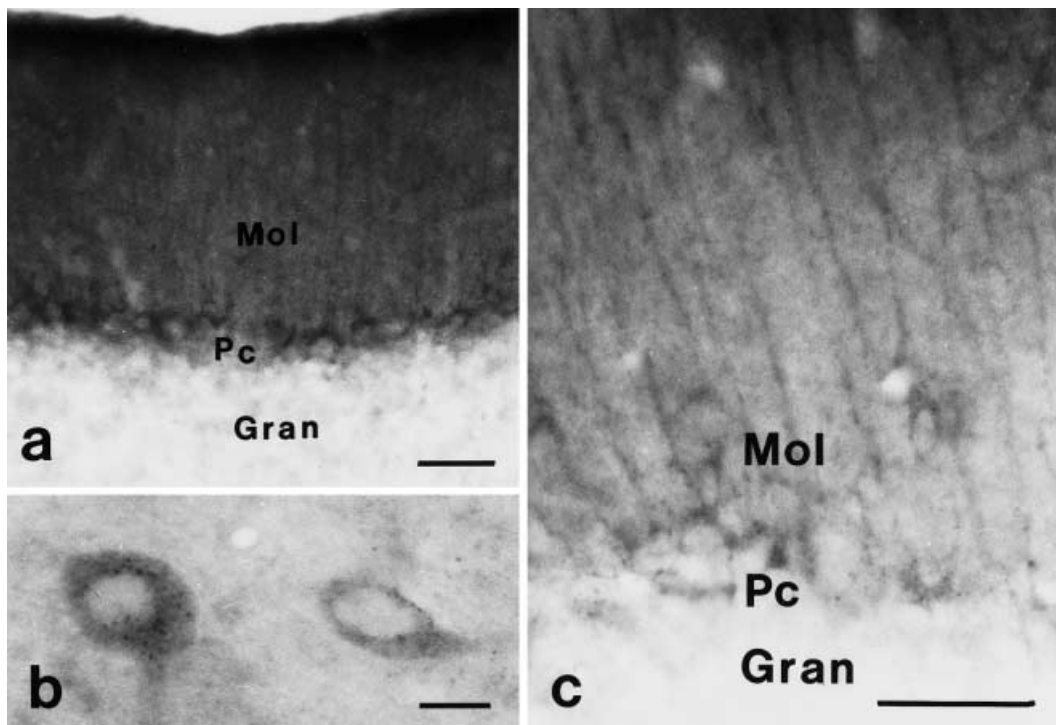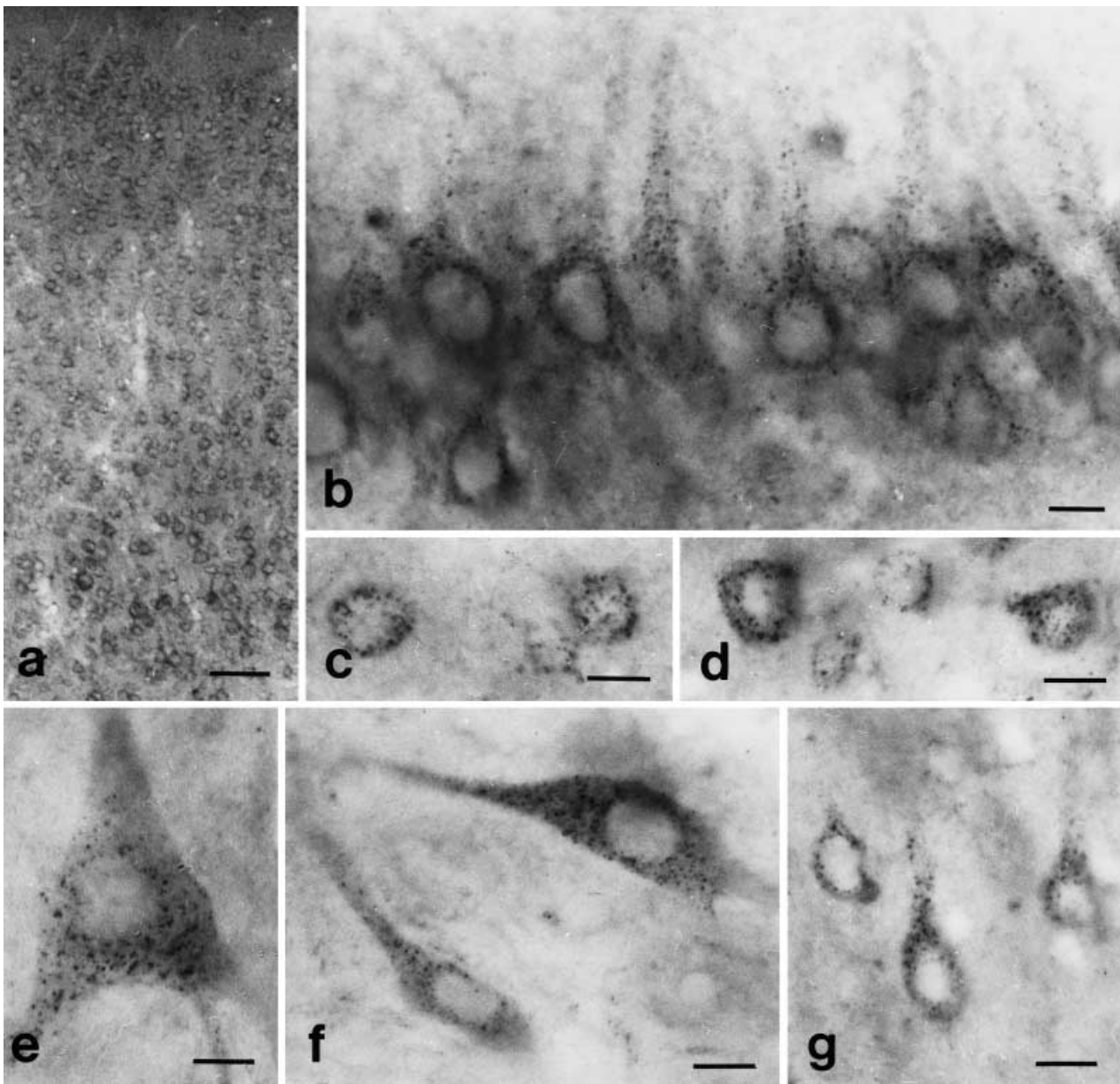
Fig. 4a–g Light microscopy of PI4K230-immunoreactive neurons in the brain and spinal cord of rats. **a** Cerebral cortex. **b** Stratum pyramidale of the hippocampus. **c,d** Layer IV of the cerebral cortex. **e** Lateral motor column of the spinal cord. **f** Lamina VII of the spinal grey matter. **g** Lamina III of the cerebral cortex. *Bars* 50 μm (**a**); 10 μm (**b–g**)

300–400 nm were scattered close to the cisterns of the rough endoplasmic reticulum (Fig. 5b,c) and/or covering the outer membrane of mitochondria (Fig. 5c). Some of them were associated with multivesicular bodies (Fig. 5d) or infrequently attached to the cell membrane in the vicinity of synaptic specialisations (Fig. 5a).

Distribution of PI4K92 immunoreactivity

To compare the distribution and appearance of PI4K230 with those of PI4K92, identical parts of the brain were immunostained under identical conditions. At the light microscopic level, the distribution of immunoreactivity for PI4K92 (Fig. 6b,d,f) was similar to that obtained for PI4K230 (Fig. 6a,c,e). The intensity of the staining, however, showed marked differences at certain locations. For instance, the immunostaining in the molecular layer of the cerebellar cortex was far more intense for PI4K92 (Fig. 6b) than for PI4K230 (Fig. 6a). In contrast to this, the density of immunostaining for PI4K230 in neurons within the cerebral cortex and spinal cord surpassed that obtained for PI4K92 (Fig. 6c–f). In addition, the granular immunoprecipitates were smaller in neurons stained for PI4K92 than in neurons stained for PI4K230 (Fig. 6c–f).

284

Fig. 5a–d Electron micrographs of PI4K230-immunoreactive granules in the cytoplasm of neurons in the ventral horn of the spinal cord of rats. The immunoprecipitates: (**a**) are attached to the cell membrane in close vicinity of a synaptic specialisation, (**b**) are located close to the cisterns of the rough endoplasmic reticulum, (**c**) are attached to the outer membrane of a mitochondrion and (**d**) cover a multivesicular body. *White asterisks* label the immunoprecipitates that represent areas immunoreactive for PI4K230. *Black asterisks* label non-immunoreactive axon terminals. *Arrows* on **a** and **c** point to synaptic contacts. *Arrowheads* on **a** point to the plasma membrane. *G* Golgi apparatus, *RER* rough endoplasmic reticulum, *m* mitochondrion, *mvb* multivesicular body. *Bars* 0.5 μm
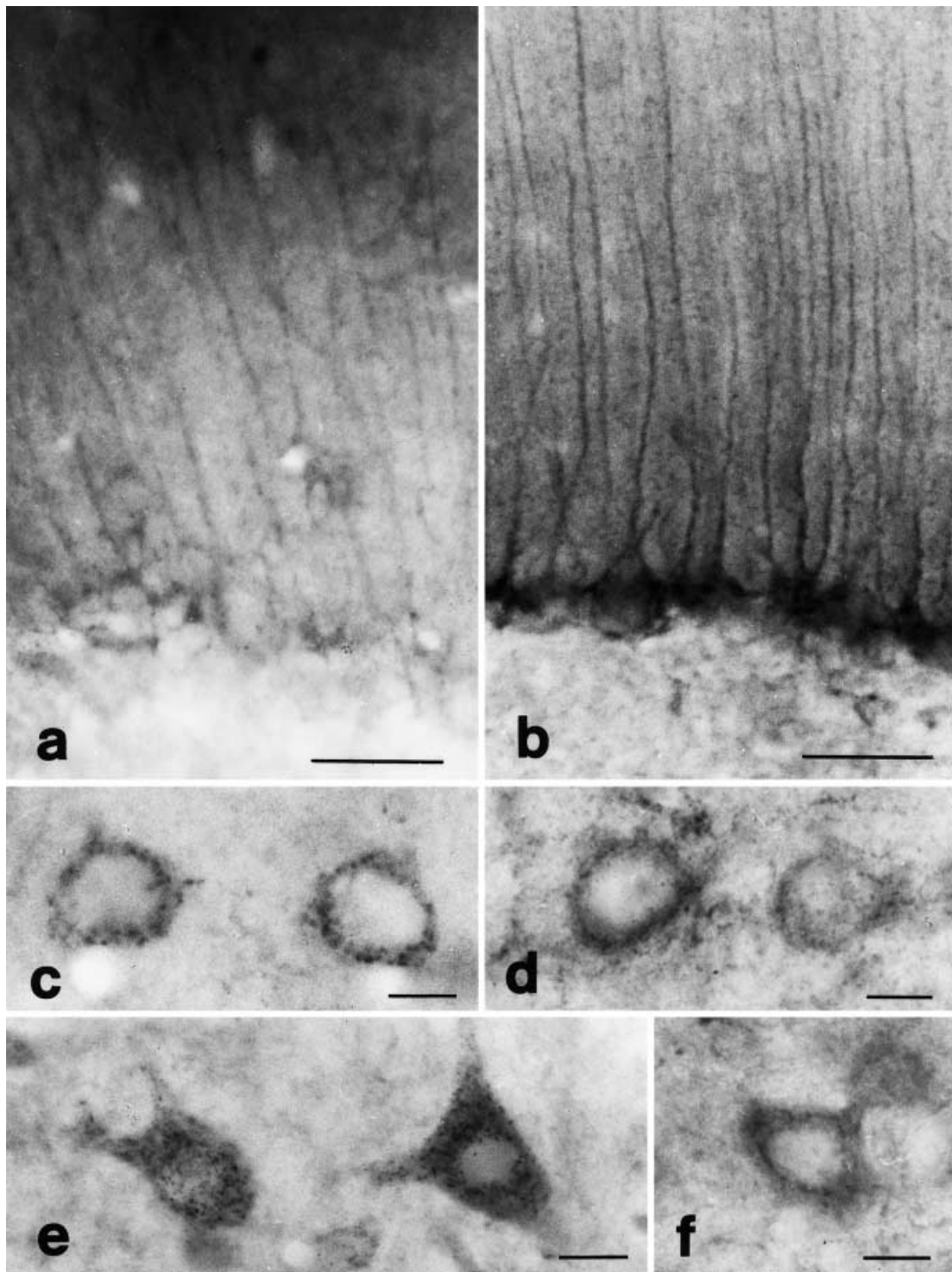
Fig. 6a–f Immunolocalisation of PI4K92 in comparison with that of PI4K230. Micrographs show cells immunostained for PI4K92 (**b,d,f**) and PI4K230 (**a,c,e**). Immunoreactive cells are: (**a,b**) in the molecular layer of the cerebellar cortex, (**c,d**) in layer IV of the cerebral cortex and (**e,f**) in lamina VII of the spinal cord. *Bars* 50 µm (**a,b**); 10 µm (**c–f**)

This difference in the size of granules was also observed in electron microscopic studies (see below).

Electron microscopy of the neurons immunostained for PI4K92 in the ventral horn of the spinal cord showed that the electron-dense immunoprecipitates covered areas in the cytoplasm that were not larger than 100–200 nm in diameter (Fig. 7). Most of these small granules were attached to the outer membrane of mitochondria (Fig. 7b) or to the membranes of the rough en-

286

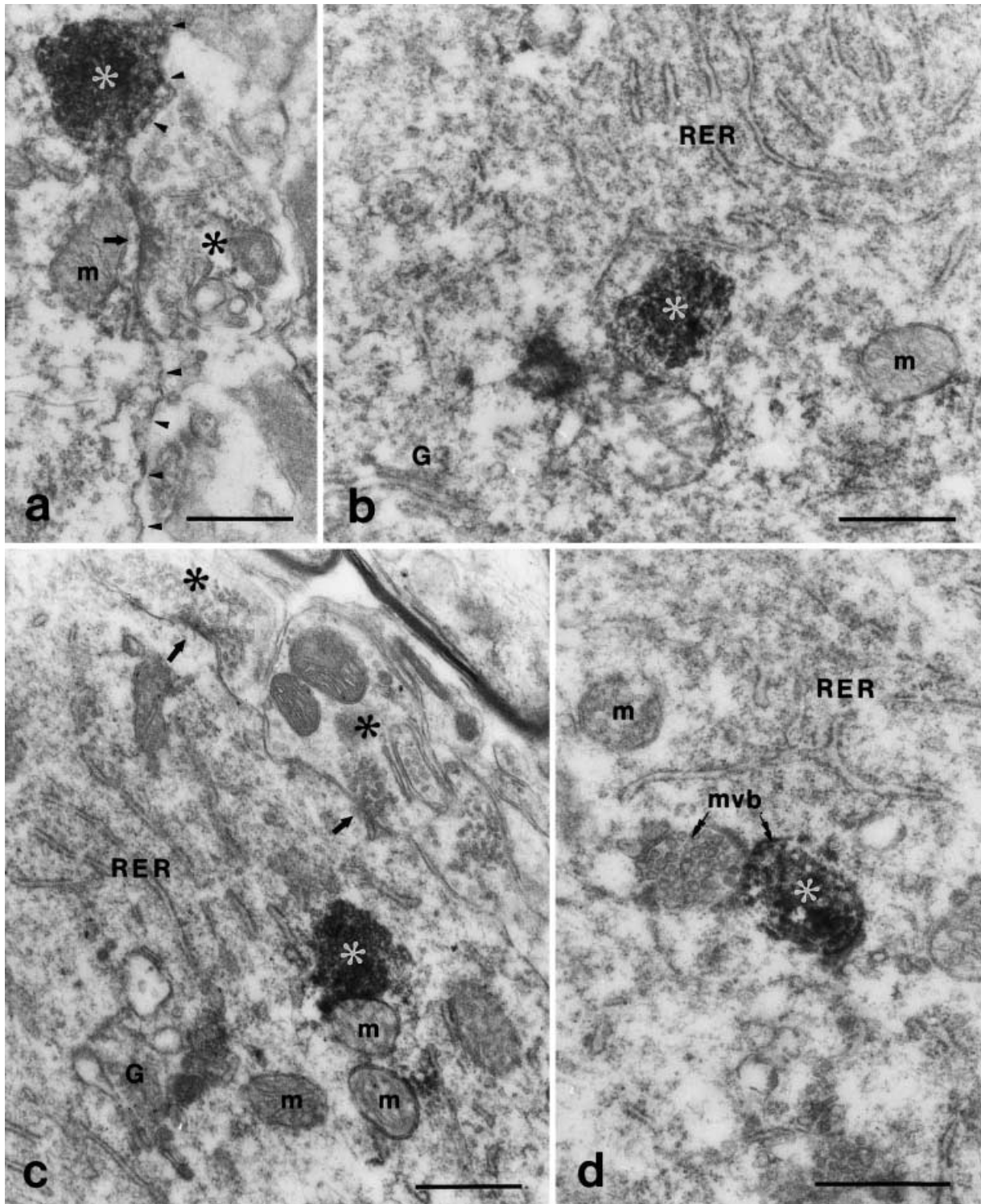**Fig. 7a–c** Electron micrographs of PI4K92-immunoreactive granules in the cytoplasm of interneurons in the ventral horn of the spinal cord of rats. The immunoprecipitates are attached to: (**a**) the outer surface of cisterns and vesicles of Golgi complexes, (**b**) outer cell membrane of a mitochondrion and (**c**) membranes of rough-surfaced endoplasmic reticulum and cytoplasmic surface of the nuclear envelope. *RER* rough-surfaced endoplasmic reticulum, *m* mitochondrion, *nucl* nucleus. *Bars* 0.5 μm
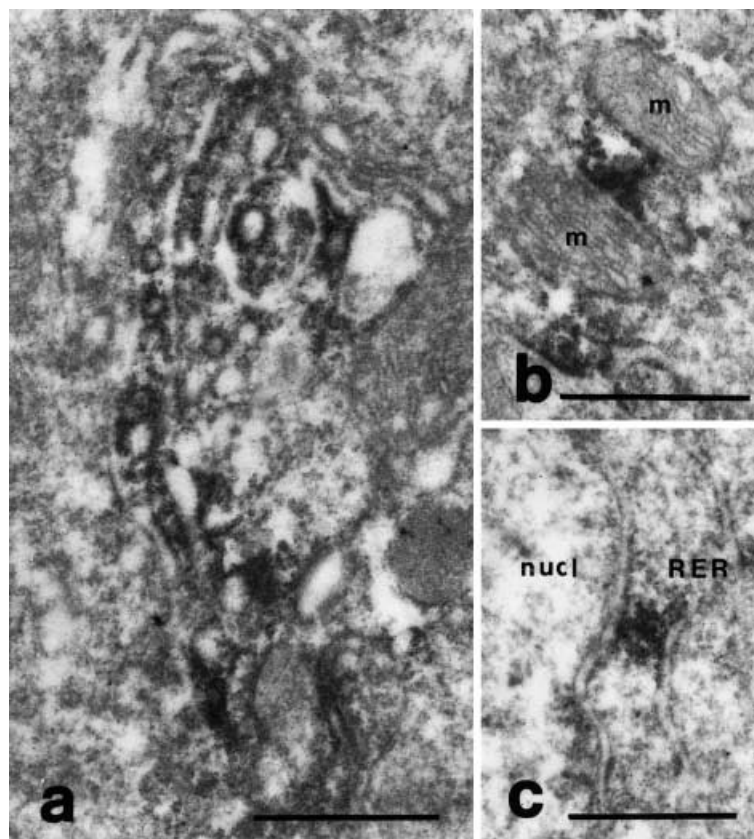
doplasmic reticulum (Fig. 7c). They were also frequently seen on the outer surface of cisterns and vesicles of Golgi complexes (Fig. 7a). Immunoprecipitates were occasionally also attached to the cytoplasmic surface of the nuclear envelope (Fig. 7c).

Discussion

It is well established that PI4K is involved in the production of the plasma membrane-bound PtdIns(4,5)P_2. The regulated hydrolysis of PtdIns(4,5)P_2 in response to extracellular signals provides the second messengers inositol(1,4,5)P_3 and diacylglycerol. A variety of studies (for review see Gehrmann and Heilmeyer 1998) lead to the hypothesis that plasma membranes contain PI4K55, the PI4K species responsible for agonist-stimulated PtdIns(4)P formation in these membranes. The localisation studies reported here are consistent with this suggestion. Our results show that both PI4K92 and PI4K230 are present in various neurons of the central nervous system, including the cerebellum, cerebral cortex, hippocampus and the spinal cord. Cell types stained for one isoform are usually also positive for the other. However, both isoforms appear solely in the cytoplasm of neurons, indicating that neither PI4K92 nor PI4K230 are involved directly in the ligand-stimulated turnover of phosphoinositides at the plasma membrane.

The absence of immunostaining for PI4K230 in the nucleus (at least at the level of sensitivity of our methods) is somewhat surprising since PI4K230 contains nuclear localisation signals (NLS; Gehrmann et al. 1996, 1999). However, recent results indicate that phosphorylation of the NLS itself or other areas of the transported protein causing its export from the nucleus (Hopper 1999) often regulate the NLS-dependent nuclear transport. Other proteins located in the cytosol are imported into the nucleus after dephosphorylation (Heist et al. 1998). One NLS of PI4K230 contains a putative phosphorylation site (T1417) for protein kinase C (PKC) and this NLS is flanked by putative phosphorylation sites for PKC (S1414), and cAMP- or cGMP-dependent protein kinases (T1432) (Gehrmann et al. 1999) making plausible its regulation by phosphorylation. In addition, some proteins with NLS show reduced or no nuclear occurrence in non-mitotic cells (Carlock et al. 1996) and in myoblasts following the differentiation into myotubes (Brown et al. 1999). Moreover, there are proteins with NLS sequence that are exclusively located in the cytoplasm (Tolerico et al. 1999). Even the cytoplasmic function of some proteins with NLS was described, for example, the regulation of the association of importin alpha with microtubules and microfilaments (Smith and Raikhel 1998) or binding to RNA (Eister et al. 1997).

The subcellular localisation of PI4K92 and PI4K230 is in accordance with the concept that phosphoinositides are involved in the regulation of the intracellular mem-

brane traffic. A growing amount of evidence indicates that, in addition to the protein machinery organising and controlling the intracellular vesicular transport via clathrin-coat, COP-coatomers and SNARE proteins (Rothman 1994; Schekman and Orci 1996), phosphoinositides also play key roles in various aspects of vesicle formation, exocytosis and endocytosis (De Camilli et al. 1996). The regulation of ARF cycling, phospholipase-D and dynamin by PtdIns(4,5)P_2 observed during vesicle formation requires spatially localised synthesis of phosphoinositides (Martin 1997). The association of PI4K with subcellular particles can provide for such focal synthesis of phosphoinositides. Indeed, endogenous or overexpressed PI4K92 was localised at the Golgi region in several cell lines (Nakagawa et al. 1996b; Wong et al. 1997). However, the subcellular localisation of overexpressed PI4K230 remained unclear. In COS-7 cells this enzyme has been found at the cytoplasmic surface of the membranes of Golgi vesicles (Nakagawa et al. 1996a), whereas a cloned variant of PI4K230, PI4K97 (Wong and Cantley 1994), was colocalised with the endoplasmic reticulum in HeLa cells (Wong et al. 1997). Our results (Figs. 5, 7) clearly show that in the native neural cells both PI4K230 and PI4K92 are generally associated with the endoplasmic reticulum and the outer membrane of some mitochondria, while only PI4K92 is associated with the Golgi membranes. The enrichment of PI4K92 in the perinuclear region and, moreover, its association with the outer surface of vesicles attached to the nuclear envelope, ergastoplasmic membranes and Golgi apparatus may indicate a possible involvement in the transfer of newly synthesised membranes and/or proteins. The appearance of PI4K230 close to the synaptic membranes and its association with some multivesicular bodies suggests a possible involvement in retrograde transport processes (Schmid and Ambron 1997), endocytosis, receptor recycling (Felder et al. 1990) and in the multivesicular body sorting pathway (Odorizzi et al. 1998). Our present findings, showing dense patches of immunoreactivity at the outer membrane of mitochondria and the immunostained cerebellar filaments suggest further functions of PI4K230 and PI4K92, as well.

Several observations suggest that the participation of PI4K isoforms in the vesicular transport, exocytosis and endocytosis of neural cells may be very complex. Experimental data show the involvement of PI4K92 in the endocytosis of muscarinic cholinergic receptors in the brain (Sorensen et al. 1998). PI4K55 seems also to be involved in the vesicular traffic playing a role in the fusion of chromaffin granules with the cell membrane (Wiedemann et al. 1996). The glutamate release from isolated small synaptic vesicles (Wiedemann et al. 1998) is also associated with the function of PI4K, although its type has not been identified.

Our results show that PI4K92 and PI4K230 are associated selectively with membranes of distinct subcellular organelles. This finding suggests that the investigated two isoforms of PI4K may be involved differently in the localised synthesis of regulatory phosphoinositides. A spatially and temporally transient appearance of PI4Ks might explain that only a part of the neurons or subcellular particles show positive staining at the same time. Consistent with this hypothesis, a higher expression level of PI4Ks was observed in the brain of embryonal rats than in adults (Nakagawa et al. 1996a,b).

References

Arneson LS, Kunz J, Anderson RA, Traub LM (1999) Coupled inositide phosphorylation and phospholipase D activation initiates clathrin-coat assembly on lysosomes. J Biol Chem 274: 17794–17805

Balla T, Downing GJ, Jaffe H, Kim S, Zolyomi A, Catt KJ (1997) Isolation and molecular cloning of wortmannin-sensitive bovine type III phosphatidylinositol 4-kinases. J Biol Chem 272: 18358–18366

Baukrowitz T, Schulte U, Oliver D, Herlitze S, Krauter T Tucker SJ, Ruppersberg JP, Fakler B (1998) PIP2 and PIP as determinants for ATP inhibition of KATP channels. Science 282: 1141–1144

Berridge MJ (1984) Inositol trisphosphate and diacylglycerol as second messengers. Biochem J 220:345–360

Boronenkov IV, Loijens JC, Umeda M, Anderson RA (1998) Phosphoinositide signaling pathways in nuclei are associated with nuclear speckles containing pre-mRNA processing factors. Mol Biol Cell 9:3547–3560

Bradford MM (1976) A rapid and sensitive method for the quantitation of microgram quantities of protein utilizing the principle of protein-dye binding. Anal Biochem 72:248–254

Brown S, McGrath MJ, Ooms LM, Gurung R, Maimone MM, Mitchell CA (1999) Characterization of two isoforms of the skeletal muscle LIM protein 1, SLIM1. Localization of SLIM1 at focal adhesions and the isoform slimmer in the nucleus of myoblasts and cytoplasm of myotubes suggests distinct roles in the cytoskeleton and in nuclear–cytoplasmic communication. J Biol Chem 274:27083–27091

Carlock L, Vo T, Lorincz M, Walker PD, Bessert D, Wisniewski D, Dunbar JC (1996) Variable subcellular localization of a neuron-specific protein during Ntera 2 differentiation into post-mitotic human neurons. Brain Res Mol Brain Res 42:202–212

Carpenter CL, Cantley LC (1990) Phosphoinositide kinases. Biochemistry 29:11147–11156

Carpenter CL, Cantley LC (1996) Phosphoinositide kinases. Curr Opin Cell Biol 8:153–158

De Camilli P, Emr SD, McPherson PS, Novick P (1996) Phosphoinositides as regulators in membrane traffic. Science 271: 1533–1539

Divecha N, Irvine RF (1995) Phospholipid signaling. Cell 80: 269–278

Downing GJ, Kim S, Nakanishi S, Catt KJ, Balla T (1996) Characterization of a soluble adrenal phosphatidylinositol 4-kinase reveals wortmannin sensitivity of type III phosphatidylinositol kinases. Biochemistry 35:3587–3594

D'Santos CS, Clarke JH, Divecha N (1998) Phospholipid signalling in the nucleus. Een DAG uit het leven van de inositide signalering in de nucleus. Biochim Biophys Acta 1436:201–232

288

Eister C, Larsen K, Gagnon J, Ruigrok RW, Baudin F (1997) Influenza virus M1 protein binds through its nuclear localization signal. J Gen Virol 78: 1589–1596

Felder S, Miller K, Moehren G, Ullrich A, Schlessinger J, Hopkins CR (1990) Kinase activity controls the sorting of the epidermal growth factor receptor within the multivesicular body. Cell 61:623–634

Gehrmann T, Heilmeyer LMG Jr (1998) Phosphatidylinositol 4-kinases. Eur J Biochem 253:357–370

Gehrmann T, Vereb G, Schmidt M, Klix D, Meyer H, Varsanyi M, Heilmeyer LMG Jr (1996) Identification of a 200 kDa polypeptide as type 3 phosphatidylinositol 4-kinase from bovine brain by partial protein and cDNA sequencing. Biochim Biophys Acta 1311:53–63

Gehrmann T, Gülkan H, Suer S, Herberg FW, Balla A, Vereb G, Mayr GW, Heilmeyer LMG Jr (1999) Functional expression and characterisation of a new human phosphatidylinositol 4-kinase PI4K230. Biochim Biophys Acta 1437:341–356

Hassl A, Aspöck H (1988) Purification of egg yolk immunoglobulins. A two-step procedure using hydrophobic interaction chromatography and gel filtration. J Immunol Methods 110: 225–228

Heist EK, Srinivasan M, Schulman H (1998) Phosphorylation at the nuclear localization signal of Ca^{2+}/calmodulin-dependent protein kinase II blocks its nuclear targeting. J Biol Chem 273: 19763–19771

Hinchliffe KA, Ciruela A, Irvine RF (1998) PIPkins, their substrates and their products: new functions for old enzymes. Biochim Biophys Acta 1436:87–104

Hopper AK (1999) Inside out regulation. Curr Biol 9:803–806

Husebye ES, Letcher AJ, Lander DJ, Flatmark T (1990) Purification and kinetic properties of a membrane-bound phosphatidylinositol kinase of the bovine adrenal medulla. Biochim Biophys Acta 1042:330–337

Khvotchev M, Sudhof TC (1998) Newly synthesized phosphatidylinositol phosphates are required for synaptic norepinephrine but not glutamate or gamma-aminobutyric acid (GABA) release. J Biol Chem 273:21451–21454

Kim D, Bang H (1999) Modulation of rat atrial G protein coupled K$^+$-channel function by phospholipids. J Physiol (Lond) 517: 59–74

Laemmli UK (1970) Cleavage of structural proteins during the assembly of the head of bacteriophage T4. Nature 227:680–685

Martin TFJ (1997) Phosphoinositides as spatial regulators of membrane traffic. Curr Opin Neurobiol 7:331–338

Martin TFJ (1998) Phosphoinositide lipids as signaling molecules: common themes for signal transduction, cytoskeletal regulation and membrane trafficking. Annu Rev Cell Dev Biol 14:231–264

Meyers R, Cantley LC (1997) Cloning and characterization of a wortmannin-sensitive human phosphatidylinositol 4-kinase. J Biol Chem 272:4384–4390

Nakagawa T, Goto K, Kondo H (1996a) Cloning, expression, and localization of 230-kDa phosphatidylinositol 4-kinase. J Biol Chem 271:12088–12094

Nakagawa T, Goto K, Kondo H (1996b) Cloning and characterization of a 92 kDa soluble phosphatidylinositol 4-kinase. Biochem J 320:643–649

Odorizzi G, Babst M, Emr SD (1998) Fab1p PtdIns(3)P 5-kinase function essential for protein sorting in the multivesicular body. Cell 95:847–858

Olsson H, Martinez-Arias W, Drobak BK, Jergil B (1995) Presence of a novel form of phosphatidylinositol 4-kinase in rat liver. FEBS Lett 361:282–286

Rao VH, Misra S, Boronenkov IV, Anderson RA, Hurley JH (1998) Structure of type IIβ phosphatidylinositol phosphate kinase: a protein kinase fold flattened for interfacial phosphorylation. Cell 94:829–929

Rothman JE (1994) Mechanisms of intracellular protein transport. Nature 372:55–63

Schekman R, Orci L (1996) Coat proteins and vesicle budding. Science 271:1526–1533

Schmid R, Ambron RT (1997) A nuclear localization signal targets proteins to the retrograde transport system, thereby evading uptake into organelles in aplysia axons. J Neurobiol 33: 151–160

Schu PV, Takegawa K, Fry MJ, Stack JH, Waterfield MD, Emr SD (1993) Phosphatidylinositol 3-kinase encoded by yeast VPS34 gene essential for protein sorting. Science 260:88–91

Shyng SL, Nichols CG (1998) Membrane phospholipid control of nucleotide sensitivity of KATP channels. Science 282:1138–1141

Smith HM, Raikhel NV (1998) Nuclear localization signal receptor importin alpha associates with cytoskeleton. Plant Cell 10:1791–1799

Sorensen SD, Linseman DA, McEwen EL, Heacock AM, Fisher SK (1998) A role for a wortmannin-sensitive phosphatidylinositol-4-kinase in the endocytosis of muscarinic cholinergic receptors. Mol Pharmacol 53:827–836

Toker A (1998) The synthesis and cellular roles of phosphoinositol 4,5-bisphosphate. Curr Opin Cell Biol 10:254–261

Tolerico LH, Benko AL, Aris JP, Stanford DR, Martin NC, Hopper AK (1999) *Saccharomyces cerevisiae* Modd5p-II contains sequences antagonistic for nuclear and cytosolic locations. Genetics 151:57–75

Wiedemann C, Schafer T, Burger MM (1996) Chromaffin granule-associated phosphatidylinositol 4-kinase activity is required for stimulated secretion. EMBO J 15:2094–2101

Wiedemann C, Schafer T, Burger MM, Sihra TS (1998) An essential role for a small synaptic vesicle-associated phosphatidylinositol 4-kinase in neurotransmitter release. J Neurosci 18: 5594–5602

Wong K, Cantley LC (1994) Cloning and characterization of a human phosphatidylinositol 4-kinase. J Biol Chem 269:28878–28884

Wong K, Meyers R, Cantley LC (1997) Subcellular locations of phosphatidylinositol 4-kinase isoforms. J Biol Chem 272: 13236–13241

Zeng XT, Hara M, Inagaki C (1994) Electrogenic and phosphatidylinositol-4-monophosphate-stimulated Cl-transport by Cl-pump in the rat brain. Brain Res 641:167–170

Zhainazarov AB, Ache BW (1999) Effects of phosphatidylinositol 4,5-bisphosphate and phosphatidylinositol 4-phosphate in a Na$^+$-gated nonselective cation channel. J Neurosci 19: 2929–2937

Characterization of Type II Phosphatidylinositol 4-Kinase Isoforms Reveals Association of the Enzymes with Endosomal Vesicular Compartments*

Andras Balla‡, Galina Tuymetova‡, Michal Barshishat‡, Miklós Geiszt§, and Tamas Balla‡¶

From the ‡Endocrinology and Reproduction Research Branch, NICHD, and §Laboratory of Host Defenses, NIAID, National Institutes of Health, Bethesda, Maryland 20892

Phosphorylation of phosphatidylinositol (PI) to PI 4-phosphate is one of the key reactions in the production of phosphoinositides, lipid regulators of several cellular functions. This reaction is catalyzed by multiple enzymes that belong either to the type II or the type III family of PI 4-kinases. Type III enzymes are structurally similar to PI 3-kinases and are sensitive to PI 3-kinase inhibitors. In contrast, the recent cloning of the first type II PI 4-kinase enzyme defined a novel enzyme family. Here we characterize a new member of this family, the type IIβ enzyme that has been identified in the NCBI data base based on its homology to the first-cloned type IIα enzyme. The type IIβ enzyme has a primary transcript size of ~3.8 kb and shows wide tissue distribution. It contains an open reading frame of 1.4 kb, encoding a protein of ~54 kDa. Sequence comparison reveals a high degree of similarity to the type IIα enzyme within the C-terminal catalytic domain but significantly lower homology within the N-terminal region. Expression of both enzyme yields increased PI 4-kinase activity that is associated with the microsomal membrane fractions and is significantly lower for the type IIβ than the type IIα form. Both enzymes use PI as their primary substrate and have no detectable activity on PI monophosphates. Epitope-tagged as well as green fluorescent protein-tagged forms of both enzymes localize primarily to intracellular membranes and show prominent co-localization with early endosomes and recycling endosomes but not with the Golgi. These compartments participate in the processing of both the transferrin receptor and the G protein-coupled AT$_{1A}$ angiotensin receptor. Our data indicate the existence of multiple forms of type II PI 4-kinase in mammalian cells and suggest that their functions are related to the endocytic pathway.

Inositol phospholipids have long been considered primarily as precursors for important messenger molecules during activation of certain G protein-coupled receptors and receptor-tyrosine kinases (1, 2). Phosphatidylinositol (PI)[1] 4-kinase and

PI 4-phosphate (PI(4)P) 5-kinase activities were believed to maintain the small PI(4,5)P$_2$ pools of the plasma membrane during increased phospholipase C activity in stimulated cells. In addition to this important signaling aspect of phosphoinositide metabolism, it has been increasingly recognized in the last decade that localized phosphoinositide changes are of crucial importance in the organization of signaling microdomains (3, 4). A growing number of kinases and phosphatases that act upon inositides have been identified in recent years (5, 6). This together with the recognition and characterization of several molecular motifs that interact with inositides to regulate a large number of signaling molecules has contributed to our changing perception of how inositides contribute to cellular signaling. In light of such localized functions, the importance of PI(4)P formation has to be reevaluated. It can now be safely assumed that PI(4)P serves not only as a synthetic intermediate in PI(4,5)P$_2$ synthesis but also as a regulatory molecule on its own right.

PI 4-kinase (PI4K) enzyme activities have long been described in several tissues and have been classified as either type II or type III activities based on the catalytic properties of the enzyme (7–9). The sensitivity of type III but not type II enzymes to PI3K inhibitors (10) predicted a similarity between the catalytic domains of the type III enzymes and the PI3K enzymes. This has been proven by cloning of the type III PI4Ks (9, 11), of which two forms have been identified, a larger 200–220-kDa α-form and a smaller 110-kDa β-form, which are homologues of the yeast Stt4 and Pik1 proteins, respectively (9). Several elegant studies indicate that Pik1 and Stt4 serve nonredundant functions in yeast (12–15). Although Pik1 has been implicated in nuclear (12) and trans-Golgi (15, 16) functions, Stt4 was found to support cell wall synthesis and stability (15, 17). Most recently, it has also been shown that the PI(4)P pool produced by Stt4 but not by Pik1 is dephosphorylated by the inositide phosphatase, Sac1, and this lipid pool determines vacuole morphology and is functionally linked to the actin cytoskeleton (18). These studies are consistent with the existence of multiple functional pools of PI(4)P and tight control of their synthesis and degradation by distinct kinases and phosphatases.

In contrast to the significant progress in the field of type III PI4Ks, relatively little is known about the functions of the type II PI4Ks. Several biochemical studies demonstrate the presence of type II PI4K activity in a number of membrane compartments and organelles and indicate that the enzyme regulates PI(4)P synthesis related to several cellular processes, most notably to secretion (19). However, the molecular identi-

---

[1] The abbreviations used are: PI, phosphatidylinositol; PIP, phosphatidylinositol monophosphate; PI(4)P, PI 4-phosphate; PI(4,5)P$_2$, PI 4,5-bisphosphate; PI4K, PI 4-kinase; EEA1, early endosomal autoanti-gen; EGFP, enhanced green fluorescent protein (GFP); HA, hemagglutinin; PBS, phosphate-buffered saline.

ties of the type II enzymes have been only recently revealed. The enzyme has been cloned based on purification of the protein from secretory granules (20) and from detergent-insoluble membrane fractions, also termed rafts (21). The latter study also indicates the existence of homologues of the cloned enzyme identified in the EST data base and is termed the cloned enzyme type IIα, indicating that it was the first member of a family of enzymes.

In the present study, we have characterized the human type IIβ PI4K enzyme and compared its features to the human type IIα protein. We found significant differences in the tissue distribution and catalytic activities of the two proteins. We also demonstrate that both enzymes associate with the endosomal vesicular compartment in several cell types and is involved in the regulation of endosomal membrane traffic in mammalian cells.

EXPERIMENTAL PROCEDURES

Materials and DNA Clones—The EST clone from the I.M.A.G.E. Consortium (image.llnl.gov) (IMAGE clone ID 2905670, dbEST ID 5108611) encoding human PI4K type IIα was obtained from ATCC (Manassas, VA). The EST from Research Genetics (AL527283, dbEST ID 7860272) encoding human PI4K type IIβ was purchased from Invitrogen. The coding sequences of the two proteins were subcloned into the pcDNA3.1 plasmid for mammalian expression and *in vitro* translation or into the pEGFP-N1 plasmid to create the GFP-fused forms of the proteins. Epitope-tagged versions of the enzymes were created from the GFP fusion constructs by replacing the entire GFP sequence with the sequence coding for the HA epitope. To create a catalytically inactive enzyme, the conserved aspartate residue within the catalytic DRG sequence (Asp-308 in type IIα and Asp-304 in type IIβ) has been mutated to alanine by the QuikChange mutagenesis kit of Stratagene. To search for longer 5′ sequences, the type IIβ form was also amplified from Marathon Ready cDNA of human leukemia, K-562. Although longer forms have not been found, a shorter variant of the type IIβ enzyme has been isolated, and this was also subcloned into the pcDNA 3.1 and pEGFP-N1 plasmids. The TNT T7 Coupled Transcription/ Translation System was obtained from Promega (Madison, WI). [γ-^{32}P]ATP (3000–6000 Ci/mmol) and [^{35}S]methionine were purchased from PerkinElmer Life Sciences. ATP, adenosine, and wortmannin were obtained from Sigma. Phosphatidylinositol was purchased from Fluka (Ronkonkoma, NY), and phosphatidylinositol phosphates were from Echelon Research Laboratories (Salt Lake City, UT). The primary antibodies against early endosomal autoantigen (EEA1) and gm130 were obtained from BD Biosciences. The Alexa-595 and Alexa-488 secondary antibodies were from Molecular Probes (Eugene, OR). The monoclonal anti-HA antibody was purchased from Covance, and the polyclonal anti-HA antibody was from Alpha Diagnostics (San Antonio, TX).

Northern Blot Analysis—Human 12-lane multiple tissue and cancer cell line Northern blots (CLONTECH) containing poly(A)$^+$-selected RNA were hybridized at 65 °C with the radiolabeled cDNA fragment using standard hybridization procedures (Amersham Biosciences). The 1.5-kbp *Eco*RI fragment containing the non-coding region of the type IIβ enzyme was used as a probe to detect the transcript for the type IIβ enzyme. For the type IIα enzyme, either a 500-bp PCR product coding for the unique N-terminal sequence or the full-length cDNA insert was used as a probe for hybridization. The cDNA fragments were labeled with the Prime-It RmT random primer labeling kit (Stratagene, La Jolla, CA). Membranes were washed twice for 15 min in 2× SSC (1× SSC = 0.15 M NaCl and 0.015 M sodium citrate) with 0.1% SDS at room temperature followed by a 30-min wash in 0.1× SSC with 0.1% SDS at 60 °C.

In Vitro Translation—One microgram of supercoiled DNA plasmid was transcribed *in vitro* and then translated in the presence of [^{35}S]methionine with the TnT-coupled reticulocyte lysate system (Promega) according to the manufacturer's instructions. The reaction products were analyzed by SDS-PAGE followed by autoradiography.

Immunocytochemistry and Confocal Microscopy—For immunostaining, COS-7 cells were grown on coverslips and fixed in 2% formaldehyde in PBS, pH 7.4, for 10 min at room temperature. After three washes with PBS (5 min each), fixed cells were incubated in blocking solution (10% FBS in PBS) for 10 min to decrease nonspecific binding of the antibodies. This blocking solution was complemented with 0.2% saponin for diluting the primary antibody (anti-EEA1 and anti-gm130,

1:250), and cells were incubated for 1 h at room temperature. After 3 washes, cells were incubated in the same buffer with a fluorescent secondary antibody (1:1000) for 1 h at room temperature. After a final washing step (3 × 5 min with blocking solution), the cells were rinsed with PBS, air-dried, and mounted on glass slides using Aqua Poly-Mount mounting medium (Polysciences, Inc.). Cells were then analyzed by confocal microscopy using an inverted Zeiss LSM-410 confocal microscope.

Immunoprecipitation of Epitope-tagged PI 4-Kinases—COS-7 cells cultured on 10-cm culture dishes were transfected with the respective HA-tagged PI 4-kinase constructs (or with GFP as control) for 48 h. Cells were lysed in 1 ml of lysis buffer (50 mM Tris/HCl, pH 7.4, 150 mM NaCl, 1 mM EDTA, 1% Nonidet P-40, 0.25% sodium deoxycholate, 1 mM dithiothreitol, 1 mM 4-(2-aminoethyl)benzenesulfonyl fluoride, 10 μg/ml leupeptin, 10 μg/ml aprotinin), and the lysates were cleared by centrifugation (14,000 × g, 15 min). After pre-clearing with 100 μl (1:1 slurry) of protein G-agarose for 30 min, 10 μg of monoclonal anti-HA antibody (MMS 101R, from Berkeley Antibody Co.) was added to the lysates, and the samples were incubated on a rotating platform at 4 °C for 2 h. The antibody was then collected on protein G-agarose beads (50 μl), and the complex was washed 3 times with 1 ml of lysis buffer before a final wash in the PI kinase buffer. The enzyme was then analyzed by Western blotting, or its activity was assayed on the beads as described below.

Assay of PI 4-Kinase—The activity of PI 4-kinase was measured as incorporation of radioactivity from [γ-^{32}P]ATP into organic solvent-extractable material as described previously (22). The standard reaction mixture for PI 4-kinase (50-μl final volume) contained 50 mM Tris/HCl, pH 7.5, 20 mM MgCl$_2$, 1 mM EGTA, 1 mM PI, 0.4% Triton X-100, 0.5 mg/ml bovine serum albumin (lipid kinase buffer), 100 μM [γ-^{32}P]ATP, and the enzyme. All assay components except [γ-^{32}P]ATP were preincubated with or without inhibitors for 10 min at room temperature. Reactions were started by the addition of [γ-^{32}P]ATP and terminated after 10 min by the addition of 3 ml of CHCl$_3$, CH$_3$OH, 37% HCl (200:100:0.75 (v/v/v)). The organic solvent phase was separated from [γ-^{32}P]ATP as described elsewhere (10), and after evaporation, its activity was determined in a liquid scintillation counter. The identity of the lipid product was assessed by TLC analysis and by further phosphorylation with a recombinant type I PIP 5-kinase (kindly provided by Drs. Jolanta Vidugiriene and Thomas F. Martin).

The substrate specificity of the enzymes was measured with lipids spotted on nitrocellulose or SAM^2® (Promega) membranes. 1–10 μg of lipid was spotted onto the membranes from a chloroform solution with or without phosphatidylserine. Dried membranes were incubated with the enzymes in the same buffer used for the kinase assays (except that it lacked PI, see above) in the presence of 100 μM [γ-^{32}P]ATP in a wet chamber for 1 h. Reactions were stopped with 50 mM EDTA, and the membranes were washed 3 times with 2 M NaCl followed by 3 washes in 2 M NaCl, 1% phosphoric acid and finally rinsed twice with distilled water. Phosphorylation of the lipids on the membrane was assessed by phosphorimaging analysis (PhosphorImager, Molecular Dynamics).

Permeabilized Cell Studies—COS-7 cells were seeded on 12-well plates (50,000 cells/well) and cultured for 2 days before transfection with LipofectAMINE 2000 according to the manufacturer's instructions. Twenty-four hours after transfection, cells were washed with PBS and incubated in 400 μl of permeabilization medium containing 110 mM KCl, 10 mM NaCl, 5 mM MgCl$_2$, 20 mM Hepes, pH 7.4, 2 mM EGTA, 0.05% bovine serum albumin, 15 μg/ml digitonin, 0.3 mM ATP, 12.5 μCi/ml [γ-^{32}P]ATP, and the various stimuli. Incubations were carried out at 37 °C for 10 min, and reactions were terminated with perchloric acid (5% final). Inositol lipids were extracted and separated by TLC as described previously (23), and their radioactivity was quantitated by phosphorimaging.

RESULTS

Molecular Characterization of Type IIβ PI4K—A search of the data base for homologues of the recently published type II PI4K revealed a protein sequence with significant homology with the type II PI4K enzyme (NCBI: 8922869). The nucleotide sequence for this polypeptide (XM003573) contained an overlapping segment with another nucleotide entry in the GenBank™ (AK023186), providing a total transcript length of 3469 bp. An EST containing the full putative coding sequence (AL527283) was obtained, and its sequencing has confirmed the identity of the full cDNA sequence deduced from the two GenBank™ sequences. This long transcript contains an open reading frame of 1503 bp (Fig. 1*A*). During our characterization
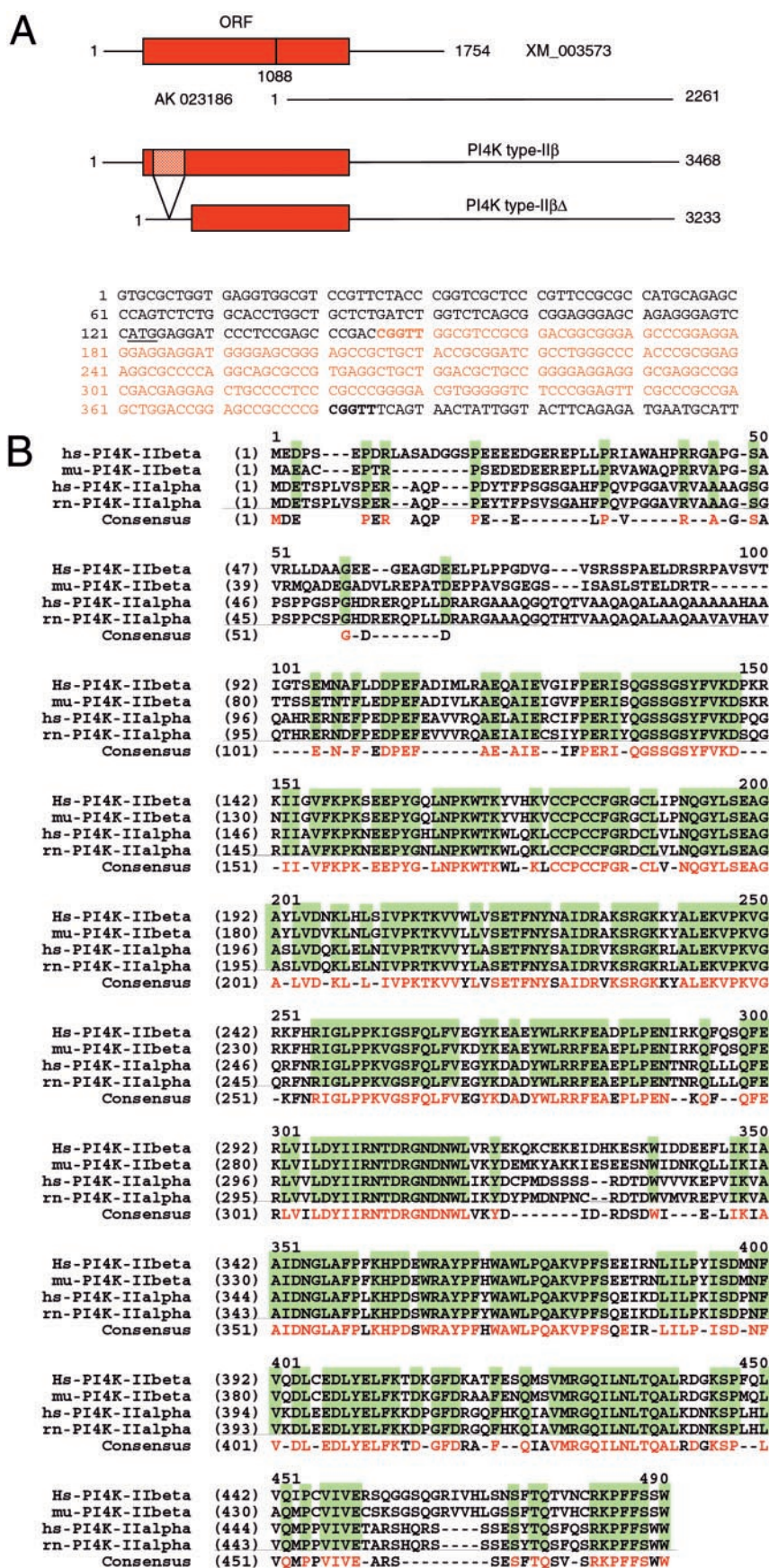
FIG. 1. **Structure and assembly of cDNAs encoding PI 4-kinase type IIβ (A) and amino acid sequence homology between the type IIβ and -α isoforms (B).** *Panel A*, The EST clone (AL527283) encompasses the two partial DNA entries in the GenBank™ encoding PI4K type IIβ. An alternative product obtained by PCR amplification from Marathon-Ready cDNA lacks the sequence labeled with *orange*, yielding an N-terminal-truncated from of the protein termed PI4K type IIβΔ. *ORF*, open reading frame. *Panel B*, sequence alignment of PI4K type IIβ and type IIα from human (*hs*), mouse (*mu*) and rat (*rn*). Conserved regions are *highlighted* with *green*.

of this sequence, Minogue *et al.* (21) reported the cloning of type IIα PI4K and also identified another protein sequence in the data base that was termed type IIβ and which is identical to the protein characterized in the present report. Therefore, we refer to this protein as the type IIβ PI 4-kinase. Fig. 1*B* shows the sequence homology between the type IIα and type IIβ enzymes.

Type II PI 4-Kinases and Endocytosis
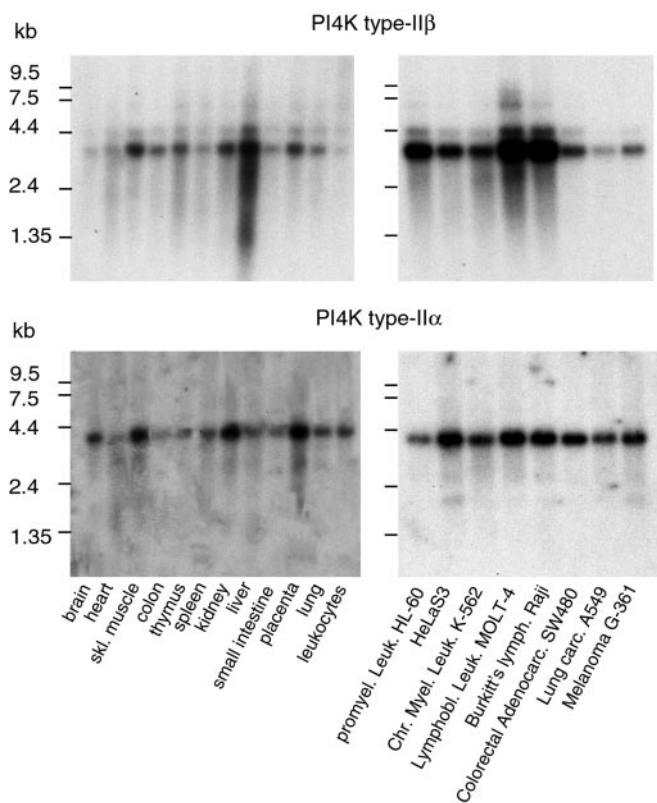
FIG. 2. **Northern analysis showing the distribution of PI4K type IIβ and PI4K type IIα mRNA in human tissues and cancer cell lines.** A human multiple-tissue Northern blot and a multiple cancer cell line Northern blot (CLONTECH) were hybridized with ³²P-labeled probes specific for the respective mRNAs. The exposure times for the type IIβ and type IIα blots were 16 h and 5 days, respectively. *skl.*, skeletal; *promyel. leuk.*, promyelocytic leukemia; *Chr.*, chronic; *Lymphobl.*, lymphoblastic; *lymph.*, lymphoma; *adenocarc.*, adenocarcinoma.

A high degree of identity and similarity is found throughout the amino acid sequence, with only the N-terminal regions more unique. Because the transcript does not contain an in-frame stop codon preceding the putative translation start-site that conforms to a Kozak sequence, we searched for possible sequences extending in the 5′ direction using Marathon-Ready cDNA from various human tissues and cells. These efforts did not find any longer 5′ sequence but repeatedly identified a shorter transcript that lacks 235 bp in the N-terminal coding sequence, yielding a 96-amino acid shorter, N-terminal-truncated variant protein. This shorter form, which we termed type IIβΔ, could be an alternatively spliced form, although the lack of typical splice donor and acceptor sequences around the variant sequence (which lies within the first exon) makes this questionable. Given the sequence repeat around the "spliced-out sequence" in the short variant, it is possible that this is not a natural product but an artifact generated during cDNA synthesis (Fig. 1*A*). This question was not further pursued in the present study, but the short variant protein has proven to be useful to provide information about the role of the N-terminal sequence in the localization of the protein (see below).

Northern analysis was performed on human tissue mRNA blots using probes based on the non-coding region of the type IIβ and either the unique N-terminal or the full sequence of the type IIα enzyme. As shown in Fig. 2, a primary transcript size of ~3.8 kb was observed for both probes specific for the respective mRNAs and an additional weaker signal at ~4.3 kb in the case of type IIβ enzyme. Both transcripts showed a relatively uniform distribution between the tissues represented on the
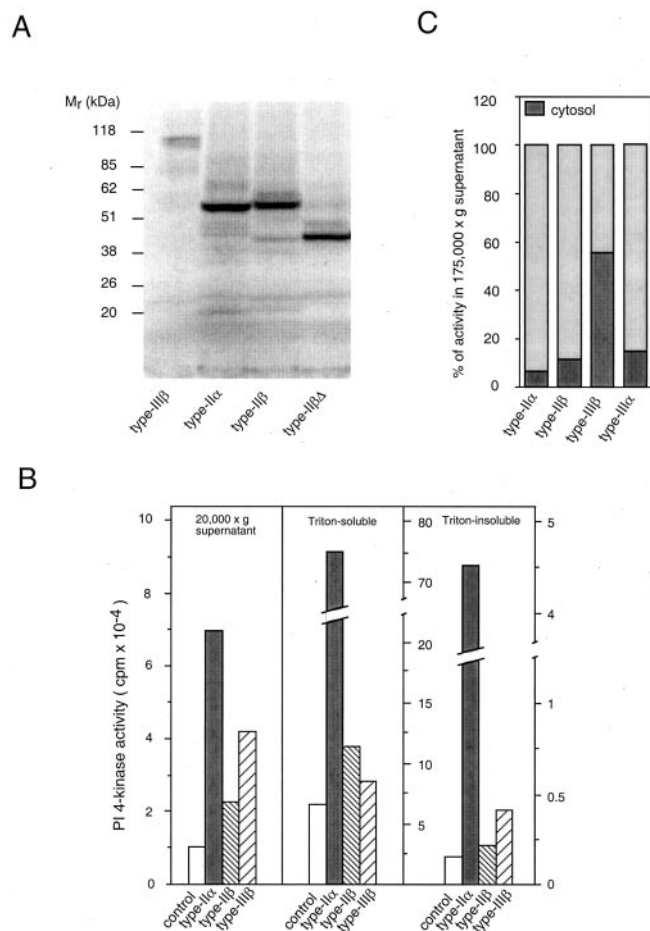
FIG. 3. ***In vitro* translation and expression of PI4K isoforms in COS-7 cells.** *Panel A*, cDNAs encoding PI4K type IIα, type IIβ, type IIβΔ, and type IIIβ were subcloned into the pcDNA3.1 mammalian expression plasmid and subjected to an *in vitro* translation reaction in the presence of [³⁵S]methionine using rabbit reticulocyte lysates. The reaction products were analyzed by SDS-PAGE. *Panel B*, COS-7 cells were transfected with the indicated plasmids (pEGFP was used as control), and after 24 h, cells were lysed, and their membranes were fractionated. PI 4-kinase activity was measured in the various fractions by an *in vitro* PI kinase assay. *Panel C*, the 20,000 × *g* supernatant was centrifuged with 175,000 × *g* to separate the light microsomal membranes from the cytosol, and the cytosolic activity was expressed as the percent of the total present in the 20,000 × *g* supernatant. Results from 3–4 representative experiments, each performed in duplicate, are shown; the error bars (less than 10%) are omitted for clarity.

blots with only a few notable differences. These were the prominent abundance of type IIβ but not type IIα mRNA in liver and the relatively low level of type IIβ mRNA in the brain and peripheral leukocytes. A weaker signal was repeatedly observed with two distinct probes specific for the type IIα enzyme sequence. Probes based on the N-terminal short splice variant sequence of type IIβΔ failed to produce a detectable signal (not shown).

Biochemical Analysis of the Expressed Proteins—The coding sequences of the three proteins (type IIα, type IIβ, and type IIβΔ) were subcloned into the mammalian expression plasmid, pcDNA3.1. Proteins were first expressed in an *in vitro* translation reaction to reveal the sizes of the expressed proteins. As shown in Fig. 3*A*, type IIα, type IIβ, and type IIβΔ were all efficiently translated to yield proteins consistent with their expected molecular sizes. Importantly, the size of the *in vitro* translated type IIβ was the same regardless of the presence or absence of the large 3′-untranslated region, confirming the correct identification of the stop codon based on the nucleotide sequence. When the enzymes were expressed in COS-7 cells, a

large increase was observed in the PI4K activity of the cell lysates when cells expressed PI4K type IIα but only a moderate increase when the type IIβ protein was expressed (Fig. 3*B*). For a comparison, the two forms of the wortmannin-sensitive type III PI 4-kinases were also expressed in these studies. Most of the overexpressed type II activity was found to be membrane-associated and was solubilized with Triton X-100, as typically found for type II PI 4-kinases (Fig. 3*B*). However, some of the type II enzyme was also associated with the Triton-insoluble fraction and was also detectable in the 20,000 × *g* supernatant. In the latter fraction, however, most of the type II enzymes (unlike the type IIIβ form) was not cytosolic and was associated with the light membranes essentially as described in (20) (Fig. 3*C*). The effect of overexpression of the type II enzymes on the phosphorylation of endogenous PI was also examined in permeabilized COS-7 cells. Expression of the type IIα enzyme caused an average 2.5-fold increase in ^{32}P-labeling of PI(4)P, whereas the type IIβ enzyme caused only about a 20% increase, consistent with its significantly lower PI 4-kinase activity compared with that of α-form (Fig. 4*B*). Even the more active type IIα enzyme evoked only a moderate increase in the labeling of PI(4,5)P$_2$. This effect was more pronounced in the presence of 10 μM wortmannin, when the endogenous type III PI 4-kinases were inhibited (Fig. 4*A*).

To investigate whether the different activities of the α- and β-forms of the type II enzymes could be caused by their different optimum assay conditions, we examined the detergent sensitivities of the two enzymes. These experiments showed an identical activation of both enzymes with Triton X-100 in the same concentration range (not shown). When HA epitope-tagged forms of the enzymes were expressed in COS-7 cells and their expression levels were analyzed by Western blot analysis, a significantly lower level of expression of the type IIβ form was observed (Fig. 5*A*). Therefore, we performed immunoprecipitation and compared the activity of equal amounts of the two enzymes based on quantitation of the Western analysis. These measurements showed that the type IIβ enzyme was about 30% as active as the type IIα form (Fig. 5*B*). The reaction products of both enzymes were run together with PI(4)P on TLC analysis and could be converted to PI(4,5)P$_2$ by a recombinant type I PIP kinase, indicating that both enzymes are *bona fide* PI 4-kinases (Fig. 5*C*).

We also examined whether the type IIβ form can use alternative inositide substrates. However, neither enzyme could use any of the phosphorylated derivatives of PI as substrate *in vitro* under our experimental conditions (not shown). Comparison of the sensitivities of the two proteins to various inhibitors revealed their complete resistance to the PI 3-kinase inhibitor, wortmannin (not shown), and a slightly higher sensitivity of the type IIβ enzyme to phenylarsine oxide but not to adenosine (Fig. 6). It is worth noting that both enzymes were significantly more resistant to phenylarsine oxide than either of the two type III PI4K enzymes, as already reported for the type IIα enzyme (20). These data suggested that the lower PI 4-kinase activity of the β-form is not due to completely different catalytic properties or substrate specificity of the two enzymes.

Localization of the Type II Enzymes to Early Endosomes—To investigate the intracellular distribution of the two isoforms of type II PI4Ks, GFP-tagged as well as epitope-tagged versions of the proteins were created by fusing the enhanced GFP protein (or the HA epitope) to the C termini of the enzymes. These constructs were expressed in COS-7 and HEK 293 cells to observe the distribution of the expressed proteins. The GFP-tagged enzymes were catalytically active, but their activities were only about 50% of their untagged counterparts (data not shown). The cellular distribution of the proteins in live COS-7
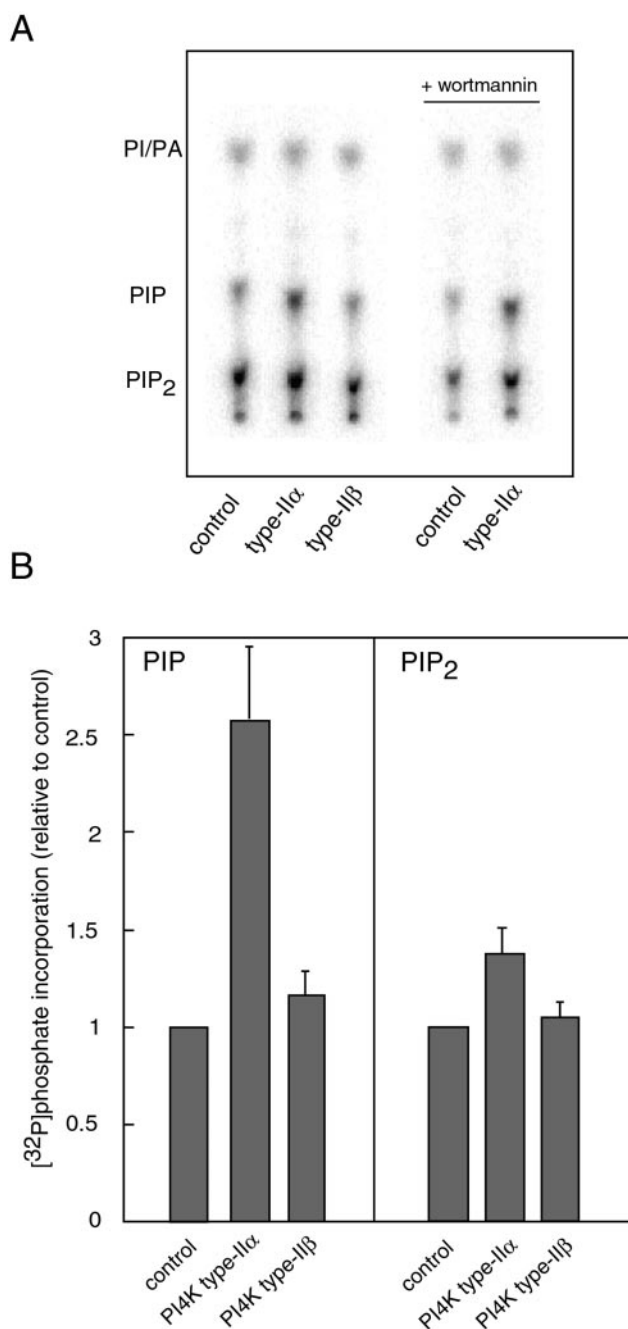
FIG. 4. **Effect of overexpression of PI4K type IIβ and type IIα on phosphorylation of endogenous lipid substrate in permeabilized COS-7 cells.** Cells were transfected with the indicated plasmids (pEGFP was used for control) for 24 h before analysis of [^{32}P]phosphate incorporation into various phospholipids from [γ-^{32}P]ATP after permeabilization with digitonin. *Panel A* shows the results of a representative TLC analysis, and *panel B* shows the summary of quantitative data from 4 similar experiments performed in duplicate. Wortmannin (10 μM) was added 10 min before permeabilization to inhibit endogenous type III PI 4-kinases. *PIP$_2$*, phosphatidylinositol biphosphate; *PA*, phosphatidic acid.

cells is shown in Fig. 7. Consistent with their tight membrane association, both type IIα and type IIβ forms were present in intracellular membranes, primarily in small vesicular structures scattered throughout the cytoplasm. Interestingly, the distribution and sizes of the vesicles positive for the type IIα enzyme were clearly dependent on the level of protein expression. Cells that expressed high levels of the protein contained larger vesicles that were concentrated mostly in the juxtanuclear compartment (Fig. 7, *A–C*). Higher expression levels
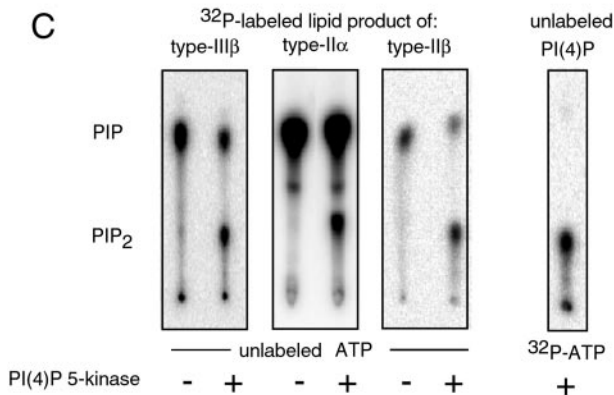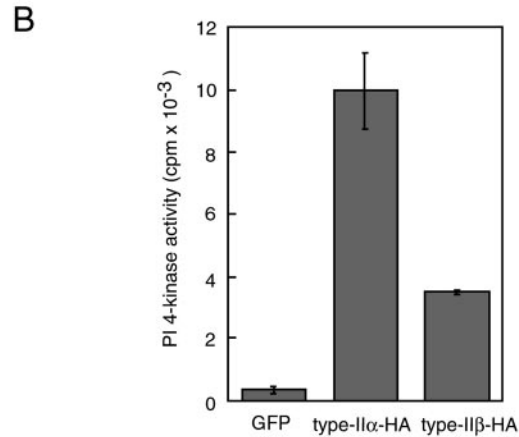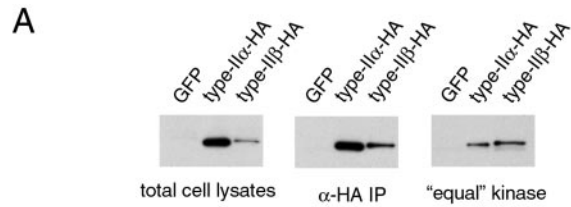
FIG. 5. **Comparison of expression levels and activities of epitope-tagged PI4K type II enzymes.** COS-7 cells were transfected with either PI4K type IIα or type IIβ, epitope-tagged at their C termini with the HA epitope. Total cell lysates as well as the immunoprecipitated (with a monoclonal anti HA antibody) proteins were analyzed by Western blotting using a polyclonal anti HA antibody (*panel A*). Based on densitometry, "equal" amounts of the two kinases were assayed for PI kinase activity (*panel B*) and again analyzed by Western blotting (*right* on *panel A*). The identity of the lipid product was determined by TLC analysis and further phosphorylation by a type I PIP 5-kinase, which converts PI(4)P but not PI(5)P to PI(4,5)P$_2$ (*panel C*).

of the type IIβ protein also caused the appearance of larger vesicles, but juxtanuclear accumulation of these enlarged vesicles was not as obvious as that of the type IIα enzyme (Fig. 7, *D–F*). Plasma membrane localization was less pronounced in the case of the type IIβ enzyme, and more of this protein was present in the cytoplasm (Fig. 7D). The shorter, type II$\beta\Delta$ enzyme, on the other hand, failed to show membrane localization and was mostly present in the cytoplasm (Fig 7, *G–I*). This result indicated that the N-terminal 96-amino acid sequence is necessary to target the protein to its specific membrane location. Immuno-cytochemical analysis of the epitope-tagged enzymes in fixed cells showed a distribution that was indistinguishable from that of the GFP-fused forms. Moreover, simultaneous detection of the GFP-tagged and epitope-tagged versions of the same expressed enzymes showed clear co-localization for both the type IIα and type IIβ enzymes (data not
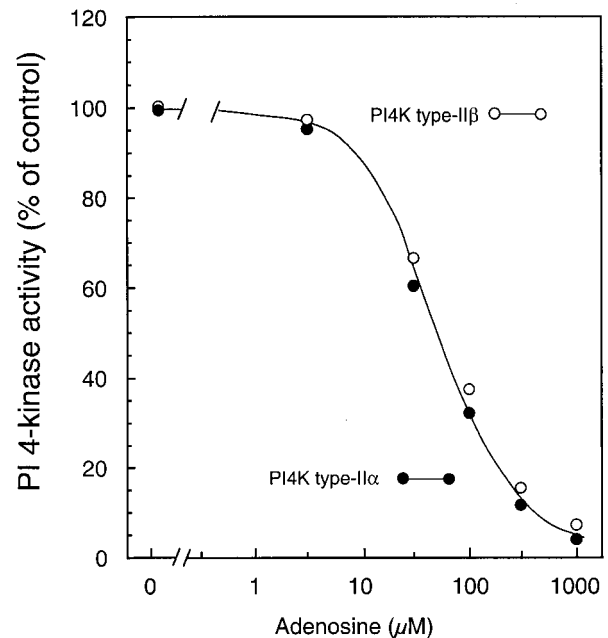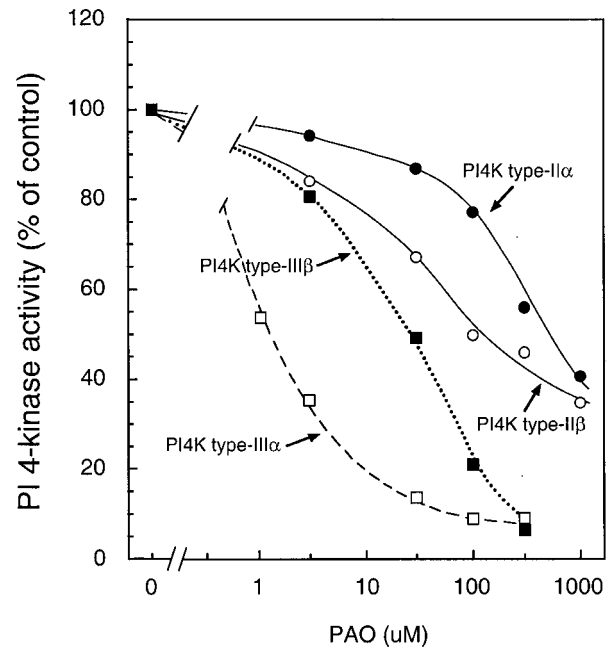
FIG. 6. **Sensitivity of the individual PI4K isoforms to phenylarsine oxide (*PAO*) and adenosine.** COS-7 cells were transfected with the indicated plasmids or pEGFP for 24 h. After lysis and fractionation (see the legend to Fig. 3), PI 4-kinase activities of the 20,000 × *g* supernatant (for the type III enzymes) or of the Triton X-100-sulubilized membranes (for the type II enzymes) were assayed after a 10-min preincubation with the indicated concentrations of inhibitors. In each case, the activity of the pEGFP-transfected control assayed under similar conditions was subtracted, and the results are expressed as the percent of the activity measured without inhibitors. The average results from two experiments are shown, and the error bars (less than 10%) are omitted for clarity.

shown). To determine the identity of the membrane compartment in which the enzymes were found, transfected COS-7 cells were fixed and subjected to immuno-cytochemistry using antibodies against known intracellular markers. These studies showed that both the α and β forms of the enzymes co-localized with the EEA1 protein in the small peripheral membrane vesicles, suggesting their association with early endosomes (Figs. 8 and 9). Similar data were obtained with the epitope-tagged
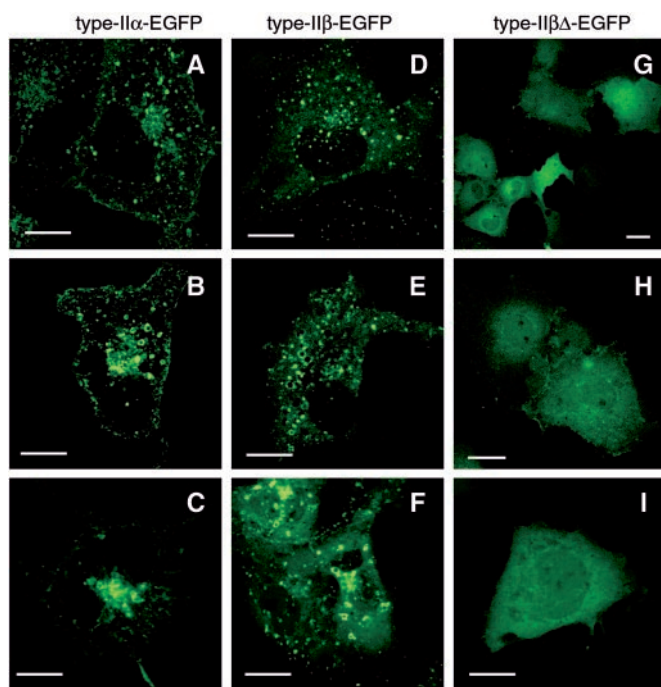
FIG. 7. **Cellular distribution of type II PI 4-kinase-EGFP isoforms, expressed in COS-7 cells.** EGFP was fused to the C termini of the two PI4K type II isoforms, and the hybrids were expressed in COS-7 cells. One day after transfection, live cells were analyzed in an inverted Zeiss LSM-410 confocal microscope. Cells expressing increasing amounts of the kinase (*panels A–C* and *D–F* from *top* to *bottom*) show larger vesicles (*B* and *E*) and, in the case of the type IIα enzyme, also show accumulation of the larger vesicles in the juxtanuclear compartment (*C*). Association of the type IIβ kinase with the intracellular vesicles requires the N-terminal 96 amino acids, since the truncated enzyme is largely cytosolic (*panels G–I*). The *bars* represent 10 μm.

FIG. 8. **Co-localization of the type IIα PI4K with the early endosome-associated autoantigen (EEA1).** COS-7 cells expressing PI4K type IIα fused to EGFP were fixed and permeabilized for immunocytochemical analysis using, EEA1 (*A–I*) and the Golgi marker, gm130 (*J–L*). Co-localization of the type IIα enzyme with EEA1 in the small punctate structures scattered around the cytoplasm is clearly evident (*A–C*). At higher expression levels, cells contain larger vesicles that are also positive for EEA1 (*D–F*). It is noteworthy that the *red* and *green* signals do not exactly overlap within the same vesicular structures, as if their distribution had some polarity (see *arrow* in *panel I*). No co-localization of the kinase is observed with the Golgi marker, gm130 (*J–L*). The *bar* represents 10 μm.

enzymes (not shown). In cells expressing high levels of the type IIα or type IIβ enzyme, the enlarged vesicles were also positive for the EEA1 protein. In contrast, no co-localization of the type IIα PI4K enzyme was observed with the Golgi marker protein, gm130, even in cells where the type IIα enzyme was found in the juxtanuclear vesicular compartment (Figs. 8 and 9). In the case of the type IIβ form, some cells showed a signal over the area of the Golgi (this was more prominent in the fixed cells), but the majority of the signal was associated with the vesicular endosomal structures (Fig. 9).

Association of Type II PI 4-Kinases with the Endocytic Pathway That Processes Both Transferrin and G Protein-coupled Receptors—To investigate whether the type II enzymes are present on the endocytic pathway through which internalized cell surface receptors are processed, we examined the uptake of Alexa-594-conjugated transferrin in COS-7 cells expressing the GFP-tagged forms of the respective type II enzymes. As shown in Fig. 10, co-localization of transferrin with either the type IIα or type IIβ enzyme was clearly demonstrable in early endosomes during endocytosis of the fluorescent ligand. At later times (>15 min), when transferrin began to accumulate in juxtanuclear recycling endosomes, it showed co-localization with the type IIα enzyme present in this compartment in cells expressing higher levels of the enzyme. The presence of high levels of the type IIα enzyme reduced the uptake of transferrin compared with non-transfected cells (Fig. 10), indicating that accumulation of vesicles in the juxtanuclear recycling compartment is probably associated with reduced recycling of transferrin receptors to the plasma membrane. A similar inhibitory effect of the type IIβ enzyme on transferrin uptake was not appreciable.

When catalytically inactive mutant forms of the enzymes

were expressed in COS-7 cells, their distribution showed subtle differences compared with their wild-type counterparts. These included a more prominent plasma membrane localization of the inactive type IIα form and the accumulation of numerous vesicles in the juxtanuclear region of the cell (Fig. 11*A*). In addition, small tubular structures were observed in some of the cells expressing high levels of the kinase-inactive proteins, and these were much more pronounced in the case of the inactive type IIβ enzyme (Fig. 11*B*). Unlike its wild-type form, kinase-inactive type IIβ did inhibit transferrin uptake (Fig. 11*B*). Nevertheless, transferrin uptake was observed in many cells expressing lower levels of the proteins after prolonged incubations (not shown). Co-localization of the GFP-tagged type IIα enzyme with G protein-coupled receptors was also examined in HEK 293 cells stably expressing the AT_{1A} angiotensin receptor. As shown in Fig. 12, after stimulation with rhodamine-conjugated angiotensin II, the ligand appeared in the vesicular compartments that were positive for type II PI4K, indicating that AT_{1A} receptors are also sorted through these PI4K-positive vesicles during agonist-induced endocytosis.
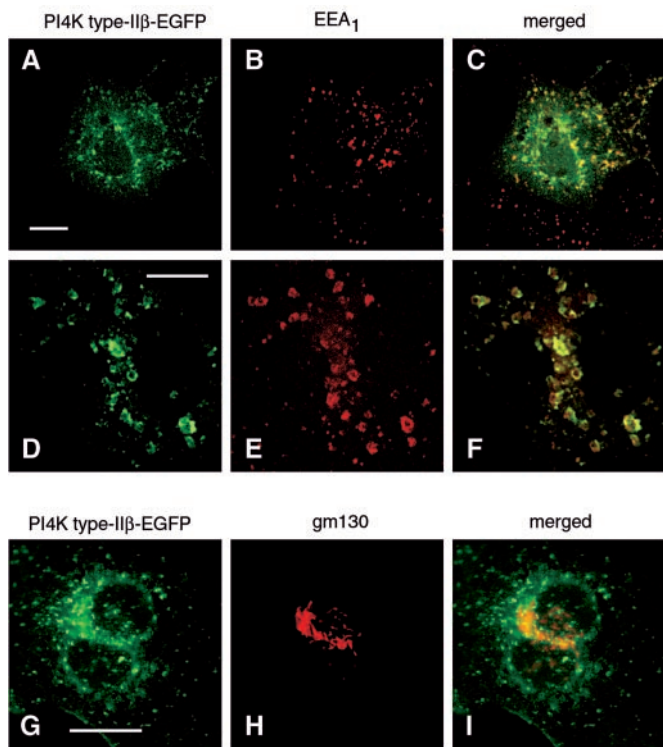
FIG. 9. **Co-localization of the type IIβ PI4K with the EEA1.** COS-7 cells expressing PI4K type IIβ fused to EGFP were fixed and permeabilized for immunocytochemical analysis using the early endosomal marker, EEA1 (*A–F*), and the Golgi marker, gm130 (*G–I*). Like type IIα, type IIβ is co-localized with EEA1 in the small punctate structures scattered around the cytoplasm (*A–C*) and in the larger vesicles that can be observed in cells expressing the kinase at higher levels (*D–F*). Again, no co-localization of the kinase is observed with the Golgi marker, gm130 (*G–I*). The *bar* represents 10 μm.

FIG. 10. **Co-localization of type II PI4K isoforms with Alexa transferrin in COS-7 cells.** COS-7 cells expressing PI4K type IIα (*A–I*) or type IIβ (*J–L*), both fused to EGFP, were incubated at 33 °C with Alexa-594-labeled transferrin for increasing periods of time. After incubation for 5–15 min, co-localization of Alexa transferrin with both the α and β forms of the kinase is observed over the early endosomes (*A–C* and *J–L*, respectively). At later times (20–30 min), transferrin also appears in the juxtanuclear recycling endosomes, where it also co-localizes with vesicles containing the type IIα kinase (*D–F*). Most of these structures are positive for the presence of the kinase in cells expressing high levels of the type IIα PI4K. Loading of the recycling endosomes with Alexa transferrin is greatly reduced in cells that express moderate to high levels of PI4K type IIα (*G–I*). The *bar* represents 10 μm.

DISCUSSION

Type II PI 4-kinase was the first PI kinase to be biochemically characterized and purified from several membrane sources, including red blood cell membranes, liver, bovine uterus, and A431 cell membranes and also from *Saccharomyces cerevisiae* (8, 9). This tightly membrane-bound enzyme is responsible for the majority of the PI 4-kinase activity found in the membranes of mammalian cells. Type II PI 4-kinases have been distinguished from other PI 4-kinases by their sensitivity to low concentrations of adenosine (K_i 10–50 μM) and micromolar concentrations of Ca^{2+} as well as to the anti-type II PI 4-kinase-neutralizing antibody, 4C5G (7). Based on these criteria, type II PI 4-kinases have been shown to be associated with virtually every membrane compartment within the cell including the plasma membrane, Golgi, secretory vesicles, and lysosomes in studies using cell or tissue fractionation (8, 9). However, the regulatory roles of these enzymes within these or any other compartments have not yet been clearly defined.

Despite their wide tissue distribution and prominent activity, the molecular identity of type II PI 4-kinases remained elusive until very recently, when two groups independently cloned the enzyme after purification of the protein from the membranes of chromaffin granules (20) and from non-caveolar membrane rafts, a subdomain of the plasma membrane (21). The reported enzymatic properties of the cloned protein are clearly consistent with it being a type II PI 4-kinase. Sequence homologues of type II PI 4-kinases have been identified in other species including *S. cerevisiae* in the NCBI data base. PI4K type IIβ, a closely related protein already noted in Minogue *et al.* (21) and characterized in this report, displayed a weaker PI 4-kinase activity than the type IIα enzyme, even after correc-

tion for its lower expression levels. Nevertheless, despite their remarkably different PI kinase activities, these two proteins have similar catalytic properties, inhibitor sensitivities, and substrate specificities. This raises the possibility that some additional members of this enzyme family may not even possess PI kinase activity and could be protein kinases similarly to the members of the PI 3-kinase-related kinases (24). It is noteworthy that the yeast homologues of the two type III PI 4-kinases, Pik1p and Stt4p, account for more than 90% of the yeast PI 4-kinase activity (15), raising the question of whether the yeast homologue of the type II PI 4-kinase possesses significant PI kinase activity. Whether any of the type II enzymes display protein kinase activity has yet to be determined, but among the possible inositide lipid substrates, these enzymes can only phosphorylate PI.

The intracellular localization of the two PI 4-kinase isoforms showed significant similarities and only subtle differences. Both enzymes were found to be associated with intracellular vesicular membranes bearing the early endosome marker, EEA1, and in some cells with the juxtanuclear recycling endo-
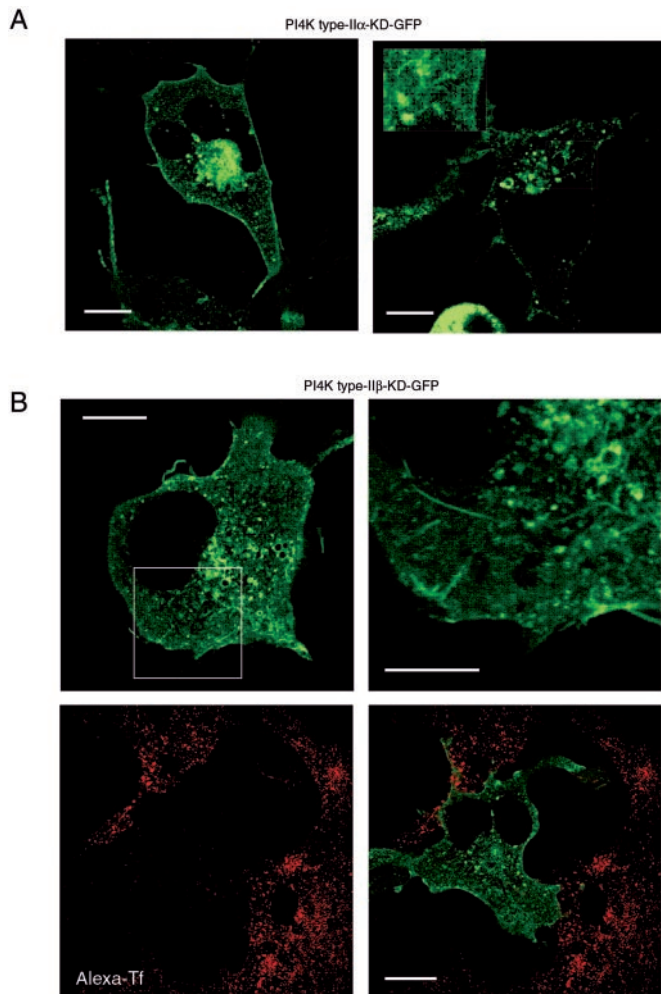
FIG. 11. **Cellular distribution of kinase-inactive type II PI 4-kinase isoforms, expressed as GFP fusion proteins in COS-7 cells.** COS-7 cells were transfected with the kinase-inactive mutants of the respective enzymes (D308A of type IIα, *panel A*, and D304A of type IIβ, *panel B*). Note the intense plasma membrane localization of the enzyme and the accumulation of juxtanuclear vesicles in *panel A*. The *inset* shows tubular structures that can be observed beneath the plasma membrane. *Panel B*, the tubular structures are more prominent with the kinase-inactive PI4K type IIβ enzyme. Also, the uptake of Alexa transferrin (*red*) (5-min pulse and 5-min chase at 37 °C) is greatly reduced in cells expressing high amounts of kinase-inactive PI4K type IIβ. The *bars* represent 10 μm.

FIG. 12. **Co-localization of type II PI4K isoforms with internalized rhodamine-angiotensin II in HEK-293 cells stably transfected with the AT$_{1A}$ angiotensin receptor.** HEK-293 cells expressing the AT$_{1A}$ angiotensin receptor were transfected with PI4K type IIα fused to EGFP. One day later, cells were incubated in the presence of rhodamine-labeled angiotensin II (*Rhod-Ang II*) at 33 °C for the indicated periods of time. Co-localization of the ligand (*red*) and the kinase (*green*) in early endosomes is evident shortly after stimulation. The *bar* represents 10 μm.

somes. The expressed type IIα enzyme fused to EGFP also clearly promoted the formation of recycling endosomes, since this compartment was prominently present in cells expressing high levels of the protein. This effect was not pronounced with the type IIβ enzyme, perhaps due to its lower PI 4-kinase activity. Association of both type II PI 4-kinases with the endosomal vesicular pathway carrying both internalized transferrin as well as the ligand of the G protein-coupled AT$_1$ angiotensin receptor was clearly demonstrable. This finding indicates that type II PI 4-kinase(s) may participate in the trafficking steps associated with clathrin-mediated endocytosis. Although the roles of Class III and Class II PI 3-kinases have been well documented in the endocytic process (25, 26), PI 4-kinases have not yet been implicated despite the known requirement for PI(4,5)P$_2$ binding to several proteins that participate in clathrin assembly (27, 28). A recent study has shown that plasma membrane removal and recycling is greatly affected by both ARF6 and the type I PIP 5-kinase (29). Because PIP 5-kinase uses PI(4)P as its substrate, type II PI 4-kinases are good candidates for producing PI(4)P in these internalized

membranes, especially since none of the type III PI 4-kinases appear to be present in these cellular compartments (30). The reported association of the type II PI 4-kinase activity with the epidermal growth factor receptor after agonist stimulation (31, 32) could also be related to the endocytosis and subsequent processing of this receptor.

Expression of kinase-inactive mutants of both proteins exerted no prominent change in cellular morphology other than what has already been observed with the kinase active forms, which is the formation of larger vesicles that often accumulated in the juxtanuclear compartment. The only clear effect of overexpressed kinase-inactive enzymes was the appearance of fine tubular structures of variable length at the cell periphery, and this effect was significantly more pronounced with the type IIβ form. Also, transferrin uptake was greatly reduced in cells expressing high levels of the inactive (but not the active) type IIβ enzyme but was also reduced in cells expressing either the active or inactive type IIα form. More studies are needed to define the exact steps in the endocytic pathway at which these enzymes may play a regulatory role.

None of the cells used in the present study display regulated secretion, a process in which PI 4-kinases have repeatedly been implicated. Therefore, it is quite possible that type II PI 4-kinases have an important function(s) in the secretory process or in any other more specialized membrane trafficking events, such as synaptic vesicle biogenesis (33). However, the wide tissue distribution of these enzymes and their presence in tissues and cells that lack regulated secretion suggest that they are involved in more basic processes of membrane dynamics. It will also be of great interest to follow the function of these proteins in membrane rafts because type II PI kinase activities have been shown to be present in such membrane subdomains (34). Given the pleiotropic functions of several members of

Type II PI 4-Kinases and Endocytosis

other inositide kinases, it is most likely that the type II enzymes are involved in multiple membrane fusion/budding events within mammalian cells.

The tissue distribution of the two enzymes does not indicate a specialized expression pattern for the individual proteins, which are probably both present simultaneously in numerous tissues and cells. The sizes of the main transcript for both proteins were 3.8–4.0 kb, in contrast to the 6.6-kb transcript size reported for PI4K type IIα (21). Because the tissue distribution for the latter transcript was found to be identical to that reported in Minogue *et al.* (21), we assume that the molecular size marker was misidentified in the latter report.

In a recent study, palmitoylation of PI4K type IIα has been shown to determine the membrane association of the protein (20). Although the palmitoylation motif of CCPCC (residues 170–174) is also present in PI4K type IIβ, the latter protein did not associate with early endosomes when lacking the N-terminal 96 amino acids. The presence of several proline residues within this part of the sequence of the type IIβ enzyme, including a PLLP motif, may be important in the localization of the protein. However, it is possible that palmitoylation is also required for proper membrane targeting.

In summary, the present study describes and characterizes a novel member of the type II PI 4-kinase family and compares its enzymatic characteristics to the recently cloned type IIα enzyme. It also demonstrates that, at least in COS-7 and HEK 293 cells, these enzymes are present in early endosomes through which both nutrient receptors and G protein-coupled receptors are processed during endocytosis. Expression of the more active type IIα enzyme also alters the distribution of membranes between the early and recycling endosomes and inhibits the rate of endocytosis of transferrin. These data suggest that this novel family of proteins is yet another addition to the increasing number of enzymes that regulate vesicular trafficking by modifying the phosphorylation state of phosphoinositides.

REFERENCES

1. Berridge, M. J. (1993) *Nature* **361,** 315–325
2. Nishizuka, Y. (1984) *Science* **225,** 1365–1370
3. Odorizzi, G., Babst, M., and Emr, S. D. (2000) *Trends Biochem. Sci.* **25,** 229–235
4. Hurley, J. H., and Meyer, T. (2001) *Curr. Opin. Cell Biol.* **13,** 146–152
5. Fruman, D. A., Meyers, R. E., and Cantley, L. C. (1998) *Annu. Rev. Biochem.* **67,** 481–507
6. Majerus, P. W., Kisseleva, M. V., and Norris, F. A. (1999) *J. Biol. Chem.* **274,** 10669–10672
7. Carpenter, C. L., and Cantley, L. C. (1990) *Biochemistry* **29,** 11147–11156
8. Pike, L. J. (1992) *Endocr. Rev.* **13,** 692–706
9. Balla, T. (1998) *Biochim. Biophys. Acta* **1436,** 69–85
10. Downing, G. J., Kim, S., Nakanishi, S., Catt, K. J., and Balla, T. (1996) *Biochemistry* **35,** 3587–3594
11. Gehrmann, T., and Heilmayer, L. G. (1998) *Eur. J. Biochem.* **253,** 357–370
12. Flanagan, C. A., Schnieders, E. A., Emerick, A. W., Kunisawa, R., Admon, A., and Thorner, J. (1993) *Science* **262,** 1444–1448
13. Yoshida, S., Ohya, Y., Goebl, M., Nakano, A., and Anrakur, Y. (1994) *J. Biol. Chem.* **269,** 1166–1171
14. Cutler, N. S., Heitman, J., and Cardenas, M. E. (1997) *J. Biol. Chem.* **272,** 27671–27677
15. Audhya, A., Foti, M., and Emr, S. D. (2000) *Mol. Biol. Cell* **11,** 2673–2689
16. Walch-Solimena, C., and Novick, P. (1999) *Nat. Cell Biol.* **1,** 523–525
17. Pramanik, A., Garcia, E., Ospina, R., Powell, M., Martinez, M., Alejo, W., McCoy, J., and Moore, C. W. (1997) *Cell. Mol. Biol.* **43,** 1007–1018
18. Foti, M., Audhya, A., and Emr, S. D. (2001) *Mol. Biol. Cell* **128,** 2396–2411
19. Martin, T. F. J., Loyet, K. M., Barry, V. A., and Kowalchik, J. A. (1997) *Biochem. Soc. Trans.* **25,** 1137–1141
20. Barylko, B., Gerber, S. H., Binns, D. D., Grichine, N., Khvotchev, M., Sudhof, T. C., and Albanesi, J. P. (2001) *J. Biol. Chem.* **276,** 7705–7708
21. Minogue, S., Anderson, J. S., Waugh, M. G., dosSantos, M., Corless, S., Cramer, R., and Hsuan, J. J. (2001) *J. Biol. Chem.* **276,** 16635–16640
22. Nakanishi, S., Catt, K. J., and Balla, T. (1995) *Proc. Natl. Acad. Sci. U. S. A.* **92,** 5317–5321
23. Balla, T., Baukal, A. J., Guillemette, G., and Catt, K. J. (1988) *J. Biol. Chem.* **263,** 4083–4091
24. Hunter, T. (1995) *Cell* **83,** 1–4
25. Simonsen, A., Lippe, R., Christoforidis, S., Gaullier, J-M., Brech, A., Callaghan, J., Toh, B-H., Murphy, C., Zerial, M., and Stenmark, H. (1998) *Nature* **394,** 494–498
26. Gaidarov, I., Smith, M. E., Domin, J., and Keen, J. H. (2001) *Mol. Cell* **7,** 443–449
27. Vallis, Y., Wigge, P., Marks, B., Evans, P. R., and McMahon, H. T. (1999) *Curr. Biol.* **9,** 257–260
28. Ford, M. G. J., Pearse, B. M. F., Higgins, M. K., Vallis, Y., Owen, D. J., Gibson, A., Hopkins, C. R., Evans, P. R., and McMahon, H. T. (2001) *Science* **291,** 1051–1055
29. Brown, F. D., Rozelle, A. L., Yin, H. L., Balla, T., and Donaldson, J. G. (2001) *J. Cell Biol.* **154,** 1007–1017
30. Wong, K., Meyers, R., and Cantley, L. C. (1997) *J. Biol. Chem.* **272,** 13236–13241
31. Cochet, C., Filhol, O., Payrastre, B., Hunter, T., and Gill, G. N. (1990) *J. Biol. Chem.* **266,** 637–644
32. Kauffmann-Zeh, A., Thomas, G. M., Ball, A., Prosser, S., Cunningham, E., Cockcroft, S., and Hsuan, J. J. (1995) *Science* **268,** 1188–1190
33. Cremona, O., and De Camilli, P. (2001) *J. Cell Sci.* **114,** 1041–1052
34. Waugh, M. G., Lawson, D., Tan, S. K., and Hsuan, J. J. (1998) *J. Biol. Chem.* **273,** 17115–17121

A Plasma Membrane Pool of Phosphatidylinositol 4-Phosphate Is Generated by Phosphatidylinositol 4-Kinase Type-III Alpha: Studies with the PH Domains of the Oxysterol Binding Protein and FAPP1

Andras Balla,* Galina Tuymetova,* Arnold Tsiomenko,* Péter Várnai,† and Tamas Balla*

*Endocrinology and Reproduction Research Branch, National Institute of Child Health and Human Development, National Institutes of Health, Bethesda, MD 20892; and †Department of Physiology, Semmelweis University, Faculty of Medicine, 1085 Budapest, Hungary

The PH domains of OSBP and FAPP1 fused to GFP were used to monitor PI(4)P distribution in COS-7 cells during manipulations of PI 4-kinase (PI4K) activities. Both domains were associated with the Golgi and small cytoplasmic vesicles, and a small fraction of OSBP-PH was found at the plasma membrane (PM). Inhibition of type-III PI4Ks with 10 μM wortmannin (Wm) significantly reduced but did not abolish Golgi localization of either PH domains. Down-regulation of PI4KIIα or PI4KIIIβ by siRNA reduced the localization of the PH domains to the Golgi and in the former case any remaining Golgi localization was eliminated by Wm treatment. PLC activation by Ca^{2+} ionophores dissociated the domains from all membranes, but after Ca^{2+} chelation, they rapidly reassociated with the Golgi, the intracellular vesicles and with the PM. PM association of the domains was significantly higher after the Ca^{2+} transient and was abolished by Wm pretreatment. PM relocalization was not affected by down-regulation of PI4KIIIβ or -IIα, but was inhibited by down-regulation of PI4KIIIα, or by 10 μM PAO, which also inhibits PI4KIIIα. Our data suggest that these PH domains detect PI(4)P formation in extra-Golgi compartments under dynamic conditions and that various PI4Ks regulate PI(4)P synthesis in distinct cellular compartments.

INTRODUCTION

Phosphoinositides have been known for some time for their signaling roles in mediating the actions of calcium-mobilizing hormones and neurotransmitters (Michell, 1975; Berridge, 1984). Phosphoinositides are also emerging as important regulators of molecular interactions critical for proper trafficking and function of cellular proteins (Martin, 1997; Odorizzi et al., 2000). There are a number of inositide kinase and phosphatase enzymes that have been shown to play a central role in the sorting of molecules to specific organelles (Fruman et al., 1998; Odorizzi et al., 2000). Phosphatidylinositol (PI) 4-kinases (PI4Ks), on the other hand, have long been considered only in the context of synthesis of polyphosphoinositides, the precursors of the PLC-generated second messengers, Ins(1,4,5)P$_3$ and diacylglycerol in agonist-stimulated cells. This picture has begun to change only when the

first two PI4Ks, Pik1 and Stt4, were cloned in yeast (Flanagan et al., 1993; Garcia-Bustos et al., 1994; Yoshida et al., 1994), and it was shown that the two proteins assumed nonredundant functions, related to Golgi to membrane trafficking and to cell-wall biogenesis, respectively (Hama et al., 1999; Walch-Solimena and Novick, 1999; Audhya et al., 2000). The mammalian homologues of the yeast enzymes, the type-III PI4ks have been identified as the wortmannin (Wm)-sensitive enzymes responsible for the synthesis of the hormone-sensitive pools of PI(4)P and PI(4,5)P$_2$ (Nakanishi et al., 1995; Downing et al., 1996). However, localizations of the two type-III enzymes in mammalian cells are not particularly consistent with their function at the plasma membrane, the type-IIIβ enzymes being localized primarily to the Golgi (Wong et al., 1997), whereas the type-IIIα is found at the ER (Wong et al., 1997) and in the pericentriolar area that possibly also contains the Golgi compartment (Nakagawa et al., 1996). In addition to being produced by type-III PI4Ks, PI(4)P is also generated by the type-II PI4Ks, a separate family of Wm-insensitive enzymes that have been cloned recently and that also exist as an α and β form (Barylko et al., 2001; Minogue et al., 2001; Balla et al., 2002; Wei et al., 2002). The localization of these latter enzymes is more complex in that the endogenous forms are found in localization to *trans*-Golgi (Wei et al., 2002; Wang et al., 2003), whereas the expressed forms are also localized to endosomes, especially in the case of the type-IIα enzyme (Balla et al., 2002). This latter enzyme has also been found in noncaveolar Rafts (Minogue et al., 2001), and in a subcompartment of the ER (Waugh et

Abbreviations used: BFA, brefeldin A; GFP, enhanced green fluorescent protein; mRFP, monomeric red fluorescent protein; OSBP, oxysterol-binding protein; PI, phosphatidylinositol; PI4K, phosphatidylinositol 4-kinase; PI(4)P, phosphatidylinositol 4-phosphate; PI(4,5)P$_2$, phosphatidylinositol 4,5-bisphosphate; PH, pleckstrin homology; Wm, wortmannin.

al., 2003) and has been purified from the secretory granules of adrenal chromaffin cells (Barylko *et al.,* 2001). The only enzyme that has been shown to translocate to the plasma membrane in stimulated cells was the type-IIβ enzyme using a Rac-dependent mechanism (Wei *et al.,* 2002). Nonetheless, type-II PI4K activity has been shown to associate with epidermal growth factor (EGF) receptors (Kauffmann-Zeh *et al.,* 1994) and with another group of membrane proteins, the tetraspanins (Berditchevski *et al.,* 1997). All of these data suggest that localization alone cannot unveil the multiple roles of the PI4Ks and there is a need for additional methods that can assess the activity of these enzymes in the various cellular compartments preferably in living cells.

Recent advances in understanding the nature of phosphoinositide-protein interactions and the detailed characterization of protein domains that specifically recognize inositol lipids (Hurley and Meyer, 2001; Lemmon, 2003) allowed dynamic imaging of several phosphoinositide species in living cells (Balla *et al.,* 2000; Balla and Varnai, 2002). Among these, the pleckstrin homology (PH) domains have been particularly popular because of their often (but not always) specific and high-affinity binding to specific phosphoinositides (Lemmon and Ferguson, 2000; Yu *et al.,* 2004). The PH domains of the OSBP and FAPP1 proteins have been shown to recognize PI(4)P very specifically in vitro (Dowler *et al.,* 2000). A detailed characterization of the cellular localization of these PH domains in yeast, on the other hand, led to the conclusion that in addition to PI(4)P, their localization is also determined by protein-protein interactions (Levine and Munro, 2002).

In the present study, we used the PH domains of the OSBP and FAPP1 proteins together with various manipulations of PI4K activities to obtain further spatial information about PI(4)P production by the distinct enzymes and about the usefulness of these PH domains for such analyses. In agreement with previous reports, our studies show that in steady state, the two PH domains detect PI(4)P formation in the Golgi by a mechanism that is also Arf1 dependent. However, our data also suggest that during de novo synthesis, both PH domains can reveal active PI(4)P formation in non-Golgi membranes and that distinct PI4Ks are responsible for the generation of this lipid in the various membrane compartments.

MATERIALS AND METHODS

Reagents

Ionomycin, Wm, and BAPTA were purchased from Calbiochem (La Jolla, CA), and brefeldin A (BFA) from Epicenter Technologies (Madison, WI). The primary antibody of gm130 was obtained from BD Transduction Laboratories (Franklin Lakes, NJ) and the monoclonal anti HA antibody (HA1.1) was form Covance (Berkley, CA). The polyclonal antibody against the type-IIα PI4K was kindly provided by Drs. Jun Guo and Pietro DeCamilli. The antibody against the PI4KIIIα was obtained by immunization of New Zeeland Rabbits with the peptide, KYLTASQLVPPDNQDTRS conjugated to KLH (Covance), and affinity purification of the immune-sera using the same peptide conjugated to Sulfolinc gel (New England Peptide, Gardner, MA) The secondary antibodies, Alexa-595 and Alexa-488 were from Molecular Probes (Eugene, OR). The lipofectamine 2000 reagent was purchased from Invitrogen (Carlsbad, CA).

DNA Constructs and Transfections

The PH domain of OSBP (residues 87–189) has been amplified from human brain cDNA (Quick-clone, Clontech, Palo Alto, CA) using the primer pairs of: fw: 5′-tttagatctggctcggctcgagagggctggctc-3′, rev: 5′-aaagaattctgccagcatcttcacagctttggc-3′. The PH domain of FAPP1 (residues 1–101) was amplified from a partial human EST clone: (IMAGE id: 287618) with the following primers: fw: 5′-aaagaattcaccatggaggggggtgttgtacaag-3′, rev: 5′-aaaggatccttagtccttgtatcagtcaaacatgc-3′. Both PH domains were subcloned into the pEGFP plasmid, pEGFP-C1 (*Bgl*II/*Eco*RI) and pEGFP-N1 (*Eco*RI/*Bam*HI) for the OSBP and FAPP1 PH-domains, respectively, in frame with the GFP protein. Mutations

were generated with the QuikChange mutagenesis kit of Stratagene (La Jolla, CA). The construct containing the transmembrane targeting sequence of the β1,4-galactosyl transferase enzyme fused to GFP (N-GT-GFP) was created from the commercially available CFP-fused construct (Clontech) by exchanging the CFP to GFP. For siRNA studies, the double-stranded RNAs corresponding to nucleotides 888–908 of human PI4KIIα (NM_018425; Wang *et al.,* 2003), 2684–2704 of PI4KIIIβ (NM_002651), and 1072–1092 of PI4KIIIα (NM_058004) were used. In some experiments, a pool of five different siRNAs (against sequences: 1072–1092, 1244–1264, 4516–4536, 6175–6195, and 6325–6345) were mixed and used to knock down the PI4KIIIα enzyme. Silencing RNAs were obtained from Qiagen (Valencia, CA). COS-7 cells (10^5 cells in 2 ml) were plated in 35-mm culture dishes 1 d before transfection with 20 μl of 20 μM siRNA using Oligofectamine (Invitrogen). After 6 h, the medium was changed to DMEM containing fetal bovine serum (FBS). Transfection with the siRNAs was repeated 24 h later, and cells were transfected with plasmid DNAs on the third day using Lipofectamine 2000. Cells were then studied on the following day either live or after fixation and immunostaining. The effect of siRNA treatment on the PI4K expression levels was also determined by Western blot analysis.

Immunocytochemistry and Confocal Microscopy

For immunostaining, COS-7 cells were grown on coverslips and fixed in 2% formaldehyde in phosphate-buffered saline (PBS; pH 7.4) for 10 min at room temperature. After three washes with PBS (5 min each), fixed cells were incubated in blocking solution (10% FBS and 0.2% Saponin in PBS) for 1 h to decrease the nonspecific binding of the antibodies and to improve the penetration of the antibodies through membranes. This blocking solution was also used for diluting the primary antibody (gm130 [1:500] or anti HA [1: 500]), and cells were incubated for 1 h. After three washes, cells were incubated in the same buffer with a fluorescent secondary antibody (1:1000) for 1 h at RT. This was followed by a last washing step (3 times for 5 min, in PBS), and then the cells were rinsed with distilled water, air-dried, and mounted on glass slides using Cytoseal 60 mounting medium (Stephens Scientific, Riverdale, NJ). Cells were then analyzed by using an inverted Zeiss LSM-410 or LSM-510 scanning laser confocal microscope (Thornwood, NY) or an Olympus IX70 inverted microscope (Melville, NY) equipped with a CCD camera (Hamamatsu, ORCA ER, Bridgewater, NJ) and a lambda DG-4 illuminator (Sutter, Novato, CA). Live cells were studied at 35°C using a temperature-controlled chamber (Harvard Instruments, Boston, MA) and an objective heater (Bioptech, Butler, PA).

Analysis of FRET in Cell Suspension

To have a quantitative measure of membrane localization of the various constructs, the CFP and YFP variants of all fusion proteins were created. These were cotransfected into COS-7 cells that were cultured in 10-cm culture dishes. One day after transfection, cells were removed from the dishes by mild trypsinization, washed, and centrifuged. Cells (~3–5 million) were then resuspended in 2 ml of the Krebs-Ringer solution described above and placed in the thermostated cuvette holder of a fluorescence spectrophotometer used for ratiometric Ca^{2+} measurements. Recordings were made using an excitation of 425 nm and calculating a ratio from the emissions detected at 525 and 475 nm (20 nm bandwidth, each). Ionomycin (10 μM) was used to activate endogenous phospholipase C to hydrolyze the phospholipids and the decrease in the 525/475 ratio was taken as an index of translocation of the domains from the membrane to the cytosol (see van Der Wal *et al.,* 2001 and Várnai and Balla, 1998 for details concerning the FRET approach, and ionomycin manipulation, respectively). Digitonin (15 μg/ml) was added at the end of the incubations so that the domains dissociate away from FRET distance. The slight baseline drift (which was increased by high Wm concentrations) was fitted for the control period and was subtracted from the traces. Traces were reproduced at least three times in independent experiments.

RESULTS

Cellular Distribution of the OSBP- and FAPP1-PH-GFP Proteins

Both PH domains were expressed as GFP fusion proteins and their positions relative to GFP were designed to follow those in their native proteins, i.e., FAPP1-PH was N-terminally and OSBP-PH C-terminally placed relative to GFP. Fusion proteins were expressed in COS-7 cells and were examined in a scanning laser confocal microscope either in live cells or after fixation with 2% paraformaldehyde. Occasionally, fixed cells were also examined in a wide-field fluorescence microscope equipped with a CCD camera. As observed earlier by the Munro group (Levine and Munro, 1998, 2001, 2002), both PH domains showed primarily Golgi localization (Figure 1). There was a sig-
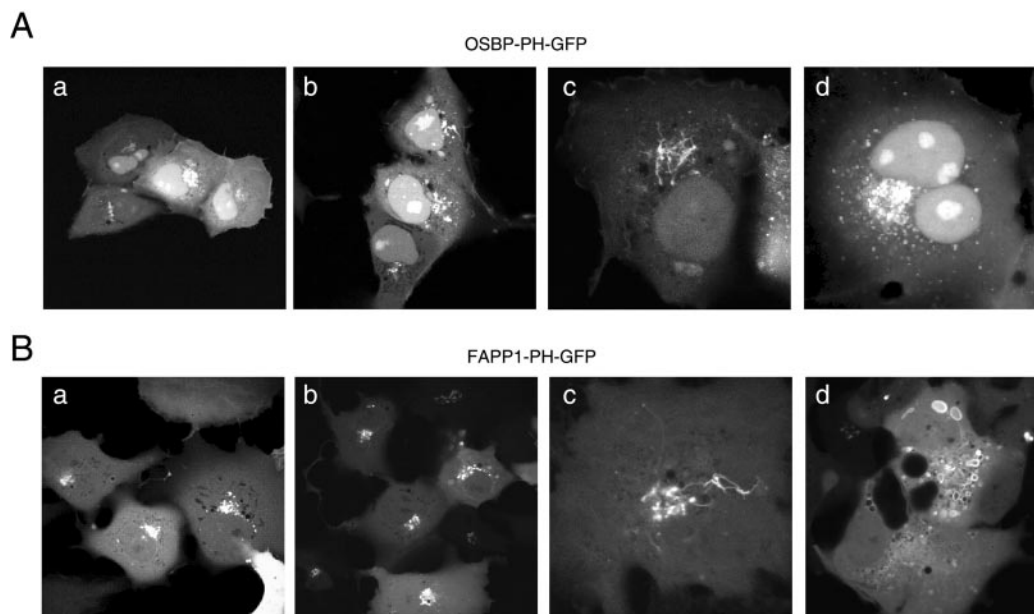
A. Balla *et al.*

Figure 1. Cellular distribution of OSBP-PH-GFP (A) and FAPP1-PH-GFP (B) expressed in COS-7 cells. Cells were transiently transfected with the indicated PH domain-GFP chimera for 24 h, and live cells were studied by confocal microscopy at 35°C. In most cells showing low-to-moderate expression levels both constructs show localization to the Golgi compartment (a and b panels in both A and B). In many cells expressing low levels of either construct dynamic tubular structures emanate from the Golgi, reminiscent of the effects of early BFA treatment (panels c). At higher expression levels, OSBP-PH showed several small vesicles around the Golgi area and also in more peripheral locations, whereas the FAPP1-PH domain generated multiple larger vesicles strongly positive for the domain in their limiting membranes (panels d on A and B, respectively). Notable difference is the nuclear accumulation of OSBP-PH but not FAPP1-PH, especially in cells expressing the protein at higher levels.

nificant heterogeneity in the morphology of cells in that some cells showed a very pronounced small vesicular distribution of OSBP-PH-GFP, especially at high expression levels, whereas in some cases a clear filamentous structure extending from the Golgi was observed (e.g., Figure 1). Such filaments were even more pronounced with the FAPP1-PH-GFP, but at higher expression levels, this construct caused the accumulation and aggregation of large cytoplasmic vesicles with FAPP1-PH-GFP in their walls and a parallel loss of Golgi localization. This was never observed with the OSBP-PH domain. A further difference between the distributions of the two proteins was the prominent nuclear accumulation of the OSBP-PH domain, which was not characteristic of the FAPP1-PH domain (Figure 1). When the distribution of the proteins was studied in fixed, rather than live cells, the localization of the OSBP-PH was very similar to that observed in live-cells, but the FAPP1-PH domain also appeared more in filamentous structures and the larger vesicular structures were not obvious in the fixed and immunostained samples. Mutant forms of the proteins (R18L-FAPP1-PH) or (R107E,R108E-OSBP-PH), which prevents their PI(4)P binding showed no localization to the Golgi (unpublished data), consistent with earlier findings (Levine and Munro, 2002).

Effects of PH Domains on Golgi Morphology and Function

Next, we analyzed whether expression of the constructs altered the Golgi morphology especially because many cells expressing either of the constructs showed a filamentous tubular structure that was reminiscent of the acute effect of

BFA on the Golgi. To assess Golgi morphology, we used either immunostaining for the endogenous *cis*-Golgi marker gm130 or the transmembrane domain of the β1,4-galactosyl transferase enzyme fused to GFP (N-GT-GFP) in live cells. As shown in Figure 2A, expression of either the OSBP- or FAPP1-PH-GFP caused tubulation and dispersion of the *cis*-Golgi marker. Importantly, the colocalization of the domains with the *cis*-Golgi marker was progressively lost in cells expressing higher levels of the fusion proteins (compare the structures shown by the arrows on Figure 2A). For a simultaneous detection of a Golgi marker with the PH domains in live cells, the latter were also created as RFP fusion proteins using the mRFP protein, which does not oligomerize (Campbell *et al.*, 2002) in place of GFP. In these studies a GFP construct containing the N-terminal segment including the transmembrane domain of the β1,4-galactosyl transferase enzyme (N-GT-GFP) was used as a Golgi marker (Yamaguchi and Fukuda, 1995). In this construct, the GFP is located in the lumen of the Golgi. This marker also revealed the tubulation caused by moderate expression of both PH domains (Figure 2B, top and middle rows) and a small extent of Golgi dispersion at higher expression levels of the FAPP1, but less so with the OSBP-PH domain (Figure 2B, bottom row).

Arf-1 Is Necessary for Localization of the OSBP and FAPP1-PH Domains to the Golgi

The localization of the OSBP- or FAPP1-PH domains to the Golgi area raised the possibility that Arf1 has an important role (direct or indirect) in determining the localization of the PH domain GFP fusion proteins. This has already been suggested by previous studies using the same PH domains

A

B
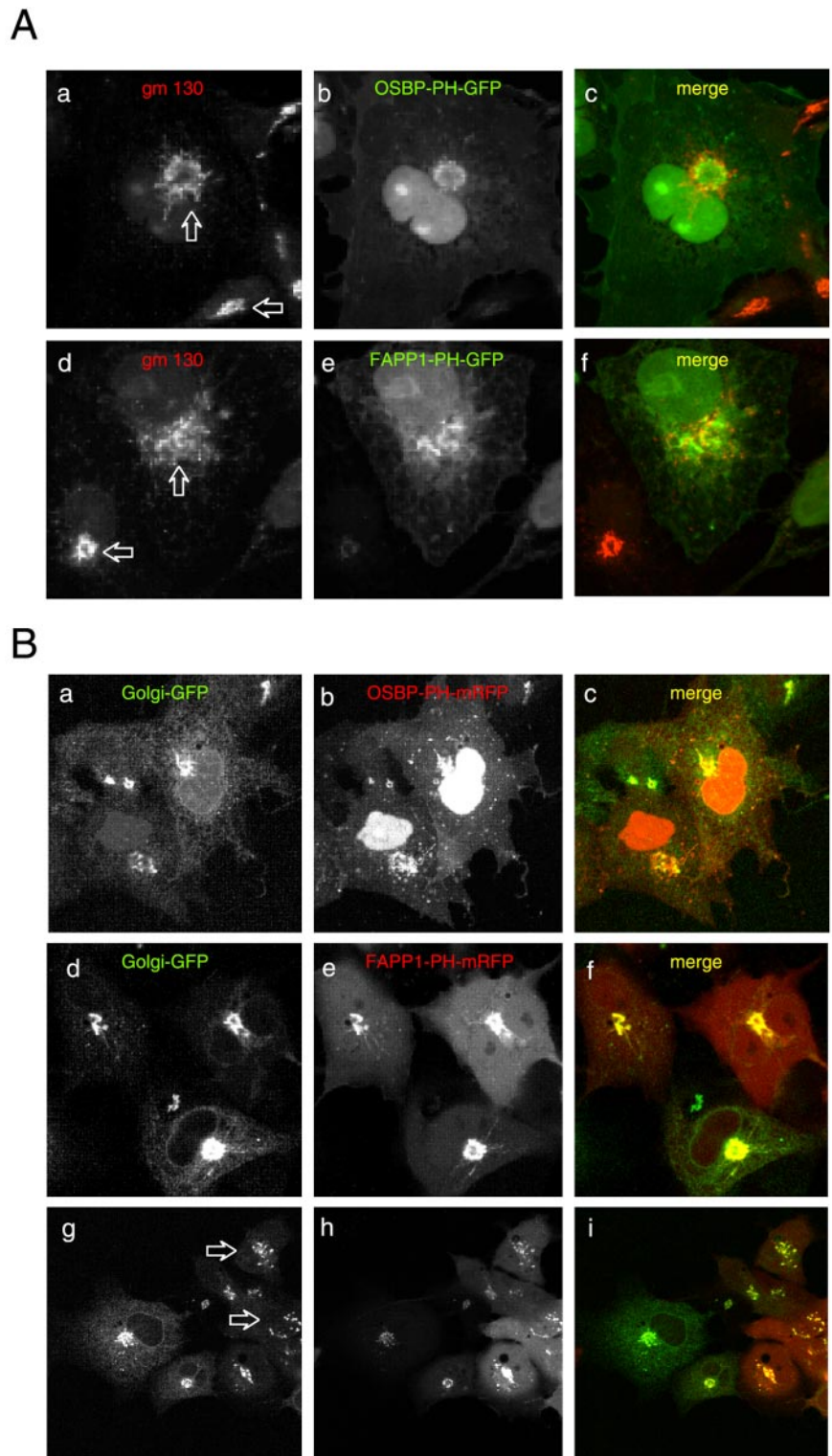
Figure 2. Effects of overexpressed OSBP- and FAPP1-PH-GFP on the distribution of Golgi markers. COS-7 cells were transfected for 24 h with either the GFP-fused (A) or the mRFP-fused (B) respective PH domains and studied either as fixed cells immunostained for the *cis*-Golgi marker, gm130 (A) or co-transfected with a GFP construct containing the N-terminal transmembrane domain of the β1,4-galactosyl transferase enzyme (Golgi-GFP) and observed live (B). Note the fragmentation and tubulation of the *cis*-Golgi marker in the cells expressing higher levels of either PH domains (compare the structures indicated by the two arrows on A) and the loss of tight colocalization observed in cells expressing the constructs at low level. (B) Similar fragmentation of the Golgi was observed in live cells expressing high levels of the FAPP1-PH-mRFP (arrows in bottom row), but this effect was not so prominent with the OSBP-PH-mRFP (top row).

(Levine and Munro, 2002; Godi *et al.,* 2004), and it has been shown that PI4K-IIIβ also associates with and is regulated by Arf1 in mammalian cells (Godi *et al.,* 1999). Therefore, we investigated whether inhibition of Arf1 GDP/GTP exchange by BFA has an effect on the localization of the OSBP- or FAPP1-PH domains. As shown in Figure 3, addition of BFA (5 μg/ml) led to the rapid release of both the FAPP1- and OSBP-PH domains from the Golgi in most of the cells. Importantly, the BFA-induced dissociation of the OSBP-PH was consistently faster than that of the FAPP1-PH (Figure 3). In contrast to the Golgi, OSBP-PH associated with small intracellular vesicles was resistant to BFA treatment and so were the large vesicles present in cells that expressed high concentrations of the FAPP1-PH domain (unpublished data).

A. Balla *et al.*

OSBP-PH
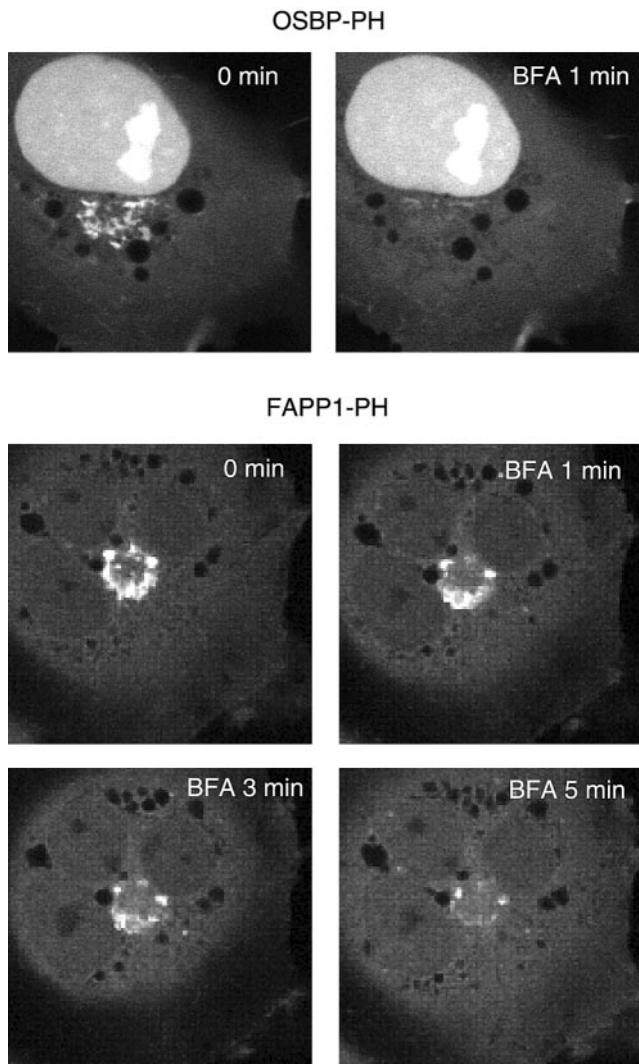
FAPP1-PH

Figure 3. Effects of brefeldin A (BFA) treatment on the localization of OSBP- and FAPP1-PH-GFP in COS-7 cells. Cells were transfected with the indicated constructs and live cells were examined by laser confocal microscopy 24 h later at 35°C. (A) After addition of BFA (5 μg/ml) OSBP-PH-GFP dissociated from the Golgi very rapidly (within 1 min), whereas the FAPP1-PH domain required a longer period (3–5 min).

Effects of PI4K Inhibition or Down-regulation on PH Domain Localization

To inhibit the activity of the type-III PI 4-kinases, we treated the cells with high concentrations (up to 10 μM) of Wm. Pretreatment of cells with 10 μM Wm at 37°C decreased the number of cells showing prominent localization at the Golgi and changed the localization to a more dispersed vesicular pool. Nonetheless, there were still a significant number of cells in which the OSBP- or FAPP1-PH domains were associated with the Golgi area after treatment of the cells for 1 h with up to 10 μM Wm and even the formation of tubular structures could be observed (Figure 4A). In some cases it was possible to find the same cell before and after Wm administration or to monitor the change in the PH domain distribution during Wm treatment (Figures 4B and 5). Overall, there was a great variability in the Wm-sensitive fraction of the Golgi localization with both PH domains.

We also used small interfering (si)RNA to evaluate the importance of the specific PI4Ks in providing the PI(4)P for localization of the PH domains. Cells were treated for 2 d with siRNA designed against PI4KIIIβ, PI4KIIα, or PI4KIIIα and transfected for 1 d with the PH-GFP constructs. PI4KIIIα knock-down cells showed no major alteration in their PH domain localization patterns (unpublished data). In case of PI4KIIIβ knock-down, a significant number of cells showed no or little Golgi localization with either PH domains and the remaining localization was found in dispersed vesicular structures that did not show the usual Golgi morphology (Figure 5A). Knock-down of the PI4KIIα also impaired Golgi localization, but its effect was not as dramatic with the FAPP1-PH domain as with OSBP-PH in the live cells (Figure 6A). When cells were fixed and immunostained for the respective kinases, it was also confirmed that in many—but not all—cells in which the kinases were largely knocked down, the Golgi localization of the PH domains was greatly reduced or eliminated (Figures 5C and 6B). However, it was important to note that in many cells after 2 d of siRNA treatment, in spite of the reduced immunostaining of either kinases, there was still localization of the PH domains (unpublished data), suggesting that in a significant fraction ($\sim$50%) of cells either of the kinases can be eliminated without a dramatic effect on the steady state distribution of the PH domains. However, when cells were chosen in which the Golgi localization of the PH domains was relatively well preserved after knock-down of PI4KIIα, this residual localization was completely eliminated by Wm (10 μM) treatment (Figure 7).

Manipulations of Cellular Ca^{2+} Affects the Distribution of OSBP and FAPP1-PH-GFP Proteins

The experiments described so far gave information on the steady state distribution of the PH domains. To determine whether rapid elimination of the inositol lipids have an effect on the distribution of the PH domains, we used activation of the endogenous PLC enzymes so that all of the PI(4,5)P$_2$ and PI(4)P is acutely eliminated from the cells. This was achieved by ionomycin treatment that has been shown to be an effective way of hydrolyzing all of the PI(4)P and PI(4,5)P$_2$ in the membranes (Várnai and Balla, 1998). As shown in Figure 8A, ionomycin treatment induced the release of the OSBP-PH domain from the membranes, including the Golgi membranes with a parallel increase in the cytoplasmic fraction of the protein. Chelation of the Ca^{2+} that decreases PLC activity, hence allowing the replenishment of the lipids via resynthesis, caused a reappearance of the PH domains at the Golgi, as well as on the surface of small vesicles in the cytoplasm and importantly, at the plasma membrane. The plasma membrane association of the PH domain was significantly stronger after the Ca^{2+} increase and chelation than prior to the ionomycin treatment (Figure 8, A and B). This plasma membrane association was much more prominent with the OSBP- than with the FAPP1-PH domain (compare Figures 8 and 9). When these experiments were performed in cells after treatment with high concentrations of Wm (1–10 μM), the association of the OSBP-PH domain with the plasma membrane was almost completely abolished, whereas some reassociation of the domain with the Golgi and the intracellular vesicles were still observed (Figure 8A). It is important to note that no prominent translocation of either PI4KIIIα or PI4KIIIβ to the plasma membrane was observed under the same conditions (unpublished data).

Because these changes were relatively robust, we tried to quantitate them using the FRET approach that we have
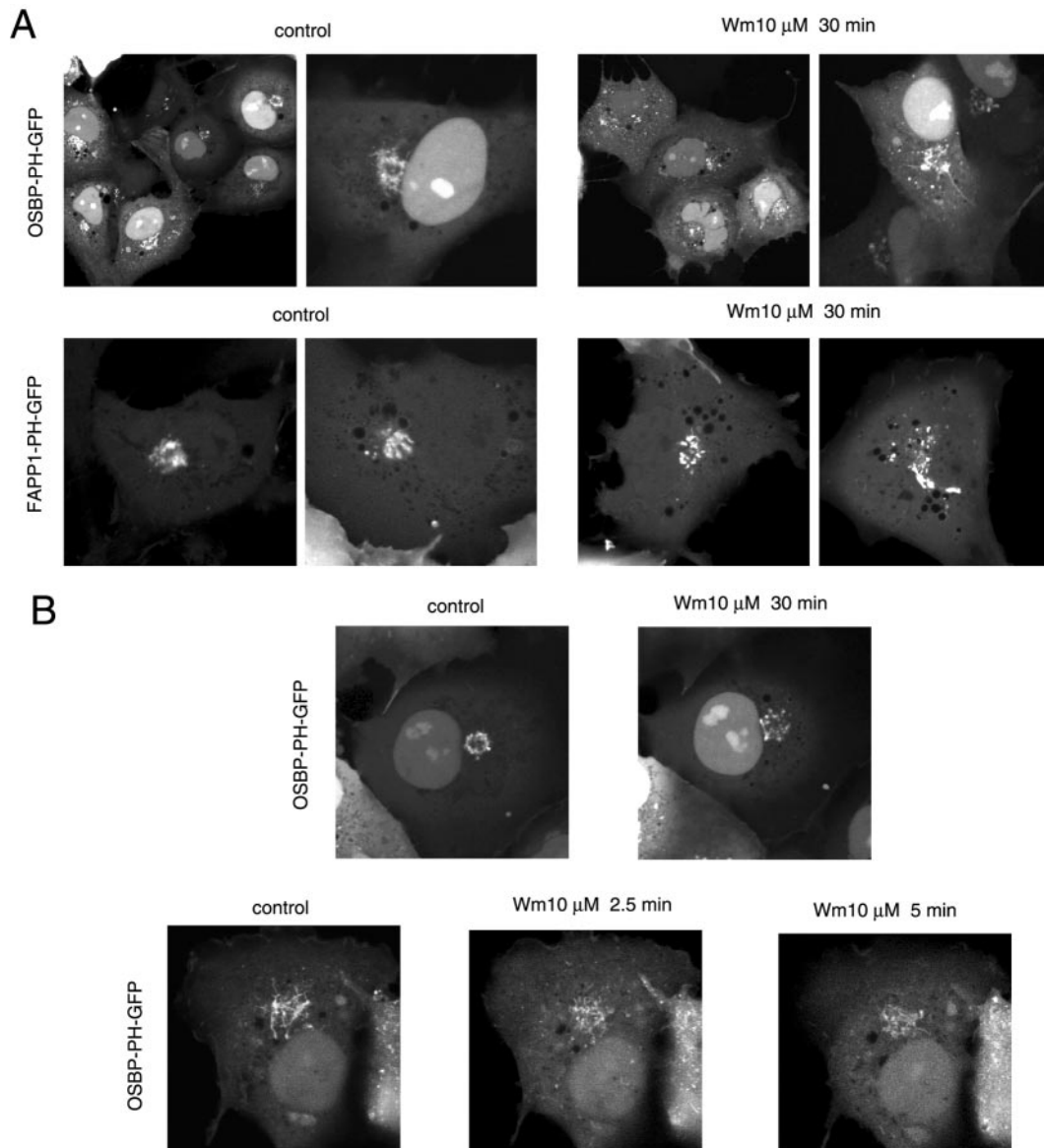
Figure 4. Effects of wortmannin (Wm) treatment on the localization of the OSBP or FAPP1-PH-GFP fusion proteins in COS-7 cells. COS-7 cells were transfected with the indicated PH-GFP construct for 24 h and studied as live cells by confocal microscopy. (A) Cells were treated with 10 μM Wm for 30 min (at 37°C) to fully inhibit the type-III PI4Ks. There was a decrease in the Golgi localization of both PH domains after Wm treatment, but there was still a significant localization in vesicular compartments, often associated with the Golgi area. In most cases these vesicles were more dispersed than those in untreated cells. (B) The difference between pre- and post-Wm treatment is illustrated in a cell that was recorded both before and after the Wm treatment. The bottom panel shows a cell that rapidly loses some of its OSBP-PH domain localization after Wm treatment. Figure 7 shows additional examples of the effects of Wm treatment on the Golgi localization.

used before (van Der Wal *et al.,* 2001; Varnai *et al.,* 2002). For this purpose, the CFP- and YFP-tagged versions of the respective PH domains were created and coexpressed in COS-7 cells. Cells were then removed from the culture plates with mild trypsinization and incubated in a fluorescence spectrophotometer for ratiometric measurements of YFP/CFP ratios using CFP excitation at 425 nm. As shown before (van Der Wal *et al.,* 2001), when the PH domains with the CFP and YFP fluorophores are bound to the membrane they are within FRET distance, whereas being in the cytoplasm they are not. Therefore, the FRET signal is a good reflection of the localization of the domains to the cellular membranes. As shown in the graph

in Figure 8A, ionomycin treatment slowly decreased the FRET signal between the OSBP-PH-YFP/OSBP-PH-CFP pairs and similarly for the FAPP1-PH-YFP/FAPP1-PH-CFP pairs (Figure 8A, graph). This signal was restored once the Ca^{2+} was removed with the Ca^{2+} chelator BAPTA or EGTA. There was clearly a larger FRET signal after the Ca^{2+} chelation observed with the FAPP1-PH domains than before ionomycin addition (Figure 9A, graph inset). This was obscured in the case of the OSBP-PH domain by the high initial FRET values probably originating from the highly concentrated presence of the domains in the nucleus (Figure 8A, graph). There was no increase in the FRET signal after BAPTA (or EGTA)

A. Balla *et al.*

Figure 5. Effects of down-regulation of the type-IIIβ PI4K by siRNA treatment on the localization of OSBP- and FAPP1-PH-GFP in live (A) and OSBP-PH-GFP in fixed (C) COS-7 cells. COS-7 cells were treated with double-stranded RNA designed to interfere with expression of PI4KIIIβ for 2 consecutive days and transfected with the PH-GFP constructs on the third day for an additional day as described in *Materials and Methods.* Cells were either studied live at 35 C (A) or analyzed after fixation and immunostaining with a polyclonal anti-PI4KIIIβ antibody (C). The arrows point to two cells in which PI4KIIIβ is largely eliminated. To determine the effect of siRNA treatment, cells treated identically with the various siRNAs directed against the three PI4K enzymes were subjected to Western blot analysis using antibodies against the respective kinases and the blots were also analyzed for actin (B). In the picture showing the effect of PI4KIIIβ knockdown the control and siRNA-treated samples were not loaded on adjacent lanes, indicated by the gap between the images. Nevertheless the images are derived from the same gel scanned and processed with identical settings.

addition without ionomycin treatment (unpublished data). Importantly, in both cases, a significant fraction (~50–60%) of the FRET increase after ionomycin and BAPTA treatment was abolished by treatment of the cells with 10 μM Wm (Figures 8A and 9A, graphs). At lower concentrations of Wm (10–100 nM) that inhibit only the PI 3-kinases, there were no inhibitory effects observed (unpublished data).

To assess the fraction of the PH domains associated with the plasma membrane, we performed FRET measurements by pairing the OSBP- or the FAPP1-PH domain CFP chimera with the YFP-fused PLCδ$_1$PH domain. Because the PLCδ$_1$PH-YFP protein localizes primarily to the plasma membrane and follows a translocation to and from the cytosol in response to ionomycin and BAPTA treatment, respectively (Várnai and Balla, 1998), the FRET between the PLCδ$_1$PH-YFP and CFP-fused OSBP- or FAPP1-PH domain reflects the interaction between these domains at the plasma membrane. This is illustrated in Figures 8 and 9 (panels B), where the translocation of the PLCδ$_1$PH-mRFP and GFP-OSBP-PH proteins were followed simultaneously during ionomycin and BAPTA treatment. As shown in Figure 8, the

FRET signal between the CFP-OSBP-PH and PLCδ$_1$PH-YFP is relatively modest under basal conditions and decreases in response to ionomycin treatment, reflecting the disappearance of the small initial association of the OSBP-PH with the plasma membrane. After BAPTA treatment, there was a large increase observed in the FRET signal, reflecting the increased association of the two PH domains at the plasma membrane. This response was, again, greatly inhibited by Wm treatment (Figure 8B, graph). Consistent with the morphological findings, the FRET signal was much smaller between the FAPP1-PH-CFP and PLCδ$_1$PH-YFP constructs (hence the noisier trace in Figure 9B, graph), indicating that FAPP1-PH barely associates with the plasma membrane under basal steady state conditions. There was also very little change after ionomycin treatment, and only after Ca^{2+} chelation was an increase in the FRET signal observed. This increase was, again, greatly inhibited by Wm treatment. These data together suggested that after a large Ca^{2+} transient, there is a significant type-III PI 4-kinase–dependent association of the OSBP-PH and to a lesser degree of the FAPP1-PH domain with the plasma membrane.
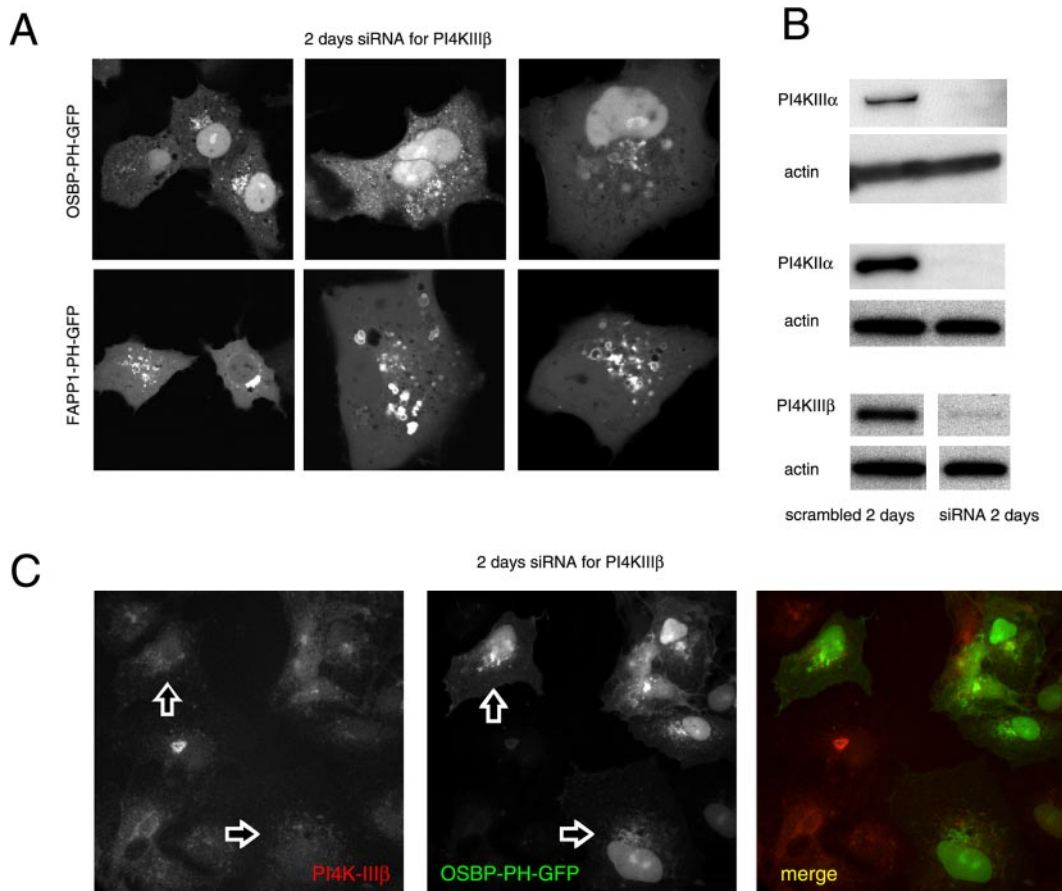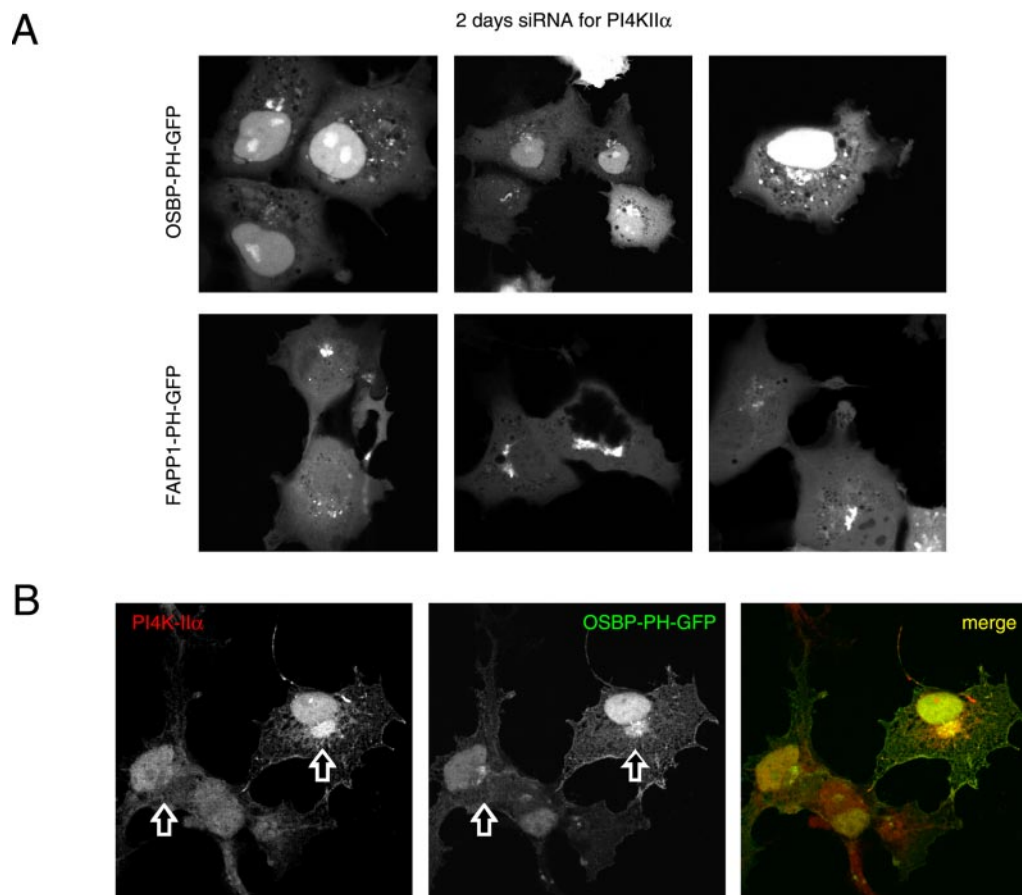
Figure 6. Effects of down-regulation of the type-IIα PI4K by siRNA treatment on the localization of OSBP- and FAPP1-PH-GFP in live (A) and OSBP-PH-GFP in fixed (B) COS-7 cells. COS-7 cells were treated with double-stranded RNA designed to interfere with expression of PI4KIIα for 2 consecutive days and transfected with the PH-GFP constructs for an additional day as described in *Materials and Methods*. Cells were either studied live at 35°C (A) or analyzed after fixation and immunostaining with a polyclonal anti-PI4KIIα antibody (B; Guo *et al.,* 2003). The arrows point to the Golgi area of two cells, one in which the PI4KIIα is largely eliminated and another in which it is still readily detectable.

The Role of PI4K Enzymes in the Redistribution of the PH Domains after Ionomycin Treatment and Ca²⁺ Chelation

To assess whether any of the two type-III PI 4-kinases was responsible for the Wm-sensitive PH domain redistribution to the plasma membrane, similar experiments were performed in COS-7 cells after down-regulation of the various PI4K isoforms by 2-d treatment with siRNA. These experiments were performed either in live cells (Figure 10) or in cells that were fixed after the ionomycin/EGTA treatment and processed for immunocytochemistry to determine the extent of knock-down (unpublished data). Down-regulation of either PI4KIIIβ or PI4KIIα failed to impair the relocalization of the PH domains to the plasma membrane after ionomycin/EGTA treatment and variably affected the Golgi localization (Figure 10, B and C). In some cells the Golgi localization was minimal; in others it was still detectable after the treatment. In contrast, down-regulation of PI4KIIIα almost completely abolished the localization of the PH domains to the small peripheral vesicles and to the plasma membrane (Figure 10D), but did not affect their relocalization to the Golgi in most cells. As an alternative to down-regulation, we also used phenylarsineoxide (PAO) at a concentration (10 μM) that preferentially inactivates the type-IIIα PI4K isoform (Balla *et al.,* 2002). Pretreatment of the cells with 10 μM PAO for 10 min did not

have any effect on steady state localization (unpublished data), but completely prevented the relocalization of the either PH domains to the plasma membrane (Figure 10E). In the case of the FAPP1- but not OSBP-PH, PAO also impaired the relocalization of the PH domain to the Golgi. The effect of PAO was reversed by simultaneous incubation with 1 mM dithiothreitol (DTT; Figure 10F) but not with β-mercaptoethanol (unpublished data). Taken together, these experiments indicated that PI4KIIIα is the enzyme that is mainly responsible for the production of PI(4)P that reaches the plasma membrane during active phosphoinositide resynthesis.

DISCUSSION

The present experiments were designed to explore whether PI 4-kinase function can be assessed at the single cell level using PH domains that recognize PI(4)P in vitro. Recent studies in yeast have concluded that the Golgi localization of the OSBP- and FAPP1-PH domains, the two domains used in the present study, are dependent both on the function of the yeast PI 4-kinase, Pik1, and on an Arf1-dependent additional component (Levine and Munro, 2002). Our present data on COS-7 cells are in complete agreement with those conclusions, in that both the lipid component and Arf1 in its

A. Balla *et al.*

control

FAPP1-PH

PI4KIIα siRNA

FAPP1-PH

Wm 0 min   Wm 5 min   Wm 15 min   Wm 30 min

control

OSBP-PH

PI4KIIα siRNA

OSBP-PH

Wm 0 min   Wm 5 min   Wm 15 min   Wm 30 min
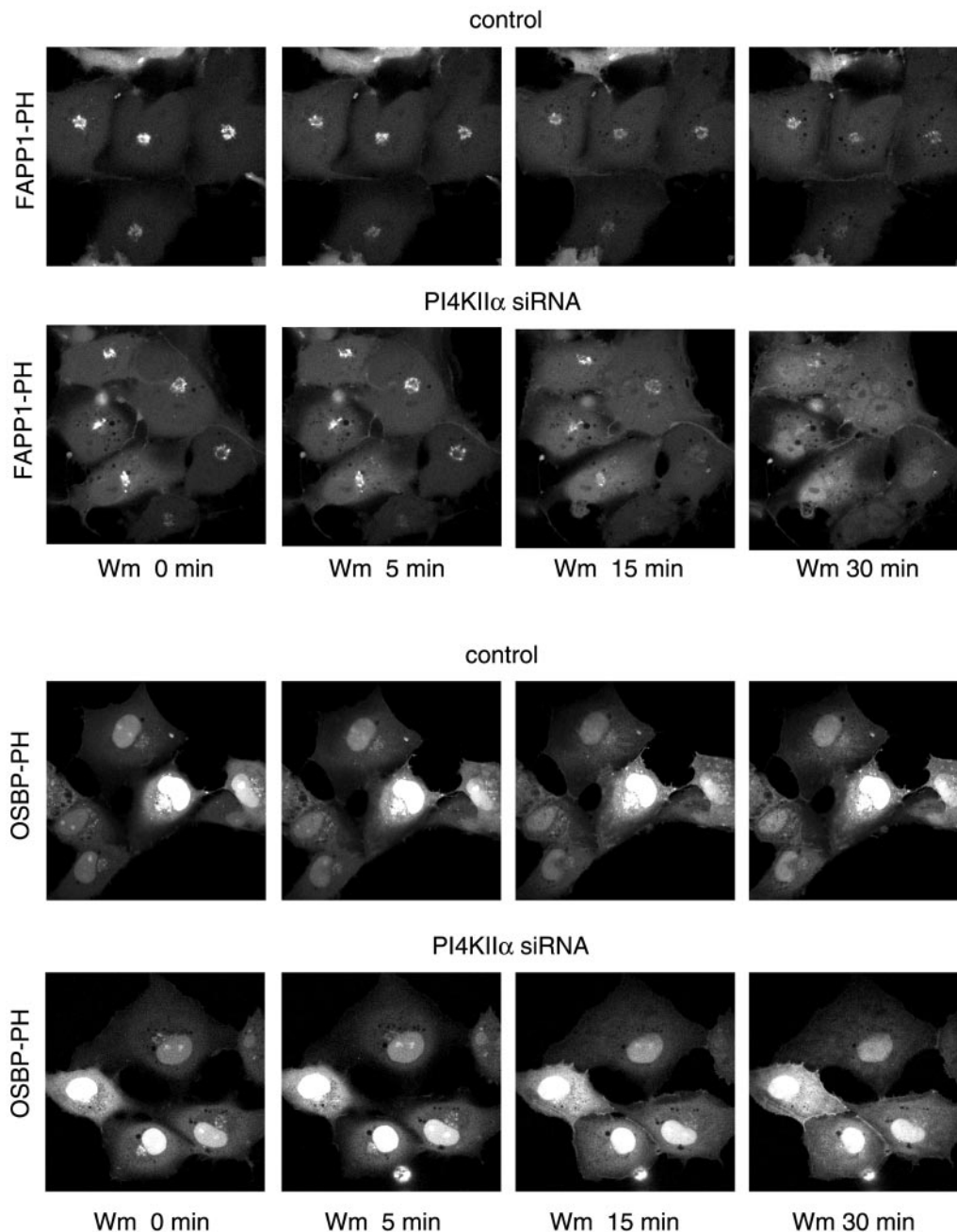
Figure 7. Effect of wortmannin treatment on the localization of the OSBP- and FAPP1-PH-GFP after 2-d treatment with siRNA against PI4KIIα. COS-7 cells were treated with siRNA and transfected with the PH domain constructs as described in the legend to Figure 5. Live cells were studied at 35°C and treated with 10 μM Wm for the indicated times. Note the complete loss of localization of the PH domains in the siRNA-treated cells but not in the controls.

GTP-bound form are necessary for efficient Golgi localization of these PH domains in steady state. However, our observations also showed that the OSBP-PH domain is also found in small vesicular compartments outside the Golgi, and the FAPP1-PH domain was also observed in a vesicular pool that became quite enlarged in cells expressing high levels of the fusion protein. Interestingly, at these extra-Golgi sites neither constructs showed the requirement for the Arf1 protein function.

An important finding of the present study was the prominent redistribution of both PH domains after Ca^{2+}-induced

PLC activation followed by Ca^{2+} removal. Both domains translocated to the cytosol in the presence of high intracellular [Ca^{2+}], and reassociated with the Golgi after Ca^{2+} chelation. However, a significant fraction of the PH domains were found in the plasma membrane after this manipulation, and this response was largely abolished by concentrations of Wm that are consistent with the involvement of type-III PI4Ks in the process. It was also noteworthy that parallel to the appearance of the PH domains at the plasma membrane, large number of small vesicles were also visible just beneath the plasma membrane. These data indicated
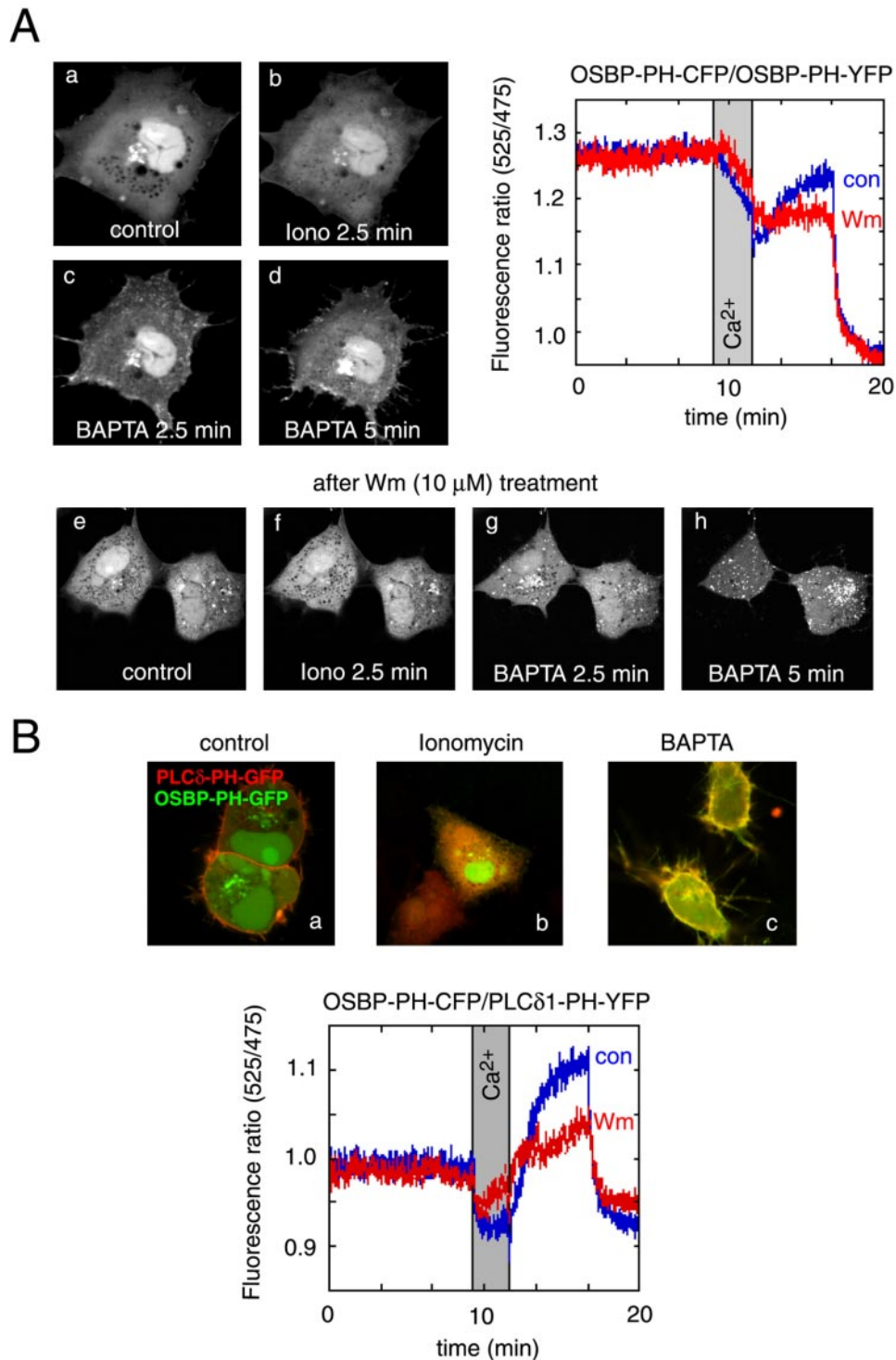
Figure 8. Effects of cytoplasmic [Ca^{2+}] increases on the distribution of the OSBP-PH-GFP fusion protein. Cells were transfected with the indicated constructs and live cells were examined by confocal microscopy (Zeiss LSM410) at 35°C. (A) Addition of ionomycin (10 μM) in the presence of 2 mM external Ca^{2+} caused the translocation of the PH domain from the Golgi to the cytoplasm. Chelation of Ca^{2+} by BAPTA restores the localization in the Golgi and induces a prominent plasma membrane localization of the PH domain. Wortmannin (Wm) pretreatment prevents the plasma membrane localization but not the vesicular localization of the PH domain after ionomycin/BAPTA treatment (A, lower series). FRET measurements between CFP- and YFP-fused OSBP-PH domains coexpressed in COS-7 cells show a high initial FRET value (probably because of the high nuclear accumulation of the constructs), which decreases after ionomycin addition, but shows a rapid increase after Ca^{2+} chelation, which is mostly sensitive to Wm (10 μM) treatment (A, graph). (B) Simultaneous monitoring of the OSBP-PH and PLCδ1-PH domain translocations by coexpression of GFP and mRFP fused PH domains, respectively. Note the prominent colocalization of the red and green signals after (but not before) the iono/BAPTA treatment. FRET measurements between the same domains fused to CFP and YFP (OSBP-PH-CFP and PLCδ1-PH-YFP) shows a small initial FRET that is abolished after ionomycin treatment and returns well above baseline after Ca^{2+} chelation. This FRET analysis shows the plasma membrane component of the OSBP-PH movement that is significantly reduced after Wm treatment.

A. Balla *et al.*

A

B
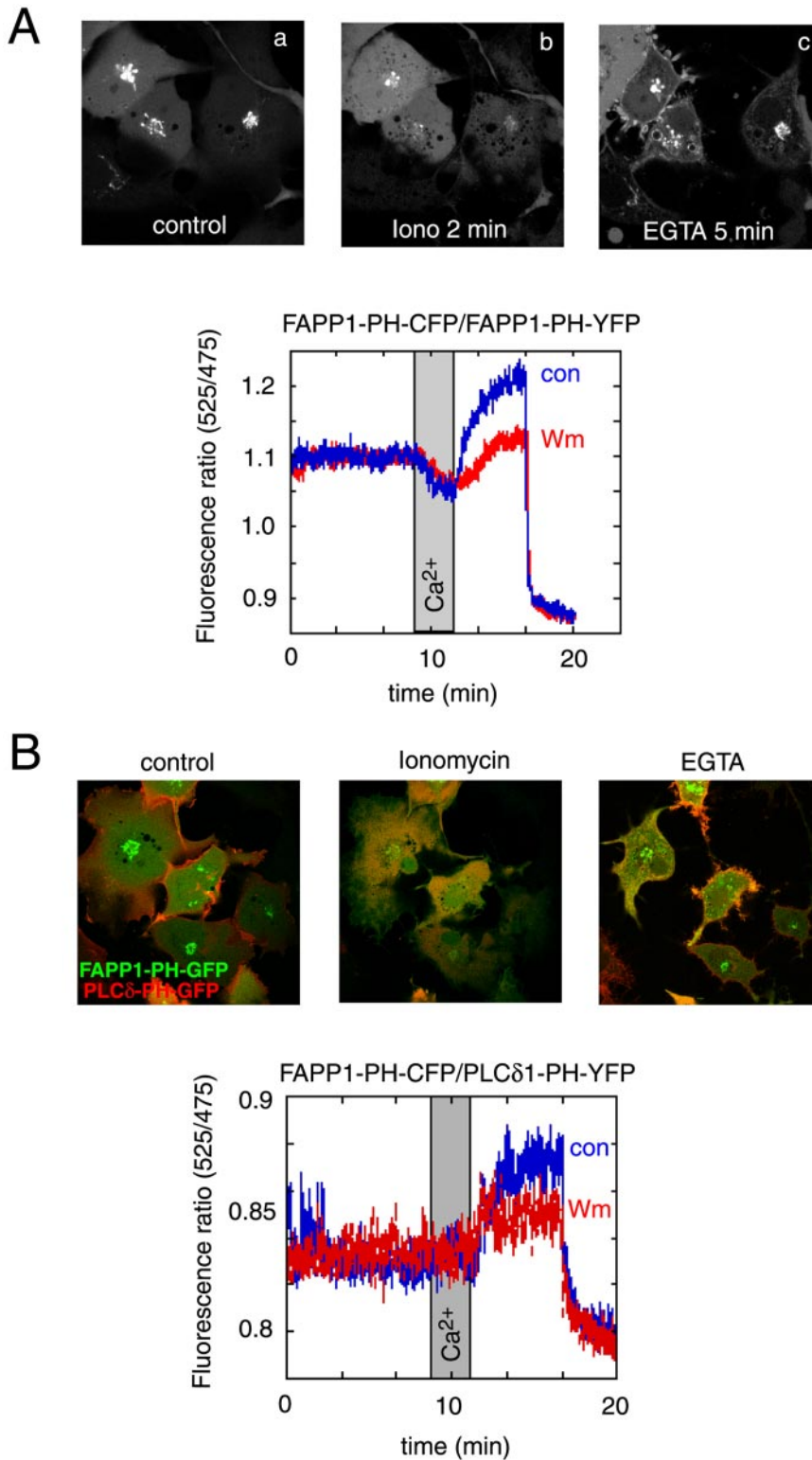
Figure 9. Effects of cytoplasmic $[Ca^{2+}]$ increases on the distribution of the FAPP1-PH-GFP fusion protein. See legend to Figure 8 for experimental details. (A) Addition of ionomycin (10 μM) in the presence of 2 mM external Ca^{2+} caused the translocation of the PH domain from the Golgi to the cytoplasm. Chelation of Ca^{2+} by EGTA restores the localization in the Golgi but the plasma membrane localization of the FAPP1-PH domain is less prominent that that of the OSBP-PH. FRET measurements between CFP- and YFP-fused FAPP1-PH domains coexpressed in COS-7 cells show a rapid decrease after ionomycin addition and show a rapid increase above basal after Ca^{2+} chelation. About 50% of this increase is sensitive to Wm (10 μM) treatment (A, graph). (B) Simultaneous monitoring of the FAPP1-PH and PLCδ1-PH domain translocations by coexpression of GFP and mRFP fused PH domains, respectively. The colocalization of the red and green signals after the iono/EGTA treatment is not as prominent as with the OSBP-PH domain. FRET measurements between the same domains fused to CFP and YFP (FAPP1-PH-CFP and PLCδ1-PH-YFP) shows no initial FRET and no change after ionomycin treatment. FRET values; however, increase above baseline after Ca^{2+} chelation. This FRET analysis shows the plasma membrane component of the FAPP1-PH movement that is smaller than with the OSBP-PH and is also significantly reduced after Wm treatment.

that PI(4)P is produced near and perhaps within the plasma membrane under these conditions and that both the OSBP- and FAPP1-PH-GFP are able to report on these changes. It is not clear at present why the localization of OSBP- or FAPP1-PH at the plasma membrane is low in resting cells. Whether this reflects low steady state PI(4)P levels at the plasma membrane or masking of this lipid by more stable

interaction(s) with other endogenous proteins are questions to be further investigated.

Given the presence of multiple PI4K isoforms in eukaryotic cells, an important question to address was whether they all contributed to the membrane localization of the OSBP- and FAPP1-PH domains. This question was approached by pharmacological means as well as by using
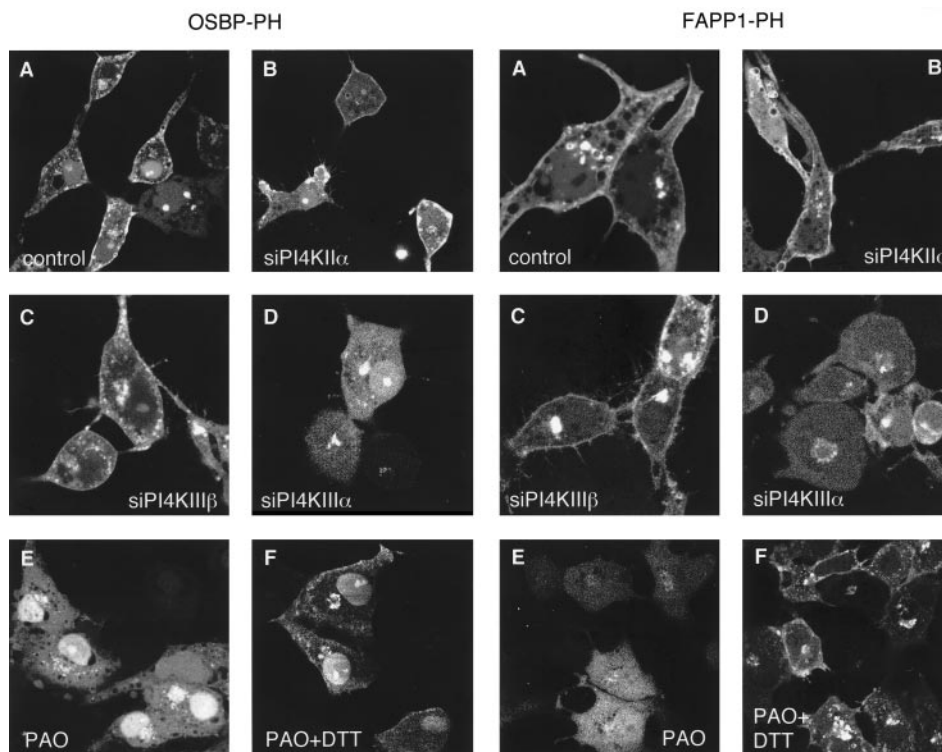
Figure 10. Relocalization of OSBP- and FAPP1PH-GFP in COS-7 cells in which PI4K isoforms were down-regulated or inhibited. Cells were treated with siRNA and transfected with the plasmid DNA as described in the legend to Figure 5. Cells were studied live on the temperature-controlled stage of a Zeiss 410 laser confocal microscope at 35°C. Cells were stimulated with ionomycin (10 μM) until most of their localized PH domains were released from the Golgi (2–3 min), at which point Ca^{2+} was chelated by the addition of EGTA (7 mM) and images were recorded after 3–7 min. When indicated, PAO (10 μM) was added 10 min before ionomycin either in the presence or absence of 1 mM DTT. Note that the prominent plasma membrane localization of both PH domains was abolished in cells treated with PAO or in which the PI4KIIIα was down-regulated.

siRNA to down-regulate the respective PI4K enzymes. These experiments showed that both the type-IIα and the Wm-sensitive type-IIIβ enzyme was involved in the Golgi localization of the PH domains. Although the endogenous type-IIIβ enzyme shows the closest colocalization with either PH domains and also with the *cis*-Golgi marker gm130, the distribution of the type-IIα enzyme is only partially overlapping with the PH domains, consistent with the reported trans-Golgi and endosomal localization of this protein (Balla *et al.,* 2002; Wei *et al.,* 2002; Wang *et al.,* 2003). In addition, the type-II enzyme (both endogenous and expressed) shows a significant amount of vesicular localization outside the Golgi, but at these sites it does not attract either of the PH domains (Balla, A., and Balla, T., unpublished observation). Based on the partial Wm sensitivity and the knock-down studies, the function of the type-IIIβ enzyme is clearly important for the Golgi localization of the PH domains. However, our data also show that the type-IIα enzyme also contributes to PI(4)P formation in the Golgi, as also have been indicated by its involvement in AP-1 recruitment (Wang *et al.,* 2003). The relative contribution of the two PI 4-kinases appeared to show a great deal of variability in the COS-7 cells, and we could not find any morphological clues to predict the predominance of one over the other.

Remarkably, however, none of these enzymes was found to be necessary for the plasma membrane localization of the PH domains during active acute PI(4)P resynthesis after a strong, Ca^{2+}-mediated PLC activation. The plasma membrane recruitment of the PH domains was Wm sensitive,

was inhibited by 10 μM PAO and was largely eliminated in cells in which the PI4KIIIα was down-regulated. These data together suggest that the type-IIIα PI 4-kinase is responsible for the generation of this plasma membrane pool of PI(4)P, at least under these extreme conditions. This enzyme has been reported to localize primarily to the ER (Wong *et al.,* 1997), a finding also confirmed by our studies, and plasma membrane localization of the enzyme was not demonstrable either in unstimulated cells or after inomycin/EGTA treatment (Balla, A., and Balla, T., unpublished observation). Nevertheless, we cannot rule out the function of PI4KIIIα at the plasma membrane, and in *Saccharomyces cerevisiae* the homologue of this enzyme, Stt4 has also been shown to generate PI(4)P at the plasma membrane for subsequent conversion to PI(4,5)P$_2$ by the yeast PIP kinase, Mss4 (Audhya and Emr, 2002). However, it is also possible that PI(4)P is produced in a sub–plasma membrane vesicular pool of ER origin and the lipid is either transported to the PM or reaches the PM through dynamic exchange of these vesicles with the PM. Answering these questions will require further analysis and could reveal important new details about the generation of phosphoinositide pools at the plasma membrane.

Recently, Godi *et al.* (2004) have reported on the localization and functions of the FAPP1 and FAPP2 proteins and the importance of the PH domains in their localization. Several findings reported in that study is relevant to the discussion of our current results. Godi *et al.* (2004) have reported that the PH domains showed only partial colocalization with the

A. Balla *et al.*

cis-Golgi marker and a better colocalization with the TGN. In our studies, using COS-7 cells, both PH domains showed almost perfect colocalization with the *cis*-Golgi marker gm130 at low expression levels, but this colocalization was not maintained in cells expressing higher levels of the proteins. Godi *et al.* (1999) also showed that Arf1 is important for the localization of both PH domains and demonstrated a direct interaction between recombinant Arf1 and the PH domains. This could explain the data obtained with BFA, but it remains to be seen whether direct interaction is the sole mechanism by which Arf1 can regulate PH domain association, because Arf1 had also been shown earlier by the same authors to be important in the recruitment of the type-IIIβ PI4K. Although the nature of the PI4Ks that contribute to the recruitment of the FAPP1 and FAPP2 proteins was not the main focus of the above study, some of the data indicated the importance of the type-IIIβ PI4K. Our data are also consistent with the involvement of the type-IIIβ PI4K enzyme in the membrane recruitment of the PH domains.

In summary, our data demonstrate that PI(4)P generation at distinct membrane compartments is regulated by distinct PI 4-kinase enzymes and this process can be visualized by the FAPP1- and OSBP-PH domains. These studies also show the importance of Ca^{2+} in regulating the dynamics of the interaction of the PH domains with the various membranes. Clearly, the restrictive, Arf1-dependent steady state Golgi localization of the PH domains was dramatically changed after a cytoplasmic Ca^{2+} challenge. Whether the localization of the PH domains in the extra-Golgi compartments requires additional proteins is yet to be determined. PI4Ks are clearly emerging as important enzymes with multifaceted functions that reach far beyond the production of PI(4)P as a simple lipid precursor of plasma membrane PI(4,5)P_2 and it may be more than coincidence that all of the known PH domains that recognize PI(4)P are found in lipid-transfer proteins, such as OSBP, FAPP2, or in the recently described CERT (Hanada *et al.*, 2003). Exploration of the identity of the kinase(s) that regulate the synthesis of PI(4)P in distinct cellular compartments should aid further studies to understand the complex functions of phosphoinositides.

ACKNOWLEDGMENTS

REFERENCES

Audhya, A., Foti, M., and Emr, S. D. (2000). Distinct roles for the yeast phosphatidylinositol 4-kinases, stt4p and pik1p, in secretion, cell growth, and organelle membrane dynamics. Mol. Biol. Cell *11*, 2673–2689.

Audhya, A., and Emr, S. D. (2002). Stt4 PI 4-kinase localizes to the plasma membrane and functions in the Pkc1-mediated MAP kinase cascade. Dev. Cell *2*, 593–605.

Balla, A., Tuymetova, G., Barshishat, M., Geiszt, M., and Balla, T. (2002). Characterization of type II phosphatidylinositol 4-kinase isoforms reveals association of the enzymes with endosomal vesicular compartments. J. Biol. Chem. *277*, 20041–20050.

Balla, T., Bondeva, T., and Varnai, P. (2000). How accurately can we image inositol lipids in live cells? Trends Pharmacol. Sci. *21*, 238–241.

Balla, T. and Varnai, P. (2002). Visualizing cellular phosphoinositide pools with GFP-fused protein-modules. Sci. STKE *125*, *PL3*, 1–16.

Barylko, B., Gerber, S. H., Binns, D. D., Grichine, N., Khvotchev, M., Sudhof, T. C., and Albanesi, J. P. (2001). A novel family of phosphatidylinositol 4-kinases conserved from yeast to humans. J. Biol. Chem. *276*, 7705–7708.

Berditchevski, F., Tolias, K. F., Wong, K., Carpenter, C. L., and Hemler, M. E. (1997). A novel link between integrins, transmembrane-4 superfamily proteins (CD63 and CD81), and phosphatidylinositol 4-kinase. J. Biol. Chem. *272*, 2595–2598.

Berridge, M. J. (1984). Inositol trisphosphate and diacylglycerol as intracellular messengers. Biochem. J. *220*, 345–360.

Campbell, R. E., Tour, O., Palmer, A. E., Steinbach, P. A., Baird, G. S., Zacharias, D. A., and Tsien, R. Y. (2002). A monomeric red fluorescent protein. Proc. Natl. Acad. Sci. USA *99*, 7877–7882.

Dowler, S., Currie, R. A., Campbell, D. G., Deak, M., Kular, G., Downes, C. P., and Alessi, D. R. (2000). Identification of pleckstrin-homology-domain-containing proteins with novel phosphoinositide-binding specificities. Biochem. J. *351*, 19–31.

Downing, G. J., Kim, S., Nakanishi, S., Catt, K. J., and Balla, T. (1996). Characterization of a soluble adrenal phosphatidylinositol 4-kinase reveals wortmannin-sensitivity of Type III phosphatidylinositol 4-kinases. Biochemistry *35*, 3587–3594.

Flanagan, C. A., Schnieders, E. A., Emerick, A. W., Kunisawa, R., Admon, A., and Thorner, J. (1993). Phosphatidylinositol 4-kinase: gene structure and requirement for yeast cell viability. Science *262*, 1444–1448.

Fruman, D. A., Meyers, R. E., and Cantley, L. C. (1998). Phosphoinositide kinases. Annu. Rev. Biochem. *67*, 481–507.

Garcia-Bustos, J. F., Marini, F., Stevenson, I., Frei, C., and Hall, M. N. (1994). PIK1, an essential phosphatidylinositol 4-kinase associated with the yeast nucleus. EMBO J. *13*, 2352–2361.

Godi, A., Pertile, P., Meyers, R., Marra, P., Di Tullio, G., Iurisci, C., Luini, A., Corda, D., and De Matteis, M. A. (1999). ARF mediates recruitment of PtdIns-4-OH kinase-β and stimulates synthesis of PtdIns(4,5)P_2 on the Golgi complex. Nat. Cell Biol. *1*, 280–287.

Godi, A., Di Campi, A., Konstantakopoulos, A., Di Tullio, G., Alessi, D. R., Kular, G. S., Daniele, T., Marra, P., Lucocq, J. M., and De Matteis, M. A. (2004). FAPPs control Golgi-to-cell-surface membrane traffic by binding to ARF and PtdIns(4)P. Nat. Cell Biol. *6*, 393–404.

Guo, J., Wenk, M. R., Pellegrini, L., Onofri, F., Benfenati, F., and De Camilli, P. (2003). Phosphatidylinositol 4-kinase type IIalpha is responsible for the phosphatidylinositol 4-kinase activity associated with synaptic vesicles. Proc. Natl. Acad. Sci. USA *100*, 3995–4000.

Hama, H., Schnieders, E. A., Thorner, J., Takemoto, J. Y., and DeWald, D. B. (1999). Direct involvement of phosphatidylinositol 4-phosphate in secretion in the yeast *Saccharomyces cerevisiae*. J. Biol. Chem. *274*, 34294–34300.

Hanada, K., Kumagai, K., Yasuda, S., Miura, Y., Kawano, M., Fukasawa, M., and Nishijima, M. (2003). Molecular machinery for non-vesicular trafficking of ceramide. Nature *426*, 803–809.

Hurley, J. H., and Meyer, T. (2001). Subcellular targeting by membrane lipids. Curr. Opin. Cell Biol. *13*, 146–152.

Kauffmann-Zeh, A., Klinger, R., Endemann, G., Waterfield, M. D., Wetzker, R., and Hsuan, J. J. (1994). Regulation of human type II phosphatidylinositol kinase activity by EGF-dependent phosphorylation and receptor association. J. Biol. Chem. *269*, 31243–31251.

Lemmon, M. A., and Ferguson, K. M. (2000). Signal-dependent membrane targeting by pleckstrin homology (PH) domains. Biochem. J. *350*, 1–18.

Lemmon, M. A. (2003). Phosphoinositide recognition domains. Traffic *4*, 201–213.

Levine, T. P., and Munro, S. (1998). The pleckstrin-homology domain of oxysterol-binding protein recognizes a determinant specific to Golgi membranes. Curr. Biol. *8*, 729–739.

Levine, T. P., and Munro, S. (2001). Dual targeting of Osh1p, a yeast homologue of oxysterol-binding protein, to both the Golgi and the nucleus-vacuole junction. Mol. Biol. Cell *6*, 1633–1644.

Levine, T. P., and Munro, S. (2002). Targeting of Golgi-specific pleckstrin homology domains involves both PtdIns 4-kinase-dependent and -independent components. Curr. Biol. *12*, 695–704.

Martin, T. F. (1997). Phosphoinositides as spatial regulators of membrane traffic. Curr. Opin. Neurobiol. *7*, 331–338.

Michell, R. H. (1975). Inositol phospholipids and cell surface receptor function. Biochim. Biophys. Acta *415*, 81–147.

Minogue, S., Anderson, J. S., Waugh, M. G., dosSantos, M., Corless, S., Cramer, R., and Hsuan, J. J. (2001). Cloning of a human type II phosphatidylino-

sitol 4-kinase reveals a novel lipid kinase family. J. Biol. Chem. *276*, 16635–16640.

Nakagawa, T., Goto, K., and Kondo, H. (1996). Cloning, expression and localization of 230 kDa phosphatidylinositol 4-kinase. J. Biol. Chem. *271*, 12088–12094.

Nakanishi, S., Catt, K. J., and Balla, T. (1995). A wortmannin-sensitive phosphatidylinositol 4-kinase that regulates hormone-sensitive pools of inositolphospholipids. Proc. Natl. Acad. Sci. USA *92*, 5317–5321.

Odorizzi, G., Babst, M., and Emr, S. D. (2000). Phosphoinositide signaling and the regulation of membrane trafficking in yeast. Trends Biochem. Sci. *25*, 229–235.

van Der Wal, J., Habets, R., Varnai, P., Balla, T., and Jalink, K. (2001). Monitoring Phospholipase C activation kinetics in live cells by FRET. J. Biol. Chem. *276*, 15337–15344.

Varnai, P., Lin, X., Lee, S. B., Tuymetova, G., Bondeva, T., Spat, A., Rhee, S. G., Hajnoczky, G., and Balla, T. (2002). Inositol lipid binding and membrane localization of isolated pleckstrin homology (PH) domains. Studies on the PH domains of phospholipase C delta 1 and p130. J. Biol. Chem. *277*, 27412–27422.

Várnai, P., and Balla, T. (1998). Visualization of phosphoinositides that bind pleckstrin homology domains: calcium-and agonist-induced dynamic changes and relationship to myo-[³H]inositol-labeled phosphoinositide pools. J. Cell Biol. *143*, 501–510.

Walch-Solimena, C., and Novick, P. (1999). The yeast phosphatidylinositol-4-OH kinase Pik1 regulates secretion at the Golgi. Nat. Cell Biol. *1*, 523–525.

Wang, Y. J., Wang, J., Sun, H. Q., Martinez, M., Sun,. Y. X., Macia, E., Kirschhausen,T.,Albanesi,J.P.,Roth,M.G.,andYin,H.L.(2003).Phosphatidylinositol 4 phosphate regulates targeting of clathrin adaptor AP-1 complexes to the Golgi. Cell *114*, 299–310.

Waugh, M. G., Minogue, S., Anderson, J. S., Balinger, A., Blumenkrantz, D., Calnan, D. P., Cramer, R., and Hsuan, J. J. (2003). Localization of a highly active pool of type II phosphatidylinositol 4-kinase in a p97/valosin-containing-protein-rich fraction of the endoplasmic reticulum. Biochem. J. *373*, 57–63.

Wei, Y. J., Sun, H. Q., Yamamoto, M., Wlodarski, P., Kunii, K., Martinez, M., Barylko, B., Albanesi, J. P., and Yin, H. L. (2002). Type II phosphatidylinositol 4-kinase beta is a cytosolic and peripheral membrane protein that is recruited to the plasma membrane and activated by Rac-GTP. J. Biol. Chem. *277*, 46586–46593.

Wong, K., Meyers, R., and Cantley, L. C. (1997). Subcellular localization of phosphatidylinositol 4-kinase isoforms. J. Biol. Chem. *272*, 13236–13241.

Yamaguchi, N., and Fukuda, M. N. (1995). Golgi retention mechanism of β-1,4-galactosyltransferase. Membrane-spanning domain-dependent homodimerization and association with α- and β-tubulins. J. Biol. Chem. *270*, 12170–12176.

Yoshida, S., Ohya, Y., Goebl, M., Nakano, A., and Anrakur, Y. (1994). A novel gene, STT4, encodes a phosphatidylionositol 4-kinase in the PKC1 protein kinase pathway of *Saccharomyces cerevisiae.* J. Biol. Chem. *269*, 1166–1171.

Yu, J. W., Mendrola, J. M., Audhya, A., Singh, S., Keleti, D., DeWald, D. B., Murray, D., Emr, S. D., and Lemmon, M. A. (2004). Genome-wide analysis of membrane targeting by *S. cerevisiae* pleckstrin homology domains. Mol. Cell *13*, 677–688.

Maintenance of Hormone-sensitive Phosphoinositide Pools in the Plasma Membrane Requires Phosphatidylinositol 4-Kinase IIIα

Andras Balla,*† Yeun Ju Kim,* Peter Varnai,*† Zsofia Szentpetery,* Zachary Knight,‡ Kevan M. Shokat,§ and Tamas Balla*

*Section on Molecular Signal Transduction, National Institute of Child Health and Human Development, National Institutes of Health, Bethesda, MD 20892; †Department of Physiology, Semmelweis University, School of Medicine, Budapest, Hungary H-1086; ‡Program in Chemistry and Chemical Biology, University of California, San Francisco, CA 94158; and §Howard Hughes Medical Institute and Department of Cellular and Molecular Pharmacology, University of California, San Francisco, CA 94158

Type III phosphatidylinositol (PtdIns) 4-kinases (PI4Ks) have been previously shown to support plasma membrane phosphoinositide synthesis during phospholipase C activation and Ca^{2+} signaling. Here, we use biochemical and imaging tools to monitor phosphoinositide changes in the plasma membrane in combination with pharmacological and genetic approaches to determine which of the type III PI4Ks (α or β) is responsible for supplying phosphoinositides during agonist-induced Ca^{2+} signaling. Using inhibitors that discriminate between the α- and β-isoforms of type III PI4Ks, PI4KIIIα was found indispensable for the production of phosphatidylinositol 4-phosphate (PtdIns4P), phosphatidylinositol 4,5-bisphosphate [PtdIns(4,5)P$_2$], and Ca^{2+} signaling in angiotensin II (AngII)-stimulated cells. Down-regulation of either the type II or type III PI4K enzymes by small interfering RNA (siRNA) had small but significant effects on basal PtdIns4P and PtdIns(4,5)P$_2$ levels in ^{32}P-labeled cells, but only PI4KIIIα down-regulation caused a slight impairment of PtdIns4P and PtdIns(4,5)P$_2$ resynthesis in AngII-stimulated cells. None of the PI4K siRNA treatments had a measurable effect on AngII-induced Ca^{2+} signaling. These results indicate that a small fraction of the cellular PI4K activity is sufficient to maintain plasma membrane phosphoinositide pools, and they demonstrate the value of the pharmacological approach in revealing the pivotal role of PI4KIIIα enzyme in maintaining plasma membrane phosphoinositides.

INTRODUCTION

Activation of cell surface receptors by a variety of stimuli initiates a cascade of molecular events ultimately eliciting a response characteristic of the target cell. One of the most studied and best-characterized signal transduction pathways is initiated by the phospholipase C-mediated breakdown of phosphatidylinositol 4,5-bisphosphate [PtdIns(4,5)P$_2$] to generate the Ca^{2+}-mobilizing messenger inositol trisphosphate (InsP$_3$) and the protein kinase C activator diacylglycerol

Abbreviations used: 5-ptase, type-IV phosphoinositide 5-phosphatase; AngII, angiotensin II; DTT, dithiothreitol; ER, endoplasmic reticulum; FAPP, four phosphate adaptor protein; FRET, fluorescence resonance energy transfer; GFP, enhanced green fluorescent protein; InsP$_3$, inositol trisphosphate; Mer, β-mercaptoethanol; mRFP, monomeric red fluorescent protein; OSBP, oxysterol binding protein; PAO, phenylarsine oxide; PI4K, phosphatidylinositol 4-kinase; PtdIns4P, phosphatidylinositol 4-phosphate; PtdIns(4,5)P$_2$, phosphatidylinositol 4,5-bisphosphate; PtdA, phosphatidic acid; PLC, phospholipase C; PH, pleckstrin homology; siRNA, small interfering RNA; Wm, wortmannin.

(Berridge and Irvine, 1984). It has long been recognized that the sustained production of these messengers requires continuous phosphorylation of phosphatidylinositol (PtdIns) to phosphatidylinositol 4-phosphate (PtdIns4P) and PtdIns(4,5)P$_2$ by phosphoinositide (PI) 4-kinase (PI4K) and PIP 5-kinase enzymes, due to the limited amount of PtdIns(4,5)P$_2$ present in the plasma membrane (Creba *et al.*, 1983). Several isoforms within the PI 4-kinase and PIP 5-kinase families have been described previously (Doughman *et al.*, 2003; Balla and Balla, 2006), and a recent study identified a splice variant of PIP 5-kinase γ as the enzyme responsible for PtdIns4P to PtdIns(4,5)P$_2$ conversion in agonist-induced Ca^{2+} signaling (Wang *et al.*, 2004). In contrast, the PI 4-kinase that generates PtdIns4P for this process so far has eluded identification.

Four PI 4-kinase enzymes have been identified in mammalian cells that belong to either the type II or type III families (Balla and Balla, 2006). Type II PI 4-kinase enzymes (α- and β-forms) are small, 56-kDa proteins that are abundant in almost all cellular membranes, and they are enriched in plasma membrane preparations. They are kept in the membrane by palmitoylation, and recent studies suggest that these enzymes have a role in post-*trans*-Golgi network trafficking (Wang *et al.*, 2003, 2007) and the endocytic processing of the epidermal growth factor receptors (Minogue *et al.*, 2006). Type III PI 4-kinases (α- and β-forms), in contrast, are soluble enzymes structurally related to PI 3-ki-

A. Balla *et al.*

nases, and they can be inhibited by higher concentrations of PI 3-kinase inhibitors, such as wortmannin (Wm). We have reported over 10 years ago that production of the agonist-sensitive phosphoinositide pools required the activity of Wm-sensitive type III PI 4-kinase enzymes (Nakanishi *et al.*, 1995). However, it is still not known which of the type III enzymes participates in the formation of the agonist-regulated PtdIns4P pools.

In the present study, we used both pharmacological and genetic approaches to interfere with the activity of all of the PI 4-kinase enzymes, and we monitored phosphoinositide changes both by conventional metabolic labeling of inositol lipids and -phosphates and by using green fluorescent protein (GFP)-tagged pleckstrin homology (PH) domains recognizing PtdIns4P and PtdIns(4,5)P_2. These results show that the PH domain of the yeast OSH2 protein is a valuable tool to monitor plasma membrane PtdIns4P pools and that PI 4-kinase IIIα is required for sustained InsP$_3$ production and Ca^{2+} signaling. Although this conclusion was supported by small interfering RNA (siRNA)-mediated gene silencing of the individual PI4K enzymes, the present studies also highlight the difficulties in obtaining conclusive data with siRNA on enzymes whose functions are near essential and emphasize the value of inhibitors to dissect the roles of these proteins in cellular signaling.

MATERIALS AND METHODS

Materials

Wortmannin and ionomycin were purchased from Calbiochem (San Diego, CA). Phenylarsine oxide (PAO), β-mercaptoethanol, dithiothreitol, and poly-lysine were obtained from Sigma-Aldrich (St. Louis, MO). Fura-2/acetoxymethyl ester (AM) and Pluronic acid were from Invitrogen (Carlsbad, CA). PIK93 was synthesized as described previously (Knight *et al.*, 2006). *Myo*-[^{3}H]inositol (60 Ci/mmol) was purchased from GE Healthcare (Little Chalfont, Buckinghamshire, United Kingdom) and ortho-[^{32}P]phosphate (9000 Ci/mmol) was from General Electric (PerkinElmer Life and Analytical Sciences, Boston, MA). The polyclonal antibody against PI4KIIIβ was purchased from UBI (Lake Placid, NY), the polyclonal antibody against PI4KIIα was a kind gift from Dr. Pietro De Camilli (Yale School of Medicine, New Haven, CT), and the anti PI4KIIIα antibody was raised in New Zealand rabbits as described previously (Balla *et al.*, 2005).

DNA Constructs and Transfections

The OSH2–2x-GFP construct was generated by amplifying the PH domain sequence of OSH2 (residues 256–424) from Saccharomyces *cerevisiae* cDNA (American Type Culture Collection, Manassas, VA) by using two primer pairs to obtain fragments flanked by XhoI/EcoRI and EcoRI/KpnI sites. These fragments were then cloned in tandem between the XhoI/KpnI sites of the pEGFP-C1 plasmid (Clontech, Mountain View, CA), with a linker (VNSKL) in between them following the design of Roy and Levine (2004). The single PH domain version of the PH domain also has been created as well as the cyan and yellow fluorescent versions of the tandem construct. The PLCδ_1PH-GFP construct (Várnai and Balla, 1998) and its color variants have been described previously (Varnai *et al.*, 2002). The OSH1-PH-GFP was kindly provided by Dr. Mark Lemmon (University of Pennsylvania, Philadelphia, PA) (Yu *et al.*, 2004), and the type IV phosphoinositide 5-phosphatase was a kind gift from Dr. Philip Majerus (Washington University, St. Louis, MO) (Kisseleva *et al.*, 2000). The constructs used for the rapamycin-inducible translocation of the type-IV phosphoinositide 5-phosphatase have been described recently (Varnai *et al.*, 2006).

The human embryonic kidney (HEK)-293AT1 cells used for these studies have been stably transfected with the hemagglutinin (HA)-AT1a and FLAG-AT1a angiotensin receptors in two rounds of selection by using G-418 and Zeocine (Zeo) (Invitrogen, Carlsbad, CA) for the two constructs, respectively. These cells were kindly provided by Drs. Alberto Jesus Olivares-Reyes and Kevin J. Catt (NICHD, NIH, Bethesda, MD). Cells were cultured in DMEM with Pen/Strep (Invitrogen) and 10% fetal bovine serum (FBS), and they have been subjected to a G-418/Zeo selection from time to time but not during cultures for the experiments.

For RNA interference (RNAi)-mediated knockdown, the cells were cultured either in 10-cm dishes (for suspension Ca^{2+} measurements), 12-well plates (for metabolic labeling studies), or 25-mm glass coverslips treated with poly-lysine (for single-cell Ca^{2+} or confocal studies). The duplexes used for treatment have been described previously (Balla *et al.*, 2005). Cells were treated with 100 nM siRNA twice in consecutive days, and they were analyzed on the fourth day after the first treatment.

Analysis of Single Cells for Fluorescence Resonance Energy Transfer (FRET), Cytoplasmic Ca²⁺ Measurements, and Confocal Microscopy

HEK-293AT1 cells were cultured on glass coverslips (3×10^5 cells/35-mm dish) pretreated with poly-lysine and transfected with the various constructs (0.5–2 μg DNA/dish) by using Lipofectamine 2000 (Invitrogen) for 24 h as described previously (Varnai *et al.*, 2005). For calcium measurements, cells were loaded with 3 μM Fura-2/AM in medium 199/Earle's balanced salt solution containing 1.2 mM CaCl$_2$, 3.6 mM KCl, 25 mM HEPES containing 1 mg/ml bovine serum albumin (BSA), 0.06% Pluronic acid, and 200 μM sulfinpyrazone, for 45 min at room temperature. Calcium measurements were performed at room temperature in a modified Krebs-Ringer buffer containing 120 mM NaCl, 4.7 mM KCl, 1.2 mM CaCl$_2$, 0.7 mM MgSO$_4$, 10 mM glucose, and Na-HEPES 10 mM, pH 7.4. An Olympus IX70 inverted microscope equipped with a Lamda-DG4 illuminator and a MicroMAX-1024BFT digital camera and the appropriate filter sets was used for Ca^{2+} analysis. The same microscope equipped with a beam-splitter (Optical Insights, Photometrics, Tucson, AZ) with a 505-nm dichroic mirror was used for FRET analysis with 435/25-nm excitation and 475/30- and 535/30-nm emission filters, respectively. Images acquired simultaneously in the two emission wavelengths in the two halves of the camera sensor chip were used to form the ratios. These ratio values were then normalized, taking their control initial values as 100 and the minimum values obtained after ionomycin (or agonist treatment if the latter was smaller) as zero.

Cells expressing the OSH2–2x-PH-GFP and PLCδ1PH-monomeric red fluorescent protein (mRFP) constructs were studied in the same modified Krebs-Ringer solution at 35°C by using a Zeiss 510Meta laser-scanning confocal microscope (Carl Zeiss, Thornwood, NY) in multitrack mode, and pictures were taken in time-series mode. Membrane localization was assessed by forming membrane/cytosol intensity ratio values from line-intensity histograms of cells in the whole series of images after acquisition. Data acquisitions for Ca^{2+} and FRET measurements and processing were performed by the MetaFluor software (Molecular Devices, Sunnyvale, CA). Postacquisition data analysis of the confocal images was performed with either the MetaView (Carl Zeiss) or the MetaMorph (Molecular Devices) software.

Cytoplasmic Ca²⁺ Measurements in Cell Suspensions

Cells grown on 10-cm culture plates were removed by mild trypsinization and loaded with 0.5 μM Fura-2/AM in the same solution described above for single Ca^{2+} measurements. Cells were then washed with the same medium without Fura-2/AM and stored at room temperature in the dark. Aliquots of cells (~5 × 10^5 cells) were centrifuged rapidly before the measurements and dispersed in 2.5 ml of the modified Krebs-Ringer buffer used for all other analysis. Ca^{2+} measurements were performed at 35°C in a PTI Deltascan spectrofluorometer (Photon Technology International, Princeton, NJ).

Analysis of Myo-[³²H]Inositol- or [³²P]Phosphate-labeled Lipids and ³H-labeled Inositol Phosphates

Cultured cells were labeled with *myo*-[^{3}H]inositol (20 μCi/ml) on 12-well culture plates in inositol-free DMEM supplemented with 2% dialyzed FBS and 1 mg/ml BSA for 24 h. For ^{32}P-phopshate labeling, the cells were labeled with 2 μCi/ml o-[^{32}P]phosphate for 3 h in phosphate-free DMEM supplemented with 1 mg/ml BSA. After *myo*-inositol labeling, the cells were washed twice with a medium without inositol, and after a 10-min preincubation, inhibitors were added for a further 10 min before stimulation with 100 nM angiotensin II (AngII) for the indicated times. Reactions were terminated by the addition of ice-cold perchloric acid (5% final concentration), and cells were kept on ice for 30 min. After scraping, and freezing/thawing, the cells were centrifuged, and the supernatant was processed for perchloric acid (PCA) extraction and analysis by high-performance liquid chromatography as described previously (Nakanishi *et al.*, 1995). The cell pellet was also processed to extract the phosphoinositides by an acidic chloroform/methanol extraction followed by thin layer chromatography (TLC) analysis essentially as described previously (Nakanishi *et al.*, 1995). ^{32}P-labeled cells were not washed after the labeling period, but they were treated in the same medium with inhibitors for 10 min followed by AngII (10^{-7} M) stimulation. Reactions were terminated by PCA, and lipids were extracted and separated as with the inositol-labeled cells.

RESULTS

Pharmacological Manipulations of Type III PI 4-Kinase Activities Affect Agonist-regulated PtdIns4P Pools

High (micromolar) concentrations of Wm have been valuable tools to demonstrate a role of type III PI4Ks in InsP$_3$/Ca^{2+} signaling. However, it is not possible to discriminate between the α- and β-forms of these PI4Ks based on their Wm sensitivities (Balla *et al.*, 1997; Knight *et al.*, 2006). There-

fore, we took advantage of the recent characterization of isoform-specific PI 3-kinase inhibitors that revealed one of the inhibitors, PIK93, as being significantly more potent against PI4KIIIβ than PI4KIIIα (Knight *et al.*, 2006). This inhibitor inhibits PI 3-kinases and clearly discriminates between the two PI 4-kinase enzymes as assessed by an in vitro PI kinase assay on the purified mammalian proteins (Knight *et al.*, 2006). Unfortunately, none of the tested inhibitors showed the opposite selectivity, i.e., inhibition of PI4KIIIα more potently than the PI4KIIIβ enzyme. Phenylarsine oxide (PAO), a sulfhydryl (SH)-reactive agent has been shown earlier to inhibit PI4Ks (Wiedemann *et al.*, 1996). PAO was found to inhibit type III PI 4-kinases, whereas it is relatively ineffective against the type II enzymes based on in vitro kinase assays of the purified proteins (Balla *et al.*, 2002; Barylko *et al.*, 2002). Among the type III enzymes, PI4KIIIα is significantly more sensitive to PAO than the type IIIβ form (Balla *et al.*, 2002). This difference was also exploited to discriminate between the two enzymes in their involvement to generate the hormone-sensitive PtdIns4P pools. It is important to emphasize that PAO is a SH-reactive agent that probably has many targets in a cell. However, in the present study, the effects of PAO have only been tested on parameters that immediately reflect PI 4-kinase functions (see below); therefore, in this narrow context the effects of PAO on the purified PI 4-kinases and PtdIns4P formation in the intact cell can be correlated with somewhat higher confidence.

Several parameters were tested with these inhibitors in HEK-293 cells stably expressing AT_{1a} angiotensin receptors (HEK-293-AT1). Cellular phosphoinositides were monitored after [^{32}P]phosphate or *myo*-[^{3}H]inositol labeling, and InsP$_3$ formation was followed from cells prelabeled with *myo*-[^{3}H]inositol. Finally, the effects of the inhibitors on AngII-induced changes in cytoplasmic Ca^{2+} concentration [Ca^{2+}]$_i$ were measured in cell suspensions with Fura-2. Figure 1 shows the effects of inhibitors on InsP$_3$ levels analyzed from *myo*-[^{3}H]inositol-labeled cells and on Ca^{2+} signaling. As shown earlier in AngII-stimulated adrenal glomerulosa cells (Nakanishi *et al.*, 1995), 10 μM Wm pretreatment greatly reduced the size of AngII-induced InsP$_3$ elevation in HEK-293-AT1 cells, and it eliminated its sustained increase. This was also reflected in the cytoplasmic Ca^{2+} changes that became transient lacking the plateau phase of Ca^{2+} rise in Wm treated cells (Figure 1B). These effects of Wm were not observed at lower concentrations (<300 nM) that already inhibit PI 3-kinases (data not shown), and they were clearly caused by the limited supply of PtdIns4P and PtdIns(4,5)P$_2$, consistent with the inhibition of a PI4K that helps replenishing these pools during a sustained phospholipase C (PLC) activation. This is demonstrated in Figure 2, where the [^{32}P]phosphate-labeled PtdIns4P and PtdIns(4,5)P$_2$ were analyzed in AngII-stimulated cells. Without the inhibitors, AngII stimulation evokes a robust PLC activation, resulting in the rapid depletion of PtdIns(4,5)P$_2$ that slowly returns toward prestimulatory levels. A similar change is observed in PtdIns4P levels due to the conversion of this lipid to PtdIns(4,5)P$_2$ by the PIP 5-kinases and its relatively slower synthesis by the PI4Ks. Pretreatment of the cells with 10 μM Wm greatly reduced the ^{32}P-labeled PtdIns4P and, hence, the AngII-induced changes observed in HEK-293-AT1 cells (Figure 1A), but it only slightly reduced basal PtdIns(4,5)P$_2$ levels. However, this treatment significantly enhanced the AngII-induced decrease in PtdIns(4,5)P$_2$ and strongly inhibited its resynthesis (Figure 2B).

These effects of Wm were not reproduced by 250 nM PIK93, which inhibits PI4KIIIβ (and the PI 3-kinases) but not PI4KIIIα (Knight *et al.*, 2006), and which was found as effec-

Figure 1. Effects of PI4K inhibitors on the kinetics of InsP$_3$ and [Ca^{2+}]$_i$ changes in HEK-293-AT1 cells stimulated with AngII. (A) HEK-293-AT1 cells were labeled with *myo*-[^{3}H]inositol for 24 h in inositol-free medium as described under *Materials and Methods*. After washing, AngII (10^{-7} M) was added to the cells for the indicated times, and reactions were terminated by PCA. Labeled inositol phosphates were extracted from the soluble fraction and separated by high-performance liquid chromatography connected to a scintillation flow detector as described previously (Nakanishi *et al.*, 1995). Data are shown are means ± range of duplicate determinations. The concentrations of the inhibitors added 10 min before AngII were 250 nM PIK93, 10 μM PAO with 1 mM β-mercaptoethanol (Mer), and 10 μM Wm. Two additional experiments were performed with the 10-min time points with similar results. (B) HEK-293-AT1 cells were loaded with Fura-2/AM, and their fluorescence monitored in a fluorescent spectrophotometer as described under *Materials and Methods*. AngII (10^{-7} M) was added at the indicated time. Pretreatment with the inhibitors for 10 min was as described in A. This result is a representative of three similar observations.

tive as 10 μM Wm in inhibiting the endoplasmic reticulum (ER)-to-Golgi transport of ceramide, a process linked to PI4KIIIβ function (Toth *et al.*, 2006). PIK93 failed to affect either the InsP$_3$ and Ca^{2+} changes or those of the ^{32}P-labeled phosphoinositides during AngII stimulation (Figures 1 and 2). The effect of PAO was tested at a concentration of 10 μM (applied in the presence of 1 mM β-mercaptoethanol to reduce its side effects). Although at this concentration PAO only partially inhibits PI4KIIIα (~80%), it was chosen because it does not yet inhibit PI4KIIIβ (Balla *et al.*, 2002). As shown in Figure 1, PAO partially mimicked the effects of Wm on both the InsP$_3$ and Ca^{2+} responses, substantially reducing the sustained phases of both signals. Also, after 10 μM PAO treatment the ^{32}P-labeled phosphoinositides showed changes similar to those observed with Wm treatment (Figure 2). All of these data were consistent with the limited supply of PtdIns4P in the presence of Wm or PAO but not PIK93, implicating the PI4KIIIα enzyme in the pro-
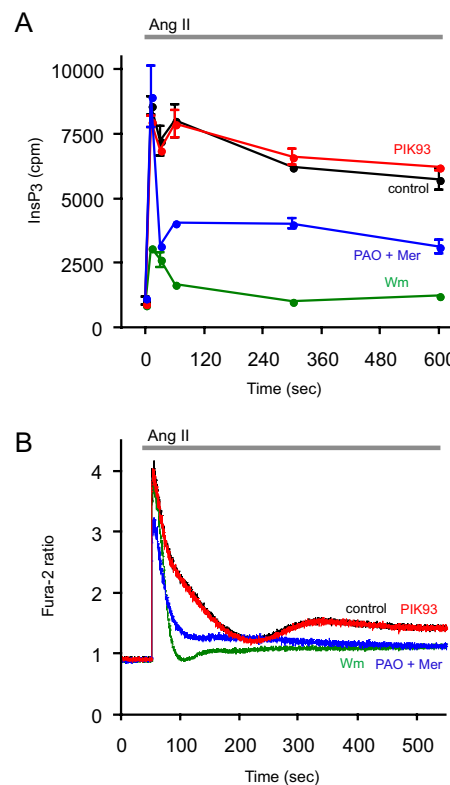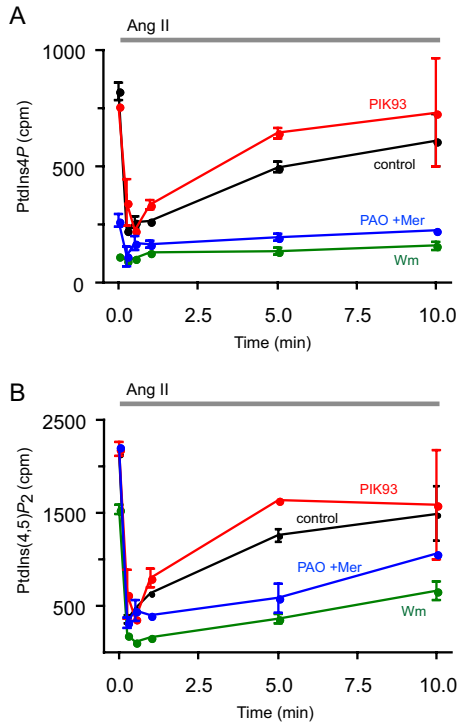
A. Balla *et al.*

Figure 2. Effects of PI4K inhibitors on the kinetics of phosphoinositide changes in HEK-293-AT1 cells stimulated with AngII. HEK-293-AT1 cells were labeled with [^{32}P]phosphate for 3 h in a phosphate-free medium as described under *Materials and Methods*. AngII (10^{-7} M) was added to the cells at the indicated times, and reactions terminated by the addition of PCA. Lipids were extracted from the cell pellets, separated by TLC, and analyzed both by a PhosphorImager and scintillation counting of the spots cut out from the plates. Data shown are means ± range of duplicate determinations. The concentrations of the inhibitors added 10 min before AngII were 250 nM PIK93, 10 μM PAO with 1 mM Mer, and 10 μM Wm. This full time course experiment was repeated from *myo*-[^{3}H]inositol-labeled cells with similar results, supporting the same conclusion.

cess, and the incomplete effects of PAO relative to Wm were consistent with the incomplete inhibition of PI4KIIIα at this concentration of the inhibitor.

Analysis of PtdIns(4,5)P$_2$ Changes in the Plasma Membrane with the PLCδ_1PH Domain

These metabolic data provided information on the overall inositide pools of the cells but only limited information on the question of which membranes contributed to these changes. In fact, when cells were labeled with *myo*-[^{3}H]inositol, a smaller fraction of the inositides showed changes with AngII and the inhibitors (data not shown), suggesting the presence of additional metabolic pools that become labeled with *myo*-[^{3}H]inositol in 24 h but not with [^{32}P]phosphate in 3 h. Therefore, further experiments were designed to monitor the phosphoinositide changes in single cells by using PH domains that recognize PtdIns4P and PtdIns(4,5)P$_2$. PtdIns(4,5)P$_2$ changes were followed in single cells by either confocal microscopy or by FRET analysis using yellow fluorescent protein (YFP) and cyan fluorescent protein (CFP)-tagged versions of the PLCδ PH domain (van Der Wal *et al.*, 2001).

Cells were stimulated with AngII for the indicated times followed by the addition of high concentration (10 μM) of ionomycin to activate PLC and to eliminate PLCδ_1PH-GFP localization and FRET (Várnai and Balla, 1998; Balla *et al.*,
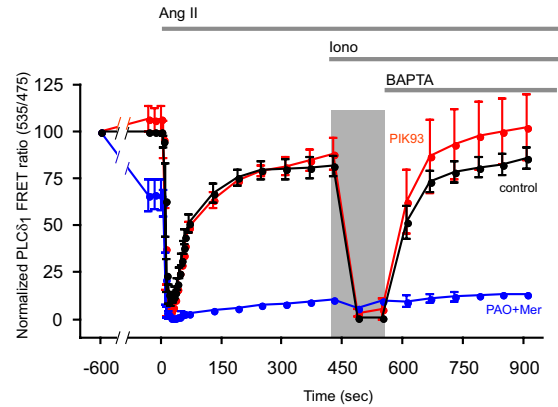

Figure 3. Effects of PI4K inhibitors on the kinetics of redistribution of PLCδ_1PH domain in HEK-293-AT1 cells stimulated with AngII. HEK-293 cells stably transfected with the AT1a angiotensin receptors were cotransfected with the PLCd1PH-CFP and -YFP constructs for 24 h. The FRET signal from individual cells was then monitored in a wide-field fluorescent microscope equipped with an emission beam splitter using 430-nm excitation and 535- and 475-nm emissions as described under *Materials and Methods*. To minimize light exposure, after the first minute of stimulation, data were collected in longer intervals. AngII (10^{-7} M) was added at the indicated time followed by 10 μM inonomycin (Iono) and 5 mM BAPTA (or EGTA). The dark bar represents the exposure of the cells to the high (extracellular) Ca^{2+} concentration after ionomycin treatment. The concentrations of the inhibitors added 10 min before AngII were 250 nM PIK93 and 10 μM PAO with 1 mM Mer. FRET was expressed as fluorescent emission ratio values (535/475 nm), and it was normalized so that the ratio value recorded before the addition of inhibitors was taken as 100% and the lowest values (after AngII or ionomycin) were taken as 0%. Means ± SEM (or range) from five, two, and three cells are shown for control, PAO + Mer, and PIK93, respectively. Similar changes were observed in two additional experiments.

2005). Subsequent addition of 1,2-bis(2-aminophenoxy)ethane-N,N,N',N'-tetraacetic acid (BAPTA) (or EGTA) was used to reverse the Ca^{2+} change and allow the PtdIns(4,5)P$_2$ pools to recover. As shown in Figure 3, the PLCδ_1PH translocation was rapid and complete after AngII treatment, and the FRET signal rapidly returned close to the baseline in control cells (black trace). Ionomycin treatment then caused the complete translocation of the probe to the cytosol from which the cells recovered slowly after Ca^{2+} chelation. These changes were not affected by preincubation of the cells with 250 nM PIK93 (Figure 3, red trace), consistent with the previous data with metabolic labeling and suggesting that PI4KIIIβ plays no significant role in this process. In contrast, 10 μM PAO (with 1 mM β-mercaptoethanol) decreased the basal FRET by ~40% and prevented the relocalization of the probe after the AngII-induced complete translocation (Figure 3, blue trace).

When the effects of Wm were tested in similar experiments, we encountered several technical difficulties. First, the inhibitory effects of Wm showed a strong light-induced reversal in single-cell experiments. At shorter excitation wavelengths, these effects were stronger, making it essentially impossible to monitor the effect of Wm on single cell Ca^{2+} responses with Fura-2. (The photon flux density is significantly lower during Ca^{2+} measurements in cell suspension; therefore, those measurements are less sensitive to this effect). In addition, a significant drift was observed in the FRET baseline during the 10 min Wm preincubation period (without illumination). Although this was partially eliminated rapidly after two to three light scans, it was difficult to assess the basal FRET values after Wm treatment.

Therefore the data on the effects of Wm (still partially inhibitory) were not included in this analysis.

Evaluation of the OSH2 PH Domain as a Probe of Plasma Membrane PtdIns4P Levels

None of the type III PI4K enzymes can be detected by immunofluorescence at the plasma membrane; yet, PtdIns4P has to be present in the plasma membrane to be converted to PtdIns(4,5)P$_2$. To obtain information on the activity rather than the steady-state cellular distribution of the PI4K enzymes, it was highly desirable to use reporter probes that monitor PtdIns4P production in single cells. PH domain-GFP chimeras with high in vitro PtdIns4P binding specificities, such as the four phosphate adaptor protein (FAPP)1 or oxysterol binding protein (OSBP) PH domains have been used for this purpose, but these probes mostly report on PtdIns4P formed in the Golgi as they also require Arf1-GTP for their Golgi recruitment (Levine and Munro, 2002; Godi *et al.*, 2004; Balla *et al.*, 2005). Although both of these PH domains can detect PtdIns4P formation in the plasma membrane under special circumstances (Balla *et al.*, 2005), they are not optimal for monitoring PtdIns4P in the plasma membrane. It has recently been shown by two independent studies that the PH domain of the yeast oxysterol binding protein homologue, OSH2 recognizes PtdIns4P in the plasma membrane, in spite of its limited specificity to bind PtdIns4P in vitro (Roy and Levine, 2004; Yu et al., 2004). Therefore, first, we wanted to determine whether the OSH2 PH domain could, in fact, be used to follow PtdIns4P changes in the plasma membrane of mammalian cells.

Expression of the single PH domain of OSH2 fused to GFP showed clear plasma membrane localization and a strong nuclear staining as described previously (Roy and Levine, 2004; Yu *et al.*, 2004). Using two PH domains in tandem fused to GFP (GFP-OSH2-PH2x) greatly reduced the nuclear localization of the construct and clearly labeled the plasma membrane (Figure 4A). Importantly, unlike in yeast cells, neither the tandem nor the single OSH2 PH domain decorated the Golgi membrane in COS-7 or HEK-293 cells (Figure 4A). In contrast, the yeast OSH1 PH domain labeled both the plasma membrane (at high expression levels) and the Golgi (Figure 4A). Because the OSH2 PH domain has limited in vitro specificity to PtdIns4P (Yu *et al.*, 2004), we were concerned that it may be recruited to the plasma membrane by PtdIns(4,5)P$_2$. The specificity question was examined with our recently developed method of acute depletion of PtdIns(4,5)P$_2$ in the plasma membrane. This approach is based on a drug induced plasma membrane recruitment of a truncated type-IV phosphoinositide 5-phosphatase (5-ptase) that was rendered cytoplasmic by mutations in its localization sequences (Varnai *et al.*, 2006). Recruitment of this cytoplasmic 5-ptase to the plasma membrane rapidly eliminated PtdIns(4,5)P$_2$ as monitored by PLCδ$_1$PH-GFP localization (Figure 4B), without elimination of the GFP-OSH2-PH2x localization (Figure 4C). This question was further analyzed in total internal reflection fluorescence experiments where the release of the PH domain from the membrane can be better quantified. These experiments showed no effect of the phosphatase recruitment on GFP-OSH2-PH2x localization while eliminating PLCδ1PH-GFP localization in COS-7 cells (Korzeniowski and Balla, unpublished observations).

In a separate set of studies performed in COS-7 cells, the wild-type 5-ptase enzyme was expressed together with the mRFP-fused PLCδ1PH domain and the GFP-OSH2-PH2x construct. This triple transfection yielded many cells in which the plasma membrane localization of the PLCδ1PH-
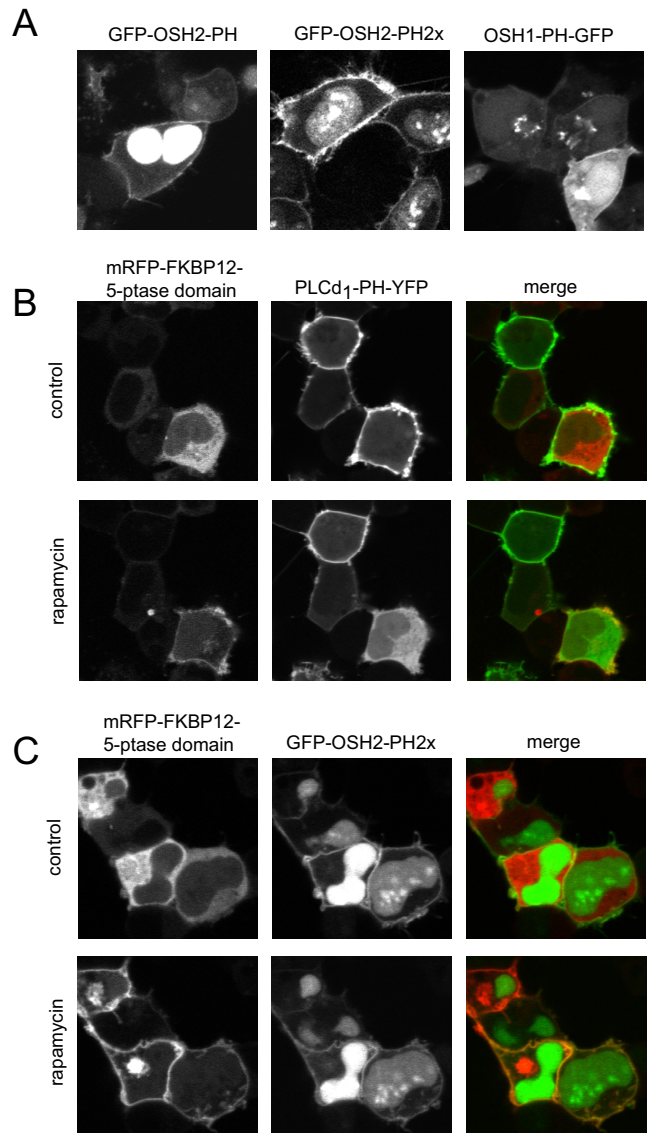
Figure 4. Localization of OSH1- and OSH2-PH domain-GFP fusion proteins in HEK-293-AT1 cells. (A) The PH domains of the yeast oxysterol-binding protein homologues OSH2 and OSH1 were fused to GFP as described under *Materials and Methods*. These constructs were transfected into HEK-293-AT1 cells and examined 24 h after transfection with live cell confocal microscopy. Note that the OSH2-PH domain binds to the plasma membrane and strongly accumulates in the nucleus but does not bind to the Golgi. A tandem PH domain of the OSH2 protein shows smaller signal in the nucleus and a strong plasma membrane binding. The OSH1-PH domain binds both the plasma membrane and the Golgi. (B) Elimination of the plasma membrane localization of PLCδ$_1$PH-GFP [monitoring PtdIns(4,5)P$_2$] by plasma membrane recruitment of a phosphoinositide 5-phosphatase. HEK-293-AT1 cells were transfected with a truncated type-IV phosphoinositide 5-phosphatase fused to mRFP and FKBP12, a plasma membrane-targeted FRB-CFP construct and the PLCδ$_1$PH-YFP reporter described in Varnai *et al.* (2006). Addition of rapamycin for 3 min recruits the otherwise cytoplasmic 5-ptase construct to the plasma membrane (left) with a concomitant elimination of PtdIns(4,5)P$_2$ and loss of PLCδ$_1$PH-YFP localization (middle). (C) The same manipulations do not eliminate the plasma membrane localization of the OSH2-PH2x-GFP, suggesting that this construct is not kept at the membrane by PtdIns(4,5)P$_2$.

A. Balla *et al.*

A

B
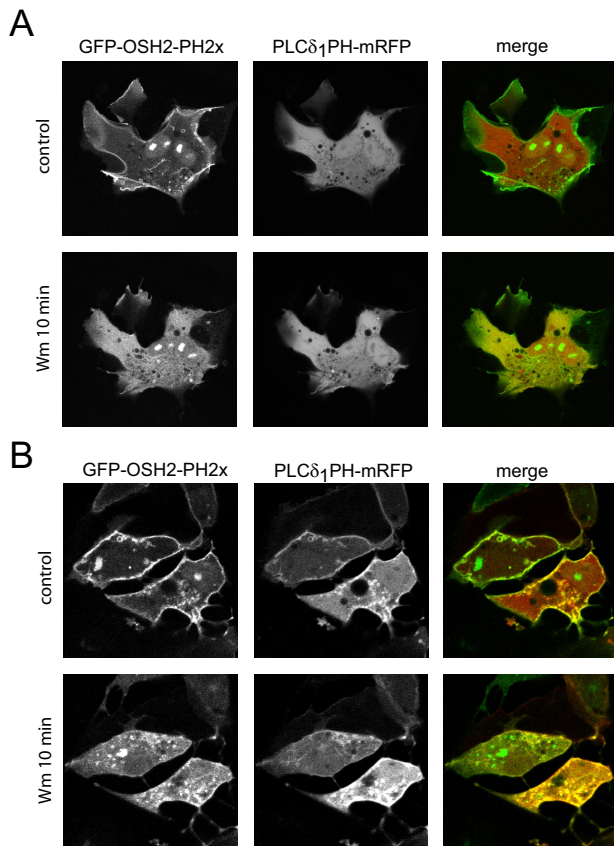
Figure 5. Localization of OSH2-PH2x-GFP to the plasma membrane is wortmannin sensitive. (A) COS-7 cells were transfected with OSH2-PH2x-GFP together with PLCδ$_1$PH-mRFP and the wild-type type IV phosphoinositide 5-phosphatase for 24 h. Cells were selected so that the PLCδ$_1$PH-mRFP showed no localization, indicating the lack of PtdIns(4,5)P$_2$ as a result of phosphatase expression. These cells still showed plasma membrane localization of OSH2-PH2x-GFP, indicating that the construct is kept in the membrane not by PtdIns(4,5)P$_2$. Addition of 10 μM Wm to such cells caused a rapid translocation of the OSH2-PH2x-GFP domain construct from the membrane to the cytosol. (B) Release of the OSH2-PH2x-GFP construct from the membrane after Wm treatment is significantly slower in control cells where PtdIns(4,5)P$_2$ is present in the membrane.

mRFP construct was eliminated indicating the depletion of PtdIns(4,5)P$_2$; yet, the localization of the OSH2-PH2x was still preserved (Figure 5A). These studies also confirmed that the OSH2-PH2x was not recruited to the membrane by PtdIns(4,5)P$_2$. When such cells were treated with 10 μM Wm, the localization of OSH2-PH2x was rapidly eliminated (Figure 5A). Lower concentrations of Wm specific for PI 3-kinases had no such effect (data not shown), indicating that the plasma membrane pool of PtdIns4P monitored by OSH2-PH2x requires the activity of type III PI 4-kinases. Notably, Wm exerted a much slower effect on OSH2-PH2x localization in cells not expressing the 5-phosphatase (Figure 5B; see below) indicating that the dephosphorylation of PtdIns(4,5)P$_2$ probably contributes to maintaining PtdIns4P levels in the membrane for a period of time when PI4K is inhibited.

The PH Domain of OSH2 Follows Agonist-induced Changes of PtdIns4P Levels

Next, we determined whether GFP-OSH2-PH2x localization is affected by agonist-induced PLC activation. HEK-293-AT1

cells were cotransfected with the PLCδ1PH-mRFP and GFP-OSH2-PH2x for simultaneous monitoring of PtdIns(4,5)P$_2$ and PtdIns4P. As shown in Figure 6, both constructs showed a rapid and transient translocation from the plasma membrane to the cytosol after AngII addition, but with notable kinetic differences. The translocation of the GFP-OSH2-PH2x occurred with a clearly measurable ($\sim$5-s) delay compared with that of PLCδ1PH-mRFP. The kinetics of changes in GFP-OSH2-PH2x localization after AngII addition was indistinguishable regardless whether cells were preincubated with 10 mM Li$^+$ or not (data not shown). Because Ins(1,4)P$_2$ levels accumulate to very high levels and remain elevated in Li$^+$-treated cells (e.g., Balla *et al.*, 1988) due to the inhibition of the phosphatase that dephosphorylates Ins(1,4)P$_2$ (Majerus *et al.*, 1999), these findings suggest that the AngII-induced translocation of the GFP-OSH2-PH2x protein from the membrane is caused by the changes in membrane PtdIns4P levels rather than increases in Ins(1,4)P$_2$ levels in the cytosol. The slight delay in the response of GFP-OSH2-PH2x compared with that of PLCδ1PH-mRFP may reflect the slower (probably Ca^{2+}-dependent) activation of the PLC isoform that hydrolyzes PtdIns4P, or a slight delay in the conversion of PtdIns4P to PtdIns(4,5)P$_2$, but the contribution of the rapid Ins(1,4,5)P$_3$ increase to PLCδ1PH-mRFP translocation can also be responsible for its faster kinetics. Nevertheless, these data together were consistent with the conclusion that the GFP-OSH2-PH2x reporter can monitor plasma membrane PtdIns4P changes during agonist activation.

Pharmacological Manipulations of the Membrane Localization of OSH2–2x-PH

In response to the PI 4-kinase inhibitors, the GFP-OSH2-PH2x domain showed changes in good agreement with the [^{32}P]phosphate and *myo*-[^{3}H]inositol labeling results: the localization of the GFP-OSH2-PH2x was monitored as a change in the membrane to cytosol ratio of fluorescence. (We also attempted to use FRET for analysis of OSH2-PH2x. However, the FRET signal was significantly smaller than with the PLCδ$_1$PH domain, which may reflect a lower abundance of PtdIns4P in the membrane or a lower density of the lipid in the membrane microdomains where it is found). The membrane-bound fluorescence of GFP-OSH2-PH2x already started to decrease during the 10-min Wm (10 μM) preincubation, and $\sim$70–80% of the membrane localization was eliminated by the end of this period. Lower concentrations of Wm (300 nM) did not show this effect (Figure 7A). Subsequent addition of AngII rapidly eliminated the remaining localization and no relocalization of the probe was observed throughout the 10-min stimulation (Figure 8A). It is important to note that the effects of Wm became almost undetectable when prolonged rapid sampling of the confocal pictures was used to follow localization of the PH domains. This was again attributed to the photolability of Wm inhibition discussed above and also observed in Warashina (1999). Ten micromolar PAO (with 1 mM β-mercaptoethanol) had a similar inhibitory effect on the basal localization, although this treatment did not evoke the same decrease as Wm did before AngII addition (Figure 7B). The effect of PAO was completely reversed by simultaneous addition of 1 mM dithiothreitol (DTT) (Figure 7B). PAO also prevented the relocalization of the GFP-OSH2-PH2x during AngII stimulation (Figure 8B). In contrast, PIK93 (250 nM) had no effect on either the basal localization of the GFP-OSH2-PH2x probe (Figure 7C) nor did it affect the response to AngII stimulation (Figure 8A).
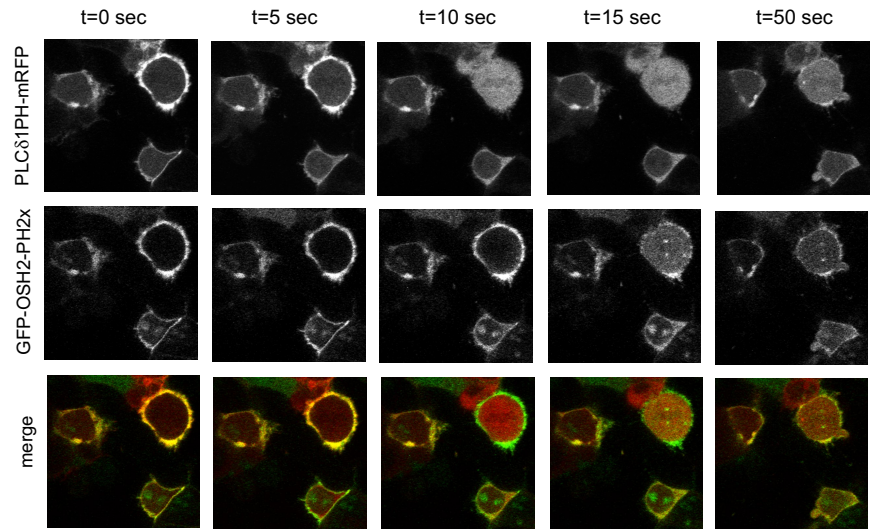
Figure 6. Angiotensin II-induced changes in membrane phosphoinositides simultaneously monitored by OSH2-PH2x-GFP and PLCδ_1PH-mRFP. HEK-293 cells stably transfected with the AT1a angiotensin receptors were cotransfected with the PLCδ_1PH-mRFP and OSH2-PH2x-GFP constructs for 24 h. Live cells were examined in a confocal microscope at 35°C during stimulation with AngII (10^{-7} M), and pictures were taken every 5 s. Note the faster response observed with the PLCδ_1PH-mRFP. Quantification of membrane/cytosolic fluorescence intensities as function of time calculated from line-intensity histograms from five to seven cells obtained in two separate experiments (means ± SEM).

Effects of RNAi-mediated Knockdown on Phosphoinositides and Ca²⁺ Signaling

The results of the pharmacological analysis pointed to PI4KIIIα as the enzyme important in the maintenance of the agonist-sensitive phosphoinositide pools of the plasma membrane. We wanted to confirm these data with RNAi-mediated gene silencing. All PI4Ks were individually knocked down, and the basal and AngII-induced changes in ^{32}P-labeled phosphoinositides and cytoplasmic Ca^{2+} were determined. These experiments showed that knockdown of either PI4Ks (confirmed in each experiments by Western blot analysis) (Figure 9A) resulted in no appreciable change in the Ca^{2+} response of the cells in response to AngII regardless of whether these measurements were performed in cells suspension or in single attached cells (data not shown). ^{32}P-labeling of cells depleted in the respective PI4Ks showed variations due to the loss of cells in the PI4K down-regulated groups (Figure 9B). To normalize for this difference, in each experiments the ratio of PtdIns4P and PtdIns(4,5)P$_2$ to the PtdIns/phosphatidic acid (PtdA) spots from unstimulated cells were calculated and compared between the control siRNA or PI4K siRNA-treated groups. After such corrections, the labeling of both PtdIns4P and PtdIns(4,5)P$_2$ showed an ~25% decrease upon depletion of either of PI4KIIα, PI4KIIIα, or PI4KIIIβ. This difference was statistically significant (p < 0.05) for all enzyme knockdowns in

PtdIns4P but only for PI4KIIα in PtdIns(4,5)P$_2$ (Figure 9C). To assess PtdIns4P and PtdIns(4,5)P$_2$ synthesis during stimulation, the level of these lipids were measured after 10 min of AngII exposure, because by this time impaired resynthesis of these lipids was expected to be detectable (see Figure 2 for full kinetics). In these experiments, we also included treatment with 250 nM PIK93 before AngII treatment for each group to determine whether compensatory changes in PI4KIIIβ (although not apparent by Western analysis) could mask the effects of PI4KIIα or PI4KIIIα knockdown. Because there was absolutely no difference between the PIK93-AngII–treated group and those only treated with AngII alone (data not shown), these measurements have been combined for statistical analysis.

As shown in Figure 9C, by 10 min of AngII treatment, PtdIns(4,5)P$_2$ and PtdIns4P levels returned to ~60–70% of their prestimulatory values (also see Figure 2) in control cells[1]. However, in cells depleted in PI4KIIIα, this value was significantly

---

[1] Because AngII treatment increases the labeling of PtdIns/PtdA, and the knockdown of the individual enzymes could also affect this response, the correction for cell loss due to knockdown of the enzymes was based on the PtdIns/PtdA values obtained in the unstimulated cells also for the in AngII-stimulated samples. We assumed that AngII treatment does not cause cell loss.
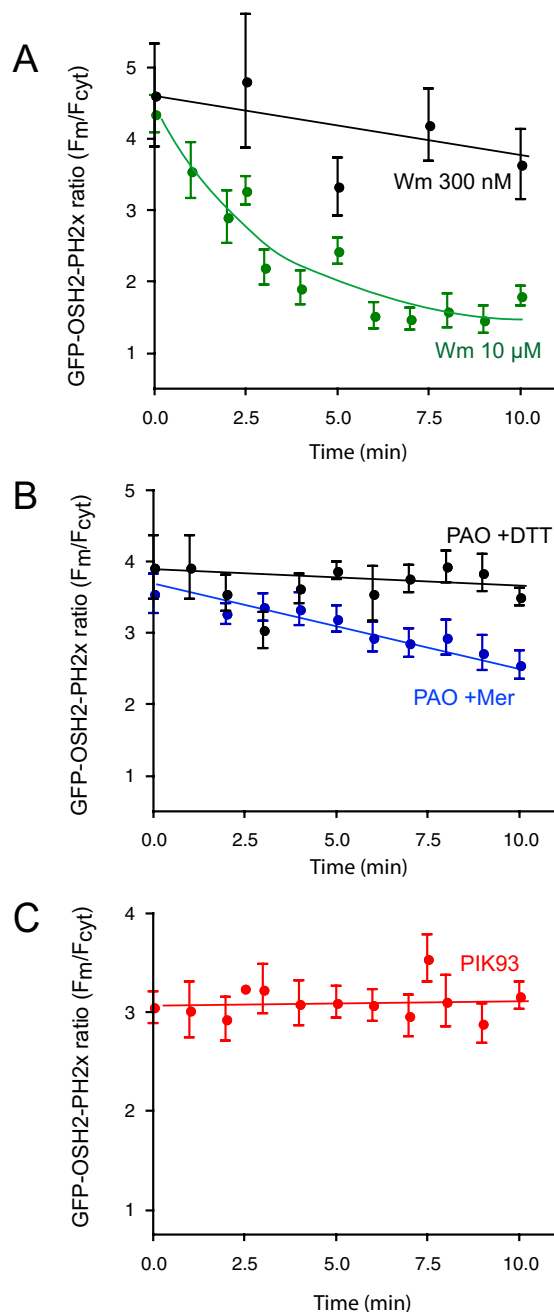
A. Balla *et al.*

Figure 7. Effects of PI4K inhibitors on the membrane localization of the OSH2-PH2x-GFP. HEK-293 cells stably transfected with the AT1a angiotensin receptors were cotransfected with the OSH2-PH2x-GFP constructs for 24 h. Live cells were examined in a confocal microscope at 35°C. Calculation of membrane/cytosolic fluorescence intensities as function of time was performed from line-intensity histograms from images taken at every minute during a 10-min incubation with the inhibitors. The concentrations of the inhibitors were 250 nM PIK93, 10 μM PAO with 1 mM Mer, 10 μM PAO with 1 mM DTT, and 10 μM or 300 nM Wm. Means $\pm$ SEM from three to 25 cells from two to four separate experiments are shown.

($p < 0.05$) lower (~50%) for both lipids, the difference being more pronounced in PtdIns(4,5)P$_2$, which could be measured with better accuracy. These differences were relatively minor and required a fine balance between siRNA treatment that still
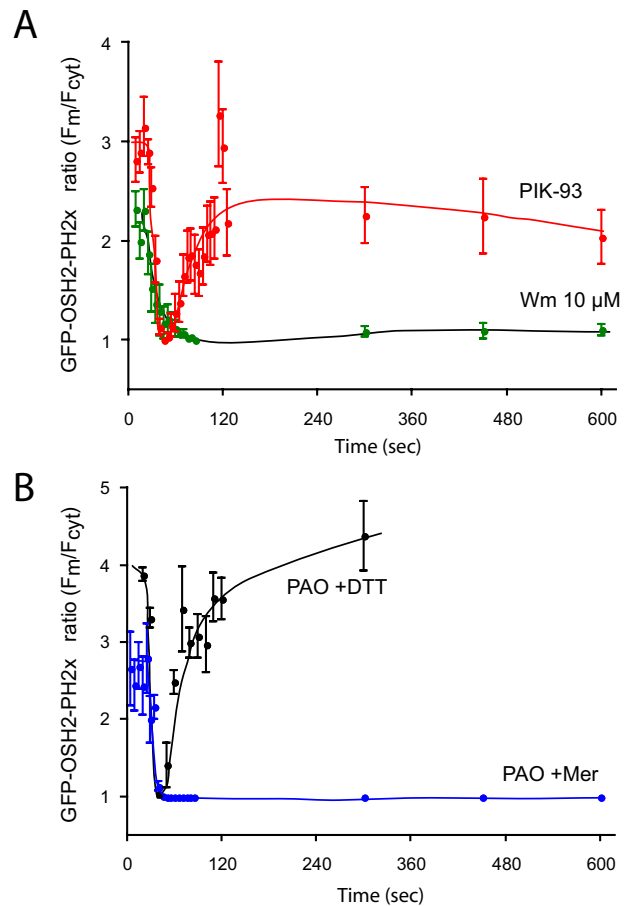
Figure 8. Effects of AngII on the membrane localization of the OSH2-PH2x-GFP after treatment with PI4K inhibitors. HEK-293 cells stably transfected with the AT1a angiotensin receptors were cotransfected with the OSH2-PH2x-GFP constructs for 24 h. Live cells were examined in a confocal microscope at 35°C. Calculation of membrane/cytosolic fluorescence intensities as function of time was performed from line-intensity histograms from images taken at the indicated times after AngII addition. The concentrations of the inhibitors applied for 10 min before AngII were 250 nM PIK93, 10 μM PAO with 1 mM Mer, and 10 μM Wm. Means $\pm$ SEM from three to 25 cells from two to four separate experiments are shown. The initial ratio values of Wm-treated cells are higher in these experiments than those shown in Figure 7 at the end of Wm treatment, because cells with still measurable OSH2-PH2x-GFP localization after Wm treatment were selected for this analysis.

preserved enough cells for analysis yet showed sufficient knockdown to capture even these small changes.

In cells labeled with *myo*-[³H]inositol, the picture was further complicated because we observed an increased labeling of PtdIns4P and PtdIns(4,5)P$_2$ (and the inositol phosphates) in cells in which PI4KIIIα was depleted. This paradoxical change was attributed to a significant decrease in the free inositol level of PI4KIIIα knockdown cells and hence an increased specific activity of the labeled inositol pool (data not shown). The reason for the consistent decrease in the level of inositol in cells depleted in PI4KIIIα is not known, and it is currently under further investigation.

DISCUSSION

In the present study, we asked the question of which of the PI4K enzymes is important for the generation of the plasma

Figure 9. Effects of knockdown of the individual PI 4-kinases on [^{32}P]phosphate labeling of phosphoinositides and their response to AngII stimulation in HEK-293-AT1 cells. HEK-293 cells stably transfected with the AT1a receptors were treated with siRNA for 3 d as described under *Materials and Methods*. The extent of knockdown was determined by Western blot analysis (A). On the fourth day, cells were labeled with [^{32}P]phosphate for 3 h in phosphate-free medium. Cells were then either t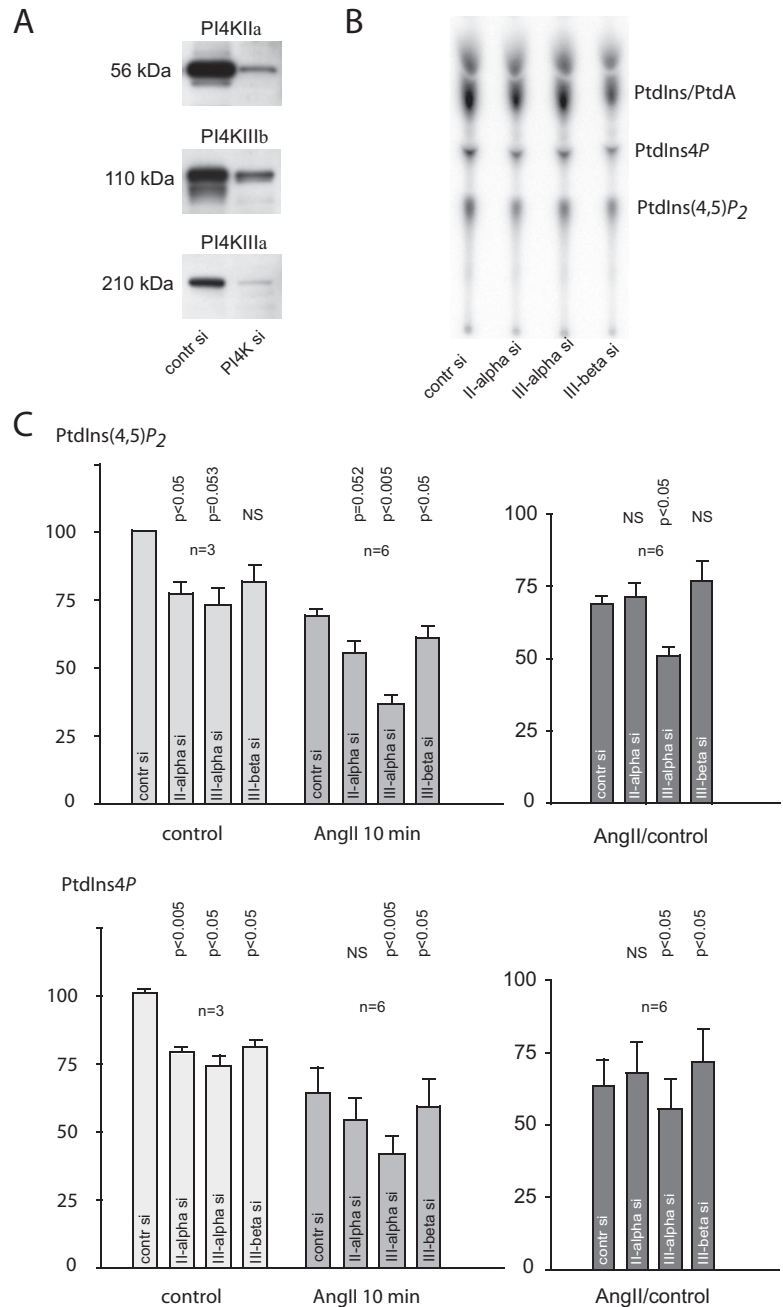reated with AngII (10^{-7} M) or saline and incubated for an additional 10 min. Reactions were terminated by PCA, and lipids were extracted from the cell pellets, separated by TLC, and analyzed by a PhosphorImager (B). Due to cell loss in the PI4K-depleted cells, the individual PtdIns4P and PtdIns(4,5)P$_2$ spots were normalized to the PtdA/PtdIns values measured in unstimulated samples of the respective groups. These ratios were then compared between the PI4K downregulated or control siRNA-treated cells in each of the three experiments performed in duplicates (C). In each experiments, the effect of 250 nM PIK93 was also determined in the AngII group. Because PIK93-treated cells showed no difference compared with those treated with AngII only, these values were pooled in the statistical analysis. Means ± SEM are shown, and the p values obtained in one-sample *t* tests compared with control siRNA-treated cells are shown above the bars.

membrane pool of PtdIns4P, the precursor of PtdIns(4,5)P$_2$ during PLC activation in agonist-stimulated cells. This question has not been thoroughly addressed before for lack of appropriate tools to investigate it properly. In a previous study, we showed that Wm-sensitive type III PI4Ks are required for the maintenance of agonist-sensitive phosphoinositide pools and hence Ins(1,4,5)P$_3$ and calcium signaling (Nakanishi *et al.*, 1995). These studies have been confirmed in other laboratories using different cell lines and different Ca^{2+}-mobilizing receptors and agonists (Willars *et al.*, 1998), but the identity of the enzyme(s) responsible for supplying PtdIns4P for the plasma membrane so far has eluded identification. The recent discovery of a PI 3-kinase inhibitor that discriminates between the type III PI4Ks has proven to be an invaluable tool to reinvestigate this question. Based on stud-

ies using ^{32}P-labeled phosphoinositides and *myo*-[^{3}H]inositol-labeled inositol phosphates and cytoplasmic Ca^{2+} measurements, we were able to show that the effects of Wm are reproduced by inhibitors of PI4KIIIα but not PI4KIIIβ. It was also important to demonstrate that the PtdIns4P pool that is affected by the PI4KIIIα enzyme is in fact in the plasma membrane. This question was especially relevant, because none of the type III PI4Ks can be found in detectable amounts in the plasma membrane by immunofluorescence analysis of COS-7 or HEK-293 cells. Based on enzymatic characterization of the plasma membrane-associated PI4K activity performed two decades ago, it was concluded that the smaller and wortmannin-insensitive type II PI4Ks are present in the plasma membrane. This is supported by more recent immunocytochemical analysis that finds only the type

A. Balla *et al.*

II enzymes partially in the plasma membrane. Of the type III enzymes, PI4KIIIβ is found in the Golgi, and PI4KIIIα in the ER/Golgi compartment (see Balla and Balla, 2006 for citation of the original studies). So, it was of particular interest that the PH domain of the OSH2 protein, one of the yeast homologues of oxysterol binding proteins, is capable of reporting on changes in the plasma membrane that are consistent with changes of PtdIns4P levels (see also Yeung *et al.*, 2006).

These studies using PH domains of PLCδ_1 and OSH2-PH2x to monitor PtdIns(4,5)P$_2$ and PtdIns4P, respectively, confirmed the conclusions of the labeling and Ca^{2+} experiments that PI4KIIIα is the enzyme necessary for the maintenance of the plasma membrane pool of these lipids. The exact mechanism how this is achieved by the enzyme that is primarily ER/Golgi localized remains to be answered, but its is quite possible that a small fraction of the enzyme is in fact found at the plasma membrane regulated by a unique mechanism, whereas the larger fraction of the protein has additional functions in the ER/Golgi compartments. It is interesting to note that in *S. cerevisiae* the Stt4p PI4K, a homologue of PI4KIIIα, was reported to generate the plasma membrane PtdIns4P pool, but unlike in mammalian cells, the yeast enzyme is primarily found in the plasma membrane or a tightly associated compartment (Audhya and Emr, 2002). Paradoxically, there are well-documented ER and vacuolar functions of Stt4p in yeast; yet, the protein has not been detected in those locations (Trotter *et al.*, 1998; Audhya *et al.*, 2000).

RNAi-mediated depletion of the individual PI4Ks has produced only small effects on ^{32}P-labeled PtdIns4P and PtdIns(4,5)P$_2$ but confirming the identity of the PI4KIIIα enzyme as one responsible for PtdIns4P and PtdIns(4,5)P$_2$ production at the plasma membrane during AngII stimulation. Although the levels of the enzymes can be knocked down to 15–30% of their original values, this level of knockdown produced only small effects in the labeled lipids and none on AngII-induced Ca^{2+} signaling. This probably reflects the fact that small amounts of these enzymes are sufficient to support the production of this signaling pool of the lipids and cells with more severe knockdown could simply be eliminated or developed adaptive mechanisms to cope with the lack of the protein. This highlights the difficulties with knockdown studies of enzymes of crucial importance and the value of inhibitors that can be tested in short-term experiments.

In recent studies, we were able to show the role of PI4Ks in other aspects of cellular PtdIns4P production where the knockdown data gave as clear results as the pharmacological approach. These included the recruitment of the FAPP1PH domain to the Golgi being mediated by both the PI4KIIIβ and PI4KIIα enzymes (Balla *et al.*, 2005), and the role of PI4KIIIβ in the ER-to-Golgi transport of ceramide (Toth *et al.*, 2006). In fact, in the former study we found that PI4KIIIα knockdown was able to decrease the plasma membrane recruitment of the FAPP1PH domain during recovery from a large Ca^{2+}-mediated PLC activation (Balla *et al.*, 2005). These studies collectively suggest that PI4Ks probably have multiple functions within the cells that are affected at different level of enzyme depletion.

Last, the experiments using the FAPP1PH, OSBP-PH, and OSH2-PH domains highlight the values and the limitations of PH domain reporters. They clearly demonstrate that specific pools of PtdIns4P are detected by the individual probes and that one reporter may not detect PtdIns4P in all locations within the cells. The FAPP1 and OSBP PH domains detect primarily the Golgi pool, although under special circumstances such as during recovery from massive Ca^{2+} induced PLC activation they can also detect PtdIns4P in the plasma membrane (Balla *et al.*, 2005). In contrast, the OSH2–2x-PH-GFP reporter detects PtdIns4P in the plasma membrane but not in the Golgi compartment in mammalian cells. Only the yeast OSH1-PH decorates both the Golgi and the plasma membrane. Importantly, the plasma membrane localization of all of the PtdIns4P reporters depends on the activity of Wm-sensitive, type III PI4Ks, and based on the current studies, specifically of the PI4KIIIα enzyme.

In summary, the present results establish PI4KIIIα as an important component of the generation of the plasma membrane pool of phosphoinositides. This conclusion is based on pharmacological studies and confirmed by RNAi-mediated gene silencing, although the latter could not decrease the enzyme levels sufficiently to appreciably impair Ca^{2+} signaling. These results also establish the OSH2-PH2x domain as a useful reporter to follow PtdIns4P changes in the plasma membrane. Further studies are in progress to identify the mechanism by which the apparently ER/Golgi localized PI4KIIIα can affect the supply of plasma membrane PtdIns4P.

ACKNOWLEDGMENTS

REFERENCES

Audhya, A., and Emr, S. D. (2002). Stt4 PI 4-kinase localizes to the plasma membrane and functions in the Pkc1-mediated MAP kinase cascade. Dev. Cell 2, 593–605.

Audhya, A., Foti, M., and Emr, S. D. (2000). Distinct roles for the yeast phosphatidylinositol 4-kinases, stt4p and pik1p, in secretion, cell growth, and organelle membrane dynamics. Mol. Biol. Cell 11, 2673–2689.

Balla, A., and Balla, T. (2006). Phosphatidylinositol 4-kinases; old enzymes with emerging functions. Trends Cell Biol. 16, 351–361.

Balla, A., Tuymetova, G., Barshishat, M., Geiszt, M., and Balla, T. (2002). Characterization of type II phosphatidylinositol 4-kinase isoforms reveals association of the enzymes with endosomal vesicular compartments. J. Biol. Chem. 277, 20041–22050.

Balla, A., Tuymetova, G., Tsiomenko, A., Varnai, P., and Balla, T. (2005). A plasma membrane pool of phosphatidylinositol 4-phosphate is generated by phosphatidylinositol 4-kinase type-III alpha: studies with the PH domains of the oxysterol binding protein and FAPP1. Mol. Biol. Cell 16, 1282–1295.

Balla, T., Baukal, A. J., Guillemette, G., and Catt, K. J. (1988). Multiple pathways of inositol polyphosphate metabolism in angiotensin-stimulated adrenal glomerulosa cells. J. Biol. Chem. 263, 4083–4091.

Balla, T., Downing, G. J., Jaffe, H., Kim, S., Zolyomi, A., and Catt, K. J. (1997). Isolation and molecular cloning of wortmannin-sensitive bovine type-III phosphatidylinositol 4-kinases. J. Biol. Chem. 272, 18358–18366.

Barylko, B., Wlodarski, P., Binns, D. D., Gerber, S. H., Earnest, S., Sudhof, T. C., Grichine, N., and Albanesi, J. P. (2002). Analysis of the catalytic domain of phosphatidylinositol 4-kinase type II. J. Biol. Chem. 277, 44366–44375.

Berridge, M. J., and Irvine, R. F. (1984). Inositol trisphosphate, a novel second messenger in cellular signal transduction. Nature 312, 315–321.

Creba, J. A., Downes, C. P., Hawkins, P. T., Brewster, G., Michell, R. H., and Kirk, C. J. (1983). Rapid breakdown of phosphatidylinositol 4-phosphate and phosphatidylinositol 4,5-bisphosphate in rat hepatocytes stimulated by vasopressin and other Ca2+-mobilizing hormones. Biochem. J. *212*, 733–747.

Doughman, R. L., Firestone, A. J., and Anderson, R. A. (2003). Phosphatidylinositol phosphate kinases put PI4,5P(2) in its place. J. Membr. Biol. *194*, 77–89.

Godi, A., Di Campi, A., Konstantakopoulos, A., Di Tullio, G., Alessi, D. R., Kular, G. S., Daniele, T., Marra, P., Lucocq, J. M., and De Matteis, M. A. (2004). FAPPs control Golgi-to-cell-surface membrane traffic by binding to ARF and PtdIns(4)P. Nat. Cell Biol. *6*, 393–404.

Kisseleva, M. V., Wilson, M. P., and Majerus, P. W. (2000). The isolation and characterization of a cDNA encoding phospholipid-specific inositol polyphosphate 5-phosphatase. J. Biol. Chem. *275*, 20110–20116.

Knight, Z. A., *et al.* (2006). A pharmacological map of the PI3-K family defines a role for p110alpha in insulin signaling. Cell *125*, 733–747.

Levine, T. P., and Munro, S. (2002). Targeting of Golgi-specific pleckstrin homology domains involves both PtdIns 4-kinase-dependent and -independent components. Curr. Biol. *12*, 695–704.

Majerus, P. W., Kisseleva, M. V., and Norris, F. A. (1999). The role of phosphatases in inositol signaling reactions. J. Biol. Chem. *274*, 10669–10672.

Minogue, S., Waugh, M. G., De Matteis, M. A., Stephens, D. J., Berditchevski, F., and Hsuan, J. J. (2006). Phosphatidylinositol 4-kinase is required for endosomal trafficking and degradation of the EGF receptor. J. Cell Sci. *119*, 571–581.

Nakanishi, S., Catt, K. J., and Balla, T. (1995). A wortmannin-sensitive phosphatidylinositol 4-kinase that regulates hormone-sensitive pools of inositol-phospholipids. Proc. Natl. Acad. Sci. USA *92*, 5317–5321.

Roy, A., and Levine, T. P. (2004). Multiple pools of phosphatidylinositol 4-phosphate detected using the pleckstrin homology domain of Osh2p. J. Biol. Chem. *279*, 44683–44689.

Toth, B., Balla, A., Ma, H., Knight, Z. A., Shokat, K. M., and Balla, T. (2006). Phosphatidylinositol 4-kinase IIIbeta regulates the transport of ceramide between the endoplasmic reticulum and Golgi. J. Biol. Chem. *281*, 36369–36377.

Trotter, P. J., Wu, W. I., Pedretti, J., Yates, R., and Voelker, D. R. (1998). A genetic screen for aminophospholipid transport mutants identifies the phosphatidylinositol 4-kinase, Stt4p, as an essential component in phosphatidylserine metabolism. J. Biol. Chem. *273*, 13189–13196.

van Der Wal, J., Habets, R., Varnai, P., Balla, T., and Jalink, K. (2001). Monitoring phospholipase C activation kinetics in live cells by FRET. J. Biol. Chem. *276*, 15337–15344.

Varnai, P., Balla, A., Hunyady, L., and Balla, T. (2005). Targeted expression of the inositol 1,4,5-triphosphate receptor (IP3R) ligand-binding domain releases Ca2+ via endogenous IP3R channels. Proc. Natl. Acad. Sci. USA *102*, 7859–7864.

Várnai, P., and Balla, T. (1998). Visualization of phosphoinositides that bind pleckstrin homology domains: calcium-and agonist-induced dynamic changes and relationship to myo-[3H]inositol-labeled phosphoinositide pools. J. Cell Biol. *143*, 501–510.

Varnai, P., Lin, X., Lee, S. B., Tuymetova, G., Bondeva, T., Spat, A., Rhee, S. G., Hajnoczky, G., and Balla, T. (2002). Inositol lipid binding and membrane localization of isolated pleckstrin homology (PH) domains. Studies on the PH domains of phospholipase C delta 1 and p130. J. Biol. Chem. *277*, 27412–27422.

Varnai, P., Thyagarajan, B., Rohacs, T., and Balla, T. (2006). Rapidly inducible changes in phosphatidylinositol 4,5-bisphosphate levels influence multiple regulatory functions of the lipid in intact living cells. J. Cell Biol. *175*, 377–382.

Wang, J., Sun, H. Q., Macia, E., Kirchhausen, T., Watson, H., Bonifacino, J. S., and Yin, H. L. (2007). PI4P promotes the recruitment of the GGA adaptor proteins to the *trans*-Golgi network and regulates their recognition of the ubiquitin sorting signal. Mol. Biol. Cell *18*, 2646–2655.

Wang, Y. J., Li, W. H., Wang, J., Xu, K., Dong, P., Luo, X., and Yin, H. L. (2004). Critical role of PIP5KIgamma 87 in InsP3-mediated Ca(2+) signaling. J. Cell Biol. *167*, 1005–1010.

Wang, Y. J., Wang, J., Sun, H. Q., Martinez, M., Sun, Y. X., Macia, E., Kirchhausen, T., Albanesi, J. P., Roth, M. G., and Yin, H. L. (2003). Phosphatidylinositol 4 phosphate regulates targeting of clathrin adaptor AP-1 complexes to the Golgi. Cell *114*, 299–310.

Warashina, A. (1999). Light-evoked recovery from wortmannin-induced inhibition of catecholamine secretion and synaptic transmission. Arch. Biochem. Biophys. *367*, 303–310.

Wiedemann, C., Schäfer, T., and Burger, M. M. (1996). Chromaffin granule-associated phosphatidylinositol 4-kinase activity is required for stimulated secretion. EMBO J. *15*, 2094–2101.

Willars, G. B., Nahorski, S. R., and Challiss, R. A. (1998). Differential regulation of muscarinic acetylcholine receptor-sensitive polyphosphoinositide pools and consequences for signaling in human neuroblastoma cells. J. Biol. Chem. *273*, 5037–5046.

Yeung, T., Terebiznik, M., Yu, L., Silvius, J., Abidi, W. M., Philip, M., Levine, T., Kapus, A., and Grinstein, S. (2006). Receptor activation alters inner surface potential during phagocytosis. Science *313*, 347–351.

Yu, J. W., Mendrola, J. M., Audhya, A., Singh, S., Keleti, D., DeWald, D. B., Murray, D., Emr, S. D., and Lemmon, M. A. (2004). Genome-wide analysis of membrane targeting by *S. cerevisiae* pleckstrin homology domains. Mol. Cell *13*, 677–688.

Design of Drug-Resistant Alleles of Type-III Phosphatidylinositol 4-Kinases Using Mutagenesis and Molecular Modeling[†]

Andras Balla,[‡,§] Galina Tuymetova,[‡] Balazs Toth,[‡] Zsofia Szentpetery,[‡] Xiaohang Zhao,[||] Zachary A. Knight,[⊥] Kevan Shokat,[⊥] Peter J. Steinbach,[#] and Tamas Balla*,[‡]

Section on Molecular Signal Transduction, Center for Developmental Neuroscience, NICHD, National Institutes of Health, Bethesda, Maryland, Department of Physiology, Faculty of Medicine, Semmelweis University, Budapest, Hungary, Center for Molecular Modeling, Division of Computational Bioscience, CIT, National Institutes of Health, Bethesda, Maryland, National Laboratory of Molecular Oncology, Cancer Institute & Hospital, Chinese Academy of Medical Sciences & Peking Union Medical College, Beijing, P. R. China, Program in Chemistry and Chemical Biology, University of California, San Francisco, California, and Howard Hughes Medical Institute and Department of Cellular and Molecular Pharmacology, University of California, San Francisco, California

ABSTRACT: Molecular modeling and site directed mutagenesis were used to analyze the structural features determining the unique inhibitor sensitivities of type-III phosphatidylinositol 4-kinase enzymes (PI4Ks). Mutation of a highly conserved Tyr residue that provides the bottom of the hydrophobic pocket for ATP yielded a PI4KIIIβ enzyme that showed greatly reduced wortmannin sensitivity and was catalytically still active. Similar substitutions were not tolerated in the type-IIIα enzyme rendering it catalytically inactive. Two conserved Cys residues located in the active site of PI4KIIIα were found responsible for the high sensitivity of this enzyme to the oxidizing agent, phenylarsine oxide. Mutation of one of these Cys residues reduced the phenylarsine oxide sensitivity of the enzyme to the same level observed with the PI4KIIIβ protein. In search of inhibitors that would discriminate between the closely related PI4KIIIα and -IIIβ enzymes, the PI3Kγ inhibitor, PIK93, was found to inhibit PI4KIIIβ with significantly greater potency than PI4KIIIα. These studies should aid development of subtype-specific inhibitors of type-III PI4Ks and help to better understand the significance of localized PtdIns4*P* production by the various PI4Ks isoforms in specific cellular compartments.

Inositol phospholipids emerge as universal regulators of membrane-associated signaling events and membrane trafficking (*2−4*). These lipids are formed from phosphatidylinositol (PtdIns[1]) by sequential phosphorylations of the hydroxyl groups in their inositol ring by inositol lipid kinases. Phosphatidylinositol 4-kinases (PI4Ks) are the enzymes that produce PtdIns4*P*, a minor regulatory lipid that was long considered only as an intermediate in the production of other phosphoinositides, such as PtdIns(4,5)P_2 and PtdIns(3,4,5)-P_3. More recently, PtdIns4*P* has been increasingly recognized as a regulatory lipid that controls the recruitment of adaptor proteins and lipid-transport proteins to ER and Golgi membranes (*5*). Therefore, interest in PI4Ks is increasing. PI4Ks are classified into two major classes: the type-II PI4Ks (-α and -β forms) are proteins of ∼56 kDa in size that are tightly associated with membranes due to their palmitoylation (*6, 7*). These enzymes have only been recently cloned and, although they represent the majority of PI4K activities associated with membranes, their functional significance has just started to emerge. Type-III PI4Ks (-α and -β forms), on the other hand, are soluble peripheral membrane proteins that are greatly conserved from plants to humans and are homologous to PI3Ks (*8−10*).

The importance of the presence of multiple PI4K enzymes in the same cell is still not fully understood, due to the lack of specific inhibitors to study the functions of the individual enzymes. Based on yeast studies, both type-III PI4Ks are essential for viability, and they assume nonredundant functions. Pik1p (the yeast orthologue of PI4KIIIβ), which is mainly localized to the Golgi, plays a role in Golgi-to-plasma membrane secretion at the late Golgi secretory pathway (*11−13*), while the functions of Stt4p (the ortholog of PI4KIIIα) are more diverse, including roles in aminophospholipid synthesis (*14*), signaling to MAP kinases via the PKC pathway (*15*), and to PLD at the plasma membrane (*16*). Much less is known about these proteins in mammalian cells,

* To whom correspondence should be addressed: National Institutes of Health, Bldg 49, Rm 6A35, 49 Convent Drive, Bethesda, MD 20892-4510, phone (301)-496-2136, fax (301)-480-8010, e-mail ballat@mail.nih.gov.

‡ NICHD, National Institutes of Health.

§ Semmelweis University.

|| Chinese Academy of Medical Sciences & Peking Union Medical College.

⊥ Program in Chemistry and Chemical Biology, University of California, and Howard Hughes Medical Institute and Department of Cellular and Molecular Pharmacology, University of California.

Division of Computational Bioscience, CIT, National Institutes of Health.

[1] Abbreviations: PAO, phenylarsine oxide; PI3K, phosphatidylinositol 3-kinase; PI4K, phosphatidylinositol 4-kinase; PtdIns, phosphatidylinositol; PtdIns4*P*, phosphatidylinositol 4-phosphate; PtdIns-(4,5)P_2, phosphatidylinositol 4,5-bisphosphate; PtdIns(3,4,5)P_3, phosphatidylinositol 3,4,5-trisphosphate; Wm, wortmannin.

but PI4KIIIβ, which is a Golgi-localized protein, is important for Golgi-to-plasma membrane secretion (*17, 18*), while PI4KIIIα appears to regulate the production of the plasma membrane pool of PtdIns4*P*, although the enzyme is primarily localized to the ER/Golgi in mammalian cells (*8, 19*). Type-II PI4Ks are mostly associated with endosomes and the TGN, and recently the type-IIα enzyme was implicated in EGF receptor trafficking and degradation (*20*).

The ideal way to study the functions of these proteins would be to use specific inhibitors for the distinct isoforms of these enzymes. Unfortunately, little effort has been exerted in this research direction. Wortmannin (*21, 22*) and LY294002 (*23*) have been invaluable tools to study PI3Ks, and their use has also contributed to our knowledge of type-III PI4Ks (*24*). However, Wm has four major disadvantages when studying the functions of PI4Ks. First, Wm inhibits PI3Ks at much lower concentrations than is necessary to inhibit the type-III PI4Ks. Second, and especially problematic, Wm cannot discriminate between PI4KIIIα and -β (*25*). Third, the effects of Wm are irreversible.[2] Finally, its dose-dependent effects are greatly influenced by the duration of its administration (*26, 27*). Phenylarsine oxide (PAO) has also been used often as a PI4K inhibitor (*28*), and while this drug has probably several cellular targets, among the PI4Ks it is most potent against the type-IIIα enzyme (*29*). The present study was undertaken to investigate the structural properties of the catalytic domains of type-III PI4Ks, in comparison with those of PI3Ks using molecular modeling. These studies combined with site-directed mutagenesis allowed the generation of PI4K enzymes that are significantly less sensitive to their commonly used inhibitors and that could be used in pharmacological rescue experiments. Moreover, these studies also identified an inhibitor that discriminates between the two closely related type-III PI4Ks. Our studies should aid efforts to search for, and possibly design, inhibitors that would specifically target individual PI4K enzymes.

EXPERIMENTAL PROCEDURES

Materials. Wortmannin and LY294002 were purchased from Calbiochem, and PIK93 was synthesized as described previously (*30*). Phosphatidylinositol and PAO were obtained from Sigma. [γ-^{32}P]ATP (6000 Ci/mmol) was from NEN (General Electric), and [^{3}H]wortmannin-17-ol (19.7 Ci/mmol) was from DuPont NEN. Unfortunately, the latter product has now been discontinued for a long time. [^{3}H]L-Serine (20-40 Ci/mmol) was from General Electric (Piscataway, NJ). All other materials were of the highest analytical grade.

Molecular Biology and Mutagenesis. The bacterial expression plasmid for GST-fused PI4KIIIβ has been described previously (*31*), and so were the HA-tagged forms of the type-II enzymes for eukaryotic expression (*29*). Bovine PI4KIIIβ was HA-tagged at the N-terminus using the pcDNA3.1-PI4KIIIβ as the template (*10*), while bovine PI4KIIIα was epitope tagged at its C-terminus in the pcDNA3.1(+) vector. For bacterial expression of a PI4KIIIα enzyme, a GST fusion construct was generated from the C-terminal fragment (residues 874−2044) of the bovine

PI4KIIIα using the pET23b plasmid (Novagen) as a backbone. This plasmid was fashioned to generate a GST fusion protein construct using the GST fragment with its original proteolytic and restriction sites from the pGEX6P (Amersham) plasmid.

Mutagenesis was performed with the QuikChange mutagensis kit of Promega following the manufacturer's instructions. After verifying the mutations with dideoxy sequencing, the mutated fragments were exchanged between the wild-type and mutated enzymes with suitable restriction sites to avoid the generation of unwanted mutations outside the sequenced regions.

Production of Proteins in Bacteria. All four PI4Ks were expressed in the BL21 strain of *E. coli*, induced, purified essentially as described earlier (*31*) and cleaved either with PrerScission or TEV protease or eluted with gluthathione.

PI Kinase Assays. PI kinase assays were performed either with the bacterially expressed and GST purified enzymes on the beads or with the enzymes expressed in COS-7 cells and immunoprecipitated from cell lysates essentially as described previously (*24, 31*). Briefly, the assay mixture contained $\sim$1 mM PtdIns in the form of Triton micelles and 0.1 mM (1−2 μCi) [γ-^{32}P]ATP in 20 mM Tris buffer (pH 7.4) and in the presence of 20 mM MgCl$_2$ and the enzyme. When inhibitors were added, they were preincubated with the enzymes for 10 min prior to the addition of ATP. Reactions were run at room temperature for 10−20 min and were terminated by the addition of 3 mL of CHCl$_3$:CH$_3$OH: *cc*HCl (200:100:0.75 (v/v). The organic solvent phase was separated from [γ-^{32}P]ATP by adding 0.6 mL of 0.6 N HCl, mixing vigorously, and letting it stand for phase separation. The upper phase (aqueous) was discarded, and 1.5 mL of CHCl$_3$:CH$_3$OH:0.6 N HCl (3:48:47, v/v) was added to the lower phase, followed by mixing and phase separation. The lower phase was then transferred to scintillation vials and, after evaporation, the radioactivity counted with Econofluor as a scintillant.

For K_m determinations, the concentration of unlabeled ATP was changed, and the incubation time was chosen to be on the linear part of the reaction kinetics. For calculations, the simple Lineweaver−Burk analysis was used.

Wortmannin Binding. Aliquots of the purified and cleaved wild-type or mutant PI4KIIIβ enzymes containing equal amounts of protein were incubated for 20 min at room temperature in a total volume of 100 μL of PBS containing 0.4 μCi of [^{3}H]WT, which corresponded to 200 nM concentration of WT. Proteins were precipitated with TCA (5% final) and subjected to SDS PAGE and Western blotting. PVDF membranes were then sprayed with ENHANCE (DuPont), and after drying they were exposed at −70 °C for 1 week.

Analysis of Protein Kinase Activity. Aliquots of the purified and cleaved wild-type or mutant PI4KIIIβ enzymes were incubated in 100 μL of 50 mM Tris-HCl pH 7.4, 100 mM NaCl, 3−10 mM MnCl2, 40 μM ATP, and 5 μCi of [γ-^{32}P]ATP for 30 min at 37 °C. Wm or DMSO was added 10 min prior to ATP. After phosphorylation, the protein was subjected to SDS PAGE, and phosphorylation was quantitated using a PhosphoImager (Molecular Dynamics).

Studies in COS-7 Cells. COS-7 cells were transfected with the indicated constructs cloned in pcDNA3.1 plasmids and

---

[2] The effects of wortmannin can be reversed by strong illumination especially with wavelengths below 450 nm (*1*).

selected in 800 μg/mL G418. Clones were tested with Western analysis to determine the expression of the protein. Cells were grown on 25 mm glass coverslips and transfected with a construct composed of the CERT-PH domain fused to mRFP for 24 h for confocal analysis. Live cells were examined at 35 °C in a Zeiss LSM510 laser confocal microscope as described in detail elsewhere (*32*). The ceramide and sphingomyelin labeling with [^{3}H]serine has been previously described (*33*). Briefly, COS-7 cells were seeded on 12 well plates at a density of 3×10^5 cells/well. After 1 day in culture, cells were incubated in a serine-free medium for 4 h before labeling with 100 μCi/mL [^{3}H]serine for 60 min. When inhibitors were used, they were added 10 min prior to labeling and they were present throughout the labeling period. Incubations were terminated by removal of the labeling medium and the addition of ice-cold 5% PCA. Lipids were extracted, deacylated and separated as described in (*33*).

Molecular Modeling of PI4Ks. Homology models of the bovine type-III PI4Ks (accession numbers: AAC48729 for β form and AAC48730 for α form) were built with either ATP, wortmannin or PIK93 bound, using the crystal structure of PI3Kγ with the particular ligand bound (pdb codes: 1e8x, 1e7u, 2chz, respectively) as template. The SegMod algorithm (*34*) implemented in the program GeneMine was used to build each model.

RESULTS

Comparison of PI3K and Type-III PI4Ks Using Sequence Alignment and Molecular Modeling. Multiple-sequence alignments of the catalytic domains of the various classes of PI 3- and 4-kinases demonstrate a large degree of conservation among these proteins (Figure 1). Such alignments are of great value to pinpoint differences that are conserved within the individual classes of the enzymes. The published X-ray structure of PI3Kγ (*35, 36*) has made it possible to analyze these differences structurally and to predict their importance for the catalytic process. We used homology-based molecular modeling to compare the structures of the catalytic domains of the two type-III PI4Ks, PI4KIIIα and PI4KIIIβ, with that of PI3Kγ. These models are built assuming that the catalytic domains of PI4Ks fold similarly to that of PI3Kγ. Figure 2A shows the model of PI4KIIIβ with residues that are identical to PI3Kγ colored red. Although the overall homology within this whole segment is only 21%, it increases closer to the ATP binding site (46% within 7 Å of ATP and 65% within 5 Å). The catalytic domains of both PI4K models are formed by two half-lobes, a smaller N-terminal and a larger C-terminal lobe (Figure 2A), with the ATP molecule sandwiched in between. The two sides are linked together by a short intervening sequence, and a highly conserved Tyr residue (Y867 in PI3Kγ) located on a long loop forms the bottom of the nucleotide binding pocket (Figure 2A). Importantly, the major contacts with the adenosine ring and the phosphate groups are highly conserved between the three molecules.

Mutagenesis of PI4KIIIβ. These sequence comparisons and the structural models were used to design a PI4K with

diminished Wm sensitivity. The advantage of such an enzyme is that it could be used in expression studies where the endogenous enzymes are inhibited by Wm treatment. Wm binds to the ATP binding site of PI3Ks and covalently attaches to Lys 833 of PI3Kγ (*37*). This Lys residue corresponds to K549 and K1791 in PI4KIIIβ and -α, respectively, shown in the model either with the ATP (Figure 2B) or Wm (Figure 3) molecules. Since this residue is essential to the binding of ATP, its mutation renders the enzyme catalytically inactive. Instead, we sought a site of Wm interaction that, when mutated, would weaken Wm binding without a major effect on ATP binding. Since the yeast orthologue of the PI4KIIIβ enzyme, Pik1p, is resistant to Wm, we reasoned that creation of such a mutant was feasible, and we looked for regions within the Wm binding pocket that differ significantly between the yeast Pik1p enzyme and other PI 3- or 4-kinases.

Two aromatic residues were found in the right position. One was the Tyr within the P866−Y867 sequence (PI3Kγ numbering) that is highly conserved between the PI 3- and type-III PI4-kinases. This Tyr residue, which corresponds to Y583 and Y1825 in PI4KIIIβ and -α, respectively, forms the bottom of the binding pocket both for ATP (Figure 2B) and for Wm (Figure 3). Remarkably, in the Pik1 homologues of lower eukaryotes these two residues are replaced by Arg-Met (Figure 1, upper panel, highlighted in deep blue). The other residue, which corresponds to F961 of PI3Kγ, faces the adenine ring and corresponds to a Ser in Pik1p and an Ile in all type-III PI 4-kinases. Mutations were generated in the bacterially expressed recombinant bovine PI4KIIIβ (*31*), and the enzymatic activities of equal amounts of enzymes were determined in the presence of 0.1 or 1 mM ATP. Substitution of the P582−Y583 sequence with Arg-Met or Leu-Met greatly reduced Wm sensitivity (Figure 4A and Table 1). However, the catalytic activities of these mutants were also sharply reduced (Table 1). In contrast, substitution of only the Tyr with Met (Pro-Met) resulted in a similarly reduced Wm sensitivity, but the activity of this mutant was much better preserved (Figure 4A and Table 1). Mutation of I670−I671 to Val-Ser (as in Pik1p) reduced Wm sensitivity but also greatly reduced the catalytic activity compared to the wild-type PI4KIIIβ (Figure 4A and Table 1).

The binding of [^{3}H]Wm and the Wm-sensitivity of the autophosphorylation (*31*) of selected PI4KIIIβ enzymes were also tested. As shown in Figure 4B, Wm binding of the Y583M mutant was negligible, and its autophosphorylation was not inhibited by 3 μM Wm, a concentration that completely eliminated the autophosphorylation of the wild-type enzyme. We also tested whether mutations of conserved Ser and Thr residues within the tail of PI4KIIIβ affect autophosphorylation or the enzyme's catalytic activity. Neither of these substitutions (S781A, T787A and T797A) affected autophosphorylation or changed significantly the catalytic property of the enzyme (data not shown).

Mutagenesis of the PI4KIIIα Enzyme. To generate a bacterially expressed enzyme, the C-terminal 1171 residues of bovine PI4KIIIα were fused to GST based on an earlier report describing this construct as the minimally active catalytic module (*38*). Expression of this protein, indeed, yielded a catalytically active enzyme that was extremely sensitive to oxidation as has been observed for the mammalian PI4KIIIα enzyme. This result, and the high sensitivity

---

[3] Although the modeling was done on the bovine PI4K sequences, in the regions shown the bovine and human protein sequence is identical.
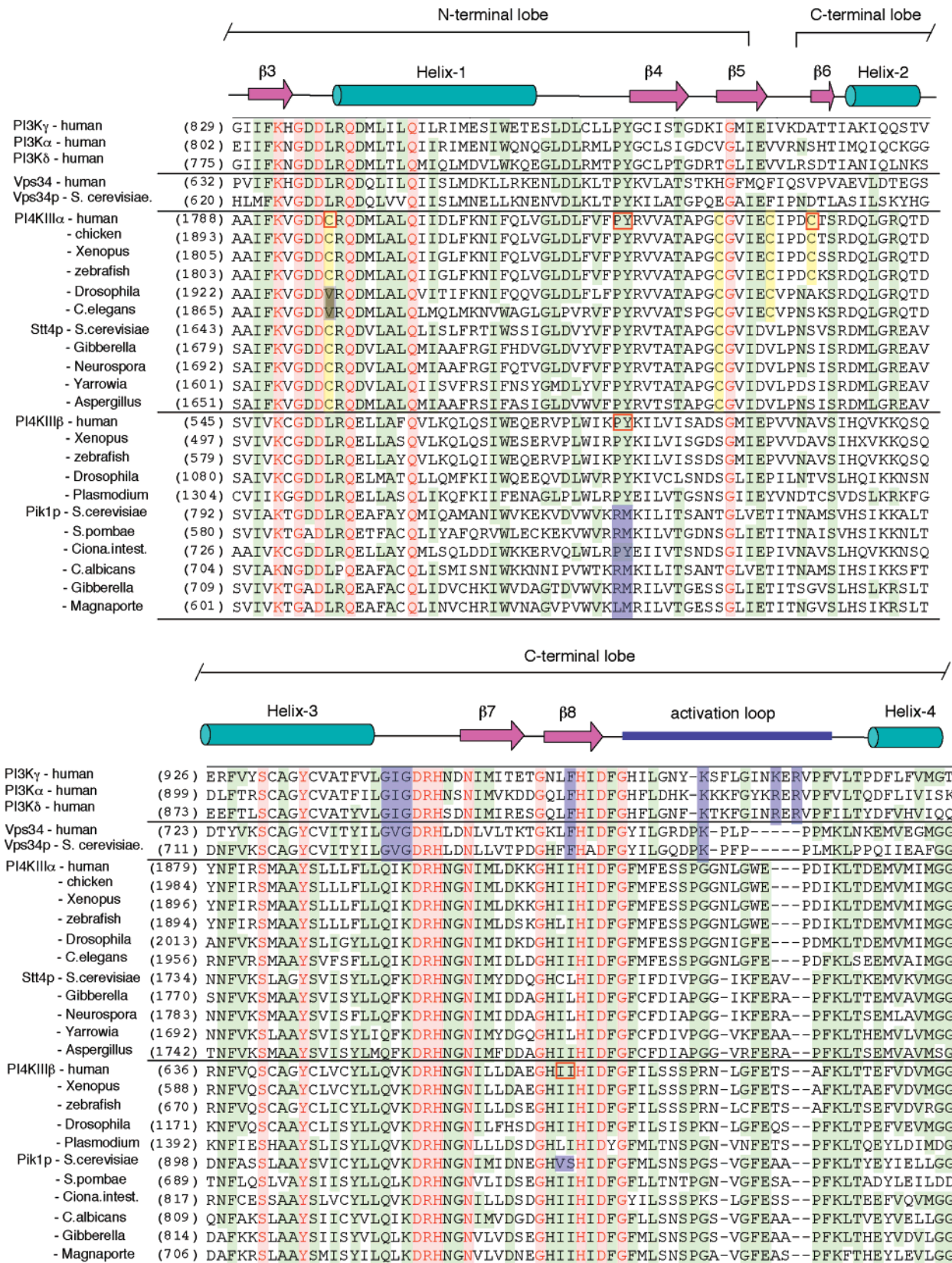
FIGURE 1: Multiple-sequence alignment of the catalytic domains of type-III PI4Ks and the human representatives of PI3Ks.[3] Residues conserved across all species and the different classes of enzymes are labeled red, while those showing limited conservation are labeled light green. Secondary structure elements based on the PI3Kγ structure are shown above the alignment. Regions of interest are highlighted with purple background and are discussed in the text. The Cys residues within PI4KIIIα are highlighted with a yellow background. Mutated residues are labeled with the red boxes. The multiple alignment was made with the Vector NTI software.

of the PI4KIIIα enzyme to the oxidizing agent PAO (*29*), prompted us to evaluate the roles of Cys residues in the high PAO sensitivity. Comparison of the sequences and models

of the two PI4Ks revealed the presence of two cysteines (C1839 and C1843) facing the adenine ring from each side in the short linker region connecting the N- and C-terminal
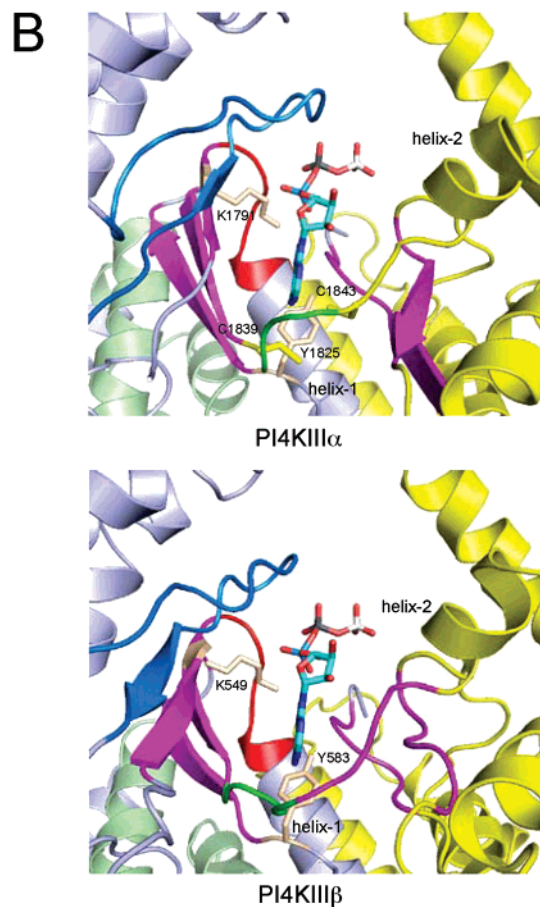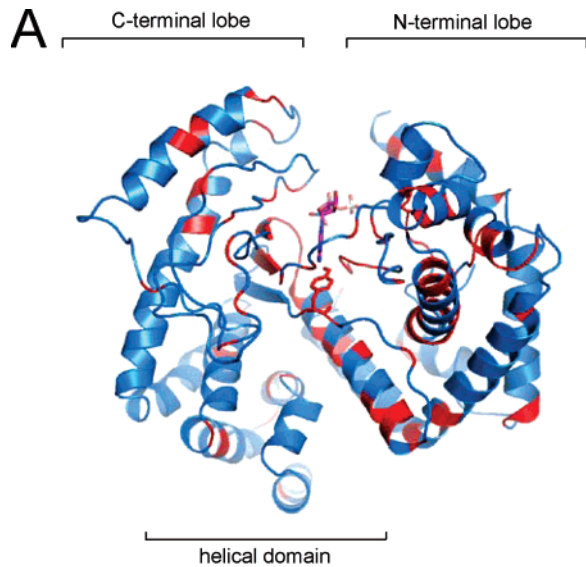
FIGURE 2: Molecular models of the catalytic domains of type-III PI4Ks based on the PI3Kγ structure bound with ATP. (A) Residues of PI4KIIIβ identical to those of PI3Kγ are colored red. The ATP binding site is formed by C- and N-terminal lobes (light blue and yellow, respectively, in panel B). In both lobes several antiparallel β-strands (purple in panel B) contribute to the sides of the nucleotide binding pocket. The all-helical domain (also called the lipid kinase unique domain) is packed against the bottom part of the C-terminal lobe (shown in light green in panel B), but it shows little sequence identity and the model has significant uncertainty in those regions. (B) Structural models of PI4KIIIα (upper) and PI4KIIIβ (lower) with ATP. The segments corresponding to the upper wall of the binding site in the C-terminal lobe are the least conserved (marine blue). Important residues that participate in ATP binding and PAO sensitivity are highlighted. The pictures were made using PyMol.
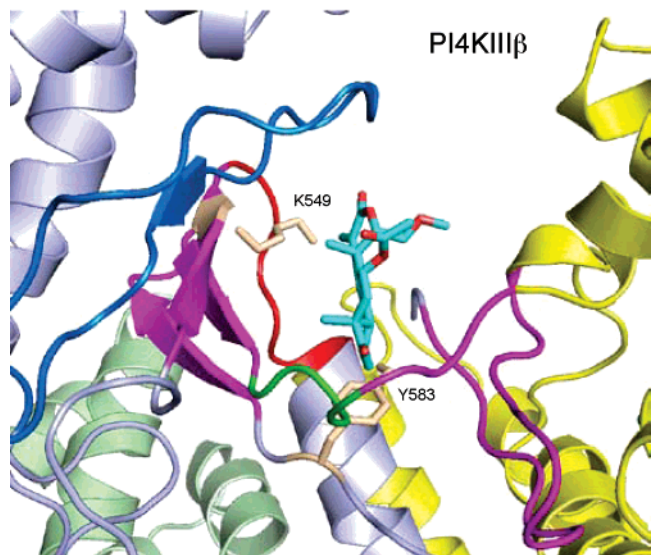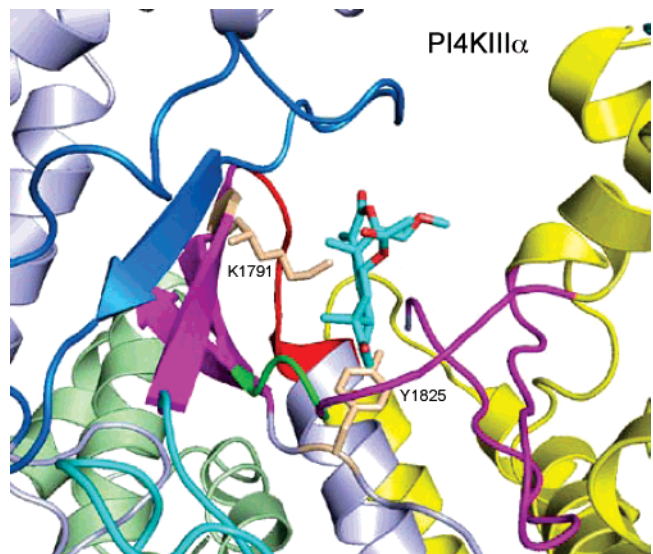
FIGURE 3: Structural models of PI4KIIIα (upper) and PI4KIIIβ (lower) with wortmannin in the binding pocket. The segments corresponding to the upper wall of the binding site in the C-terminal lobe are the least conserved (marine blue). The Lys residue that covalently binds Wm and the conserved Tyr are highlighted. The pictures were made using PyMol.

lobes of the catalytic pocket. (Figures 1 and 2B). Also tested was an additional Cys (C1796) that is also highly conserved within the Gly-Asp-Asp-Cys-Lys segment of PI4KIIIα and that corresponds to a Leu in all PI3Ks and PI4KIIIβ enzymes (Figure 1A). Substitution of C1796 with either Ser or Leu yielded an enzyme with no catalytic activity. However, substitution of Cys1843 with Ser did not diminish the catalytic activity of the enzyme, but reduced its PAO sensitivity to the level that was observed with the PI4KIIIβ enzyme (Figure 5A). Interestingly, the mutant enzyme showed a slight enhancement of activity by low concentrations of PAO for which we do not have an explanation. However, this substitution failed to protect the enzyme from oxidation as judged by the rapid loss of activity without DTT. It is notable that the PI4KIIIα homologues of yeast and fungi lack both of these cysteines and the *Drosophila* and *Caenorhabditis elegans* homologues lack one of them, probably making these enzymes less sensitive to PAO, but this was not tested experimentally.

Balla et al.
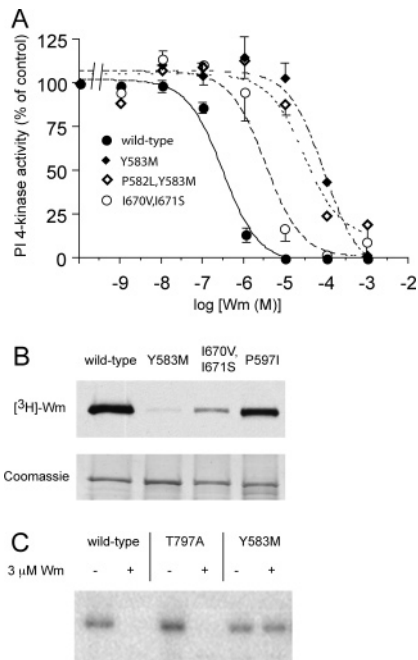
FIGURE 4: Inhibitory dose−response curves for wortmannin (Wm) in wild-type and mutant forms of recombinant PI4KIIIβ expressed in bacteria as GST fusion proteins. The enzymes were preincubated with the indicated concentrations of Wm for 10 min before the addition of [γ-^{32}P]ATP (0.1 mM final) to the kinase buffer that contained 1 mM PtdIns as substrate. See Experimental Procedures for details. (A) Activity values are expressed as percent of the activity found without Wm (DMSO). Means ± SEM of 3−6 determinations are shown. For the K_m and relative V_{max} values see Table 1. Wortmannin binding (B) and autophosphorylation (C) of recombinant PI4KIIIβ mutants. Note the reduced Wm binding to mutants (Y583M; I670V, I671S; P597I) that show decreased Wm sensitivity and the complete inhibition of the autophosphorylation by 3 μM Wm in the wild-type or tail mutant enzyme but not in the Y583M mutant.

Table 1: Summary of Kinetic Parameters of the Mutant PI4KIIIβ Enzymes[a]

| | IC$_{50}$ | | | |
	Wm (μM)	LY294002 (mM)	ATP K_m (mM)	rel V_{max} (% of wt)
PI4KIIIβ (wt)	0.32	0.30	0.5	100
I670V, I671S	3.53	1.00	1.0	2.2
I670L, I671F	0.27	0.21	0.9	∼10[a]
P597I	0.12	1.00	0.8	1.0
P582L, Y583M	31.0	nd[b]	nd	∼1.0[a]
P582R, Y583M	48.2	nd	nd	∼1.0[a]
Y583M	93.8	1.00	2.3	90

[a] Estimated values based on relative initial activity measured using same amounts of enzymes. [b] Not determined.

Identification of Inhibitors That Discriminate between PI4KIIIα and -β. Wortmannin has been a valuable tool to discriminate between the functions of type-II and type-III PI 4-kinases. Although Wm also inhibits PI3Ks, comparison of the doses of Wm that affect a particular cellular function can help determine whether the process is mediated by PI 3- or 4-kinases. Unfortunately, Wm is almost equipotent on PI4KIIIα and -β, and therefore, the functions of these proteins cannot be discriminated by Wm. It would be very useful to identify inhibitors that discriminate between the two proteins. During a recent screen of a chemically diverse panel of PI 3-kinase inhibitors, we identified the phenylthiazole compound, PIK93, as a potent inhibitor of PI4KIIIβ
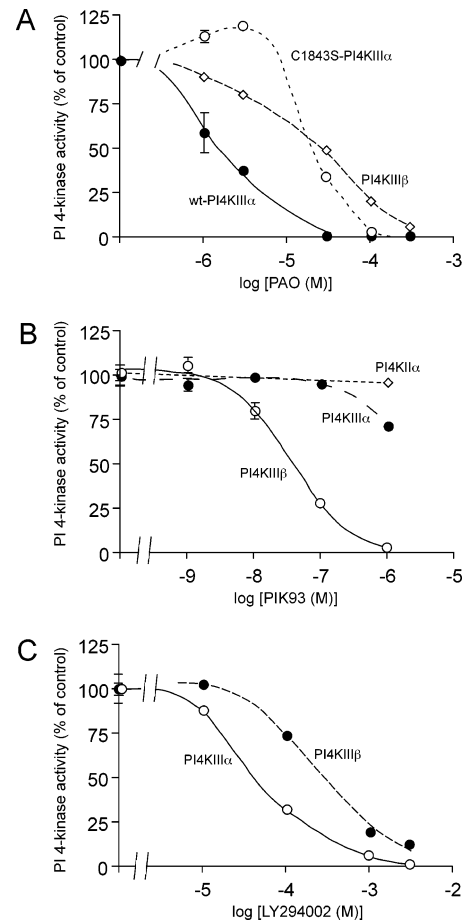
FIGURE 5: Differential inhibitor sensitivity of type-III PI4Ks. (A) PI4KIIIα shows high sensitivity to the alkylating agent, phenylarsine oxide (PAO), due to the presence of two exposed cysteins in the ATP binding pocket. Mutation of one of these residues (C1843S) significantly reduces the PAO sensitivity of the enzyme. Representative of two similar observations performed in duplicate. (B) PI4KIIIβ (but not PI4KIIIα) is highly sensitive to the PI3K inhibitor, PIK93, while the type-II PI4Kα shows complete resistance. Representative results from two similar observations performed in duplicate. (C) The sensitivities of both PI4Ks to LY294002 are low, but PI4KIIIα is more sensitive to the compound than PI4KIIIβ. Representative results are shown from two similar observations.

(*30*). As shown in Figure 5B, this compound was about 100-fold more potent against PI4KIIIβ than against PI4KIIIα (tested at 0.1 mM ATP concentration), and it was ineffective against the type-II PI4Ks. The PIK93 sensitivity of the PI4KIIIβ Y583M mutant was also tested and showed greatly reduced sensitivity to the inhibitor (not shown). We also examined the other widely used PI3K inhibitor, LY 294002, with the two PI 4-kinases. As shown in Figure 5C, LY 294002 showed low potency against either PI4K, but it was still more potent against the PI4KIIIα enzyme.

Expression of the Mutant Enzymes in Mammalian Cells. The Y583M mutation was then created in the bovine PI4KIIIβ enzyme in the mammalian expression plasmid so that the activity of the enzyme expressed in COS-7 cells could be tested. The Y583M mutant mammalian enzyme was catalytically still active and was not inhibited by Wm at concentrations that completely inhibited the endogenous or the expressed wild-type PI4KIIIβ (not shown). Interestingly, the Y583G substituted enzyme that showed an even better activity than the Y583M mutant in the bacterially expressed

recombinant protein (not shown) had only negligible activity when expressed in COS-7 cells. Our explanation for this discrepancy was that the folding of the mutant enzyme must have been affected at the higher temperature and/or in the different redox environment of the COS-7 cells, but these possibilities have not been pursued further in the present study. When the corresponding mutation (Y1825M) was created in the full-length bovine PI4KIIIα, it had negligible catalytic activity, in spite of the protein being expressed at levels equivalent to wild-type (not shown). The C1843S mutation in the full-length PI4KIIIα construct showed similarly reduced PAO sensitivity and an activity comparable to the wild-type enzyme (not shown).

The value of a Wm-insensitive PI4K enzyme was next evaluated in COS-7 cells stably expressing either the wild-type or the Y583M PI4KIIIβ enzyme. We chose to examine the Wm-sensitivity of the conversion of ceramide (Cer) to sphingomyelin (SM) in [³H]serine-labeled cells that we recently demonstrated as dependent on PI4KIIIβ (*33*). This is due to the requirement of the ceramide transfer protein (CERT) pleckstrin homology (PH) domain to bind PtdIns4*P* for Golgi interaction (*39*). First we tested the localization of the CERT-PH-mRFP construct in COS-7 cells in which we knocked down the PI4KIIα enzyme so that PtdIns4*P* formation in the Golgi is primarily dependent on PI4KIIIβ. As shown in Figure 6A, under these conditions, 10 *μ*M Wm rapidly reduced the Golgi localization of CERT-PH-mRFP either in untransfected control COS-7 cells or in cells expressing the wild-type enzyme (the latter not shown). In contrast, in cells expressing the Y583M mutant enzyme, a significant localization of the PH domain was still observed after treatment with Wm. Similarly, the conversion of Cer to SM showed a significantly reduced Wm sensitivity in cells expressing the Y583M mutant enzyme, compared either to control COS-7 cells or to those expressing the wild-type protein (Figure 6B). These experiments have confirmed that the Wm-sensitivity of Cer to SM conversion is due to the inhibition of the PI4KIIIβ enzyme and showed that this approach can be applied to other questions related to PI4KIIIβ function.

DISCUSSION

Mutagenesis and modeling of the type-III PI4Ks based on the crystal structure of PI3Kγ have provided several important clues concerning the catalytic properties and inhibitor sensitivities of these enzymes. Even before their cloning, these proteins had been predicted to be relatives of PI3Ks based on their sensitivities to PI3K inhibitors, most notably, wortmannin (*24, 25*). Following their molecular cloning, sequence comparisons have proven the high homology between the catalytic domains of these enzymes, and the solved PI3Kγ structure provided a good template for modeling.

Inhibitor Sensitivities. Analysis of the Wm sensitivity of the various groups of the PI3- and 4-kinases revealed significant differences, even though the Lys residue that reacts covalently with Wm in the ATP binding pocket is highly conserved in all of these proteins. In this regard it was significant that Pik1p, the yeast orthologue of PI4KIIIβ shows very low sensitivity to Wm. This suggested that it might be possible to generate mutations that could decrease
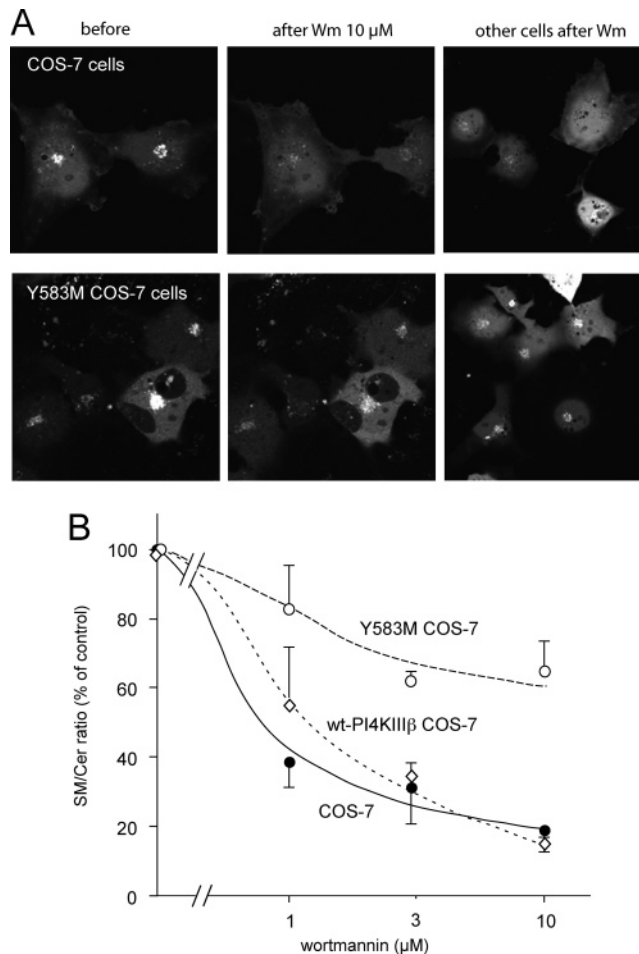
FIGURE 6: Wortmannin-resistance of ceramide transport to the Golgi in COS-7 cells stably expressing Y583M mutant PI4KIIIβ. COS-7 cells were stably transfected with either the wild-type or the Y583M mutant PI4KIIIβ. (A) Cells were treated with siRNA to downregulate the type-II PI4Ka enzyme (*19*) so that the recruitment of the CERT-PH domain to the Golgi is mostly dependent on PI4KIIIβ. In such cells, the localization of the CERT-PH-mRFP protein to the Golgi is largely eliminated after 10 min treatment with 10 *μ*M Wm in control cells (upper panels), but not in cells expressing the Y583M mutant PI4KIIIβ (lower panels). (B) The conversion of ceramide (Cer) to sphingomyelin (SM) is inhibited by Wm in control cells but not in cells expressing the Y583M mutant enzyme. Cells were labeled with [³H]serine, and the labeled sphingolipids were separated after glycerophospholipids were eliminated by alkaline methanolysis. Note the slight shift in the Wm-sensitivity in cells overexpressing the wild-type enzyme but a resistance in cells expressing the mutant. Means ± SEM of three experiments each performed in duplicate.

Wm sensitivity without losing the catalytic activity. Comparison of the sequences of numerous PI3- and -4-kinases in regions that form the ATP binding pocket, together with the molecular models, pointed to a unique variation conserved within the family of yeast and fungal Pik1p proteins. A ProTyr residue pair that is highly conserved in all PI3- and 4-kinases was replaced by an ArgMet sequence. This Tyr has a special position as it forms the bottom of the binding pocket encompassing the adenine ring. While the ArgMet substitution in the bovine PI4KIIIβ yielded a catalytically compromised enzyme, the ProMet mutant retained reasonable activity, and it was also transferable to enzymes expressed in mammalian cells. Remarkably, the same mutation was not tolerated in the PI4KIIIα enzyme

Balla et al.

for reasons that are not obvious based on comparisons of the three models or sequences. However, the mutations of the same residue in PI3Kα also resulted in a catalytically inactive enzyme (*40*). Our finding is also consistent with the lack of any published report on Wm-resistant PI4KIIIα and the high sensitivity of the yeast orthologue, Stt4p, to this inhibitor (*41*). Also, no substitution corresponding to this Y residue is found in any of the homologue sequences retrieved from various genomes.

The extreme sensitivity of the PI4KIIIα enzyme to PAO (*29*) as well as to oxidation suggested that this enzyme has reactive pairs of SH groups in close proximity at a solvent-exposed surface. Comparison of the PI4K structural models and analysis of the multiple-sequence alignment pointed to two Cys residues (C1839 and C1843) in the short loop connecting the N- and C-terminal lobes of the ATP binding pocket in PI4KIIIα but not in that of PI4KIIIβ. Interestingly, these Cys residues are only present in the vertebrate enzymes. Indeed, the C1843S mutation significantly decreased the PAO sensitivity of the enzyme to a level comparable to that of PI4KIIIβ, without changing the sensitivity of the enzyme to oxidation (judged by rapid loss of activity without DTT). We assume that the high sensitivity of the enzymes to oxidation is related to two other Cys residues found in close proximity (C1796 and C1834) that are also present in almost all of the PI4KIIIα enzymes from yeast to humans (C1796 is not found in *Drosophila* and *C. elegans*). Since the C1796S mutation made the enzyme inactive, the validity of this hypothesis cannot be tested.

Substrate Preference. Although substrate preference of the PI4Ks was not directly tested experimentally, it is very likely that it is determined by the activation loop and the adjacent sequences. PI4Ks, like the PtdIns specific class III PI3Ks, only phosphorylate PtdIns. Both the PI4K enzymes and class III PI3Ks lack the positive residues within the activation loop characteristic of class I PI3Ks (Figure 1). Instead, they contain several Pro residues and a Lys at the C-terminally adjacent sequence. It is certainly the activation loop that also determines the position of the inositol ring in PtdIns to expose the OH to be phosphorylated, as observed with both the PI3Kγ (*42*) and PIP kinases (*43*).

Inibitor Selectivities and Possibilities for New Inhibitors. These studies further analyzed the sensitivities of PI4Ks to PI3K inhibitors, especially to PIK93, the inhibitor recently described as significantly more potent on PI4KIIIβ than PI4KIIIα (*30*). The higher sensitivity of the β enzyme can be attributed to sequence differences in a segment corresponding to the "selectivity pocket" of PI3Kγ (*30*). While this part of the molecule shows relatively low sequence identity and therefore the model has significant ambiguity there, it is almost certainly the region relevant for subtype-specific inhibition. These and other differences, such as the presence of the two cysteines within the ATP binding site in PI4KIIIα, suggest that there is a good possibility that specific PI4K inhibitors can be developed. Such inhibitors would greatly facilitate studies on the role of the various PI4Ks in the cell since the contribution of these enzymes to the production of PtdIns4*P* in specific cellular compartments is not known. Most studies on this topic have relied on the use of PI3K inhibitors exploiting the difference in sensitivity between PI4Ks and PI3Ks to these drugs. Unfortunately, knock down of the individual enzymes, the only approach

that would selectively eliminate the function of the proteins, has many drawbacks due to the exposure of cells to the depletion of the protein for several days as opposed to minutes when using inhibitors.

Until more selective inhibitors become available, the experiments performed in COS-7 cells stably transfected with the Wm-resistant Pi4KIIIβ mutant enzymes showed the value of this chemical-genetic approach. The insensitivity of the mutant enzyme to Wm allows a selective assessment of PI4KIIIβ functions when the endogenous type-III PI4Ks are acutely inhibited. Although this approach will not alleviate the need for specific PI4K inhibitors, it may still facilitate progress in the field of biochemistry and cell biology of PI4Ks.

REFERENCES

1. Warashina, A. (1999) Light-evoked recovery from wortmannin-induced inhibition of catecholamine secretion and synaptic transmission, *Arch. Biochem. Biophys. 367*, 303−310.
2. Balla, T. (2006) Phosphoinositide-derived messengers in endocrine signaling, *J. Endocrinol. 188*, 135−153.
3. Di Paolo, G., and De Camilli, P. (2006) Phosphoinositides in cell regulation and membrane dynamics, *Nature 443*, 651−657.
4. Roth, M. G. (2004) Phosphoinositides in constitutive membrane traffic *Physiol. Rev. 84*, 699−730.
5. De Matteis, M. A., Di Campli, A., and Godi, A. (2005) The role of the phosphoinositides at the Golgi complex, *Biochim. Biophys. Acta 1744*, 396−405.
6. Minogue, S., Anderson, J. S., Waugh, M. G., dosSantos, M., Corless, S., Cramer, R., and Hsuan, J. J. (2001) Cloning of a human type II phosphatidylinositol 4-kinase reveals a novel lipid kinase family, *J. Biol. Chem. 276*, 16635−16640.
7. Barylko, B., Gerber, S. H., Binns, D. D., Grichine, N., Khvotchev, M., Sudhof, T. C., and Albanesi, J. P. (2001) A novel family of phosphatidylinositol 4-Kinases conserved from yeast to humans, *J. Biol. Chem. 276*, 7705−7708.
8. Nakagawa, T., Goto, K., and Kondo, H. (1996) Cloning, expression and localization of 230 kDa phosphatidylinositol 4-kinase, *J. Biol. Chem. 271*, 12088−12094.
9. Meyers, R., and Cantley, L. C. (1997) Cloning and characterization of a wortmannin-sensitive human phosphatidylinositol 4-kinase, *J. Biol. Chem. 272*, 4384−4390.
10. Balla, T., Downing, G. J., Jaffe, H., Kim, S., Zolyomi, A., and Catt, K. J. (1997) Isolation and molecular cloning of wortmannin-sensitive bovine type-III phosphatidylinositol 4-kinases, *J. Biol. Chem. 272*, 18358−18366.
11. Flanagan, C. A., Schnieders, E. A., Emerick, A. W., Kunisawa, R., Admon, A., and Thorner, J. (1993) Phosphatidylinositol 4-kinase: gene structure and requirement for yeast cell viability, *Science 262*, 1444−1448.
12. Hama, H., Schnieders, E. A., Thorner, J., Takemoto, J. Y., and DeWald, D. B. (1999) Direct involvement of phosphatidylinositol 4-phosphate in secretion in the yeast Saccharomyces cerevisiae, *J. Biol. Chem. 274*, 34294−34300.
13. Walch-Solimena, C., and Novick, P. (1999) The yeast phosphatidylinositol-4-OH kinase Pik1 regulates secretion at the Golgi, *Nat. Cell Biol. 1*, 523−525.
14. Trotter, P. J., Wu, W. I., Pedretti, J., Yates, R., and Voelker, D. R. (1998) A genetic screen for aminophospholipid transport mutants identifies the phosphatidylinositol 4-kinase, Stt4p, as an essential component in phosphatidylserine metabolism, *J. Biol. Chem. 273*, 13189−13196.
15. Audhya, A., and Emr, S. D. (2002) Stt4 PI 4-kinase localizes to the plasma membrane and functions in the Pkc1-mediated MAP kinase cascade, *Dev. Cell 2*, 593−605.
16. Tabuchi, M., Audhya, A., Parsons, A. B., Boone, C., and Emr, S. D. (2006) The PI(4,5)P2 and TORC2 binding proteins, Slm1 and Slm2, function in sphingolipid regulation, *Mol. Biol. Cell 26*, 5861−5875.
17. Godi, A., Pertile, P., Meyers, R., Marra, P., Di Tullio, G., Iurisci, C., Luini, A., Corda, D., and De Matteis, M. A. (1999) ARF mediates recruitment of PtdIns-4-OH kinase-beta and stimulates synthesis of PtdIns(4,5)P2 on the Golgi complex, *Nat. Cell Biol. 1*, 280−287.

18. Fabbri, A., Tsai-Morris, C. H., Luna, S., Fraioli, F., and Dufau, M. L. (1985) Opiate receptors are present in the rat testis. Identification and localization in Sertoli cells, *Endocrinology 117*, 2544−2546.

19. Balla, A., Tuymetova, G., Tsiomenko, A., Varnai, P., and Balla, T. (2005) A plasma membrane pool of phosphatidylinositol 4-phosphate is generated by phosphatidylinositol 4-kinase type-III alpha: studies with the PH domains of the oxysterol binding protein and FAPP1, *Mol. Biol. Cell 16*, 1282−1295.

20. Minogue, S., Waugh, M. G., De Matteis, M. A., Stephens, D. J., Berditchevski, F., and Hsuan, J. J. (2006) Phosphatidylinositol 4-kinase is required for endosomal trafficking and degradation of the EGF receptor, *J. Cell Sci. 119*, 571−581.

21. Yano, H., Nakanishi, S., Kimura, K., Hanai, N., Saitoh, Y., Fukui, Y., Nonomura, Y., and Matsuda, Y. (1993) Inhibition of histamine secretion by wortmannin through the blockade of phosphatidylinositol 3-kinase in RBL-2H3 cells, *J. Biol. Chem. 268*, 25846−25856.

22. Arcaro, A., and Wymann, M. P. (1993) Wortmannin is a potent phosphatidylinositol 3-kinase inhibitor: the role of phosphatidylinositol 3,4,5-trisphosphate in neutrophil responses, *Biochem. J. 296*, 297−301.

23. Vlahos, C. J., Matter, W. F., Hui, K. Y., and Brown, R. F. (1994) A specific inhibitor of phosphatidylinositol 3-kinase, 2-(4-morpholinyl)-8-phenyl-4H-1-benzopyran-4-one (LY294002), *J. Biol. Chem. 269*, 5241−5248.

24. Nakanishi, S., Catt, K. J., and Balla, T. (1995) A wortmannin-sensitive phosphatidylinositol 4-kinase that regulates hormone-sensitive pools of inositolphospholipids, *Proc. Natl. Acad. Sci. U.S.A. 92*, 5317−5321.

25. Downing, G. J., Kim, S., Nakanishi, S., Catt, K. J., and Balla, T. (1996) Characterization of a soluble adrenal phosphatidylinositol 4-kinase reveals wortmannin-sensitivity of Type III phosphatidylinositol 4-kinases, *Biochemistry 35*, 3587−3594.

26. Wymann, M. P., Bulgarelli-Leva, G., Zvelebil, M. J., Pirola, L., Vanhaesebroeck, B., Waterfield, M. D., and Panayotou, G, (1996) Wortmannin inactivates phosphoinositide 3-kinase by covalent modification of Lys-802, a residue involved in the phosphate transfer reaction, *Mol. Cell. Biol. 16*, 1722−1733.

27. Hashimoto, Y., Ogihara, A., Nakanishi, S., Matsuda, Y., Kurokawa, K., and Nonomura, Y. (1992) Two thrombin-activated Ca2+ channels in human platelets, *J. Biol. Chem. 267*, 17078−17081.

28. Wiedemann, C., Schäfer, T., and Burger, M. M. (1996) Chromaffin granule-associated phosphatidylinositol 4-kinase activity is required for stimulated secretion, *EMBO J. 15*, 2094−2101.

29. Balla, A., Tuymetova, G., Barshishat, M., Geiszt, M., and Balla, T. (2002) Characterization of type II phosphatidylinositol 4-kinase isoforms reveals association of the enzymes with endosomal vesicular compartments, *J. Biol. Chem. 277*, 20041−22050.

30. Knight, Z. A., Gonzalez, B., Feldman, M. E., Zunder, E. R., Goldenberg, D. D., Williams, O., Loewith, R., Stokoe, D., Balla, A., Toth, B., Balla, T., Weiss, W. A., Williams, R. L., and Shokat, K. M. (2006) A Pharmacological Map of the PI3-K Family Defines a Role for p110alpha in Insulin Signaling, *Cell 125*, 733−747.

31. Zhao, X. H., Bondeva, T., and Balla, T. (2000) Characterization of recombinant phosphatidylinositol 4-kinase beta reveals auto- and heterophosphorylation of the enzyme, *J. Biol. Chem. 275*, 14642−14648.

32. Varnai, P., and Balla, T. (2007) Visualization and manipulation of phosphoinositide dynamics in live cells using engineered protein domains, *Pfluegers Arch*.

33. Toth, B., Balla, A., Ma, H., Knight, Z. A., Shokat, K. M., and Balla, T. (2006) Phosphatidylinositol 4-kinase IIIbeta regulates the transport of ceramide between the endoplasmic reticulum and Golgi, *J. Biol. Chem. 281*, 36369−36377.

34. Levitt, M. (1992) Accurate modeling of protein conformation by automatic segment matching, *J. Mol. Biol. 226*, 507−533.

35. Walker, E. H., Perisic, O., Ried, C., Stephens, L., and Williams, R. L. (1999) Structural insights into phosphoinositide 3-kinase catalysis and signaling, *Nature 402*, 313−320.

36. Walker, E. H., Pacold, M. E., Perisic, O., Stephens, L., Hawkins, P. T., Wymann, M. P., and Williams, R. L. (2000) Structural determinants of phosphoinositide 3-kinase inhibition by wortmannin, LY294002, quercetin, myricetin, and staurosporine, *Mol. Cell 6*, 909−919.

37. Thelen, M., Wymann, M. P., and Langen, H. (1994) Wortmannin binds specifically to 1-phosphatidylinositol 3-kinase while inhibiting guanine nucleotide-binding protein- coupled receptor signaling in neutrophil leukocytes, *Proc. Natl. Acad. Sci. U.S.A. 91*, 4960−4964.

38. Heilmeyer, L. M., Jr., Vereb, G., Jr., Vereb, G., Kakuk, A., and Szivak, I. (2003) Mammalian phosphatidylinositol 4-kinases, *IUBMB Life 55*, 59−65.

39. Hanada, K., Kumagai, K., Yasuda, S., Miura, Y., Kawano, M., Fukasawa, M., and Nishijima, M. (2003) Molecular machinery for non-vesicular trafficking of ceramide, *Nature 426*, 803−809.

40. Alaimo, P. J., Knight, Z. A., and Shokat, K. M. (2005) Targeting the gatekeeper residue in phosphoinositide 3-kinases, *Bioorg. Med. Chem. 13*, 2825−2836.

41. Cutler, N. S., Heitman, J., and Cardenas, M. E. (1997) STT4 is an essential phosphatidylinositol 4-kinase that is a target of wortmannin in Saccharomyces cerevisiae, *J. Biol. Chem. 272*, 27671−27677.

42. Bondeva, T., Pirola, L., Bulgarelli-Leva, G., Rubio, I., Wetzker, R., and Wymann, M. P. (1998) Bifurcation of lipid and protein kinase signals of PI3Kgamma to the protein kinases PKB and MAPK, *Science 282*, 293−296.

43. Kunz, J., Wilson, M. P., Kisseleva, M., Hurley, J. H., Majerus, P. W., and Anderson, R. A. (2000) The activation loop of phosphatidylinositol phosphate kinases determines signaling specificity, *Mol. Cell 5*, 1−11.

Demonstration of Angiotensin II-induced Ras Activation in the *trans*-Golgi Network and Endoplasmic Reticulum Using Bioluminescence Resonance Energy Transfer-based Biosensors*

András Balla[‡1]**, László Sándor Erdélyi**[‡]**, Eszter Soltész-Katona**[‡]**, Tamas Balla**[§]**, Péter Várnai**[‡]**, and László Hunyady**[‡¶2]

From the ‡*Department of Physiology, Faculty of Medicine, Semmelweis University, H-1444 Budapest, Hungary, the* §*Section on Molecular Signal Transduction, Program for Developmental Neuroscience, Eunice Kennedy Shriver NICHD, National Institutes of Health, Bethesda, Maryland 20892, and the* ¶*Laboratory of Neurobiochemistry and Molecular Physiology, Semmelweis University and Hungarian Academy of Sciences, H-1444 Budapest, Hungary*

Previous studies have demonstrated that molecules of the Ras signaling pathway are present in intracellular compartments, including early endosomes, the endoplasmic reticulum (ER), and the Golgi, and suggested that mitogens can regulate Ras activity in these endomembranes. In this study, we investigated the effect of angiotensin II (AngII) on intracellular Ras activity in living HEK293 cells expressing angiotensin type 1 receptors (AT$_1$-Rs) using newly developed bioluminescence resonance energy transfer biosensors. To investigate the subcellular localization of AngII-induced Ras activation, we targeted our probes to various intracellular compartments, such as the trans-Golgi network (TGN), the ER, and early endosomes. Using these biosensors, we detected AngII-induced Ras activation in the TGN and ER, but not in early endosomes. In cells expressing a cytoplasmic tail deletion AT$_1$-R mutant, the AngII-induced response was enhanced, suggesting that receptor internalization and β-arrestin binding are not required for AngII-induced Ras activation in endomembranes. Although we were able to demonstrate EGF-induced Ras activation in the plasma membrane and TGN, but not in other endomembranes, AG1478, an EGF receptor inhibitor, did not affect the AngII-induced response, suggesting that the latter is independent of EGF receptor transactivation. AngII was unable to stimulate Ras activity in the studied compartments in cells expressing a G protein coupling-deficient AT$_1$-R mutant (^{125}DRY^{127} to ^{125}AAY^{127}). These data suggest that AngII can stimulate Ras activity in the TGN and ER with a G protein-dependent mechanism, which does not require β-arrestin-mediated signaling, receptor internalization, and EGF receptor transactivation.

The small G proteins, such as Ras, Rho, and Rac, are central players of many signal transduction pathways that regulate a wide variety of cell functions. The small G proteins are monomeric GTPases, serve as molecular switches, and regulate a wide variety of functions, such as gene expression, cell proliferation, cytoskeleton dynamics, the cell cycle, and vesicular transport (1). The >100 mammalian small G proteins are classified into several families, including the Ras and Rho families. Generally, their GDP-bound form is inactive, and upon stimulatory effect, GDP will be changed to GTP, and this activated form will interact with downstream signaling partners. GDP/GTP conversion is stimulated by a guanine nucleotide exchange factor, whereas small G protein inactivation is facilitated by GTPase-activating proteins (2, 3). Small G proteins are active in association with a cellular membrane, and according to the well established model, an extracellular stimulus causes the activation of the Ras and Rho proteins via plasma membrane receptors (3). Activated Ras proteins activate Raf protein kinases, leading to MAPK pathway signalization (4). Raf proteins are the main and direct effectors of Ras proteins, and activated Raf kinases stimulate MEKs.

Membrane localization on the cytoplasmic leaflet of cellular membranes is mediated by post-translational modifications with a lipid moiety on their C-terminal tail. The C-terminal hypervariable regions of Ras isoforms contain the motifs for different plasma membrane signaling nanocluster associations. K-Ras localizes in a cholesterol-independent nanocluster with the help of its polybasic domain, which associates electrostatically with plasma membrane lipids. This association can be disrupted by PKC phosphorylation of Ras, which also causes mitochondrial translocation (5, 6). Recent studies have shown that Ras isoforms can also associate with different cellular membranes (7). It has been shown that targeting of Ras proteins to the plasma membrane is preceded by their localization to endomembranes, such as the endoplasmic reticulum (ER)[3] and Golgi (8). Early studies also demonstrated that elements of Ras signaling can be detected in endosomes (9) and have an important role in the MAPK signaling of growth factor receptors, including the EGF recep-

---

[3] The abbreviations used are: ER, endoplasmic reticulum; GPCR, G protein-coupled receptor; AngII, angiotensin II; AT$_1$-R, angiotensin type 1 receptor; BRET, bioluminescence resonance energy transfer; RBD, Ras-binding domain; TGN, *trans*-Golgi network.

Angiotensin II Induces Ras Activation in the ER and Golgi

tor (10–12). Furthermore, it was shown that internalized growth factor receptors can selectively activate endosomal H-Ras (but not K-Ras) signaling (13). Although it is generally accepted that the Ras signal generation predominantly occurs at the plasma membrane (14), it seems that the plasma membrane is not the sole platform for Ras signal generation (15). In addition to the well established role of the endosomal compartment in growth factor receptor signaling, recent data suggest that Ras signaling in other endomembranes may also have physiological roles. For example, a recent study proposed that Ras signaling in the Golgi has an effect on thymocyte selection (16). The demonstration of the presence of various elements of Ras signaling in intracellular compartments, including the Golgi and ER, raises the possibility that Ras signal generation can also occur in these compartments (7).

Ras also can be activated by G protein-coupled receptors (GPCRs). Angiotensin II (AngII) is an octapeptide hormone that is the main effector of the renin-angiotensin system and mediates its physiological and pathological effects. AngII can bind and activate two types of angiotensin receptors (angiotensin type 1 and 2 receptors). The angiotensin type 1 receptor (AT_1-R) is a typical seven-transmembrane GPCR, and the G protein-mediated "classical" signaling mechanisms are responsible for the majority of AngII-evoked cellular responses. These signaling mechanisms have a wide spectrum, including second messenger generation (Ca^{2+} signal via inositol 1,4,5-trisphosphate and diacylglycerol), activation of small G proteins and cytoplasmic tyrosine kinases, regulation of ion channels, and transactivation of growth factor receptors. After binding to the AT_1-R, a heterotrimeric G protein (G_q) mediates the hydrolysis of phosphatidylinositol 4,5-bisphosphate by phosphoinositide-specific phospholipase Cβ, resulting in the generation of second messengers (17). It is well established that extracellular stimulus of the AT_1-R can lead to activation of various small G proteins, including Ras, either through transactivation of a tyrosine kinase receptor (mainly via the EGF receptor) or through transactivation independently (18–20). Not only does endocytosis of GPCRs regulate the activity of plasma membrane receptors (21, 22), but it can also initiate signaling pathways, such as MAPK activation (23). In this study, we investigated whether agonist stimulation of a GPCR, the AT_1-R, can lead to intracellular Ras activation and compared these responses with those of the EGF receptor.

Recently, a wide range of FRET-based approaches were used to examine Ras and other signal transduction mechanisms (24, 25). To investigate Ras activation in various locations inside cells upon agonist stimulation of the AT_1-R, we have developed several intra- and intermolecular probes for bioluminescence resonance energy transfer (BRET) measurements in living cell experiments based on previous FRET-based studies (26, 27). We show that Ras signal generation can be detected not only in the plasma membrane but also in intracellular compartments, such as the *trans*-Golgi and ER, in response to AngII stimulation.

EXPERIMENTAL PROCEDURES

Materials—Molecular biology enzymes were obtained from Fermentas (Burlington, Canada), Stratagene (La Jolla, CA), and Invitrogen. Cell culture dishes and plates for BRET measurements were purchased from Geiner Bio-One GmbH (Kremsmunster, Austria). Lipofectamine 2000 and coelenterazine h were from Invitrogen. Unless stated otherwise, all other chemicals and reagents were purchased from Sigma. HEK293 cells were from American Type Culture Collection (Manassas, VA).

Molecular Biology—For the construction of our intramolecular BRET probes, we followed the design of the Raichu (Ras and interacting protein chimeric unit) FRET probes from the Matsuda laboratory (26, 27). The cDNA parts of the constructs were generated by amplification either from a respective expressed sequence tag clone (German Resource Center for Genome Research (RZPD), Berlin, Germany) or from H295R human cell line cDNA by PCR. For the intramolecular BRET probes, the order of the domains was similar to that in the Raichu probes (26). We used the pEYFP-C1 plasmid backbone (Clontech, Mountain View, CA), and the fluorescent acceptor protein (YFP) was followed by H-Ras, the Ras-binding domain (RBD) of Raf-1, and luciferase (see Fig. 1 for schematic representation). We have previously shown that the Raf-1 RBD (amino acids 51–131) is able to recognize activated Ras but is not capable of being recruited to the plasma membrane (28), which makes this RBD suitable for utilizing in targeted biosensors. We used *Renilla* luciferase as the energy donor by subcloning the codon-humanized *Renilla* luciferase from pRluc-N2 (PerkinElmer Life Sciences). The intermolecular BRET probes were derived from their respective intramolecular probes by splitting them between Ras and the RBD of Raf-1 by adding suitable start and stop codon sequences. Targeting was achieved by placing a targeting signal at either the N- or C-terminal end of the probe. We used several previously described targeting motifs to target our BRET probes (29). Targeting to the plasma membrane was achieved using various distinct tags. We fused C*AAX* motifs from Ras proteins C-terminally as described (26, 30). Briefly, the tK tag (K-Ras C*AAX* targeting motif, tail K-Ras), KMSKDGKKKKK-KSKTKCVIM, consists of the membrane-targeting C*AAX* motif and hypervariable regions of K-Ras (GenBank accession number NM_004985). The tHL tag (tail H-Ras long, KLNPP-DESGPGCMSCKCVLS) consists of the membrane-targeting C*AAX* motif and hypervariable regions of H-Ras (accession number NM_005343), whereas the tHS tag (tail H-Ras short, CMSCKCVLS) consists of the membrane-targeting C*AAX* motif but without the hypervariable regions of H-Ras. The MP (MyrPalm) and PP (PalmPalm) tags targeting to plasma membrane rafts were based on the design of Zacharias *et al.* (31), where the MP tag is the N-terminal amino acid sequence (MGCIKSKRKDNLNDDE) from Lyn kinase (accession number NM_002350), and the PP tag is the N-terminal amino acid sequence (MLCCMRRTKQ) from GAP43 (accession number NM_002045) (31). Targeting to the Golgi surface was achieved by fusing the full-length *trans*-Golgi network protein 2 (also known as TGN38; accession number NM_006464)

(32), and targeting to the ER surface was achieved by adding segment 233–250 of the yeast Ubc6 protein (accession number NM_001178991) or the C-terminal segment 521–587 of the Sac1 phosphoinositide phosphatase (accession number NM_014016) (29, 33). Endosomal targeting was done by fusing the probes C-terminally with the FYVE domain (segment 1253–1411) of EEA1 (early endosome antigen 1; accession number NM_3566). Mutagenesis was performed using standard mutagenesis conditions. After verifying the mutations with dideoxy sequencing, the mutated fragment was exchanged between the wild-type and mutated portions with suitable restriction sites to avoid the generation of unwanted mutations outside the sequenced regions. pcDNA3.1-AT$_{1A}$-R, pcDNA3.1-AT$_{1A}$-RΔ319 (with Tyr^{319} substituted with a stop codon), and pcDNA3.1-DRY/ AAY-AT$_{1A}$-R (with the highly conserved ^{125}DRY^{127} sequence mutated to ^{125}AAY^{127}) were described previously (34–36).

Cell Culture and Transfection—The experiments were performed on the HEK293 cell line. The cells were cultured in DMEM with penicillin/streptomycin (Invitrogen) and 10% heat-inactivated FBS in 5% CO$_2$ at 37 °C. The cells were cultured in plastic dishes, trypsinized prior to transfection, and transiently transfected using Lipofectamine 2000 (Invitrogen), and plated on polylysine-pretreated white 96-well plates at a density of 1×10^5 cells/well for BRET measurements. The DNA amount was 0.2–0.4 μg/well; the amount of Lipofectamine 2000 was 0.5 μl/well.

BRET Measurements—We monitored the molecular interactions of either two parts of a biosensor (intramolecular probes) or two proteins (intermolecular probes) by BRET measurements. The measurements were performed after 24 h of transfection on white 96-well plates. Before BRET measurements, the HEK293 cells were switched to serum-free medium (DMEM with 0.1% BSA) for several hours (4–6 h) to render the cells quiescent. The medium of the cells was changed prior to measurements to a modified Krebs-Ringer buffer containing 120 mM NaCl, 4.7 mM KCl, 1.8 mM CaCl$_2$, 0.7 mM MgSO$_4$, 10 mM glucose, and 10 mM NaHEPES (pH 7.4), and the BRET measurements were performed at 37 °C. The BRET measurements were started after the addition of the cell-permeable substrate coelenterazine at a final concentration of 5 μM, and the counts were recorded using a Berthold Mithras LB 940 multilabel reader, which allows for the detection of signals using filters at 485- and 530-nm wavelengths. The detection time was 0.25–0.5 s. The BRET ratios were calculated as the 530/485 nm ratio. The measurements were done in triplicate. The BRET records are the average of at least three independent experiments. BRET ratios were base line-corrected to the vehicle curve using GraphPad Prism software. The approximate BRET ratio of the YFP-deficient intramolecular RasBRET-tK probe was ~0.8 (data not shown).

Confocal Microscopy—The localization and distribution of the targeted probes were analyzed using a Zeiss LSM 510 confocal laser scanning microscope in living cells plated on polylysine-pretreated glass coverslips (3×10^5 cells/35-mm dish).

RESULTS

Generation and Optimization of RasBRET Probes to Measure Ras Activation upon AngII Stimulation in HEK293 cells—To study Ras activation after AngII or EGF stimulation in intracellular compartments, we first established a BRET-based Ras activity measurement using newly developed probes. For the detection of Ras activation, HEK293 cells were chosen for our studies because this cell line is broadly used for angiotensin receptor studies (20, 23, 37). Moreover, this cell type has endogenous EGF receptors, and Ras activation upon EGF treatment could be detected using BRET measurements. Stimulation of endogenous EGF receptors by EGF yielded a robust and prolonged response in Ras activation as assessed in the plasma membrane by the intramolecular RasBRET-tK probe (see details under "Experimental Procedures") (Fig. 1*A*), which was designed as the BRET version of the Raichu-Ras fusion protein (26). The probes indicate when the respective Ras becomes loaded with GTP because the RBD of Raf-1 increases its affinity dramatically for Ras upon GTP loading. This results in conformational changes that bring the energy acceptor close to the donor, as was shown by the developers of the corresponding FRET probes (38). Compared with EGF treatment, Ras activation upon AngII stimulation resulted in a transient and smaller response in HEK293 cells (Fig. 1*A*).

To optimize the probe, tags were used to target it to different plasma membrane microdomains, including non-raft domains (tK), caveolae/rafts (tHS and tHL) (39), and plasma membrane raft domains (MP and PP) (31). The localization and distribution of the targeted probes in HEK293 cells were verified by confocal microscopy (Fig. 1, *lower panels*). Among these targeting sequences, the MP-targeted version of the intramolecular probe yielded the most sensitive probe (Fig. 1*B*) (data not shown for the others). To further improve the sensitivity of the detection of Ras activation in the plasma membrane, an intermolecular variant of the MP-targeted RasBRET probe (the energy donor and acceptor are in different polypeptide chains; MP-YFP-Ras + RBD-luciferase) (see "Experimental Procedures" and Fig. 1*C*) was constructed. Fig. 1*C* shows that this setup yielded a greatly improved and very sensitive probe for measuring Ras activation. The higher signal-to-noise ratio of the intermolecular biosensor can be explained by the high basal BRET signal of the intramolecular probes (~1.4 *versus* ~1.1) because, in these constructs, the donor and acceptor are in the same molecule. The cytosolic (spatially unbiased) intermolecular plasmid pair for RasBRET (non-targeted YFP-Ras plus RBD-luciferase) had the lowest absolute level of the BRET signal (~0.9).

We validated that the change in the BRET signal using the intermolecular MP-RasBRET probe in our experimental protocol is dependent on the activation state of Ras (hence, the interaction of Ras and the Raf RBD) by performing measurements with mutated Ras domains in the probe. Fig. 2 shows that, by utilizing the "active" form of the intermolecular MP-RasBRET probe pair (G12V), we detected the maximal absolute level of the BRET signal. In contrast, when we applied the "inactive" Ras S17N mutation, the extent of the BRET signal was lower than the base line of the wild-type probe, showing

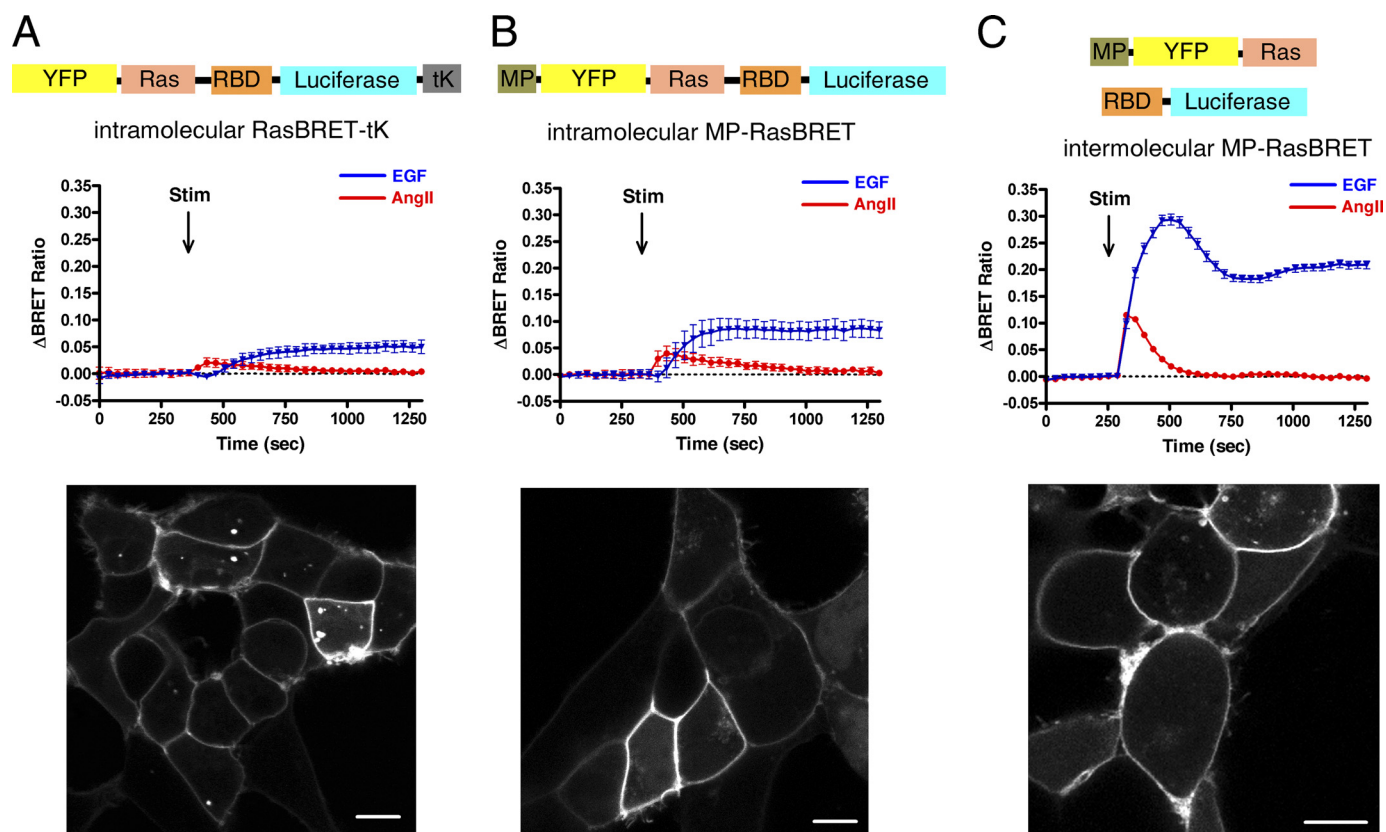## Angiotensin II Induces Ras Activation in the ER and Golgi

FIGURE 1. **Ras activation upon AngII and EGF stimulation in HEK293 cells.** *A*, intramolecular RasBRET-tK; *B*, intramolecular MP-RasBRET; *C*, intermolecular MP-RasBRET. *Upper rows*, schematic representation of the arrangement of the RasBRET probes. *Middle rows*, BRET assay of plasma membrane-targeted Ras-BRET probes. HEK293 cells were transfected with the plasmids of the indicated probes and with the AT_{1A}-R, and after 24 h, the serum-starved cells were exposed to 50 ng/ml EGF (*blue traces*), 100 nM AngII (*red traces*), or vehicle (*dotted lines*) at the indicated time points. The BRET records are the average of at least three independent experiments. The means $\pm$ S.E. are shown ($n = 3$). *Lower rows*, the representative confocal micrographs show the localization and cellular distribution of the indicated probes in HEK293 cells. YFP fluorescence was detected using a Zeiss LSM 510 confocal microscope. *Stim*, stimulation. *Scale bars* = 10 μm.
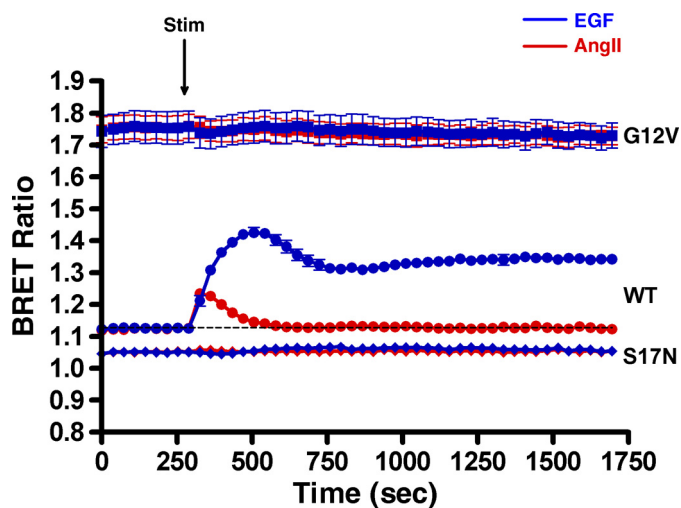

FIGURE 2. **Validation of the BRET measurement approach for agonist-stimulated Ras activation by mutated MP-RasBRET probe pairs.** HEK293 cells were transfected with intermolecular RasBRET pairs. The wild-type (●), active G12V (■), and inactive S17N (♦) MP-RasBRET probes are shown. HEK293 cells were transfected with the plasmids of the indicated probes and with the AT_{1A}-R, and after 24 h, the serum-starved cells were exposed to 50 ng/ml EGF (*blue trace*), 100 nM AngII (*red trace*), or vehicle (*dashed line*) at the indicated time points. The BRET records are an average of at least three independent experiments. The means $\pm$ S.E. are shown ($n = 3$). *Stim*, stimulation.

that Ras was partially active in control cells. Because the optimization of BRET biosensors showed that the intermolecular MP-RasBRET probe resulted in the best Ras activation biosensors, we used the intermolecular BRET approach in our later work, and therefore, all subsequent data represent results using intermolecular BRET biosensors.

Ras Activation in the Plasma Membrane after AngII Stimulation of Different AT_1-R Mutants—After optimization and validation of our BRET strategy, experiments were performed with RasBRET probes in HEK293 cells cotransfected with the wild-type AT_{1A}-R, the tail deletion AT_{1A}-RΔ319 mutant (which is unable to internalize) (40), or the AT_1-R-DRY/AAY mutant (which is unable to couple to $G\alpha_q$ and initiate inositol phosphate signaling) (35, 37). As shown in Fig. 3, AngII stimulation of the wild-type AT_1-R caused transient Ras activation in the plasma membrane, which was rapidly terminated because of the receptor desensitization and internalization. However, when the desensitization or internalization was reduced in cells expressing the AT_{1A}-RΔ319 mutant, Ras activation was enhanced and prolonged. We did not detect significant Ras activation when utilizing the AT_1-R-DRY/AAY mutant, which suggests that the AngII-induced Ras activation is predominantly G protein-mediated.

Subcellular Localization of Ras Activation—In the next set of experiments, the effect of extracellular stimuli on intracel-
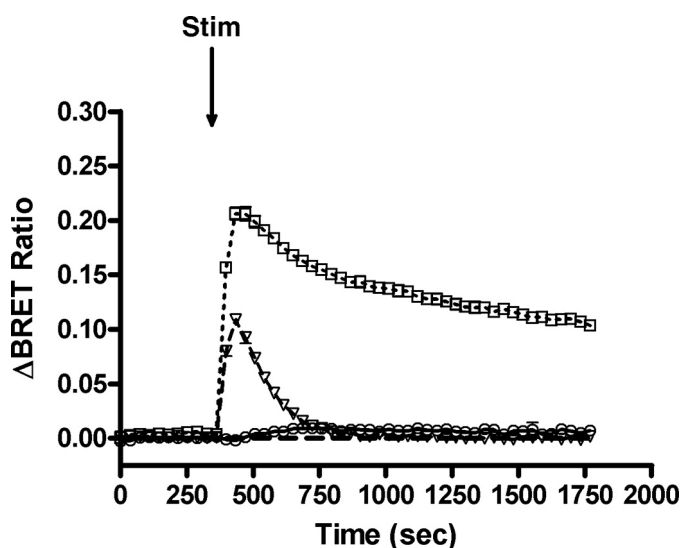
FIGURE 3. **Ras activation upon agonist stimulation of different AT_1-R mutants.** HEK293 cells were cotransfected with intermolecular MP-RasBRET and the wild-type AT_{1A}-R, AT_{1A}-RΔ319, or AT_{1A}-R-DRY/AAY plasmid. The serum-starved cells were exposed to 100 nM AngII (*open triangles, dashed line* for the wild-type AT_{1A}-R, *open rectangles, dotted line* for AT_{1A}-RΔ319, and *open circles* for AT_{1A}-R-DRY/AAY) or vehicle (*dashed line*) at the indicated time points. The BRET records are an average of at least three independent experiments. The means ± S.E. are shown ($n = 3$). *Stim*, stimulated.

lular Ras activation was examined. To investigate specifically the possible compartmentalized Ras signaling processes, we targeted our probes to the surface of intracellular organelles using previously described targeting motifs (29). These motifs were placed at either the N or C terminus of the respective probes as described under "Experimental Procedures." We used intermolecular probe pairs in which one of the interacting partners (either YFP-Ras or RBD-luciferase) was tagged with the targeting sequence while the other polypeptide was not targeted to organelles and was therefore expressed in the cytosol. The micrographs (confocal microscopic images) in Fig. 4 demonstrate that all probes were properly expressed in the targeted compartment. HEK293 cells were cotransfected with the AT_{1A}-R (wild-type AT_{1A}-R, AT_{1A}-RΔ319 or AT_{1A}-R-DRY/AAY) and with the indicated intermolecular probes targeted to various compartments, such as the *trans*-Golgi network (TGN), the ER, and endosomes.

EGF- and AngII-induced Ras activation was detected in the Golgi using YFP-Ras targeted to the TGN (the targeting sequence was fused to the N terminus of YFP-Ras, and RBD-luciferase was cytosolic) (Fig. 4A). AngII caused a rapid and transient Ras activation in the TGN (Fig. 4A). In contrast to the Ras activation in the plasma membrane, where AngII stimulation resulted in a much smaller response compared with EGF-evoked activation, the changes in the BRET ratios in the TGN were quite similar for EGF and AngII, suggesting that the relative Ras activation efficacy of AngII may be higher than that of EGF in this compartment. It is also important to note that the response to AngII consistently occurred more rapidly then the EGF-induced response. To assess the compartmentalized Ras signaling upon agonist stimulation, we compared the data obtained using the wild-type AT_1-R and an internalization-deficient AT_1-R mutant (AT_{1A}-RΔ319)

coexpressed with various BRET probes in HEK293 cells. Our data show that the AngII-induced Ras activation in the TGN is not a consequence of receptor internalization because the internalization-deficient AT_1-R mutant showed prolonged, rather than inhibited, Ras activation compared with the wild-type AT_1-R (Fig. 4A).

We also detected Ras activation on the surface of the ER using both Ubc6- and Sac1- targeted intermolecular probes. In these constructs, the ER-targeting sequences were fused to the C terminus of the RBD-luciferase part while the YFP-Ras part was cytosolic. Interestingly, only AngII stimulation activated Ras in the ER, whereas EGF was not able to show this effect (Fig. 4B). The kinetics and characteristics of the AngII-induced Ras activation in the ER were indistinguishable when Sac1- or Ubc6-targeting sequences were used (Fig. 4B; only the results with the Sac1-targeted probe are shown). These data also suggest that the AngII-induced response is independent of EGF receptor transactivation. Similar to Ras activation detected in the TGN, the AngII-induced Ras activation was more sustained in the ER in cells expressing the internalization-deficient AT_{1A}-RΔ319 mutant compared with the wild-type receptor.

Although EGF receptor activation in endosomes was detected by resonance energy transfer measurements in previous studies (11), our RasBRET probe targeted with the FYVE domain to endosomes (the targeting sequence was fused to the C terminus of RBD-luciferase while YFP-Ras is cytosolic) was not able to detect EGF- or AngII-induced Ras activation in endosomes (Fig. 4C). Based on these data, it is possible that endosomal Ras activation occurs away from the targeted phosphatidylinositol 3-phosphate-containing microdomain of this organelle.

Mechanism of AngII-induced Ras Activation—In the cells of the cardiovascular system, AngII-induced Ras activation (and hence, MAPK activation) is mostly the consequence of the transactivation of receptor tyrosine kinases, such as the EGF receptor. However, in some other cell types, AngII-induced ERK activation is independent of EGF receptor transactivation (17). It has been demonstrated that phosphorylation of ERK1/2 upon AngII stimulation in HEK293 cells, but not in C9 hepatic cells, is EGF receptor transactivation-independent, but Ras activation was not investigated (20). In our experiments using HEK293 cells, the EGF receptor kinase inhibitor AG1478 abolished the EGF-evoked Ras activation in the plasma membrane, but it had no inhibitory effect on the AngII-induced Ras activation in the plasma membrane (Fig. 5A). The AngII-induced Ras activation in the TGN was not affected (Fig. 5 B). These data suggest that Ras activation in HEK293 cells is primarily independent of EGF receptor transactivation but requires G protein coupling because AngII stimulation of cells expressing the AT_1-R-DRY/AAY mutant failed to initiate Ras signaling in the plasma membrane (Fig. 3) and in the intracellular organelles studied (data not shown).

DISCUSSION

Small G proteins are central players in many signal transduction pathways and regulate a wide variety of cell functions. It is well known that stimulation of GPCRs, including the

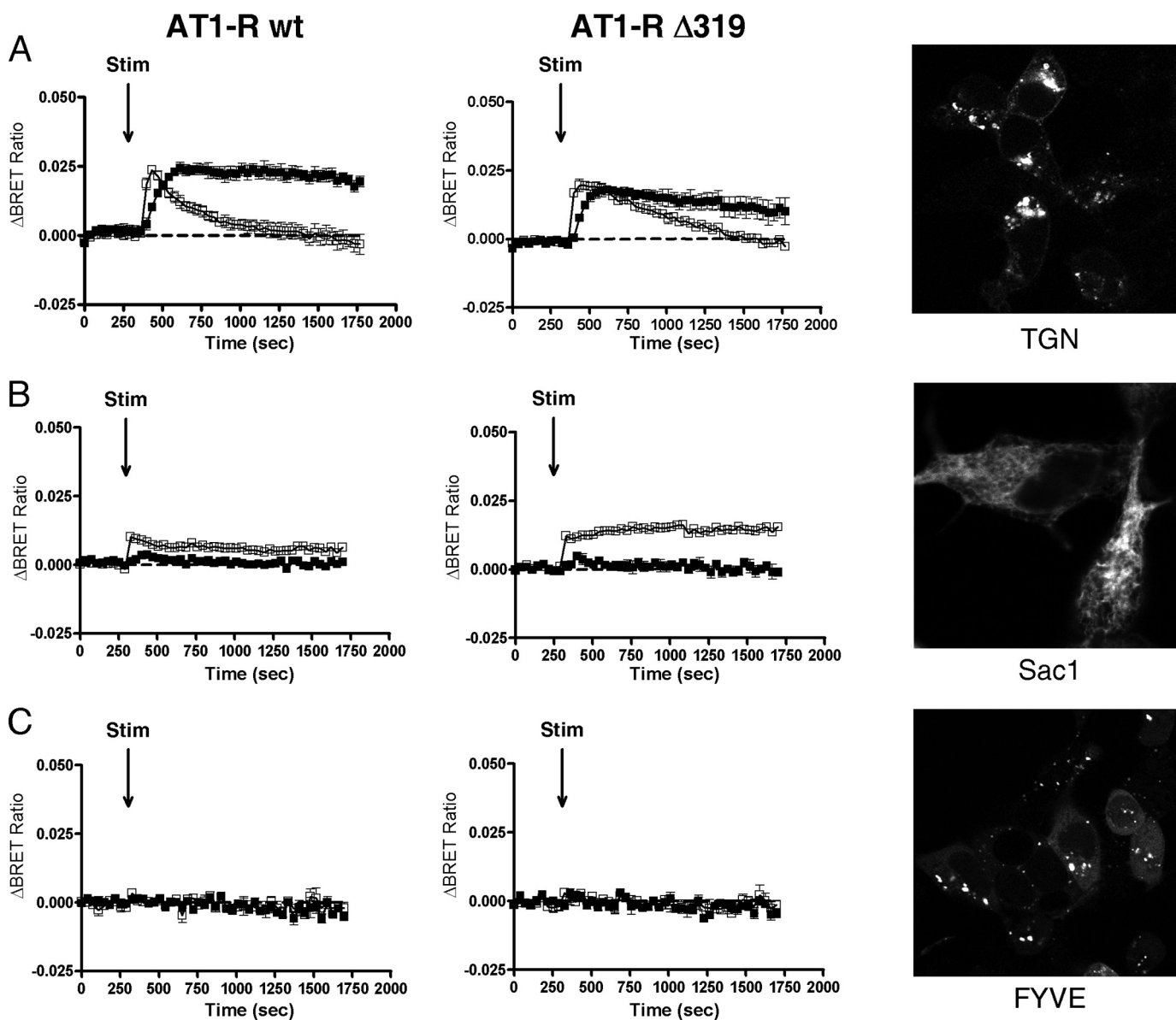*Angiotensin II Induces Ras Activation in the ER and Golgi*

FIGURE 4. **Ras activation in intracellular organelles.** HEK293 cells were cotransfected with the indicated intermolecular RasBRET probes along with either the wild-type AT$_{1A}$-R (*left panels*) or AT$_{1A}$-RΔ319 (*middle panels*) plasmid. HEK293 cells were exposed to 50 ng/ml EGF (*filled symbols*), 100 nM AngII (*open symbols*), or vehicle (*dashed lines*) at the indicated time points. The BRET records are an average of at least three independent experiments, each performed in triplicate. The means ± S.E. are shown (*n* = 3). *A–C*, Ras activation in the TGN, the ER, and endosomes, respectively. The representative confocal micrographs (*right panels*) show the localization and cellular distribution of the various probes in HEK293 cells that were transfected with the plasmids of the indicated probes. YFP fluorescence was detected using a Zeiss LSM 510 confocal microscope. Because the endosome- and ER-targeting sequences are located at the C terminus of RBD-luciferase, the micrographs for endosomes and the ER show the cellular distribution of the intramolecular versions of RasBRET-Sac1 and RasBRET-FYVE, respectively. *Stim*, stimulated.

AT$_1$-R, can lead to activation of various small G proteins, such as Ras (1, 17). Although it is generally believed that the signal generation of GPCRs occurs at the plasma membrane, the presence of small G proteins in intracellular organelles has already been demonstrated (7), and in this study, we examined whether AngII-induced Ras activation can be detected on the surface of intracellular membranes by targeting biosensors to various compartments. BRET and FRET probes report energy transfer from an energy donor (*Renilla* luciferase in BRET and cyan fluorescent protein in FRET applications) to YFP when Ras becomes loaded with GTP and interacts with its effector during Ras activation. In our studies, we used BRET measurements because BRET has several advan-

tages compared with FRET microscopy. For example, BRET is a more quantitative method because it can be performed on a large population of cells. BRET is also more sensitive compared with FRET because the excitation light causes a high background in FRET measurements. Our BRET probes were targeted to plasma membrane microdomains and intracellular organelles, including the ER and Golgi, using specific targeting sequences to assess the effect of hormonal stimulation on Ras activity in these compartments.

AngII induced a transient Ras activation in the plasma membrane, which was much smaller compared with the EGF-induced response (Fig. 1). This finding is consistent with the fact that EGF is a more effective Ras activator than AngII;
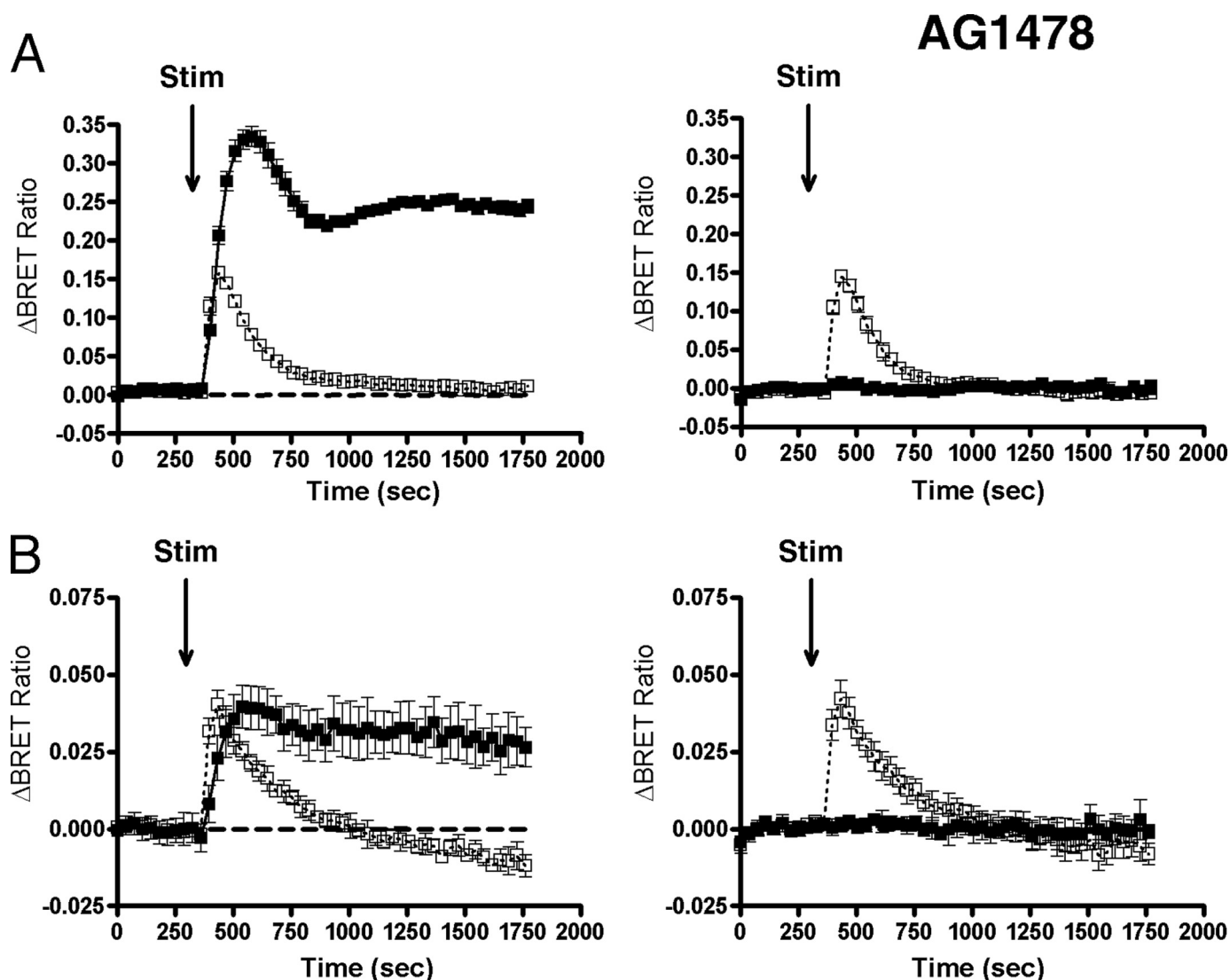
FIGURE 5. **Mechanism of Ras activation upon AngII stimulation is independent of EGF receptor transactivation in HEK293 cells.** HEK293 cells were transfected with the AT_{1A}-R and with the plasmid pair of the intermolecular MP-RasBRET (*A*) or TGN-RasBRET (*B*), and after 24 h, the serum-starved cells were pretreated for 30 min prior to BRET measurement either with vehicle (*left panels*) or with 1 μM AG1478 (*right panels*). After the pre-treatment, the cells were exposed to 50 ng/ml EGF (*filled symbols*), 100 nM AngII (*open symbols, dotted lines*), or vehicle (*dashed* traces) at the indi-cated time points. The BRET records are an average of at least three independent experiments, each performed in triplicate. The means $\pm$ S.E. are shown ($n = 3$). *Stim*, stimulated.

however, it is possible that the incomplete transfection effi-ciency of the angiotensin receptor-containing plasmid also contributed to this finding. Kinetically, EGF receptor activa-tion also produced more prolonged Ras activation compared with the AngII-induced response. However, it is also notewor-thy that our initial studies with intramolecular BRET probes showed that the AngII-induced Ras activation in the plasma membrane was more rapid than the EGF-induced response (Fig. 1, *A* and *B*).

The sensitivity of intramolecular RasBRET probes was not sufficient to detect Ras activation in intracellular organelles (data not shown). In the intramolecular BRET probes, the energy donor and acceptor are in the same molecule, and their molecular proximity causes high initial (background) levels and a low dynamic range of these biosensors. On the other hand, in intermolecular RasBRET probes, the energy donor and acceptor are in distinct polypeptide chains, which

results in a much better signal-to-noise ratio (Fig. 1). In this study, we were able to demonstrate that AngII stimulation not only increased Ras activity in the plasma membrane but also activated it in intracellular compartments, such as the TGN and ER (Fig. 4). Endocytosis of receptors, including both tyro-sine kinase receptors and GPCRs, not only regulates their ac-tivity but also initiates signaling pathways, such as MAPK ac-tivation (23). Although AT_1-R- and EGF receptor-generated signaling in endosomes has been reported (11, 41), our endo-somal targeted probes were not able to demonstrate Ras sig-naling on endosomes (Fig. 4*C*). This fact calls for cautious evaluation of the BRET and FRET measurements because negative results with BRET or FRET biosensors certainly do not report the nonexistence of the investigated events but rather reflect the unsuitable or non-optimal arrangement of interacting partners and energy donors and acceptors of the applied biosensors. It is also possible that the FYVE domain-

Angiotensin II Induces Ras Activation in the ER and Golgi

targeted biosensor and the elements of Ras signaling are localized in distinct microdomains of endosomes, preventing the interactions of these probes.

Mitogen-induced Ras activation in the Golgi has been demonstrated using a Raf-1-based FRET sensor (42). Chiu *et al.* have shown that rapid and transient plasma membrane Ras activation is followed by a slower and sustained Ras response in the Golgi. A possible explanation for the different kinetics of EGF-induced Ras activation in the Golgi in this report compared with the more rapid response observed in our study is the difference in the targeting strategies because our probe was targeted to the TGN. We also detected AngII-induced rapid and transient Ras activation in the TGN. AngII was a relatively efficient activator of Ras in the TGN because the amplitude of the AngII and EGF responses in the TGN was comparable, whereas EGF caused a much larger response in the plasma membrane. AngII caused a more prolonged activation of Ras in the TGN in cells expressing the internalization-deficient AT_{1A}-RΔ319 mutant, which is consistent with the impaired desensitization of this receptor (43) and argues against the role of receptor endocytosis in AngII-induced Ras activation in the TGN. Similarly, as was shown previously, EGF-induced endomembrane-associated Ras activation is also independent of EGF receptor endocytosis in COS-1 cells (42).

The Ras activation in the ER is surprising in many respects. It is remarkable that only AngII stimulation activated Ras, but EGF receptor stimulation was not able to produce this effect (Fig. 4*B*). This result provides evidence that the effect of AngII in the ER is independent of EGF receptor transactivation. Although mitogen-induced Ras signaling in the ER has been reported in COS-1 cells (42), we did not observe a major effect of EGF receptor activation on Ras activity in the ER in HEK293 cells (Fig. 4*B*). Similar to the TGN, AngII caused a more prolonged activation of ER-targeted Ras in cells expressing the internalization-deficient AT_{1A}-RΔ319 mutant, suggesting that the effect of AngII on Ras activation is also internalization-independent in this compartment.

Our data demonstrate that AngII stimulates Ras activity in the Golgi and ER, which raises the question as to the function of Ras activation in these compartments. The most obvious answer is that Ras has multiple and widespread functions, and the compartmentalized signaling can provide the complexity of downstream pathways with different kinetics. Activation of small G proteins in endosomes is not surprising because this cellular membrane compartment is derived from the plasma membrane, and it is possible that the signaling continues after internalization of the plasma membrane receptor (and extracellular ligand) on the cytosolic surface of the endosomes. Activated GPCRs also bind β-arrestin molecules. In the case of many GPCRs, including the AT_1-R, β-arrestin binding of the internalized receptor persist in the endosomes. Because β-arrestin can facilitate the activation of signaling complexes, this mechanism can also cause signaling, including activation of MAPKs, on the surface of endosomes (17, 21, 41). Ras activation on the surface of endomembranes, such as the ER and Golgi, is much more surprising because these compartments are not derived from the plasma membrane. Because the presence of agonist-bound receptors in the Golgi and ER is un-

likely after a short stimulation of the receptor, it can be assumed that Ras activation in these compartments occurs with a different mechanism compared with the plasma membrane.

The mechanism of AngII-induced Ras activation in the plasma membrane is cell type-dependent (17). In vascular smooth muscle cells and many other cell types, transactivation of EGF receptors plays a major role in the mitogen effects of AngII (17, 44). In our study, AG1478, an EGF receptor kinase inhibitor, eliminated all EGF-induced responses but had no effect on AngII-induced Ras activation in the Golgi and ER, similar to that in the plasma membrane, in HEK293 cells (Fig. 5). This finding is consistent with previous studies that demonstrated that AngII-induced ERK activation and mitogen signaling are independent of EGF receptor transactivation in these cells (20). We did not detect significant AngII-induced Ras activation in cells expressing the AT_1-R-DRY/AAY mutant, suggesting that the response, both in the plasma membrane (Fig. 3) and in endomembranes (data not shown), is predominantly G protein-mediated. Considering its rapid timing, it is likely that the effect of AngII on Ras activation in the TGN and ER is mediated by soluble messengers, similar to the previously reported similar effects of growth factors and lysophosphatidic acid (7, 45, 46). In cells expressing the internalization-deficient AT_{1A}-RΔ319 mutant, AngII caused more prolonged Ras activation both in the plasma membrane (Fig. 3) and in endomembranes (Fig. 4), which is probably caused by the impaired desensitization of this mutant receptor (43). These data are also consistent with our conclusion that AngII-induced Ras activation in the Golgi and ER is G protein-mediated and does not require receptor internalization or β-arrestin-mediated signaling.

This study has demonstrated the wide-scale effects of AngII on Ras activation and emphasizes that Ras can signal from distinct compartments of cellular membranes to ensure functional diversity but not redundancy of its signaling. The better understanding of the signaling properties of the AT_1-R may provide additional clues to improve the therapeutic potential of drugs that target this receptor.

REFERENCES

1. Takai, Y., Sasaki, T., and Matozaki, T. (2001) *Physiol. Rev.* **81,** 153–208
2. García-Mata, R., and Burridge, K. (2007) *Trends Cell Biol.* **17,** 36–43
3. Buday, L., and Downward, J. (2008) *Biochim. Biophys. Acta* **1786,** 178–187
4. Vojtek, A. B., Hollenberg, S. M., and Cooper, J. A. (1993) *Cell* **74,** 205–214
5. Bivona, T. G., Quatela, S. E., Bodemann, B. O., Ahearn, I. M., Soskis, M. J., Mor, A., Miura, J., Wiener, H. H., Wright, L., Saba, S. G., Yim, D., Fein, A., Pérez de Castro, I., Li, C., Thompson, C. B., Cox, A. D., and Philips, M. R. (2006) *Mol. Cell* **21,** 481–493
6. Plowman, S. J., Ariotti, N., Goodall, A., Parton, R. G., and Hancock, J. F. (2008) *Mol. Cell. Biol.* **28,** 4377–4385
7. Mor, A., and Philips, M. R. (2006) *Annu. Rev. Immunol.* **24,** 771–800
8. Choy, E., Chiu, V. K., Silletti, J., Feoktistov, M., Morimoto, T., Michaelson, D., Ivanov, I. E., and Philips, M. R. (1999) *Cell* **98,** 69–80
9. Di Guglielmo, G. M., Baass, P. C., Ou, W. J., Posner, B. I., and Bergeron, J. J. (1994) *EMBO J.* **13,** 4269–4277
10. Wang, Y., Pennock, S., Chen, X., and Wang, Z. (2002) *Mol. Cell. Biol.* **22,**

7279–7290

11. Sorkin, A., McClure, M., Huang, F., and Carter, R. (2000) *Curr. Biol.* **10,** 1395–1398

12. Vieira, A. V., Lamaze, C., and Schmid, S. L. (1996) *Science* **274,** 2086–2089

13. Roy, S., Wyse, B., and Hancock, J. F. (2002) *Mol. Cell. Biol.* **22,** 5128–5140

14. Augsten, M., Pusch, R., Biskup, C., Rennert, K., Wittig, U., Beyer, K., Blume, A., Wetzker, R., Friedrich, K., and Rubio, I. (2006) *EMBO Rep.* **7,** 46–51

15. Plowman, S. J., and Hancock, J. F. (2005) *Biochim. Biophys. Acta* **1746,** 274–283

16. Daniels, M. A., Teixeiro, E., Gill, J., Hausmann, B., Roubaty, D., Holmberg, K., Werlen, G., Holländer, G. A., Gascoigne, N. R., and Palmer, E. (2006) *Nature* **444,** 724–729

17. Hunyady, L., and Catt, K. J. (2006) *Mol. Endocrinol.* **20,** 953–970

18. Ohtsu, H., Suzuki, H., Nakashima, H., Dhobale, S., Frank, G. D., Motley, E. D., and Eguchi, S. (2006) *Hypertension* **48,** 534–540

19. Higuchi, S., Ohtsu, H., Suzuki, H., Shirai, H., Frank, G. D., and Eguchi, S. (2007) *Clin. Sci.* **112,** 417–428

20. Shah, B. H., Yesilkaya, A., Olivares-Reyes, J. A., Chen, H. D., Hunyady, L., and Catt, K. J. (2004) *Mol. Endocrinol.* **18,** 2035–2048

21. Ferguson, S. S. (2001) *Pharmacol. Rev.* **53,** 1–24

22. Hunyady, L. (1999) *J. Am. Soc. Nephrol.* **10,** Suppl. 11, S47–S56

23. Daaka, Y., Luttrell, L. M., Ahn, S., Della Rocca, G. J., Ferguson, S. S., Caron, M. G., and Lefkowitz, R. J. (1998) *J. Biol. Chem.* **273,** 685–688

24. Bivona, T. G., and Philips, M. R. (2005) *Methods* **37,** 138–145

25. Kiyokawa, E., Hara, S., Nakamura, T., and Matsuda, M. (2006) *Cancer Sci.* **97,** 8–15

26. Mochizuki, N., Yamashita, S., Kurokawa, K., Ohba, Y., Nagai, T., Miyawaki, A., and Matsuda, M. (2001) *Nature* **411,** 1065–1068

27. Nakamura, T., Kurokawa, K., Kiyokawa, E., and Matsuda, M. (2006) *Methods Enzymol.* **406,** 315–332

28. Bondeva, T., Balla, A., Várnai, P., and Balla, T. (2002) *Mol. Biol. Cell* **13,** 2323–2333

29. Várnai, P., and Balla, T. (2007) *Pflugers Arch.* **455,** 69–82

30. Fukano, T., Sawano, A., Ohba, Y., Matsuda, M., and Miyawaki, A. (2007) *Cell. Struct. Funct.* **32,** 9–15

31. Zacharias, D. A., Violin, J. D., Newton, A. C., and Tsien, R. Y. (2002) *Science* **296,** 913–916

32. Szentpetery, Z., Várnai, P., and Balla, T. (2010) *Proc. Natl. Acad. Sci. U.S.A.* **107,** 8225–8230

33. Várnai, P., Balla, A., Hunyady, L., and Balla, T. (2005) *Proc. Natl. Acad. Sci. U.S.A.* **102,** 7859–7864

34. Smith, R. D., Baukal, A. J., Zolyomi, A., Gaborik, Z., Hunyady, L., Sun, L., Zhang, M., Chen, H. C., and Catt, K. J. (1998) *Mol. Endocrinol.* **12,** 634–644

35. Gáborik, Z., Jagadeesh, G., Zhang, M., Spät, A., Catt, K. J., and Hunyady, L. (2003) *Endocrinology* **144,** 2220–2228

36. Gáborik, Z., Mihalik, B., Jayadev, S., Jagadeesh, G., Catt, K. J., and Hunyady, L. (1998) *FEBS Lett.* **428,** 147–151

37. Wei, H., Ahn, S., Shenoy, S. K., Karnik, S. S., Hunyady, L., Luttrell, L. M., and Lefkowitz, R. J. (2003) *Proc. Natl. Acad. Sci. U.S.A.* **100,** 10782–10787

38. Ohba, Y., Kurokawa, K., and Matsuda, M. (2003) *EMBO J.* **22,** 859–869

39. Prior, I. A., Harding, A., Yan, J., Sluimer, J., Parton, R. G., and Hancock, J. F. (2001) *Nat. Cell Biol.* **3,** 368–375

40. Balmforth, A. J., Lee, A. J., Bajaj, B. P., Dickinson, C. J., Warburton, P., and Ball, S. G. (1995) *Eur. J. Pharmacol.* **291,** 135–141

41. Luttrell, L. M., Roudabush, F. L., Choy, E. W., Miller, W. E., Field, M. E., Pierce, K. L., and Lefkowitz, R. J. (2001) *Proc. Natl. Acad. Sci. U.S.A.* **98,** 2449–2454

42. Chiu, V. K., Bivona, T., Hach, A., Sajous, J. B., Silletti, J., Wiener, H., Johnson, R. L., 2nd, Cox, A. D., and Philips, M. R. (2002) *Nat. Cell Biol.* **4,** 343–350

43. Olivares-Reyes, J. A., Smith, R. D., Hunyady, L., Shah, B. H., and Catt, K. J. (2001) *J. Biol. Chem.* **276,** 37761–37768

44. Eguchi, S., Numaguchi, K., Iwasaki, H., Matsumoto, T., Yamakawa, T., Utsunomiya, H., Motley, E. D., Kawakatsu, H., Owada, K. M., Hirata, Y., Marumo, F., and Inagami, T. (1998) *J. Biol. Chem.* **273,** 8890–8896

45. Bivona, T. G., Pérez De Castro, I., Ahearn, I. M., Grana, T. M., Chiu, V. K., Lockyer, P. J., Cullen, P. J., Pellicer, A., Cox, A. D., and Philips, M. R. (2003) *Nature* **424,** 694–698

46. Arozarena, I., Matallanas, D., Berciano, M. T., Sanz-Moreno, V., Calvo, F., Muñoz, M. T., Egea, G., Lafarga, M., and Crespo, P. (2004) *Mol. Cell. Biol.* **24,** 1516–1530

Demonstration of Angiotensin II-induced Ras Activation in the *trans*-Golgi Network and Endoplasmic Reticulum Using Bioluminescence Resonance Energy Transfer-based Biosensors

András Balla, László Sándor Erdélyi, Eszter Soltész-Katona, Tamas Balla, Péter Várnai
and László Hunyady

Access the most updated version of this article at doi: 10.1074/jbc.M110.176933

Alerts:
- When this article is cited
- When a correction for this article is posted

Click here to choose from all of JBC's e-mail alerts

This article cites 46 references, 17 of which can be accessed free at
http://www.jbc.org/content/286/7/5319.full.html#ref-list-1

Mapping of the Localization of Type 1 Angiotensin Receptor in Membrane Microdomains Using Bioluminescence Resonance Energy Transfer-based Sensors*[S]

András Balla[‡1], **Dániel J. Tóth**[‡], **Eszter Soltész-Katona**[‡], **Gyöngyi Szakadáti**[‡], **László Sándor Erdélyi**[‡], **Péter Várnai**[‡], and **László Hunyady**[‡§¶2]

From the [‡]*Department of Physiology, Faculty of Medicine, and the* [§]*Laboratory of Neurobiochemistry and Molecular Physiology, Semmelweis University, Budapest H-1444, Hungary and the* [¶]*Hungarian Academy of Sciences, H-1444 Budapest, Hungary*

Background: Agonists can affect the subcellular localization of G protein-coupled receptors (GPCRs).
Results: Subcellular localization of AT1 angiotensin receptor rapidly changes in response to ligand binding.
Conclusion: Agonists have diverse effects on the subcellular dynamics of wild type and mutant AT1-Rs.
Significance: This study demonstrates that the effects of ligands on subcellular localization of GPCRs in living cells can be investigated by BRET.

Initiation and termination of signaling of the type I angiotensin receptor (AT_1-R) can lead to dynamic changes in its localization in plasma membrane microdomains. Several markers were recently developed to investigate membrane microdomains. Here, we used several YFP-labeled fusion constructs (*i.e.* raft or non-raft plasma membrane markers) to analyze the agonist-induced changes in compartmentalization of AT_1-R, including internalization or lateral movement between plasma membrane compartments in response to stimulation using bioluminescence resonance energy transfer measurements. Our data demonstrate that angiotensin II (AngII) stimulus changes the microdomain localization of wild type or mutated (DRY → AAY or TSTS → AAAA) AT_1-Rs co-expressed with the fluorescent probes in HEK293 cells. The comparison of the trafficking of AT_1-R upon AngII stimulus with those of [Sar^1,Ile^8]AngII or [Sar^1,Ile^4,Ile^8]AngII stimulus revealed different types of changes, depending on the nature of the ligand. The observed changes in receptor compartmentalization of the AT_1-R are strikingly different from those of 5HT-2C and EGF receptors, which demonstrate the usefulness of the bioluminescence resonance energy transfer-based measurements in the investigation of receptor trafficking in the plasma membrane in living cell experiments.

Studies during recent decades have revealed that the plasma membrane is not a uniform structure but rather a mosaic of microdomains, and this is a key concept of our current understanding of compartmentalized signaling. Membrane rafts are specific microdomains of the plasma membrane, which differ in their compositions from the rest of the plasma membrane (1). These cholesterol- and sphingolipid-rich plasma membrane microdomains play important roles in compartmentalization of cellular functions. Membrane rafts are frequently referred to as lipid rafts, whereas the rest of the plasma membrane can be called non-raft lipid domains or disordered membranes. The cholesterol- and sphingolipid-rich lipid rafts comprise up to 50% of the plasma membrane (2), their sizes are 10–200 nm, and they contain proteins clustered within them. The detergent-insoluble lipid rafts contain proteins that are modified posttranslationally by acylation or glycosylphosphatidylinositol modification but not by prenylation. Formation of rafts requires cholesterol; thus, cholesterol depletion by β-methylcyclodextrin treatment is widely used for disruption of lipid rafts.

Membrane microdomains are located in both leaflets of the plasma membrane. The Ras small G proteins are associated with inner leaflet clusters, as revealed by various methods, such as transmission electron microscopy and fluorescence recovery after photobleaching (3, 4). H-Ras and K-Ras are homologous proteins, but their C-terminal tails are significantly different. These C-terminal tails anchor the Ras proteins to the plasma membrane, but the different C termini of the Ras isoforms cause different interactions with membranes that can lead to distinct signaling outcomes. It was demonstrated that the GDP-bound H-Ras is located in lipid rafts, whereas the K-Ras is found in cholesterol-insensitive, non-raft lipid domains (4), and the different CAAX domains of the Ras proteins are targeted to distinct plasma membrane microdomains (5). It was also demonstrated by a fluorescence resonance energy transfer (FRET) approach that a lipid anchor on a fluorescent protein is sufficient to sequester the protein to different microdomains within the plasma membrane (6). Zacharias *et al.* (6) constructed several probes, in which the yellow fluorescent protein (YFP)

[S] This article contains supplemental Figs. 1–3.
[1] Supported in part by the János Bolyai Research Scholarship of the Hungarian Academy of Sciences.
[2] To whom correspondence should be addressed: Dept. of Physiology, Semmelweis University, Faculty of Medicine, P.O. Box 259, H-1444 Budapest, Hungary. Tel.: 36-1-266-9180; Fax: 36-1-266-6504; E-mail: Hunyady@eok.sote.hu.

was fused with short peptides containing consensus sequences for acylation, such as myristoylation and palmitoylation (MP-YFP).[3] FRET measurements have revealed that the MP-YFP probe is clustered to membrane rafts, and β-methyl-cyclodextrin treatment interfered with its localization (6).

AngII is an octapeptide hormone, which is the main effector of the renin-angiotensin system and can bind and activate type 1 (AT$_1$-R) and type 2 angiotensin receptors. AT$_1$-R is a typical heptahelical, G protein-coupled receptor (GPCR), and the G protein-mediated "classical" signaling mechanisms are responsible for the majority of AngII-evoked cellular responses. These signaling mechanisms have a wide spectrum, including generation of second messengers (Ca^{2+} signal via inositol 1,4,5-trisphosphate, diacylglycerol), activation of small G proteins and cytoplasmic tyrosine kinases, regulation of ion channels, and transactivation of growth factor receptors. After binding of AngII to AT$_1$-R, activation of heterotrimeric G proteins, G$_{q/11}$, mediates the hydrolysis of PtdIns(4,5)P$_2$ by phosphoinositide-specific phospholipase Cβ, which leads to generation of second messengers (7). The down-regulation of this signaling includes several consecutive or parallel processes, such as desensitization, internalization into intracellular vesicles, and degradation of the receptors. Internalization of AT$_1$-R is regulated by phosphorylation by GPCR kinases (GRKs), which promotes β-arrestin binding (7). Changes in the plasma membrane localization of AT$_1$-R occur during the initiation and termination of signaling and also provide the possibility of resensitization that allows response to new extracellular stimuli.

Although membrane rafts are hot topics in the literature, their existence remains challenged (8). It is well established that some structural motifs of plasma membrane proteins are responsible for targeting into membrane microdomains, and several membrane markers were recently developed to investigate these microdomains (6). Although the concept of membrane rafts is based on biochemical experiments utilizing various detergent extraction methods, we decided to use another approach to investigate the relation of AT$_1$-R to membrane microdomains in living cells. Earlier studies have demonstrated that AngII stimulation of AT$_1$-R promotes association and trafficking of the receptors into caveolin-enriched/lipid rafts in vascular smooth muscle cells (9–11). Instead of focusing on the characterization of the biophysical and biochemical nature of the plasma membrane microdomains during AT$_1$-R action, we followed the distribution of the AT$_1$-Rs after ligand stimulus. FRET- and bioluminescence resonance energy transfer (BRET)-based methods are widely used to study oligomerization and protein-protein interactions of GPCRs (12, 13). The main advantage of these methods is that the measurements can

be performed in living cells. For instance, it was shown by using FRET imaging in living cells that the neurokinin-1 receptors reside in very small (~10-nm) membrane microdomains that are cholesterol-sensitive (14). We have constructed and used several YFP-labeled fusion constructs (*i.e.* raft or non-raft plasma membrane markers) to analyze the details of AT$_1$-R trafficking, such as internalization or lateral movement between plasma membrane compartments upon stimulus in BRET measurements. Recently, a very similar targeting strategy was used to label different membrane microdomains (raft-targeted and non-raft-targeted reporters) to investigate the spatial compartmentalization in PI3K/Akt signaling (15). The BRET probes report energy transfer from *Renilla* luciferase to YFP, hence the molecular proximity of two fusion proteins. The BRET method is very sensitive due to the lack of excitation light, which results in low background (13, 16).

Using BRET experiments, we demonstrated that AT$_1$-R changes its distribution between membrane microdomains in response to AngII stimulus in HEK293 cells. We also examined mutated AT$_1$-Rs (either DRY/AAY mutation or TSTS/A mutation) co-expressed with fluorescent probes of different microdomains in order to determine the G protein- and phosphorylation-dependent steps in AT$_1$-R trafficking. It was also revealed that the dynamics of AT$_1$-R is different using diverse ligands of the receptor. The stimulus of AT$_1$-R with peptide angiotensin analogues, such as [Sar^1,Ile^8]AngII or [Sar^1,Ile^4,Ile^8]AngII, caused different changes in localization of AT$_1$-R compared with AngII, whereas the non-peptide angiotensin antagonist candesartan led to complete inhibition of AT$_1$-R trafficking.

EXPERIMENTAL PROCEDURES

Materials—Molecular biology enzymes were obtained from Fermentas (Burlington, Canada), Stratagene (La Jolla, CA), and Invitrogen. Cell culture dishes and plates for BRET measurements were purchased from Greiner (Kremsmunster, Austria). Lipofectamine 2000 and coelenterazine h were from Invitrogen. The candesartan was obtained from Toronto Research Chemicals. The [Sar^1,Ile^8]AngII (SI-AngII) and [Sar^1,Ile^4,Ile^8]AngII (SII-AngII) were purchased from Bachem AG (Bubendorf, Switzerland). Unless otherwise stated, all other chemicals and reagents were purchased from Sigma. The human embryonic kidney (HEK293) cells were from ATCC (American Type Culture Collection, Manassas, VA).

Molecular Biology—For the construction of YFP-labeled constructs, the plasmid backbones of eYFP-C1 or eYFP-N1 (Clontech, Mountain View, CA) were used. The cDNA of the eYFP-tagged β-arrestin2 (β-arrestin2-YFP) and eYFP-tagged AT$_1$-R (AT$_1$-R-YFP) were constructed as described previously (17). AT$_1$-R-Rluc was constructed by replacing the eYFP coding region in AT$_1$-R-YFP with *Renilla* luciferase. The luciferase-tagged 5-hydroxytryptamine receptor-2C receptor (5HT-2C-R) was constructed by subcloning the receptor cDNA into the codon humanized *Renilla* luciferase pRluc-N1 vector (PerkinElmer Life Sciences). The luciferase-tagged epidermal growth factor receptor (EGF-R) was constructed by replacing the eYFP coding region in EGF-R-YFP with *Renilla* luciferase. The MP targeting to plasma membrane rafts was based on the

---

[3] The abbreviations used are: MP-YFP, myristoylated and palmitoylated YFP; AngII, angiotensin II; BRET, bioluminescence resonance energy transfer; GPCR, G protein-coupled receptor; GRK, GPCR kinase; 5HT, serotonin (5-hydroxytryptamine); AT$_1$-R, type 1 angiotensin receptor; 5HT-2C-R, type 2C serotonin receptor; KR-YFP, YFP-labeled CAAX domain of K-Ras; PLC, phospholipase C; PH, pleckstrin homology; PLCδ1-PH-YFP, YFP-tagged phospholipase Cδ1 PH domain; PtdIns(4,5)P$_2$, phosphatidylinositol 4,5-bisphosphate; HEK, human embryonic kidney; eYFP, enhanced YFP; EGF-R, EGF receptor; SI-AngII, [Sar^1,Ile^8]AngII; SII-AngII, [Sar^1,Ile^4,Ile^8]AngII; DRY/AAY, D125A/R126A mutation; TSTS/A, T332A/S335A/T336A/S338A mutation.

Localization of AT$_1$-R in Membrane Microdomains

design of Zacharias *et al.* (6), where the MP tag was the N-terminal MGCIKSKRKDNLNDDE amino acid sequence from Lyn kinase (accession number NM_002350). In order to target the eYFP to the disordered plasma membrane microdomains, we have fused C-terminally the CAAX motif from the K-Ras small G protein, KMSKDGKKKKKKSKTKCVIM, consisting of the membrane targeting CAAX motif and hypervariable regions of K-Ras (accession number NM_004985). The eYFP-tagged phospholipase Cδ1 PH domain (PLCδ1-PH-YFP) was constructed as described previously (18). The eYFP-labeled full-length Rab5 was constructed by replacing the eGFP coding region with eYFP in Rab5-GFP, as described previously (19). The GRK2-YFP construct was a generous gift from Dr. Marc G. Caron (Duke University Medical Center).

Mutagenesis was performed using standard site-directed mutagenesis techniques. After verifying the mutations with dideoxy sequencing, the mutated fragment was exchanged between the wild type and mutated portion with suitable restriction sites to avoid the generation of unwanted mutations outside the sequenced regions. The DRY/AAY mutation of the AT$_{1A}$-R (the highly conserved $D^{125}R^{126}Y^{127}$ was mutated to $A^{125}A^{126}Y^{127}$) and the TSTS/A mutant of the AT$_{1A}$-R ($T^{332}S^{335}T^{336}S^{338}$ was substituted with alanine residues) were described earlier (20, 21).

Cell Culture and Transfection—The experiments were performed on the HEK293 cell line. The cells were cultured in DMEM with penicillin/streptomycin (Invitrogen) and 10% heat-inactivated fetal bovine serum (FBS) in 5% CO$_2$ at 37 °C. The cells were cultured in plastic dishes, trypsinized prior to transfection, transiently transfected by using Lipofectamine 2000 (Invitrogen), and plated on polylysine-pretreated white 96-well plates at a density of 1×10^5 cells/well for BRET measurements. The DNA amounts were 0.25 μg of Rluc-containing construct/well and 0.0625 μg of YFP-containing construct/well; the amount of Lipofectamine 2000 was 0.5 μl/well.

BRET Measurement—We used a *Renilla* luciferase-fused receptor as the energy donor and an eYFP-tagged protein as the acceptor. The BRET measurements were performed after 24 h of the transfection on white 96-well plates. The medium of the cells was changed prior to measurements to a modified Krebs-Ringer buffer containing 120 mM NaCl, 4.7 mM KCl, 1.8 mM CaCl$_2$, 0.7 mM MgSO$_4$, 10 mM glucose, and 10 mM Na-HEPES, pH 7.4, and the BRET measurements were performed at 37 °C. The BRET measurements were started after the addition of the cell-permeable substrate, coelenterazine h (Invitrogen), at a final concentration of 5 μM, and the counts were recorded by using a Berthold Mithras LB 940 multilabel reader using filters at 485- and 530-nm wavelengths; the detection time was 0.25–0.5 s. The BRET ratios were calculated as the 530 nm/485 nm ratio. Measurements were done in triplicate. The BRET records are averages of at least three independent experiments. BRET ratios were base line-corrected to the vehicle curve using GraphPad Prism software.

Confocal Microscopy—The localization and distribution of the targeted probes were analyzed using a Zeiss LSM 510 confocal laser-scanning microscope in living cells plated on polylysine-pretreated glass coverslips (3×10^5 cells/35-mm dish).

RESULTS

BRET Assay for Detection of Changes in Compartmental Localization of AT$_1$-R—To detect the agonist-induced trafficking of AT$_1$-R, our strategy was to use *Renilla* luciferase-labeled AT$_1$-R, and we followed the BRET ratio of its interaction with a YFP-labeled protein counterpart. When the HEK293 cells co-expressing wild type AT$_1$-R-luciferase and β-arrestin2-YFP were exposed to 100 nM AngII, the BRET ratio (Fig. 1*A*, *magenta trace*) elevated between the β-arrestin2-YFP and wild type AT$_1$-R-luciferase, showing that the β-arrestin binds to the activated AT$_1$-R. The internalized AT$_1$-R then appears in the endocytic route, which could be detected with the energy transfer between the Rab5-YFP (as early endosome marker) and the wild type AT$_1$-R-luciferase (Fig. 1*B*, *magenta trace*). To further analyze the compartmentalization of the receptors, we also used plasma membrane-targeted biosensors to investigate the possibility of the compartmentalized signaling of AT$_1$-R. We used MP-YFP to label the lipid rafts (6), whereas the YFP-labeled CAAX domain of K-Ras (KR-YFP) was used as the marker of the non-raft lipid domains (disordered plasma membrane) (4, 5, 15). When MP-YFP was used, the BRET ratio between this construct and wild type AT$_1$-R-luciferase dropped in response to AngII stimulation (Fig. 1*C*, *magenta trace*). However, when KR-YFP was used, we measured a significant BRET signal elevation prior to the drop in BRET ratio (Fig. 1*D*, *magenta trace*). The observed changes in the BRET ratio upon stimulus of AT$_1$-R-luciferase using either MP-YFP or KR-YFP are not a consequence of protein overexpression because gradual reduction of the DNA amounts used for the transfection, resulting in very low counts in the BRET measurements, did not alter the shapes and extents of the BRET ratio changes (supplemental Fig. 1). Because the cytosolic YFP and AT$_1$-R are not in the same compartment, the stimulus of the AT$_1$-R-luciferase by 100 nM AngII did not change the BRET ratio (Fig. 1*E*, *magenta trace*). We also have investigated the binding of GRK2 to AT$_1$-R upon stimulus because this GRK isoform is mostly responsible for AT$_1$-R phosphorylation and β-arrestin recruitment in HEK293 cells (22). When the cells were exposed to 100 nM AngII, the BRET ratio immediately elevated between the GRK2-YFP and wild type AT$_1$-R-luciferase (Fig. 1*G*, *magenta trace*). The time resolution of the BRET measurement allowed us to demonstrate that the agonist-induced binding of GRK2 to the AT$_1$-R precedes the binding of β-arrestin2 to the receptor. Stimulation of the wild type AT$_1$-R-luciferase evokes the binding of both the GRK2-YFP and β-arrestin2-YFP, but it is observable that the *red trace* of GRK2 precedes the *black trace* of β-arrestin2 (Fig. 1*G*), a phenomenon that was shown earlier by Hasbi *et al.* (23), using the oxytocin receptor, another GPCR.

Compartmentalization of Mutant AT$_1$-Rs—The dissimilar BRET curves of MP-YFP or KR-YFP with the AT$_1$-R-luciferase raised the possibility that we could monitor the compartmentalization of AT$_1$-R between different plasma membrane compartments in living cells immediately in response to agonist stimulus. We further investigated whether the trafficking of the receptor is altered using mutant AT$_1$-Rs (Fig. 1, DRY/AAY AT$_1$-R (*green traces*) and TSTS/A AT$_1$-R (*blue traces*)). It was revealed that the compartmentalization of DRY/AAY AT$_1$-R is
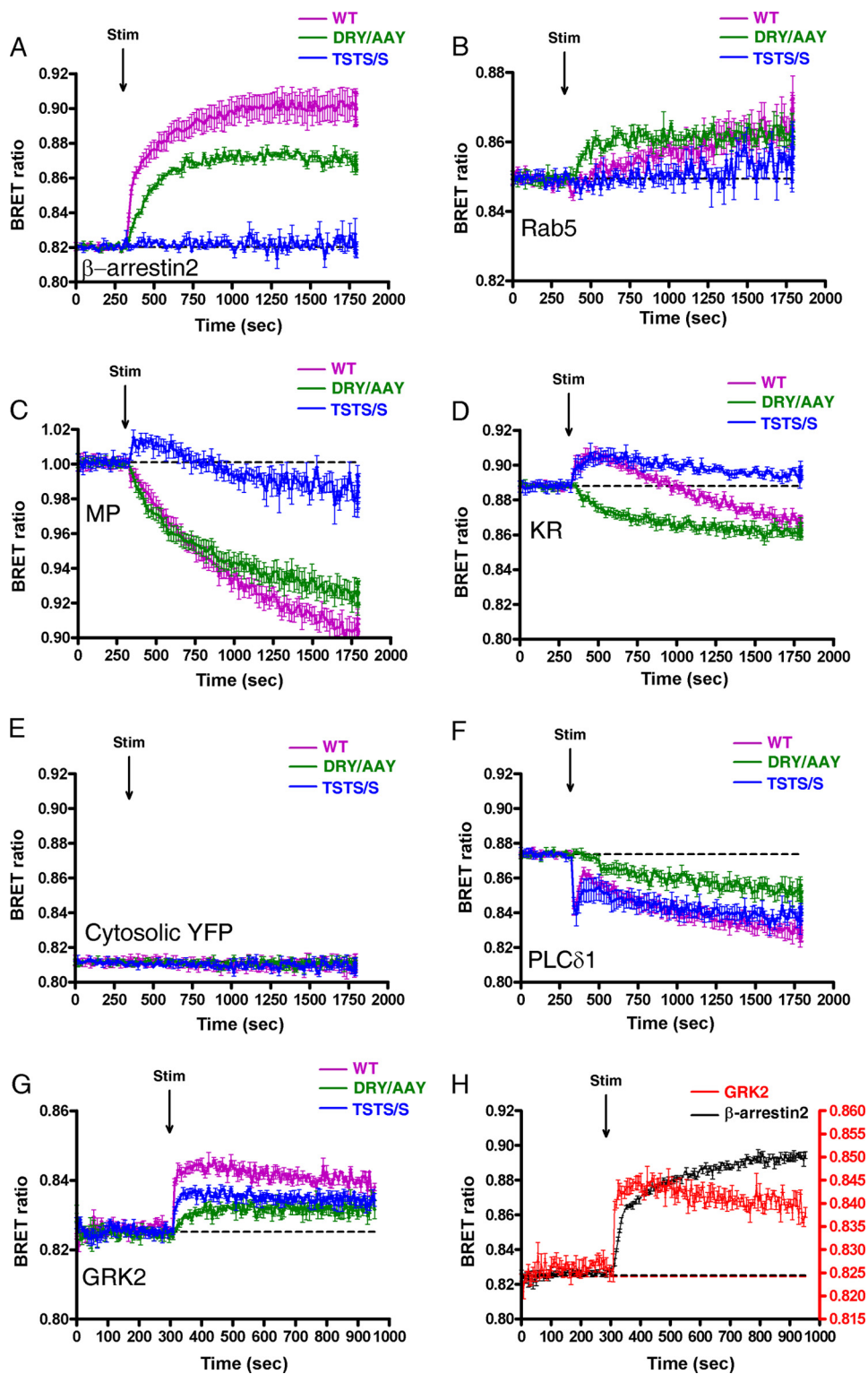
FIGURE 1. **BRET assay between AT₁-R and different proteins upon AngII stimulation in HEK293 cells.** HEK293 cells were transfected with the plasmids of the indicated AT₁-R-luciferase (*magenta trace*, wild type; *green trace*, DRY/AAY mutant; *blue trace*, TSTS/A mutant) and with the indicated YFP-fused proteins, and after 24 h, the cells were exposed to 100 nM AngII or vehicle (*dashed line*) at the indicated time points. BRET pairs were as follows: β-arrestin2-YFP and the indicated AT₁-R-luciferase (*A*), Rab5-YFP and the indicated AT₁-R-luciferase (*B*), MP-YFP and the indicated AT₁-R-luciferase (*C*), KR-YFP and the indicated AT₁-R-luciferase (*D*), untargeted YFP and the indicated AT₁-R-luciferase (*E*), PLCδ1-PH-YFP and the indicated AT₁-R-luciferase (*F*), and GRK2-YFP and the indicated AT₁-R-luciferase (*G*). *H*, HEK293 cells were transfected with the plasmids of the wild type AT₁-R-luciferase and either β-arrestin2-YFP (*black trace*) or GRK2-YFP (*red trace*), and after 24 h, the cells were exposed to 100 nM AngII or vehicle (*dashed line*). The *left y axis* is for β-arrestin2, and the *right y axis* is for GRK2. The BRET records are averages of at least three independent experiments. Mean values ± S.E. (*error bars*) are shown (*n* = 3).

Localization of AT$_1$-R in Membrane Microdomains

dramatically changed compared with wild type AT$_1$-R. When the DRY/AAY AT$_1$-R-luciferase was exposed to 100 nM AngII, the β-arrestin binding of the AngII-bound DRY/AAY mutant receptor was slightly decreased (Fig. 1*A*, *green trace*). The AngII-stimulated DRY/AAY mutant receptor was also able to translocate to Rab5 endocytic compartments (Fig. 1*B*, *green trace*). The BRET ratio also dropped immediately with MP-YFP using DRY/AAY AT$_1$R-luciferase (Fig. 1*C*, *green trace*), similar to the wild type AT$_1$-R-luciferase (Fig. 1*C*, *magenta trace*). The BRET ratio decreased after the stimulation of HEK293 cells with 100 nM AngII when we studied the interaction of DRY/AAY AT$_1$-R-luciferase and KR-YFP (Fig. 1*D*, *green trace*). In this case, the decrease in BRET ratio was immediate and did not show the initial elevation we observed using the wild type AT$_1$-R and the KR-YFP (Fig. 1*D*, *magenta trace*). We also determined the compartmentalization of another AT$_1$-R mutant, TSTS/A. In agreement with earlier findings (21, 24), this receptor was not able to bind β-arrestin, and its AngII-induced internalization was significantly reduced (Fig. 1, *A* and *B*, *blue traces*). Because the internalization of the TSTS/A AT$_1$-R is impaired compared with the wild type AT$_1$-R, we observed a reduction in the late decrease in the BRET ratios (Fig. 1, *C* and *D*, *blue traces*). We think that the late component of the BRET signal is the consequence of the internalization of the AT$_1$-R, resulting in depletion of the receptor in the plasma membrane. This assumption is confirmed using AT$_1$-R-luciferase and PLCδ1-PH-YFP as BRET pairs. The PH domain of PLCδ1 binds to PtdIns(4,5)P$_2$ in the plasma membrane (18). When the HEK293 cells co-expressing wild type AT$_1$-R-luciferase and PLCδ1-PH-YFP were exposed to 100 nM AngII, the BRET ratio dropped very quickly, which was followed by an increase (Fig. 1*F*, *magenta trace*). The graph shows that the rapid initial dissociation (BRET ratio drop) of AT$_1$-R-luciferase and PLCδ1-PH-YFP is followed by a transient association (a short BRET ratio increase) and a more prolonged dissociation (prolonged BRET ratio decrease) of these proteins. The initial drop in the BRET signal reflects that agonist-induced activation of AT$_1$-R caused G$_{q/11}$ activation and PtdIns(4,5)P$_2$ breakdown, resulting in the release of PLCδ1-PH-YFP from the plasma membrane. After a short period of time, the ratio began to increase because PtdIns(4,5)P$_2$ resynthesis occurs very rapidly, and the majority of the PLCδ1-PH-YFP molecules rebind to the plasma membrane. This elevation in the BRET signal is followed by a slow decrease, which suggests that the AT$_1$-R-luciferase and the PLCδ1-PH-YFP start to diverge from each other again, reflecting the internalization of the receptor. When HEK293 cells co-expressing DRY/AAY mutant AT$_1$-R-luciferase and PLCδ1-PH-YFP were exposed to 100 nM AngII, the BRET ratio decreased slowly without the fast initial dissociation (Fig. 1*F*, *green trace*), which is consistent with the fact that the stimulus of the DRY/AAY AT$_1$-R does not result in PtdIns(4,5)P$_2$ breakdown and release of PLCδ1-PH-YFP from the plasma membrane (Fig. 1*F*), but the DRY/AAY AT$_1$-R internalizes upon stimulus (Fig. 1*B*, *green trace*). We also investigated the effects of AngII on the binding of mutant AT$_1$-Rs to GRK2. The TSTS/A mutant AT$_1$-R mutant was able to bind to GRK2, although the binding was reduced, whereas the β-arrestin2 binding of this mutant was not detectable (Fig. 1, *A* and *G*, *blue*
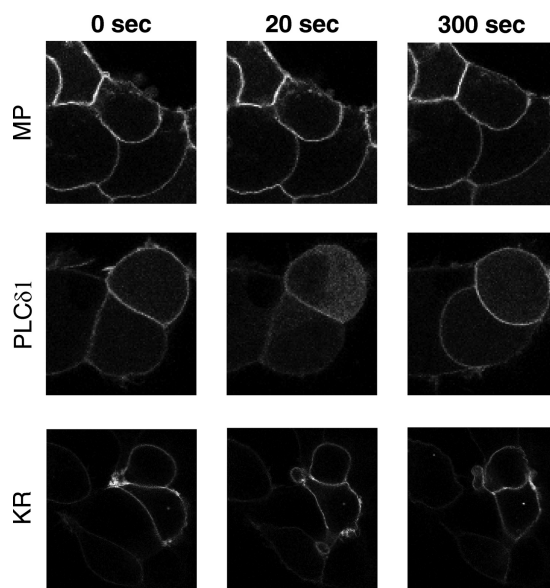

FIGURE 2. **Effects of AngII stimulation on the distribution of MP-YFP, PLCδ1-PH-YFP, and KR-YFP in HEK293 cells.** The cells were transfected with the AT$_1$-R-luciferase and with the indicated YFP-fused proteins. After 24 h, the cells were exposed to 100 nM AngII. The probes were visualized by laser-scanning confocal microscopy (Zeiss LSM510). The representative confocal micrographs show the localization and cellular distribution of the indicated probes before (0 s) and 20 or 300 s after the AngII treatment. The YFP fluorescence was detected by Zeiss LSM510 confocal microscope. *Bars*, 10 μm.

traces). Interestingly, the DRY/AAY AT$_1$-R mutant is less capable of binding to GRK2, although the β-arrestin2 binding of this mutant is very similar to the wild type receptor (Fig. 1, *A* and *G*, *green traces*).

Effect of Agonist Stimulation on Distribution of Plasma Membrane Markers—We examined the distribution of MP-YFP, PLCδ1-PH-YFP, and KR-YFP in HEK293 cells in response to AngII stimulation. As shown in Fig. 2, the AngII stimulus did not affect noticeably the distribution and amount of either MP-YFP or KR-YFP in the plasma membrane. In contrast, PLCδ1-PH-YFP is temporarily translocated to the cytoplasm and then returns to the plasma membrane, reflecting its PtdIns(4,5)P$_2$ level (18). Taken together, we can conclude that the largest proportion of the observed changes in the BRET ratio using MP-YFP or KR-YFP along with AT$_1$-R-luciferase probably reflect the alterations in the AT$_1$-R distribution. Based on our data, we cannot rule out that the possibility that distributions of the MP-YFP or KR-YFP are not altered during the experiments, although this cannot be resolved by confocal microscopy.

Compartmentalization of AT$_1$-Rs Using Various Ligands—We further investigated whether the binding of different ligands to the AT$_1$-R leads to dissimilar changes upon stimulus. SII-AngII is a biased peptide agonist of the AT$_1$-R, which is not able to activate G proteins but can stimulate G protein-independent mechanisms, such as β-arrestin binding and consequent ERK activation (25, 26). Stimulation of AT$_1$-R with this peptide caused different compartmentalization of AT$_1$-R compared with the effects of AngII (Fig. 3). It is shown in Fig. 3, *A* and *B*, that motion of the AT$_1$-R is impaired using SII-AngII, but the receptor is able to internalize, which is consistent with previous reports that SII-AngII can induce AT$_1$-R internaliza-
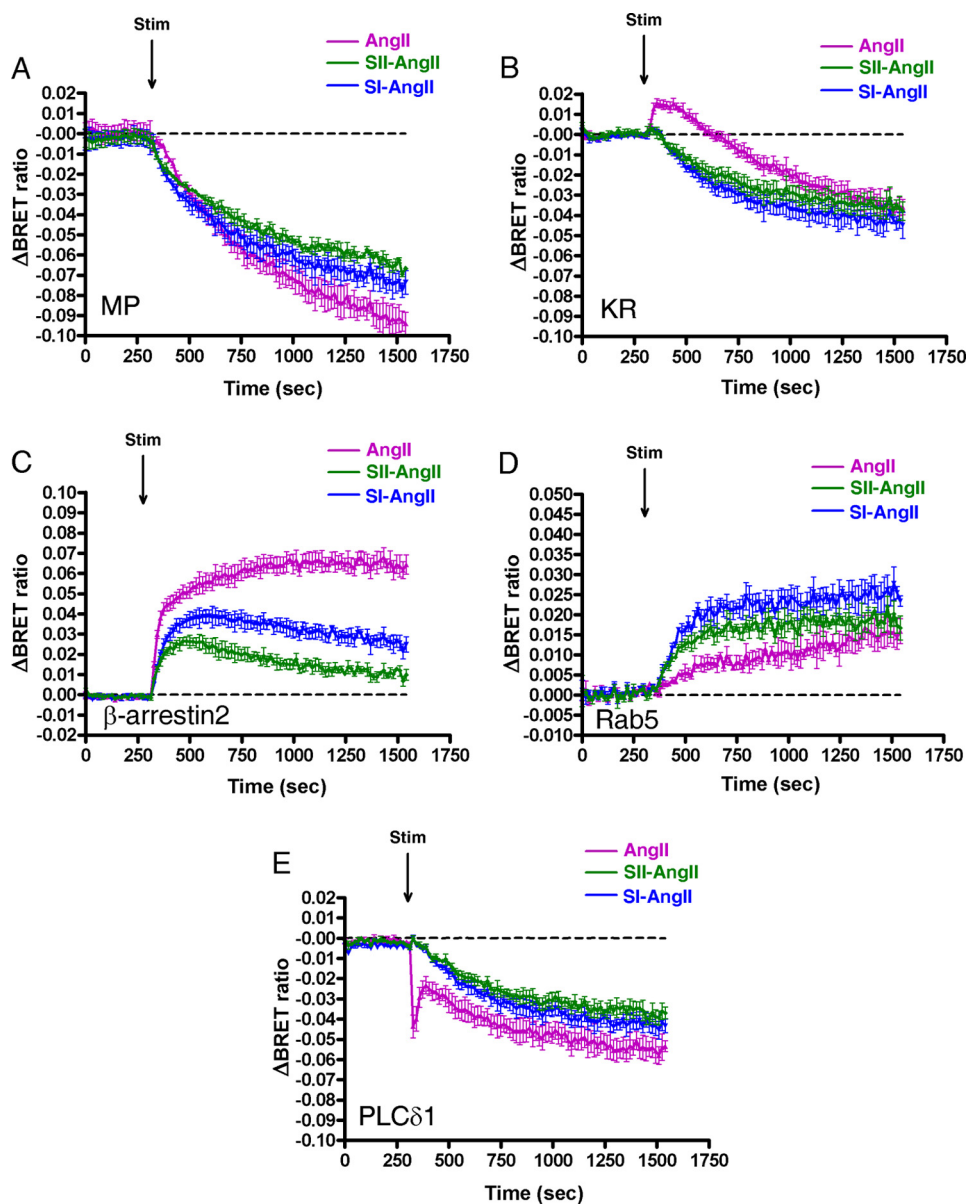
FIGURE 3. **Effects of angiotensin peptides on the BRET interaction between AT$_1$-R and different proteins in HEK293 cells.** HEK293 cells were transfected with the plasmids of the AT$_1$-R-luciferase and the indicated YFP-fused proteins, and after 24 h, the cells were exposed to either 100 nM AngII (*magenta trace*), 100 nM SI-AngII (*blue trace*), 10 μM SII-AngII (*black trace*), or vehicle (*dashed line*) at the indicated time points. BRET pairs were as follows: MP-YFP and wild type AT$_1$-R-luciferase (*A*); KR-YFP and wild type AT$_1$-R-luciferase (*B*); β-arrestin2-YFP and wild type AT$_1$-R-luciferase (*C*); Rab5-YFP and wild type AT$_1$-R-luciferase (*D*); PLCδ1-PH-YFP and wild type AT$_1$-R-luciferase (*E*). The BRET records are averages of three independent experiments. Mean values ± S.E. (*error bars*) are shown (*n* = 3).

tion (27). The BRET ratio drops with the MP-YFP immediately after SII-AngII stimulation (Fig. 3*A*, *green trace*), and the kinetics of this process seems to be more rapid compared with AngII stimulus (Fig. 3*A*, *magenta trace*). It is remarkable that the BRET ratio between KR-YFP and AT$_1$-R-luciferase upon SII-AngII treatment decreases immediately, without the initial elevation compared with AngII stimulation (Fig. 3*B*). This observation is very reminiscent of the AngII stimulus of DRY/AAY AT$_1$-R with KR-YFP (Fig. 1*D*, *green trace*). The SII-AngII-induced binding of AT$_1$-R-luciferase to β-arrestin2 is impaired compared with the effect of AngII stimulation (Fig. 3*C*). In addition, a higher increase in the BRET interaction between Rab5-YFP and AT$_1$-R-luciferase was observed after SII-AngII treatment compared with AngII stimulation (Fig. 3*D*), which is

similar to the results obtained in the studies for AngII-induced association of wild type and DRY/AAY mutant AT$_1$-R-luciferase with Rab5-YFP (Fig. 1*B*). Because the SII-AngII stimulus of AT$_1$-R does not activate G$_q$-mediated PtdIns(4,5)P$_2$ breakdown, the BRET ratio with the PLCδ1-PH-YFP decreases immediately and continually without an initial peak in the drop (Fig. 3*E*, *green trace*). The SI-AngII is an octapeptide angiotensin analog, which is an antagonist of AT$_1$-R (28), but it was shown earlier that it is able to initiate receptor internalization (29). Stimulation of AT$_1$-R-luciferase with SI-AngII also caused altered receptor compartmentalization compared with AngII stimulation (Fig. 3). Because the SI-AngII is an AT$_1$-R antagonist, stimulation with this analog does not result in PtdIns(4,5)P$_2$ hydrolysis (Fig. 3*B*, *blue trace*). In addition, treat-

Localization of AT$_1$-R in Membrane Microdomains

ment of AT$_1$-R with a non-peptide AT$_1$-R antagonist, cande-sartan, did not change the distribution of AT$_1$-R, and the pre-treatment of HEK293 cells with candesartan prior to BRET measurement completely inhibited the trafficking of AT$_1$-R in response to AngII stimulation (Fig. 4).

BRET Assay for Detection of Compartmentalization of 5HT-2C-R and EGF-R—The preceding results suggest that the plasma membrane compartmentalization of a receptor could be mapped by the help of BRET measurements. Next, we tested the agonist-induced compartmentalization of other membrane receptors using our BRET approach to compare their kinetics with those of AT$_1$-R. We analyzed the agonist-induced dynamics of 5HT-2C-R (supplemental Fig. 2) and EGF-R (supplemental Fig. 3). The 5HT-2C-R (30) also couples to G$_q$ protein, similarly to the AT$_1$-R. After serotonin (5-hydroxytryptamine, 5HT) binding, the receptor bound β-arrestin2 (Fig. 5C) and became internalized, as shown by the elevation of the BRET ratio between Rab5 and 5HT-2C-R (supplemental Fig. 2D). The internalization was also apparent using the plasma membrane-located MP-YFP and KR-YFP (supplemental Fig. 2, A and B). However, in contrast to AT$_1$-R, we could not detect a strikingly different distribution change between using MP-YFP and KR-YFP. The EGF-R is a growth factor receptor with tyrosine kinase activity, which is widely used for the study of receptor internalization (31). In contrast to GPCRs, such as AT$_1$-R or 5HT-2C-R, the EGF-R does not interact with β-arrestin (supplemental Fig. 3C) but internalizes upon EFG treatment (supplemental Fig. 3D). Similarly to 5HT-2C-R, we also did not observe different distribution change between using MP-YFP and KR-YFP with EGF-R-luciferase (supplemental Fig. 3, A and B).

DISCUSSION

In the present study, we have investigated the compart-mentalization of the AT$_1$-R in the plasma membrane in response to ligand binding. Instead of biochemical charac-terization of AT$_1$-R localization in the plane of the plasma membrane, we used a BRET-based approach to investigate the distribution of the receptor in response to hormone stimulus. We used several YFP-labeled fusion constructs and *Renilla* luciferase fused receptors as intermolecular probe pairs in BRET measurements.

Interactions of YFP-labeled fusion constructs (plasma mem-brane targeted markers, β-arrestin, GRK2, and Rab5) with luciferase-tagged AT$_1$-Rs were evaluated to follow the com-partmentalization of the receptor. MP-YFP and YFP-labeled CAAX domain of K-Ras (KR-YFP) were used to label the lipid rafts (6) and non-raft lipid domains (disordered plasma mem-brane), respectively (4, 5, 15). Because our goal was to analyze the agonist-induced changes in receptor compartmentalization in live cells, we did not measure the actual distribution of the YFP-labeled markers in our HEK293 cells by biochemical prep-aration methods, such as detergent solubilization and ultracen-trifugation. To achieve our goal, we used BRET-based probes, assuming that, although the MP-YFP and KR-YFP are appar-ently uniformly localized in the inner surface of the plasma membrane (see the confocal images of Fig. 2), they probably differently label submicroscopic microdomains (4–6, 15). The
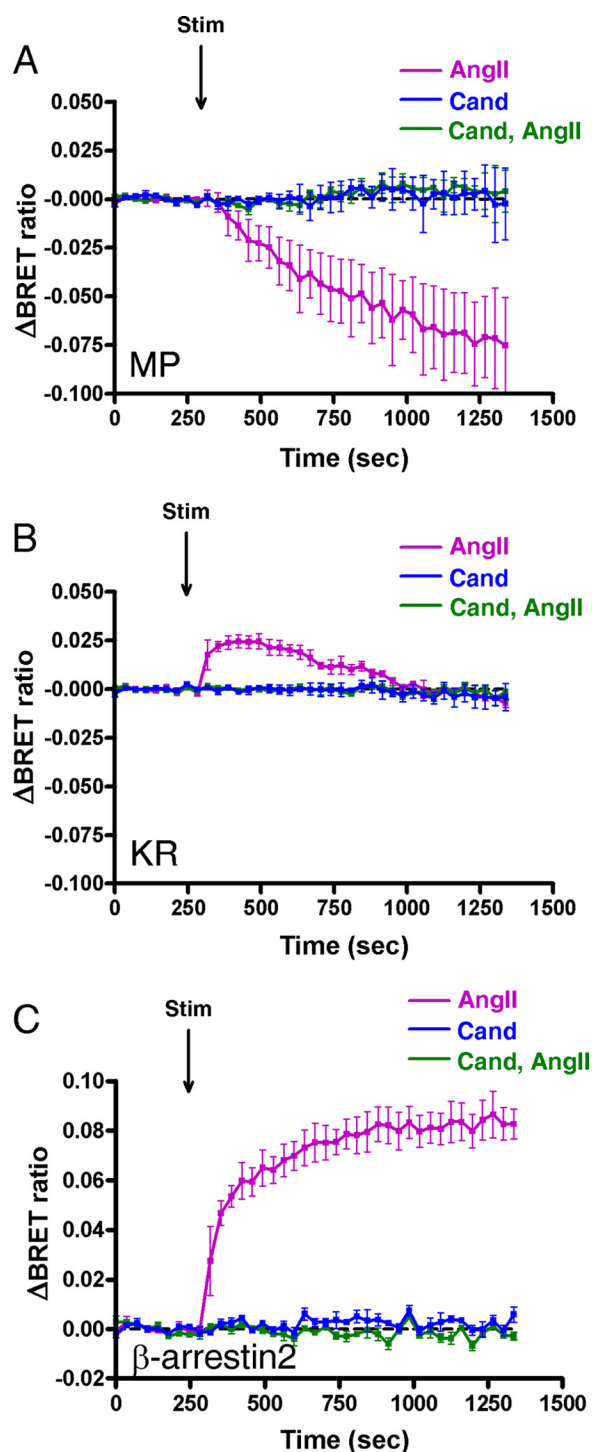

FIGURE 4. **Effects of AngII and candesartan on the BRET interaction between AT$_1$-R and different proteins in HEK293 cells.** HEK293 cells were transfected with the plasmids of the AT$_1$-R-luciferase and the indicated YFP-fused proteins, and after 24 h, the cells were exposed to either 100 nM cande-sartan (*blue trace*) or 100 nM AngII without pretreatment (*magenta trace*) or with 100 nM candesartan pretreatment for 10 min (*green trace*). BRET pairs were as follows: MP-YFP and wild type AT$_1$-R-luciferase (*A*), KR-YFP and wild type AT$_1$-R-luciferase (*B*), and β-arrestin2-YFP and wild type AT$_1$-R-luciferase (*C*). The BRET records are averages of three independent experiments. Mean values $\pm$ S.E. (*error bars*) are shown ($n = 3$).

different properties of these microdomains also manifested when their interaction was studied with AT$_1$-R-luciferase in BRET measurements in living cells (Fig. 1). These data demon-
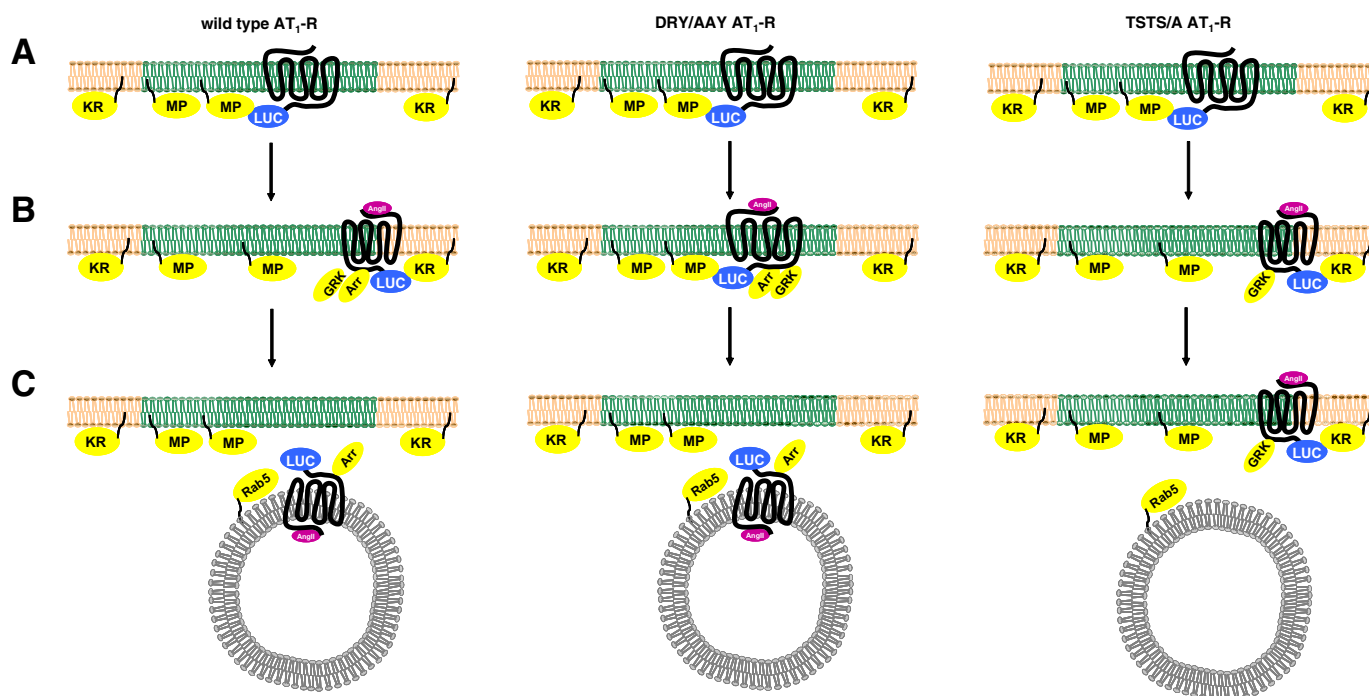
FIGURE 5. **Compartmentalized AT$_1$-R signaling in the plasma membrane.** *A*, plasma membrane localization of the indicated AT$_1$-Rs in unstimulated cells. *B*, changes immediately after the ligand treatment. *C*, localization of the receptors 5 min after the stimulus. The plasma membrane and endosome are shown.

strate that AT$_1$-R probably is not distributed uniformly in the native plasma membrane but is instead localized in specific microdomains. The changes in compartmentalization of AT$_1$-Rs are different when followed by various plasma membrane markers in BRET measurements. Our BRET experiments indicate that the localization of the AT$_1$-R rapidly changes after AngII stimulation in HEK293 cells (Figs. 1 and 3). However, we cannot exclude the possibility that the BRET ratio changes can be also the result of the lateral diffusion of YFP-labeled biosensors because the membrane microdomains are not static structures. It is noteworthy that the absolute level of BRET signal is higher when using MP-YFP compared with KR-YFP (∼1.0 *versus* ∼0.89; the absolute BRET ratio is ∼0.82 when using cytosolic YFP and the AT$_1$-R-luciferase). The higher basal BRET signal could reflect that the unstimulated AT$_1$-R-luciferase is preferably located in the plasma membrane microdomain marked by MP-YFP in resting conditions.

We also examined the agonist-induced changes in compartmentalization of mutated AT$_1$-Rs (DRY/AAY or TSTS/A mutation) in order to determine the G protein- and phosphorylation-dependent steps in AT$_1$-R trafficking. Comparing the data, which were obtained utilizing either wild type or mutated AT$_1$-R co-expressed with the fluorescent probes in HEK293 cells, revealed changes in their distribution between membrane microdomains in response to AngII stimulation. It is also possible that the initial BRET ratio elevation between wild type AT$_1$-R-luciferase and KR-YFP upon AngII stimulus is the consequence of the change of the distribution of the KR-YFP (the energy acceptor molecules are enriched during AT$_1$-R action). The compartmentalization of DRY/AAY AT$_1$-R, which is not able to activate G$_{q/11}$ protein (20), is dramatically changed compared with wild type AT$_1$-R. Stimulation of DRY/AAY AT$_1$-R did not result in PtdIns(4,5)P$_2$ breakdown and concomitant

release of PLCδ1-PH-YFP from the plasma membrane (Fig. 1*F*), but DRY/AAY AT$_1$-R internalizes upon stimulus, in agreement with previous reports that DRY/AAY AT$_1$-R undergoes internalization after AngII stimulation (20, 26). The β-arrestin binding of the AngII-bound DRY/AAY mutant receptor is G protein-independent (Fig. 1*A*) as was shown earlier (26, 32, 33). It seems that the rapid distribution change of AT$_1$-R-luciferase in response to AngII stimulus between the MP-YFP and KR-YFP is G protein-dependent. The BRET ratio between DRY/AAY AT$_1$-R-luciferase and the KR-YFP decreased after AngII stimulation without the initial elevation, contrary to the wild type AT$_1$-R (Fig. 1*D*). In addition, the decline in the BRET ratio seemed more immediate when interaction of DRY/AAY AT$_1$R-luciferase was studied with MP-YFP compared with the wild type AT$_1$-R-luciferase (Fig. 1*C*) or when MP-YFP and AT$_1$-R-luciferase were studied upon SII-AngII or SI-AngII stimuli (Fig. 3*A*). TSTS/A mutant AT$_1$-R is not able to bind β-arrestin2, and its internalization is significantly reduced in response to AngII (21, 24). We also confirmed these properties of this mutant and also showed that the TSTS/A AT$_1$-R still anchors GRK2 (Fig. 1, *A*, *B*, and *G*). Because the internalization of the TSTS/A AT$_1$-R is reduced compared with wild type AT$_1$-R, the late decrease component is similarly slower, which is consistent with our conclusion that this component is caused by the internalization of the receptor (Fig. 1, *C*, *D*, and *F*).

Our studies also revealed that treatment of AT$_1$-R with either [Sar^1,Ile^8]AngII or [Sar^1,Ile^4,Ile^8]AngII caused different changes in the compartmentalization of AT$_1$-R compared with the effect of AngII (Fig. 3), whereas candesartan did not induce changes in microdomain localization or trafficking of AT$_1$-R (Fig. 4). The biased agonist, SII-AngII, is not able to activate G proteins but can stimulate G protein-independent mechanisms, such as β-arrestin binding and ERK activation (25, 26).

Localization of AT$_1$-R in Membrane Microdomains

According to our data, the rapid distribution change of AT$_1$-R-luciferase upon stimulus between plasma membrane markers is G protein-dependent or reflects the different conformational change of the receptor using distinct ligands. The binding of an antagonist (SI-AngII) to AT$_1$-R also caused altered compartmentalization of the receptor compared with AngII stimulus (Fig. 3), which supports the idea that the agonist-induced compartmentalization of the AT$_1$-Rs in the plasma membrane is G protein-dependent and/or requires the physiological conformational change.

Based on our findings, we propose that the AT$_1$-R preferably localized in raft domains in resting cells. According to the model, the stimulation of wild type AT$_1$-R with AngII causes conformational change and redistribution of the receptor in the plasma membrane as well as binding to GRK2 and β-arrestin2, which leads to internalization of the receptor (Fig. 5, *left column*). In the case of stimulation of wild type AT$_1$-R with SII-AngII or stimulation of DRY/AAY mutant AT$_1$-R with AngII, cause another conformational change and the redistribution of the receptor is bypassed (Fig. 5, *middle column*). This leads to accelerated association with Rab5. In contrast, stimulation of TSTS/AAY mutant AT$_1$-R with AngII causes similar conformational change and redistribution of the receptor as in the case of the wild type receptor. This mutant is not able to bind β-arrestin2, which results in impaired internalization, leading to the sustained "mislocalization" of the receptor among the membrane microdomains (Fig. 5, *right column*). Taken together, it is likely that the AT$_1$-R is not uniformly located in the plasma membrane but is compartmentalized. The AT$_1$-R-luciferase prefers the MP-YFP-labeled microdomains (raft domains), contrary to KR-YFP-labeled non-raft microdomains. The examined mutations (DRY/AAY and TSTS/A) in the receptors did not change this uneven distribution pattern. Interestingly, the AngII stimulus evoked different distribution changes of the wild type and the mutated receptors with the YFP biomarkers. The data showed that G$_q$ protein activation is essential for the proper compartmentalization of the AT$_1$-R. Lack of G$_q$ activation inhibits the appearance of the receptor in the non-raft microdomains (or the KR-YFP accumulation close to the receptor) and accelerates the association with Rab5. It also seems that the endocytosis of the receptor can occur by distinct mechanisms, depending on the G$_q$ coupling. It is also possible that other mutations or pathological conditions can induce mislocalization of the receptors that can provoke altered signaling.

We also examined the compartmentalization of other receptors, such as 5HT-2C-R and EGF-R (supplemental Figs. 2 and 3). The 5HT-2C-R is also coupled to G$_q$ protein, similarly to the AT$_1$-R (30), whereas the EGF-R is a tyrosine kinase receptor and is widely used for the study of receptor internalization (31). It is important to note that the compartmentalization of AT$_1$-R is strikingly different from those of 5HT-2C-R and EGF-R, which underlines the usefulness of the BRET-based approach to investigate the dynamics of receptor compartmentalization in living cell experiments. Taken together, these studies provided valuable information about the distribution and dynamics of AT$_1$-R upon ligand binding among membrane microdomains.

REFERENCES

1. Jacobson, K., Mouritsen, O. G., and Anderson, R. G. (2007) Lipid Rafts. At a crossroad between cell biology and physics. *Nat. Cell Biol.* **9,** 7–14
2. Hao, M., Mukherjee, S., and Maxfield, F. R. (2001) Cholesterol depletion induces large scale domain segregation in living cell membranes. *Proc. Natl. Acad. Sci. U.S.A.* **98,** 13072–13077
3. Plowman, S. J., Muncke, C., Parton, R. G., and Hancock, J. F. (2005) H-Ras, K-Ras, and inner plasma membrane raft proteins operate in nanoclusters with differential dependence on the actin cytoskeleton. *Proc. Natl. Acad. Sci. U.S.A.* **102,** 15500–15505
4. Niv, H., Gutman, O., Kloog, Y., and Henis, Y. I. (2002) Activated K-Ras and H-Ras display different interactions with saturable nonraft sites at the surface of live cells. *J. Cell Biol.* **157,** 865–872
5. Prior, I. A., Muncke, C., Parton, R. G., and Hancock, J. F. (2003) Direct visualization of Ras proteins in spatially distinct cell surface microdomains. *J. Cell Biol.* **160,** 165–170
6. Zacharias, D. A., Violin, J. D., Newton, A. C., and Tsien, R. Y. (2002) Partitioning of lipid-modified monomeric GFPs into membrane microdomains of live cells. *Science* **296,** 913–916
7. Hunyady, L., and Catt, K. J. (2006) Pleiotropic AT1 receptor signaling pathways mediating physiological and pathogenic actions of angiotensin II. *Mol. Endocrinol.* **20,** 953–970
8. Shaw, A. S. (2006) Lipid rafts. Now you see them, now you don't. *Nat. Immunol.* **7,** 1139–1142
9. Ishizaka, N., Griendling, K. K., Lassègue, B., and Alexander, R. W. (1998) Angiotensin II type 1 receptor. Relationship with caveolae and caveolin after initial agonist stimulation. *Hypertension* **32,** 459–466
10. Linder, A. E., Thakali, K. M., Thompson, J. M., Watts, S. W., Webb, R. C., and Leite, R. (2007) Methyl-beta-cyclodextrin prevents angiotensin II-induced tachyphylactic contractile responses in rat aorta. *J. Pharmacol. Exp. Ther.* **323,** 78–84
11. Ushio-Fukai, M., and Alexander, R. W. (2006) Caveolin-dependent angiotensin II type 1 receptor signaling in vascular smooth muscle. *Hypertension* **48,** 797–803
12. Giepmans, B. N., Adams, S. R., Ellisman, M. H., and Tsien, R. Y. (2006) The fluorescent toolbox for assessing protein location and function. *Science* **312,** 217–224
13. Szidonya, L., Cserzo, M., and Hunyady, L. (2008) Dimerization and oligomerization of G-protein-coupled receptors. Debated structures with established and emerging functions. *J. Endocrinol.* **196,** 435–453
14. Meyer, B. H., Segura, J. M., Martinez, K. L., Hovius, R., George, N., Johnsson, K., and Vogel, H. (2006) FRET imaging reveals that functional neurokinin-1 receptors are monomeric and reside in membrane microdomains of live cells. *Proc. Natl. Acad. Sci. U.S.A.* **103,** 2138–2143
15. Gao, X., Lowry, P. R., Zhou, X., Depry, C., Wei, Z., Wong, G. W., and Zhang, J. (2011) PI3K/Akt signaling requires spatial compartmentalization in plasma membrane microdomains. *Proc. Natl. Acad. Sci. U.S.A.* **108,** 14509–14514
16. Marullo, S., and Bouvier, M. (2007) *Trends Pharmacol. Sci.* **28,** 362–365
17. Turu, G., Szidonya, L., Gáborik, Z., Buday, L., Spät, A., Clark, A. J., and Hunyady, L. (2006) Differential β-arrestin binding of AT1 and AT2 angiotensin receptors. *FEBS Lett.* **580,** 41–45
18. Várnai, P., and Balla, T. (1998) Visualization of phosphoinositides that bind pleckstrin homology domains. Calcium- and agonist-induced dynamic changes and relationship to myo-[^{3}H]inositol-labeled phosphoinositide pools. *J. Cell Biol.* **143,** 501–510
19. Hunyady, L., Baukal, A. J., Gaborik, Z., Olivares-Reyes, J. A., Bor, M., Szaszak, M., Lodge, R., Catt, K. J., and Balla, T. (2002) Differential PI 3-kinase dependence of early and late phases of recycling of the internalized AT1 angiotensin receptor. *J. Cell Biol.* **157,** 1211–1222
20. Gáborik, Z., Jagadeesh, G., Zhang, M., Spät, A., Catt, K. J., and Hunyady, L. (2003) The role of a conserved region of the second intracellular loop in

AT1 angiotensin receptor activation and signaling. *Endocrinology* **144,** 2220–2228

21. Qian, H., Pipolo, L., and Thomas, W. G. (2001) Association of β-arrestin 1 with the type 1A angiotensin II receptor involves phosphorylation of the receptor carboxyl terminus and correlates with receptor internalization. *Mol. Endocrinol.* **15,** 1706–1719

22. Kim, J., Ahn, S., Ren, X. R., Whalen, E. J., Reiter, E., Wei, H., and Lefkowitz, R. J. (2005) Functional antagonism of different G protein-coupled receptor kinases for β-arrestin-mediated angiotensin II receptor signaling. *Proc. Natl. Acad. Sci. U.S.A.* **102,** 1442–1447

23. Hasbi, A., Devost, D., Laporte, S. A., and Zingg, H. H. (2004) Real-time detection of interactions between the human oxytocin receptor and G protein-coupled receptor kinase-2. *Mol. Endocrinol.* **18,** 1277–1286

24. Hunyady, L., Bor, M., Balla, T., and Catt, K. J. (1994) Identification of a cytoplasmic Ser-Thr-Leu motif that determines agonist-induced internalization of the AT1 angiotensin receptor. *J. Biol. Chem.* **269,** 31378–31382

25. Noda, K., Feng, Y. H., Liu, X. P., Saad, Y., Husain, A., and Karnik, S. S. (1996) The active state of the AT1 angiotensin receptor is generated by angiotensin II induction. *Biochemistry* **35,** 16435–16442

26. Wei, H., Ahn, S., Shenoy, S. K., Karnik, S. S., Hunyady, L., Luttrell, L. M., and Lefkowitz, R. J. (2003) Independent β-arrestin 2 and G protein-mediated pathways for angiotensin II activation of extracellular signal-regulated kinases 1 and 2. *Proc. Natl. Acad. Sci. U.S.A.* **100,** 10782–10787

27. Holloway, A. C., Qian, H., Pipolo, L., Ziogas, J., Miura, S., Karnik, S., South-well, B. R., Lew, M. J., and Thomas, W. G. (2002) Side chain substitutions within angiotensin II reveal different requirements for signaling, internalization, and phosphorylation of type 1A angiotensin receptors. *Mol. Pharmacol.* **61,** 768–777

28. Aumelas, A., Sakarellos, C., Lintner, K., Fermandjian, S., Khosla, M. C., Smeby, R. R., and Bumpus, F. M. (1985) Studies on angiotensin II and analogs. Impact of substitution in position 8 on conformation and activity. *Proc. Natl. Acad. Sci. U.S.A.* **82,** 1881–1885

29. Conchon, S., Monnot, C., Teutsch, B., Corvol, P., and Clauser, E. (1994) Internalization of the rat AT1a and AT1b receptors. Pharmacological and functional requirements. *FEBS Lett.* **349,** 365–370

30. Becamel, C. (2008) 5-Hydroxytryptamine receptor 2C. *UCSD-Nature Molecule Pages*, doi:10.1038/mp.a000152.000101

31. Sorkin, A., and Goh, L. K. (2008) Endocytosis and intracellular trafficking of ErbBs. *Exp. Cell Res.* **314,** 3093–3106

32. Szidonya, L., Süpeki, K., Karip, E., Turu, G., Várnai, P., Clark, A. J., and Hunyady, L. (2007) AT1 receptor blocker-insensitive mutant AT1A angiotensin receptors reveal the presence of G protein-independent signaling in C9 cells. *Biochem. Pharmacol.* **73,** 1582–1592

33. Bonde, M. M., Hansen, J. T., Sanni, S. J., Haunsø, S., Gammeltoft, S., Lyngsø, C., and Hansen, J. L. (2010) Biased signaling of the angiotensin II type 1 receptor can be mediated through distinct mechanisms. *PloS One* **5,** e14135

balla.andras:3

Investigation of the Fate of Type I Angiotensin Receptor after Biased Activation Ⓢ

Gyöngyi Szakadáti, András D. Tóth, Ilona Oláh, László Sándor Erdélyi, Tamas Balla, Péter Várnai, László Hunyady, and András Balla

Department of Physiology, Semmelweis University, Faculty of Medicine, Budapest, Hungary (G.S., A.D.T., I.O., L.S.E., P.V., L.H., A.B.), Magyar Tudományos Akadémia–Semmelweis Egyetem Laboratory of Molecular Physiology, Hungarian Academy of Sciences and Semmelweis University, Budapest, Hungary (L.S.E., P.V., L.H., A.B.); and Section on Molecular Signal Transduction, Program for Developmental Neuroscience, Eunice Kennedy Shriver National Institute of Child Health and Human Development, National Institutes of Health, Bethesda, Maryland (T.B.)

ABSTRACT

Biased agonism on the type I angiotensin receptor (AT_1-R) can achieve different outcomes via activation of G protein–dependent and –independent cellular responses. In this study, we investigated whether the biased activation of AT_1-R can lead to different regulation and intracellular processing of the receptor. We analyzed β-arrestin binding, endocytosis, and subsequent trafficking steps, such as early and late phases of recycling of AT_1-R in human embryonic kidney 293 cells expressing wild-type or biased mutant receptors in response to different ligands. We used *Renilla* luciferase–tagged receptors and yellow fluorescent protein–tagged β-arrestin2, Rab5, Rab7, and Rab11 proteins in bioluminescence resonance energy transfer measurements to follow the fate of the receptor after stimulation. We found that not only is the signaling of the receptor different upon using selective ligands, but the fate within the cells is also determined by the type of the stimulation. β-arrestin binding and the internalization kinetics of the angiotensin II–stimulated AT_1-R differed from those stimulated by the biased agonists. Similarly, angiotensin II–stimulated wild-type AT_1-R showed differences compared with a biased mutant AT_1-R (DRY/AAY AT_1-R) with regards to β-arrestin binding and endocytosis. We found that the differences in the internalization kinetics of the receptor in response to biased agonist stimulation are due to the differences in plasma membrane phosphatidylinositol 4,5-bisphosphate depletion. Moreover, the stability of the β-arrestin binding is a major determinant of the later fate of the internalized AT_1-R receptor.

Introduction

Ligand binding to receptors can initiate several parallel signal transduction pathways, leading to various final outcomes in the same cell. It has been recognized that several ligands are capable of selectively initiating distinct signal transduction pathways from the same receptor, leading to the concept of biased agonism. It is well accepted that biased agonism is an important feature of G protein–coupled receptors (GPCRs), and it is proposed that development of biased agonists can serve a new therapeutic approach (Whalen et al., 2011). The binding of agonists to GPCRs initiates the G protein–mediated pathway, which results in the production of second messengers. The downregulation of activated receptors involves several consecutive or parallel processes, such as desensitization, followed by internalization into vesicles and recycling or degradation. Receptor internalization is regulated by GPCR kinases (GRKs), with subsequent binding of β-arrestin (Lefkowitz, 2007). The β-arrestin binding not only mediates desensitization and internalization, but also triggers additional signal transduction pathways, which are often called G protein–independent signaling routes.

Angiotensin II (AngII) is the main effector of the renin-angiotensin system and can activate the type 1 (AT_1-R) angiotensin receptor. After binding to AT_1-R, the $G_{q/11}$ protein mediates the activation of phosphoinositide-specific phospholipase Cβ (PLCβ) and hydrolysis of phosphatidylinositol 4,5-bisphosphate [PtdIns(4,5)P_2] (Hunyady and Catt, 2006). Binding of AngII also triggers events leading to regulation of AT_1-R, such as desensitization, internalization, degradation, and recycling to the cell surface (Hunyady et al., 2000; Ferguson, 2001). Desensitization and internalization of AT_1-R

are regulated by phosphorylation by GRKs, which promote β-arrestin binding and additional dynamin-dependent steps (Anborgh et al., 2000; Qian et al., 2001). Although a considerable amount of knowledge has been gained in understanding the mechanisms involved in the biased agonism of GPCRs (Godin and Ferguson, 2012; Reiter et al., 2012), less information is available about the fate (intracellular processing) of the receptors after biased activation.

The Rab proteins are key players in vesicular transport mechanisms, with the individual isoforms marking distinct vesicles in the endocytic and exocytic compartments (Zerial and McBride, 2001). Internalization, recycling, and degradation of receptors involve different Rab proteins, such as Rab5, Rab7, and Rab11 (Seachrist and Ferguson, 2003). It was shown that Rab5, Rab7, and Rab11 work together to regulate the vesicular trafficking of AT$_1$-R (Dale et al., 2004). We have shown in confocal microscopy studies using green fluorescent protein (GFP)–tagged AT$_1$-R that AngII stimulates rapid translocation of the receptor to Rab5 early endosomes, and subsequently to juxtanuclear Rab11 vesicles (Hunyady et al., 2002).

Studies of the G protein–independent signaling of AT$_1$-R have been accelerated by several approaches. Mutations within the highly conserved Asp^{125}Arg^{126}Tyr^{127} sequence of AT$_1$-R (DRY/AAY mutation) abrogated G protein coupling, yet such receptors can initiate ERK1/2 activation (Wei et al., 2003; Szidonya et al., 2007; Hansen et al., 2008). The development and utilization of a biased AT$_1$-R agonist, [Sar^1,Ile^4,Ile^8]AngII (SII-AngII), further widened the possibilities to investigate G protein–independent mechanisms (Holloway et al., 2002). Stimulation of AT$_1$-R by SII-AngII does not activate G proteins, but stimulates G protein–independent mechanisms and is also able to induce internalization of the receptor (Luttrell et al., 2001; Wei et al., 2003). SII-AngII is a widely used tool to study the biased agonism of AT$_1$-R in spite of its relatively low affinity to AT$_1$-R. Recently, new biased peptide ligands of AT$_1$-R were discovered such as TRV120023 (Sar-Arg-Val-Tyr-Lys-His-Pro-Ala-OH) and TRV120027 (Sar-Arg-Val-Tyr-Ile-His-Pro-D-Ala-OH), which have higher receptor binding affinities than SII-AngII (Violin et al., 2010). These TRV peptides selectively activate the β-arrestin–mediated signaling pathway and possess beneficial effects on cardiac contractility and performance (Violin et al., 2010; Kim et al., 2012). The favorable properties and potential clinical applications of TRV120027 are further investigated in trials for the treatment of acute heart failure (Soergel et al., 2013; Violin et al., 2014).

We used a bioluminescence resonance energy transfer (BRET)–based approach to investigate the fate of the receptor in response to stimuli. We used fluorescently labeled constructs marking the molecular steps during internalization and luciferase-fused receptors in BRET measurements. Our results demonstrate that biased agonists or stimulation of a biased receptor with the native AngII (AT$_1$-R–DRY/AAY) yield(s) different fates of the activated receptors in terms of β-arrestin binding, internalization, and appearance in various intracellular compartments. Our findings also suggest that the intracellular processing of AT$_1$-R is dependent on the type of activation and affinity of ligand binding to AT$_1$-R. Bias ligand–bound receptors are unable to couple to G$_q$ proteins and activate PLCβ to show accelerated internalization due to a lack of PtdIns(4,5)P_2 hydrolysis in the plasma membrane. In contrast, the degradation and recycling of the internalized receptor is mainly determined by the strength of β-arrestin binding.

Materials and Methods

Cell culture dishes and plates for BRET measurements were purchased from Greiner (Kremsmunster, Austria). Coelenterazine h was from either Invitrogen (Carlsbad, CA) or Regis Technologies (Morton Grove, IL). SII-AngII was purchased from Bachem AG (Bubendorf, Switzerland). The TRV120023 and TRV120027 peptides were synthesized by Proteogenix (Schiltigheim, France) to more than 98% purity. Wortmannin (Wm) was purchased from Calbiochem (San Diego, CA), PIK93 was obtained from Sigma-Aldrich (St. Louis, MO), and the A1 inhibitor was synthesized as described (Bojjireddy et al., 2014). Rapamycin was obtained from Merck (Darmstadt, Germany). Unless otherwise stated, all other chemicals and reagents were purchased from Sigma-Aldrich. The human embryonic kidney (HEK) 293 cells were from American Type Culture Collection (Manassas, VA).

DNA Constructs. For the construction of yellow fluorescent protein (YFP)–labeled constructs, the plasmid backbones of eYFP-C1 or eYFP-N1 (Clontech, Mountain View, CA) were used. The cDNA of the eYFP-tagged β-arrestin2 (β-arrestin2–YFP) and *Renilla* luciferase (Rluc)–tagged AT$_1$-Rs (AT$_1$-R–Rluc and AT$_1$-R–DRY/AAY–Rluc) were constructed as described previously (Turu et al., 2006; Balla et al., 2012). The eYFP-labeled full-length Rab5, Rab7, and Rab11 were constructed by replacing the eGFP-coding region with eYFP in the GFP-tagged constructs as described previously (Hunyady et al., 2002). The eYFP-tagged PLCδ1 pleckstrin homology (PH) domain was constructed as described previously (Varnai and Balla, 1998), whereas the PLCδ1-PH–super *Renilla* luciferase (Sluc) was constructed by replacing the eYFP coding region with sequence of super *Renilla* luciferase (Woo and von Arnim, 2008). The constructs of the rapamycin-inducible heterodimerization system (PM-FRB-mRFP and mRFP-FKBP-5ptase) were constructed as described previously (Toth et al., 2012). The expression vector of dominant-negative (DN) mutant GRK2 (K220M) was kindly provided by Dr. S. S. G. Ferguson (Ferguson et al., 1995).

Cell Culture and Transfection. The experiments were performed on the HEK293 cell line. The cells were cultured in Dulbecco's modified Eagle's medium with Pen/Strep (Invitrogen) and 10% heat-inactivated fetal bovine serum in 5% CO$_2$ at 37°C. For BRET experiments, the cells were cultured in plastic dishes, trypsinized prior to transfection, transiently transfected by using Lipofectamine 2000 (Invitrogen), and plated on poly-lysine pretreated white 96-well plates in 1×10^5 cells/well density for BRET measurements. The DNA amounts were 0.25 μg Rluc-containing construct/well and 0.0625–0.125 μg YFP-containing construct/well. The amount of Lipofectamine 2000 was 0.5 μl/well. For suspension of Ca^{2+} measurements and the mitogen-activated protein kinase assay, the HEK293 cells were cultured in 10-cm dishes and six-well plates, respectively. The cells were transiently transfected with Lipofectamine 2000 according to the manufacturer's protocol.

BRET Measurement. We used a *Renilla* luciferase–fused receptor as the energy donor and an eYFP-tagged protein as the acceptor. The BRET measurements were performed after 24 hours of the transfection on white 96-well plates. The medium of the cells was changed prior to measurements to a modified Krebs-Ringer buffer containing 120 mM NaCl, 4.7 mM KCl, 1.8 mM CaCl$_2$, 0.7 mM MgSO$_4$, 10 mM glucose, and Na-HEPES 10 mM, pH 7.4, and the BRET measurements were performed at 37°C. The BRET measurements were started after addition of the cell-permeable substrate coelenterazine h (Invitrogen or Regis Technologies) at a final concentration of 5 μM, and the counts were recorded by using either Berthold Mithras LB 940 (Bad Wildbad, Germany) or Varioskan Flash (Thermo Scientific, Waltham, MA) readers that allow the detection of signals using filters at 485- and 530-nm wavelengths. The detection time was 0.25–0.5 seconds. The BRET ratios were calculated as a 530/485 nm ratio. Measurements were done

in triplicates. The plotted BRET curves are the average of at least three independent experiments. BRET ratios were baseline corrected to the vehicle curve using GraphPad Prism software (La Jolla, CA). The approximate BRET ratio using the cytosolic eYFP and AT$_1$-R–Rluc pair is ~0.8 (data not shown).

Cytoplasmic Ca^{2+} Measurements in Cell Suspensions. HEK293 cells were transfected with the various constructs (6 μg DNA/10-cm dish) by using Lipofectamine 2000. After 24 hours, the cells grown on 10-cm culture plates were removed by mild trypsinization, and aliquots of cells (~10^6 cells) were loaded with 2 μM Fura-2/acetoxymethyl ester in Dulbecco's modified Eagle's medium containing 1.2 mM CaCl$_2$, 3.6 mM KCl, and 25 mM HEPES containing 1 mg/ml bovine serum albumin, 0.06% Pluronic acid, and 200 μM sulfinpyrazone for 45 minutes at room temperature. Cells were then washed with the same medium without Fura-2/acetoxymethyl ester and stored at room temperature in the dark. The cells were centrifuged rapidly before the measurements and dispersed in 3 ml of the modified Krebs-Ringer buffer used for all other analysis. Calcium measurements were performed at room temperature in a PTI Deltascan spectrofluorometer (Photon Technology International, Princeton, NJ).

ERK1/2 Mitogen-Activated Protein Kinase Assay. Twenty-four hours after transfection, the HEK293 cells were serum starved for 4 hours and stimulated for 5 minutes with 100 nM AngII or 10 μM SII-AngII. Cells were scraped into an SDS sample buffer containing protease and phosphatase inhibitors, briefly sonicated, boiled, and separated on SDS-polyacrilamide gels. The proteins were transferred to polyvinylidene fluoride membranes and incubated with the appropriate primary (Santa Cruz Biotechnology, Santa Cruz, CA) and secondary (Cell Signaling, Danvers, MA) antibodies. The antibodies were visualized by enhanced chemiluminescence using Immobilion Western HRP substrate reagents (Millipore, Billerica, MA).

Confocal Microscopy. AT$_1$-R–GFP stably expressing HEK293 cells (Hunyady et al., 2002) was plated on polylysine-pretreated glass coverslips (3 × 10^5 cells/35-mm dish). After 24 hours, the localization and distribution of the receptor were analyzed using a Zeiss LSM 710 confocal laser-scanning microscope (Carl Zeiss, Oberkochen, Germany).

Postacquisition data analysis of the confocal images was performed with either ZEN (Carl Zeiss) or MetaMorph (Molecular Devices, Sunnyvale, CA) software. Quantification of the internalization of AT$_1$-R–GFP (location in intracellular vesicles, which are clearly separated from the plasma membrane) as a function of time was calculated from a morphometric analysis by MetaMorph software obtained in seven separate experiments.

Results

BRET Assay for the Detection of Agonist-Induced Internalization of AT$_1$-R. Our previous results raised the possibility that biased stimulation of AT$_1$-R can lead to different fates of the internalized receptor (Balla et al., 2012). To investigate this question in more detail, we analyzed the proximity of the receptor with different Rab proteins used as markers of the steps along the endocytotic/recycling/degradation pathways of the internalized receptors. Rab5-YFP is a marker for early endosomes and Rab7-YFP is that for the multivesicular body/late endosome, whereas Rab11-YFP marks the late recycling route (Zerial and McBride, 2001). As shown in Fig. 1A, we detected an elevated BRET ratio between AT$_1$-R–Rluc and Rab5-YFP after both AngII and SII-AngII stimulation (black filled and gray open symbols, respectively), which indicates receptor-mediated endocytosis. In our previous studies (Balla et al., 2012), we noted that at the early phase after stimulation, SII-AngII induced a more robust colocalization of the receptor with Rab5 endosomes compared with AngII stimulation (Fig. 1A, gray open symbols; also in Supplemental Fig. 6C). Therefore, we investigated the effects of newly developed biased agonists on the internalization and sequential intracellular trafficking steps of AT$_1$-R. Figure 1B shows that stimulation with both 1 μM TRV120023 (TRV3) and 1 μM TRV120027 (TRV7) yielded BRET curves
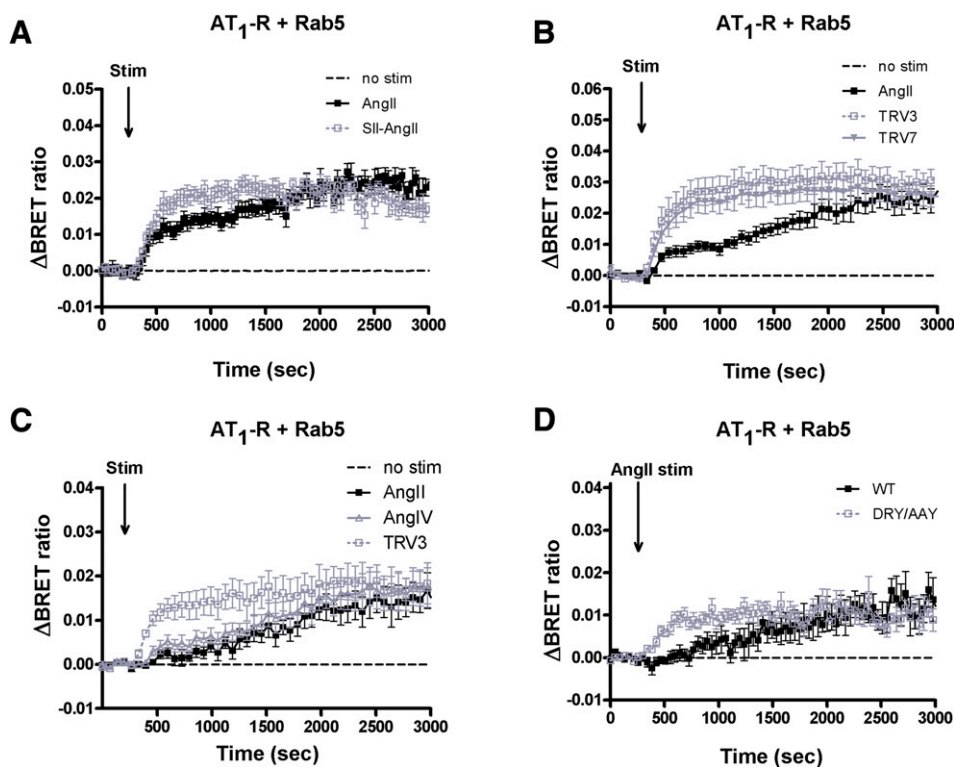
Fig. 1. BRET assay between wild-type AT$_1$-R and Rab5 upon stimulation (Stim) in HEK293 cells. (A–C) HEK293 cells were transfected with the plasmids of AT$_1$-R–Rluc and YFP-fused Rab5 protein, and after 24 hours, the cells were exposed to either 100 nM AngII (black-filled squares), (A) 10 μM SII-AngII (gray open symbols), (B) 1 μM TRV120023 (TRV3; gray open squares) or 1 μM TRV120027 (TRV7; gray-filled triangles); (C) 10 μM AngIV (gray open triangles) or 1 μM TRV3 (gray open squares), or vehicle (dashed lines) at the indicated time points. (D) HEK293 cells were transfected with the plasmids of the indicated receptor Rluc (WT, wild type, black-filled symbols; DRY/AAY mutant, gray open symbols) and Rab5-YFP, and after 24 hours, the cells were exposed to either 100 nM AngII or vehicle (dashed line) at the indicated time points. The BRET records are the average of at least three independent experiments. Mean values ± S.E.M. are shown (n = 3).

between the receptor and Rab5 that were very reminiscent of those evoked by SII-AngII. Taken together, the results shown in Fig. 1, A and B suggest that biased stimulation apparently accelerated the internalization of AT$_1$-R. Since both SII-AngII and the TRV compounds have a lower affinity than AngII, we also tested a low affinity, but unbiased agonist, the hexapeptide angiotensin IV (AngIV) (Le et al., 2002) on the internalization rate of AT$_1$-R. In contrast to the biased agonists, AngIV stimulation evoked a very similar BRET interaction of the receptor with Rab5 containing endosomes as the AngII-initiated response (Fig. 1C).

It is well established that AT$_1$-R–induced G$_q$ activation causes PLC-mediated hydrolysis of the membrane PtdIns(4,5)P_2, which can be monitored by following the translocation of PLCδ1-PH-GFP from the plasma membrane to the cytosol (Varnai and Balla, 1998). We confirmed that AngIV at the concentration used (10 μM) is able to initiate G$_q$ activation and PtdIns(4,5)P_2 hydrolysis in BRET measurements. AngIV, similarly to AngII, decreased the BRET ratio between the PLCδ1-PH domains fused with YFP and Sluc. When the PH domains are bound to the plasma membrane, they are within BRET distance, whereas being in the cytoplasm, they are not; therefore, the decreased BRET signal reflects the dissociation of the PtdIns(4,5)P_2 sensor domains from the plasma membrane due to the breakdown of PtdIns(4,5)P_2. The lipid is slowly resynthesized, causing the reappearance of the probes in the plasma membrane (BRET ratio increase) (Supplemental Fig. 1). It has been well documented that AngII stimulation of the DRY/AAY mutant receptor leads to biased activation, similar to that seen during SII-AngII stimulation of wild-type receptors (Wei et al., 2003). Figure 1D shows that AngII stimulation of the AT$_1$-R–DRY/AAY–Rluc caused a similar BRET interaction with Rab5-YFP as the biased ligand stimulation of the wild-type receptor (Fig. 1, A and B). This result suggested that the AngII-induced internalization of the mutant receptor occurs faster than with the wild-type AT$_1$-R. To demonstrate that the properties of the luciferase-tagged receptors are similar to those of the untagged receptors, we analyzed calcium signaling and extracellular signal-regulated kinase activation. The results showed that both of these responses were comparable with the untagged and Rluc-tagged receptors and that neither SII-AngII nor the DRY/AAY receptor stimulated by AngII showed Ca^{2+} responses, yet they displayed a reduced but still detectable ERK1/2 activation (Supplemental Fig. 2). These data together suggested that the tagged receptors function similarly to the nontagged AT$_1$-Rs.

Characterization of the Biased Agonist–Induced Internalization of AT$_1$-R. We also investigated the agonist-induced internalization of the receptor with confocal microscopy using HEK293 cells stably expressing AT$_1$-R–GFP. Figure 2 demonstrates the slightly faster internalization of a biased-activated receptor. More receptors were detectable in intracellular vesicles after 4-minute stimulation with either SII-AngII or TRV120023 (TRV3) compared with AngII stimulation.

We then investigated the possibility that the more rapid internalization of the SII-AngII–stimulated receptor is the result of the use of an alternative endocytic pathway(s). We used 300 mM sucrose treatment to inhibit clathrin-mediated endocytosis (Heuser and Anderson, 1989). At this concentration (300 mM), sucrose significantly diminished the BRET

ratio increase between the receptor and Rab5 after stimulation with either AngII or SII-AngII, which suggested that both ligands initiated a primarily clathrin-mediated endocytic mechanism (Supplemental Fig. 3, A and B). We also studied the effect of filipin, which is widely used for the inhibition of the clathrin-independent caveolae-mediated pathway (Orlandi and Fishman, 1998). During stimulation of the cells with 100 nM AngII or 10 μM SII-AngII, the preincubation of cells with filipin did not change the BRET ratio kinetic between Rab5 and AT$_1$-R (Supplemental Fig. 3C).

Next, we analyzed whether the faster rate of Rab5 recruitment is the consequence of the absence of classic (G protein–dependent) calcium signaling in biased-stimulated AT$_1$-R. We used BAPTA-AM pretreatment to blunt the evoked calcium signal. As shown in Supplemental Fig. 4A, BAPTA-AM pretreatment did not alter the kinetics of Rab5 recruitment. We confirmed that BAPTA-AM pretreatment was sufficient to inhibit the calcium signal in HEK293 cells (Supplemental Fig. 4B).

Effect of Biased Stimulation on the Association of AT$_1$-R with β-Arrestin2. Next, we investigated the possible involvement of β-arrestin2 in the altered internalization of AT$_1$-R when the receptor is activated by biased agonists. Both SII-AngII and the TRV compounds were able to cause β-arrestin2 recruitment, although the biased agonists evoked smaller responses than AngII stimulation (Fig. 3, A and B). It is noteworthy that the AngII-induced binding of β-arrestin2 appeared more sustained than that evoked by the biased agonists, (Fig. 3, A and B, gray symbols; also in Supplemental Fig. 6A, gray symbols). Here, AngIV caused a similar type of AT$_1$-R–β-arrestin2 BRET interaction as the low-affinity biased agonists (Fig. 3C). We also measured complete concentration-response curves to check that the used agonist concentrations are maximally effective. Supplemental Figure 5 demonstrates that 100 nM of AngII induced maximal PtdIns(4,5)P_2 hydrolysis (Supplemental Fig. 5A) and β-arrestin2 binding (Supplemental Fig. 5B). AngIV was maximally effective with a 10 μM concentration in PtdIns(4,5)P_2 breakdown and β-arrestin2 recruitment assays (Supplemental Fig. 5, A and B). Ten micromolars of SII-AngII and 1 μM concentrations of TRV compounds evoked maximal β-arrestin binding (Supplemental Fig. 5B), but did not cause detectable PtdIns(4,5)P_2 hydrolysis (Supplemental Fig. 1) or vasoconstriction in wire myography experiments using mouse aortic rings (data not shown).

The BRET curve of the AngII-induced β-arrestin binding of DRY/AAY–AT$_1$-R is very reminiscent of that of the wild-type receptor, and the amplitude is ~75% of the wild-type counterpart (Fig. 3D, black-filled symbols). We also compared the effects of stimulation of AT$_1$-R–DRY/AAY–Rluc with SII-AngII and AngII. Stimulation of AT$_1$-R–DRY/AAY–Rluc with SII-AngII resulted in slightly weaker and less stable β-arrestin binding than the AngII-induced response (Supplemental Fig. 6). Yet, the translocations to Rab5 endosomes of AT$_1$-R–DRY/AAY–Rluc in response to either SII-AngII or AngII stimulation were almost identical (Supplemental Fig. 6).

Effect of Inhibitors of Phosphatidylinositol Kinases on the Agonist-Induced AT$_1$-R Endocytosis. Next, we investigated the role of PtdIns(4,5)P_2 in the regulation of AT$_1$-R internalization. PtdIns(4,5)P_2 is located on the inner leaflet of the plasma membrane and is important in both signal transduction processes and the endocytosis of cell surface
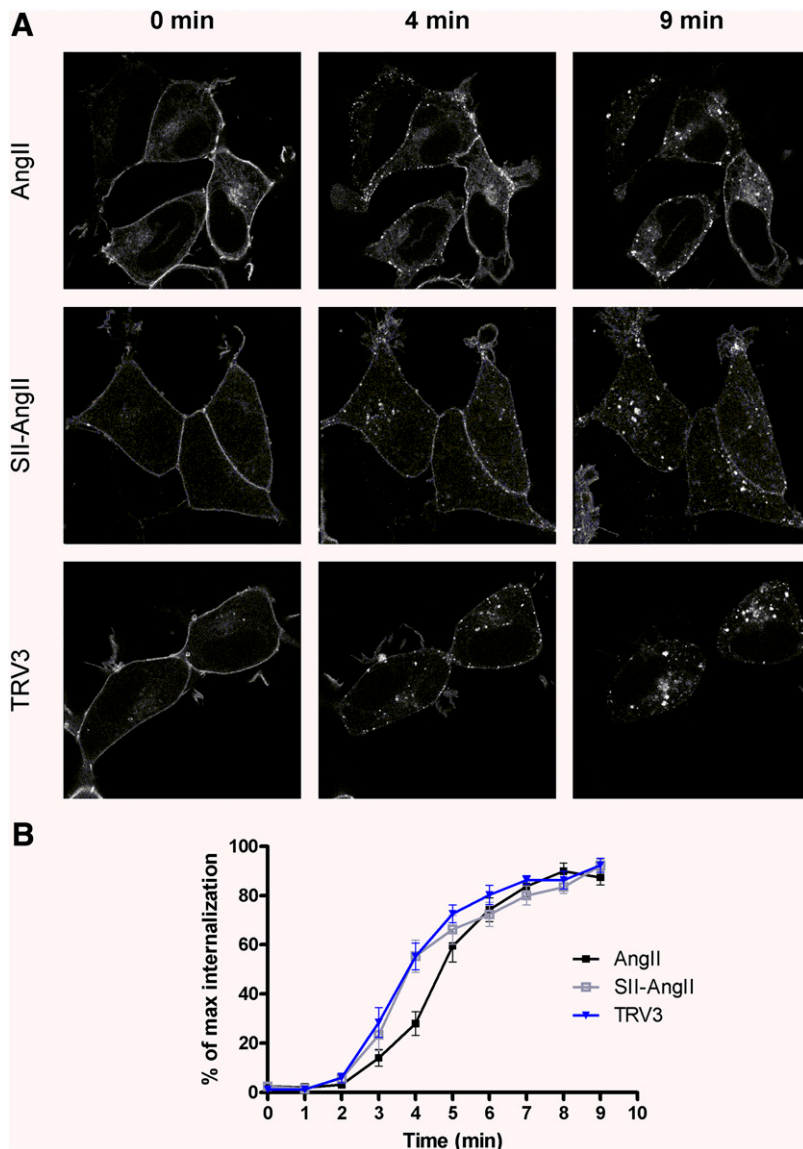
Fig. 2. Effect of agonist stimulation on the distribution of AT_1-R–GFP in HEK293 cells. (A) AT_1-R–GFP stably expressing HEK293 cells were exposed to either 100 nM AngII (upper row of micrographs), 10 μM SII-AngII (middle row of micrographs), or 1 μM TRV120023 (TRV3; lower row of micrographs), and the GFP fluorescence was detected by a Zeiss LSM 710 confocal laser-scanning microscope. The representative confocal micrographs show the localization and cellular distribution of AT_1-R before (0 minutes) and 4 or 9 minutes after agonist treatment. (B) Quantification of the internalization of AT_1-R–GFP as a function of time, which was calculated from a morphometric analysis by MetaMorph software obtained in seven separate experiments (mean $\pm$ S.E.M.).

receptors, including GPCRs (Toth et al., 2012). Several phosphatidylinositol kinases are involved in the maintenance of the plasma membrane PtdIns(4,5)P_2 (Balla and Balla, 2006; Balla, 2013). Among these, phosphatidylinositol-4 kinases (PI4Ks) control the first step in PtdIns(4,5)P_2 synthesis (Balla et al., 2005, 2008). First, we examined the effect of low and high concentrations of Wm (the former selectively inhibits most phosphatidylinositol-3 kinases; the latter also inhibits type III PI4Ks). Figure 4 shows that 100 nM Wm did not alter the agonist-induced endocytosis of AT_1-R. In contrast, 10 μM Wm was able to diminish AngII- and AngIV-induced endocytosis (Fig. 4, A and C), but not the internalization evoked by the biased agonists (Fig. 4B). This result suggested the involvement of PI4Ks rather than phosphatidylinositol-3 kinases, and therefore we tested more selective inhibitors of the individual PI4K isoforms. PIK-93 inhibits PI4KIIIβ/PI4KB, but to a much lesser degree than PI4KA (Balla et al., 2008), whereas a compound, A1, inhibits PI4KIIIα/PI4KA more potently than PI4KB (Bojjireddy et al., 2014). Using these inhibitors and following the BRET signal

between the receptor and Rab5, the activity of PI4KIIIα was found to be necessary for the AngII- and AngIV-induced endocytosis, but not for the biased agonist–induced response (Fig. 5), whereas PI4KIIIβ was found not to be responsible for the maintenance of PtdIns(4,5)P_2 involved in the regulation of endocytosis.

Plasma Membrane PtdIns(4,5)P_2 Depletion Affects AT_1-R Internalization upon Unbiased or Biased Activation. We also investigated the role of PtdIns(4,5)P_2 in the stimulation-evoked Rab5 recruitment of AT_1-R. First, we used a plasma membrane PtdIns(4,5)P_2 depletion system, as described earlier (Toth et al., 2012). The appearance of AT_1-R in early endosomes was followed by BRET measurements between AT_1-R–Rluc and fluorescently tagged Rab5 in cells coexpressing the rapamycin-inducible PtdIns(4,5)P_2 depletion system. Briefly, addition of rapamycin induces heterodimerization between the plasma membrane–targeted FRB and cytoplasmic FK506 binding protein; thus, the 5ptase domain is translocated to the plasma membrane, where it degrades PtdIns(4,5)P_2. We confirmed the efficiency of this
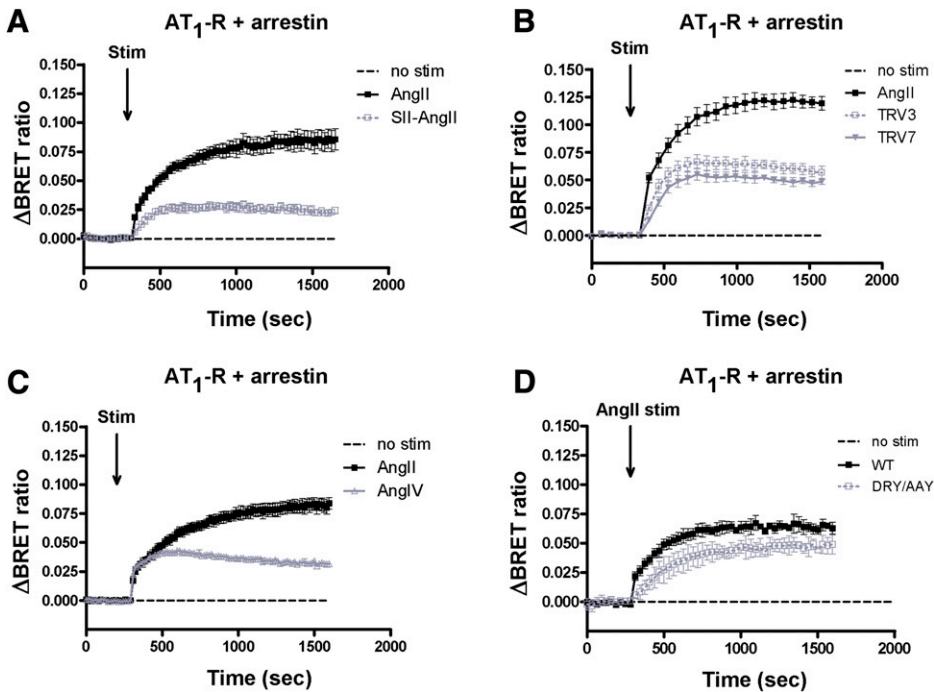
Fig. 3. BRET assay between AT$_1$-R and β-arrestin2 upon agonist stimulation (Stim) in HEK293 cells. HEK293 cells were transfected with AT$_1$-R–luciferase and β-arrestin2–YFP, and after 24 hours, the cells were exposed to 100 nM AngII (black-filled squares), (A) 10 μM SII-AngII (gray open symbols), (B) 1 μM TRV120023 (TRV3; gray open squares) or 1 μM TRV120027 (TRV7; gray-filled triangles), (C) 10 μM AngIV (gray open triangles), or vehicle (dashed lines) at the indicated time points. (D) HEK293 cells were transfected with the plasmids of the indicated receptor Rluc (WT, wild type, black-filled symbols; DRY/AAY mutant, gray open symbols) and β-arrestin2–YFP, and after 24 hours, the cells were exposed to either 100 nM AngII or vehicle (dashed line) at the indicated time points. The BRET records are the average of at least three independent experiments. Mean values $\pm$ S.E.M. are shown (n = 3).

method in BRET measurements using YFP- and Sluc-tagged phospholipase Cδ1 PH domain sensors (data not shown). The depletion of plasma membrane PtdIns(4,5)P_2 completely blocked both unbiased or biased activation–induced AT$_1$-R Rab5 recruitment (Supplemental Figs. 6B and 7A).

We also performed experiments using a dominant-negative GRK2 construct to show the role of PtdIns(4,5)P_2 in the regulation of AT$_1$-R internalization. It was demonstrated that DN-GRK2 significantly blunts the receptor activation–induced PLCβ activity (Carman et al., 1999; Sallese et al., 2000), and we confirmed that overexpression of DN-GRK2 (GRK2-K220M) decreased the AT$_1$-R stimulation–induced plasma membrane PtdIns(4,5)P_2 hydrolysis in HEK293 cells (Supplemental Fig. 8A). Figure 6 shows that overexpression of DN-GRK2 accelerated AngII-evoked AT$_1$-R internalization, but had no effect on the biased agonist (TRV120023)–induced
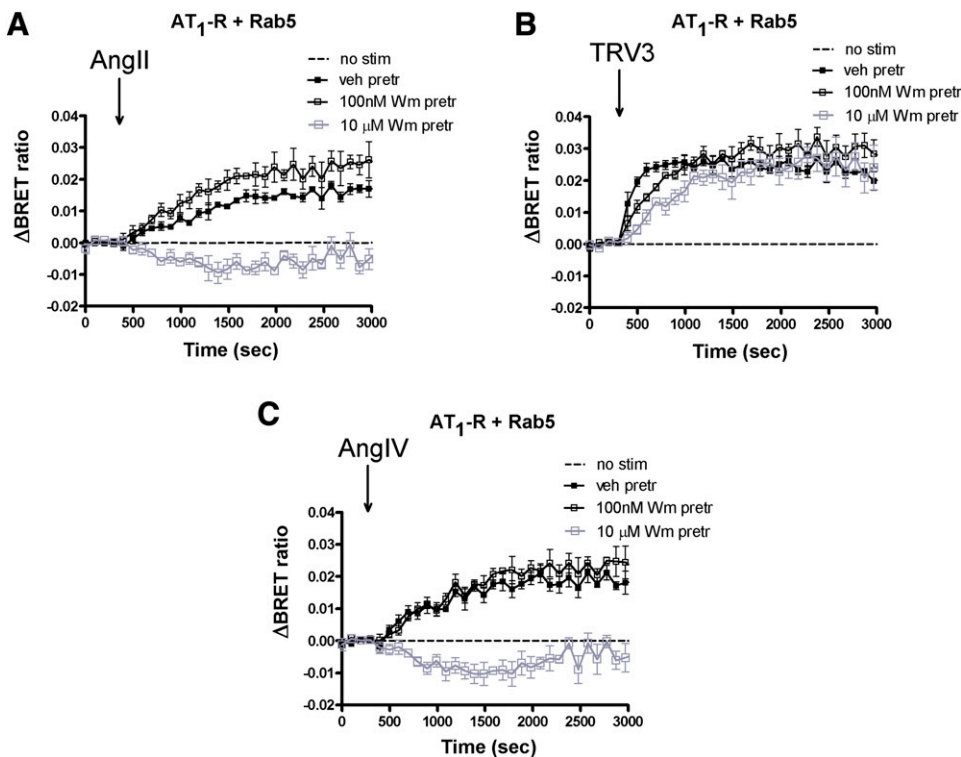

Fig. 4. Effect of wortmannin on the agonist-induced internalization of AT$_1$-R in HEK293 cells. HEK293 cells were transfected with the plasmids of AT$_1$-R–Rluc and Rab5-YFP proteins, and after 24 hours, the experiments were carried out. Cells were pretreated (pretr) for 10 minutes with vehicle (veh) BRET medium (black-filled symbols) or BRET medium supplemented with 100 nM wortmannin (black open symbols) or 10 μM wortmannin (gray open symbols) and exposed to either vehicle (dashed line), 100 nM AngII (A), 1 μM TRV120023 (TRV3) (B), or 10 μM AngIV (C) at the indicated time points. The BRET curves are the average of three independent experiments, each performed in triplicate. Mean values $\pm$ S.E.M. are shown (n = 3). Stim, stimulation.
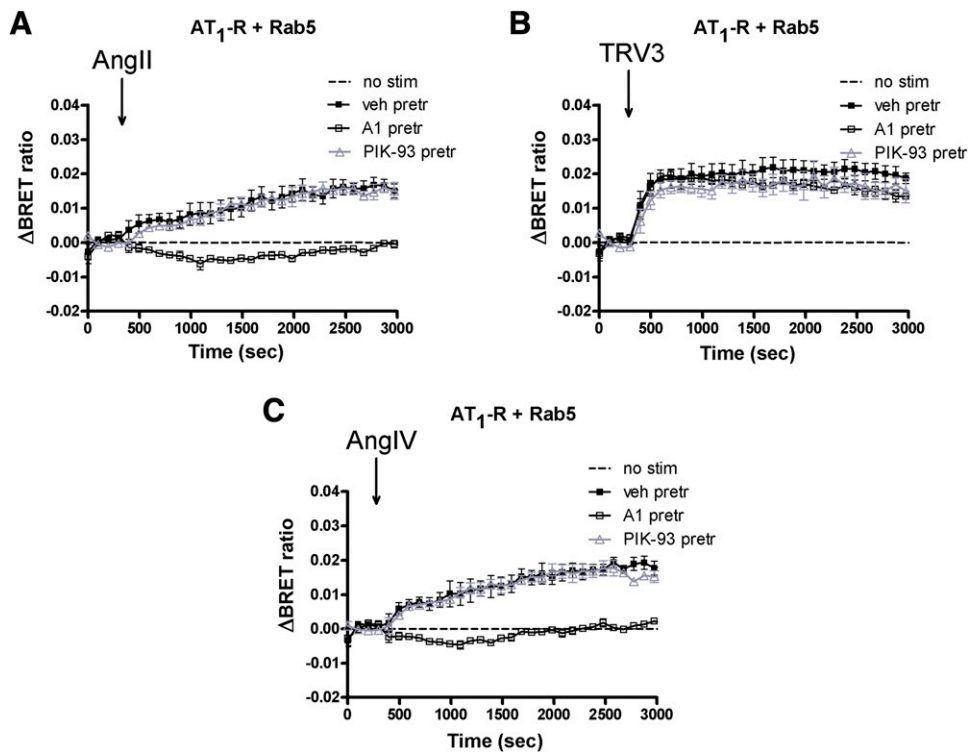
A
AT$_1$-R + Rab5

AngII

- - - no stim
- veh pretr
- A1 pretr
- PIK-93 pretr

B
AT$_1$-R + Rab5

TRV3

- - - no stim
- veh pretr
- A1 pretr
- PIK-93 pretr

C
AT$_1$-R + Rab5

AngIV

- - - no stim
- veh pretr
- A1 pretr
- PIK-93 pretr

Fig. 5. Effect of A1 and PIK-93 on the agonist-induced internalization of AT$_1$-R in HEK293 cells. HEK293 cells were transfected with the plasmids of the AT$_1$-R–Rluc and Rab5-YFP proteins, and after 24 hours, the experiments were carried out. Cells were pretreated (pretr) for 10 minutes with vehicle (veh) BRET medium (black-filled symbols) or BRET medium supplemented with 10 nM A1 (black open squares) or 250 nM PIK-93 (gray open triangles) and exposed to either vehicle (dashed line), 100 nM AngII (A), 1 μM TRV120023 (TRV3) (B), or 10 μM AngIV (C) at the indicated time points. The BRET curves are the average of three independent experiments, each performed in triplicate. Mean values $\pm$ S.E.M. are shown ($n = 3$). Stim, stimulation.

response. The overexpression of DN-GRK2 did not affect the β-arrestin2 binding properties (Supplemental Fig. 8B), which supports that not only GRK2 but other GRK isoforms, such as GRK3/5/6, could be involved in receptor phosphorylation and β-arrestin2 recruitment in HEK293 cells (Kim et al., 2005).

BRET Assay for Detection of Intracellular Processing of AT$_1$-R. Our results suggested that biased stimulation of AT$_1$-R can lead to altered intracellular processing of the internalized receptor. To investigate this possibility, we

AT$_1$-R + Rab5

Stim

- - - no stim
- AngII
- TRV3
- - - no stim (DN-GRK2)
- AngII (DN-GRK2)
- TRV3 (DN-GRK2)

Fig. 6. Effects of attenuation of plasma membrane PtdIns(4,5)P_2 hydrolysis on BRET curves between AT1-R and Rab5 or β-arrestin2. HEK293 cells were transfected with plasmids encoding DN-GRK2, AT$_1$-R–Rluc, and Rab5-YFP. After 24 hours, the cells were exposed to either 100 nM AngII (red trace), 1 μM TRV120023 (TRV3; blue trace), or vehicle (dashed lines) at the indicated time point. The BRET records are the average of three independent experiments. Mean values $\pm$ S.E.M. are shown ($n = 3$). Stim, stimulation.

performed a BRET experiment to follow AT$_1$-R inside the cell using various markers of endomembranes, such as Rab7 and Rab11, as the markers of degradation and recycling pathways, respectively. As discussed earlier, Rab7-YFP is used to detect the multivesicular body/late endosome pathway and Rab11-YFP is a marker of the late recycling route. As shown in Fig. 7, we detected an elevated BRET ratio with Rab7-YFP following both AngII and biased agonist (SII-AngII, TRV120023, and TRV120027) stimulation. Enhanced initial BRET interactions were detected after stimulation with biased ligands between AT$_1$-R and Rab5 (Fig. 1) and both the Rab7- and Rab11-containing compartments (Fig. 7). The amplitudes of the association of Rab7 and the receptor were in good correlation with the initiated β-arrestin binding upon stimulation with various ligands (Figs. 3 and 7, A, C, and E). In the case of Rab11-YFP and AT$_1$-R–Rluc, AngII stimulus caused an initial decrease in the BRET ratio, but after ~15 minutes of stimulation, the ratio started to elevate (Fig. 7, B, D, and F; black-filled symbols). The low-affinity agonists caused increased colocalization with Rab11 endosomes after ~5–10 minutes of the stimulation, which is strikingly different from the AngII-evoked response, where the increased BRET ratio was preceded by a period of ~15-minute BRET decrease (Fig. 7, B, D, and F). We also analyzed whether the calcium signal of AT$_1$-R is partially responsible for the intracellular processing of the receptor. However, BAPTA-AM pretreatment did not modify the association of AT$_1$-R with Rab4, Rab7, and Rab11 (data not shown), arguing against the role of Ca^{2+} signal generation in this process.

Discussion

In the present study, we investigated and analyzed the consequences of biased activation of AT$_1$-R, focusing on
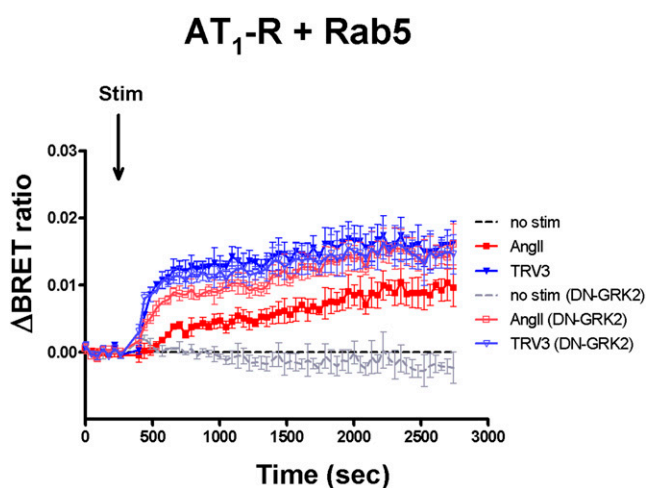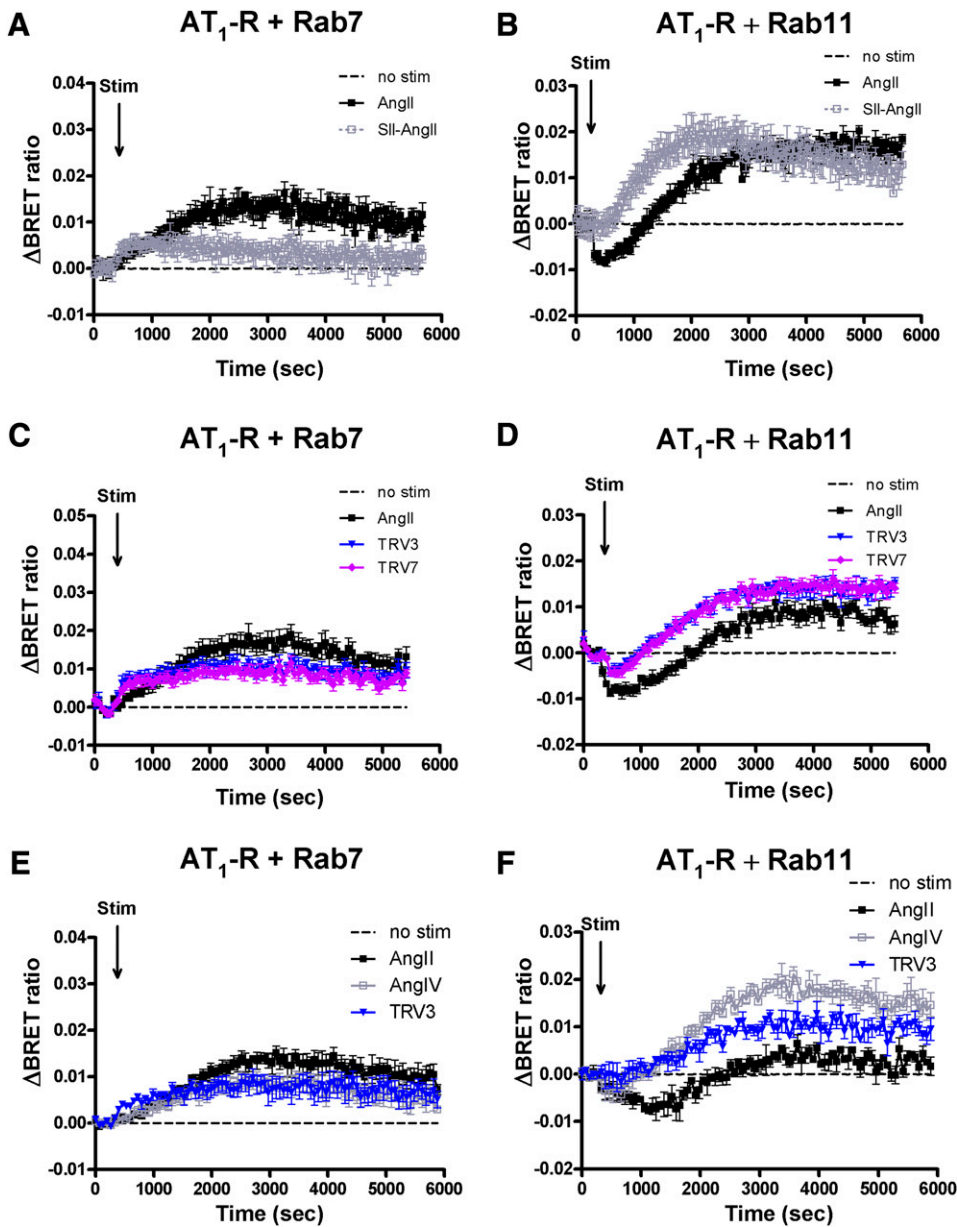
Fig. 7. BRET assay between AT$_1$-R and different Rab proteins upon agonist stimulation (Stim) in HEK293 cells. HEK293 cells were transfected with the plasmids of AT$_1$-R–Rluc and the indicated YFP-fused Rab proteins, and after 24 hours, the cells were exposed to either 100 nM AngII (black-filled symbols), (A and B) 10 μM SII-AngII (gray open symbols), (C and D) 1 μM TRV120023 (TRV3; blue traces), 1 μM TRV120027 (TRV7; purple traces), (E and F) 10 μM AngIV (gray open squares), 1 μM TRV3 (blue traces), or vehicle (dashed lines) at the indicated time points. BRET pairs: (A, C, and E) Rab7-YFP and AT$_1$-R–Rluc; (B, D, and F) Rab11-YFP and AT$_1$-R–Rluc. The BRET records are the average of at least three independent experiments. Mean values $\pm$ S.E.M. are shown ($n = 3$).

β-arrestin binding and intracellular processing of wild-type as well as DRY/AAY mutant AT$_1$-Rs. Agonist activation of most GPCRs, such as AT$_1$-R, initiates phosphorylation of the receptor by G protein–coupled receptor kinases. The phosphorylated carboxyl-terminal tail of the receptor recruits the cytosolic adaptor protein, β-arrestin, and uncouples the receptor from the corresponding heterotrimeric G protein. The receptor bound to β-arrestin is also sorted from the plasma membrane into endocytic vesicles. Receptor internalization can occur by several mechanisms, such as via clathrin-coated vesicles, or by other vesicles, including caveolae (Maxfield and McGraw, 2004). GPCRs, which internalize via the chlathrin-mediated pathway, require agonist binding and subsequent β-arrestin binding to become endocytosed. The adaptor between the phosphorylated receptor and endocytotic machinery is the β-arrestin molecule itself (Ferguson, 2001). AT$_1$-Rs are internalized predominantly via the chlathrin-mediated pathway at physiologic hormone concentrations,

but β-arrestin–independent internalization was also reported at higher AngII concentrations (Zhang et al., 1996; Gaborik et al., 2001).

We used a BRET-based approach to investigate the distribution of the receptor in response to ligands that possess biased agonist properties. We used several YFP-labeled fusion constructs and *Renilla* luciferase–fused receptors as intermolecular probe pairs in BRET measurements. After the addition of AngII, the BRET ratios are increased between AT$_1$-R and Rab5 and Rab7, which are signs of a traveling receptor through endosomes decorated with those proteins (Figs. 1 and 7). Since the DRY/AAY mutation of the receptor or the use of biased agonists (such as SII-AngII, TRV120023, and TRV120027) fail to achieve G protein activation (Gaborik et al., 2003; Wei et al., 2003; Violin et al., 2010), differences were expected in the fate of AT$_1$-R after biased activation. All biased agonists (SII-AngII, TRV120023, and TRV120027) induced colocalization of AT$_1$-R

with Rab5 endosomes (indicating internalization of the receptor), which was apparently more robust than the AngII-evoked responses (Fig. 1). The low-affinity unbiased AT$_1$-R agonist AngIV caused a very similar internalization as AngII (Fig. 1C). Our results did not prove the role of either fundamentally different endocytic routes (Supplemental Fig. 3) or a G$_q$ activation–initiated calcium signal (Supplemental Fig. 4) in the background of the dissimilar rate of endocytosis after bias activation of AT$_1$-R. We were also not able to demonstrate correlation between β-arrestin binding and the accelerated internalization of AT$_1$-R after stimulation with biased agonists (Fig. 3). Moreover, it seems that the course of AT$_1$-R–β-arrestin2 recruitment may correlate with the affinity of the ligand since it is known that SII-AngII, TRV120023, and TRV120027 have a significantly lower affinity than AngII (Bonde et al., 2010; Violin et al., 2010), and also the low-affinity unbiased AT$_1$-R agonist AngIV caused a similarly reduced and less stable AT$_1$-R–β-arrestin2 recruitment as the biased agonists (Fig. 3C). We used various concentrations of agonists to check their effects (Supplemental Fig. 5) since locally produced AngII levels in many target tissues are at least one order of magnitude higher than the concentration of circulating AngII (Danser, 2003).

Since both AngII and AngIV initiated PtdIns(4,5)P_2 breakdown in our system, whereas the biased agonists did not (Supplemental Fig. 1), we investigated the role of PtdIns(4,5)P_2 in the regulation of AT$_1$-R internalization. The pharmacological approach revealed that PI4KIIIα is responsible for the maintenance of the PtdIns(4,5)P_2 pool, which is involved in receptor-mediated endocytosis since both 10 μM wortmannin and 10 nM A1 were able to suspend the endocytosis after AngII or AngIV stimulation of AT$_1$-R (Figs. 4 and 5). The inhibitory effect of the inhibition of PtdIns(4,5)P_2 resynthesis by the blockade of PI4KIIIα activity on AT$_1$-R endocytosis is consistent with the observation that PtdIns(4,5)P_2 depletion by a rapamycin-inducible heterodimerization system also interfered with GPCR internalization (Supplemental Fig. 7) (Toth et al., 2012).

Several studies have investigated the roles of different Rab proteins, such as Rab4, Rab5, Rab7, and Rab11, in AT$_1$-R intracellular processing (Hunyady et al., 2002; Seachrist et al., 2002; Seachrist and Ferguson, 2003; Dale et al., 2004). We extended those studies using biased agonists in living cell experiments. It is important to emphasize in the interpretation of the results of the previous studies and our recent studies that a given intracellular vesicle may contain more than one isoform of Rab proteins (Sonnichsen et al., 2000).

Rab4 shows an overlapping distribution in early endosomes with Rab5 and in recycling endosomes with Rab11. In our studies, the BRET curves of Rab4 and Rab5 with AT$_1$-R were very similar, which suggests that Rab4 is partly located in Rab4/Rab5-positive endosomes (data not shown) in HEK293 cells. As mentioned above, Rab7 is localized to both late endosomal and lysosomal compartments as well (Bucci et al., 2000). Rab7 is important in the regulation of the intracellular processing of GPCRs routing the receptors from early endosomes to late endosomal and lysosomal compartments. It seems that the biased agonists and AngIV-induced receptor trafficking did not prefer the association with Rab7 compartments as much as the AngII-induced mechanism (Fig. 7). Our data raise the possibility that the association

with Rab7 is mainly determined by the affinity of the ligands toward the receptor (Fig. 7, A, C, and E). Rab11 is also located in several compartments, such as perinuclear recycling endosomes and the trans-Golgi network, where it influences the slow endosomal recycling and endosome to trans-Golgi network trafficking, respectively. It was demonstrated earlier by confocal (Hunyady et al., 2002) and fluorescence resonance energy transfer microscopy (Li et al., 2008) that Rab4 and Rab11 together coordinate the recycling of AT$_1$-R. During early recycling, the receptor associated mostly with Rab4, and during late-stage recycling, it associated mostly with Rab11. That is in concert with our results, which show that the association of AT$_1$-R with Rab11 is a latter event after stimulation. AngII stimulus caused a drop in the BRET ratio between Rab11-YFP and AT$_1$-R–Rluc, but after ~15 minutes of stimulation, the ratio started to increase (Fig. 7, B, D, and F; black-filled symbols). This phenomenon could raise the possibility that some fraction of the overexpressed receptor is already located in Rab11 intracellular compartments in HEK293, and after stimulus, these receptors shift to other compartments, which results in the drop in BRET ratio. It is known that Rab11 is a very important player, not just in the regulation of the endocytic recycling compartment, but also in the regulation of the biosynthetic recycling compartment (Saraste and Goud, 2007); moreover, Rab11 regulates exocytosis of vesicles at the plasma membrane (Takahashi et al., 2012). It is possible that AngII stimulation initiates a mechanism, which translocates the preformed or previously endocytosed receptors to the cell surface regulating the responsiveness of the cells.

Interestingly, the association with Rab11 is very dissimilar in the case of stimulation with the other agonists (biased agonists and AngIV), where the association starts at an earlier time point after the stimulation (Fig. 7, B, D, and F). The dissimilarity between AngII and the other ligands suggest that the ligand affinity and strength of arrestin binding can determine the later fate of the stimulated receptor.

Taken together, the wild-type and DRY/AAY mutant AT$_1$-Rs and also the AngII or biased agonist–stimulated receptors differ in their sorting between intracellular compartments. Our data suggest that neither the reduced arrestin binding, fundamentally different internalization routes, nor the calcium signal (Supplemental Figs. 3 and 4), but rather the transient depletion of the plasma membrane PtdIns(4,5)P_2 pool, is responsible for the reduced rate of AngII-induced AT$_1$-R endocytosis compared with the biased agonist–induced responses (Figs. 4 and 5; Supplemental Figs. 7 and 8). Even though the main determinant of the endocytic rate is the presence or absence of PLC activation, the later fate of AT$_1$-R within the cells seems mainly dependent on the course of β-arrestin binding to the stimulated receptor. The hormonal responsiveness of tissues and cells is dynamic and determined by the delicate balance between externalization (delivery mechanisms, which transport the receptors from the intracellular compartments to the plasma membrane) and internalization pathways of the receptors. It is very promising that the delicate balance between receptor resensitization/externalization and desensitization/internalization can be modified by biased agonists, which raises the possibility of applying biased ligands in diseases where intracellular receptor processing should be changed.

References

Anborgh PH, Seachrist JL, Dale LB, and Ferguson SS (2000) Receptor/beta-arrestin complex formation and the differential trafficking and resensitization of beta2-adrenergic and angiotensin II type 1A receptors. *Mol Endocrinol* 14:2040–2053.
Balla A and Balla T (2006) Phosphatidylinositol 4-kinases: old enzymes with emerging functions. *Trends Cell Biol* 16:351–361.
Balla A, Kim YJ, Varnai P, Szentpetery Z, Knight Z, Shokat KM, and Balla T (2008) Maintenance of hormone-sensitive phosphoinositide pools in the plasma membrane requires phosphatidylinositol 4-kinase IIIalpha. *Mol Biol Cell* 19:711–721.
Balla A, Tóth DJ, Soltész-Katona E, Szakadáti G, Erdélyi LS, Várnai P, and Hunyady L (2012) Mapping of the localization of type 1 angiotensin receptor in membrane microdomains using bioluminescence resonance energy transfer-based sensors. *J Biol Chem* 287:9090–9099.
Balla A, Tuymetova G, Tsiomenko A, Várnai P, and Balla T (2005) A plasma membrane pool of phosphatidylinositol 4-phosphate is generated by phosphatidylinositol 4-kinase type-III alpha: studies with the PH domains of the oxysterol binding protein and FAPP1. *Mol Biol Cell* 16:1282–1295.
Balla T (2013) Phosphoinositides: tiny lipids with giant impact on cell regulation. *Physiol Rev* 93:1019–1137.
Bojjireddy N, Botyanszki J, Hammond G, Creech D, Peterson R, Kemp DC, Snead M, Brown R, Morrison A, and Wilson S et al. (2014) Pharmacological and genetic targeting of the PI4KA enzyme reveals its important role in maintaining plasma membrane phosphatidylinositol 4-phosphate and phosphatidylinositol 4,5-bisphosphate levels. *J Biol Chem* 289:6120–6132.
Bonde MM, Hansen JT, Sanni SJ, Haunsø S, Gammeltoft S, Lyngsø C, and Hansen JL (2010) Biased signaling of the angiotensin II type 1 receptor can be mediated through distinct mechanisms. *PLoS ONE* 5:e14135.
Bucci C, Thomsen P, Nicoziani P, McCarthy J, and van Deurs B (2000) Rab7: a key to lysosome biogenesis. *Mol Biol Cell* 11:467–480.
Carman CV, Parent JL, Day PW, Pronin AN, Sternweis PM, Wedegaertner PB, Gilman AG, Benovic JL, and Kozasa T (1999) Selective regulation of Galpha(q/11) by an RGS domain in the G protein-coupled receptor kinase, GRK2. *J Biol Chem* 274:34483–34492.
Dale LB, Seachrist JL, Babwah AV, and Ferguson SS (2004) Regulation of angiotensin II type 1A receptor intracellular retention, degradation, and recycling by Rab5, Rab7, and Rab11 GTPases. *J Biol Chem* 279:13110–13118.
Danser AH (2003) Local renin-angiotensin systems: the unanswered questions. *Int J Biochem Cell Biol* 35:759–768.
Ferguson SS (2001) Evolving concepts in G protein-coupled receptor endocytosis: the role in receptor desensitization and signaling. *Pharmacol Rev* 53:1–24.
Ferguson SS, Ménard L, Barak LS, Koch WJ, Colapietro AM, and Caron MG (1995) Role of phosphorylation in agonist-promoted beta 2-adrenergic receptor sequestration. Rescue of a sequestration-defective mutant receptor by beta ARK1. *J Biol Chem* 270:24782–24789.
Gáborik Z, Jagadeesh G, Zhang M, Spät A, Catt KJ, and Hunyady L (2003) The role of a conserved region of the second intracellular loop in AT1 angiotensin receptor activation and signaling. *Endocrinology* 144:2220–2228.
Gáborik Z, Szaszák M, Szidonya L, Balla B, Paku S, Catt KJ, Clark AJ, and Hunyady L (2001) Beta-arrestin- and dynamin-dependent endocytosis of the AT1 angiotensin receptor. *Mol Pharmacol* 59:239–247.
Godin CM and Ferguson SS (2012) Biased agonism of the angiotensin II type 1 receptor. *Mini Rev Med Chem* 12:812–816.
Hansen JL, Aplin M, Hansen JT, Christensen GL, Bonde MM, Schneider M, Haunsø S, Schiffer HH, Burstein ES, and Weiner DM et al. (2008) The human angiotensin AT(1) receptor supports G protein-independent extracellular signal-regulated kinase 1/2 activation and cellular proliferation. *Eur J Pharmacol* 590:255–263.
Heuser JE and Anderson RG (1989) Hypertonic media inhibit receptor-mediated endocytosis by blocking clathrin-coated pit formation. *J Cell Biol* 108:389–400.
Holloway AC, Qian H, Pipolo L, Ziogas J, Miura S, Karnik S, Southwell BR, Lew MJ, and Thomas WG (2002) Side-chain substitutions within angiotensin II reveal different requirements for signaling, internalization, and phosphorylation of type 1A angiotensin receptors. *Mol Pharmacol* 61:768–777.
Hunyady L, Baukal AJ, Gaborik Z, Olivares-Reyes JA, Bor M, Szaszak M, Lodge R, Catt KJ, and Balla T (2002) Differential PI 3-kinase dependence of early and late phases of recycling of the internalized AT1 angiotensin receptor. *J Cell Biol* 157:1211–1222.
Hunyady L and Catt KJ (2006) Pleiotropic AT1 receptor signaling pathways mediating physiological and pathogenic actions of angiotensin II. *Mol Endocrinol* 20:953–970.
Hunyady L, Catt KJ, Clark AJ, and Gáborik Z (2000) Mechanisms and functions of AT(1) angiotensin receptor internalization. *Regul Pept* 91:29–44.

Kim J, Ahn S, Ren XR, Whalen EJ, Reiter E, Wei H, and Lefkowitz RJ (2005) Functional antagonism of different G protein-coupled receptor kinases for beta-arrestin-mediated angiotensin II receptor signaling. *Proc Natl Acad Sci USA* 102:1442–1447.
Kim KS, Abraham D, Williams B, Violin JD, Mao L, and Rockman HA (2012) β-Arrestin-biased AT1R stimulation promotes cell survival during acute cardiac injury. *Am J Physiol Heart Circ Physiol* 303:H1001–H1010.
Le MT, Vanderheyden PM, Szaszák M, Hunyady L, and Vauquelin G (2002) Angiotensin IV is a potent agonist for constitutive active human AT1 receptors. Distinct roles of the N-and C-terminal residues of angiotensin II during AT1 receptor activation. *J Biol Chem* 277:23107–23110.
Lefkowitz RJ (2007) Seven transmembrane receptors: something old, something new. *Acta Physiol (Oxf)* 190:9–19.
Li H, Li HF, Felder RA, Periasamy A, and Jose PA (2008) Rab4 and Rab11 coordinately regulate the recycling of angiotensin II type 1 receptor as demonstrated by fluorescence resonance energy transfer microscopy. *J Biomed Opt* 13:031206.
Luttrell LM, Roudabush FL, Choy EW, Miller WE, Field ME, Pierce KL, and Lefkowitz RJ (2001) Activation and targeting of extracellular signal-regulated kinases by beta-arrestin scaffolds. *Proc Natl Acad Sci USA* 98:2449–2454.
Maxfield FR and McGraw TE (2004) Endocytic recycling. *Nat Rev Mol Cell Biol* 5:121–132.
Orlandi PA and Fishman PH (1998) Filipin-dependent inhibition of cholera toxin: evidence for toxin internalization and activation through caveolae-like domains. *J Cell Biol* 141:905–915.
Qian H, Pipolo L, and Thomas WG (2001) Association of beta-arrestin 1 with the type 1A angiotensin II receptor involves phosphorylation of the receptor carboxyl terminus and correlates with receptor internalization. *Mol Endocrinol* 15:1706–1719.
Reiter E, Ahn S, Shukla AK, and Lefkowitz RJ (2012) Molecular mechanism of β-arrestin-biased agonism at seven-transmembrane receptors. *Annu Rev Pharmacol Toxicol* 52:179–197.
Sallese M, Mariggiò S, D'Urbano E, Iacovelli L, and De Blasi A (2000) Selective regulation of Gq signaling by G protein-coupled receptor kinase 2: direct interaction of kinase N terminus with activated galphaq. *Mol Pharmacol* 57:826–831.
Saraste J and Goud B (2007) Functional symmetry of endomembranes. *Mol Biol Cell* 18:1430–1436.
Seachrist JL and Ferguson SS (2003) Regulation of G protein-coupled receptor endocytosis and trafficking by Rab GTPases. *Life Sci* 74:225–235.
Seachrist JL, Laporte SA, Dale LB, Babwah AV, Caron MG, Anborgh PH, and Ferguson SS (2002) Rab5 association with the angiotensin II type 1A receptor promotes Rab5 GTP binding and vesicular fusion. *J Biol Chem* 277:679–685.
Soergel DG, Subach RA, Cowan CL, Violin JD, and Lark MW (2013) First clinical experience with TRV027: pharmacokinetics and pharmacodynamics in healthy volunteers. *J Clin Pharmacol* 53:892–899.
Sönnichsen B, De Renzis S, Nielsen E, Rietdorf J, and Zerial M (2000) Distinct membrane domains on endosomes in the recycling pathway visualized by multicolor imaging of Rab4, Rab5, and Rab11. *J Cell Biol* 149:901–914.
Szidonya L, Süpeki K, Karip E, Turu G, Várnai P, Clark AJ, and Hunyady L (2007) AT1 receptor blocker-insensitive mutant AT1A angiotensin receptors reveal the presence of G protein-independent signaling in C9 cells. *Biochem Pharmacol* 73:1582–1592.
Takahashi S, Kubo K, Waguri S, Yabashi A, Shin HW, Katoh Y, and Nakayama K (2012) Rab11 regulates exocytosis of recycling vesicles at the plasma membrane. *J Cell Sci* 125:4049–4057.
Tóth DJ, Tóth JT, Gulyás G, Balla A, Balla T, Hunyady L, and Várnai P (2012) Acute depletion of plasma membrane phosphatidylinositol 4,5-bisphosphate impairs specific steps in endocytosis of the G-protein-coupled receptor. *J Cell Sci* 125:2185–2197.
Turu G, Szidonya L, Gáborik Z, Buday L, Spät A, Clark AJ, and Hunyady L (2006) Differential beta-arrestin binding of AT1 and AT2 angiotensin receptors. *FEBS Lett* 580:41–45.
Várnai P and Balla T (1998) Visualization of phosphoinositides that bind pleckstrin homology domains: calcium- and agonist-induced dynamic changes and relationship to myo-[3H]inositol-labeled phosphoinositide pools. *J Cell Biol* 143:501–510.
Violin JD, Crombie AL, Soergel DG, and Lark MW (2014) Biased ligands at G-protein-coupled receptors: promise and progress. *Trends Pharmacol Sci* 35:308–316.
Violin JD, DeWire SM, Yamashita D, Rominger DH, Nguyen L, Schiller K, Whalen EJ, Gowen M, and Lark MW (2010) Selectively engaging β-arrestins at the angiotensin II type 1 receptor reduces blood pressure and increases cardiac performance. *J Pharmacol Exp Ther* 335:572–579.
Wei H, Ahn S, Shenoy SK, Karnik SS, Hunyady L, Luttrell LM, and Lefkowitz RJ (2003) Independent beta-arrestin 2 and G protein-mediated pathways for angiotensin II activation of extracellular signal-regulated kinases 1 and 2. *Proc Natl Acad Sci USA* 100:10782–10787.
Whalen EJ, Rajagopal S, and Lefkowitz RJ (2011) Therapeutic potential of β-arrestin- and G protein-biased agonists. *Trends Mol Med* 17:126–139.
Woo J and von Arnim AG (2008) Mutational optimization of the coelenterazine-dependent luciferase from Renilla. *Plant Methods* 4:23.
Zerial M and McBride H (2001) Rab proteins as membrane organizers. *Nat Rev Mol Cell Biol* 2:107–117.
Zhang J, Ferguson SS, Barak LS, Ménard L, and Caron MG (1996) Dynamin and beta-arrestin reveal distinct mechanisms for G protein-coupled receptor internalization. *J Biol Chem* 271:18302–18305.

Address correspondence to: Dr. László Hunyady, H-1444 Budapest, P. O. Box 259, Hungary. E-mail: Hunyady@eok.sote.hu

MOL #97030

Supplementary data file

Article's title: Investigation of the fate of type I angiotensin receptor after biased activation

Authors: Gyöngyi Szakadáti, András D. Tóth, Ilona Oláh, László Sándor Erdélyi, Tamas Balla, Péter Várnai, László Hunyady, András Balla

Department of Physiology (G.S., A.D.T., I.O., L.S.E., P.V., L.H. A.B.), Semmelweis University, Faculty of Medicine, H-1444 Budapest, Hungary

MTA-SE Laboratory of Molecular Physiology (L.S.E., P.V., L.H. A.B.), Hungarian Academy of Sciences and Semmelweis University, H-1094 Budapest, H-1094 Budapest, Hungary

Section on Molecular Signal Transduction (T.B.), Program for Developmental Neuroscience, Eunice Kennedy Shriver National Institute of Child Health and Human Development, National Institutes of Health, Bethesda, MD 20892

Running title: Fate of biased activated AT_1-receptor

Supplemental Figure 1.
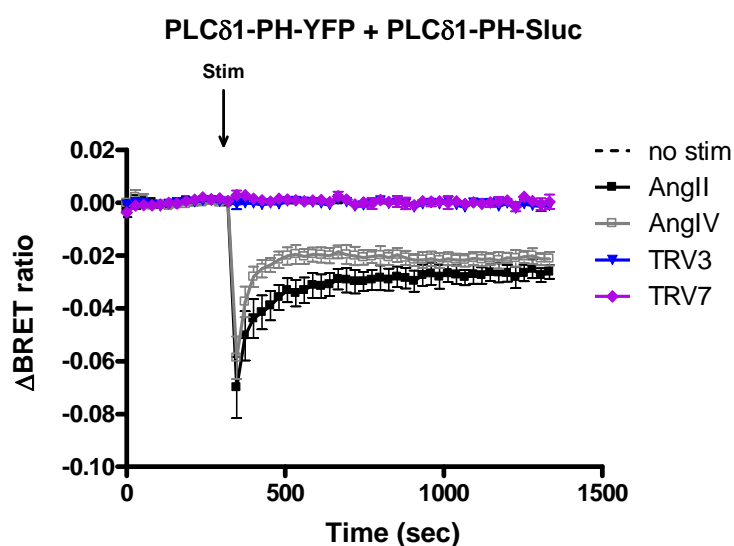
Supplemental Figure 1. Effects of AT$_1$-R agonist stimulation on PtdIns(4,5)P_2 breakdown in HEK293 cells. HEK293 cells were transfected with the plasmids of the AT$_1$-R, PLCδ1-PH-YFP and PLCδ1-PH-Sluc, and after 24 hours the cells were exposed to either 100 nM AngII (black trace), 1 μM TRV120023 (labeled as TRV3, blue trace), 1 μM TRV120027 (labeled as TRV7, purple trace), 10 μM AngIV (grey trace), or vehicle (dashed lines) at the indicated time point. The BRET records are average of 3 independent experiments. Mean values $\pm$ SEM are shown (n = 3).

Supplemental Figure 2.
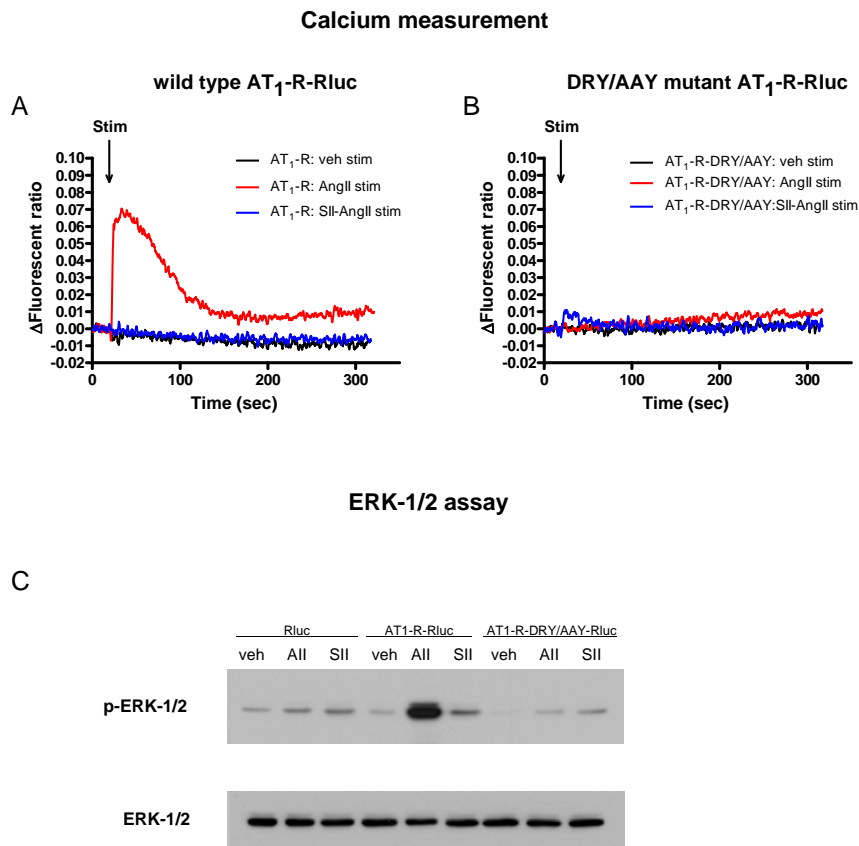
Supplemental Figure 2. Functional analysis of the AT_1-R-Rluc and AT_1-R-DRY/AAY-Rluc. HEK293 cells were transfected with the plasmids of the indicated AT_1-R-luciferase (wild type or DRY/AAY mutant), and after 24 hours the cells were used for studies. (A-B) Cytoplasmic Ca^{2+} measurement. The Fura-2-loaded HEK293 cells were exposed to either 100 nM AngII (red trace), 10 μM SII-AngII (blue trace), or vehicle (black trace) at the indicated time points. The curves are representative of 3 independent experiments. (C) ERK-1/2 MAPK activation. HEK293 cells were exposed to vehicle, 100 nM AngII or 10 μM SII-AngII for 5 min. The western blot is a representative of 3 independent experiments.

3

Supplemental Figure 3.
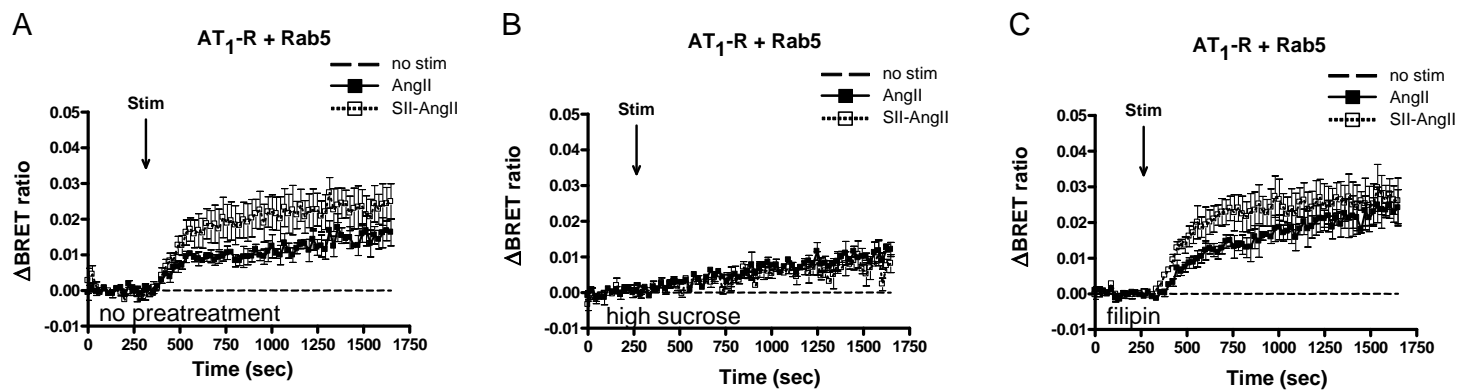
Supplemental Figure 3. BRET assay between AT$_1$-R and Rab5 upon either AngII or SII-AngII stimulation in HEK293 cells. HEK293 cells were transfected with the plasmids of the AT$_1$-R-Rluc and with Rab5-YFP proteins, and after 24 hours the experiments were carried out. Cells were pretreated for 30 min with vehicle BRET medium (**A**), BRET medium supplemented with 300 mM sucrose (**B**), or 5 μg/ml filipin (**C**) and exposed to either vehicle (dashed line) or 100 nM AngII (black filled symbols) or 10 μM SII-AngII (grey open symbols) at the indicated time points. The BRET curves are average of 3 independent experiments, each performed in triplicates. Mean values ± SEM are shown (n = 3).

Supplemental Figure 4.
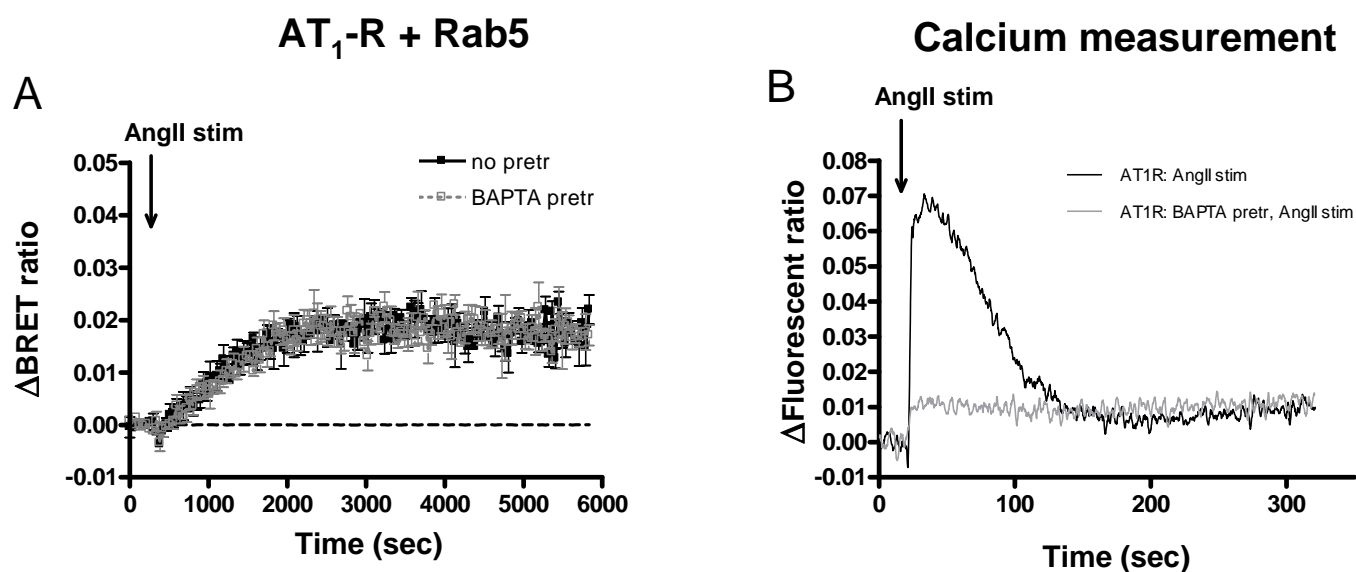
Supplemental Figure 4. Effect of intracellular Ca^{2+} chelation on AT$_1$-R internalization upon AngII stimulation in HEK293 cells. HEK293 cells were transfected with the plasmids of the AT$_1$-R-Rluc and with either Rab5-YFP (A) or PLCδ1-PH-YFP (C), and after 24 hours the cells were pretreated for 30 min with either vehicle BRET medium (black traces) or BRET medium supplemented with 10 μM BAPTA-AM for 30-45 min (grey traces) and exposed to either vehicle (dashed line, A and B) or 100 nM AngII (A-C) or 10 μM ionomycin (C) at the indicated time points. The BRET curves (A and C) are average of 3 independent experiments, each performed in triplicates, mean values ± SEM are shown (n = 3); the fluorescent ratio curves for the cytoplasmic Ca^{2+} measurements (B) are representative of 3 independent experiments.

Supplemental Figure 5.
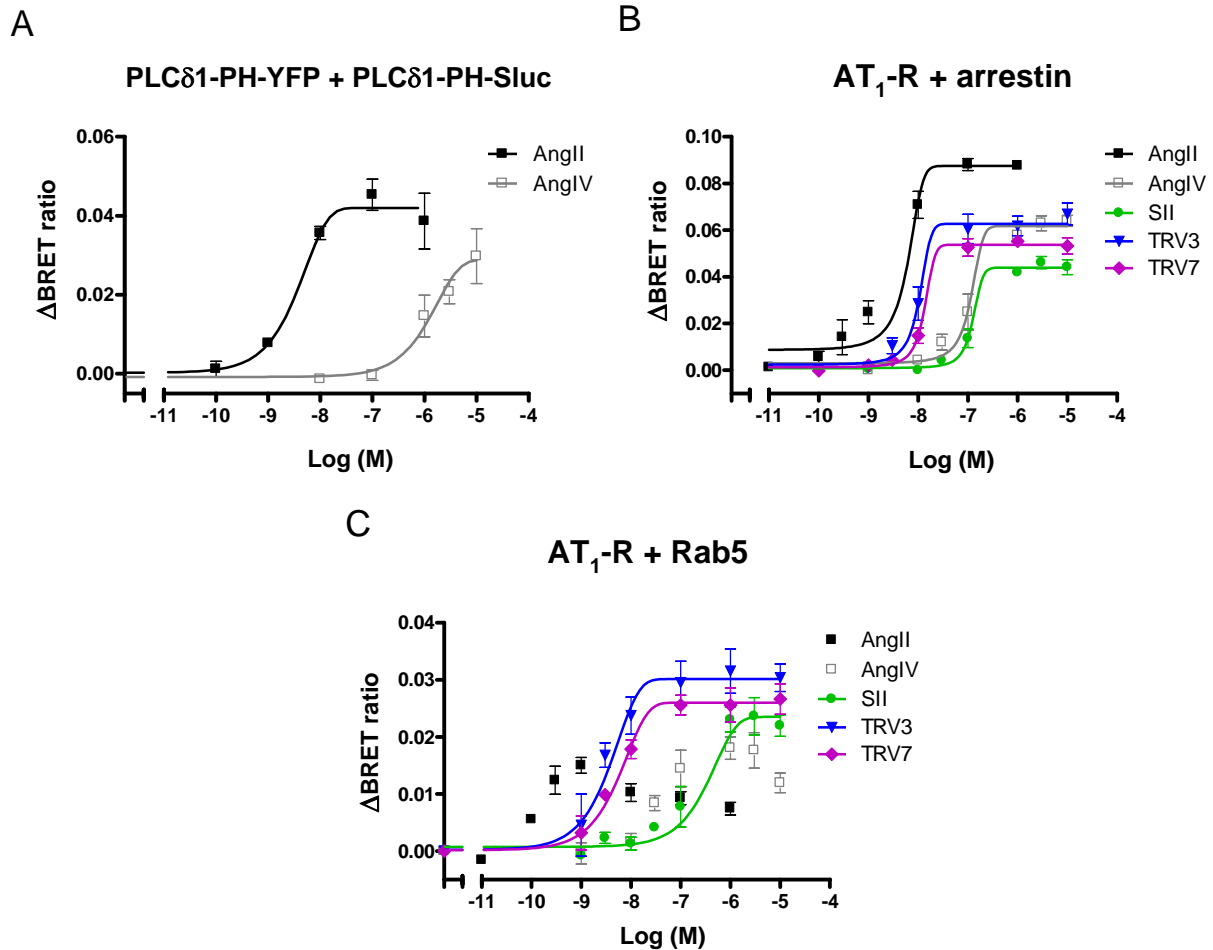
**Supplemental Figure 5. Dose-response curves of AT$_1$-R induced PtdIns(4,5)P_2 hydrolysis (A), β-arrestin2 binding (B), and Rab5 recruitment (C) in HEK293 cells.** HEK293 cells were transfected with the plasmids of the AT$_1$-R, PLCδ1-PH-YFP and PLCδ1-PH-Sluc (A), AT$_1$-R-Rluc and β-arrestin2-YFP (B), AT$_1$-R-Rluc and Rab5-YFP (C) and after 24 hours the cells were exposed to various concentrations of AngII, AngIV, SII-AngII, TRV120023 (labeled as TRV3), TRV120027 (labeled as TRV7). The BRET records are average of 3 independent experiments, and the following data points were used for the calculations: (A) BRET values in the first minute after stimulation, (B) BRET values between 5-6 minutes after stimulation, (C) BRET values between 9-11 minutes after stimulation. Mean values ± SEM are shown (n = 3).

MOL #97030

Supplemental Figure 6.
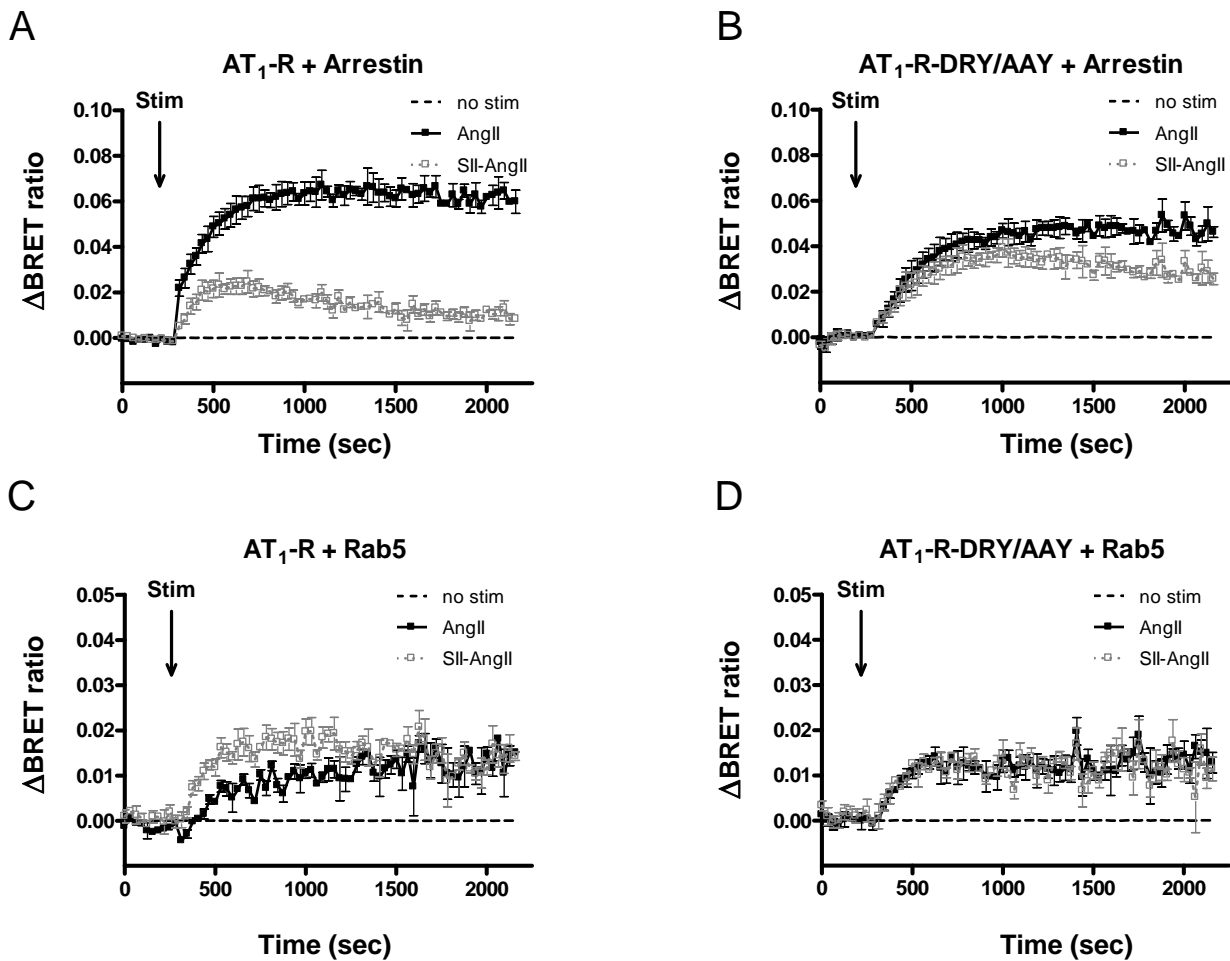
Supplemental Figure 6. BRET assay between wild type or mutant AT$_1$-Rs and β-arrestin2 or Rab5 upon either AngII or SII-AngII stimulation in HEK293 cells. HEK293 cells were transfected with the plasmids of the indicated receptor-Rluc and with either β-arrestin2-YFP (A-B) or Rab5-YFP (C-D), and after 24 hours the cells were exposed to either vehicle (dashed line) or 100 nM AngII (black filled symbols) or 10 μM SII-AngII (grey open symbols) at the indicated time points. BRET pairs: (A) AT$_1$-R-Rluc and β-arrestin2-YFP; (B) AT$_1$-R-DRY/AAY-Rluc and β-arrestin2-YFP; (C) AT$_1$-R-Rluc and Rab5-YFP; (D) AT$_1$-R-DRY/AAY-Rluc and Rab5-YFP. The BRET records are average of at least 3 independent experiments. Mean values ± SEM are shown (n = 3).

7

Supplemental Figure 7.
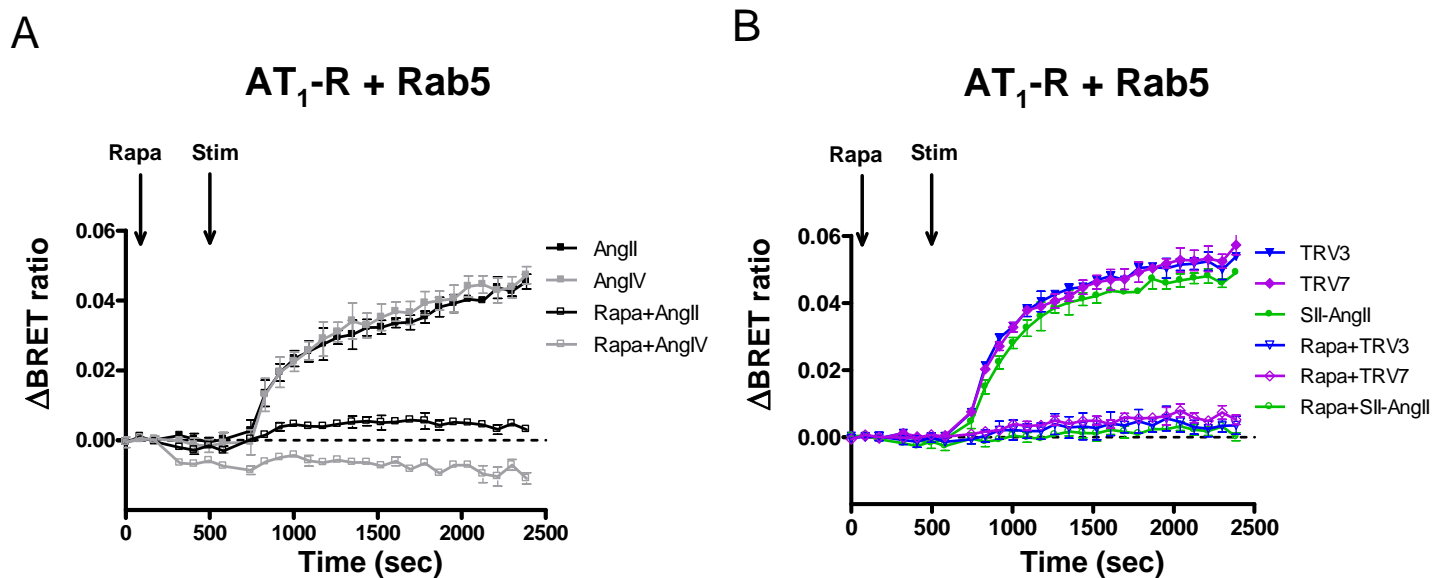
Supplemental Figure 7. Plasma membrane PtdIns(4,5)P_2 depletion effects AT$_1$-R internalization. HEK293T cells were transfected with plasmids encoding AT1-R-Rluc, Venus-Rab5, PM-FRB-mRFP and mRFP-FKBP-5ptase. After 24 hours the cells were pretreated with either rapamycin (300 nM) or vehicle (DMSO) for 5 minutes, followed by stimulation with the indicated agonists (100 nM AngII, 1 μM TRV120023, 1 μM TRV120027, 10 μM SII-AngII or 10 μM AngIV) and (A) Rab5 recruitment and (B) β-arrestin2 binding were detected in BRET measurements.

Supplemental Figure 8.

A

B
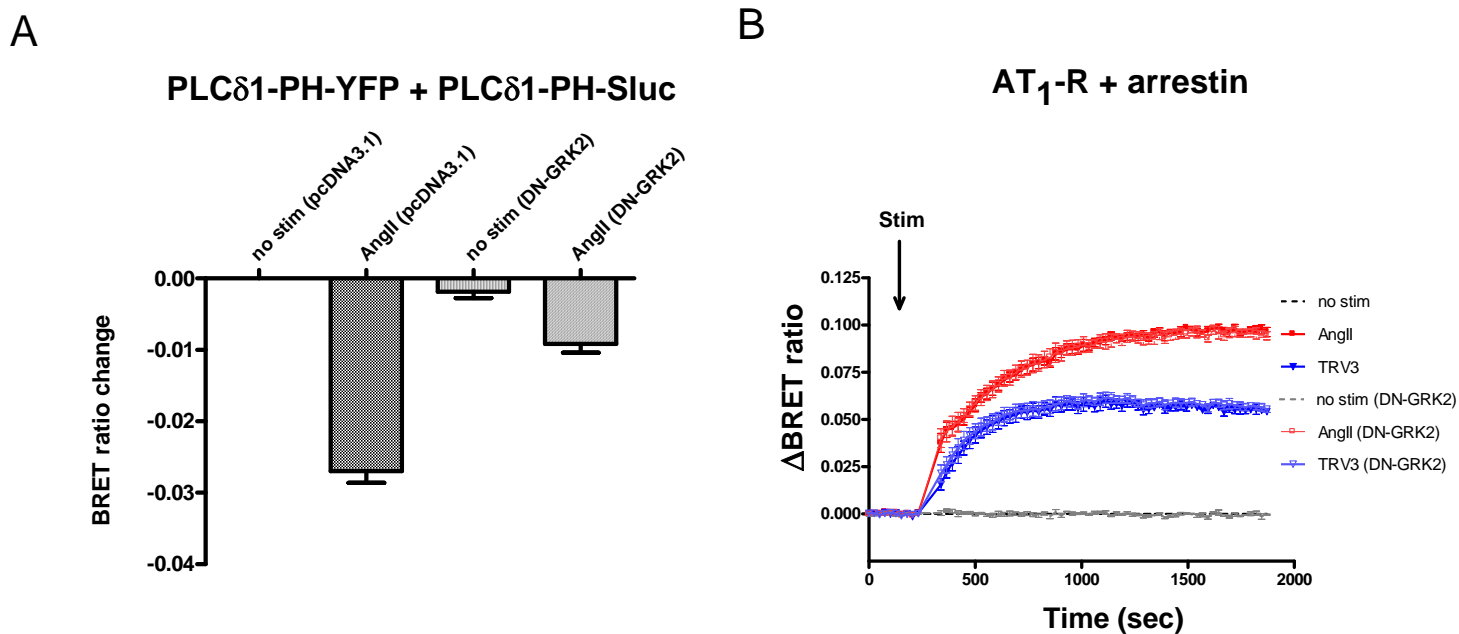
Supplemental Figure 8. Effects of DN-GRK overexpression on plasma membrane PtdIns(4,5)P_2 hydrolysis and β-arrestin2 binding of AT$_1$-R. HEK293 cells were transfected with plasmids encoding (A) DN-GRK2, AT$_1$-R, PLCδ1-PH-YFP and PLCδ1-PH-Sluc, or (B) DN-GRK2, AT$_1$-R-Rluc and β-arrestin2-YFP. (A) The cells were exposed to 100 nM AngII and the PtdIns(4,5)P_2 hydrolysis caused BRET ratio change was detected for three minutes. (B) The cells were exposed to either 100 nM AngII (red trace), 1 μM TRV120023 (labeled as TRV3, blue trace), or vehicle (dashed lines) at the indicated time point. The BRET records are average of 3 independent experiments. Mean values ± SEM are shown (n = 3).

cells

Article

Characterization of Type 1 Angiotensin II Receptor Activation Induced Dual-Specificity MAPK Phosphatase Gene Expression Changes in Rat Vascular Smooth Muscle Cells

Janka Borbála Gém [1,†], Kinga Bernadett Kovács [1,†], Laura Szalai [1,2], Gyöngyi Szakadáti [1], Edit Porkoláb [1,2], Bence Szalai [1], Gábor Turu [1,2], András Dávid Tóth [1,2,3], Mária Szekeres [1,4], László Hunyady [1,2,*] and András Balla [1,2,*]

1   Department of Physiology, Faculty of Medicine, Semmelweis University, 1085 Budapest, Hungary; gem.janka@phd.semmelweis.hu (J.B.G.); kovacs.kinga@phd.semmelweis.hu (K.B.K.); laura.szalai42@gmail.com (L.S.); szakadati.gyongyi@gmail.com (G.S.); porkolabeda@gmail.com (E.P.); ben.szalai@gmail.com (B.S.); turu.gabor@med.semmelweis-univ.hu (G.T.); toth.andras1@med.semmelweis-univ.hu (A.D.T.); szekeres.maria@med.semmelweis-univ.hu (M.S.)
2   MTA-SE Laboratory of Molecular Physiology, Hungarian Academy of Sciences and Semmelweis University, 1085 Budapest, Hungary
3   Department of Internal Medicine and Hematology, Semmelweis University, 1085 Budapest, Hungary
4   Department of Morphology and Physiology, Faculty of Health Sciences, Semmelweis University, 1085 Budapest, Hungary
*   Correspondence: hunyady.laszlo@med.semmelweis-univ.hu (L.H.); balla.andras@med.semmelweis-univ.hu (A.B.); Tel.: +36-1-459-1500/60401 (L.H.); +36-1-459-1500/60450 (A.B.); Fax: +36-1-266-6504 (L.H.); +36-1-266-6504 (A.B.)
†   These authors contributed equally to this work.

Abstract: Activation of the type I angiotensin receptor (AT1-R) in vascular smooth muscle cells (VSMCs) plays a crucial role in the regulation of blood pressure; however, it is also responsible for the development of pathological conditions such as vascular remodeling, hypertension and atherosclerosis. Stimulation of the VSMC by angiotensin II (AngII) promotes a broad variety of biological effects, including gene expression changes. In this paper, we have taken an integrated approach in which an analysis of AngII-induced gene expression changes has been combined with the use of small-molecule inhibitors and lentiviral-based gene silencing, to characterize the mechanism of signal transduction in response to AngII stimulation in primary rat VSMCs. We carried out Affymetrix GeneChip experiments to analyze the effects of AngII stimulation on gene expression; several genes, including *DUSP5*, *DUSP6*, and *DUSP10*, were identified as upregulated genes in response to stimulation. Since various dual-specificity MAPK phosphatase (DUSP) enzymes are important in the regulation of mitogen-activated protein kinase (MAPK) signaling pathways, these genes have been selected for further analysis. We investigated the kinetics of gene-expression changes and the possible signal transduction processes that lead to altered expression changes after AngII stimulation. Our data shows that the upregulated genes can be stimulated through multiple and synergistic signal transduction pathways. We have also found in our gene-silencing experiments that epidermal growth factor receptor (EGFR) transactivation is not critical in the AngII-induced expression changes of the investigated genes. Our data can help us understand the details of AngII-induced long-term effects and the pathophysiology of AT1-R. Moreover, it can help to develop potential interventions for those symptoms that are induced by the over-functioning of this receptor, such as vascular remodeling, cardiac hypertrophy or atherosclerosis.

Keywords: angiotensin II (AngII); dual-specificity MAPK phosphatase (DUSP); epidermal growth factor receptor (EGFR); G protein-coupled receptor (GPCR); mitogen-activated protein kinase (MAPK); type 1 angiotensin receptor (AT$_1$-R); vascular smooth muscle cell (VSMC)

1. Introduction

Angiotensin II (AngII) is an octapeptide hormone that is the main effector of the renin-angiotensin system, and participates in the physiological and pathological mechanisms leading to cardiovascular diseases. The resulting pathophysiological changes, such as vascular remodeling, atherosclerosis and hypertension, are mainly due to the exaggerated action of AngII, which results in hyperplasia and hypertrophy in the cardiovascular tissues [1]. AngII most importantly acts through the type 1 angiotensin II receptor (AT_1-R), a versatile G protein-coupled receptor (GPCR) that is able to promote a broad variety of biological effects, both short-term and long-term [1,2]. AngII regulates the vascular tone in vascular smooth muscle cells (VSMCs) and it is also an important regulator of cell proliferation and vascular remodeling. The AT_1-R largely acts via heterotrimeric $G_{q/11}$ activation in VSMCs, resulting in second messenger generation (Ca^{2+} signal via inositol trisphosphate and diacylglycerol) upon agonist binding. This "classical" $G_{q/11}$ protein-mediated signaling mechanism is responsible for the majority of AngII-evoked physiological responses in target cells, but AT_1-R is able to activate $G_{i/o}$ or $G_{12/13}$ proteins as well [3,4]. In addition, there are other AT_1-R-mediated signaling mechanisms that are AngII-induced and independent of G protein coupling [5].

AngII stimulation also triggers the activation of receptor tyrosine kinases, among which EGFR transactivation plays the most important role in the cardiovascular system [1]. EGFR transactivation is mediated by matrix metalloprotease activation, which causes the shedding of heparin-binding epidermal growth factor-like growth factor (HB–EGF) resulting in agonist release and binding to EGFR [6,7]. The EGFR transactivation has been proven to be an important factor in the long-term effects of AngII in VSMCs, including cell proliferation. It is also responsible for the development of several pathophysiological conditions in the cardiovascular system, such as vascular remodeling and atherosclerosis [1]. In addition to EGFR transactivation, platelet-derived growth factor receptor and insulin-like growth factor I receptor transactivation appears to be important in cardiovascular cells [1].

The vascular smooth muscle is one of the main targets of AngII. Its stimulation activates numerous signaling pathways that cause contraction and could also result in gene expression changes in VSMCs (Supplementary Figure S1). Although much is understood regarding the mechanisms involved in the regulation of AngII-induced gene expression in various cells [8–13], less information is available about the signal transduction pathways involved in primary VSMCs. In this work, we used rat primary isolated VSMCs for our studies to provide more relevant results than we could achieve by studying immortalized cell lines. Although rat primary VSMCs can be maintained up to 20–30 passages, it was demonstrated that primary cultured VSMCs undergo phenotypic modulations [14]. These changes can manifest as early as 7–9 days into primary cell culturing [15]. We carried out the experiments up to 3 passages in order to keep the molecular machinery of the cells as similar to their in vivo conditions as possible.

Mitogen-activated protein kinases (MAPKs), such as ERK1/2, JNK, and p38 MAPK, play an important role in the regulation of various functions in VSMCs and they are general mediators of AngII-evoked cellular responses [16]. The MAPKs require dual phosphorylation of both threonine and tyrosine residues within their activation motif for activation by MAPK kinases. The duration and the magnitude of MAPK activation determine cellular functions such as cell proliferation, gene expression, differentiation, cell death, and metabolism. The activation states of MAPKs are primarily regulated by a family of dual-specificity MAPK phosphatases (DUSPs). DUSPs can dephosphorylate both threonine and tyrosine residues within their activation loop. In addition, they control the duration and the spatiotemporal properties of the MAPK pathways; hence, they are important regulators of MAPK signaling in the cells [17,18]. Interestingly, the binding of DUSPs to MAPKs does not require the phosphorylated, active state of the MAPKs; thus, DUSPs can regulate the availability of various MAPKs and they serve as versatile regulators of MAPK signaling. To date, at least 11 DUSPs have been described in the regulation of activity patterns of MAPKs. DUSPs can be divided into three subfamilies, based on domain structure and subcellular

localization [18,19]. DUSP1, DUSP2, DUSP4 and DUSP5 are localized in the nucleus where they can dephosphorylate all three MAPKs, whereas DUSP6, DUSP7 and DUSP9 largely dephosphorylate ERK1/2 MAPK in the cytoplasm. DUSP8, DUSP10, DUSP14 and DUSP16 can be localized in both the nucleus and the cytoplasm, and they mainly regulate the JNK and p38 MAPKs, except for DUSP8, which is more specific for ERK1/2 [20]. The various DUSPs are transiently induced by cellular stresses, or mitogens such as growth factors, and affect the activity of MAPKs. It is well established that their activity and expression are dependent on the regulated MAPKs, thus providing a feedback loop [18].

In the present study, we have sought to investigate the change in transcriptome and identify novel, potentially important but not yet well-characterized proteins that are involved in the action of AngII using primary VSMCs up to their 3 passages. Our transcriptome analysis revealed the upregulation of several DUSP genes, such as *DUSP4*, *5*, *6*, *10*, and *14*. In our further analysis, we have chosen one DUSP gene from each subfamily (based on their intracellular localization), such as *DUSP5*, *DUSP6*, and *DUSP10*, to investigate gene expression changes in response to AngII stimulation.

2. Materials and Methods

2.1. Materials

Cell culture dishes and plates were purchased from Greiner (Kremsmunster, Austria). Unless otherwise stated, all molecular biology and cell-culture reagents were from Thermo Fisher Scientific (Waltham, MA, USA). Fast Start Essential DNA Green Master Mix was sourced from Roche Applied Science (Basel, Switzerland). The RNeasy Plus Mini Kit was from Qiagen (Hilden, Germany). To maintain cell cultures, Dulbecco's Modified Eagle Medium (DMEM) was purchased from Biosera (Nuaille, France). Heat-inactivated fetal bovine serum, Glutamax and penicillin/streptomycin were supplied by Invitrogen (Carlsbad, CA, USA). Immobilon Western Chemiluminescent HRP substrate was purchased from Merck-Millipore (Billerica, MA, USA), Radiance Plus Femtogram HRP substrate was obtained from Azure Biosystems (Dublin, CA, USA). Glycerol, sodium dodecyl sulfate (SDS) and 40% acrylamide/bis solution were obtained from Serva (Heidelberg, Germany). Tween 20 and 2-mercapto-ethanol, bromophenol blue, phosphatase inhibitor cocktail 2 were purchased from Sigma-Aldrich (St. Louis, MO, USA). The protease inhibitor cOmplete used in sample preparation for immunoblotting was obtained from Roche Applied Science (Basel, Switzerland). Immunoblot signals were detected with an Azure c600 device (Azure Biosystems, Dublin, CA, USA). The Lenti-X Concentrator kit was from Takara Bio (Kusatsu, Japan). To measure lentivirus concentrations, we used a Lentivirus Titer Kit (Applied Biological Materials, Vancouver, Canada). AngII, EGF, AG1024, AG538, AG1478, BAPTA-AM, CK59, Gefitinib, MMP-2/MMP-9 Inhibitor II, PD98059 and PF 562271 were purchased from Sigma-Aldrich (St. Louis, MO, USA). YM-254890 was obtained from Wako Chemicals (Neuss, Germany). TRV120023 (Sar-Arg-Val-Tyr-Lys-His-Pro-Ala-OH) peptide was synthesized by Proteogenix (Schiltigheim, France) to more than 98% purity. Gefitinib, Sorafenib and Sunitinib were synthesized by Vichem Chemie Research Ltd. (Budapest, Hungary) as members of NCL (Nested Chemical Library). The purity of the compounds was > 99%, determined by LC-MS and NMR. Anti-pERK1/2, anti-pEGFR, anti-mouse-HRP and anti-rabbit-HRP were sourced from Cell Signaling Technologies (Danvers, MA, USA). Anti-α-actin, anti-β-actin antibodies and DAPI (4′,6-diamidino-2-phenylindole, dihydrochloride) were obtained from Sigma-Aldrich (St. Louis, MO, USA). Alexa Fluor 488 conjugated anti-mouse IgG was obtained from Invitrogen (Carlsbad, CA, USA).

The human embryonic kidney (HEK293T) cells were sourced from ATCC (ATCC CRL-3216; American Type Culture Collection, Manassas, VA, USA). Unless otherwise stated, all other chemicals and reagents were purchased from Sigma-Aldrich (St. Louis, MO, USA).

2.2. Animals

Male Wistar rats were used for the preparation of primary VSMCs (170–250 g, Charles River Laboratories-Semmelweis University, Budapest, Hungary). They were kept on a

standard semisynthetic diet. The animals were then sacrificed by decapitation and rapid bleeding. The investigation conformed to the Guide for the Care and Use of Laboratory Animals (NIH, 8th edition, 2011) as well as to national legal and institutional guidelines for animal care. They were approved by the Animal Care Committee of the Semmelweis University, Budapest, and by the Hungarian authorities (No. 001/2139-4/2012). All procedures followed legal and institutional guidelines of animal care.

2.3. Isolation of VSMCs

The rat VSMCs were isolated according to the standard explant method [21]. Briefly, to isolate appropriate amounts of cells for our experiments, over a one-week period, two animals were sacrificed by decapitation and rapid bleeding. After removal of the connective tissue and the adherent fat, the thoracic aorta was excised. The aorta was cut into small sections and the VSMCs were allowed to grow out from the explant for 7–14 days. The VSMCs were maintained by passaging with trypsin and were used between passages 2 and 3 (typically, the experiments were performed at passage 3). We used 4–5 million cells weekly for our experiments. The expression of smooth muscle α-actin was confirmed by immunochemistry (Supplementary Figure S1A). The isolated VSMCs exhibited a normal response to AngII stimulation, such as calcium signals and ERK activation (Supplementary Figure S1B, other data not shown).

2.4. Cell Culture

The experiments were conducted on a rat aortic primary isolated VSMC cell line, whereas the lentiviral particles were made using the HEK293T cell line. The cells were subcultured in DMEM supplemented with 10% heat-inactivated fetal bovine serum, 1% Glutamax and 100 IU/mL penicillin/streptomycin, in 5% CO_2 at 37 °C. For each experiment, VSMCs were transferred onto 6-well plates and were used at approximately 90% confluency. Before the experiments, VSMCs were made quiescent by incubating them in serum-free DMEM for 16–24 h.

2.5. Affymetrix GeneChip

After serum deprivation, VSMCs were stimulated with 100 nM AngII for 2 h at 37 °C, then the cells were lysed in Trizol reagent. The quality control of the RNA samples was checked using an Agilent BioAnalyzer RNA Nano lab chip before the array experiments. The total RNA isolation and the Affymetrix Rat Gene 1.0 ST GeneChip Array (Affymetrix, Santa Clara, CA, USA) analysis were performed by UD-GenoMed Medical Genomic Technologies Ltd., University of Debrecen, Debrecen, Hungary). Hybridization and an image scan were performed according to the protocol of UD-GenoMed Medical Genomic Technologies Ltd. The microarray experiment was performed in triplicate. Raw CEL files were background-corrected and normalized using the *oligo* R package [22], and differential expression (Angiotensin II-Vehiculum) analysis was performed using the *limma* R package [22]. We used *PROGENy* pathway activity analysis tool to identify AngII induced pathway activity changes [23,24]. Calculated *PROGENy* pathway activity scores were normalized to null distribution (created by 10,000 random permutations of gene names) to create pathway activity z-scores.

2.6. DNA Constructs

For the construction of gene-silencing transfer plasmids, pLKO.1 puro vector was used. This was a gift from Dr. Bob Weinberg (Addgene plasmid #8453; http://n2t.net/addgene:8453; access date: 9 December 2021; RRID: Addgene_8453) [25]. The AgeI and EcoRI restriction sites of the pLKO.1 puro vector and the following sequences transcribing short-hairpin RNAs, specific to rat EGFR, were used: shRNA#1: 5′-GCATAGGCATTGGTGAATTTA-3′ shRNA#2: 5′-GGAAATCACCTATGTGCAAAG-3′ or scrambled sequence (control). The oligos were obtained from Sigma-Aldrich.

2.7. RNA Extraction and Real-Time PCR

Cells were washed twice with sterile PBS (137 mM NaCl; 2.7 mM KCl 2.7; 10.1 mM Na_2HPO_4; 1.8 mM KH_2PO_4, pH 7.4), and the total RNA was isolated with an RNeasy Plus Mini kit from Qiagen. RNA concentrations were determined spectrophotometrically via absorbance at 260 nm and purity was assessed by the 260/280 and 230/260 nm ratios. Reverse transcription from total RNA was carried out using a RevertAid Reverse Transcription Kit according to the manufacturer's instructions. Gene expression levels were quantified by quantitative real-time PCR (qRT-PCR). The measurements were performed using the SYBR Green method (SYBR Green I Master, Roche, Basel, Switzerland) using a LightCycler 480. The primers were synthesized by Sigma-Aldrich and designed so that the amplicon sizes were between 100 and 200 base pairs. Efficiency for each primer pair was determined by using serial dilutions of the PCR product.

The thermal cycling program started with pre-incubation at 95 °C for 5 min, followed by amplification via 45 cycles of 10 s at 95 °C, 5 s at 62 °C and 15 s at 72 °C, melting curve 5 s at 95 °C, 1 min at 65 °C and 97 °C, and cooling for 30 s at 40 °C. Fluorescence data including melting curves were obtained. The cycle threshold (Ct) was calculated via the second derivative method using LightCycler 480 Software. ΔCt represents the difference in Ct values obtained between the reference and the tested samples. For normalization, the glyceraldehyde-3-phosphate dehydrogenase (*GAPDH*) housekeeping gene was used. Gene expression levels were plotted against the *GAPDH* expression level. Fold ratios of gene expression were calculated as follows: ratio = $E^{\Delta Ct \, target \, gene}/E^{\Delta Ct \, GAPDH}$. The following primers were used for qRT-PCR determinations (5′-3′): GAPDH: Forward CCT GCA CCA CCA ACT GCT TAG, Reverse CAG TCT TCT GAG TGG CAG TGA TG; DUSP5: Forward GGC AAG GTC CTG GTT CAC TGT, Reverse GTT GGG AGA GAC CAC GCT CCT; DUSP6: Forward ATC ACT GGA GCC AAA ACC TG, Reverse CGT TCA TGG ACA AGT TGA GC; DUSP10 Forward GGC AAA GAA CCC CTG GTA TT, Reverse AGA AAC AGG AAG GGC AGG AT; EGFR Forward CAT CCA GTG CCA TCC AGA AT, Reverse CTT CCA GAC CAG GGT GTT GT.

2.8. Treatment Protocols

Before the experiments, VSMCs were made quiescent by incubating in serum-free DMEM for 16–24 h. For the time-dependency determinations, the serum-starved cells were stimulated with 100 nM AngII for 1–6 h. During the examination of inhibitor effects, the cells were pretreated with the appropriate inhibitor for 30 min, then stimulated for 2 h with 100 nM AngII or 50 ng/mL EGF. BAPTA-AM and RO31-8425 pretreatments were used for 10 min before the 2-h agonist stimulation of the cells.

2.9. Lentivirus Production

Lentiviruses were produced by co-transfecting HEK293T cells on 10-cm dishes with pLKO.1puro transfer, the pCMV-VSV-G envelope and pCMV-dR8.2 packaging plasmids (gift from Dr. Bob Weinberg, [25], purchased from Addgene) using the calcium phosphate precipitation method. In summary, plasmid DNAs were mixed in sterile distilled water, then 2.5 M $CaCl_2$ was added (final concentration: 125 mM) and the solution was mixed dropwise with 2× HEPES-buffered solution [HBS] (42 mM HEPES, 15 mM D-glucose, 1.4 mM Na_2HPO_4, 10 mM KCl, 274 mM NaCl 274 mM, pH 7.1). This mixture was added dropwise to attached cells and the medium was replaced with fresh complete DMEM after 6 h. After 48 h had passed post-transfection, the cell medium was collected and centrifuged for 10 min at 3000 rpm, the supernatant was filtered and the lentiviral vector particles were purified and concentrated with a Lenti-X concentrator kit (Takara). After concentration, the viral particles were resuspended in sterile phosphate-buffered saline and the titer of the samples was measured with a qPCR Lentivirus titer kit from Applied Biological Materials (Vancouver, Canada). The samples were stored at −80 °C until the infection of cells.

2.10. Lentiviral Infection of VSMCs

Briefly, 2×10^5–2.5×10^5 primary vascular smooth muscle cells/well were plated on-6-well plates, and the cells were infected the next day. The same titers of lentiviral preparations, diluted in complete DMEM + 8 µg/mL Polybrene (Sigma-Aldrich), were used to infect the VSMCs. The cells were subjected to the experiments 48 h after infection.

2.11. Immunoblot Analysis

After the agonist stimulation of the VSMCs, cells were scraped with $2 \times$ concentrated Laemmli buffer (Tris-Cl pH 6.8, glycerol, SDS, 2-mercapto-ethanol, bromophenol blue), supplemented with protease and phosphatase inhibitors. This cell lysate was briefly sonicated, then boiled, and equal amounts of samples were loaded into 12% SDS-polyacrylamide gels. The proteins were transferred to PVDF membranes using 80V for 2 h during the process. The PVDF membranes were then blocked with a 5% blocking solution (nonfat dried milk diluted in PBS-T). The membranes were then incubated with either pEGFR or pERK1/2 primary antibodies, depending on the experiment. Following PBS-T washing, these membranes were incubated with the appropriate anti-rabbit IgG secondary antibody. As a loading control, β-actin labeling was used. The signals were visualized with enhanced chemiluminescence, using Immobilon Western HRP substrate reagents, and were then detected with an Azure c600 device.

2.12. Immunofluorescence Staining

The immunostaining was performed according to the following protocol: the VSMCs were gently washed, once, before fixation with 3.7% paraformaldehyde solution for 15 min. After quenching the fixation solution in three washing steps, the cells were permeabilized using 0.1% Triton X-100 (Sigma-Aldrich) and incubated in 0.1% sodium-borohydride solution for 15 min. The cells were then incubated in 1% BSA (Sigma-Aldrich) containing blocking solution for 30 min, then immunolabelled using anti-α-smooth muscle actin (Sigma-Aldrich) and Alexa Fluor 488 conjugated secondary antibodies (Invitrogen). Cell nuclei were stained by DAPI (4′,6-diamidino-2-phenylindole, dihydrochloride; Sigma-Aldrich). Photomicrographs were taken using a Leica DMI6000B inverted microscope.

2.13. Statistical Analysis

We analyzed gene expression data, collected from qRT-PCR measurements, using multiple linear regression with a 95% confidence interval in order to determine the significance of inhibitor treatments, stimuli and their interaction on the dependent variable, which is the fold-change value of a given gene of interest. In the case of Figures 2, 4D–F and 6A, ordinary one-way ANOVA analyses were performed to compare stimulated or lentiviral infected groups to control groups. Statistical analysis and graph plotting were carried out with GraphPad Prism 9.1.2 software. The sample size (*n*) in the figure legends refers to the number of independent experiments (biological replicates). Unless otherwise stated, data are presented as mean $\pm$ SE.

3. Results

3.1. Affymetrix GeneChip Analysis of the AngII Upregulated Genes in VSMCs

In the present study, we used the Affymetrix GeneChip Rat Gene 1.0 ST array to compare the gene expression profiles of the vehicle and 100 nM AngII-treated VSMCs after 2 h of treatment. We used rat primary isolated VSMCs in their second passage, in order to get physiologically relevant data. In order to demonstrate that these relatively early-passage young cells possess the expected properties of VSMCs, we performed smooth muscle α-actin immunostaining and agonist stimulation of these early passage cells. Our data confirmed that these cells showed characteristic features of VSMCs, such as the expression of smooth muscle α-actin and showed a typical ERK1/2 activation pattern in response to 50 ng/mL EGF or 100 nM AngII stimulation (Supplementary Figure S1).

We performed differential expression (DE) analysis between the AngII- and vehicle-treated microarray samples using *limma* [21]. AngII led to the significant upregulation (false discovery rate, based on the Benjamini–Hochberg correction < 0.05, $\log_2$ fold change > 1) of 74 genes (Figure 1A). We found 4 DUSP isoforms among the significantly upregulated genes, namely, DUSP4, DUSP5, DUSP6 and DUSP10 (log2 fold change values: 1.01, 2.66, 2.01 and 1.23, FDR (false discovery rate): 2.5×10^{-04}, 3×10^{-06}, 5×10^{-06} and 5.2×10^{-05}, respectively). We performed a pathway activity analysis using the *PROGENy* tool to ensure a more unbiased analysis of AngII-induced gene expression changes [22,23]. *PROGENy* identifies upstream pathways regulating the observed gene expression changes for 14 pathways (Figure 1B). *PROGENy* analysis revealed that AngII treatment significantly increased the MAPK and EGFR pathways (Figure 1B, z-scores of pathway activities: 21.22 and 22.86, respectively (see the Materials and Methods section for further details)), and also led to a modest increase in another receptor tyrosine kinase pathway (VEGFR) and TGFβ.
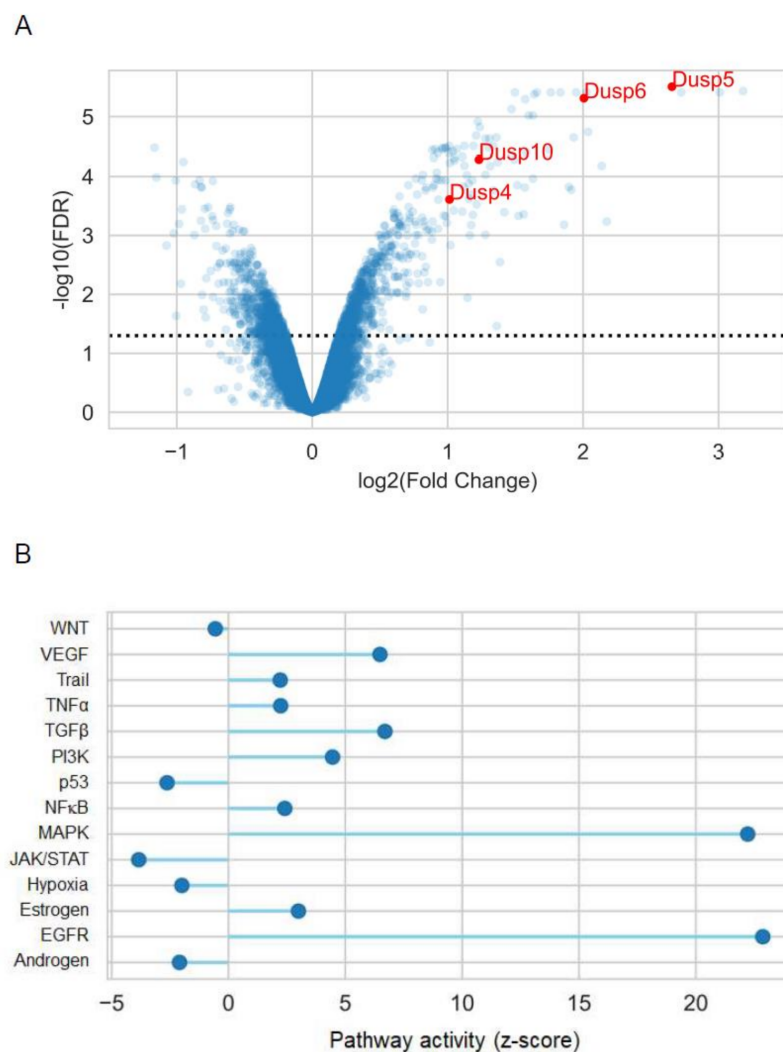
A

B

Figure 1. AngII-induced gene expression changes in VSMCs. (**A**) Differential expression (DE) analysis was performed between 2-hour AngII- and vehicle-treated samples. The microarray experiment was performed in triplicate. The results of DE analysis are shown as a volcano plot (*x*-axis: log2 fold change, *y*-axis: −log10 (FDR, false discovery rate), based on the Benjamini–Hochberg correction of p-values. Selected members of the DUSP family are color-coded and text-labeled. The dotted line shows the significance threshold (FDR < 0.05) (**B**) *PROGENy* pathway analysis of an AngII-induced gene expression signature. Pathway activity was calculated for 14 PROGENy pathways (*x*-axis) and normalized to z-scores (*y*-axis), based on a random permutation of gene labels.

In summary, our microarray analysis revealed that AngII increased the activity of MAPK and EGFR pathways in VSMCs. We found several DUSP isoforms, important negative regulators of the MAPK pathway, among the most significantly overexpressed genes, corresponding to a plausible negative feedback mechanism [26].

3.2. qRT-PCR Measurements Validate the Affymetrix Array Results Regarding the Upregulation of DUSP5, DUSP6, and DUSP10 Gene Expressions, in Response to AngII Stimulation. Time Kinetics of Gene Expression Changes, in Response to the AngII Stimulation of VSMCs

We used qRT-PCR determinations to confirm the effect of AngII stimulation on the expression levels of certain DUSP isoforms. The transcriptome analysis revealed the upregulation of several DUSP genes, such as *DUSP 5, 6, 10, 4,* and *14*. We selected one DUSP from each subfamily of DUSPs, namely, DUSP5, DUSP6, and DUSP10 for our studies. We aimed to validate the Affymetrix GeneChip results, and we also wanted to determine the time course of the AngII-induced DUSP5 (Figure 2A), DUSP6 (Figure 2B) and DUSP10 (Figure 2C) expression-level upregulation. VSMCs were stimulated at different points of time from 1 to 6 h with 100 nM of AngII, then the mRNA levels were measured via real-time PCR. In the case of DUSP5 and DUSP10, we observed the highest mRNA levels 2 h after the stimulation. The mRNA levels of DUSP6 were strongly elevated after the first hour, peaked at 2 h, and remained continuously elevated, although they showed a slightly reduced tendency at later time points. Based on the qRT-PCR results, we chose 2-hour-long stimulations for our further experiments concerning the analysis of gene expression changes.
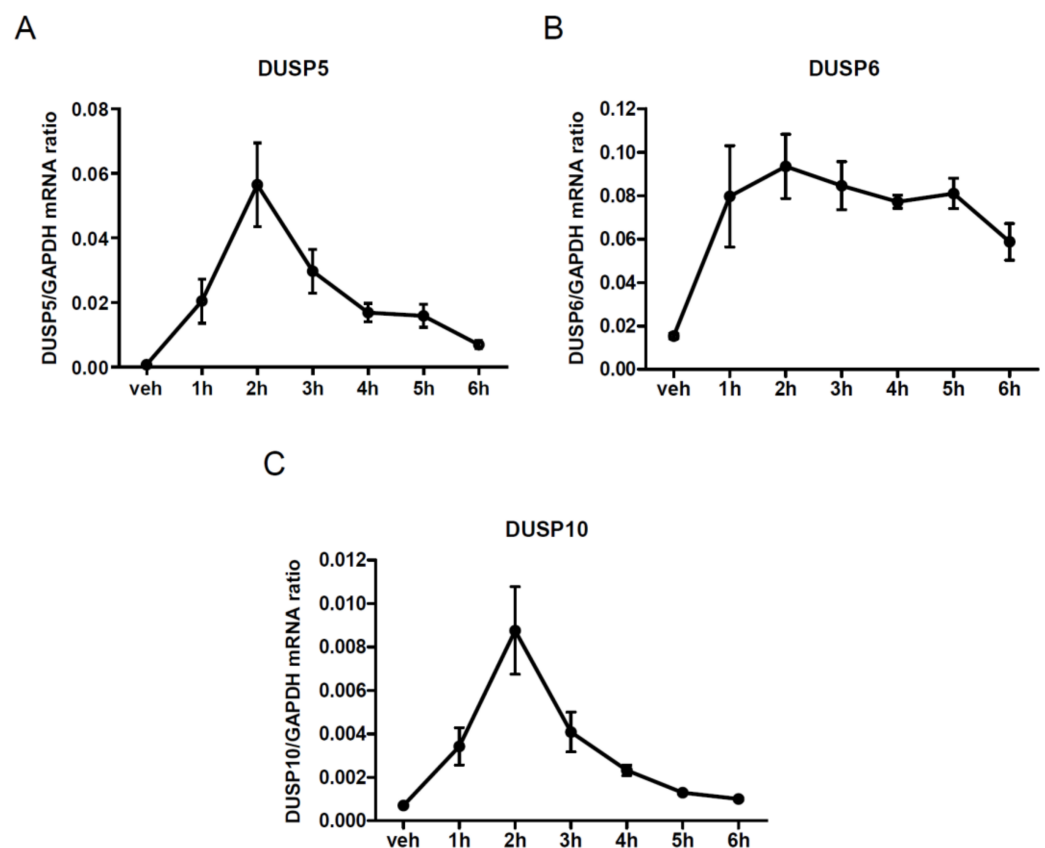

Figure 2. Time-dependent effect of AngII stimulation on gene expression in VSMCs. VSMCs were serum-depleted for 24 h, then cells were treated for various lengths of time intervals with 100 nM AngII, beside a control group treated with the vehicle. Time kinetics of (**A**) DUSP5, (**B**) DUSP6, and (**C**) DUSP10 expression levels are shown. The mRNA abundance was calculated via normalization to the *GAPDH* housekeeping gene and measured using real-time PCR. Mean values ± SE are shown (*n* = 5–6).

3.3. Investigation of Signaling Pathways Involved in AngII-Mediated Responses

Next, we wanted to determine which receptor type and coupling G protein is responsible for the expression changes. Theoretically, AngII can stimulate and mediate its effect via two distinct GPCRs, the AT_1 and AT_2 angiotensin receptors in VSMCs [27]. The AT_1-R is much more important and is abundantly expressed in vessels. In order to exclude the potential role of the AT_2 angiotensin receptor in the investigated gene expression changes, we applied candesartan, a selective AT_1-R antagonist with insurmountable binding properties. As shown in Figure 3, the candesartan (10 µM) pretreatment completely blocked the AngII-mediated upregulation of DUSP levels. This data indicated that AT_1-R mediates the observed AngII-induced gene expression changes that mostly couple to the $G_{q/11}$ heterotrimeric G protein in VSMCs [1].
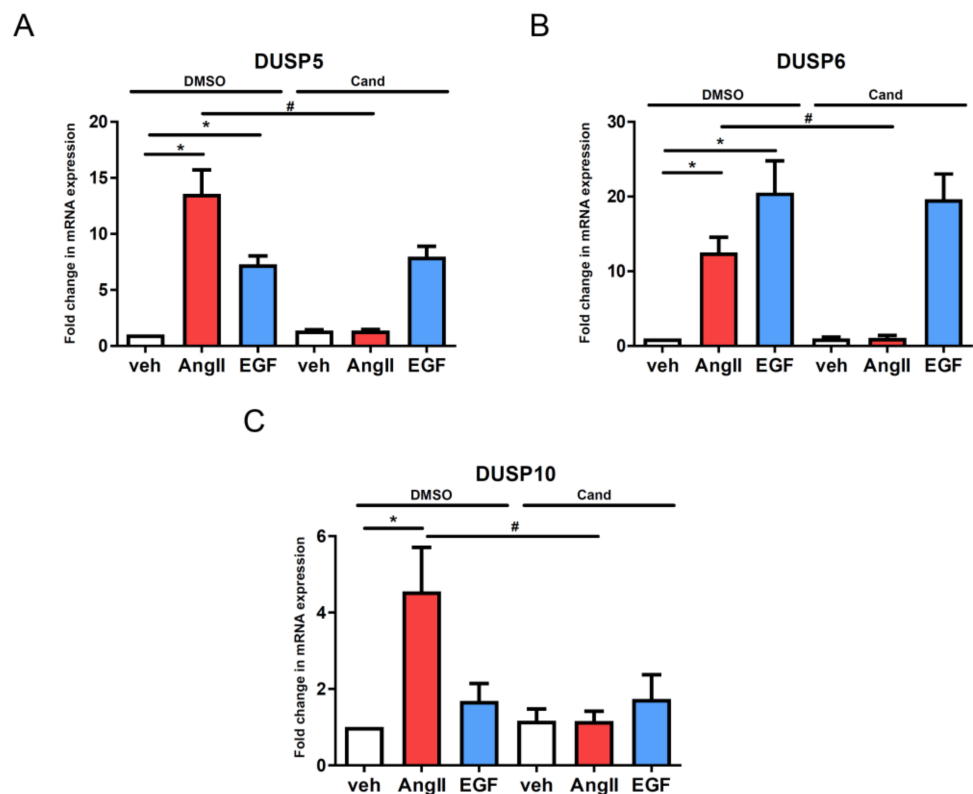

Figure 3. Effect of AT_1-R antagonist treatment on the agonist-induced gene expression changes of the DUSP isoform in vascular smooth muscle cells. Serum-starved cells were incubated with 10 µM candesartan (Cand) or DMSO as a control for 30 min, then the cells were exposed to either 100 nM AngII (red columns) or 50 ng/mL EGF (blue columns) or the vehicle (white columns) for 2 h. Standardization was made against the *GAPDH* housekeeping gene. The mRNA levels of DUSP5 (**A**), DUSP6 (**B**) and DUSP10 (**C**) were normalized to values of DMSO vehicle samples and expressed as fold change. Mean values ± SE are shown. Significance was determined with multiple linear regression. $p < 0.05$ was considered as statistically significant. *: statistically significant from vehicle stimulation. #: statistically significant from DMSO-pretreated agonist-induced response. The values are from four independent experiments ($n = 4$).

It has previously been reported that only the G protein-dependent mechanism of AT_1-R seems to be important in AngII-induced hypertrophy in VSMCs [28]. In addition to the $G_{q/11}$ activation mechanism, it is well documented that AT_1-R can also couple to the $G_{i/o}$ and $G_{12/13}$ heterotrimeric proteins, leading to the inhibition of adenylyl cyclase, the activation of Rho-kinase and phospholipase D, and the regulation of Ca^{2+} channels [29]. We used YM-254890, a selective $G_{q/11}$ inhibitor, to investigate the role of $G_{q/11}$-mediated pathways. Figure 4 demonstrates that 1 µM of YM-254890 completely wiped out the

AngII-mediated gene expression upregulation in all the examined DUSPs. We also used pertussis toxin (PTX) pretreatment (100 ng/mL for 18 h) to inhibit G_i protein activation and to assess the potential role of the G_i protein in the induced gene expression changes. Our results show that the PTX evoked only partial inhibition of the AngII-induced gene expression changes, emphasizing the primary role of $G_{q/11}$ activation (data not shown). We also wanted to evaluate the possible role of β-arrestin-mediated signaling in the regulation of AngII-induced expression changes. TRV120023 peptide is a biased agonist of AT_1-R that triggers no or partial activation of G proteins but it induces β-arrestin-mediated signaling via β-arrestin binding [30–32]. In contrast to 100 nM AngII stimulation, using 3 μM TRV120023 as an AT_1-R agonist did not evoke significant gene expression changes, which reflects the finding that DUSP upregulation is initiated exclusively in a G-protein-dependent manner (Figure 4).
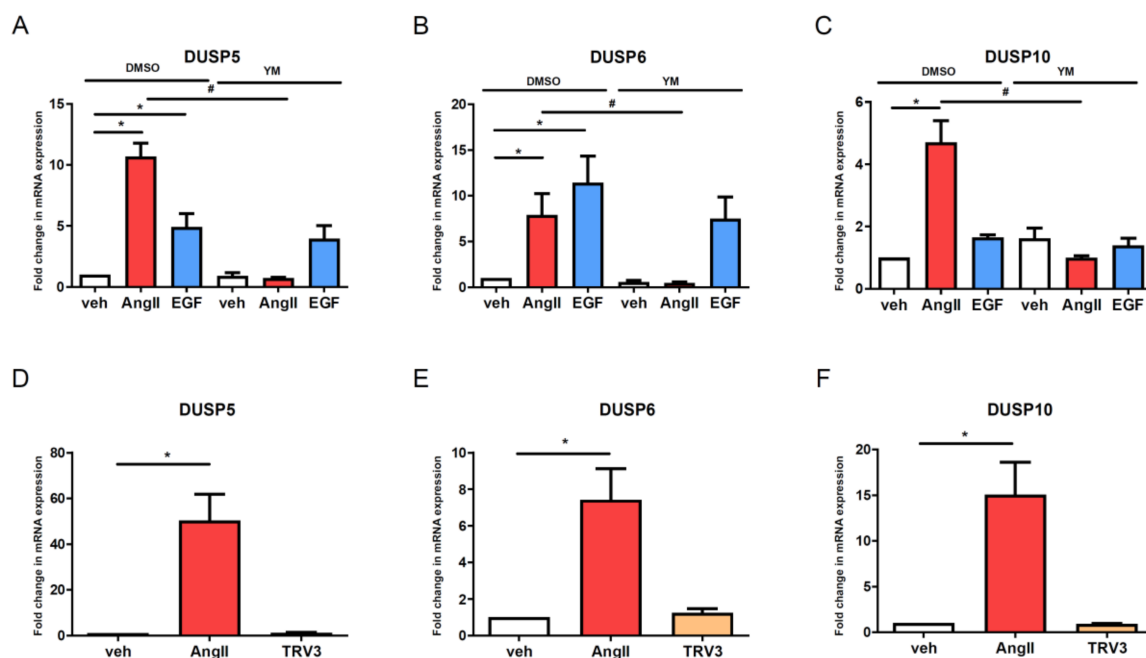

Figure 4. Evaluation of the contribution of G-protein-dependent and independent mechanisms in the AT_1-receptor stimulation on induced changes in DUSP levels in vascular smooth muscle cells. Serum-depleted VSMCs were incubated with 1 μM YM-254890 (YM) or DMSO as a control for 30 min, then the cells were exposed to either 100 nM AngII (red columns) or 50 ng/mL EGF (blue columns) or vehicle (white columns) for 2 h (**A**–**C**). The serum-starved VSMCs were exposed to either the vehicle (white columns) or 100 nM AngII I (red columns) or 3 μM TRV120023 (beige columns) for 2 h (**D**–**F**). RNA was isolated from VSMCs, then converted to cDNA. cDNA levels of DUSP5 (**A**,**D**), DUSP6 (**B**,**E**) and DUSP10 (**C**,**F**) were measured by qRT-PCR. Standardization was established against the *GAPDH* housekeeping gene. Mean values ± SE are shown. Significance was determined via multiple linear regressions. $p < 0.05$ was considered as statistically significant. *: statistically significant from vehicle stimulation. #: statistically significant from DMSO pretreated agonist-induced response (**A**–**C**). In the case of **D**–**F**, significance was determined with a one-way ANOVA-test (* $p < 0.05$). The values are from four or five independent experiments ($n = 4$–5).

3.4. Effect of EGF Stimulation and EGFR Tyrosine Kinase Inhibitors on Agonist-Induced Expression of DUSP Genes

Since EGF-receptor transactivation plays an important role in the AngII-induced cell responses in VSMCs, we investigated the effect of direct EGF-receptor stimulation on DUSP gene-expression changes. Figure 5 demonstrates that 50 ng/mL of EGF stimulation caused a significant increase in DUSP5 and DUSP10 expression levels but this was to a lesser extent than the 100 nM AngII stimulus-evoked response (Figure 5A,C). In the case of DUSP6 mRNA levels, we observed a similar increase in both EGF- and AngII-stimulated groups

(Figure 5B). In order to determine the role and contribution of EGFR transactivation in the AngII-induced changes, we pretreated the VSMCs with either 1 μM AG1478 or 2.5 μM gefitinib, two widely used EGFR tyrosine kinase inhibitors. As expected, these inhibitors completely blocked the EGF-induced increase of DUSP5, DUSP6, and DUSP10 mRNA levels (Figure 5). It is noteworthy that neither candesartan nor YM-254890 evoked a significant effect on the EGF-induced increase in DUSP expression levels, showing the specificity of the candesartan and YM-254890 on AngII-induced responses (Figures 3 and 4A–C). It is important to note that although the AngII-induced upregulation of DUSP levels was significantly blunted by AG1478 and gefitinib pretreatment, these inhibitory effects were not total.
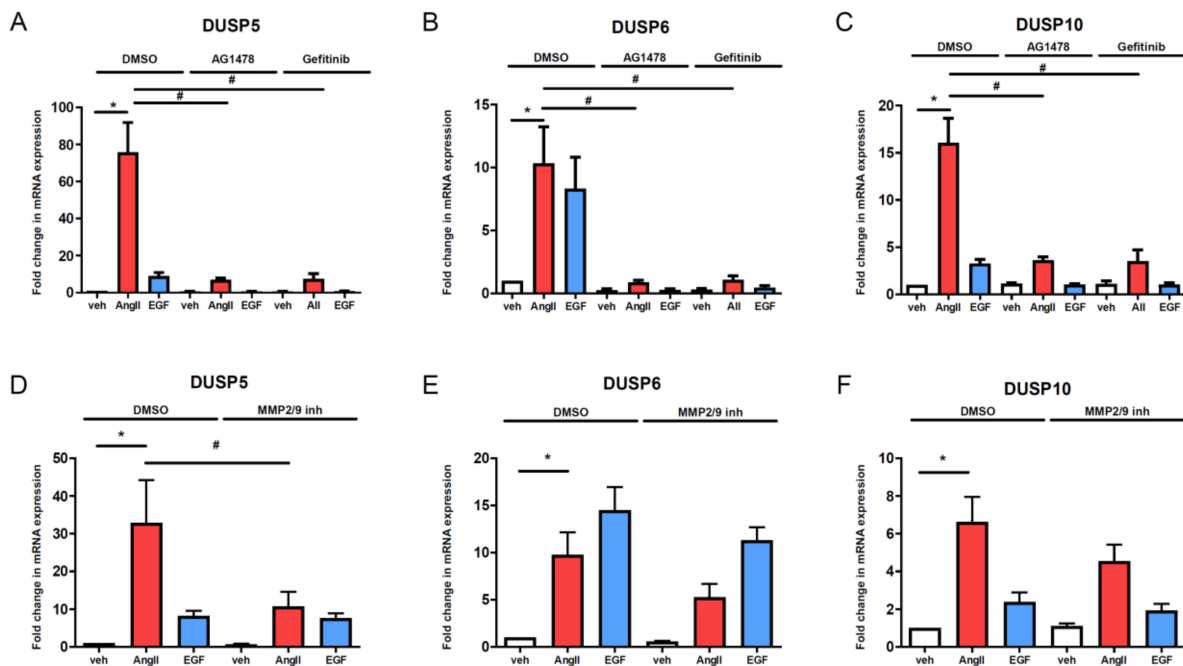

Figure 5. Effect of EGFR transactivation on the gene expressional changes of DUSP isoforms in VSMCs. Serum starved cells were incubated with either 1 μM AG1478 (**A–C**) or 2.5 μM gefitinib (**A–C**), or 1 μM MMP-2/MMP-9 Inhibitor II (**D–F**) beside the control treated with DMSO for 30 min, then the cells were exposed to either 100 nM AngII (red columns) or 50 ng/mL EGF (blue columns) or vehicle (white columns) for 2 h. mRNA levels of DUSP5 (**A,D**), DUSP6 (**B,E**) and DUSP10 (**C,F**) were measured by qPCR. Standardization was made against the *GAPDH* housekeeping gene. The mRNA levels were normalized to values of DMSO vehicle samples and expressed as fold change. The values are from three-six independent experiments. Mean values ± S.E. are shown. Significance was determined with multiple linear regression. $p < 0.05$ was considered as statistically significant. *: statistically significant from vehicle stimulation. #: statistically significant from DMSO-pretreated agonist-induced response. The values are from three to six independent experiments (*n* = 3–6).

3.5. Inhibition of Matrix Metalloproteinases Has a Moderate Effect on AngII-Induced DUSP Upregulation

It is well documented that the matrix metalloproteinases are key mediators of AngII-induced transactivation of EGFR in VSMCs and are important effectors of AngII-mediated vascular remodeling [1,6,7]. Among the MMPs, MMP-2 and MMP-9 appear to play the most important role in cardiovascular cells and, using a highly selective inhibitor, MMP-2/MMP-9 Inhibitor II potently inhibited EGFR transactivation in VSMCs [7,33]. As expected, the MMP-2/MMP-9 Inhibitor II had no significant effect on direct EGFR activation-induced gene expression changes in DUSP genes (Figure 5D–F, blue columns). On the other hand, the MMP-2/MMP-9 Inhibitor II reduced the AngII-induced increase in DUSP5 but the inhibitory effect was not complete (Figure 5D, red column). Moreover, the MMP-2/MMP-9

Inhibitor II had no significant effect on AngII-induced DUSP6 and DUSP10 upregulations (Figure 5E,F, red columns).

3.6. The Role of Calcium Signaling and Calcium-Dependent Kinases in the Upregulation of DUSP Levels

The stimulation of AT1 and EGF receptors induces a cytosolic calcium-level increase via the phospholipase β and γ activation mechanisms [1,34,35]. The agonist-induced calcium signal initiates several important regulatory mechanisms, such as the activation of protein kinase C, proline-rich tyrosine kinase 2 (Pyk2) and calcium/calmodulin-dependent protein kinase in VSMCs [36–38]. We used 50 µM BAPTA-AM (a permeant calcium chelator) pretreatment prior to agonist stimulation, to investigate the role of intracellular calcium in the regulation of DUSP mRNA levels. The results of the calcium chelation by BAPTA-AM demonstrate that the induced intracellular calcium elevation is essential for the observed upregulation of *DUSP* genes in response to both AngII and EGF stimulations in VSMCs (Supplementary Figure S2A–C). In order to further explore calcium signal-related mechanisms, we applied a specific calcium/calmodulin-dependent protein kinase II (CaMKII) inhibitor, CK59. CaMKII plays an important role in AngII-induced vascular reactivity, hypertrophy in VSMCs, and vascular remodeling [39,40]. Supplementary Figure S2D–F illustrates that the inhibition of CaMKII with 50 µM CK59 significantly attenuated the AngII-induced DUSP5 mRNA level increase but not the response caused by EGF. In the case of DUSP6 and DUSP10, the CK59 also significantly reduced the AngII-induced gene expression upregulations but the effect was much lower in the EGF-stimulated cells (Supplementary Figure S2D–F). To evaluate the role of the calcium-dependent protein kinase C (PKC), we employed the RO31-8425 compound, which is a highly selective inhibitor of PKC [41]. Pretreatment with the RO31-8425 PKC inhibitor (1 µM for 10 min) reduced the AngII- but not the EGFR-induced DUSP5 mRNA level increase (Supplementary Figure S3A–C). The inhibition of PKC resulted in a greatly reduced effect of AngII in DUSP6 and DUSP10 upregulation, whereas EGF-induced effects were moderately inhibited (Supplementary Figure S3A–C). Next, we investigated the involvement of Pyk2, a regulator of EGFR transactivation in VSMCs. We assessed the role of Pyk2 in the AngII induced upregulation of DUSPs by applying PF-562271, a potent ATP-competitive FAK and Pyk2 kinase inhibitor. Pretreatment of the cells with 1 µM PF-562271 slightly but not significantly reduced the AngII-induced upregulation of DUSP5 and DUSP6 (Supplementary Figure S3D,E); the PF-562271 pretreatment did not influence the AngII-mediated gene expressional increase of DUSP10 either (Supplementary Figure S3F).

3.7. Silencing of EGFR in VSMCs Using a Lentiviral shRNA System

AngII stimulation can result in the much higher upregulation of DUSP5 and DUSP10 mRNA levels than direct EGFR stimulation by EGF (i.e., Figure 3A,B, red vs blue solid columns). The relative ineffectiveness of matrix metalloproteinase inhibition (Figure 5D–F) raised the possibility that AngII-induced DUSP upregulation is not entirely EGFR-transactivation-dependent. The effects of EGFR inhibitors (AG1478 and gefitinib in Figure 5A–C) on AngII-induced changes may reflect the off-target effects of these inhibitors [42–44]. In order to check the role of EGFR in AngII-induced DUSP upregulations, we decided to use the short hairpin RNA (shRNA)-based silencing of EGFR expression via RNA interference. As primary VSMC cultures are hard to transfect conventionally, we transduced VSMCs with pLKO.1 puro lentiviral constructs to produce siRNA specific to EGFR. First, we prepared two sets of lentiviruses containing different constructs. Following infection, we examined *EGFR* mRNA levels via real-time PCR (Figure 6A) and EGFR protein levels via Western blot analysis (Figure 6B). The results indicate that both constructs successfully reduced the expression and the protein levels of EGFR. Briefly, shEGFR#2 was slightly more effective; therefore, we used this in our next experiments.
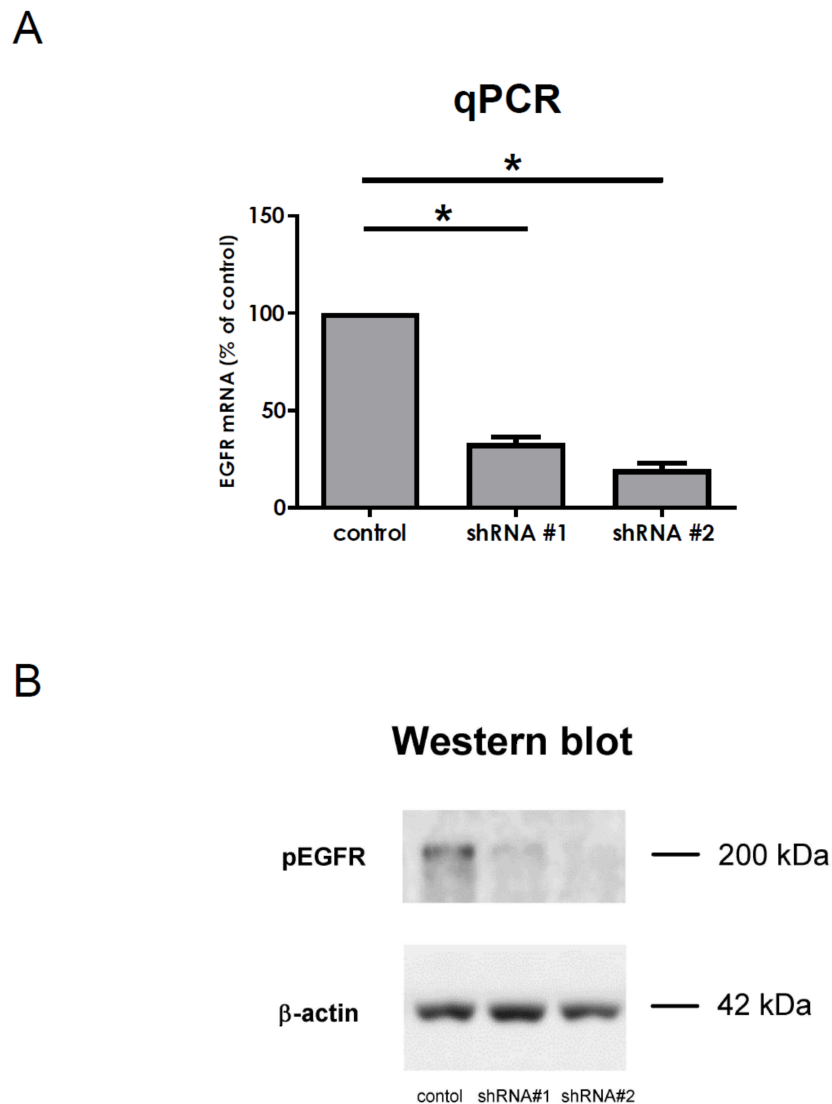
A

qPCR

B

Western blot

Figure 6. Silencing EGFR expression with shRNA constructs via lentiviral infection. VSMCs were infected with either shEGFR#1 or shEGFR#2 lentiviral constructs for 48 h. Control-group cells were infected with a lentivirus coding-scrambled shRNA sequence. (**A**) *EGFR* gene expression levels were measured by a real-time PCR. Mean values $\pm$ SE are shown. Significance was calculated with an ordinary one-way ANOVA test (* $p < 0.05$). (**B**) In the image, 5 min of 50 ng/mL EGF stimulation-induced phospho-EGFR levels were measured by Western blot analysis. Anti-β-actin staining was used as a loading control. The Western blots shown are representative of three independent experiments ($n = 3$).

The results shown in Figure 7 demonstrate that the shRNA silencing of EGFR has less effect on AngII-mediated gene expression changes than pharmacological inhibition. After waiting for 48 h after lentiviral infection with shRNA coding particles, VSMCs were stimulated with AngII or EGF, apart from a control group treated with the vehicle. The mRNA levels of DUSP isoforms were measured by real-time PCR. As expected, the silencing of EGFR completely wiped out the EGF stimulation-mediated DUSP level upregulations (Figure 7, blue columns). In contrast, the gene silencing of EGFR did not lead to such a dramatic blockade in the AngII-induced increase in DUSP mRNA levels, compared to the effect of AG1478 and gefitinib (Figure 7, red columns vs. Figure 5A–C, red columns). Moreover, the silencing of EGFR only caused a significant effect regarding the AngII-induced

DUSP5 mRNA increase (Figure 7A, red columns) but in the case of DUSP6 and DUSP10, the EGFR silencing did not cause statistically significant effects (Figure 7B,C, red columns).
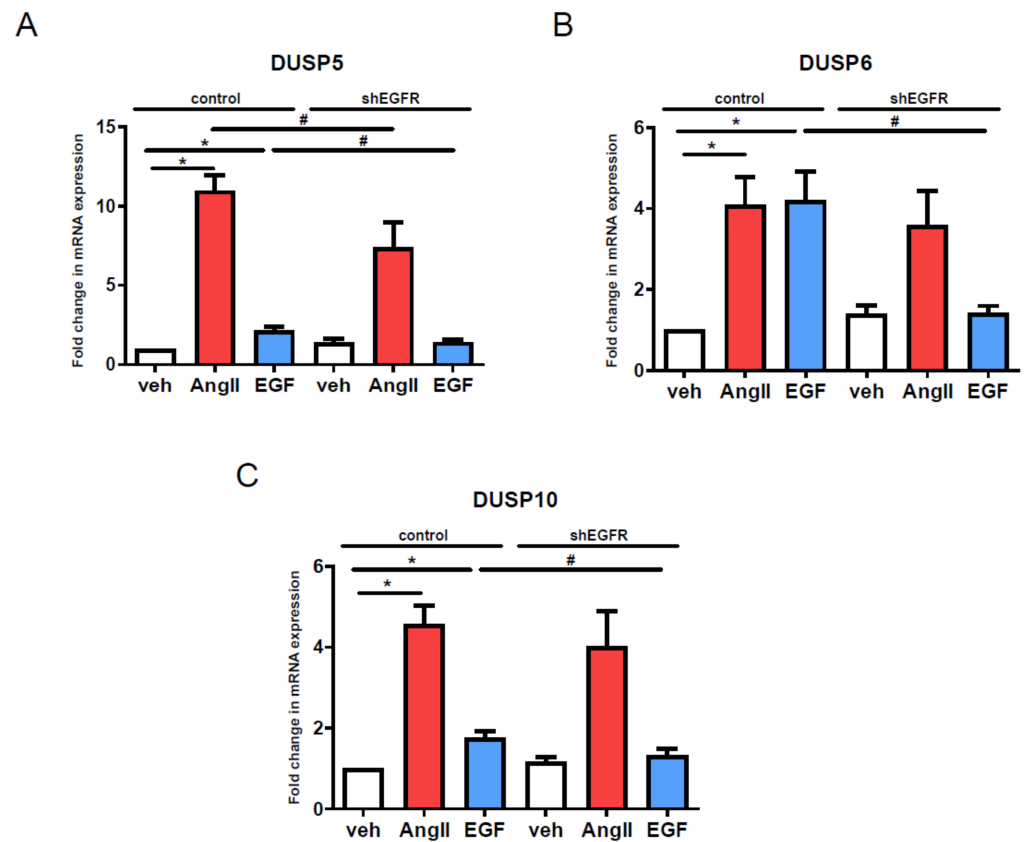

Figure 7. Effects of EGFR silencing on the gene expression responses to AngII and EGF stimuli in VSMCs. Primary vascular smooth muscle cells were infected with either scrambled (control) or shEGFR#2 (shEGFR) shRNA coding lentiviral particles for 48 h. Infected cells were stimulated for 2 h with either 100 nM AngII (red columns), or 50 ng/mL EGF (blue columns) or vehicle (white columns) after 24 h of serum starvation. RNA was isolated from VSMCs, then converted to cDNA. cDNA levels of DUSP5 (**A**), DUSP6 (**B**) and DUSP10 (**C**) were measured by qRT-PCR. Standardization was made against the *GAPDH* housekeeping gene. The mRNA levels were normalized to values of control virus-infected and vehicle-stimulated samples and expressed as fold change. Mean values ± S.E. are shown. Significance was determined with multiple linear regression. $p < 0.05$ was considered as statistically significant. *: Statistically significant from vehicle stimulation. #: Statistically significant from control virus-infected agonist-induced response. The values are from four independent experiments ($n = 4$).

3.8. Role of Other Growth Factor Receptor Transactivation Mechanisms in the AngII-Induced Gene Expression Changes

Although EGFR transactivation is considered to be the major growth factor receptor transactivation mechanism in VSMCs, the stimulation of AT_1-R has also been confirmed to transactivate other growth factor receptors, including the platelet-derived growth factor receptor (PDGFR) and the insulin-like growth factor I receptor (IGF-IR) [45,46]. Inhibition of PDGFR with sunitinib or sorafenib pretreatments (Supplementary Figure S4A–C) and inhibition of IGF-IR with AG1024 or AG538 pretreatments (Supplementary Figure S4D–F) did not cause such robust effects as EGFR inhibition with AG1478 or gefitinib (Figure 5A–C) on AngII-induced DUSP expression levels. Only the sorafenib caused a significant reduction in AngII-induced gene expression changes, in the case of *DUSP10,* among these investigated drugs (Supplementary Figure S4C). These results indicate that PDGFR or IGF-IR transactivation is not a major signaling route to lead to AngII-induced upregulation of the investigated DUSP genes.

3.9. Effect of Simultaneous AngII and EGF Stimuli on DUSP Levels in VSMCs

We used a different approach to confirm that AngII-induced gene expression changes are not exclusively EGFR transactivation-dependent. We stimulated the AT_1-R and the EGFR together by applying simultaneous 100 nM AngII and 50 ng/mL EGF stimuli of vascular smooth muscle cells. Surprisingly, the DUSP5 level was robustly upregulated. The DUSP5 expression level increased ~2.24-fold in response to simultaneous AngII and EGF stimuli compared to single AngII stimulation, and ~6.38-fold compared to only EGF stimulation (Figure 8A). Although the simultaneous AngII and EGF stimulations caused the highest increase in the DUSP6 level (Figure 8B), the combined effect of receptor agonists was not so striking as in the case of DUSP5. Similar to the evoked effect on DUSP5 level by simultaneous receptor activations, the DUSP10 mRNA level was also significantly upregulated by combined AngII and EGF stimulations; the DUSP10 expression level increased ~1.69-fold compared to only AngII stimulation, and ~4.17-fold compared to only EGF stimulation (Figure 8C). These results clearly demonstrate that there are synergistic pathways that may amplify each other, leading to robust gene expression changes in VSMCs, as in the case of DUSP5 and DUSP10 expression levels.
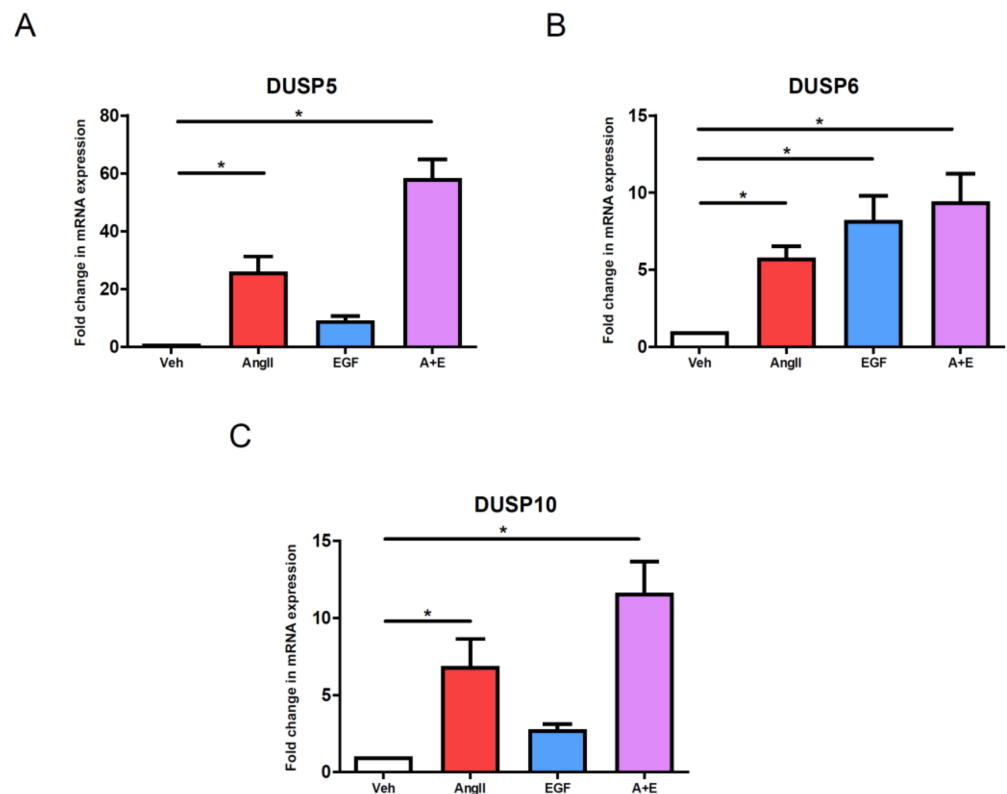

Figure 8. DUSP expression changes after simultaneous AngII and EGF stimuli in VSMCs. Serum-starved cells were exposed to either vehicle (white columns), or 100 nM AngII (red columns), or 50 ng/mL EGF (blue columns), or simultaneously 100 nM AngII and 50 ng/mL EGF (purple columns) for 2 h. RNA was isolated from VSMCs, then converted to cDNA. cDNA levels of DUSP5 (**A**), DUSP6 (**B**) and DUSP10 (**C**) were measured by qRT-PCR. The mRNA levels were normalized to values of DMSO vehicle samples and expressed as a fold change. Mean values $\pm$ SE are shown. Significance was determined with multiple linear regression (* $p < 0.05$). The values are from seven independent experiments ($n = 7$).

3.10. Effect of MAPK Signaling Inhibition on AngII-Induced DUSP Gene Upregulations

Since the activity and expression of various DUSP isoforms are dependent on MAPKs [18], we aimed to evaluate the role of MAPKs in AngII-induced DUSP expression changes. We pretreated the cells with the PD98059 MEK inhibitor to assess the potential role of ERK1/2

MAPKs in the AngII-evoked responses. The inhibition of the MEK significantly reduced the DUSP5 mRNA level increase upon AngII stimulation (Supplementary Figure S5A). Due to the dramatic effect of the PD98059 MEK inhibitor on basal DUSP6 and DUSP10 levels, the role of ERK1/2 MAPKs in AngII-induced DUSP6 and DUSP10 changes cannot be clearly established (Supplementary Figure S5B,C). On the contrary, the p38 MAPK inhibitor (SB202190) effectively reduced all the investigated AngII stimulation-caused DUSP mRNA level increases in VSMCs, whereas its inactive analog, SB202474, had no effect (Supplementary Figure S5D–F). These results indicate the important role of p38 MAPK signaling in the regulation of expression levels of DUSP5, DUSP6 and DUSP10 isoforms.

4. Discussion

Sustained AngII actions can lead to hypertension, vascular remodeling and atherosclerosis [1]; therefore, an evaluation of AngII-induced gene expression changes is important to clarify. New data can reveal previously unidentified mechanisms and new therapeutic agents to ameliorate AngII-triggered cardiovascular symptoms. Our results provide novel insights into the transcriptomic effects of AngII in primary rat VSMCs. The major findings of the present study are: (1) analyzing the transcriptomic effects and the gene expression changes of various DUSP isoforms in response to AngII stimulations of primary vascular smooth muscle cells and (2) demonstrating that AT_1-R and EGFR can initiate synergistic signaling pathways to induce gene expression changes. These findings support the notion that AT_1-R is capable of activating multiple signaling pathways that may be responsible for various cell responses.

Recent studies have already elucidated the importance of AngII-regulated gene expression changes in many cell types [8–13]. In this present study, we used rat primary VSMCs up to 3 passages in order to approximate them more closely to their physiological functions. We investigated the transcriptomic effect of AngII by stimulating serum-deprived early-passage VSMCs with the vehicle or 100 nM AngII for two hours. We found many genes that were significantly upregulated or downregulated after AngII stimulation by using the Affymetrix GeneChip assay (Figure 1). In agreement with the previous gene-chip results, numerous earlier-described genes were identified in VSMCs [9,10]. The activation of AT_1-R is followed by events leading to the downregulation of AT_1-R; in addition, the initiated signal transduction steps can be attenuated by various mechanisms, i.e., the phosphorylated proteins undergo dephosphorylation reactions. Our data demonstrate that Ang-II upregulates numerous genes, including dual-specificity phosphatases (DUSPs), which, in turn, can regulate the long-term MAPK signaling mechanisms of AT_1-R. Since the effect of AngII on DUSP gene expressions has not been reported, we wanted to investigate their roles in AngII signaling, and to identify which arm of the AT_1-R signaling pathway is responsible for these effects. Among the identified genes, we have chosen to analyze one member from each subfamily of DUSP isoforms, namely, DUSP5, DUSP6 and DUSP10. Real-time PCR measurements demonstrated that the expression levels of the investigated DUSP genes increased 1 h after AngII stimulation, peaked at 2 h and persisted for up to 6 h (Figure 2). In the case of DUSP6, the kinetics of the expression were slightly different from those of DUSP5 and DUSP10, which indicates that the involved signaling pathways may vary in terms of the different AngII-evoked responses. We analyzed the possible signal transduction mechanisms that are responsible for the upregulation of the DUSP genes, in response to the AngII stimulation of VSMCs. The results revealed that the AngII effects are due to AT_1-R activation caused by $G_{q/11}$ protein coupling (Figure 4A–C). The activated AT_1-Rs interact with β-arrestins that serve as organizers/scaffold platforms of signaling complexes, such as the activation of the MAP kinase cascade [47]. In order to evaluate the possible role of β-arrestin-mediated signaling in the regulation of expression changes, we applied TRV120023, a β-arrestin-biased AT_1-R agonist, and the results indicated that β-arrestin has no significant role in the regulation of DUSP expression levels (Figure 4D–F). Since the G_q-dependent signaling of AT_1-R activation leads to calcium signal and the activation of many calcium-dependent kinases in VSMCs, we investigated the effect of a

calcium chelator, BAPTA-AM, and specific inhibitors of CaMKII, PKC, and Pyk2. The results demonstrated that the calcium signal and CaMKII play an essential role in all the investigated DUSP expression changes (Supplementary Figure S2D–F), whereas PKC and Pyk2 calcium-dependent kinases play no significant role in the AngII-induced DUSP5 and DUSP6 mRNA-level changes (Supplementary Figure S3). The DUSP10 level seems to be regulated only by PKC, not by Pyk2 activity (Supplementary Figure S3).

EGFR is a receptor tyrosine kinase, which is a key regulator in cardiovascular functions and plays many roles in VSMCs [48]. The stimulation of EGFR leads not just to the activation of Src family kinases and MAPKs promoting VSMC proliferation but also the calcium signal potentiating myogenic tone [49,50]. EGF stimulation was able to induce the DUSP6 mRNA level to a similar extent as the AngII but the EGF was less effective in the regulation of DUSP5 and DUSP10 levels (Figure 2). EGF-induced upregulation was wiped out by small-molecule EGFR kinase inhibitors (AG1478 and gefitinib), whereas the AngII-induced changes were significantly diminished by AG1478 or gefitinib pretreatment (Figure 4A–C). The results regarding the inhibition of matrix metalloproteinases revealed that EGFR transactivation has no exclusive role in the regulation of AngII-induced DUSP mRNA levels, which finding was further confirmed in EGFR gene-silencing experiments (Figure 5D–F and Figure 7). Our experiments also proved that PDGFR or IGFIR transactivation has no significant role in the AngII-induced DUSP mRNA level changes, and only sorafenib caused a significant reduction in AngII-induced gene expression changes in the case of *DUSP10* (Supplementary Figure S4). The AngII-induced EGFR transactivation depends on calcium signal, calcium-dependent Pyk2 and cytoplasmic Src-like tyrosine kinases [37,51,52]. Among the investigated DUSP isoforms, the *DUSP5* upregulation is, at least partly, EGFR transactivation-dependent since either the inhibition of MMP enzymes by MMP-2/MMP-9 Inhibitor II or the silencing of EGFR by shRNA significantly reduced the effect of AngII stimulation. It is important to note that simultaneous AngII and EGF stimuli cause augmented DUSP levels compared to single AngII treatments (Figure 8), which indicates a synergistic role of EGFR- and AT_1-R-induced signaling pathways and/or synergism of transcriptional factors in the regulation of DUSP levels. We may consider at least two mechanisms that lead to the upregulation of *DUSP* genes, an EGFR-dependent and an EGFR-independent mechanism. The EGFR transactivation-independent mechanisms are supported by the results that demonstrate less-efficient DUSP5 and DUSP10 upregulation by direct EGF stimulation compared to the AngII effect (Figure 3), and the partial effects of MMP2/9 inhibition and EGFR silencing (Figure 5A–C and Figure 7).

Mitogen-activated protein kinases (MAPKs) are important regulators of numerous cell functions including proliferation, apoptosis, and differentiation. Initially, the DUSP enzymes are considered as negative regulators of MAPK pathways [18], but it is possible that the various DUSPs and changes in their expression level can regulate/orchestrate the pattern of MAPK activation in response to repeated AngII stimuli. The gene expression induction of the various DUSPs in response to AngII stimulation is ultimately mediated by MAPK activity, primarily by ERK1/2 and p38 MAPKs (Supplementary Figure S5). It is possible that the AngII-induced DUSP5, DUSP6 and DUSP10 increase regulates the MAPK signaling in the long term in the VSMCs. The induced DUSPs may alter the MAPK signaling outcome (magnitude and duration) of subsequent stimulations. Both nuclear-localized DUSP5 and cytoplasmic DUSP6 are known to be induced by ERK1/2 activity and they play an important role in the negative feedback loop to limit ERK1/2 activation. DUSP5 specifically interacts with and inactivates ERK1/2 but the DUSP5 itself is also regulated by ERK1/2 activity, i.e., the transcription of DUSP5 mRNA is dependent on the phosphorylation of Elk-1 by ERK1/2 [53]. The overexpression of DUSP5 in cardiomyocytes results in ERK1/2 inactivation and the reduction of agonist-dependent hypertrophy [54], but it was recently demonstrated that although DUSP5 terminates nuclear ERK signaling and anchors ERK in the nucleus, DUSP5 increases the ERK activation in MEF cells [55]. DUSP6 is primarily located in the cytoplasm, binds to the activated ERK1/2, and causes the cytoplasmic retention of the inactivated ERK1/2 in the cytoplasm to play a role in the

spatiotemporal regulation of MAPK activity [56]. It was demonstrated that *DUSP6* gene expression and *DUSP6* mRNA stability are controlled by the MEK-ERK1/2 pathways [57]. The DUSP6 KO mice showed increased basal ERK1/2 phosphorylation in multiple tissues and showed increased heart weight; however, this did not result in increased or prolonged ERK1/2 activation in response to stimulation, suggesting that DUSP6 is responsible for the fine-tuning of basal ERK1/2 activity [58]. Based on these findings, it is highly possible that DUSP5 and DUSP6 regulate the nucleo-cytoplasmic shuttling of ERK1/2, together sequestering the dephosphorylated ERK either in the nucleus or in the cytoplasm [18]. Our demonstrated results suggest that these DUSP isoforms can play an essential role in the regulation of MAPK signaling patterns in VSMCs. DUSP10, also called MKP-5, can be found in both the nucleus and cytoplasm, and is capable of regulating multiple MAPK pathways, including JNK, p38, and ERK1/2 MAPKs [59]. Among those pathways, the activated JNK and p38 MAPKs are more effectively dephosphorylated by DUSP10 than the ERK1/2 [60]. Interestingly, DUSP10 not only inactivates ERK MAPKs but also interacts with them. DUSP10 is capable of retaining ERK MAPKs in the cytoplasm and downregulating ERK-dependent transcription [61]. The multiple roles of DUSP10 in the regulation of MAPK signaling are also indicated in a study where the knockdown of DUSP10 inhibited acute EGF-stimulated ERK activation that could be reversed by the pharmacological inhibition of p38 MAPK, suggesting that DUSP10 may modulate crosstalk between the ERK1/2 and p38 MAPK pathways [62]. It is important to note that the expression of DUSP10 is elevated in various diseases, such as atherosclerosis [63], which may be the case in other pathophysiological conditions induced by the over-activation of AT_1-R. It is also possible that due to the not-exclusive substrate preference of certain DUSPs (i.e., DUSP10) and the crosstalk mechanisms in parallel MAPK pathways, the AngII stimulation-induced DUSPs can suppress or modify certain types of MAPKs, thus shaping the pattern/interplay of the MAPK network after repeated hormone stimuli. The confirmation of this possibility requires further study. In addition, the upregulated DUSP enzymes may regulate not just MAPKs but other proteins, either by dephosphorylating them and/or by binding to them. AngII-activated MAPK signaling also has implications in the phenotypic switching of VSMCs [64]. Since VSMC plasticity is an important factor in the physiological and pathological processes of the vasculature, we find that it is worthwhile to study the role of DUSPs in this context.

Our studies using the pharmacological inhibition of various signaling elements and the gene silencing of EGFR revealed that there is not an exclusive, or predominant, signal transduction pathway in primary rat VSMCs that leads to or may explain the investigated DUSP gene expression changes, and our experimental data shed light on the complex interplay/regulation among the signaling pathways. Our data showed that AngII-induced gene expression regulation is much more complex than we originally thought, due to the multiple signaling pathways that mediate them. The regulation of expression changes is very complex and is probably determined by the interplay of the involved signaling cascades. According to our data, different mechanisms can lead to the expression changes; classical $G_{q/11}$ activation initiated the Ca^{2+}-dependent mechanism, which induces EGFR transactivation-dependent and independent mechanisms. Further studies are needed to establish how the contributory signaling pathways could be successfully targeted in the treatment of diseases caused by AT_1-R over-activation.

The pleiotropic effects of AngII on vascular smooth muscle cells contribute to the development of numerous cardiovascular diseases, such as hypertension, cardiac hypertrophy, and atherosclerosis. Our data provided new insights into the physiology of VSMCs in response to AngII stimulation, and a better understanding of the mechanisms of AT_1-R-mediated gene expression changes in primary VSMCs can lead to the development of novel types of drugs for the treatment of cardiovascular and other diseases. In addition, the AT_1-R is a prototypical GPCR, with its pleiotropic action of mechanisms, so the described and revealed mechanisms can be considered valid in the case of other GPCRs in VSMCs.

References

1. Forrester, S.J.; Booz, G.W.; Sigmund, C.D.; Coffman, T.M.; Kawai, T.; Rizzo, V.; Scalia, R.; Eguchi, S. Angiotensin II Signal Transduction: An Update on Mechanisms of Physiology and Pathophysiology. *Physiol. Rev.* **2018**, *98*, 1627–1738. [CrossRef] [PubMed]

2. Toth, A.D.; Turu, G.; Hunyady, L.; Balla, A. Novel Mechanisms of G-Protein-Coupled Receptors Functions: AT1 Angiotensin Receptor Acts as a Signaling Hub and Focal Point of Receptor Cross-Talk. *Best Pr. Res. Clin. Endocrinol. Metab.* **2018**, *32*, 69–82. [CrossRef] [PubMed]

3. Hunyady, L.; Catt, K.J. Pleiotropic AT1 Receptor Signaling Pathways Mediating Physiological and Pathogenic Actions of Angiotensin II. *Mol. Endocrinol.* **2006**, *20*, 953–970. [CrossRef]

4. Sauliere, A.; Bellot, M.; Paris, H.; Denis, C.; Finana, F.; Hansen, J.T.; Altie, M.F.; Seguelas, M.H.; Pathak, A.; Hansen, J.L.; et al. Deciphering Biased-Agonism Complexity Reveals a New Active AT1 Receptor Entity. *Nat. Chem. Biol.* **2012**, *8*, 622–630. [CrossRef] [PubMed]

5. Wei, H.; Ahn, S.; Shenoy, S.K.; Karnik, S.S.; Hunyady, L.; Luttrell, L.M.; Lefkowitz, R.J. Independent Beta-Arrestin 2 and G Protein-Mediated Pathways for Angiotensin II Activation of Extracellular Signal-Regulated Kinases 1 and 2. *Proc. Natl. Acad. Sci. USA* **2003**, *100*, 10782–10787. [CrossRef]

6. Mifune, M.; Ohtsu, H.; Suzuki, H.; Nakashima, H.; Brailoiu, E.; Dun, N.J.; Frank, G.D.; Inagami, T.; Higashiyama, S.; Thomas, W.G.; et al. G Protein Coupling and Second Messenger Generation Are Indispensable for Metalloprotease-Dependent, Heparin-Binding Epidermal Growth Factor Shedding through Angiotensin II Type-1 Receptor. *J. Biol. Chem.* **2005**, *280*, 26592–26599. [CrossRef]

7. Saito, S.; Frank, G.D.; Motley, E.D.; Dempsey, P.J.; Utsunomiya, H.; Inagami, T.; Eguchi, S. Metalloprotease Inhibitor Blocks Angiotensin II-Induced Migration through Inhibition of Epidermal Growth Factor Receptor Transactivation. *BioChem. Biophys. Res. Commun.* **2002**, *294*, 1023–1029. [CrossRef]

8. Szekeres, M.; Turu, G.; Orient, A.; Szalai, B.; Supeki, K.; Cserzo, M.; Varnai, P.; Hunyady, L. Mechanisms of Angiotensin II-Mediated Regulation of Aldosterone Synthase Expression in H295R Human Adrenocortical and Rat Adrenal Glomerulosa Cells. *Mol. Cell. Endocrinol.* **2009**, *302*, 244–253. [CrossRef] [PubMed]

9. Leung, A.; Trac, C.; Jin, W.; Lanting, L.; Akbany, A.; Saetrom, P.; Schones, D.E.; Natarajan, R. Novel Long Noncoding RNAs Are Regulated by Angiotensin II in Vascular Smooth Muscle Cells. *Circ. Res.* **2013**, *113*, 266–278. [CrossRef]

10. Jin, W.; Reddy, M.A.; Chen, Z.; Putta, S.; Lanting, L.; Kato, M.; Park, J.T.; Chandra, M.; Wang, C.; Tangirala, R.K.; et al. Small RNA Sequencing Reveals MicroRNAs That Modulate Angiotensin II Effects in Vascular Smooth Muscle Cells. *J. Biol. Chem.* **2012**, *287*, 15672–15683. [CrossRef]

11. Christensen, G.L.; Knudsen, S.; Schneider, M.; Aplin, M.; Gammeltoft, S.; Sheikh, S.P.; Hansen, J.L. AT(1) Receptor Galphaq Protein-Independent Signalling Transcriptionally Activates Only a Few Genes Directly, but Robustly Potentiates Gene Regulation from the Beta2-Adrenergic Receptor. *Mol. Cell. Endocrinol.* **2011**, *331*, 49–56. [CrossRef]

12. Szekeres, M.; Nadasy, G.L.; Turu, G.; Supeki, K.; Szidonya, L.; Buday, L.; Chaplin, T.; Clark, A.J.; Hunyady, L. Angiotensin II-Induced Expression of Brain-Derived Neurotrophic Factor in Human and Rat Adrenocortical Cells. *Endocrinology* **2010**, *151*, 1695–1703. [CrossRef] [PubMed]

13. Nogueira, E.F.; Vargas, C.A.; Otis, M.; Gallo-Payet, N.; Bollag, W.B.; Rainey, W.E. Angiotensin-II Acute Regulation of Rapid Response Genes in Human, Bovine, and Rat Adrenocortical Cells. *J. Mol. Endocrinol.* **2007**, *39*, 365–374. [CrossRef] [PubMed]

14. Eguchi, S.; Hirata, Y.; Imai, T.; Kanno, K.; Marumo, F. Phenotypic Change of Endothelin Receptor Subtype in Cultured Rat Vascular Smooth Muscle Cells. *Endocrinology* **1994**, *134*, 222–228. [CrossRef] [PubMed]

15. Chamley-Campbell, J.H.; Campbell, G.R.; Ross, R. Phenotype-Dependent Response of Cultured Aortic Smooth Muscle to Serum Mitogens. *J. Cell Biol.* **1981**, *89*, 379–383. [CrossRef] [PubMed]

16. Mehta, P.K.; Griendling, K.K. Angiotensin II Cell Signaling: Physiological and Pathological Effects in the Cardiovascular System. *Am. J. Physiol. Cell Physiol.* **2007**, *292*, C82–C97. [CrossRef]

17. Patterson, K.I.; Brummer, T.; O'Brien, P.M.; Daly, R.J. Dual-Specificity Phosphatases: Critical Regulators with Diverse Cellular Targets. *BioChem. J.* **2009**, *418*, 475–489. [CrossRef]

18. Caunt, C.J.; Keyse, S.M. Dual-Specificity MAP Kinase Phosphatases (MKPs): Shaping the Outcome of MAP Kinase Signalling. *FEBS J.* **2013**, *280*, 489–504. [CrossRef]

19. Liu, R.; Molkentin, J.D. Regulation of Cardiac Hypertrophy and Remodeling through the Dual-Specificity MAPK Phosphatases (DUSPs). *J. Mol. Cell. Cardiol.* **2016**, *101*, 44–49. [CrossRef] [PubMed]

20. Liu, R.; van Berlo, J.H.; York, A.J.; Vagnozzi, R.J.; Maillet, M.; Molkentin, J.D. DUSP8 Regulates Cardiac Ventricular Remodeling by Altering ERK1/2 Signaling. *Circ. Res.* **2016**, *119*, 249–260. [CrossRef] [PubMed]

21. Elliott, K.J.; Eguchi, S. In Vitro Assays to Determine Smooth Muscle Cell Hypertrophy, Protein Content, and Fibrosis. *Methods Mol. Biol.* **2017**, *1614*, 147–153. [CrossRef]

22. Ritchie, M.E.; Phipson, B.; Wu, D.; Hu, Y.; Law, C.W.; Shi, W.; Smyth, G.K. Limma Powers Differential Expression Analyses for RNA-Sequencing and Microarray Studies. *Nucleic Acids Res.* **2015**, *43*, e47. [CrossRef]

23. Holland, C.H.; Szalai, B.; Saez-Rodriguez, J. Transfer of Regulatory Knowledge from Human to Mouse for Functional Genomics Analysis. Biochim. Biophys. *Acta Gene Regul. Mech.* **2020**, *1863*, 194431. [CrossRef]

24. Schubert, M.; Klinger, B.; Klünemann, M.; Sieber, A.; Uhlitz, F.; Sauer, S.; Garnett, M.J.; Blüthgen, N.; Saez-Rodriguez, J. Perturbation-Response Genes Reveal Signaling Footprints in Cancer Gene Expression. *Nat. Commun.* **2018**, *9*, 20. [CrossRef] [PubMed]

25. Stewart, S.A.; Dykxhoorn, D.M.; Palliser, D.; Mizuno, H.; Yu, E.Y.; An, D.S.; Sabatini, D.M.; Chen, I.S.; Hahn, W.C.; Sharp, P.A.; et al. Lentivirus-Delivered Stable Gene Silencing by RNAi in Primary Cells. *RNA* **2003**, *9*, 493–501. [CrossRef]

26. Szalai, B.; Saez-Rodriguez, J. Why Do Pathway Methods Work Better than They Should? *FEBS Lett.* **2020**, *594*, 4189–4200. [CrossRef] [PubMed]

27. Cosentino, F.; Savoia, C.; De Paolis, P.; Francia, P.; Russo, A.; Maffei, A.; Venturelli, V.; Schiavoni, M.; Lembo, G.; Volpe, M. Angiotensin II Type 2 Receptors Contribute to Vascular Responses in Spontaneously Hypertensive Rats Treated with Angiotensin II Type 1 Receptor Antagonists. *Am. J. Hypertens.* **2005**, *18*, 493–499. [CrossRef]

28. Ohtsu, H.; Higuchi, S.; Shirai, H.; Eguchi, K.; Suzuki, H.; Hinoki, A.; Brailoiu, E.; Eckhart, A.D.; Frank, G.D.; Eguchi, S. Central Role of Gq in the Hypertrophic Signal Transduction of Angiotensin II in Vascular Smooth Muscle Cells. *Endocrinology* **2008**, *149*, 3569–3575. [CrossRef]

29. Kawai, T.; Forrester, S.J.; O'Brien, S.; Baggett, A.; Rizzo, V.; Eguchi, S. AT1 Receptor Signaling Pathways in the Cardiovascular System. *Pharm. Res.* **2017**, *125*, 4–13. [CrossRef]

30. Violin, J.D.; DeWire, S.M.; Yamashita, D.; Rominger, D.H.; Nguyen, L.; Schiller, K.; Whalen, E.J.; Gowen, M.; Lark, M.W. Selectively Engaging Beta-Arrestins at the Angiotensin II Type 1 Receptor Reduces Blood Pressure and Increases Cardiac Performance. *J. Pharm. Exp. Ther.* **2010**, *335*, 572–579. [CrossRef]

31. Szakadati, G.; Toth, A.D.; Olah, I.; Erdelyi, L.S.; Balla, T.; Varnai, P.; Hunyady, L.; Balla, A. Investigation of the Fate of Type I Angiotensin Receptor after Biased Activation. *Mol. Pharm.* **2015**, *87*, 972–981. [CrossRef]

32. Devost, D.; Sleno, R.; Petrin, D.; Zhang, A.; Shinjo, Y.; Okde, R.; Aoki, J.; Inoue, A.; Hebert, T.E. Conformational Profiling of the AT1 Angiotensin II Receptor Reflects Biased Agonism, G Protein Coupling, and Cellular Context. *J. Biol. Chem.* **2017**, *292*, 5443–5456. [CrossRef] [PubMed]

33. Odenbach, J.; Wang, X.; Cooper, S.; Chow, F.L.; Oka, T.; Lopaschuk, G.; Kassiri, Z.; Fernandez-Patron, C. MMP-2 Mediates Angiotensin II-Induced Hypertension under the Transcriptional Control of MMP-7 and TACE. *Hypertension* **2011**, *57*, 123–130. [CrossRef] [PubMed]

34. Schreier, B.; Dohler, M.; Rabe, S.; Schneider, B.; Schwerdt, G.; Ruhs, S.; Sibilia, M.; Gotthardt, M.; Gekle, M.; Grossmann, C. Consequences of Epidermal Growth Factor Receptor (ErbB1) Loss for Vascular Smooth Muscle Cells from Mice with Targeted Deletion of ErbB1. *Arter. Thromb. Vasc. Biol.* **2011**, *31*, 1643–1652. [CrossRef]

35. Zou, Z.G.; Rios, F.J.; Neves, K.B.; Alves-Lopes, R.; Ling, J.; Baillie, G.S.; Gao, X.; Fuller, W.; Camargo, L.L.; Gudermann, T.; et al. Epidermal Growth Factor Signaling through Transient Receptor Potential Melastatin 7 Cation Channel Regulates Vascular Smooth Muscle Cell Function. *Clin. Sci.* **2020**, *134*, 2019–2035. [CrossRef]

36. Shah, B.H.; Catt, K.J. Calcium-Independent Activation of Extracellularly Regulated Kinases 1 and 2 by Angiotensin II in Hepatic C9 Cells: Roles of Protein Kinase Cdelta, Src/Proline-Rich Tyrosine Kinase 2, and Epidermal Growth Receptor Trans-Activation. *Mol. Pharm.* **2002**, *61*, 343–351. [CrossRef]

37. Andreev, J.; Galisteo, M.L.; Kranenburg, O.; Logan, S.K.; Chiu, E.S.; Okigaki, M.; Cary, L.A.; Moolenaar, W.H.; Schlessinger, J. Src and Pyk2 Mediate G-Protein-Coupled Receptor Activation of Epidermal Growth Factor Receptor (EGFR) but Are Not Required for Coupling to the Mitogen-Activated Protein (MAP) Kinase Signaling Cascade. *J. Biol. Chem.* **2001**, *276*, 20130–20135. [CrossRef]

38. Eguchi, S.; Iwasaki, H.; Inagami, T.; Numaguchi, K.; Yamakawa, T.; Motley, E.D.; Owada, K.M.; Marumo, F.; Hirata, Y. Involvement of PYK2 in Angiotensin II Signaling of Vascular Smooth Muscle Cells. *Hypertension* **1999**, *33*, 201–206. [CrossRef]

39. Li, H.; Li, W.; Gupta, A.K.; Mohler, P.J.; Anderson, M.E.; Grumbach, I.M. Calmodulin Kinase II Is Required for Angiotensin II-Mediated Vascular Smooth Muscle Hypertrophy. *Am. J. Physiol. Heart Circ. Physiol.* **2010**, *298*, H688–H698. [CrossRef] [PubMed]

40. Prasad, A.M.; Nuno, D.W.; Koval, O.M.; Ketsawatsomkron, P.; Li, W.; Li, H.; Shen, F.Y.; Joiner, M.L.; Kutschke, W.; Weiss, R.M.; et al. Differential Control of Calcium Homeostasis and Vascular Reactivity by Ca^{2+}/Calmodulin-Dependent Kinase II. *Hypertension* **2013**, *62*, 434–441. [CrossRef]

41. Bit, R.A.; Davis, P.D.; Elliott, L.H.; Harris, W.; Hill, C.H.; Keech, E.; Kumar, H.; Lawton, G.; Maw, A.; Nixon, J.S.; et al. Inhibitors of Protein Kinase C. 3. Potent and Highly Selective Bisindolylmaleimides by Conformational Restriction. *J. Med. Chem.* **1993**, *36*, 21–29. [CrossRef]

42. Booij, T.H.; Klop, M.J.; Yan, K.; Szantai-Kis, C.; Szokol, B.; Orfi, L.; van de Water, B.; Keri, G.; Price, L.S. Development of a 3D Tissue Culture-Based High-Content Screening Platform That Uses Phenotypic Profiling to Discriminate Selective Inhibitors of Receptor Tyrosine Kinases. *J. Biomol. Screen.* **2016**, *21*, 912–922. [CrossRef] [PubMed]

43. Verma, N.; Rai, A.K.; Kaushik, V.; Brunnert, D.; Chahar, K.R.; Pandey, J.; Goyal, P. Identification of Gefitinib Off-Targets Using a Structure-Based Systems Biology Approach; Their Validation with Reverse Docking and Retrospective Data Mining. *Sci. Rep.* **2016**, *6*, 33949. [CrossRef] [PubMed]

44. Brehmer, D.; Greff, Z.; Godl, K.; Blencke, S.; Kurtenbach, A.; Weber, M.; Muller, S.; Klebl, B.; Cotten, M.; Keri, G.; et al. Cellular Targets of Gefitinib. *Cancer Res.* **2005**, *65*, 379–382. [PubMed]

45. Du, J.; Sperling, L.S.; Marrero, M.B.; Phillips, L.; Delafontaine, P. G-Protein and Tyrosine Kinase Receptor Cross-Talk in Rat Aortic Smooth Muscle Cells: Thrombin- and Angiotensin II-Induced Tyrosine Phosphorylation of Insulin Receptor Substrate-1 and Insulin-like Growth Factor 1 Receptor. *BioChem. Biophys Res. Commun.* **1996**, *218*, 934–939. [CrossRef]

46. Heeneman, S.; Haendeler, J.; Saito, Y.; Ishida, M.; Berk, B.C. Angiotensin II Induces Transactivation of Two Different Populations of the Platelet-Derived Growth Factor Beta Receptor. Key Role for the P66 Adaptor Protein Shc. *J. Biol. Chem.* **2000**, *275*, 15926–15932. [CrossRef] [PubMed]

47. Lefkowitz, R.J. Seven Transmembrane Receptors: Something Old, Something New. *Acta Physiol.* **2007**, *190*, 9–19. [CrossRef]

48. Makki, N.; Thiel, K.W.; Miller, F.J. The Epidermal Growth Factor Receptor and Its Ligands in Cardiovascular Disease. *Int. J. Mol. Sci.* **2013**, *14*, 20597–20613. [CrossRef] [PubMed]

49. Yin, X.; Polidano, E.; Faverdin, C.; Marche, P. Role of L-Type Calcium Channel Blocking in Epidermal Growth Factor Receptor-Independent Activation of Extracellular Signal Regulated Kinase 1/2. *J. Hypertens.* **2005**, *23*, 337–350. [CrossRef]

50. Tomas, A.; Futter, C.E.; Eden, E.R. EGF Receptor Trafficking: Consequences for Signaling and Cancer. *Trends Cell Biol.* **2014**, *24*, 26–34. [CrossRef]

51. Bokemeyer, D.; Schmitz, U.; Kramer, H.J. Angiotensin II-Induced Growth of Vascular Smooth Muscle Cells Requires an Src-Dependent Activation of the Epidermal Growth Factor Receptor. *Kidney Int.* **2000**, *58*, 549–558. [CrossRef] [PubMed]

52. Eguchi, S.; Numaguchi, K.; Iwasaki, H.; Matsumoto, T.; Yamakawa, T.; Utsunomiya, H.; Motley, E.D.; Kawakatsu, H.; Owada, K.M.; Hirata, Y.; et al. Calcium-Dependent Epidermal Growth Factor Receptor Transactivation Mediates the Angiotensin II-Induced Mitogen-Activated Protein Kinase Activation in Vascular Smooth Muscle Cells. *J. Biol. Chem.* **1998**, *273*, 8890–8896. [CrossRef]

53. Buffet, C.; Catelli, M.G.; Hecale-Perlemoine, K.; Bricaire, L.; Garcia, C.; Gallet-Dierick, A.; Rodriguez, S.; Cormier, F.; Groussin, L. Dual Specificity Phosphatase 5, a Specific Negative Regulator of ERK Signaling, Is Induced by Serum Response Factor and Elk-1 Transcription Factor. *PLoS ONE* **2015**, *10*, e0145484. [CrossRef] [PubMed]

54. Ferguson, B.S.; Harrison, B.C.; Jeong, M.Y.; Reid, B.G.; Wempe, M.F.; Wagner, F.F.; Holson, E.B.; McKinsey, T.A. Signal-Dependent Repression of DUSP5 by Class I HDACs Controls Nuclear ERK Activity and Cardiomyocyte Hypertrophy. *Proc. Natl. Acad. Sci. USA* **2013**, *110*, 9806–9811. [CrossRef] [PubMed]

55. Kidger, A.M.; Rushworth, L.K.; Stellzig, J.; Davidson, J.; Bryant, C.J.; Bayley, C.; Caddye, E.; Rogers, T.; Keyse, S.M.; Caunt, C.J. Dual-Specificity Phosphatase 5 Controls the Localized Inhibition, Propagation, and Transforming Potential of ERK Signaling. *Proc. Natl. Acad. Sci. USA* **2017**, *114*, E317–E326. [CrossRef] [PubMed]

56. Karlsson, M.; Mathers, J.; Dickinson, R.J.; Mandl, M.; Keyse, S.M. Both Nuclear-Cytoplasmic Shuttling of the Dual Specificity Phosphatase MKP-3 and Its Ability to Anchor MAP Kinase in the Cytoplasm Are Mediated by a Conserved Nuclear Export Signal. *J. Biol. Chem.* **2004**, *279*, 41882–41891. [CrossRef] [PubMed]

57. Bermudez, O.; Jouandin, P.; Rottier, J.; Bourcier, C.; Pages, G.; Gimond, C. Post-Transcriptional Regulation of the DUSP6/MKP-3 Phosphatase by MEK/ERK Signaling and Hypoxia. *J. Cell. Physiol.* **2011**, *226*, 276–284. [CrossRef]

58. Maillet, M.; Purcell, N.H.; Sargent, M.A.; York, A.J.; Bueno, O.F.; Molkentin, J.D. DUSP6 (MKP3) Null Mice Show Enhanced ERK1/2 Phosphorylation at Baseline and Increased Myocyte Proliferation in the Heart Affecting Disease Susceptibility. *J. Biol. Chem.* **2008**, *283*, 31246–31255. [CrossRef]

59. Jimenez-Martinez, M.; Stamatakis, K.; Fresno, M. The Dual-Specificity Phosphatase 10 (DUSP10): Its Role in Cancer, Inflammation, and Immunity. *Int. J. Mol. Sci.* **2019**, 20. [CrossRef]

60. Theodosiou, A.; Smith, A.; Gillieron, C.; Arkinstall, S.; Ashworth, A. MKP5, a New Member of the MAP Kinase Phosphatase Family, Which Selectively Dephosphorylates Stress-Activated Kinases. *Oncogene* **1999**, *18*, 6981–6988. [CrossRef] [PubMed]

61. Nomura, M.; Shiiba, K.; Katagiri, C.; Kasugai, I.; Masuda, K.; Sato, I.; Sato, M.; Kakugawa, Y.; Nomura, E.; Hayashi, K.; et al. Novel Function of MKP-5/DUSP10, a Phosphatase of Stress-Activated Kinases, on ERK-Dependent Gene Expression, and Upregulation of Its Gene Expression in Colon Carcinomas. *Oncol. Rep.* **2012**, *28*, 931–936. [CrossRef] [PubMed]

62. Finch, A.R.; Caunt, C.J.; Perrett, R.M.; Tsaneva-Atanasova, K.; McArdle, C.A. Dual Specificity Phosphatases 10 and 16 Are Positive Regulators of EGF-Stimulated ERK Activity: Indirect Regulation of ERK Signals by JNK/P38 Selective MAPK Phosphatases. *Cell. Signal.* **2012**, *24*, 1002–1011. [CrossRef] [PubMed]

63. Luo, L.J.; Liu, F.; Wang, X.Y.; Dai, T.Y.; Dai, Y.L.; Dong, C.; Ge, B.X. An Essential Function for MKP5 in the Formation of Oxidized Low Density Lipid-Induced Foam Cells. *Cell. Signal.* **2012**, *24*, 1889–1898. [CrossRef] [PubMed]

64. Montezano, A.C.; Nguyen Dinh Cat, A.; Rios, F.J.; Touyz, R.M. Angiotensin II and Vascular Injury. *Curr. Hypertens. Rep.* **2014**, *16*, 431. [CrossRef] [PubMed]

Article

An Unexpected Enzyme in Vascular Smooth Muscle Cells: Angiotensin II Upregulates Cholesterol-25-Hydroxylase Gene Expression

Kinga Bernadett Kovács [1], Laura Szalai [1,2], Pál Szabó [3], Janka Borbála Gém [1], Szilvia Barsi [1], Bence Szalai [1,4], Bernadett Perey-Simon [1], Gábor Turu [1,2], András Dávid Tóth [1,2,5], Péter Várnai [1,2], László Hunyady [1,2,4,*,†] and András Balla [1,2,*,†]

[1] Department of Physiology, Semmelweis University, 1094 Budapest, Hungary
[2] ELKH-SE Laboratory of Molecular Physiology, Eötvös Loránd Research Network and Semmelweis University, 1085 Budapest, Hungary
[3] Research Center for Natural Sciences, Center for Structural Study, MS Metabolomics Laboratory, 1117 Budapest, Hungary
[4] Research Centre for Natural Sciences, Institute of Enzymology, 1117 Budapest, Hungary
[5] Department of Internal Medicine and Haematology, Semmelweis University, 1088 Budapest, Hungary
[*] Correspondence: hunyady.laszlo@med.semmelweis-univ.hu (L.H.); balla.andras@med.semmelweis-univ.hu (A.B.); Tel.: +36-1-459-1500 (ext. 60401) (L.H.); +36-1-459-1500 (ext. 60450) (A.B.)
[†] These authors contributed equally to this work.

Abstract: Angiotensin II (AngII) is a vasoactive peptide hormone, which, under pathological conditions, contributes to the development of cardiovascular diseases. Oxysterols, including 25-hydroxycholesterol (25-HC), the product of cholesterol-25-hydroxylase (CH25H), also have detrimental effects on vascular health by affecting vascular smooth muscle cells (VSMCs). We investigated AngII-induced gene expression changes in VSMCs to explore whether AngII stimulus and 25-HC production have a connection in the vasculature. RNA-sequencing revealed that *Ch25h* is significantly upregulated in response to AngII stimulus. The *Ch25h* mRNA levels were elevated robustly (~50-fold) 1 h after AngII (100 nM) stimulation compared to baseline levels. Using inhibitors, we specified that the AngII-induced *Ch25h* upregulation is type 1 angiotensin II receptor- and $G_{q/11}$ activity-dependent. Furthermore, p38 MAPK has a crucial role in the upregulation of *Ch25h*. We performed LC-MS/MS to identify 25-HC in the supernatant of AngII-stimulated VSMCs. In the supernatants, 25-HC concentration peaked 4 h after AngII stimulation. Our findings provide insight into the pathways mediating AngII-induced *Ch25h* upregulation. Our study elucidates a connection between AngII stimulus and 25-HC production in primary rat VSMCs. These results potentially lead to the identification and understanding of new mechanisms in the pathogenesis of vascular impairments.

Keywords: angiotensin II; atherosclerosis; cholesterol-25-hydroxylase; 25-hydroxycholesterol; vascular smooth muscle cell

1. Introduction

Cardiovascular disease (CVD) is the most common cause of death despite the decrease in CVD mortality throughout the years [1,2]. Atherosclerosis is one of the causative factors leading to the development of CVD. Both angiotensin II (AngII) and oxysterols are implicated in the pathological processes underlying atherosclerosis [3,4]. The present study aims to elucidate a connection between AngII and oxysterol production in primary vascular smooth muscle cells (VSMCs).

AngII is a vasoactive peptide hormone, which is the main effector molecule of the renin–angiotensin–aldosterone system (RAAS). Under physiological conditions, the RAAS regulates blood pressure through the alteration of blood volume and vascular resistance [5].

AngII exerts its physiological effects on VSMCs mainly through type 1 angiotensin II receptor (AT1R), which is a 7-transmembrane domain, G protein-coupled receptor (GPCR). The activated AT1R interacts with $G_{q/11}$, $G_{12/13}$, and G_i heterotrimeric G proteins; hence, the activated signalization pathways upon ligand binding are diverse. The most characteristic is $G_{q/11}$ signalization, which results in intracellular Ca^{2+} release and thus leads to VSMC contraction on tissue-level vasoconstriction [3]. It is well established that the AT1R signalization pathways in the vasculature are pleiotropic and involve growth factor receptor transactivation as well as the activation of numerous kinases [3]. The disrupted RAAS function, excessive AngII production, or AT1R activity promote pathological processes such as vascular remodeling [6]. AngII promotes reactive oxygen species (ROS) production, VSMC hypertrophy, proliferation and migration, collagen synthesis, the structural modification of vessel walls, and tumor necrosis factor-alpha (TNF-α) expression [7–12]. It is clear that AngII and AT1R signalization have serious implications for CVD. Yet, the exact signalization mechanisms and the induced cellular processes are not yet fully understood.

Oxysterols are the products of enzymatic or non-enzymatic reactions [13] and, similarly to AngII, can have detrimental effects on the vasculature [4,14,15]. For example, 25-hydroxycholesterol (25-HC) is the product of the cholesterol-25-hydroxylase (CH25H) enzyme, and it has several roles in various physiological functions. Indeed, 25-HC has been shown to possess a negative regulatory effect on cholesterol synthesis by inhibiting the proteolysis of sterol regulatory element-binding protein (SREBP) precursors, thus preventing the transcriptional events needed for cholesterol synthesis [16].

The oxysterol 25-HC is widely studied for its significant immunological properties, one of which is a strong antiviral action. It is exerted through the inhibition of viral entry, which has been described in the case of vesicular stomatitis virus (VSV), human immunodeficiency virus (HIV), Nipah virus (NiV), Ebola virus (EBOV), and Zika virus (ZIKV) [17,18]. Recently it was reported that 25-HC blocks the entry of severe acute respiratory syndrome coronavirus 2 (SARS-CoV-2), SARS-CoV, and Middle East respiratory syndrome coronavirus (MERS-CoV) [19]. CH25H and its oxysterol product are also mediators of innate immune responses. Following Toll-like receptor (TLR) agonist stimulus, CH25H induction and subsequent 25-HC production occur in dendritic cells and macrophages, which is regulated by type I interferons [20,21]. In vivo experiments revealed that TLR activation also results in elevated serum 25-HC levels in mice [20]. Oxysterols, including 25-HC, were found in the aortic tissue of hypercholesterolemic rabbits [22]. These hydroxylated products are also present in atherosclerotic plaques and are involved in atherosclerosis pathogenesis [14]. This is due to their role in promoting inflammatory cytokine production, foam cell formation, increasing matrix metalloproteinase-9 (MMP-9) expression, and contributing to vascular dysfunction through pro-oxidant effects [4,15,23]. In atherosclerotic lesions, macrophages express the chemokine interleukin-8 (IL-8), which is promoted by 25-HC in a dose-dependent and TLR-independent manner [24,25]. In macrophages, a proinflammatory response to 25-HC is triggered by the binding of 25-HC to integrins and the subsequent activation of focal adhesion kinase (FAK) signalization [26]. It was also demonstrated that 25-HC was able to induce ROS production in VSMCs [27]. The apoptotic effect of 25-HC on VSMCs has been described in primary cells derived from rabbits and chickens as well as in human VSMC cell lines [28–31]. It has been shown that 25-HC induces apoptosis via increased Ca^{2+} uptake of VSMCs [29] and, in addition, 25-HC promotes protein kinase A (PKA) dependent Bax phosphorylation and its subsequent translocation to the mitochondria, which leads to ROS production and the activation of the mitochondrial pathway of apoptosis [27]. VSMC apoptosis is notable in symptomatic plaques. It prominently occurs in the necrotic core and fibrous cap of atherosclerotic plaques; as a consequence, the fibrous cap grows thinner and, therefore, the risk of lesion rupture increases [32]. Another hallmark of atherosclerotic plaque formation is the phenotypic change and calcification of VSMCs, and these processes are also promoted by 25-HC [4,33].

Here, we present the novel findings that AngII stimulus markedly upregulates *Ch25h* expression through AT1R activation in rat primary VSMCs and, as a result of enzyme activity, 25-HC is present in the supernatant of cultured primary rat VSMCs.

2. Results

2.1. AngII Induces Upregulation of Ch25h Gene Expression in Primary Rat VSMCs

To investigate transcriptomic changes associated with AngII-stimulation in rat VSMCs, we carried out RNA-sequencing (RNA-seq). Serum-deprived VSMCs were stimulated with 100 nM AngII or vehicle for 2 h. After preprocessing the RNA-seq data, we performed differential expression (DE) analysis (see Section 4). Considering the role of oxysterols and 25-HC in atherogenic processes [14,15], we were especially curious about how AngII affects *Ch25h* expression. *Ch25h*, which encodes the CH25H protein that catalyzes the formation of 25-HC, is significantly (p-value = 7.88×10^{-4}, false discovery rate (FDR) corrected p-value < 0.1 based on Benjamini–Hochberg correction) upregulated in AngII stimulated samples. We found that *Ch25h* has the 10th highest $\log_2$FC among significantly (FDR < 0.1) upregulated genes (Figure 1A). *Ch25h* upregulation was significantly induced by AngII stimulation (Figure 1B), while no *Ch25h* mRNA was detected in vehicle-stimulated samples. The expression in AngII-stimulated samples increased to 0.74 TPM (Figure 1B).
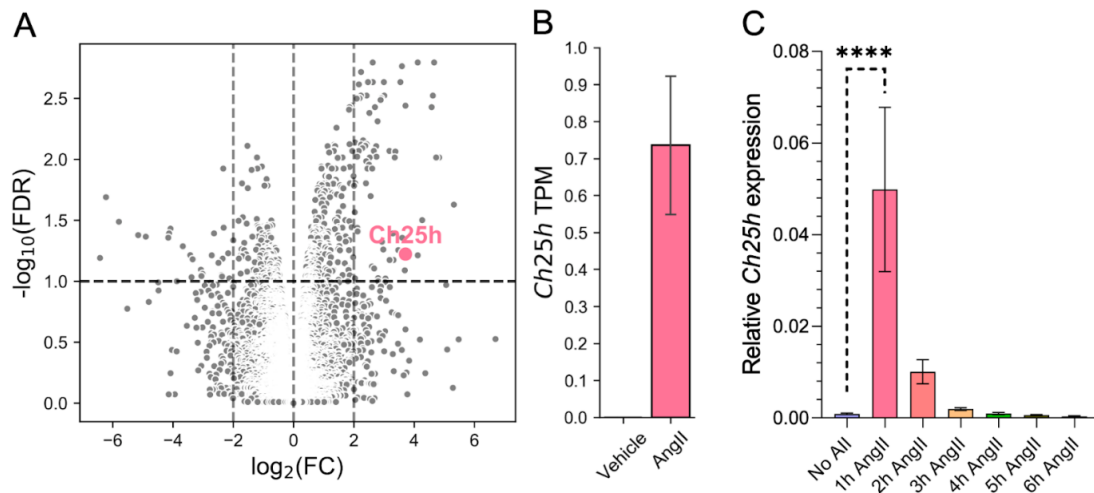

Figure 1. *Ch25h* gene expression is upregulated by AngII stimulus in rat VSMCs. (**A**) Serum-deprived VSMCs were stimulated with 100 nM AngII or treated with vehicle for 2 h. The results of the DE analysis of RNA-sequenced samples are shown as a volcano plot (x-axis: $\log_2$(FC, fold change) q, y-axis: $-\log_{10}$ (FDR, false discovery rate) based on the Benjamini–Hochberg correction of p-values. Of the significantly upregulated genes, the *Ch25h* is marked in pink. The horizontal line represents the significance threshold (FDR < 0.1). (**B**) The mean transcript per million (TPM) values of the *Ch25h* in 2 h AngII-stimulated (TPM = 0.74) VMSCs were changed compared to vehicle-treated (TPM = 0) VMSCs. (**C**) Serum-deprived VSMCs were stimulated with 100 nM AngII for 1, 2, 3, 4, 5, and 6 h or not stimulated. Total mRNA was isolated from these cells. Following cDNA preparation, qRT-PCR was performed. *Ch25h* mRNA levels are presented relative to *Gapdh*. Values are plotted as the mean $\pm$ SEM of n = 5 independent experiments. Data were analyzed using multiple linear regression, **** $p < 0.0001$.

To verify the RNA-seq results, we measured *Ch25h* mRNA levels in VSMCs using qRT-PCR. VSMCs were stimulated with 100 nM AngII for various time periods, namely 1, 2, 3, 4, 5, and 6 h or not stimulated. Our data show that *Ch25h* mRNA levels indeed increased in response to the AngII stimulus. *Ch25h* mRNA levels peaked 1 h after stimulus resulting in a more than fifty-fold increase compared to the baseline *Ch25h* mRNA levels (Figure 1C). Henceforth, we chose the 1 h stimulation time point to further analyze *Ch25h* expression characteristics in VSMCs.

2.2. AngII-Induced Ch25h Upregulation Is AT1R and G$_{q/11}$ Activity-Dependent in Primary Rat VSMCs

In order to determine the role of AT1R in *Ch25h* upregulation, we treated VSMCs with 10 μM candesartan AT1R antagonist for 30 min prior to 1 h 100 nM AngII stimulus. As expected, the candesartan pretreatment completely inhibited the AngII-induced *Ch25h* upregulation (Figure 2A). AT1R activation triggers signalization pathways typically through the G$_{q/11}$ protein. To investigate the role of the G$_{q/11}$ function in the upregulation of *Ch25h*, we utilized two approaches: the inhibition of the G$_{q/11}$ pathway and the selective activation of the β-arrestin pathway. We pretreated the VSMCs with 1 μM YM-254890 G$_{q/11}$ inhibitor for 30 min and then stimulated the cells with 100 nM AngII for 1 h. In a separate set of experiments, the VSMCs were stimulated with 3 μM TRV120023 (TRV3) peptide for one hour. TRV3 is a β-arrestin-biased AT1R agonist, and upon its receptor binding, the induced signalization does not include G$_{q/11}$ protein activation [34–37]. Our qRT-PCR data indicate that YM-254890 pretreatment completely prevented *Ch25h* upregulation (Figure 2A), and TRV3 stimulus did not increase the mRNA level of *Ch25h* (Figure 2B).
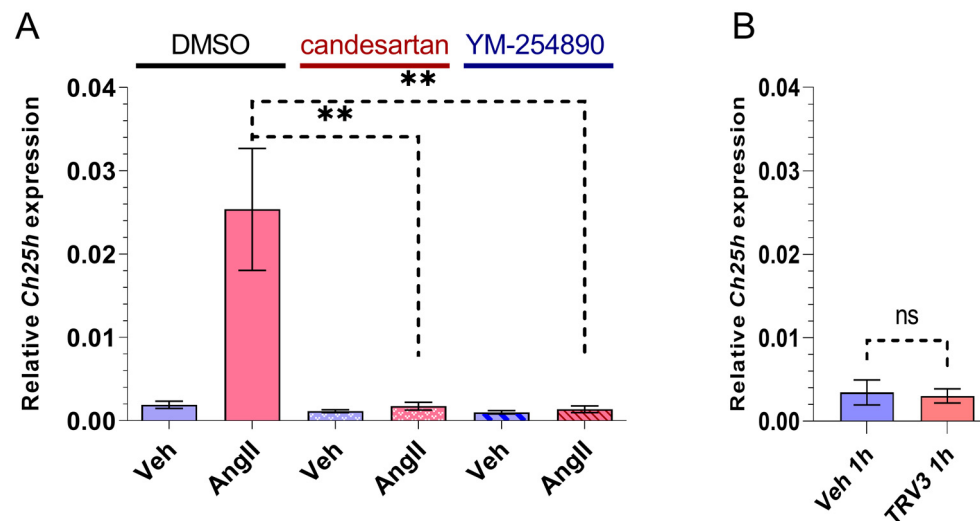

Figure 2. Effect of AT1R blocker, G$_{q/11}$ inhibitor, and β-arrestin biased agonist on *Ch25h* gene expression in rat VSMCs. (**A**) Serum-deprived VSMCs were treated with 10 μM candesartan or 1 μM YM-254890 for 30 min, whereas the negative control group received DMSO treatment. Subsequently, VSMCs were stimulated with 100 nM AngII or vehicle (Veh) for 1 h. *Ch25h* mRNA levels were measured using qRT-PCR. *Ch25h* mRNA levels are presented relative to *Gapdh*. Values are plotted as the mean ± SEM of n = 4–5 independent experiments. Data were analyzed using multiple linear regression, ** $p < 0.01$. (**B**) Serum-deprived VSMCs were stimulated with 3 μM TRV120023 (TRV3) or vehicle (Veh) for 1 h. *Ch25h* mRNA levels are presented relative to *Gapdh*. Values are plotted as the mean ± SEM of n = 3 independent experiments. The unpaired *t*-test showed no significant changes in *Ch25h* expression between groups, (ns: not significant).

2.3. Role of MAP Kinase Family Kinases in AngII-Induced Ch25h Upregulation in Primary Rat VSMCs

Our data suggest that G$_{q/11}$-mediated signaling pathways have a crucial role in *Ch25h* upregulation. MAP kinase family members such as ERK1/2, p38 mitogen-activated protein kinase (p38 MAPK), and c-Jun N-terminal kinase (JNK) are activated upon AT1R activation [3], mostly via G$_{q/11}$ activation [38,39]. To explore the involved signaling events downstream of G$_{q/11}$ protein activation, we used several MAPK family kinase inhibitors to assess the role of various MAPKs (Figure 3A–C). We used MEK inhibitor PD98059 (20 μM) for the elimination of ERK1/2 activity, SB202190 (50 μM) for p38 MAPK activity inhibition, and JNK-IN-8 (1 μM) to inhibit JNKs. VSMCs were pretreated for 30 min with one of the kinase inhibitors or DMSO as the control. Then, the VSMCs were stimulated with 100 nM AngII or vehicle for 1 h. *Ch25h* mRNA levels were assessed using qRT-PCR

measurements. Figure 3A demonstrates that the PD98059 pretreatment caused slightly reduced AngII-induced *Ch25h* upregulation; however, this reduction was not significant. MEK and ERK1/2 activation might have some role in AngII-induced *Ch25h* upregulation, but this effect is not prominent. JNK-IN-8 (IN-8) pretreatment caused virtually no difference in *Ch25h* expression upon AngII stimulus compared to the DMSO-treated group (Figure 3B). In contrast, SB202190 pretreatment resulted in a significantly lower *Ch25h* expression in the AngII stimulated group (Figure 3C) compared to the DMSO control. Based on this result, it seems that p38 MAPK has a substantial role in AngII-induced *Ch25h* upregulation in VSMCs.
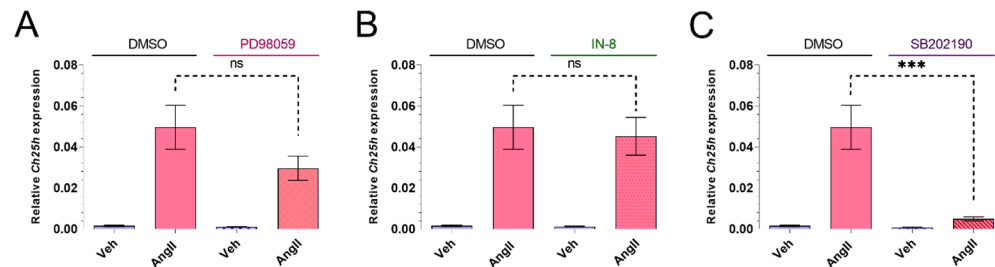

Figure 3. Effect of MAP kinase family inhibitors on *Ch25h* gene expression in rat VSMCs. (**A**) Serum-deprived VSMCs were treated with 20 μM PD98059, (**B**) 1 μM JNK-IN-8 (IN-8), or (**C**) 50 μM SB202190 for 30 min. The negative control group was treated with DMSO for 30 min in each experiment. Following treatment, VSMCs were stimulated with 100 nM AngII or vehicle (Veh) for 1 h. *Ch25h* mRNA levels are shown relative to *Gapdh*. Values are plotted as the mean ± SEM of n = 6 independent experiments. Data were analyzed using multiple linear regression, *** $p < 0.001$, ns (not significant).

2.4. AngII-Induced Ch25h Upregulation Is Independent of NOX Activation in Primary Rat VSMCs

AngII is able to induce NADPH oxidase (NOX) activity, which leads to increased ROS production [7,40]. Rat VSMCs express the NOX1 and NOX4 isoforms [40,41]. In order to investigate whether AngII-induced ROS production has any role in the subsequent upregulation of Ch25h, we used a diphenyleneiodonium chloride (DPI) pretreatment. DPI is a potent compound that inhibits the activity of NOX isoforms that are expressed in VSMCs [42]. We treated the VSMCs for 30 min with 5 μM DPI before the 1 h AngII (100 nM) stimulation. Our qRT-PCR measurements showed no significant difference between the DMSO- and DPI-treated groups (Figure 4).

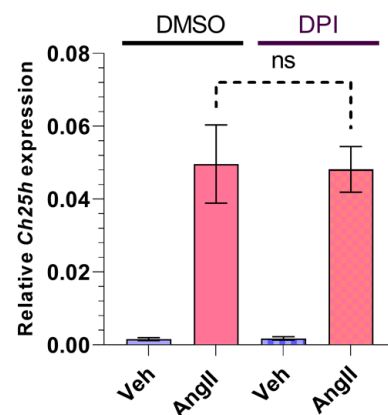**Figure 4.** Effect of NOX inhibitor on *Ch25h* gene expression in rat VSMCs. Serum-deprived VSMCs were treated with 5 μM DPI or DMSO for 30 min. Following treatment, VSMCs were stimulated with 100 nM AngII or vehicle (Veh) for 1 h. *Ch25h* mRNA levels are shown relative to *Gapdh*. Values are plotted as the mean ± SEM of n = 5 independent experiments. Data were analyzed using multiple linear regression, ns (not significant).

2.5. Subcellular Localization of CH25H Protein in Rat VSMC Cell Line and Primary Rat VSMCs

Based on the literature data, mouse and human CH25H proteins both localize to the endoplasmic reticulum (ER) and the Golgi compartment in transfected COS cells [16]. We investigated the subcellular localization of rat CH25H both in the A7R5 rat VSMC cell line (Figure 5A) and in primary rat VSMCs (Figure 5B) utilizing fluorescent proteins fused to either CH25H or an organelle marker protein. We created a DNA construct to transiently overexpress Cerulean-labeled CH25H fusion protein in cells alongside an mRFP-labeled phosphatidylinositol-3-phosphatase SAC1 (SAC1) fusion protein that localizes to the ER. Twenty-four hours after transfection, the cells were examined using confocal microscopy. Confocal images were analyzed with the JACoP plugin [43] to assess the colocalization of the two signals. The average values of Pearson's correlation coefficient were 0.83 ± 0.038 and 0.85 ± 0.01 in the case of A7R5 and rat VSMCs, respectively. These Pearson's correlation coefficient values indicate acceptable colocalization of signals. These results show that Cerulean-CH25H and mRFP-SAC1 colocalize, which confirms the ER localization of CH25H both in A7R5 cells and in primary VSMCs (Figure 5A,B). Additionally, we investigated the localization of Cerulean-CH25H to the Golgi using mRFP-TGN38 and mRFP-Giantin fusion proteins. Data obtained in these experiments show that CH25H and the Golgi markers do not colocalize (Supplementary Figure S2).
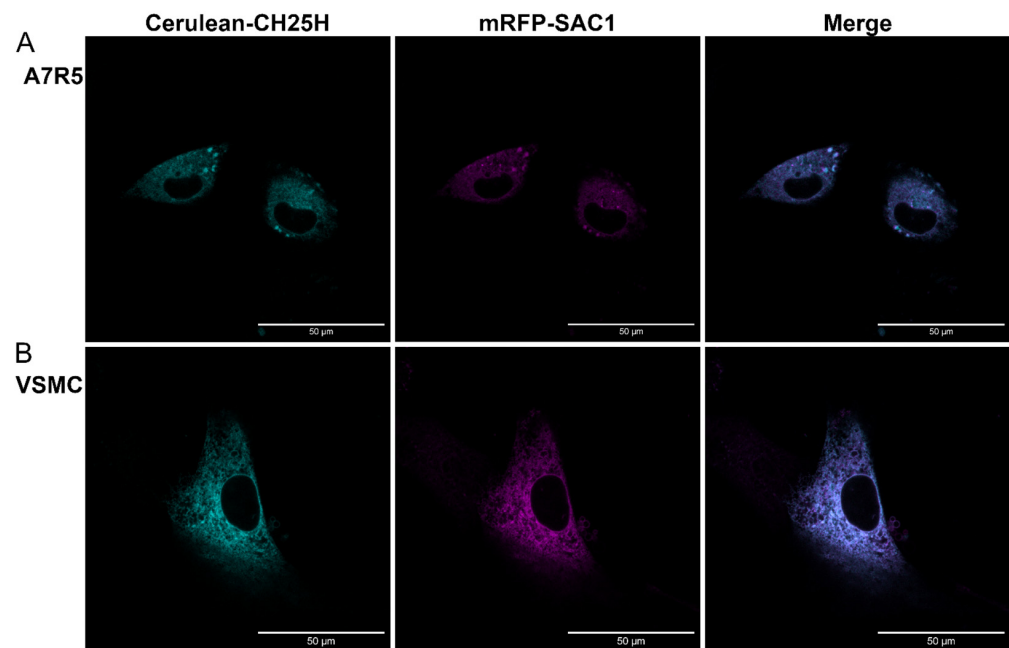

Figure 5. CH25H localizes to the endoplasmic reticulum in the A7R5 rat VSMC cell line and =primary rat VSMCs. (**A**) A7R5 cells and (**B**) primary rat VSMCs were cotransfected with DNA constructs encoding Cerulean-CH25H (cyan) and mRFP-SAC1 (magenta) fusion proteins. Twenty-four hours post-transfection, cells were examined using a Zeiss LSM710 confocal laser-scanning microscope. Merged images and colocalization analysis of signals show good colocalization of SAC1 endoplasmic reticulum marker and CH25H. Pearson's correlation coefficient in A7R5 cells: 0.83 ± 0.038 = mean $\pm$ SEM, and in rat VSMCs: 0.85 ± 0.01 = mean $\pm$ SEM, n = 5 independent experiments. Fiji software was used for image processing and colocalization analysis. Scale bars represent 50 μm.

2.6. The Presence of 25-HC in VSMC Supernatant following AngII Stimulus

It is known that 25-HC, the product of the CH25H enzyme, is capable of binding cell surface molecules and is able to induce various cell responses [26,27,33]; hence, it can function in the extracellular compartment. To find out whether VSMCs could be a source of extracellular 25-HC, we investigated the 25-HC levels in the supernatant of cultured rat VSMCs in response to AngII treatment (Figure 6). The examination of 25-HC levels also serves as an indicator of endogenous CH25H enzyme expression and activity in VSMCs.

In order to detect 25-HC, the VSMCs were stimulated with 1 μM AngII for 2, 4, 8, 16, and 24 h or not stimulated. After the hormone stimulation, 1 mL of the supernatants was collected and subjected to LC-MS/MS measurement. The 25-HC concentrations were progressively increased reaching a peak at the 4 h time point (8.2 ng/mL on average) then returning to baseline levels 16 h post-AngII stimulation (Figure 6). We observed a significant, approximately 8-fold increase in the 25-HC level of VSMC supernatants 4 h after the AngII stimulus compared to the non-stimulated VSMC supernatants.
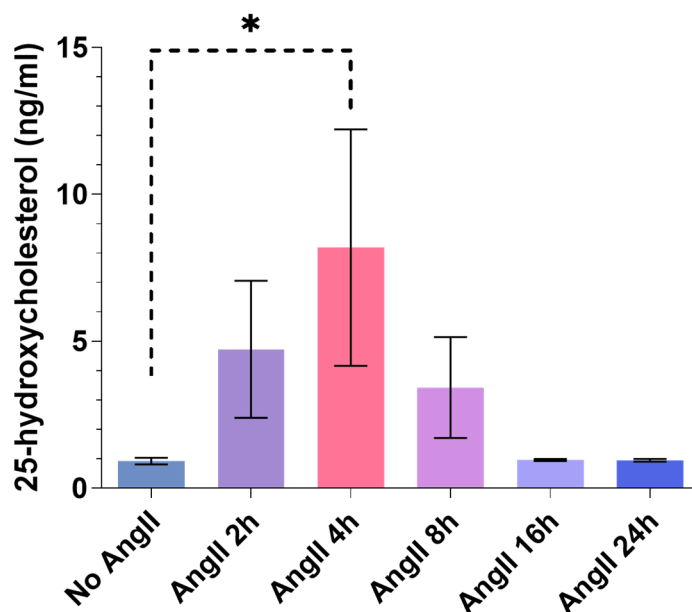

Figure 6. The 25-HC content of AngII-stimulated rat VSMC supernatant. Serum-deprived VSMCs were stimulated with 1 μM AngII for 2, 4, 8, 16, and 24 h or not stimulated. A total of 1 mL of supernatant of the cells was collected and subjected to LC-MS/MS analysis in order to identify 25-HC content and concentration. The 25-HC concentration is expressed in ng/mL. Concentration values are plotted as the mean ± SEM of n = 3 independent experiments. Data were analyzed using multiple linear regression, * $p < 0.05$.

3. Discussion

In this study, we present the following findings: (1) AngII induces significant upregulation of *Ch25h* in primary rat VSMCs, (2) *Ch25h* upregulation is mediated by AT1R through $G_{q/11}$ signaling and not via a β-arrestin-mediated mechanism, (3) p38 MAPK has a substantial role in *Ch25h* upregulation, (4) CH25H localizes to the ER in rat VSMCs, and (5) AngII stimulus promotes 25-HC production in primary rat VSMCs. Prior works show that AngII causes gene expression changes in various cell types [44–47]. Gene expression patterns shape cellular functions and are influenced by external stimuli [48]. Considering the role of AngII in the mediation of vascular remodeling [49] and its ability to activate diverse signalization pathways [3,50], it is crucial to better understand the long-term cellular responses induced by AngII. We examined gene expression changes promoted by AngII in rat primary VSMCs to clarify which genes are affected in response to AngII stimulus and to learn which pathways are involved in these gene expression changes.

In this paper, we show for the first time the upregulation of *Ch25h* expression by AngII in primary rat VSMCs. Our RNA-seq data shows significant upregulation of *Ch25h* in samples stimulated with AngII for 2 h compared to the vehicle-stimulated group (Figure 1A,B). According to our qRT-PCR measurements, *Ch25h* mRNA levels were the highest 1 h after the AngII stimulus, and 3 h after the AngII stimulus, *Ch25h* mRNA levels of the stimulated and non-stimulated groups were similar (Figure 1C). This result suggests that AngII-induced *Ch25h* upregulation is not sustained for longer periods of time in VSMCs. In contrast, various authors found that in different types of macrophages, the increase in

Ch25h expression occurs 4 or 6 h post-stimulus [20,21,51]. In those cells, lipopolysaccharide (LPS) induces *Ch25h* upregulation in a type I IFN- and STAT1-dependent manner [21]. Taken together, these findings suggest that the *Ch25h* upregulation in VSMCs may be regulated in a different manner since *Ch25h* mRNA levels increase much quicker and transiently in VSMCs than in macrophages. This invites further study of *Ch25h* gene regulation in VSMCs.

We investigated the role of AT1R and different signalization pathways in the AngII-induced upregulation of *Ch25h* in VSMCs. AT1R activation is essential for the upregulation of *Ch25h*. This is demonstrated by the fact that the treatment of VSMCs with the AT1R antagonist candesartan completely wiped out the AngII-induced *Ch25h* mRNA level increase (Figure 2A). To distinguish between the various signalization pathways activated by AngII binding to AT1R, we used YM-254890 (a $G_{q/11}$ protein inhibitor) and TRV120023 (a β-arrestin-biased agonist of AT1R) treatments. The inhibition of $G_{q/11}$ obliterated *Ch25h* upregulation, whereas the TRV120023 treatment was not able to induce a *Ch25h* gene expression increase (Figure 2A,B). Based on these results, we conclude that *Ch25h* upregulation in response to AngII stimulus is exclusively AT1R and $G_{q/11}$ activity-dependent in VSMCs.

$G_{q/11}$ activation leads to inositol 1,4,5-trisphosphate (IP_3) dependent Ca^{2+} release and diacylglycerol (DAG) production and, subsequently, ERK1/2 activation in cells [52]. Furthermore, it is well established that AngII stimulus can result in p38 MAPK and JNK activation [3]. This knowledge is especially interesting in light of one study by Bauman et al. where they demonstrated that the inhibition of p38 or JNK MAPK attenuated TLR4-mediated *Ch25h* mRNA increase in macrophages [20]. Considering the above-mentioned literature data, we examined the effects of SB202190, a p38 MAPK inhibitor, and JNK-IN-8, a JNK inhibitor. We found that SB202190 but not JNK-IN-8 inhibited the AngII-induced *Ch25h* upregulation (Figure 3B,C). These results indicated the role of p38 MAPK in *Ch25h* upregulation in VSMCs. In our experiments with the PD98059 MEK inhibitor, the AngII-induced *Ch25h* upregulation was somewhat affected by the inhibitor. However, the decrease in *Ch25h* mRNA levels in the PD98059-treated group was not significantly different from the DMSO-treated control cells (Figure 3A). This suggests that MEK and ERK1/2 activation are not essential in the upregulation of *Ch25h* expression in VSMCs, as the inhibition of these kinases was not effective to prevent *Ch25h* upregulation. Our findings point out that p38 MAPK signaling pathways are important in *Ch25h* gene expression regulation in VSMCs, but to fully understand their details further research is needed.

Based on the literature data we entertained the idea that NOX activation might play a role in AngII-induced *Ch25h* upregulation [13,53,54]. We found that DPI (a widely used NOX inhibitor) pretreatment did not have any effect on AngII-induced *Ch25h* mRNA increase. This suggests that NOX activity is not involved in the processes leading to *Ch25h* upregulation in VSMCs (Figure 4).

We examined the subcellular localization of CH25H in rat VSMCs. We found that the Cerulen-CH25H fusion protein and the mRFP-SAC1 ER marker fusion protein colocalized in both A7R5 cells and primary rat VSMCs (Figure 5A,B). This result shows that CH25H localizes to the ER both in the A7R5 VSMC cell line and in primary rat VSMCs, which is in line with previous information about the subcellular localization of the enzyme in other species [16].

The functional CH25H promotes the production of 25-HC which, by passing through the cell membrane, can act on several cell types both physiologically and pathologically [4,15,24,26,27]. Furthermore, 25-HC production is primarily the result of CH25H enzyme activity [13]. We measured 25-HC levels in the supernatant of AngII-stimulated primary rat VSMC cultures to determine whether the upregulation of *Ch25h* is associated with increased activity of the enzyme. Our results demonstrate that VSMCs indeed released 25-HC, the product of the CH25H enzyme, into their media (Figure 6). The 25-HC concentrations were at a peak 4 h after the AngII stimulation reached an average of 8.2 ng/mL. Following the 4 h time point, the 25-HC levels decreased, which may be due to its degradation or because of the reduced activity of CH25H over time. We

observed a clear increase in supernatant 25-HC levels of cells stimulated with AngII for 2 and 4 h compared to non-stimulated cells. The 25-HC levels were decreasing from the 8 h time point onward. This trend is consistent in all of our experiments (Figure 6). Based on this result, we conclude that the observed 25-HC is the product of enzyme activity, and it is not generated by non-enzymatic reactions. This result shows that the CH25H enzyme is active in VSMCs.

Another notable finding is that 25-HC concentrations in VSMC supernatants varied in the ng/mL range. Studies involving 25-HC treatments usually utilize 25-HC concentrations ranging from 5 μg/mL to 50 μg/mL [27–31], which are thousand-fold higher concentrations than our measurements indicate. It is important to note that our 25-HC concentration data were obtained from VSMC supernatants of 1 mL volume. The released 25-HC dilutes under such conditions. In the interstitial compartments of the aortic vessel walls, the dilution would not be so prominent, meaning that the 25-HC concentration could be much higher in vivo. This allows 25-HC to be an efficient autocrine or paracrine mediator. Furthermore, 25-HC is able to directly bind cell surface proteins such as $\alpha 5\beta 1$ and $\alpha v\beta 3$ integrins [26]. $\alpha 5\beta 1$ is expressed by VSMCs and is involved in processes of vascular injury [55]. Based on the findings of this study, we are eager to determine the effects of VSMC-produced 25-HC in the vasculature. Moreover, the possible functions of 25-HC intracellularly in VSMCs call for further investigation.

4. Materials and Methods

4.1. Materials

Cell culture plates were obtained from Greiner (Kremsmunster, Austria). μ-Slide 8 well plates were from Ibidi (Fitchburg, WI, USA). Reagents and biochemicals used during VSMC preparation were purchased from Duchefa Biochemie (Haarlem, The Netherlands) and Serva (Heidelberg, Germany). Collagenase type I was obtained from Worthington (Lakewood, NJ, USA). Dulbecco's Modified Eagle Medium (DMEM) cell culture medium and fetal bovine serum (FBS) were supplied by Biosera (Nuaille, France). The Opti-MEM medium used during transfection procedures was purchased from Gibco (Dublin, Ireland). Penicillin–Streptomycin (Sigma-Aldrich, Darmstadt, Germany) and GlutaMAX (Gibco) were used to supplement the cell culture medium. Molecular biology reagents, RevertAid Reverse Transcription Kit, GeneJet Gel Extraction Kit, and the restriction and ligase enzymes were purchased from Thermo Fisher Scientific (Waltham, MA, USA). AngII and the inhibitors used in our study, namely: candesartan, SB202190, PD98059, and DPI were purchased from Sigma-Aldrich (St. Louis, MO, USA). JNK-IN-8 was purchased from Selleckchem (Houston, TX, USA). YM-254890 was obtained from Wako Chemicals (Neuss, Germany). TRV120023 (Sar-Arg-Val-Tyr-Lys-His-Pro-Ala-OH) peptide was synthesized by Proteogenix (Schiltigheim, France) to more than 98% purity. For total RNA isolation, Qiagen's (Hilden; Germany) RNeasy Plus Mini kit was used. Quantitative real-time PCR (qRT-PCR) reactions were prepared using the SYBR Green Kit (LightCycler 480 SYBR Green I Master) from Roche (Basel, Switzerland). Primer oligos were synthesized by Sigma-Aldrich. Paraformaldehyde was from Polysciences (Warrington, PA, USA), other reagents, and the primer monoclonal anti-Actin, α-Smooth Muscle, clone 1A4 antibody used in immunocytochemistry were supplied by Sigma-Aldrich. Fluorophore-conjugated secondary antibodies and Lipofectamine 2000 transfection reagent were from Invitrogen (Carlsbad, CA, USA). FuGENE 6 transfection reagent was supplied by Promega (Madison, WI, USA). NEB10 competent *E. coli* was obtained from BioLabs (Ipswich, MA, USA). Unless otherwise stated, all other chemicals and reagents were purchased from Sigma-Aldrich Merck (St. Louis, MO, USA). The mRFP-SAC1 DNA construct was a kind gift from Dr. Péter Várnai (Semmelweis University).

4.2. Animals

Male Wistar rats (170–250 g, Charles River Laboratories-Semmelweis University, Budapest) were fed a standard semisynthetic diet. Our research conforms to the Guide for the Care and Use of Laboratory Animals (NIH, 8th edition, 2011) as well as national

legal and institutional guidelines for animal care. This study was approved by the Animal Care Committee of Semmelweis University, Budapest, and by Hungarian authorities (No. 001/2139–4/2012). All procedures followed legal and institutional guidelines for animal care.

4.3. Isolation of Primary Rat VSMCs

VSMCs were isolated from 40–50 day old male Wistar rats weighing 170–250 g. VSMCs were prepared according to the standard explant method [56]. Briefly, animals were sacrificed by decapitation and fast bleeding. The thoracic aorta was excised and placed in a modified Krebs–Ringer solution (120 mM NaCl (Duchefa Biochemie); 4.7 mM KCl (Duchefa Biochemie); 1.8 mM $CaCl_2$ (Duchefa Biochemie); 0.7mM $MgSO_4$ (Fluka; Sleez; Hanover; Germany); 10 mM glucose (Serva); and 10 mM Na-HEPES (Serva). Following the removal of connective tissue and adherent fat, the aorta was cut into 1 mm sections, and aorta-rings were digested with collagenase (Collagenase type I., Worthington) for 25 min at 37 °C. VSMCs were allowed to grow onto 10 cm cell culture plates from the explants for 7–14 days incubated at 5% CO_2 and 37 °C. VSMCs were cultured in Dulbecco's modified Eagle media (DMEM High Glucose W/ L-Glutamine W/Sodium Pyruvate; Biosera) containing 10% fetal bovine serum (FBS; Biosera), 1% penicillin–streptomycin (Sigma-Aldrich), and 1% GlutaMAX (Gibco). The VSMCs were passaged with trypsin (EuroClone, Milan, Italy) and were used between passages 2 and 3. Typically, the experiments were performed at the third passage. The expression of smooth muscle α-actin was confirmed using immunochemistry.

4.4. Next-Generation RNA Sequencing

Primary rat VSMCs were serum deprived overnight prior to hormone stimulus. VSMCs were stimulated with 100 nM AngII for 2 h at 37 °C. VSMCs were washed twice with cold sterile PBS (137 mM NaCl; 2.7 mM KCl 2.7; 10.1 mM Na_2HPO_4; 1.8 mM KH_2PO_4, pH 7.4). Cell lysis was carried out using Trizol reagent (Thermo Fisher Scientific, Waltham, MA, USA). Total RNA isolation and next-generation RNA sequencing were performed using UD-GenoMed Medical Genomic Technologies Ltd., University of Debrecen, Debrecen, Hungary.

4.5. Differential Expression Analysis

As a result of RNA-sequencing, raw data were obtained in the fastq format. The data were processed using kallisto v0.46.2, a program for quantifying the abundance of reads with high accuracy [57]. The quantification is obtained in transcripts per million (TPM) and estimated counts. Ensembl Rnor_6.0 reference transcriptome was used for indexing. From transcript level abundances, differential expression between control and stimulated samples were calculated using the voom, lmFit, and eBayes functions of the *limma* R package v3.50.1 [58].

4.6. Inhibitor Treatments and Hormone Stimulation of VSMCs

Before the experiments, the VSMCs were serum deprived overnight using DMEM supplemented with 0.1% bovine serum albumin (BSA; Sigma-Aldrich). VSMCs were pretreated with either dimethyl sulfoxide (DMSO) vehicle or various inhibitors separately: 10 µM candesartan, 1 µM JNK-IN-8 (IN-8), 50 µM SB202190, 20 µM PD98059 (Sigma-Aldrich), 1 µM YM-254890 (Wako Chemicals), and 5 µM DPI (Sigma-Aldrich). Pretreatment lasted for 30 min. Following pretreatment, VSMCs were stimulated with 100 nM AngII or vehicle for 1 h. In the other sets of experiments, the VSMCs were stimulated with either vehicle or 3 µM TRV120023 (TRV3; Proteogenix) for 1 h. To assess time dependency of *Ch25h* mRNA expression, VSMCs were stimulated with 100 nM AngII for 1, 2, 3, 4, 5, and 6 h or not stimulated.

For the detection of 25-HC, VSMCs were stimulated with 1 µM AngII for 2, 4, 8, 16, and 24 h or not stimulated. The experiments were performed in duplicates. After the hormone stimulation, the supernatants were collected and subjected to LC-MS/MS measurement.

4.7. RNA Isolation from VSMCs and cDNA Preparation

VSMCs were washed twice with cold, sterile PBS, and the total RNA was isolated using the RNeasy Plus Mini kit from (Qiagen). RNA concentrations were determined with spectrophotometry at 260 nm, and purity was assessed using the 260/280 and 230/260 nm ratios. For cDNA preparation, 0.1 μg/μL total RNA dilution was used. Reverse transcription was carried out with the RevertAid Reverse Transcription Kit (Thermo Fisher Scientific) according to manufacturer's instructions.

4.8. Quantitative Real-Time PCR (qRT-PCR)

We quantified mRNA levels using quantitative real-time PCR (qRT-PCR). qRT-PCR reactions were prepared using SYBR Green Kit (LightCycler 480 SYBR Green I Master; Roche) according to manufacturer's instructions. The measurements were carried out with the LightCycler 480 instrument (Roche). We assessed target gene expression levels relative to the glyceraldehyde-3-phosphate dehydrogenase (*Gapdh*) mRNA level. The following primers were used for qRT-PCR determinations: *Gapdh*: Forward: 5′ CCTGCACCAC-CAACTGCTTAG 3′, Reverse 5′CAGTCTTCTGAGTGGCAGTGATG 3′; *Ch25h*: Forward: 5′ GCGTTGGCTACCCAATACAT 3′; Reverse: 5′ GTGAGTGGACCACGGAAAGT 3′. The thermal cycling program was as follows: pre-incubation starts at 95 °C for 5 min, followed by amplification 45 cycles of 10 s at 95 °C, 5 s at 62 °C, and 15 s at 72 °C, melting curve 5 s at 95 °C, 1 min at 65 °C and 97 °C, and cooling 30 s at 40 °C. Fluorescence data including melting curves were obtained. The cycle threshold (Ct) was calculated with the second derivative method using LightCycler 480 Software. ΔCt is the difference in Ct values obtained between the reference and the tested samples. Fold ratios of gene expression were calculated as follows: Ratio = $E^{\Delta Ct\ target\ gene}/E^{\Delta Ct\ GAPDH}$.

4.9. DNA Constructs

We constructed DNA plasmids to express fluorescently tagged CH25H protein. We created a Cerulean-labeled plasmid construct using the backbones of pEYFP-N1-Cerulean (Clontech, Mountain View, CA). In order to amplify the entire *Ch25h* ORF region, the cDNA sample of VSMCs stimulated with AngII for 1 h was used as a template. The following primers were used during PCR amplification: forward 5′ ATATATGGCCTGC-CACAACGTTTCG 3′; reverse 5′ ATATAGTCTGTTTCTTCTTCTGGTTCAAGTG 3′. The PCR product was electrophoresed, purified using the GeneJet Gel Extraction Kit (Thermo Fisher Scientific), and subjected to a second round of PCR amplification with primers containing restriction enzyme sites. Forward primer containing EcoRI site: 5′ ATAT-GAATTCGCCACCATGGCCTGCCACAACGTTTCG 3′. Reverse primer containing AgeI site: 5′ ATATACCGGTCTGTTTCTTCTTCTGGTTCAAG 3′. This PCR product and the pEYFP-N1-Cerulean backbone were then digested with EcoRI and AgeI restriction enzymes (Thermo Fisher Scientific) according to manufacturer's instructions. *Ch25h* insert and pEYFP-N1-Cerulean were then incubated overnight at 16 °C with T4 ligase and T4 ligase buffer (Thermo Fisher Scientific). The completed Cerulean-CH25H plasmid construct was cloned in NEB10 bacteria (BioLabs).

4.10. Transfection

A7R5 rat aortic VSMCs (American Type Culture Collection, Rockville, MD, USA) were plated onto μ-Slide 8 well plate (Ibidi) in a 1×10^5 cells/well density. The next day, A7R5 cells were cotransfected with Cerulean-CH25H and mRFP-SAC1 fusion protein expressing DNA constructs (0.15 μg DNA/well) using Lipofectamine 2000 transfection reagent and Opti-MEM (Gibco) according to manufacturer's instructions. In a separate set of experiments, A7R5 cells were cotransfected with Cerulean-CH25H and mRFP-TGN38 or Cerulean-CH25H and mRFP-Giantin fusion protein expressing DNA constructs using the transfection protocol described above.

In the case of primary rat VSMCs, the cells were plated onto μ-Slide 8 well plate in a 1×10^5 cells/well density. Transfection took place the following day. VSMCs were

cotransfected with Cerulean-CH25H and mRFP-SAC1 constructs (0.5 μg DNA/well) using FuGENE 6 transfection reagent (Promega) applying a 3:1 = FuGENE 6:DNA ratio. We followed the manufacturer's instructions during the transfection procedure.

4.11. Immunocytochemistry

To assess the homogeneity and purity of the primary rat VSMC cultures used in our experiments, smooth muscle alpha-actin was labeled (Supplementary Figure S1). Cells were washed with cold, sterile PBS and then fixed using 4% paraformaldehyde (PFA; Polysciences) for 15 min. Following fixation, VSMCs were permeabilized with 0.1% Triton X-100 for 5 min then incubated in 0.1% sodium–borohydride solution for 15 min. VSMCs were incubated for 30 min in a blocking solution containing 1% bovine serum albumin (Sigma-Aldrich). Immunolabeling took place with anti-smooth muscle alpha-actin monoclonal mouse primary antibody (A2547; Sigma-Aldrich) alongside Alexa Fluor 488-conjugated anti-Mouse IgG secondary antibody. Between each step, cells were washed three times with PBS. To label cell nuclei, TO-PRO3 nucleic acid stain was used (Thermo Fisher Scientific).

4.12. Microscopy

For the imaging of fluorescently labeled smooth muscle alpha-actin in rat VSMC samples and the fluorescent signal of fusion protein expressing cotransfected A7R5 and rat VSMC samples, a Zeiss LSM 710 (Oberkochen, Germany) confocal laser-scanning microscope was used. Imaging of the transfected cells was carried out 24 h after cotransfection. The obtained images were processed with Fiji 1.53q software [59]. Colocalization analysis was carried out using the JACoP plugin, and Pearson's correlation coefficient values were used to define colocalization [43].

4.13. Liquid Chromatography–Tandem Mass Spectrometry (LC-MS/MS)

A total of 900 μL of methanol was used for 300 μL of supernatant samples for protein precipitation. The supernatants were obtained from 6-well plates, in which the cells were cultured in 1 mL of medium. The samples were vortexed and centrifuged for 5 min at 13,000 rpm. A total of 100 μL of supernatant was pipetted into a micro-vial and used for quantitation. LC-MS/MS measurements were run on a Sciex 6500QTrap mass spectrometer coupled with an Agilent 1100 HPLC system. A Kinetex EVO-C18, 50 × 2.1 mm, 5 μm HPLC column was applied using water and acetonitrile (both containing 0.1% formic acid) in that gradient elution mode. The flow rate was 600 μL/min. The mass spectrometer was operated in positive APCI ionization. The needle current was set to 3 μA. Curtain, evaporating, and drying gases were 40, 30, and 20 psi, respectively. Quantitation was completed in the MRM mode using ion transitions: 382.5/367.2, 367.2/161.3, 385.2/159, and 367.3/159. The dwell time for each transition was 150 msec.

4.14. Statistical Analysis

Statistical analysis and graph plotting were carried out using GraphPad Prism 9.1.2 (San Diego, CA, USA) software. The sample size is given in the figure legends as n = the number of independent experiments. Data are shown as mean $\pm$ SEM. Gene expression data obtained from qRT-PCR measurements were analyzed using multiple linear regression with a 95% confidence interval in order to determine the significance of inhibitor treatments, stimuli, and their interaction with the dependent variable. The 25-HC concentration values were analyzed using multiple linear regression. In the case of data displayed in Figure 2B, an unpaired *t*-test was used to compare the control and the stimulated group.

5. Conclusions

In this study, we report that AngII promoted the upregulation of *Ch25h* in VSMCs. *Ch25h* expression in VSMCs was dependent on AT1R and subsequent $G_{q/11}$ activation. Our experiments using various inhibitors showed the substantial role of p38 MAPK in *Ch25h* upregulation induced by AngII. CH25H localized to the ER of VSMCs. Our data demonstrated

that 25-HC concentration was elevated in the supernatants of AngII-stimulated VSMCs, meaning that the CH25H enzyme was active in VSMCs. Our work elucidates the effect of AngII on gene expression changes in VSMCs and invites further studies of CH25H—an enzyme having primarily immunological functions—in the context of the vasculature.

References

1. Virani, S.S.; Alonso, A.; Aparicio, H.J.; Benjamin, E.J.; Bittencourt, M.S.; Callaway, C.W.; Carson, A.P.; Chamberlain, A.M.; Cheng, S.; Delling, F.N.; et al. Heart Disease and Stroke Statistics—2021 Update: A Report From the American Heart Association. *Circulation* **2021**, *143*, e254–e743. [CrossRef] [PubMed]
2. Timmis, A.; Townsend, N.; Gale, C.P.; Torbica, A.; Lettino, M.; Petersen, S.E.; Mossialos, E.A.; Maggioni, A.P.; Kazakiewicz, D.; May, H.T.; et al. European Society of Cardiology: Cardiovascular Disease Statistics 2019. *Eur. Heart J.* **2020**, *41*, 12–85. [CrossRef] [PubMed]
3. Forrester, S.J.; Booz, G.W.; Sigmund, C.D.; Coffman, T.M.; Kawai, T.; Rizzo, V.; Scalia, R.; Eguchi, S. Angiotensin II Signal Transduction: An Update on Mechanisms of Physiology and Pathophysiology. *Physiol. Rev.* **2018**, *98*, 1627–1738. [CrossRef]
4. Gargiulo, S.; Gamba, P.; Testa, G.; Leonarduzzi, G.; Poli, G. The role of oxysterols in vascular ageing. *J. Physiol.* **2016**, *594*, 2095–2113. [CrossRef] [PubMed]
5. Karnik, S.S.; Unal, H.; Kemp, J.R.; Tirupula, K.C.; Eguchi, S.; Vanderheyden, P.M.L.; Thomas, W. International Union of Basic and Clinical Pharmacology. XCIX. Angiotensin Receptors: Interpreters of Pathophysiological Angiotensinergic Stimuli. *Pharmacol. Rev.* **2015**, *67*, 754–819. [CrossRef]
6. Weir, M.R.; Dzau, V.J. The renin-angiotensin-aldosterone system: A specific target for hypertension management. *Am. J. Hypertens.* **1999**, *12*, 205–213. [CrossRef]
7. Griendling, K.K.; Minieri, C.A.; Ollerenshaw, J.D.; Alexander, R.W. Angiotensin II stimulates NADH and NADPH oxidase activity in cultured vascular smooth muscle cells. *Circ. Res.* **1994**, *74*, 1141–1148. [CrossRef]
8. Berk, B.C.; Vekshtein, V.; Gordon, H.M.; Tsuda, T. Angiotensin II-stimulated protein synthesis in cultured vascular smooth muscle cells. *Hypertension* **1989**, *13*, 305–314. [CrossRef]
9. Owens, A.P.; Subramanian, V.; Moorleghen, J.J.; Guo, Z.; McNamara, C.A.; Cassis, L.A.; Daugherty, A. Angiotensin II Induces a Region-Specific Hyperplasia of the Ascending Aorta Through Regulation of Inhibitor of Differentiation 3. *Circ. Res.* **2010**, *106*, 611–619. [CrossRef]
10. Kato, H.; Suzuki, H.; Tajima, S.; Ogata, Y.; Tominaga, T.; Sato, A.; Saruta, T. Angiotensin II stimulates collagen synthesis in cultured vascular smooth muscle cells. *J. Hypertens.* **1991**, *9*, 17–22. [CrossRef]
11. Ford, C.M.; Li, S.; Pickering, J.G. Angiotensin II Stimulates Collagen Synthesis in Human Vascular Smooth Muscle Cells. *Arter. Thromb. Vasc. Biol.* **1999**, *19*, 1843–1851. [CrossRef] [PubMed]
12. Kalra, D.; Sivasubramanian, N.; Mann, D.L. Angiotensin II Induces Tumor Necrosis Factor Biosynthesis in the Adult Mammalian Heart Through a Protein Kinase C–Dependent Pathway. *Circulation* **2002**, *105*, 2198–2205. [CrossRef] [PubMed]
13. Pannu, P.S.; Allahverdian, S.; Francis, G.A. Oxysterol generation and liver X receptor-dependent reverse cholesterol transport: Not all roads lead to Rome. *Mol. Cell. Endocrinol.* **2013**, *368*, 99–107. [CrossRef] [PubMed]
14. Brown, A.J.; Jessup, W. Oxysterols and atherosclerosis. *Atherosclerosis* **1999**, *142*, 1–28. [CrossRef] [PubMed]

15. Poli, G.; Biasi, F.; Leonarduzzi, G. Oxysterols in the pathogenesis of major chronic diseases. *Redox Biol.* **2013**, *1*, 125–130. [CrossRef]

16. Lund, E.G.; Kerr, T.A.; Sakai, J.; Li, W.-P.; Russell, D.W. cDNA Cloning of Mouse and Human Cholesterol 25-Hydroxylases, Polytopic Membrane Proteins That Synthesize a Potent Oxysterol Regulator of Lipid Metabolism. *J. Biol. Chem.* **1998**, *273*, 34316–34327. [CrossRef]

17. Liu, S.-Y.; Aliyari, R.; Chikere, K.; Li, G.; Marsden, M.D.; Smith, J.K.; Pernet, O.; Guo, H.; Nusbaum, R.; Zack, J.A.; et al. Interferon-Inducible Cholesterol-25-Hydroxylase Broadly Inhibits Viral Entry by Production of 25-Hydroxycholesterol. *Immunity* **2012**, *38*, 92–105. [CrossRef]

18. Li, C.; Deng, Y.-Q.; Wang, S.; Ma, F.; Aliyari, R.; Huang, X.-Y.; Zhang, N.-N.; Watanabe, M.; Dong, H.-L.; Liu, P.; et al. 25-Hydroxycholesterol Protects Host against Zika Virus Infection and Its Associated Microcephaly in a Mouse Model. *Immunity* **2017**, *46*, 446–456. [CrossRef]

19. Wang, S.; Li, W.; Hui, H.; Tiwari, S.K.; Zhang, Q.; Croker, B.A.; Rawlings, S.; Smith, D.; Carlin, A.F.; Rana, T.M. Cholesterol 25-Hydroxylase inhibits SARS -CoV-2 and other coronaviruses by depleting membrane cholesterol. *EMBO J.* **2020**, *39*, e106057. [CrossRef]

20. Bauman, D.R.; Bitmansour, A.D.; McDonald, J.G.; Thompson, B.M.; Liang, G.; Russell, D.W. 25-Hydroxycholesterol secreted by macrophages in response to Toll-like receptor activation suppresses immunoglobulin A production. *Proc. Natl. Acad. Sci. USA* **2009**, *106*, 16764–16769. [CrossRef]

21. Park, K.; Scott, A.L. Cholesterol 25-hydroxylase production by dendritic cells and macrophages is regulated by type I interferons. *J. Leukoc. Biol.* **2010**, *88*, 1081–1087. [CrossRef] [PubMed]

22. Hodis, H.N.; Crawford, D.W.; Sevanian, A. Cholesterol feeding increases plasma and aortic tissue cholesterol oxide levels in parallel: Further evidence for the role of cholesterol oxidation in atherosclerosis. *Atherosclerosis* **1991**, *89*, 117–126. [CrossRef] [PubMed]

23. Gold, E.S.; Ramsey, S.A.; Sartain, M.J.; Selinummi, J.; Podolsky, I.; Rodriguez, D.J.; Moritz, R.L.; Aderem, A. ATF3 protects against atherosclerosis by suppressing 25-hydroxycholesterol–induced lipid body formation. *J. Exp. Med.* **2012**, *209*, 807–817. [CrossRef]

24. Liu, Y.; Hultén, L.M.; Wiklund, O. Macrophages Isolated from Human Atherosclerotic Plaques Produce IL-8, and Oxysterols May Have a Regulatory Function for IL-8 Production. *Arter. Thromb. Vasc. Biol.* **1997**, *17*, 317–323. [CrossRef] [PubMed]

25. Erridge, C.; Webb, D.J.; Spickett, C.M. 25-Hydroxycholesterol, 7β-hydroxycholesterol and 7-ketocholesterol upregulate interleukin-8 expression independently of Toll-like receptor 1, 2, 4 or 6 signalling in human macrophages. *Free Radic. Res.* **2007**, *41*, 260–266. [CrossRef]

26. Pokharel, S.M.; Shil, N.K.; Gc, J.B.; Colburn, Z.T.; Tsai, S.-Y.; Segovia, J.A.; Chang, T.-H.; Bandyopadhyay, S.; Natesan, S.; Jones, J.C.R.; et al. Integrin activation by the lipid molecule 25-hydroxycholesterol induces a proinflammatory response. *Nat. Commun.* **2019**, *10*, 1–17. [CrossRef]

27. Appukuttan, A.; Kasseckert, S.A.; Kumar, S.; Reusch, H.P.; Ladilov, Y. Oxysterol-induced apoptosis of smooth muscle cells is under the control of a soluble adenylyl cyclase. *Cardiovasc. Res.* **2013**, *99*, 734–742. [CrossRef]

28. Nishio, E.; Watanabe, Y. Oxysterols Induced Apoptosis in Cultured Smooth Muscle Cells through CPP32 Protease Activation and bcl-2 Protein Downregulation. *Biochem. Biophys. Res. Commun.* **1996**, *226*, 928–934. [CrossRef]

29. Ares, M.P.; Thyberg, J.; Juntti-Berggren, L.; Berggren, P.O.; Diczfalusy, U.; Kallin, B.; Björkhem, I.; Orrenius, S.; Nilsson, J. Ca2+ channel blockers verapamil and nifedipine inhibit apoptosis induced by 25-hydroxycholesterol in human aortic smooth muscle cells. *J. Lipid Res.* **1997**, *38*, 2049–2061. [CrossRef]

30. Yin, J.; Chaufour, X.; McLachlan, C.; McGuire, M.; White, G.; King, N.J.C.; Hambly, B. Apoptosis of vascular smooth muscle cells induced by cholesterol and its oxides in vitro and in vivo. *Atherosclerosis* **2000**, *148*, 365–374. [CrossRef]

31. Perales, S.; Alejandre, M.J.; Palomino-Morales, R.; Torres, C.; Iglesias, J.; Linares, A. Effect of Oxysterol-Induced Apoptosis of Vascular Smooth Muscle Cells on Experimental Hypercholesterolemia. *J. Biomed. Biotechnol.* **2009**, *2009*, 1–8. [CrossRef] [PubMed]

32. Bennett, M.R.; Sinha, S.; Owens, G.K. Vascular Smooth Muscle Cells in Atherosclerosis. *Circ. Res.* **2016**, *118*, 692–702. [CrossRef] [PubMed]

33. Dong, Q.; Chen, Y.; Liu, W.; Liu, X.; Chen, A.; Yang, X.; Li, Y.; Wang, S.; Fu, M.; Ou, J.-S.; et al. 25-Hydroxycholesterol promotes vascular calcification via activation of endoplasmic reticulum stress. *Eur. J. Pharmacol.* **2020**, *880*, 173165. [CrossRef] [PubMed]

34. Violin, J.D.; DeWire, S.M.; Yamashita, D.; Rominger, D.H.; Nguyen, L.; Schiller, K.; Whalen, E.J.; Gowen, M.; Lark, M.W. Selectively Engaging β-Arrestins at the Angiotensin II Type 1 Receptor Reduces Blood Pressure and Increases Cardiac Performance. *Experiment* **2010**, *335*, 572–579. [CrossRef] [PubMed]

35. Devost, D.; Sleno, R.; Pétrin, D.; Zhang, A.; Shinjo, Y.; Okde, R.; Aoki, J.; Inoue, A.; Hébert, T.E. Conformational Profiling of the AT1 Angiotensin II Receptor Reflects Biased Agonism, G Protein Coupling, and Cellular Context. *J. Biol. Chem.* **2017**, *292*, 5443–5456. [CrossRef]

36. Szakadáti, G.; Tóth, A.D.; Oláh, I.; Erdélyi, L.S.; Balla, T.; Várnai, P.; Hunyady, L.; Balla, A. Investigation of the fate of type I angiotensin receptor after biased activation. *Mol. Pharmacol.* **2015**, *87*, 972–981. [CrossRef]

37. Turu, G.; Balla, A.; Hunyady, L. The Role of β-Arrestin Proteins in Organization of Signaling and Regulation of the AT1 Angiotensin Receptor. *Front. Endocrinol.* **2019**, *10*, 519. [CrossRef]

38. Yamauchi, J.; Nagao, M.; Kaziro, Y.; Itoh, H. Activation of p38 Mitogen-activated Protein Kinase by Signaling through G Protein-coupled Receptors. *J. Biol. Chem.* **1997**, *272*, 27771–27777. [CrossRef]

39. Nagao, M.; Yamauchi, J.; Kaziro, Y.; Itoh, H. Involvement of Protein Kinase C and Src Family Tyrosine Kinase in Gαq/11-induced Activation of c-Jun N-terminal Kinase and p38 Mitogen-activated Protein Kinase. *J. Biol. Chem.* **1998**, *273*, 22892–22898. [CrossRef]

40. Brown, D.I.; Griendling, K.K. Nox proteins in signal transduction. *Free Radic. Biol. Med.* **2009**, *47*, 1239–1253. [CrossRef]

41. Durgin, B.G.; Straub, A.C. Redox control of vascular smooth muscle cell function and plasticity. *Lab. Investig.* **2018**, *98*, 1254–1262. [CrossRef] [PubMed]

42. Augsburger, F.; Filippova, A.; Rasti, D.; Seredenina, T.; Lam, M.; Maghzal, G.; Mahiout, Z.; Jansen-Dürr, P.; Knaus, U.G.; Doroshow, J.; et al. Pharmacological characterization of the seven human NOX isoforms and their inhibitors. *Redox Biol.* **2019**, *26*, 101272. [CrossRef] [PubMed]

43. Bolte, S.; Cordelières, F.P. A guided tour into subcellular colocalization analysis in light microscopy. *J. Microsc.* **2006**, *224*, 213–232. [CrossRef] [PubMed]

44. Kirat, D.; Shousha, S. Angiotensin II up-regulates monocarboxylate transporters expression in the rat adrenal gland. *Cell. Mol. Biol.* **2016**, *62*, 24–29. [PubMed]

45. Domińska, K.; Kowalska, K.; Matysiak, Z.E.; Płuciennik, E.; Ochędalski, T.; Piastowska-Ciesielska, A.W. Regulation of mRNA gene expression of members of the NF-κB transcription factor gene family by angiotensin II and relaxin 2 in normal and cancer prostate cell lines. *Mol. Med. Rep.* **2017**, *15*, 4352–4359. [CrossRef]

46. Tone, A.; Shikata, K.; Ogawa, D.; Sasaki, S.; Nagase, R.; Sasaki, M.; Yozai, K.; Usui, H.K.; Okada, S.; Wada, J.; et al. Changes of gene expression profiles in macrophages stimulated by angiotensin II—Angiotensin II induces MCP-2 through AT1-receptor. *J. Renin-Angiotensin-Aldosterone Syst.* **2007**, *8*, 45–50. [CrossRef]

47. Gém, J.B.; Kovács, K.B.; Szalai, L.; Szakadáti, G.; Porkoláb, E.; Szalai, B.; Turu, G.; Tóth, A.D.; Szekeres, M.; Hunyady, L.; et al. Characterization of Type 1 Angiotensin II Receptor Activation Induced Dual-Specificity MAPK Phosphatase Gene Expression Changes in Rat Vascular Smooth Muscle Cells. *Cells* **2021**, *10*, 3538. [CrossRef]

48. Pascual-Ahuir, A.; Fita-Torró, J.; Proft, M. Capturing and Understanding the Dynamics and Heterogeneity of Gene Expression in the Living Cell. *Int. J. Mol. Sci.* **2020**, *21*, 8278. [CrossRef]

49. Bhatta, A.; Yao, L.; Toque, H.A.; Shatanawi, A.; Xu, Z.; Caldwell, R.B. Angiotensin II-Induced Arterial Thickening, Fibrosis and Stiffening Involves Elevated Arginase Function. *PLoS ONE* **2015**, *10*, e0121727. [CrossRef]

50. Tóth, A.D.; Turu, G.; Hunyady, L.; Balla, A. Novel mechanisms of G-protein-coupled receptors functions: AT1 angiotensin receptor acts as a signaling hub and focal point of receptor cross-talk. *Best Pract. Res. Clin. Endocrinol. Metab.* **2018**, *32*, 69–82. [CrossRef]

51. Madenspacher, J.H.; Morrell, E.D.; Gowdy, K.M.; McDonald, J.G.; Thompson, B.M.; Muse, G.W.; Martinez, J.; Thomas, S.Y.; Mikacenic, C.; Nick, J.A.; et al. Cholesterol-25-hydroxylase promotes efferocytosis and resolution of lung inflammation. *J. Clin. Investig.* **2020**, *5*, e137189. [CrossRef] [PubMed]

52. Mizuno, N.; Itoh, H. Functions and Regulatory Mechanisms of Gq-Signaling Pathways. *Neurosignals* **2009**, *17*, 42–54. [CrossRef] [PubMed]

53. Komati, R.; Spadoni, D.; Zheng, S.; Sridhar, J.; Riley, K.E.; Wang, G. Ligands of Therapeutic Utility for the Liver X Receptors. *Molecules* **2017**, *22*, 88. [CrossRef] [PubMed]

54. Liu, Y.; Wei, Z.; Ma, X.; Yang, X.; Chen, Y.; Sun, L.; Ma, C.; Miao, Q.R.; Hajjar, D.P.; Han, J.; et al. 25-Hydroxycholesterol activates the expression of cholesterol 25-hydroxylase in an LXR-dependent mechanism. *J. Lipid Res.* **2018**, *59*, 439–451. [CrossRef] [PubMed]

55. Pickering, J.G.; Chow, L.H.; Li, S.; Rogers, K.A.; Rocnik, E.F.; Zhong, R.; Chan, B.M. α5β1 Integrin Expression and Luminal Edge Fibronectin Matrix Assembly by Smooth Muscle Cells after Arterial Injury. *Am. J. Pathol.* **2000**, *156*, 453–465. [CrossRef] [PubMed]

56. Elliott, K.J.; Eguchi, S. In Vitro Assays to Determine Smooth Muscle Cell Hypertrophy, Protein Content, and Fibrosis. In *The Renin-Angiotensin-Aldosterone System Methods and Protocols*; Springer: Berlin/Heidelberg, Germany, 2017; Volume 1614, pp. 147–153. [CrossRef]

57. Bray, N.L.; Pimentel, H.; Melsted, P.; Pachter, L. Near-optimal probabilistic RNA-seq quantification. *Nat. Biotechnol.* **2016**, *34*, 525–527. [CrossRef]

58. Law, C.W.; Chen, Y.; Shi, W.; Smyth, G.K. Voom: Precision weights unlock linear model analysis tools for RNA-seq read counts. *Genome Biol.* **2014**, *15*, R29. [CrossRef]

59. Schindelin, J.; Arganda-Carreras, I.; Frise, E.; Kaynig, V.; Longair, M.; Pietzsch, T.; Preibisch, S.; Rueden, C.; Saalfeld, S.; Schmid, B.; et al. Fiji: An open-source platform for biological-image analysis. *Nat. Methods* **2012**, *9*, 676–682. [CrossRef]

Phosphatidylinositol 4-kinases: old enzymes with emerging functions

Andras Balla and Tamas Balla

Endocrinology and Reproduction Research Branch, NICHD, National Institutes of Health, Bethesda, MD 20892, USA

Phosphoinositides account for only a tiny fraction of cellular phospholipids but are extremely important in the regulation of the recruitment and activity of many signaling proteins in cellular membranes. Phosphatidylinositol (PtdIns) 4-kinases generate PtdIns 4-phosphate, the precursor of important regulatory phosphoinositides but also an emerging regulatory molecule in its own right. The four mammalian PtdIns 4-kinases regulate a diverse array of signaling events, as well as vesicular trafficking and lipid transport, but the mechanisms by which their lipid product PtdIns 4-phosphate controls these processes is only beginning to unfold.

Introduction

Phosphoinositides are derivatives of phosphatidylinositol (PtdIns) in which one or more of the -OH groups at the 3-, 4- and 5-position of the inositol ring are esterified with a phosphate group in all possible combinations (Figure 1). Several kinases and phosphatases that interconvert phosphoinositides have been identified, along with an increasing number of protein modules that can recognize specific isomers of these lipid molecules. The latter include PH, PTB, ENTH, FYVE, PX, FERM and CALM domains, covered in several recent reviews [1–3]. These studies have outlined a new regulatory paradigm, in which phosphoinositides control a variety of cellular signaling and trafficking processes by recruiting regulatory proteins to signaling complexes organized in cellular membranes.

PtdIns 4-kinases catalyze the production of PtdIns 4-phosphate [PtdIns4P] from PtdIns, the first step in the formation of PtdIns(4,5)P_2 and PtdIns(3,4,5)P_3, two lipid products whose functions as regulatory molecules are best understood. PtdIns(4,5)P_2 is the main substrate of the phospholipase C (PLC) enzymes, yielding inositol 1,4,5-trisphosphate [Ins(1,4,5)P_3] and diacylglycerol (DAG), two important messengers in Ca^{2+} signaling [4]. PtdIns(4,5)P_2 also controls several types of ion channel and enzymes, such as phospholipase D (PLD), and interacts with proteins that link membranes to the actin cytoskeleton [3,5]. PtdIns(3,4,5)P_3, generated from PtdIns(4,5)P_2 by the class I PtdIns 3-kinases, regulates a wide range of processes, such as cell metabolism and the antiapoptotic pathway via the serine/threonine kinase Akt

but also controls tyrosine kinases, such as Btk and guanine exchange factors for small GTP-binding proteins [6]. Because the production of these signaling phosphoinositides relies upon both the activity of their synthesizing enzymes and their precursor supply, PtdIns 4-kinases have a pivotal role in cellular regulation.

Four distinct PtdIns 4-kinases have been identified in mammalian cells (Table 1); however, despite their central position in phosphoinositide synthesis, their regulation has been poorly understood until recently. Studies in yeast demonstrated that the three distinct yeast PtdIns 4-kinases mediate largely nonredundant functions by producing PtdIns4P in specific cellular compartments. These studies also showed the importance of PtdIns4P as a regulatory lipid as well as a precursor for PtdIns(4,5)P_2. Studies in mammalian cells also revealed that the four PtdIns 4-kinases localize to distinct membrane compartments and have specific roles in vesicle trafficking and Golgi function, where PtdIns4P rather than PtdIns(4,5)P_2 is the regulatory lipid molecule. These developments, together with the identification of PH domains that specifically recognize PtdIns4P, indicate that PtdIns 4-kinases have much broader functions than previously thought.

In this review we summarize the current knowledge on PtdIns 4-kinases, with emphasis on important questions concerning their functions and regulations. For example, why do cells require more than one form of the enzyme to produce the same lipid product? Do the localization and recruitment mechanisms of the individual enzymes determine the signaling roles of PtdIns4P in different compartments? Which of the functions of the PtdIns 4-kinases are mediated by PtdIns4P *per se*, and which ones are affected indirectly, through PtdIns(4,5)P_2 or PtdIns(3,4,5)P_3 formation? How are these functions distributed among the various forms of the enzymes, which include type III (PI4KIIIα and PI4KIIIβ) and type II (PI4KIIα and PI4KIIβ) enzymes? Many of these questions cannot be fully answered at present but their implications reveal enough to justify the efforts to learn more about these proteins.

PI4KIIIα

Yeast PI4KIIIα

The yeast ortholog of PtdIns 4-kinase type III-α (PI4KIIIα), Stt4p, was first identified as a protein affecting staurosporine sensitivity [7]. Although *STT4* is an essential gene in most yeast strains, some can survive

Corresponding author: Balla, T. (ballat@mail.nih.gov).
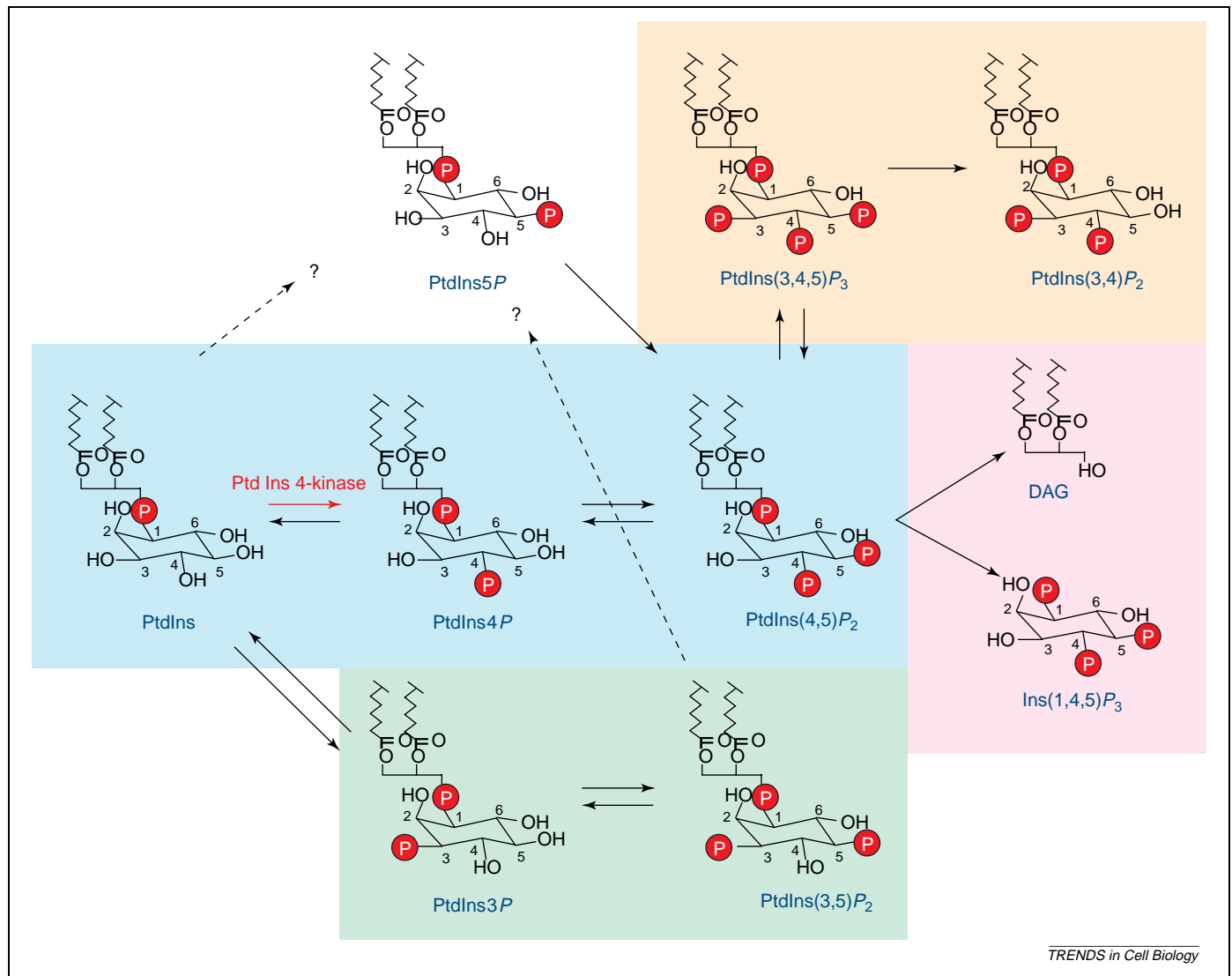Available online 21 June 2006

Figure 1. Metabolic routes of phosphoinositide production. Phosphoinositides can be phosphorylated at different positions on the inositol ring of PtdIns. The classical pathway leading to DAG and Ins(1,4,5)P_3 formation is shown on the blue and pink backgrounds. The class I PtdIns 3-kinase products produced mainly at the plasma membrane are shown on an orange background, whereas the pathway in which the 3-phosphorylated lipids are formed by class III PtdIns 3-kinases is shown on a green background. The red arrow indicates the conversion step catalyzed by PtdIns 4-kinases. The source of PtdIns(5)P is still not firmly established, as indicated by the question marks. The acyl side chains on the glycerol backbone are curtailed.

its deletion in the presence of osmotic stabilizers [7,8]. Stt4p is important for maintaining cell wall integrity and proper organization of the actin cytoskeleton [8]. In temperature-sensitive *stt4* mutants, the total cellular levels of PtdIns4P and PtdIns(4,5)P_2 are decreased by ~50% at the nonpermissive temperature and cells display a unique change in morphology with fused and collapsed large vacuoles [8].

Table 1. Distinctive features of the different forms of PtdIns 4-kinase

Features	PI4KIIα	PI4KIIβ	PI4KIIIα	PI4KIIIβ
Other names	PI4KII; PI4K55; 56 kDa type II PtdIns 4-kinase	PI4KII; PI4K55; 56 kDa type II PtdIns 4-kinase	Pik4ca; PI4K230; PtdIns 4-kinase α	Pik4cb; PI4K92; PtdIns 4-kinase β
Yeast homolog	Lsb6p (Pik2p)	Lsb6p (Pik2p)	Stt4p	Pik1p
Apparent molecular weight	55–56 kDa	55–56 kDa	210 kDa	110 kDa
Calculated molecular weight	54 kDa	55 kDa	230 kDa	92 kDa
Wortmannin	Insensitive	Insensitive	IC_{50} 50–300 nM	IC_{50} 50–300 nM
LY-294002	Insensitive	Insensitive	IC_{50} 50–100 μM	IC_{50} 100 μM
Phenylarsine oxide	$IC_{50} > 100$ μM	$IC_{50} > 100$ μM	IC_{50} 1–5 μM	$IC_{50} \sim 30$ μM
Ca^{2+}	Inhibits	Inhibits	No direct effect	No direct effect
K_i (adenosine)	10–70 μM	10–70 μM	Millimolar	Millimolar
Triton X-100	Activates	Activates	Activates	Activates
K_m (ATP)	10–50 μM	10–50 μM	~700 μM	~400 μM
K_m (PtdIns)	~20–60 μM	~20–60 μM	~100 μM	~100 μM

Functions of Stt4p at the plasma membrane

Yeast Stt4p is localized to the plasma membrane, where its product PtdIns4P is converted to PtdIns(4,5)P_2 by the only yeast PtdIns 5-kinase Mss4p [9]. Mss4p can rescue some temperature-sensitive *stt4* mutants by helping to generate sufficient PtdIns(4,5)P_2 in spite of a reduced supply of PtdIns4P. Plasma membrane PtdIns(4,5)P_2 is important in yeast signaling in several ways. First, it is hydrolyzed by the single yeast PLC enzyme that is activated by hypo-osmotic stress. However, in yeast, Ins(1,4,5)P_3 is not a calcium-mobilizing messenger – because there are no Ins(1,4,5)P_3 receptors present – but serves as a precursor for inositol hexakisphosphate synthesis [10]. Further-more, unlike the classical protein kinase Cs (PKCs) of mammalian cells, yeast Pkc1 is not stimulated by Ca^{2+} and DAG but is activated by a different sequence of events, in which PtdIns(4,5)P_2 has a central role. PtdIns(4,5)P_2 interacts with the PH domain of the yeast guanine nucleotide exchange factor Rom2p, thereby recruiting this protein to the plasma membrane. Rom2 is an activator of the small GTP-binding protein Rho1, which, in turn, regulates the yeast Pkc1. Because Stt4p is required for the synthesis of PtdIns(4,5)P_2, a link exists between Stt4p and Pkc1, the major target in yeast of the protein kinase inhibitor staurosporine [9]. Yeast Pkc1 also controls the transcription of key enzymes of cell wall biosynthesis, establishing the relationship between Stt4p function and cell wall integrity [11].

Another important protein recruited to the plasma membrane by PtdIns(4,5)P_2 is the yeast PLD Spo14p, another enzyme involved in the regulation of the actin cytoskeleton and vesicular trafficking. It was recently shown that Stt4p is required for PLD recruitment [12]. In this capacity, some of the nonclassical PtdIns transfer proteins (PITPs), termed Sec14 homologs, provide Stt4p with its PtdIns substrate. This process takes place in highly specialized membrane compartments, where the endoplasmic reticulum (ER) membranes containing the Sec14 homolog protein(s) are adjacent to the plasma membrane [12], suggesting that Stt4p might also regulate lipid transfer between the ER and plasma membrane.

Localization of Stt4p to the plasma membrane

The mechanism by which Stt4p is kept in the plasma membrane is not fully understood. However, recent studies looking for proteins that complement tempera-ture-sensitive alleles of *stt4* that are not rescued by Mss4p have identified two proteins, suppressor of four kinase (Sfk1p) and Ict1p [9]. Sfk1p physically associates with Stt4p and helps to localize the enzyme to the plasma membrane. Surprisingly, deletion of *SFK1* does not yield any obvious phenotype [9] suggesting that additional proteins must contribute to the membrane targeting of Stt4p. The mechanism of rescue by Ict1p is not clear at present but it does not seem to act through Stt4p localization.

Possible roles of Stt4p in other membrane compartments

The presence of Stt4p in the ER is not prominent in yeast, yet evidence suggests that the enzyme also has roles in the ER. The PtdIns4P pool generated by Stt4p is depho-sphorylated mainly by the ER-localized inositol lipid phosphatase Sac1p [13]. Stt4p is also important in regulating the conversion of phosphatidylserine (PtdSer) to phosphatidylethanolamine at the ER and Golgi inter-face. The mechanism of this effect is not fully understood but it is possible that Stt4p regulates PtdSer transfer between these membranes [14].

PI4KIIIα in higher organisms

In contrast to yeast, PI4KIIIα is mainly localized to the ER in mammalian cells [15] but the expressed enzyme is detected in the pericentriolar area over the Golgi [16] and also in the nucleolus [17] (Figure 2). A green fluorescent protein (GFP)-tagged form of the *Arabidopsis thaliana* PI4KIIIα homolog *At*PI4Kα1 is also found in the intra-cellular perinuclear ER membrane when expressed in Sf9 insect cells [18]. Mammalian PI4KIIIα shows highest expression in the nervous system [16,19], and immuno-histochemical analysis of ventral horn neurons of rat spinal cord shows a punctate granular staining in the cytoplasm. These puncta correspond to unique membra-nous clusters associated with various organelles such as multivesicular bodies, mitochondria and the ER, as shown by electron microscopic analysis [20]. It was also reported that the mammalian enzyme associates with an ER- and Golgi-localized PITP, PITPnm, presumably helping to supply the enzyme with its substrate [21]. In spite of the localization data, the role(s) of PI4KIIIα in the ER in mammalian cells is completely unknown.

By contrast, ample evidence suggests that PI4KIIIα functions in the plasma membrane in vertebrate cells. Rat liver plasma membrane fractions contain a small percen-tage of the enzyme [22], and PI4KIIIα is also part of the signaling complex associated with the P2X7 ion channels [23]. It was recently shown that the production of a plasma membrane pool of PtdIns4P is mediated by PI4KIIIα [24]. Because the PtdIns(4,5)P_2 pools that are hydrolyzed by PLC enzymes after stimulation of either G-protein-coupled or tyrosine kinase receptors are synthesized by wortmannin (Wm)-sensitive type III PtdIns 4-kinases [25] (Box 1), it is likely – although not yet formally proven – that PI4KIIIα supports the Ins(1,4,5)P_3–Ca^{2+} signaling cascade (Figure 3a). Mammalian PITP-α is also essential to maintain the PtdIns(4,5)P_2 pool during agonist-induced PLC activation [26], suggesting that PITPs provide PI4KIIIα with its PtdIns substrate at the membrane.

PI4KIIIβ

Yeast PI4KIIIβ

The yeast ortholog of PI4KIIIβ is encoded by an essential gene, *PIK1* [8,27,28]. Inactivation of *PIK1* by temperature-sensitive alleles or by other mutations causes a significant decrease (up to 50%) in total cellular PtdIns4P and PtdIns(4,5)P_2 levels [8,29]. Morphologically, tempera-ture-sensitive *pik1* strains show ring-shaped structures corresponding to exaggerated Golgi membranes, fragmen-tation of the vacuole and a defect in the polarization of actin at the budding pole of the cells at the nonpermissive temperature [8,29]. Multinucleation of such cells also suggests a defect in cytokinesis [29].
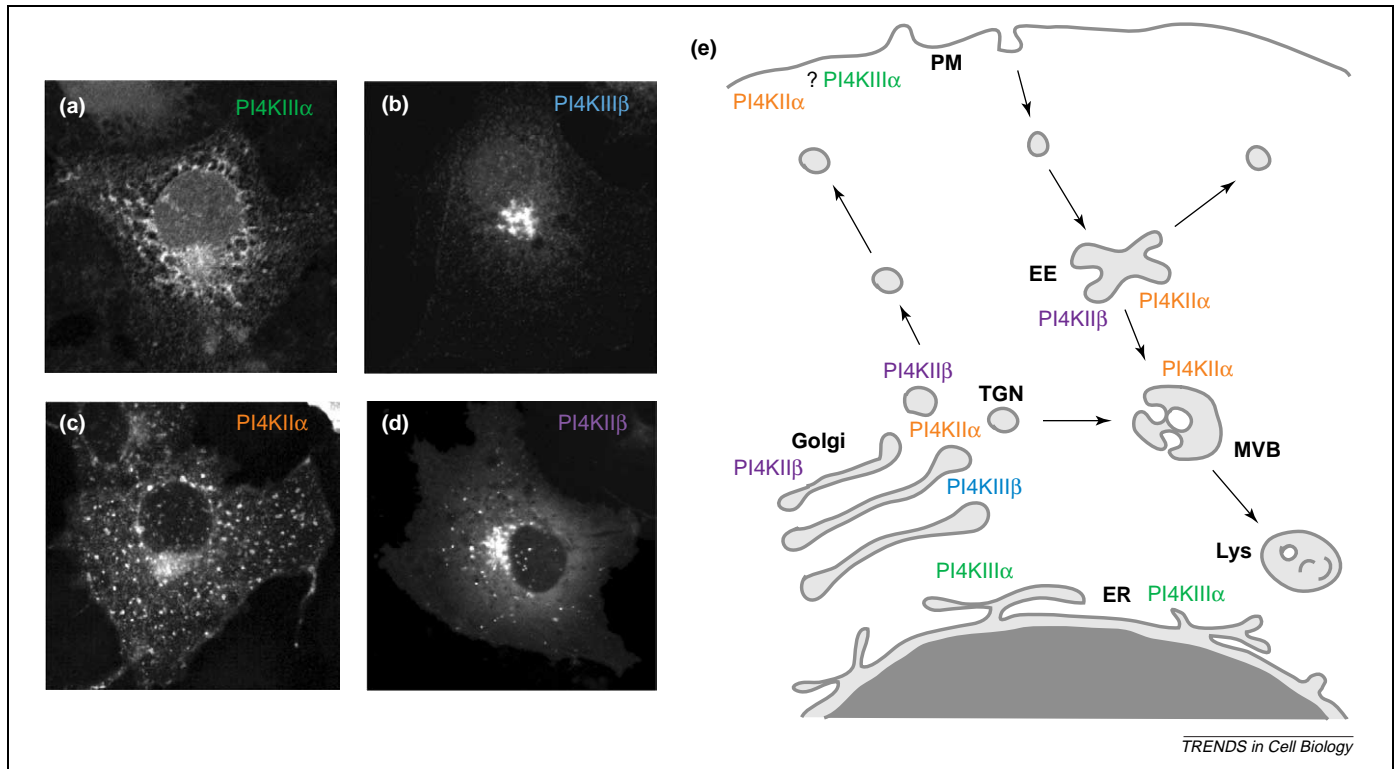
Figure 2. Cellular localization of PtdIns 4-kinases. Localization of **(a)** HA epitope-tagged PI4KIIIα, **(b)** immunostained endogenous PI4KIIIβ, **(c)** PI4KIIα–GFP and **(d)** PI4KIIβ–GFP expressed at low levels in live COS-7 cells. PI4KIIIα shows localization at the nuclear membrane and perinuclear ER, although the characteristic peripheral tubular ER localization is not pronounced. PI4KIIIβ is Golgi localized (see Ref. [46] for more details). Both type II enzymes localize to the Golgi and TGN and to endosomes, the latter being more prominent with PI4KIIα. Localization of endogenous PI4KIIα is similar [24,63,64], although in some reports the TGN localization dominates over the endosomes [62]. **(e)** The major routes of vesicular transport steps. Abbreviations: EE, early endosomes; Lys, lysosome; MVB, multivesicular body; PM, plasma membrane.

Pik1 and Golgi function

Pik1p localizes to the Golgi and the nucleus [28–30] and is a key regulator of vesicular trafficking in the late secretory pathway [8,29,31]. This notion is also supported by genetic interactions found between certain temperature-sensitive *pik1* mutants and several genes that act on late ER to Golgi trafficking steps, and also with the small GTP-binding protein Arf1 [29]. A significantly slower rate of transport from the Golgi to the vacuole in *pik1* mutants indicates multiple trafficking defects from the Golgi compartment [8,29]. A recent synthetic lethality screen identified the Golgi-associated Rab-GTPase Ypt31p (a Rab11 homolog) and its GTPase-activating protein Gyp2p as downstream targets of Pik1p function, and these

<div style="background-color:#fdf6d3">

Box 1. The history of PtdIns 4-kinases

The first reports on PtdIns kinase activity appeared in the early 1960s, showing that it was enriched in the plasma membrane. It was also recognized that similar activities were present in other subcellular fractions, with unique sensitivities to stimulation by selected detergents (see Michell [81] for a historical perspective on these early studies). These studies were followed in the early 1980s by several reports on a 56 kDa PtdIns 4-kinase activity isolated from plasma membrane preparations of a variety of cells and tissues (e.g. reviewed by Pike [61]). Whitman *et al.* distinguished type I and type II PtdIns kinase activities in fibroblasts based on their different sensitivities to detergents and adenosine. It was a major surprise and breakthrough when the same group reported that the type-I kinase phosphorylated PtdIns at the 3- rather than the 4-position of the inositol ring, leaving only the 56 kDa type II kinase as a *bona fide* PtdIns 4-kinase (reviewed in Ref. [82]). At about the same time, another enzyme, termed type III PtdIns 4-kinase was described in bovine brain, with a larger size (>200 kDa), low sensitivity to adenosine and high K_m for ATP [82] (Table 1). A soluble PtdIns 4-kinase activity showing sensitivity to Wm, the then newly identified potent PtdIns 3-kinase inhibitor, was described and it was suggested that this soluble activity, rather than the membrane-bound Wm-resistant type II enzyme, supplied the PtdIns(4,5)P_2 during agonist stimulation [25]. Subsequent studies found that two

distinct proteins of 110 kDa and ~210 kDa in size, both showing the properties of type III PtdIns 4-kinase, contributed to the Wm-sensitive soluble activity [83].

The first PtdIns 4-kinase cloned was the yeast Pik1p enzyme, which revealed its extensive sequence homology with PtdIns 3-kinases within the catalytic domain [27,28]. Subsequently, another yeast PtdIns 4-kinase, Stt4p, was cloned [7], and a shorter human variant of this protein was isolated by homology cloning and named PI4Kα [84]. The 210 kDa enzyme was first purified from bovine brain, revealing its homology with the yeast Stt4p [85]. Both type III PtdIns 4-kinases were first cloned by homology cloning from rat [16,86], shortly followed by the cloning of the human and bovine proteins (see Balla [83] and Gehrmann and Heilmayer [85] for original citations). The most frequently used terms for these enzymes are listed in Table 1. Cloning of the 56 kDa type II PtdIns 4-kinase was achieved only a few years ago, when two groups independently purified the proteins and cloned the enzyme [57,58]. Two more homologous sequences were found in the human genome, one identifying PI4KIIβ [58,60] and a third on chromosome 17 with no corresponding expressed sequence tag sequence, suggesting that the latter might be a pseudogene. More details on the history of PtdIns 4-kinases, including original citations, can be found in several reviews published over the years [17,61,82,83,85].
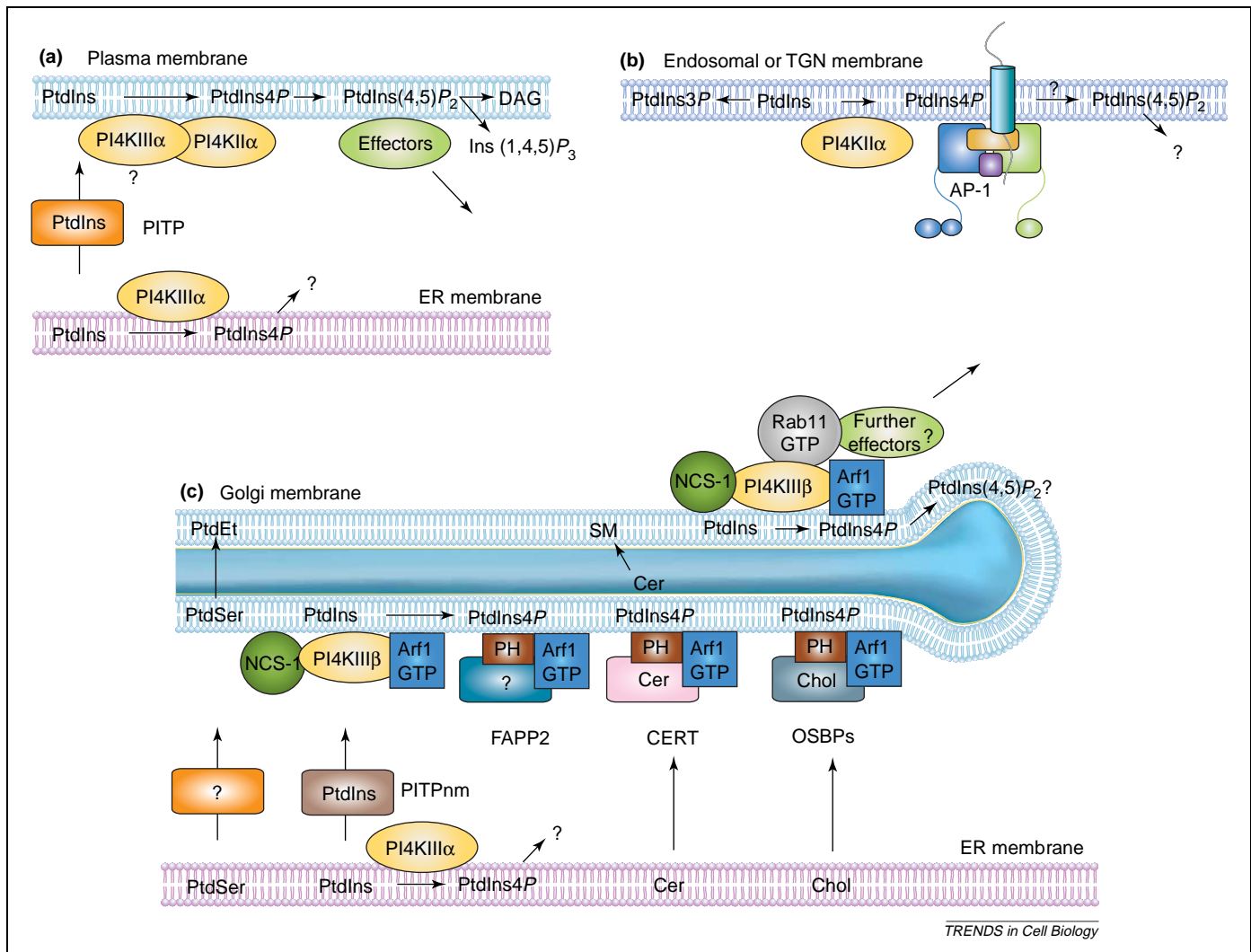
</div>

Figure 3. The functions of PtdIns 4-kinases at different membrane compartments. **(a)** The plasma membrane pool of PtdIns4P is generated by the Wm-sensitive PI4KIIIα and also by the Wm-resistant type II PtdIns 4-kinase enzymes. However, the PtdIns(4,5)P_2 pool for receptor-mediated production of DAG and Ins(1,4,5)P_3 is mostly produced from PtdIns4P made by the Wm-sensitive PI4KIIIα enzyme [25]. PtdIns(4,5)P_2 also recruits and regulates several signaling proteins (effectors), including adaptors for endocytosis, proteins that regulate actin polymerization but also control ion channels and enzymes, such as PLD. One of the classical PITPs is also likely to support the function of the PtdIns 4-kinase in this process [26]. **(b)** The type II PtdIns 4-kinase localized at the TGN helps to recruit the AP-1 adaptor protein and hence functions in protein sorting. This enzyme (and perhaps the type IIβ form, not shown) is likely to affect additional, yet to be identified, target molecules in other endosomal membranes. It is not clear whether the PtdIns4P has to be converted to PtdIns(4,5)P_2 to regulate endocytic functions. **(c)** PI4KIIIβ recruitment to the Golgi requires Arf1–GTP and, in yeast, the NCS-1 homolog frequenin. PI4KIIIβ acts at multiple steps in the Golgi and helps to engage effectors (probably including Rab11) that regulate budding and fission, and most of which still await identification. Based on the already identified PtdIns4P-binding molecules, PtdIns4P formed in the Golgi, together with Arf1–GTP, is thought to regulate nonvesicular lipid transport between the ER and the Golgi (see De Matteis *et al*. [46] for further details). The contribution of PtdIns4P formed in the ER to this process is not known, as indicated by the question mark. The manner in which the OSBPs, CERT and FAPP1 and -2 contributes to proper Golgi function is also not known. PITPnm is associated with PI4KIIIα and it is possible that the ER-bound enzyme also regulates the transport of certain lipids between the ER and Golgi or other membranes. This has not been documented in mammalian cells but in yeast Stt4p regulates the decarboxylation of PtdSer, probably affecting a transport step between the ER and the Golgi. Abbreviations: Cer, ceramide; Chol, cholesterol; PtdEt, phosphatidylethanolamine; SM, sphingomyelin.

proteins are also important components of the vesicular transport process [32]. Collectively, these studies have firmly established Pik1p as a key enzyme in maintaining the secretory function and normal morphology of the Golgi, and suggest that PtdIns4P is a regulatory lipid at this site.

Golgi and nuclear localization of Pik1
The mechanism by which Pik1p is localized to the Golgi in yeast was revealed recently. Yeast frequenin (Frq1p), the homolog of the small calcium-binding protein neuronal calcium sensor (NCS) 1 [33], physically interacts with Pik1p and is able to rescue a temperature-sensitive allele

of the enzyme [34]. The Frq1p-binding site was mapped between residues 125–169 of Pik1p, a region that immediately follows the lipid kinase unique (LKU) domain characteristic of PtdIns 3-kinases and type III PtdIns 4-kinases [35] (Box 2 and Figure I). Recent studies demonstrated that Frq1p is essential for Pik1p Golgi localization [30], and showed that Pik1p also shuttles between the nucleus and the cytoplasm. Both the Golgi and nuclear localization of the enzyme are required for viability [30]. Together with a recent report on the nucleocytoplasmic shuttling of the PtdIns kinase Mss4p [36], these data suggest that nuclear PtdIns(4,5)P_2 has an important but not fully understood role in yeast. Because

Box 2. Structural features of PtdIns 4-kinases

Type III PtdIns 4-kinases are structural relatives of PtdIns 3-kinases, with a high degree of conservation between their catalytic domains explaining the sensitivity of these proteins to Wm. Additionally, PtdIns 3-kinases and type III PtdIns 4-kinases contain a lipid kinase unique (LKU) domain that is predicted to be a helical structure (Figure I). Adjacent to the C-terminus of the LKU domain is the Frq-binding site in Pik1p that shows some level of conservation between Pik1p and the vertebrate PI4KIIIβ. Another region that shows homology between Pik1p and PI4KIIIβ (Hom2), as well as some similarity to the LKU, was identified as the Rab-binding site in mammalian and *Arabidopsis* PI4KIIIβ [43,56]. The Hom2 region follows a Ser-rich segment that contains several phosphorylation sites, including the one phosphorylated by PKD [45]. A splice variant of PI4KIIIβ extends the serine-rich region with an extra 15-residue Ser-rich cassette [83]. Both Pik1p and PI4KIIIβ contain proline-rich sequences at the N-terminus, the importance of which is unknown. There are several basic stretches within PI4KIIIβ that could serve as nuclear localization signals and Leu-rich nuclear export signals [17] but it has not been formally proven that these contribute to the nucleocytoplasmic shuttling of the enzyme.

PI4KIIIα also contains an LKU domain and a PH domain sandwiched between the LKU and the catalytic domain [84], although this PH domain is not recognized by most algorithms. The PH domain of the PI4KIIIα homolog, *At*PI4Kα1, was shown to bind PtdIns4*P* and to exert negative feedback on the activity of the enzyme [18]. PI4KIIIα also has proline-rich sequences close to its N-terminus, and contains Leu-rich regions and a putative nuclear localization and nuclear export signal [85] within its N-terminal half. It was claimed that PI4KIIIα has an SH3 domain at the N-terminus [16] but this has not been substantiated by sequence analysis. A bipartite nuclear localization signal, as well as Leu-rich putative nuclear export signals, was also described in the protein but whether these are functional is yet to be determined [17].

Type II PtdIns 4-kinases are smaller proteins with a kinase domain that shows little sequence homology with those of the type III enzymes. Their kinase domain contains two stretches that are highly conserved from yeast to human, with a longer insert present in the yeast and *Drosophila* enzyme. The conserved cysteine-rich domain that is palmitoylated lies within the catalytic domain, keeping the catalytic site close to the membrane where the PtdIns substrate is located [57]. The biggest sequence diversity between PI4KIIα and -β is found in the N-terminus, where the β enzyme contains a highly acidic region, whereas the α enzyme is especially rich in prolines.
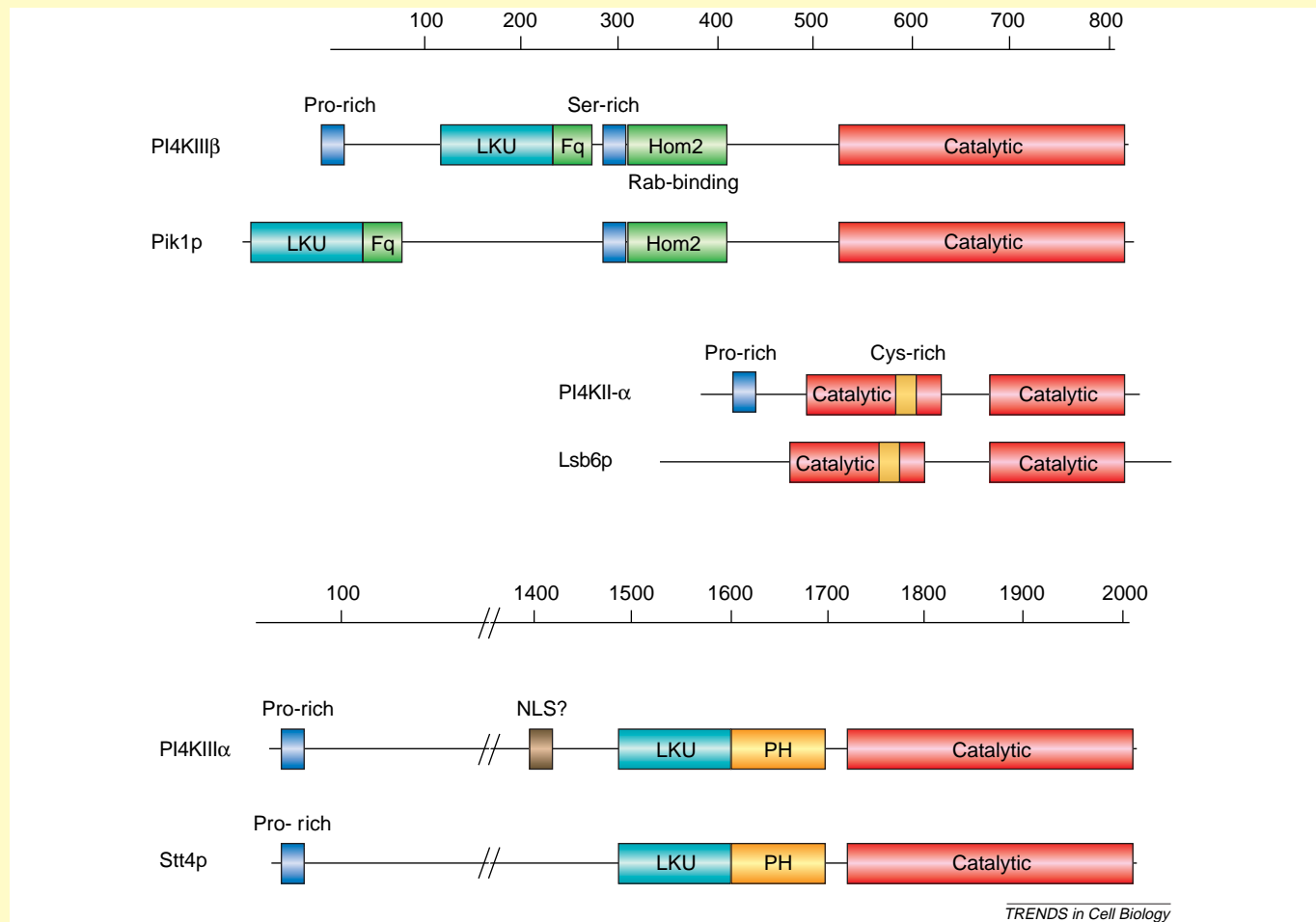

Figure I. Structural features of PtdIns 4-kinases. The scales indicate length of proteins in amino acids.

there is no evidence in yeast for the formation of PtdIns(4,5)P_2 in the Golgi from the PtdIns4*P* made by Pik1p (Mss4p is not enriched in the Golgi), the Pik1p-dependent proportion of PtdIns(4,5)P_2 could well be the product of the nuclear actions of these two enzymes.

PI4KIIIβ in higher organisms – Golgi-related functions

Mammalian PI4KIIIβ is also primarily Golgi localized [15,37] (Figure 2) and can be found in the nucleus [38]. PI4KIIIβ regulates Golgi-to-plasma membrane trafficking in Madin–Darby canine kidney cells, where it regulates

both the intra-Golgi transport of influenza hemagglutinin and the basolateral delivery of the vesicular stomatitis virus (VSV) G protein [39]. Kinase-inactive forms of PI4KIIIβ also inhibit the Golgi-to-plasma membrane delivery of the VSV-G protein in nonpolarized cells [40]. Recruitment of PI4KIIIβ to the Golgi is regulated by the small GTP-binding protein Arf1 [37] but the enzyme also interacts with and is regulated by NCS-1 [41,42]. Unlike yeast Frq1, NCS-1 does not primarily localize to the Golgi, and it is not known to what extent (if any) NCS-1 contributes to the recruitment of PI4KIIIβ to the Golgi in mammalian cells [33]. The GTP–bound form of Rab11 also binds PI4KIIIβ (at residues 401–516) (see Figure I in Box 2) but this interaction neither regulates PI4KIIIβ nor recruits the enzyme to the Golgi, and, in fact, PI4KIIIβ is required to recruit Rab11 [43]. PI4KIIIβ is phosphorylated at multiple sites [44], and phosphorylation of Ser258 and Ser266 was shown to affect the Golgi recruitment of the protein during recovery from brefeldin A treatment [17]. A recent study showed that phosphorylation of PI4KIIIβ at Ser268 by protein kinase D (PKD) is important for its kinase activity and its ability to support post-Golgi transport of the VSV-G protein but it is not necessary for Golgi recruitment of the protein [45].

How does PtdIns4P regulate Golgi functions?
The molecular details of how PI4KIIIβ affects the Golgi have only recently begun to emerge [46]. PI4KIIIβ lipid products, together with Arfs and other small GTP-binding proteins, such as Rab11, are likely to recruit several effectors (e.g. some of the clathrin adaptors and other, as yet unidentified, proteins) to promote the budding and cleavage of Golgi-derived transport vesicles (Figure 3c). Intensive efforts to identify proteins with PtdIns4P recognition so far have yielded only four candidates whose PH domains specifically recognize PtdIn(4)P [47]. Three of these, oxysterol-binding proteins (OSBPs), phosphoinositol 4-phosphate adaptor protein-2 (FAPP2) and ceramide transport protein (CERT), are lipid transport proteins possessing lipid-binding motifs. OSBP binds oxysterols and cholesterol [48], CERT transfers ceramide between the ER and the trans-Golgi network (TGN) [49] and FAPP2 has a glycolipid-transfer-protein-homology domain [40,47]. FAPP proteins are recruited to the TGN via their PH domains through interaction with both PtdIns4P and Arf1, and are required for efficient Golgi-to-plasma membrane delivery of the VSV-G protein [40]. FAPP2 is also crucial for the apical, but not basolateral, delivery of the influenza hemagglutinin [50]. Although it is becoming clear that lipid transport, such as that mediated by PITPs OSBPs and FAPP proteins is essential for the maintenance of the vesicular transport process (Figure 3c), the molecular details of how these proteins are linked to Golgi-derived vesicle budding and the secretion process have yet to be elucidated.

PI4KIIIβ and secretion
PtdIns 4-kinases are also present in secretory granules and synaptic vesicles [2,3] but the identities of the kinase(s) at these sites are not yet known. A few data suggest that PI4KIIIβ is important for regulated exocytosis: NCS-1 increases glucose-induced insulin secretion by increasing the readily releasable vesicular pool in pancreatic β cells, an effect that requires PI4KIIIβ [51]. Whether NCS-1 localizes the kinase to the plasma membrane or the exocytic vesicles is not known but association of the two proteins at these sites is highly probable. In another study, reducing the level of PI4KIIIβ with RNA interference inhibited nutrient-induced insulin secretion [52]. Because NCS-1 was discovered as a protein regulating synaptic development and plasticity [33], it is a reasonable assumption that PI4KIIIβ also functions in the genesis, transport and/or exocytosis of synaptic vesicles [2].

Phenotypes of organisms lacking PI4KIIIβ
Few studies are available on the role of PI4KIIIβ at the level of the whole organism. In *Drosophila*, disruption of the gene encoding PI4KIIIβ, named *four wheel drive*, results in male infertility owing to a defect in cytokinesis during spermatogenesis [53]. Because PtdIns(4,5)P_2 is important in the formation of the cleavage furrow during cytokinesis [54,55], it seems that *four wheel drive* is the only PtdIns 4-kinase that can supply the PtdIns4P for cytokinesis during spermatogenesis in *Drosophila*. An important function of PI4KIIIβ was recently revealed in *A. thaliana*: AtPI4Kβ1 (and its sister, AtPI4Kβ2) was found to facilitate the budding of vesicles from the TGN and to associate with the TGN-localized RabA4b protein (a Rab11 homolog of *A. thaliana*) at the region corresponding to the Rab11 interaction site in PI4KIIIβ (see Figure I in Box 2). This process is essential for polarized secretion and is necessary for root hair growth. In the same study, it was also shown that the *Arabidopsis* homolog of frequenin interacts with the N-terminal domain of AtPI4Kβ1 and probably confers Ca^{2+} regulation to the enzyme [56]. These results exemplify how specific Golgi transport defects are manifested at the level of the whole plant.

Type II PtdIns 4-kinases
Early biochemical studies on PtdIns 4-kinases mostly characterized the type II PtdIns 4-kinases from mammalian tissues (Box 1), yet the cloning of the genes corresponding to this group of proteins was a relatively late development after purification of the protein [57,58]. Two forms of the enzymes are expressed in vertebrates, type IIα and type IIβ, with very similar features. They will be discussed together because little information unique to type IIβ is available, and yeast and other lower organisms have only one form of the protein.

Possible role(s) of type II PtdIns 4-kinases at the plasma membrane
Type II PtdIns 4-kinases are tightly membrane-bound proteins, owing to their palmitoylation on a conserved stretch of cysteine residues [57] (see Figure I in Box 2). A significantly larger fraction of PI4KIIβ than PI4KIIα is cytosolic, in spite of the high degree of conservation within their cysteine-rich domains [59,60]. Whether this reflects a different degree of steady-state palmitoylation remains to be determined. Early studies isolated type II PtdIns 4-kinase activities from the plasma membrane and the

enzyme was also shown to be associated with epidermal growth factor (EGF) receptors in A431 cells [61]. This, together with the requirement for PtdIns 4-kinase function at the plasma membrane, has led to the logical assumption that type II PtdIns 4-kinases contribute to the generation of the membrane pool of PtdIns(4,5)P_2. It came as a surprise, therefore, that the majority of PI4KIIα and -β enzymes localizes to intracellular membranes, mostly to TGN and endosomes based on immunocytochemical analysis [60,62] (Figure 2). Recent studies revealed that the enzyme is also present in late endosomes [63] and in a vesicular pool rich in the adaptor protein AP-3 [64]. However, type II enzymes are clearly present in the plasma membrane, either under basal conditions (PI4KIIα) or after platelet-derived growth factor stimulation (PI4KIIβ), the latter being mediated by a Rac-dependent mechanism [59]. These data, together with early findings, indicate that type II PtdIns 4-kinases make up a significant fraction of the plasma membrane PtdIns 4-kinase activities and are responsible for the Wm-insensitive component of PtdIns(4,5)P_2 synthesis (Figure 3a). Based on mass measurements, ∼50% of the total cellular PtdIns(4,5)P_2 pool is synthesized via Wm-sensitive PtdIns 4-kinases [65] but the fraction of this that is found in the different membranes has yet to be determined.

Functions of type II PtdIns 4-kinases in endomembranes

Consistent with their endosomal localization, evidence suggests that type II PtdIns 4-kinases regulate intracellular trafficking events. Knockdown of PI4KIIα abolished the Golgi recruitment of the heterotetrameric adaptor AP-1 [62], and impaired the recruitment of AP-3 in endosomes [64] (Figure 3b). Whereas the latter effects required PtdIns4P but not PtdIns(4,5)P_2, PI4KIIα was also needed for the late-Golgi transport of VSV-G and influenza hemagglutinin but this effect was independent of AP-1 recruitment and was supported by PtdIns(4,5)P_2 [62]. The possible role of type II PtdIns 4-kinases in transferrin receptor endocytosis and recycling has been raised [60], and recent studies have shown that PI4KIIα has a major role in EGF receptor degradation in the late endosomal pathway [63]. Type II PtdIns 4-kinase activities were found in association with several other membrane proteins, including the T cell receptor [66] and some of the tetraspanins, such as CD63 [67], and these interactions might help to keep the kinase within active signaling complexes. Phosphorylation of type-II PtdIns 4-kinases by PKD has been reported but it is not known how this affects PtdIns 4-kinase activity [68]. Because PKD also phosphorylates PI4KIIIβ at the Golgi [45], it has yet to be seen whether PKD enzymes regulate both of these PtdIns 4-kinases.

Regulation of type II PtdIns 4-kinases

Regulation of the type II PtdIns 4-kinases is poorly understood. Calcium inhibits both type II PtdIns 4-kinases (Table 1), and membrane association increases PI4KIIβ activity [59]. Membrane cholesterol content and the small amphipathic wasp-venom peptide mastoparan (also an activator of some heterotrimeric G proteins) increases PI4KIIα activity [69] but the relevance of these

observations to the control of the enzymes is still unknown. The yeast ortholog Lsb6p (also termed Pik2p) shows moderate PtdIns 4-kinase activity and makes little contribution to the overall PtdIns4P production of yeast cells under normal growth conditions [70,71]. Importantly, inactivation of *LSB6* causes only a mild alteration in the trafficking of the endocytosed mating factor receptor. This defect is rescued by a construct that does not contain the catalytic domain but requires regions that interact with Las17p, the yeast homolog of Wiskott–Aldrich syndrome protein that is important for the regulation of actin polymerization [72]. It is possible that Lsb6p acts as a scaffold and regulates the movements of vesicles, and its lipid kinase activity might not be crucial for normal functions in yeast.

Little is known about type II PtdIns 4-kinases in other organisms. It is curious, however, that *Arabidopsis* contains eight genes encoding proteins with homology to the type II PtdIns 4-kinases, six of which having ubiquitin as part of their coding sequence [73]. Because ubiquitination is an important means of tagging proteins, including EGF receptors, destined for endocytosis and degradation [74], this observation is a further hint that type II PtdIns 4-kinases are regulators of endocytosis, and that they might direct endocytosed proteins for degradation.

Concluding remarks and future perspectives

Being the gatekeepers for the production of most phosphoinositides, PtdIns 4-kinases are of the utmost significance in the organization of eukaryotic cells. They control signaling events by regulating PtdIns(4,5)P_2 synthesis in the plasma membrane and the nucleus, and regulate vesicular trafficking and protein secretion from the Golgi via generation of PtdIns4P. These enzymes also regulate endocytosis, probably through production of PtdIns(4,5)P_2 at the plasma membrane, and determine the fate of endocytosed cargo by directing membrane proteins for degradation, perhaps by producing PtdIns4P as the signaling molecule and recruiting adaptor proteins. PtdIns 4-kinases also organize lipid transfer between membranes and thereby affect membrane lipid composition. PtdIns 4-kinases, therefore, emerge not just as simple providers of the precursor for PtdIns(4,5)P_2 synthesis, but also as the enzymes that generate PtdIns4P as a signaling molecule. Identification of further proteins regulated by PtdIns4P is one of the keys to a better understanding of this aspect of PtdIns 4-kinase function.

Many questions concerning PtdIns 4-kinases remain to be clarified. There are several important cellular processes in which PtdIns 4-kinase involvement can be suspected. These include the priming of secretory vesicles, exocytosis and membrane retrieval of synaptic vesicles [2], and translocation of Glut4 to the plasma membrane [75]. Identification of the PtdIns 4-kinases involved and determination of the exact molecular steps they affect are important tasks to be accomplished. It is evident that some processes in the cell are regulated by more than one PtdIns 4-kinase. For example, three forms of the enzymes regulate actin polymerization but each one in its distinctive way, and both PI4KIIIβ and PI4KIIα affects trafficking from the late Golgi. The involvement of PtdIns

4-kinases in specific processes is determined by their localization and local regulation, and it is a future challenge to resolve these for each enzyme and each compartment. Questions related to the nucleocytoplasmic shuttling of PI4KIIIβ are still open: is this process cell cycle related? How is this enzyme (and perhaps the other PtdIns 4-kinases [17]) integrated in the nuclear phosphoinositide cycle [76]? The functional significance of plasma membrane PtdIns(4,5)P_2 pools, generated either via the type II or type IIIα PtdIns 4-kinases, also deserves further investigation.

The relative contribution of the individual enzymes in the functions of different cell types and in distinct signaling pathways of multicellular organisms is an important area of investigation, as is the possible role of the enzymes in human disease or animal pathology. PI4KIIIα was identified as one of the genes specifically overexpressed in highly invasive pancreatic carcinoma cells [77], and polymorphism in the *PI4KIIIα* gene showed loose association with schizophrenia in one study [78]. The *PI4KIIIα* gene is located on human chromosome 22q11, close to the region that has been linked to schizophrenia [79]. Deletions within this region are also responsible for the 22q11 deletion syndromes, characterized by congenital heart defects, velopharyngeal dysfunctions and immunodeficiency [80]. Two extra partial copies of the *PI4KIIIα* gene containing exons coding only for the C-terminal half of the enzyme are found in this area of human and primate, but not other mammalian, chromosomes. These observations certainly warrant further studies on this enzyme in human pathology related to chromosome 22q11 aberrations.

The PtdIns 4-kinases were one of the first inositide kinase activities discovered, and for a long time these enzymes have been reluctant to reveal their secrets. However, renewed interest in these proteins will ensure that this will not remain so for long.

Acknowledgements

References
1 Carlton, J.G. and Cullen, P.J. (2005) Coincidence detection in phosphoinositide signaling. *Trends Cell Biol.* 15, 540–547
2 Wenk, M.R. and De Camilli, P. (2004) Protein–lipid interactions and phosphoinositide metabolism in membrane traffic: insights from vesicle recycling in nerve terminals. *Proc. Natl. Acad. Sci. U. S. A.* 101, 8262–8269
3 Czech, M.P. (2003) Dynamics of phosphoinositides in membrane retrieval and insertion. *Annu. Rev. Physiol.* 65, 791–815
4 Berridge, M.J. and Irvine, R.F. (1984) Inositol trisphosphate, a novel second messenger in cellular signal transduction. *Nature* 312, 315–321
5 Halstead, J.R. *et al.* (2005) An emerging role for PtdIns(4,5)P_2-mediated signalling in human disease. *Trends Pharmacol. Sci.* 26, 654–660
6 Wymann, M.P. and Marone, R. (2005) Phosphoinositide 3-kinase in disease: timing, location, and scaffolding. *Curr. Opin. Cell Biol.* 17, 141–149
7 Yoshida, S. *et al.* (1994) A novel gene, STT4, encodes a phosphatidylinositol 4-kinase in the PKC1 protein kinase pathway of *Saccharomyces cerevisiae*. *J. Biol. Chem.* 269, 1166–1171
8 Audhya, A. *et al.* (2000) Distinct roles for the yeast phosphatidylinositol 4-kinases, Stt4p and Pik1p, in secretion, cell growth, and organelle membrane dynamics. *Mol. Biol. Cell* 11, 2673–2689
9 Audhya, A. and Emr, S.D. (2002) Stt4 PI 4-kinase localizes to the plasma membrane and functions in the Pkc1-mediated MAP kinase cascade. *Dev. Cell* 2, 593–605
10 Perera, N.M. *et al.* (2004) Hypo-osmotic stress activates Plc1p-dependent phosphatidylinositol 4,5-bisphosphate hydrolysis and inositol hexakisphosphate accumulation in yeast. *J. Biol. Chem.* 279, 5216–5226
11 Levin, D.E. (2005) Cell wall integrity signaling in *Saccharomyces cerevisiae*. *Microbiol. Mol. Biol. Rev.* 69, 262–291
12 Routt, S.M. *et al.* (2005) Nonclassical PITPs activate PLD via the Stt4p PtdIns-4-kinase and modulate function of late stages of exocytosis in vegetative yeast. *Traffic* 6, 1157–1172
13 Foti, M. *et al.* (2001) Sac1 lipid phosphatase and stt4 phosphatidylinositol 4-kinase regulate a pool of phosphatidylinositol 4-phosphate that functions in the control of the actin cytoskeleton and vacuole morphology. *Mol. Biol. Cell* 12, 2396–2411
14 Trotter, P.J. *et al.* (1998) A genetic screen for aminophospholipid transport mutants identifies the phosphatidylinositol 4-kinase, Stt4p, as an essential component in phosphatidylserine metabolism. *J. Biol. Chem.* 273, 13189–13196
15 Wong, K. *et al.* (1997) Subcellular localization of phosphatidylinositol 4-kinase isoforms. *J. Biol. Chem.* 272, 13236–13241
16 Nakagawa, T. *et al.* (1996) Cloning, expression and localization of 230 kDa phosphatidylinositol 4-kinase. *J. Biol. Chem.* 271, 12088–12094
17 Heilmeyer, L.M., Jr. *et al.* (2003) Mammalian phosphatidylinositol 4-kinases. *IUBMB Life* 55, 59–65
18 Stevenson-Paulik, J. *et al.* (2003) Differential regulation of two *Arabidopsis* type III phosphatidylinositol 4-kinase isoforms. A regulatory role for the pleckstrin homology domain. *Plant Physiol.* 132, 1053–1064
19 Gehrmann, T. *et al.* (1996) Identification of a 200 kDa polypeptide as type 3 phosphatidylinositol 4-kinase from bovine brain by partial protein and cDNA sequencing. *Biochim. Biophys. Acta* 1311, 53–63
20 Balla, A. *et al.* (2000) Immunohistochemical localisation of two phosphatidylinositol 4-kinase isoforms, PI4K230 and PI4K92, in the central nervous system of rats. *Exp. Brain Res.* 134, 279–288
21 Aikawa, Y. *et al.* (1999) Involvement of PITPnm, a mammalian homologue of *Drosophila* rdgB, in phosphoinositide synthesis on Golgi membranes. *J. Biol. Chem.* 274, 20569–20577
22 Ekblad, L. and Jergil, B. (2001) Localization of phosphatidylinositol 4-kinase isoenzymes in rat liver plasma membrane domains. *Biochim. Biophys. Acta* 1531, 209–221
23 Kim, M. *et al.* (2001) Proteomic and functional evidence for a P2$_{X7}$ receptor signalling complex. *EMBO J.* 20, 6347–6358
24 Balla, A. *et al.* (2005) A plasma membrane pool of phosphatidylinositol 4-phosphate is generated by phosphatidylinositol 4-kinase type-III alpha: studies with the PH domains of the oxysterol binding protein and FAPP1. *Mol. Biol. Cell* 16, 1282–1295
25 Nakanishi, S. *et al.* (1995) A wortmannin-sensitive phosphatidylinositol 4-kinase that regulates hormone-sensitive pools of inositol phospholipids. *Proc. Natl. Acad. Sci. U. S. A.* 92, 5317–5321
26 Thomas, G.M.H. *et al.* (1993) An essential role of phosphatidylinositol transfer protein in phospholipase C-mediated inositol lipid signaling. *Cell* 74, 919–928
27 Flanagan, C.A. *et al.* (1993) Phosphatidylinositol 4-kinase: gene structure and requirement for yeast cell viability. *Science* 262, 1444–1448
28 Garcia-Bustos, J.F. *et al.* (1994) PIK1, an essential phosphatidylinositol 4-kinase associated with the yeast nucleus. *EMBO J.* 13, 2352–2361
29 Walch-Solimena, C. and Novick, P. (1999) The yeast phosphatidylinositol-4-OH kinase Pik1 regulates secretion at the Golgi. *Nat. Cell Biol.* 1, 523–525
30 Strahl, T. *et al.* (2005) Yeast phosphatidylinositol 4-kinase, Pik1, has essential roles at the Golgi and in the nucleus. *J. Cell Biol.* 171, 967–979

31 Hama, H. *et al.* (1999) Direct involvement of phosphatidylinositol 4-phosphate in secretion in the yeast *Saccharomyces cerevisiae*. *J. Biol. Chem.* 274, 34294–34300

32 Sciorra, V.A. *et al.* (2005) Synthetic genetic array analysis of the PtdIns 4-kinase Pik1p identifies components in a Golgi-specific Ypt31/rab-GTPase signaling pathway. *Mol. Biol. Cell* 16, 776–793

33 Hilfiker, S. (2003) Neuronal calcium sensor-1: a multifunctional regulator of secretion. *Biochem. Soc. Trans.* 31, 828–832

34 Hendricks, K.B. *et al.* (1999) Yeast homologue of neuronal frequenin is a regulator of phosphatidylinositol 4-OH-kinase. *Nat. Cell Biol.* 1, 234–241

35 Huttner, I.G. *et al.* (2003) Molecular interactions of yeast frequenin (Frq1) with the phosphatidylinositol 4-kinase isoform, Pik1. *J. Biol. Chem.* 278, 4862–4874

36 Audhya, A. and Emr, S.D. (2003) Regulation of PI4,5P$_2$ synthesis by nuclear-cytoplasmic shuttling of the Mss4 lipid kinase. *EMBO J.* 22, 4223–4236

37 Godi, A. *et al.* (1999) ARF mediates recruitment of PtdIns-4-OH kinase-beta and stimulates synthesis of PtdIns(4,5)P$_2$ on the Golgi complex. *Nat. Cell Biol.* 1, 280–287

38 de Graaf, P. *et al.* (2002) Nuclear localization of phosphatidylinositol 4-kinase beta. *J. Cell Sci.* 115, 1769–1775

39 Bruns, J.R. *et al.* (2002) Multiple roles for phosphatidylinositol 4-kinase in biosynthetic transport in polarized Madin-Darby canine kidney cells. *J. Biol. Chem.* 277, 2012–2018

40 Godi, A. *et al.* (2004) FAPPs control Golgi-to-cell-surface membrane traffic by binding to ARF and PtdIns(4)P. *Nat. Cell Biol.* 6, 393–404

41 Weisz, O.A. *et al.* (2000) Overexpression of frequenin, a modulator of phosphatidylinositol 4-kinase, inhibits biosynthetic delivery of an apical protein in polarized Madin-Darby canine kidney cells. *J. Biol. Chem.* 275, 24341–24347

42 Haynes, L.P. *et al.* (2005) Interaction of neuronal calcium sensor-1 and ADP-ribosylation factor 1 allows bidirectional control of phosphatidylinositol 4-kinase beta and trans-Golgi network-plasma membrane traffic. *J. Biol. Chem.* 280, 6047–6054

43 de Graaf, P. *et al.* (2004) Phosphatidylinositol 4-kinasebeta is critical for functional association of rab11 with the Golgi complex. *Mol. Biol. Cell* 15, 2038–2047

44 Suer, S. *et al.* (2001) Human phosphatidylinositol 4-kinase isoform PI4K92. Expression of the recombinant enzyme and determination of multiple phosphorylation sites. *Eur. J. Biochem.* 268, 2099–2106

45 Hausser, A. *et al.* (2005) Protein kinase D regulates vesicular transport by phosphorylating and activating phosphatidylinositol-4 kinase IIIbeta at the Golgi complex. *Nat. Cell Biol.* 7, 880–886

46 De Matteis, M.A. *et al.* (2005) The role of the phosphoinositides at the Golgi complex. *Biochim. Biophys. Acta* 1744, 396–405

47 Dowler, S. *et al.* (2000) Identification of pleckstrin-homology-domain-containing proteins with novel phosphoinositide-binding specificities. *Biochem. J.* 351, 19–31

48 Im, Y.J. *et al.* (2005) Structural mechanism for sterol sensing and transport by OSBP-related proteins. *Nature* 437, 154–158

49 Hanada, K. *et al.* (2003) Molecular machinery for non-vesicular trafficking of ceramide. *Nature* 426, 803–809

50 Vieira, O.V. *et al.* (2005) FAPP2 is involved in the transport of apical cargo in polarized MDCK cells. *J. Cell Biol.* 170, 521–526

51 Gromada, J. *et al.* (2005) Neuronal calcium sensor-1 potentiates glucose-dependent exocytosis in pancreatic beta cells through activation of phosphatidylinositol 4-kinase beta. *Proc. Natl. Acad. Sci. U. S. A.* 102, 10303–10308

52 Waselle, L. *et al.* (2005) Role of phosphoinositide signaling in the control of insulin exocytosis. *Mol. Endocrinol.* 19, 3097–3106

53 Brill, J.A. *et al.* (2000) A phospholipid kinase regulates actin organization and intercellular bridge formation during germline cytokinesis. *Development* 127, 3855–3864

54 Field, S.J. *et al.* (2005) PtdIns(4,5)P$_2$ functions at the cleavage furrow during cytokinesis. *Curr. Biol.* 15, 1407–1412

55 Wong, R. *et al.* (2005) PIP2 hydrolysis and calcium release are required for cytokinesis in *Drosophila* spermatocytes. *Curr. Biol.* 15, 1401–1406

56 Preuss, M.L. *et al.* (2006) A role for the RabA4b effector protein, PI4Kβ1 in polarized expansion of root hair cells in *Arabidopsis*. *J. Cell Biol.* 172, 991–998

57 Barylko, B. *et al.* (2001) A novel family of phosphatidylinositol 4-kinases conserved from yeast to humans. *J. Biol. Chem.* 276, 7705–7708

58 Minogue, S. *et al.* (2001) Cloning of a human type II phosphatidylinositol 4-kinase reveals a novel lipid kinase family. *J. Biol. Chem.* 276, 16635–16640

59 Wei, Y.J. *et al.* (2002) Type II phosphatidylinositol 4-kinase beta is a cytosolic and peripheral membrane protein that is recruited to the plasma membrane and activated by Rac-GTP. *J. Biol. Chem.* 277, 46586–46593

60 Balla, A. *et al.* (2004) (2002) Characterization of type II phosphatidylinositol 4-kinase isoforms reveals association of the enzymes with endosomal vesicular compartments. *J. Biol. Chem.* 277, 1–20050

61 Pike, L.J. (1992) Phosphatidylinositol 4-kinases and the role of polyphosphoinositides in cellular regulation. *Endocr. Rev.* 13, 692–706

62 Wang, Y.J. *et al.* (2003) Phosphatidylinositol 4 phosphate regulates targeting of clathrin adaptor AP-1 complexes to the Golgi. *Cell* 114, 299–310

63 Minogue, S. *et al.* (2006) Phosphatidylinositol 4-kinase is required for endosomal trafficking and degradation of the EGF receptor. *J. Cell Sci.* 119, 571–581

64 Salazar, G. *et al.* (2005) Phosphatidylinositol-4-kinase type II alpha is a component of adaptor protein-3-derived vesicles. *Mol. Biol. Cell* 16, 3692–3704

65 Várnai, P. and Balla, T. (1998) Visualization of phosphoinositides that bind pleckstrin homology domains: calcium-and agonist-induced dynamic changes and relationship to myo-[3H]inositol-labeled phosphoinositide pools. *J. Cell Biol.* 143, 501–510

66 Srivastava, R. *et al.* (2006) Type II phosphatidylinositol 4-kinase beta associates with TCR-CD3 zeta chain in Jurkat cells. *Mol. Immunol.* 43, 454–463

67 Berditchevski, F. *et al.* (1997) A novel link between integrins, transmembrane-4 superfamily proteins (CD63 and CD81), and phosphatidylinositol 4-kinase. *J. Biol. Chem.* 272, 2595–2598

68 Nishikawa, K. *et al.* (1998) Association of protein kinase Cµ with type II phosphatidylinositol 4-kinase and type I phosphatidylinositol-4-phosphate 5-kinase. *J. Biol. Chem.* 273, 23126–23133

69 Waugh, M.G. *et al.* (2006) Lipid and peptide control of phosphatidylinositol 4-kinase IIalpha activity on Golgi-endosomal rafts. *J. Biol. Chem.* 281, 3757–3763

70 Han, G.S. *et al.* (2002) The *Saccharomyces cerevisiae LSB6* gene encodes phosphatidylinositol 4-kinase activity. *J. Biol. Chem.* 277, 47709–47718

71 Shelton, S.N. *et al.* (2003) *Saccharomyces cerevisiae* contains a type II phosphoinositide 4-kinase. *Biochem. J.* 371, 533–540

72 Chang, F.S. *et al.* (2005) A WASp-binding type II phosphatidylinositol 4-kinase required for actin polymerization-driven endosome motility. *J. Cell Biol.* 171, 133–142

73 Mueller-Roeber, B. and Pical, C. (2002) Inositol phospholipid metabolism in *Arabidopsis*. Characterized and putative isoforms of inositol phospholipid kinase and phosphoinositide-specific phospholipase C. *Plant Physiol.* 130, 22–46

74 Haglund, K. *et al.* (2003) Distinct monoubiquitin signals in receptor endocytosis. *Trends Biochem. Sci.* 28, 598–603

75 Shisheva, A. (2003) Regulating Glut4 vesicle dynamics by phosphoinositide kinases and phosphoinositide phosphatases. *Front. Biosci.* 8, s945–s946

76 Irvine, R.F. (2003) Nuclear lipid signalling. *Nat. Rev. Mol. Cell Biol.* 4, 349–360

77 Ishikawa, S. *et al.* (2003) Identification of genes related to invasion and metastasis in pancreatic cancer by cDNA representational difference analysis. *J. Exp. Clin. Cancer Res.* 22, 299–306

78 Saito, T. *et al.* (2003) Polymorphism screening of PIK4CA: possible candidate gene for chromosome 22q11-linked psychiatric disorders. *Am J Med Genet B Neuropsychiatr Genet* 116, 77–83

79 Bassett, A.S. *et al.* (2003) The schizophrenia phenotype in 22q11 deletion syndrome. *Am. J. Psychiatry* 160, 1580–1586

80 Yamagishi, H. and Srivastava, D. (2003) Unraveling the genetic and developmental mysteries of 22q11 deletion syndrome. *Trends Mol. Med.* 9, 383–389

81 Michell, B. (1995) Early steps along the road to inositol-lipid-based signalling. *Trends Biochem. Sci.* 20, 326–329

82 Carpenter, C.L. and Cantley, L.C. (1990) Phosphoinositide kinases. *Biochemistry* 29, 11147–11156

83 Balla, T. (1998) Phosphatidylinositol 4-kinases. *Biochim. Biophys. Acta* 1436, 69–85

84 Wong, K. and Cantley, L.C. (1994) Cloning and characterization of a human phosphatidylinositol 4-kinase. *J. Biol. Chem.* 269, 28878–28884

85 Gehrmann, T. and Heilmayer, L.G. (1998) Phosphatidylinositol 4-kinases. *Eur. J. Biochem.* 253, 357–370

86 Nakagawa, T. *et al.* (1996) Cloning and characterization of a 92 kDa soluble phosphatidylinositol 4-kinase. *Biochem. J.* 320, 643–649

Contents lists available at ScienceDirect

Best Practice & Research Clinical Endocrinology & Metabolism

journal homepage: www.elsevier.com/locate/beem

1

Novel mechanisms of G-protein-coupled receptors functions: AT$_1$ angiotensin receptor acts as a signaling hub and focal point of receptor cross-talk

András D. Tóth, MD, Lecturer [a],
Gábor Turu, MD, PhD, Assistant professor [a, b],
László Hunyady, MD, PhD, DSc, Professor, Head of the Department of Physiology [a, b, *],
András Balla, PhD, Associate professor [a, b]

[a] Department of Physiology, Faculty of Medicine, Semmelweis University, Budapest, Hungary
[b] MTA-SE Laboratory of Molecular Physiology, Hungarian Academy of Sciences and Semmelweis University, Budapest, Hungary

ARTICLE INFO

AT$_1$ angiotensin receptor (AT$_1$R), a prototypical G protein-coupled receptor (GPCR), is the main receptor, which mediates the effects of the renin-angiotensin system (RAS). AT$_1$R plays a crucial role in the regulation of blood pressure and salt-water homeostasis, and in the development of pathological conditions, such as hypertension, heart failure, cardiovascular remodeling, renal fibrosis, inflammation, and metabolic disorders. Stimulation of AT$_1$R leads to pleiotropic signal transduction pathways generating arrays of complex cellular responses. Growing amount of evidence shows that AT$_1$R is a versatile GPCR, which has multiple unique faces with distinct conformations and signaling properties providing new opportunities for functionally selective pharmacological targeting of the receptor. Biased ligands of AT$_1$R have been developed to selectively activate the β-arrestin pathway, which may have therapeutic benefits compared to the conventional angiotensin converting enzyme inhibitors and angiotensin receptor blockers. In this review, we provide a summary about the most recent findings

and novel aspects of the AT_1R function, signaling, regulation, dimerization or oligomerization and its cross-talk with other receptors, including epidermal growth factor (EGF) receptor, adrenergic receptors and CB_1 cannabinoid receptor. Better understanding of the mechanisms and structural aspects of AT_1R activation and cross-talk can lead to the development of novel type of drugs for the treatment of cardiovascular and other diseases.

© 2018 Published by Elsevier Ltd.

Introduction

The octapeptide (Asp—Arg—Val—Tyr—Ile—His—Pro—Phe) hormone angiotensin II plays a crucial role in the maintenance of blood pressure and fluid homeostasis. It is produced by a two-step cleavage process from the precursor angiotensinogen by protease enzymes, namely renin and angiotensin convertase enzyme (ACE). The AngII effects are mediated by two distinct G protein-coupled receptors (GPCRs), the AT_1 and AT_2 angiotensin receptors, but there is a substantial difference in their importance in favor of the former. The AT_1R is expressed in numerous tissues and mediates the "classical" physiological actions of circulating AngII on mechanisms including blood pressure regulation, salt-water balance, aldosterone secretion and effects on the central nervous system, such as thirst sensation and regulation of sympathetic outflow [1,2]. In addition, increased AT_1R activity has been associated with the development of several pathological conditions, including hypertension, heart failure, vascular remodeling, diabetic nephropathy, atherosclerosis, and inflammation [2]. Therefore, dampening of AT_1R activity has enormous therapeutic benefits and has been successfully exploited in the last decades using ACE inhibitors and AT_1R blockers. However, application of these drugs also hinders the beneficial functions of AT_1R. In recent years, novel drug compounds with different pharmacodynamic properties were discovered, which are able to selectively activate specific signaling pathways of AT_1R. These compounds may reduce side effects and/or have advantageous actions in treatment of diseases and could open a new era in AT_1R-targeted therapies.

In addition, a substantial knowledge has been gained about the main properties of AT_1R, such as ligand preference, signaling, regulation, and trafficking. However, it is less known how AT_1R and other plasma membrane receptors affect each other's function, and how these crosstalk mechanisms can be utilized in the clinical practice. The new results in the field of receptor crosstalk can reveal not just new drug targets, but can also explain certain interactions between pharmaceutical compounds. In this review, we highlight the traditional and novel features of AT_1 angiotensin receptor (AT_1R), which is a prototypical GPCR, and can be considered as paradigm for other GPCRs not only in its pleiotropic functions and action of mechanisms but also in its clinical importance and druggability.

Prototypical and unique GPCR functions of AT_1R

Structural aspects of AT_1R functions

AT_1R is a member of the rhodopsin family of GPCRs, and shares their common structural architecture [1]. It possesses an extracellular N terminus, an intracellular C terminus and seven highly hydrophobic transmembrane α-helices (H1-7), connected by three extra- and intracellular loops (ECL1-3 and ICL1-3, respectively). Ligands of GPCRs can be classified as agonists or antagonists. Agonists are capable to induce structural rearrangements in the receptor, achieving an active conformation of the GPCR, whereas antagonists stabilize the inactive state. Our understanding of the structural aspects of GPCR activation has improved strikingly in recent years thanks to the growing numbers of high-resolution GPCR structures. Surprisingly, despite the relatively low sequence homology between GPCRs, the conformational features of the transmembrane helices are considerably conserved [3]. In

contrast, the composition of ligand binding pockets is diverse among GPCRs, which ensures the specific recognition of receptor ligands. Accordingly, our knowledge of the interaction between AT_1R and its specific antagonists (or more precisely: inverse agonists) has hugely improved by the first crystal structures of AT_1R in complex with the AT_1R antagonists ZD7155 and olmesartan [4,5]. In good agreement with the previous results of site-directed mutagenesis studies, the ligand binding pocket of AT_1R is formed by several key residues of ECL2 and the transmembrane helices H1, H2, H3 and H7. With the help of docking simulations, these structures could explain the different binding properties of various receptor blockers. For instance, losartan, an antagonist with a relatively low binding affinity, forms only one salt bridge with the ligand binding pocket, whereas candesartan, an antagonist with insurmountable binding, is speculated to engage AT_1R with two additional salt bridges [4]. The knowledge of the antagonist-stabilized state may also help to predict the conformational changes of the agonist-stimulated AT_1R.

Signal transducers of AT_1R

Heterotrimeric G proteins initiate the first wave of GPCR signaling (Fig. 1) [6]. Upon agonist activation, the Gα subunit binds to the core region of active GPCRs via the opened cytosolic cavity. This interaction triggers nucleotide exchange of Gα from GDP to GTP and dissociation of Gα from Gβγ. The
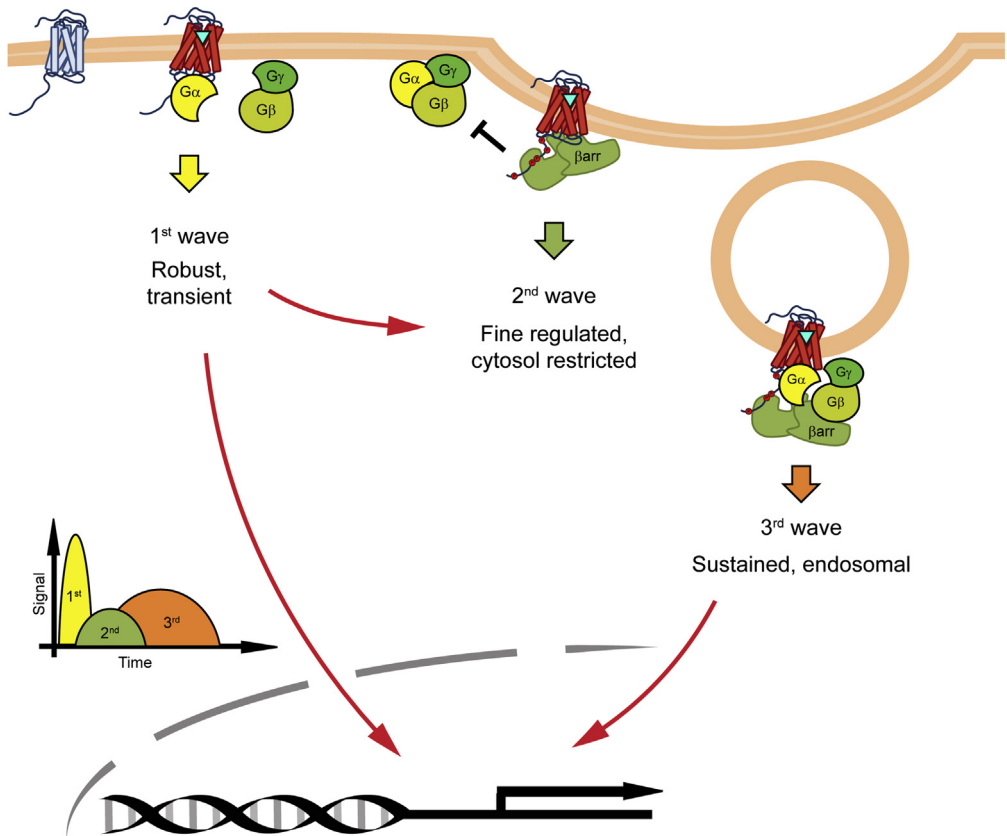
Fig. 1. Signal generation of ligand stimulated GPCR. The activation of a GPCR usually initiates multiple and complex signaling pathways in the target cells. The first wave of signaling depends on the G protein coupling and second messenger production. The β-arrestin binding not just decouple the receptor from G protein but serving as a signaling scaffold initiates the slightly delayed second, β-arrestin-mediated wave of receptor signaling. Recent evidences revealed that the internalized receptors are also capable to organize a third wave of signaling, which results in sustained cell response.

separated subunits modulate the activity of downstream effector proteins to induce robust signaling cascades. These signaling mechanisms have wide spectra, including second messenger generation, activation of small G proteins and cytoplasmic tyrosine kinases, regulation of ion channels or trans-activation of growth factor receptors. Likewise, G protein-mediated signaling pathways are responsible for the vast majority of AT_1R-evoked cellular responses [1]. AngII stimulation of AT_1R is able to activate not just one but various G proteins, such as $G_{q/11}$, $G_{i/o}$, or $G_{12/13}$ [7]. $G_{q/11}$ protein induces the hydrolysis of phosphatidylinositol 4,5-bisphosphate (PIP_2) into the second messenger inositol trisphosphate (IP_3) and diacylglycerol (DAG) by activation of phospholipase Cβ, IP_3 triggers intracellular Ca^{2+} mobilization via binding and opening its calcium channel receptor. Ca^{2+} is a central regulator of many intracellular proteins and, in co-operation with DAG, also leads to the activation of various protein kinase C (PKC) isoforms [1,2]. Meanwhile, the signal transduction via $G_{i/o}$ and $G_{12/13}$ proteins lead to inhibition of adenylyl cyclase, regulation of L- and T-type Ca^{2+} channels and activation of phospholipase D, Rho GTPases or Rho kinase. It seems that the $G_{q/11}$-mediated signal transduction mechanisms of AT_1R prevail in the major physiological target tissues, including kidney, adrenal cortex, vascular smooth muscle and cardiac cells [2].

The first wave of signaling is terminated by the elimination of the GTP bound to Gα and by distinct mechanisms of desensitization [8]. In the course of homologous desensitization, GRK enzymes recognize and phosphorylate agonist-bound GPCRs on serine/threonine residues of the receptor C-tail and/or ICL loops. The phosphorylation contributes to receptor desensitization through promotion of high affinity binding of arrestin proteins [9]. Moreover, since GRKs have a large number of non-receptor targets, they may also act as effectors of GPCR signaling [10]. Although the phosphorylation target sites of the seven GRK isoforms show substantial overlap, there are marked differences as well. It was demonstrated that distinct ligands of the $β_2AR$ initiate different phosphorylation patterns in the cytoplasmic tail of the receptor, "barcode", due to alternative interaction with GRK2 and/or GRK6 [11]. Similarly, different phosphorylation barcode by GRK2/3 and GRK5/6 were suggested in the case of AT_1R [12,13]. In addition, the C-tail of AT_1R contains several consensus PKC phosphorylation sites [14]. Phosphorylation by PKC can be induced by activation other plasma membrane receptors and occurs not only in the active but the inactive state of the receptor. This mechanism of regulation of AT_1R sensitivity is termed as heterologous desensitization.

GRK-phosphorylation of agonist-bound AT_1R is followed by the recruitment of β-arrestins. β-arrestins are multi-functional adaptor proteins of GPCRs. The two β-arrestins (β-arrestin1 and β-arrestin2) are expressed ubiquitously in mammalian tissues, and show high sequence and structural homology [9]. Their major roles are identical, but several isoform-specific functions were also reported (reviewed in [15]). They bind receptors in a two-step process [16]. First, β-arrestins interact with receptor-attached phosphates, then dock to the intrahelical cavity of the activated GPCR. The binding of β-arrestin to the GPCR core sterically prevents the further activation of G proteins. Moreover, activated β-arrestins can interact with numerous adaptor proteins involved in the endocytic cargo transport [8]. Association of β-arrestin with the $β_2$-appendage of adaptor protein 2 induces translocation of the GPCR-β-arrestin complex to clathrin-coated pits, which step is followed by internalization mediated by clathrin-coated vesicles. AT_1R interacts with β-arrestins in sustained manner, due to strong interaction of β-arrestins with phosphorylated C-terminal serine/threonine clusters [17,18]. Because of the stable interaction, AT_1R and β-arrestins internalize together as a complex. This allows β-arrestins to govern the intracellular trafficking of the receptor [8]. Basically, receptors can have two fates after endocytosis (Fig. 2). They can be degraded in lysosomes or be recycled to the plasma membrane via fast and/or slow recycling endosomes. During recycling, the receptor ligands detach from the receptor due to lower pH in endosomes, and the receptor is dephosphorylated by protein phosphatases. These processes induce resensitization of the receptor, i.e. they are able to respond to agonists again. Sustained β-arrestin binding of AT_1R favors late endosomal and lysosomal trafficking, inducing its down-regulation [8]. Furthermore, β-arrestin-independent and caveolae-mediated internalization routes of AT_1R have also been described [19].

Initially, β-arrestins were considered only as negative regulators of GPCR functions by mediating receptor desensitization and internalization. It is now widely-accepted that they have much broader roles, as they are central organizers of distinct signaling cascades [16]. As scaffolds, they orchestrate a vast array of signaling proteins, such as various mitogen-activated protein kinases (MAPK),

phosphoinositide 3-kinase, Akt or protein phosphatase 2A [16,20,21]. In that function, β-arrestins fine tune a second wave of GPCR signaling. This signaling is substantially different from the first wave regarding its temporal, spatial and mechanistic features [6]. One of the most known β-arrestin-mediated function is the modulation of MAPK activation. Various MAPK cascade members are regulated by β-arrestins upon AT_1R activation, including Raf1, MEK, ERK, p38 MAPK and JNK [16]. The formation of AT_1R–β-arrestin–MAPK complexes alter the localization of MAPK activation. These complexes keep activated MAPKs away from the nucleus, thereby preventing the induction of their transcriptional response [20]. On the other hand, the β-arrestin-bound MAPK complexes can phosphorylate and regulate other target proteins, which are brought in proximity as well by β-arrestins. β-arrestins were shown to interact with hundreds of signaling proteins, indicating that β-arrestins are central regulators of complex signaling networks [22,23]. Among a wide range of functions, β-arrestins regulate cytoskeletal rearrangements, chemotaxis, or protein synthesis. In the light of these observations, it is not surprising that β-arrestins were demonstrated to mediate a plethora of AT_1R effects, such as positive inotropy in the heart, cardiac hypertrophy or proliferation of cardiomyocytes [24–26].

Interestingly, β-arrestins show a remarkable degree of conformational plasticity [9]. They can adopt multiple active conformations with distinct signaling properties. An important determinant of the β-arrestin conformation is the receptor C-terminal phosphorylation barcode [16]. Different phosphorylation motifs induce distinct β-arrestin conformational changes, which provides the possibility to evoke distinct AT_1R induced cellular responses [12]. In addition, activated β-arrestins are ubiquitinated by ubiquitin ligases, such as Mdm2 [27]. Interestingly, the ubiquitination patterns of β-arrestin may differ in the distinct active conformations, which may contribute to the fine regulation of β-arrestin-mediated response [27].

Recent data suggest that the β-arrestin-mediated second signaling wave is dependent on G proteins, suggesting that β-arrestins, in fact, broaden the signaling options of G proteins by governing their signaling in time and space [28]. Interestingly, several GPCRs have been reported to generate a third, sustained signaling wave from endosomes after internalization [29,30]. Interestingly, GPCR–G protein–β-arrestin supercomplexes have been identified to be responsible for the sustained endosomal signaling [31]. In contrast to the generally believed competition between G proteins and β-arrestins, in this complex Gα binds to the receptor core and β-arrestin interacts with the phosphorylated C-tail of the same receptor. These results were obtained with G_s protein-coupled GPCRs, and it would be curious to investigate whether the mainly G_q-coupled AT_1R could form such complexes as well. These data shed light on the complex interplay between the GPCR transducers and suggest that spatiotemporal features of signaling are more prominent than they were previously supposed.

In addition to the above-mentioned effectors, GPCRs also have numerous other interacting partners. These proteins can be either plasma membrane proteins such as ion channels, transporters, various serine/threonine-specific protein kinases, cytoskeletal proteins, Src homology and PDZ domain-containing proteins, small G proteins or extracellularly located adhesion molecules [32]. Accordingly, AT_1R was shown to interact with wide spectra of other proteins beside G proteins and β-arrestins, such as AT_1R-associated protein (ATRAP), phospholipase Cγ, JAK2 or other GPCRs, just to name a few, which may also take important parts in the complex pleiotropic effects of AT_1R in the target tissues of the renin-angiotensin system (RAS) [1].

Biased agonism of AT_1R

β-arrestin binding and internalization of AT_1R and other GPCRs does not require G protein activation [28,33–35]. Although recent data suggest that β-arrestin-mediated signaling of GPCRs requires G protein activation [28], β-arrestin binding and its effect on receptor regulation is G protein independent, therefore compounds that selectively activate G proteins and β-arrestin binding (biased or functional selective compounds) can modify the intracellular fate of receptors, which may have therapeutic relevance. It was speculated that AT_1R may adopt multiple active conformations with distinct signaling properties, and conformation-specific targeting of AT_1R could offer the intriguing possibility of pathway-selective intervention. Evidence for this concept is the successful development of β-arrestin-biased peptide agonists [36]. These peptides induced no or partial activation of G proteins, while they triggered efficient receptor phosphorylation and β-arrestin
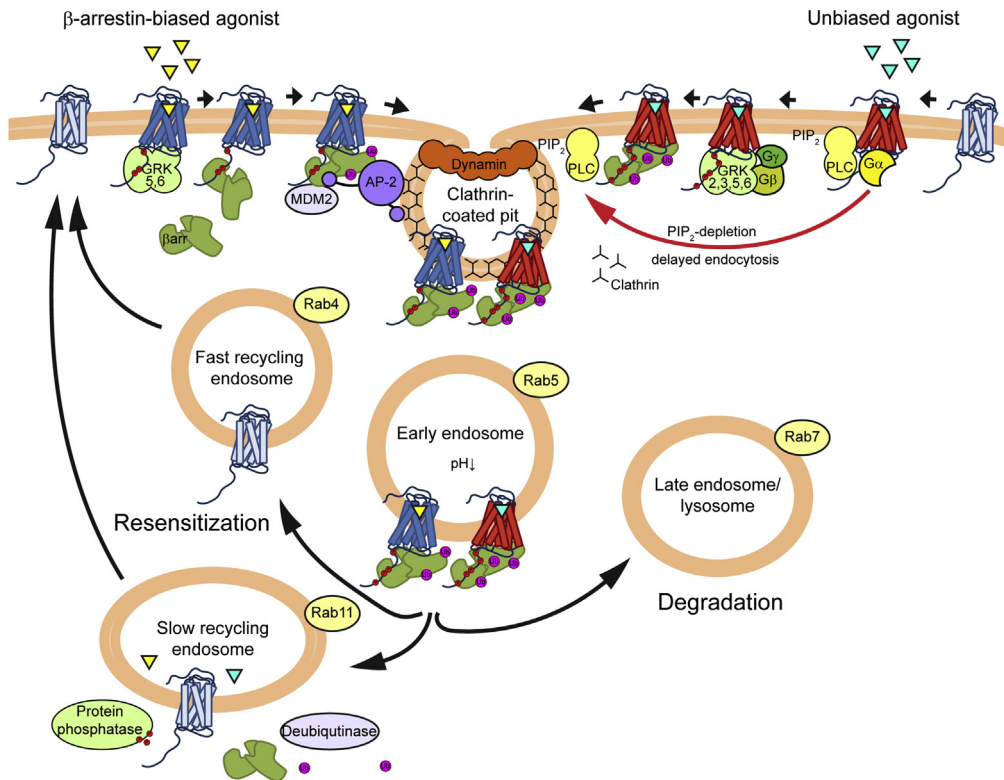
Fig. 2. **Intracellular trafficking of AT$_1$R**. Agonist stimulation of AT$_1$R leads to endocytosis predominantly via a β-arrest- and dynamin-dependent mechanism. The internalized receptors can either be degraded through the late endosomal/lysosomal route or be resensitized and recycled to the cell surface by recycling endosomes. The β-arrest-biased AT$_1$R peptides promote distinct and accelerated trafficking of the receptor due to the lack of PIP$_2$ depletion in the plasma membrane and the different β-arrest binding properties.

recruitment (Fig. 3A–B) [7,35]. Using AT$_1$R conformational biosensors, it was demonstrated that the conformations stabilized by β-arrest-biased peptides are indeed distinct from that of the AngII-induced conformation [37]. These biased peptides lack the aromatic amino acid in position 8, the indispensable residue for adoption of the G protein-activating conformation of AT$_1$R. The first such a peptide was [Sar^1,Ile^4,Ile^8]-AngII, which was then followed by a series of higher-affinity ligands including, TRV120023 or TRV120027 [38]. These peptides revolutionized AT$_1$R pharmacology and unveiled new aspects of AT$_1$R functions [39]. In addition, they show not only selective activation of the β-arrest-mediated signaling pathway but change the intracellular trafficking of AT$_1$R [40,41]. The altered intracellular fate upon treatment with β-arrest-biased compounds may be explained by the interesting finding that they also induce a different active conformation of the β-arrest [42,43]. In addition, lack of G$_q$-dependent hydrolysis of PIP$_2$, a known determinant of endocytosis [44], accelerates internalization of the receptor, which may have profound effects on the spatio-temporal features of signaling (Fig. 2) [40,45]. Moreover, these results offer the intriguing possibility that biased agonists could be applied in diseases where the intracellular receptor processing should be changed. The unique pharmacodynamic properties of biased agonists were also demonstrated *in vivo*, as they possessed beneficial effects on cardiac contractility and performance [38,46]. Unfortunately, although promising results were obtained with TRV120027 for the treatment of acute heart failure in animal studies [39,47], it failed to deliver the expected results in a Phase II clinical trial [48]. However, long-term treatment with another β-arrest-biased peptide, TRV120067 was
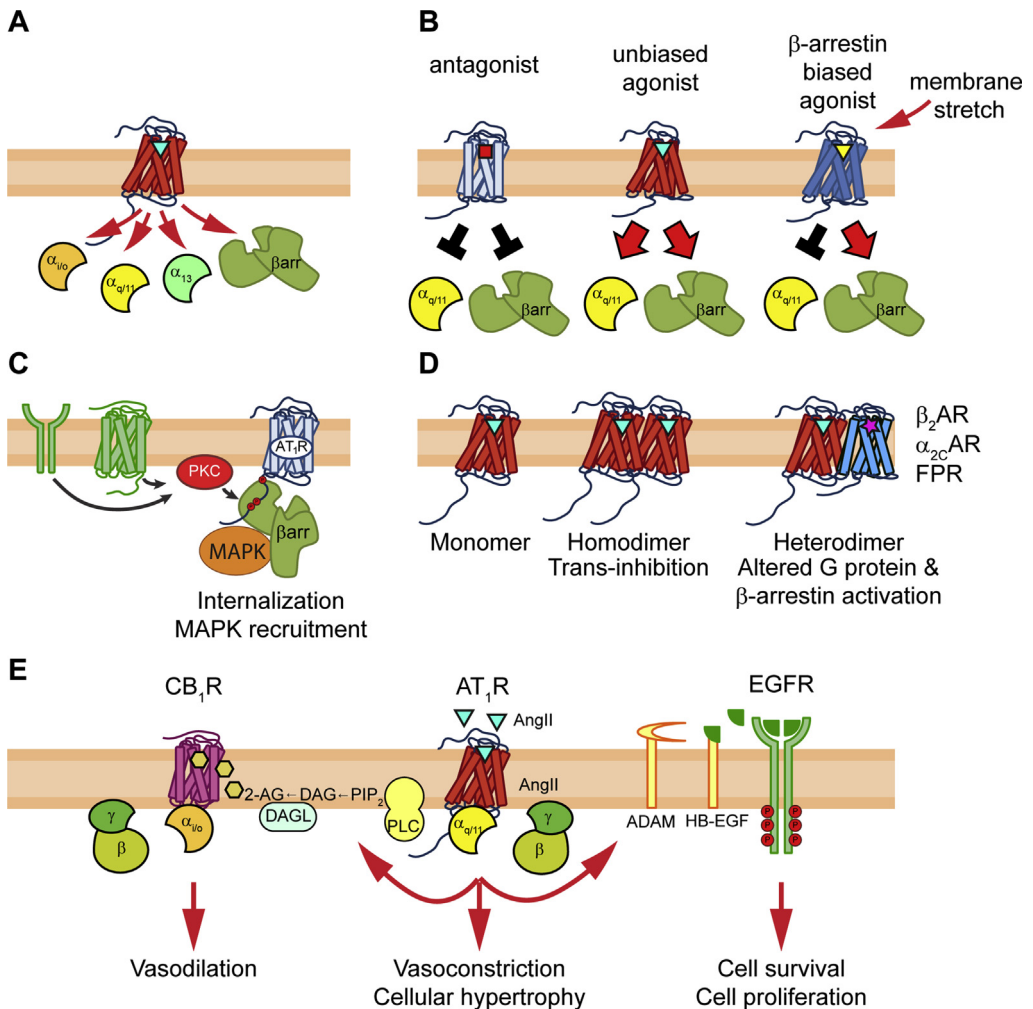
Fig. 3. Pleiotropic functions of AT₁R signaling. AT₁R acts as multifaceted organizer of signal transduction processes. (A) AT₁R can interact with various effector proteins, including $G_{q/11}$, $G_{i/o}$, $G_{12/13}$ proteins and β-arrestin molecules. (B) Binding of ligands with different pharmacodynamic properties or membrane stretch can promote distinct conformational rearrangements in the receptor, leading to alternative signaling outcomes: blockade or activation of distinct downstream effectors. (C) The inactive AT₁R acts as a focal point of signaling of other plasma membrane receptors via β-arrestin recruitment. (D) AT₁R can function in distinct molecular compositions. Homodimerization of AT₁R induces allosteric trans-inhibition in the dimer partners, whereas the heterodimerization with other receptors can alter the G protein preference and/or the β-arrestin binding properties. (E) Transactivation mechanisms driven by AT₁R. In many cell types, A₁R acts also via transactivation of other receptors, including growth factor receptor trans-activation (i.e. EGFR) and GPCR transactivation (i.e. CB₁R).

shown to have benefits compared to losartan treatment in a mouse model of dilated cardiomyopathy [49]. This suggests that chronic treatment with biased agonists could still be useful in the therapeutic strategies of some cardiovascular diseases. Although β-arrestin-mediated signaling pathways were mostly suggested to be beneficial, β-arrestin activation could also have adverse side effects. In the treatment of certain conditions, such as aldosterone overproduction, the preferable medicines will still probably be the full antagonists of AT₁R, such as candesartan or valsartan, since the use of β-arrestin-biased compounds may lead to aldosterone escape [50], due to the fact that the aldosterone production is partly β-arrestin mediated in response to AngII [51].

AT$_1$R as a stretch mechano-sensor

There is a growing number of evidence that AT$_1$R not only behaves as a hormone receptor, but also serves as a sensor of membrane stretch [52–55]. In that function, AT$_1$R is activated in the absence of ligand binding and shows biased signaling properties. Upon osmotic stretch, AT$_1$R binds β-arrestin in a G$_{i/o}$ activity dependent manner, but does not activate G$_{q/11}$ proteins [55]. These processes are followed by the transactivation of epidermal growth factor receptor (EGFR) and activation of ERK [55]. This mechanism was suggested to mediate the Frank-Starling law of the heart, i.e. the enhanced contraction response upon increased ventricular filling [56].

AT$_1$R as a signaling hub

It was generally believed that the signal transduction of AT$_1$R requires ligand binding and/or adoption of its active conformation. As reviewed above, activated AT$_1$R induces a plethora of signaling pathways, in contrast to inactive AT$_1$R, which was thought to be silent in terms of signaling. It has been demonstrated that pharmacological activation of PKC causes β-arrestin2 recruitment to AT$_1$R even in the absence of receptor agonists [57]. Moreover, stimulation of either epidermal growth factor receptor or a distinct G$_{q/11}$-coupled GPCR, such as α$_{1A}$-adrenergic receptor or endogenous purinergic receptors could exert the same effect, proving that the interaction can be triggered at physiological levels of PKC activation (Fig. 3C). It was also found that this heterologous mechanism of β-arrestin recruitment to AT$_1$R was not sensitive to treatment with the inverse agonist candesartan, showing that this process does not require the active state of the receptor. However, it depends on stable association between the PKC-phosphorylated serine/threonine clusters in the receptor's C-terminus and two conserved phosphate-binding lysines of β-arrestin2. Using β-arrestin2 conformational biosensors it was demonstrated that β-arrestin2 binds to PKC-phosphorylated AT$_1$R in a distinct conformation. Moreover, this conformation is also active functionally, since it triggers MAPK recruitment and receptor internalization with altered intracellular receptor trafficking. Taken together, the unliganded, but phosphorylated AT$_1$R is able to recruit β-arrestins and consequently, the inactive AT$_1$R may also participate in signaling as a scaffold protein [57]. This mechanism could be particularly important in the cases of receptors, like α$_{1A}$-adrenergic receptor, which do not interact with β-arrestins, since the presence of AT$_1$R could aid them to initiate β-arrestin dependent signaling. Since phosphorylation of AT$_1$R is induced by a variety of other receptors, the β-arrestin activation by heterologously-phosphorylated AT$_1$R may represent a central cross-talk mechanism for regulation of signal transduction.

Transactivation mechanisms driven by AT$_1$R

Cannabinoid receptor regulation by AT$_1$R

Cannabinoid receptors (CB$_1$ and CB$_2$ receptors) were first recognized as the targets of the phytocannabinoid tetrahydrocannabinol, the active compound of marijuana [58,59]. Later on, anandamide and 2-arachidonoyl glycerol (2-AG) were described as the main endocannabinoids produced in brain and other tissues [60]. The role of 2-AG as a cannabinoid receptor ligand was an intriguing finding, since it is produced from DAG by DAG lipase (DAGL) [61]. Since DAG is produced after G$_q$ protein activation, and DAGL is expressed widely in many tissues, we have hypothesized that AT$_1$R stimulation may lead to production of 2-AG. Indeed, 2-AG is produced in cell culture models after stimulation of the AT$_1$R with AngII, leading to activation of the CB$_1$ cannabinoid receptor (CB$_1$R) in both autocrine and paracrine manner (Fig. 3E) [62,63]. Moreover, it has been shown later, that in different arteries [64–67] and central nervous system AT$_1$R function is altered by CB$_1$R activation, which effects are dependent on DAGL activity [68]. AngII itself induces contraction in rat and mouse aorta and coronary, renal, skeletal, muscle and pulmonary arteries, and this effect is attenuated through the parallel induction of 2-AG production and activation of CB$_1$R [64–67]. This mechanism may serve as a fine-tuning negative feedback regulation in the vasomotor system, dampening the effects of many G$_q$-coupled receptors in vascular smooth muscle cells (VSMCs), which may serve as a protection mechanism from

overactivation. Although the interaction between the RAS and the cannabinoid system seems to be present in the arteries, identification of the precise cellular location of the individual elements requires additional studies.

AT_1R-CB_1R interaction is not limited to the regulation of endocannabinoid release. In rat astrocytes, AngII-induced PKC-mediated phosphorylation and heterologous desensitization of the cannabinoid receptors [69]. In these cells, CB_1R activity inhibits the MAP kinase pathway, and desensitization may regulate the balance between active and inactive receptors after activation through endocannabinoid release. Alternatively, CB_1R receptor signaling bias might be regulated through PKC-mediated phosphorylation, although these aspects of the interaction have not been yet investigated. On the other hand, AT_1R-CB_1R heterodimerization has also been reported in Neuro2A cells, where AT_1R-induced full ERK1/2 required expression of the CB_1R [70]. Together, these data show that there may be multiple levels of interaction between RAS and the cannabinoid system, which may be distinct in different tissues and cell types. They also suggest that autocrine and paracrine activations of CB_1R might be not just spatially, but also functionally different.

EGFR transactivation by AT_1R

It is very characteristic for the AT_1R that several cellular responses upon AngII stimulation are mediated by receptor tyrosine kinases, among which the EGFR plays the most important role in the cardiovascular system [71] and in other tissues, such as hepatocytes [72]. The EGFR transactivation is mediated via calcium signal and matrix metalloprotease (ADAM) activation, which causes the cleavage of heparin-binding epidermal growth factor-like growth factor (HB–EGF) resulting in agonist release for the EGFR stimulation (Fig. 3E) [73]. It turned out that this mechanism is crucial for several pathological effects of AngII, including cardiac and vascular remodeling, and the pharmacological inhibition of ADAM17 can be promising new possibility in treatment of hypertension [74]. Although EGFR transactivation seems to be the most important among growth factor receptor transactivation pathways, other growth factor receptors including insulin-like growth factor I receptor, and platelet-derived growth factor receptor transactivation mechanisms in physiological target cells, such as VSMCs, were demonstrated in response to AngII stimulation [75].

Dimer formation of AT_1R with other GPCRs

It is now widely accepted that AT_1R is capable to form higher order complexes, i.e homodimers/oligomers and heterodimers/oligomers with other GPCRs. Several GPCR–AT_1R heterodimers were published, including adiponectin receptor [76], α_{2C}-adrenergic receptor ($\alpha_{2C}AR$) [77], apelin receptor [78], β_2AR [79], bradykinin B_2 receptor [80], CB_1 cannabinoid receptor [70], chemokine (C–C Motif) receptor 2 [81], prostaglandin $F_{2\alpha}$ receptor [82] and purinergic $P2Y_6$ receptor [83]. Interestingly, several dimers have been associated with altered ability to activate G protein and/or β-arrestins (Fig. 3D). For instance, several studies have demonstrated that homodimerization has negative allosteric effect on AT_1R function [84–86], and recently the structural requirements of homodimer formation were proposed [87]. In addition, heterodimerization between the mainly $G_{i/o}$-coupled $\alpha_{2C}AR$ and G_q-coupled AT_1R was shown to change their G protein preference, and switches to G_s proteins and cAMP signaling [77]. Furthermore, altered pharmacological profile of the heterodimerized AT_1R and β_2AR has been demonstrated. Antagonist binding of either receptor was found to induce trans-inhibition of the other protomer, i.e. one antagonist could block the G protein activation of both receptors [79]. The $AT_1R-\beta_2AR$ heterodimer also influences the β-arrestin binding properties [88]. Dual agonist occupancy potentiates the β_2AR–β-arrestin recruitment without affecting the β-arrestin binding of AT_1R. β-arrestin biased AT_1R agonists, in contrast to the conventional AT_1R antagonists, could also evoke this phenomenon [88]. These results suggest that some pharmacological effects of β-arrestin-biased AT_1R agonists may be transmitted by the regulation of β_2AR leading to unexpected side effects of these drugs. However, it must be noted that physical interaction between receptor dimer partners, was mostly demonstrated using methods prone to inherent errors, and several parallel independent experimental approaches, as well as careful experimental design [89] is needed to verify many of these findings.

AT$_1$R in diseases

The overactivity of AT$_1$R is detrimental, induces pathophysiological conditions, and frequently associated with various diseases especially in the cardiovascular system and in the kidney. Due to the complexity of the AT$_1$R signaling, the various cell/tissue/organ dysfunctions could be promoted by several parallel mechanisms. The growth factor transactivation (mainly EGFR) is accounted as the key player in AngII-induced maleficent cardiac and vascular hyperplasia and hypertrophy [90]. In addition, excessive AngII-induced reactive oxygen species (ROS) production can lead to oxidative stress within the cells by promoting lipid, protein, and nucleic acid oxidations. Depending on the type of cells the oxidative stress itself can result in endothelial dysfunction, cardiovascular remodeling, hypertension, cardiac and vascular smooth muscle cell hypertrophy, diabetes, atherosclerosis [91]. AngII also induces inflammatory signals [92], and the proinflammatory actions of AT$_1$R were implicated in the development of several diseases including hypertension, myocardial and renal fibrosis [93,94]. On top of the cardiovascular and renal symptoms, the deleterious AngII signaling is also implicated in metabolic diseases and diabetes based on the results of clinical studies using various AT$_1$R blockers [95,96]. The mechanisms which lead to those conditions are not fully understood, although it is well established that insulin resistance can be caused by excessive AngII action and the blockade of RAS improves the insulin sensitivity [97].

Concluding remarks

In recent years, the high-resolution crystal structures of antagonist-bound AT$_1$R greatly improved our understanding of the molecular aspects of AT$_1$R functions. However, there is still an urgent need for the structures of both unbiased and biased agonist-bound AT$_1$Rs, which could aid the development of biased compounds with better pharmacodynamic profile. Although TRV120027 failed in a trial of acute heart failure, investigation of biased drugs in other diseases is highly desirable to answer whether these compounds be could be applied in clinical practice. The new insights of receptor cross-talk mechanisms showed that AT$_1$R is much more complex than previously appreciated. Further studies are needed to answer whether the cross-talk mechanisms of AT$_1$R could be successfully targeted in the treatment of diseases.

Practice points

- Recent results of biased agonism help to understand how different drugs acting on the same GPCR can have different pharmacological effects.
- The wide array of therapeutic effects of ACE inhibitors and AT$_1$R blockers, including blood pressure control, renoprotection, amelioration of peripheral inflammation, and beneficial effects in metabolic disorders, are mediated not only by dampening RAS activity but most likely also by hindering the endocannabinoid and growth factor receptor tyrosine kinase pathways.
- Drug interactions can be caused by receptor cross-talk mechanisms.
- Exploitations of receptor interactions and biased agonism offer the possibility of new therapeutic strategies in the near future.

Research agenda

- Determination of high-resolution structures of unbiased and biased agonist-bound AT$_1$R
- Elucidation of the spatiotemporal properties of AT$_1$R actions and the role of internalized receptors in G protein activation and signaling
- Development of novel biased AT$_1$R agonists with better pharmacokinetic and dynamic profiles
- Investigation of the effects of biased compounds in different disease models

Conflicts of interest

The authors declare that there is no conflict of interest.

Acknowledgements

References

[1] Hunyady L, Catt KJ. Pleiotropic AT1 receptor signaling pathways mediating physiological and pathogenic actions of angiotensin II. Mol Endocrinol 2006;20:953–70. https://doi.org/10.1210/me.2004-0536.

[2] Karnik SS, Unal H, Kemp JR, et al. International union of basic and clinical pharmacology. XCIX. Angiotensin receptors: interpreters of pathophysiological angiotensinergic stimuli. Pharmacol Rev 2015;67:754–819. https://doi.org/10.1124/pr.114.010454.

[3] Carpenter B, Tate CG. Active state structures of G protein-coupled receptors highlight the similarities and differences in the G protein and arrestin coupling interfaces. Curr Opin Struct Biol 2017;45:124–32. https://doi.org/10.1016/j.sbi.2017.04.010.

*[4] Zhang H, Unal H, Gati C, et al. Structure of the Angiotensin receptor revealed by serial femtosecond crystallography. Cell 2015;161:833–44. https://doi.org/10.1016/j.cell.2015.04.011.

[5] Zhang H, Unal H, Desnoyer R, et al. Structural basis for ligand recognition and functional selectivity at angiotensin receptor. J Biol Chem 2015;290:29127–39. https://doi.org/10.1074/jbc.M115.689000.

[6] Grundmann M, Kostenis E. Temporal bias: time-encoded dynamic GPCR signaling. Trends Pharmacol Sci 2017;38:1110–24. https://doi.org/10.1016/j.tips.2017.09.004.

*[7] Saulière A, Bellot M, Paris H, et al. Deciphering biased-agonism complexity reveals a new active AT1 receptor entity. Nat Chem Biol 2012;8:622–30. https://doi.org/10.1038/nchembio.961.

[8] Moore CAC, Milano SK, Benovic JL. Regulation of receptor trafficking by GRKs and arrestins. Annu Rev Physiol 2007;69:451–82. https://doi.org/10.1146/annurev.physiol.69.022405.154712.

[9] Gurevich EV, Gurevich VV. Arrestins: ubiquitous regulators of cellular signaling pathways. Genome Biol 2006;7:236. https://doi.org/10.1186/gb-2006-7-9-236.

[10] Gurevich EV, Tesmer JJG, Mushegian A, et al. G protein-coupled receptor kinases: more than just kinases and not only for GPCRs. Pharmacol Ther 2012;133:40–69. https://doi.org/10.1016/j.pharmthera.2011.08.001.

[11] Nobles KN, Xiao K, Ahn S, et al. Distinct phosphorylation sites on the β(2)-adrenergic receptor establish a barcode that encodes differential functions of β-arrestin. Sci Signal 2011;4:ra51. https://doi.org/10.1126/scisignal.2001707.

[12] Kim J, Ahn S, Ren X-R, et al. Functional antagonism of different G protein-coupled receptor kinases for beta-arrestin-mediated angiotensin II receptor signaling. Proc Natl Acad Sci U S A 2005;102:1442–7. https://doi.org/10.1073/pnas.0409532102.

[13] Zimmerman B, Beautrait A, Aguila B, et al. Differential β-arrestin-dependent conformational signaling and cellular responses revealed by angiotensin analogs. Sci Signal 2012;5:ra33. https://doi.org/10.1126/scisignal.2002522.

[14] Hunyady L, Bor M, Balla T, et al. Identification of a cytoplasmic Ser-Thr-Leu motif that determines agonist-induced internalization of the AT1 angiotensin receptor. J Biol Chem 1994;269:31378–82.

[15] Srivastava A, Gupta B, Gupta C, et al. Emerging functional divergence of β-arrestin isoforms in GPCR function. Trends Endocrinol Metab 2015;26:628–42. https://doi.org/10.1016/j.tem.2015.09.001.

[16] Peterson YK, Luttrell LM. The diverse roles of arrestin Scaffolds in G Protein-coupled receptor signaling. Pharmacol Rev 2017;69:256–97. https://doi.org/10.1124/pr.116.013367.

[17] Oakley RH, Laporte SA, Holt JA, et al. Differential affinities of visual arrestin, beta arrestin1, and beta arrestin2 for G protein-coupled receptors delineate two major classes of receptors. J Biol Chem 2000;275:17201–10. https://doi.org/10.1074/jbc.M910348199.

[18] Wei H, Ahn S, Barnes WG, et al. Stable interaction between beta-arrestin 2 and angiotensin type 1A receptor is required for beta-arrestin 2-mediated activation of extracellular signal-regulated kinases 1 and 2. J Biol Chem 2004;279:48255–61. https://doi.org/10.1074/jbc.M406205200.

[19] Hunyady L, Catt KJ, Clark AJL, et al. Mechanisms and functions of AT(1) angiotensin receptor internalization. Regul Pept 2000;91:29–44.

*[20] Luttrell LM, Roudabush FL, Choy EW, et al. Activation and targeting of extracellular signal-regulated kinases by beta-arrestin scaffolds. Proc Natl Acad Sci U S A 2001;98:2449–54. https://doi.org/10.1073/pnas.041604898.

[21] Beaulieu J-M, Sotnikova TD, Marion S, et al. An Akt/beta-arrestin 2/PP2A signaling complex mediates dopaminergic neurotransmission and behavior. Cell 2005;122:261–73. https://doi.org/10.1016/j.cell.2005.05.012.

[22] Xiao K, McClatchy DB, Shukla AK, et al. Functional specialization of beta-arrestin interactions revealed by proteomic analysis. Proc Natl Acad Sci U S A 2007;104:12011–6. https://doi.org/10.1073/pnas.0704849104.

[23] Xiao K, Sun J-P, Kim J, et al. Global phosphorylation analysis of beta-arrestin-mediated signaling downstream of a seven transmembrane receptor (7TMR). Proc Natl Acad Sci U S A 2010;107:15299–304. https://doi.org/10.1073/pnas.1008461107.

[24] Zhai P, Yamamoto M, Galeotti J, et al. Cardiac-specific overexpression of AT1 receptor mutant lacking G alpha q/G alpha i coupling causes hypertrophy and bradycardia in transgenic mice. J Clin Invest 2005;115:3045–56. https://doi.org/10.1172/JCI25330.

[25] Aplin M, Christensen GL, Schneider M, et al. The angiotensin type 1 receptor activates extracellular signal-regulated kinases 1 and 2 by G protein-dependent and -independent pathways in cardiac myocytes and langendorff-perfused hearts. Basic Clin Pharmacol Toxicol 2007;100:289–95. https://doi.org/10.1111/j.1742-7843.2007.00063.x.

[26] Aplin M, Christensen GL, Schneider M, et al. Differential extracellular signal-regulated kinases 1 and 2 activation by the angiotensin type 1 receptor supports distinct phenotypes of cardiac myocytes. Basic Clin Pharmacol Toxicol 2007;100: 296–301. https://doi.org/10.1111/j.1742-7843.2007.00064.x.

[27] Shenoy SK, Lefkowitz RJ. β-Arrestin-mediated receptor trafficking and signal transduction. Trends Pharmacol Sci 2011;32: 521–33. https://doi.org/10.1016/j.tips.2011.05.002.

*[28] Grundmann M, Merten N, Malfacini D, et al. Lack of beta-arrestin signaling in the absence of active G proteins. Nat Commun 2018;9:341. https://doi.org/10.1038/s41467-017-02661-3.

[29] Feinstein TN, Wehbi VL, Ardura JA, et al. Retromer terminates the generation of cAMP by internalized PTH receptors. Nat Chem Biol 2011;7:278–84. https://doi.org/10.1038/nchembio.545.

[30] Wehbi VL, Stevenson HP, Feinstein TN, et al. Noncanonical GPCR signaling arising from a PTH receptor-arrestin-Gβγ complex. Proc Natl Acad Sci U S A 2013;110:1530–5. https://doi.org/10.1073/pnas.1205756110.

*[31] Thomsen ARB, Plouffe B, Cahill TJ, et al. GPCR-G protein-β-arrestin super-complex mediates sustained G protein signaling. Cell 2016;166:907–19. https://doi.org/10.1016/j.cell.2016.07.004.

[32] Sokolina K, Kittanakom S, Snider J, et al. Systematic protein-protein interaction mapping for clinically relevant human GPCRs. Mol Syst Biol 2017;13:918.

*[33] Hunyady L, Baukal AJ, Balla T, et al. Independence of type I angiotensin II receptor endocytosis from G protein coupling and signal transduction. J Biol Chem 1994;269:24798–804.

[34] Gáborik Z, Jagadeesh G, Zhang M, et al. The role of a conserved region of the second intracellular loop in AT1 angiotensin receptor activation and signaling. Endocrinology 2003;144:2220–8. https://doi.org/10.1210/en.2002-0135.

*[35] Wei H, Ahn S, Shenoy SK, et al. Independent beta-arrestin 2 and G protein-mediated pathways for angiotensin II activation of extracellular signal-regulated kinases 1 and 2. Proc Natl Acad Sci U S A 2003;100:10782–7. https://doi.org/10.1073/pnas.1834556100.

[36] Holloway AC, Qian H, Pipolo L, et al. Side-chain substitutions within angiotensin II reveal different requirements for signaling, internalization, and phosphorylation of type 1A angiotensin receptors. Mol Pharmacol 2002;61:768–77.

*[37] Devost D, Sleno R, Pétrin D, et al. Conformational profiling of the AT1 angiotensin II receptor reflects biased agonism, G protein coupling, and cellular context. J Biol Chem 2017;292:5443–56. https://doi.org/10.1074/jbc.M116.763854.

[38] Violin JD, DeWire SM, Yamashita D, et al. Selectively engaging β-arrestins at the angiotensin II type 1 receptor reduces blood pressure and increases cardiac performance. J Pharmacol Exp Ther 2010;335:572–9. https://doi.org/10.1124/jpet.110.173005.

[39] Violin JD, Crombie AL, Soergel DG, et al. Biased ligands at G-protein-coupled receptors: promise and progress. Trends Pharmacol Sci 2014;35:308–16. https://doi.org/10.1016/j.tips.2014.04.007.

[40] Szakadáti G, Tóth AD, Oláh I, et al. Investigation of the fate of type I angiotensin receptor after biased activation. Mol Pharmacol 2015;87:972–81. https://doi.org/10.1124/mol.114.097030.

[41] Namkung Y, Le Gouill C, Lukashova V, et al. Monitoring G protein-coupled receptor and β-arrestin trafficking in live cells using enhanced bystander BRET. Nat Commun 2016;7:12178. https://doi.org/10.1038/ncomms12178.

[42] Shukla AK, Violin JD, Whalen EJ, et al. Distinct conformational changes in beta-arrestin report biased agonism at seven-transmembrane receptors. Proc Natl Acad Sci U S A 2008;105:9988–93. https://doi.org/10.1073/pnas.0804246105.

*[43] Lee M-H, Appleton KM, Strungs EG, et al. The conformational signature of β-arrestin2 predicts its trafficking and signalling functions. Nature 2016;531:665–8. https://doi.org/10.1038/nature17154.

[44] Tóth DJ, Tóth JT, Gulyás G, et al. Acute depletion of plasma membrane phosphatidylinositol 4,5-bisphosphate impairs specific steps in endocytosis of the G-protein-coupled receptor. J Cell Sci 2012;125:2185–97. https://doi.org/10.1242/jcs.097279.

[45] Balla A, Tóth DJ, Soltész-Katona E, et al. Mapping of the localization of type 1 angiotensin receptor in membrane microdomains using bioluminescence resonance energy transfer-based sensors. J Biol Chem 2012;287:9090–9. https://doi.org/10.1074/jbc.M111.293944.

[46] Kim K-S, Abraham D, Williams B, et al. β-Arrestin-biased AT1R stimulation promotes cell survival during acute cardiac injury. Am J Physiol Heart Circ Physiol 2012;303:H1001–10. https://doi.org/10.1152/ajpheart.00475.2012.

[47] Boerrigter G, Lark MW, Whalen EJ, et al. Cardiorenal actions of TRV120027, a novel ß-arrestin-biased ligand at the angiotensin II type I receptor, in healthy and heart failure canines: a novel therapeutic strategy for acute heart failure. Circ Heart Fail 2011;4:770–8. https://doi.org/10.1161/CIRCHEARTFAILURE.111.962571.

[48] Pang PS, Butler J, Collins SP, et al. Biased ligand of the angiotensin II type 1 receptor in patients with acute heart failure: a randomized, double-blind, placebo-controlled, phase IIB, dose ranging trial (BLAST-AHF). Eur Heart J 2017;38:2364–73. https://doi.org/10.1093/eurheartj/ehx196.

[49] Ryba DM, Li J, Cowan CL, et al. Long-term biased β-arrestin signaling improves cardiac structure and function in dilated cardiomyopathy. Circulation 2017;135:1056–70. https://doi.org/10.1161/CIRCULATIONAHA.116.024482.

[50] Lymperopoulos A, Aukszi B. Angiotensin receptor blocker drugs and inhibition of adrenal beta-arrestin-1-dependent aldosterone production: implications for heart failure therapy. World J Cardiol 2017;9:200–6. https://doi.org/10.4330/wjc.v9.i3.200.

[51] Lymperopoulos A, Rengo G, Zincarelli C, et al. An adrenal beta-arrestin 1-mediated signaling pathway underlies angiotensin II-induced aldosterone production in vitro and in vivo. Proc Natl Acad Sci U S A 2009;106:5825–30. https://doi.org/10.1073/pnas.0811706106.

[52] Zou Y, Akazawa H, Qin Y, et al. Mechanical stress activates angiotensin II type 1 receptor without the involvement of angiotensin II. Nat Cell Biol 2004;6:499–506. https://doi.org/10.1038/ncb1137.

[53] Hunyady L, Turu G. The role of the AT1 angiotensin receptor in cardiac hypertrophy: angiotensin II receptor or stretch sensor? Trends Endocrinol Metab 2004;15:405–8. https://doi.org/10.1016/j.tem.2004.09.003.

[54] Rakesh K, Yoo B, Kim I-M, et al. beta-Arrestin-biased agonism of the angiotensin receptor induced by mechanical stress. Sci Signal 2010;3:ra46. https://doi.org/10.1126/scisignal.2000769.

[55] Wang J, Hanada K, Gareri C, et al. Mechanoactivation of the angiotensin II type 1 receptor induces β-arrestin-biased signaling through Gαi coupling. J Cell Biochem 2017. https://doi.org/10.1002/jcb.26552.

[56] Abraham DM, Davis RT, Warren CM, et al. β-Arrestin mediates the Frank-Starling mechanism of cardiac contractility. Proc Natl Acad Sci U S A 2016;113:14426–31. https://doi.org/10.1073/pnas.1609308113.

*[57] Tóth AD, Prokop S, Gyombolai P, et al. Heterologous phosphorylation-induced formation of a stability lock permits regulation of inactive receptors by β-arrestins. J Biol Chem 2018;293:876–92. https://doi.org/10.1074/jbc.M117.813139.

[58] Munro S, Thomas KL, Abu-Shaar M. Molecular characterization of a peripheral receptor for cannabinoids. Nature 1993; 365:61–5. https://doi.org/10.1038/365061a0.

[59] Matsuda LA, Lolait SJ, Brownstein MJ, et al. Structure of a cannabinoid receptor and functional expression of the cloned cDNA. Nature 1990;346:561–4. https://doi.org/10.1038/346561a0.

[60] Mechoulam R, Ben-Shabat S, Hanus L, et al. Identification of an endogenous 2-monoglyceride, present in canine gut, that binds to cannabinoid receptors. Biochem Pharmacol 1995;50:83–90.

[61] Bisogno T, Howell F, Williams G, et al. Cloning of the first sn1-DAG lipases points to the spatial and temporal regulation of endocannabinoid signaling in the brain. J Cell Biol 2003;163:463–8. https://doi.org/10.1083/jcb.200305129.

[62] Turu G, Simon A, Gyombolai P, et al. The role of diacylglycerol lipase in constitutive and angiotensin AT1 receptor-stimulated cannabinoid CB1 receptor activity. J Biol Chem 2007;282:7753–7. https://doi.org/10.1074/jbc.C600318200.

[63] Turu G, Várnai P, Gyombolai P, et al. Paracrine transactivation of the CB1 cannabinoid receptor by AT1 angiotensin and other Gq/11 protein-coupled receptors. J Biol Chem 2009;284:16914–21. https://doi.org/10.1074/jbc.M109.003681.

[64] Szekeres M, Nádasy GL, Turu G, et al. Angiotensin II induces vascular endocannabinoid release, which attenuates its vasoconstrictor effect via CB1 cannabinoid receptors. J Biol Chem 2012;287:31540–50. https://doi.org/10.1074/jbc.M112.346296.

[65] Szekeres M, Nádasy GL, Turu G, et al. Endocannabinoid-mediated modulation of Gq/11 protein-coupled receptor signaling-induced vasoconstriction and hypertension. Mol Cell Endocrinol 2015;403:46–56. https://doi.org/10.1016/j.mce.2015.01.012.

[66] Karpińska O, Baranowska-Kuczko M, Kloza M, et al. Activation of CB1 receptors by 2-arachidonoylglycerol attenuates vasoconstriction induced by U46619 and angiotensin II in human and rat pulmonary arteries. Am J Physiol Regul Integr Comp Physiol 2017;312:R883–93. https://doi.org/10.1152/ajpregu.00324.2016.

[67] Szekeres M, Nádasy GL, Soltész-Katona E, et al. Control of myogenic tone and agonist induced contraction of intramural coronary resistance arterioles by cannabinoid type 1 receptors and endocannabinoids. Prostaglandins Other Lipid Mediat 2018;134:77–83. https://doi.org/10.1016/j.prostaglandins.2017.10.001.

[68] Gyires K, Rónai AZ, Zádori ZS, et al. Angiotensin II-induced activation of central AT1 receptors exerts endocannabinoid-mediated gastroprotective effect in rats. Mol Cell Endocrinol 2014;382:971–8. https://doi.org/10.1016/j.mce.2013.10.002.

[69] Haspula D, Clark MA. MAPK activation patterns of AT1R and CB1R in SHR versus Wistar astrocytes: evidence of CB1R hypofunction and crosstalk between AT1R and CB1R. Cell Signal 2017;40:81–90. https://doi.org/10.1016/j.cellsig.2017.09.002.

[70] Rozenfeld R, Gupta A, Gagnidze K, et al. AT1R-CB₁R heteromerization reveals a new mechanism for the pathogenic properties of angiotensin II. EMBO J 2011;30:2350–63. https://doi.org/10.1038/emboj.2011.139.

[71] Eguchi S, Numaguchi K, Iwasaki H, et al. Calcium-dependent epidermal growth factor receptor transactivation mediates the angiotensin II-induced mitogen-activated protein kinase activation in vascular smooth muscle cells. J Biol Chem 1998; 273:8890–6.

[72] Olivares-Reyes JA, Shah BH, Hernández-Aranda J, et al. Agonist-induced interactions between angiotensin AT1 and epidermal growth factor receptors. Mol Pharmacol 2005;68:356–64. https://doi.org/10.1124/mol.104.010637.

[73] Mifune M, Ohtsu H, Suzuki H, et al. G protein coupling and second messenger generation are indispensable for metalloprotease-dependent, heparin-binding epidermal growth factor shedding through angiotensin II type-1 receptor. J Biol Chem 2005;280:26592–9. https://doi.org/10.1074/jbc.M502906200.

[74] Takayanagi T, Forrester SJ, Kawai T, et al. Vascular ADAM17 as a novel therapeutic target in mediating cardiovascular hypertrophy and perivascular fibrosis induced by angiotensin II. Hypertens (Dallas, Tex 1979) 2016;68:949–55. https://doi.org/10.1161/HYPERTENSIONAHA.116.07620.

[75] Du J, Sperling LS, Marrero MB, et al. G-protein and tyrosine kinase receptor cross-talk in rat aortic smooth muscle cells: thrombin- and angiotensin II-induced tyrosine phosphorylation of insulin receptor substrate-1 and insulin-like growth factor 1 receptor. Biochem Biophys Res Commun 1996;218:934–9. https://doi.org/10.1006/bbrc.1996.0165.

[76] Zha D, Cheng H, Li W, et al. High glucose instigates tubulointerstitial injury by stimulating hetero-dimerization of adiponectin and angiotensin II receptors. Biochem Biophys Res Commun 2017;493:840–6. https://doi.org/10.1016/j.bbrc.2017.08.047.

[77] Bellot M, Galandrin S, Boularan C, et al. Dual agonist occupancy of AT1-R-α2C-AR heterodimers results in atypical Gs-PKA signaling. Nat Chem Biol 2015;11:271–9. https://doi.org/10.1038/nchembio.1766.

[78] Siddiquee K, Hampton J, McAnally D, et al. The apelin receptor inhibits the angiotensin II type 1 receptor via allosteric trans-inhibition. Br J Pharmacol 2013;168:1104–17. https://doi.org/10.1111/j.1476-5381.2012.02192.x.

[79] Barki-Harrington L, Luttrell LM, Rockman HA. Dual inhibition of beta-adrenergic and angiotensin II receptors by a single antagonist: a functional role for receptor-receptor interaction in vivo. Circulation 2003;108:1611–8. https://doi.org/10.1161/01.CIR.0000092166.30360.78.

[80] AbdAlla S, Lother H, Quitterer U. AT1-receptor heterodimers show enhanced G-protein activation and altered receptor sequestration. Nature 2000;407:94–8. https://doi.org/10.1038/35024095.

[81] Ayoub MA, Zhang Y, Kelly RS, et al. Functional interaction between angiotensin II receptor type 1 and chemokine (C-C motif) receptor 2 with implications for chronic kidney disease. PLoS One 2015;10:e0119803. https://doi.org/10.1371/journal.pone.0119803.

[82] Goupil E, Fillion D, Clément S, et al. Angiotensin II type I and prostaglandin F2α receptors cooperatively modulate signaling in vascular smooth muscle cells. J Biol Chem 2015;290:3137–48. https://doi.org/10.1074/jbc.M114.631119.

[83] Nishimura A, Sunggip C, Tozaki-Saitoh H, et al. Purinergic P2Y6 receptors heterodimerize with angiotensin AT1 receptors to promote angiotensin II-induced hypertension. Sci Signal 2016;9:ra7. https://doi.org/10.1126/scisignal.aac9187.

[84] Hansen JL, Theilade J, Haunsø S, et al. Oligomerization of wild type and nonfunctional mutant angiotensin II type I receptors inhibits galphaq protein signaling but not ERK activation. J Biol Chem 2004;279:24108—15. https://doi.org/10.1074/jbc.M400092200.

[85] Karip E, Turu G, Süpeki K, et al. Cross-inhibition of angiotensin AT1 receptors supports the concept of receptor oligomerization. Neurochem Int 2007;51:261—7. https://doi.org/10.1016/j.neuint.2007.05.018.

[86] Szalai B, Barkai L, Turu G, et al. Allosteric interactions within the AT₁ angiotensin receptor homodimer: role of the conserved DRY motif. Biochem Pharmacol 2012;84:477—85. https://doi.org/10.1016/j.bcp.2012.04.014.

[87] Young BM, Nguyen E, Chedrawe MAJ, et al. Differential contribution of transmembrane domains IV, V, VI, and VII to human angiotensin II type 1 receptor homomer formation. J Biol Chem 2017;292:3341—50. https://doi.org/10.1074/jbc.M116.750380.

[88] Tóth AD, Gyombolai P, Szalai B, et al. Angiotensin type 1A receptor regulates β-arrestin binding of the β2-adrenergic receptor via heterodimerization. Mol Cell Endocrinol 2017;442:113—24. https://doi.org/10.1016/j.mce.2016.11.027.

[89] Szalai B, Hoffmann P, Prokop S, et al. Improved methodical approach for quantitative BRET Analysis of G Protein coupled receptor dimerization. PLoS One 2014;9:e109503. https://doi.org/10.1371/journal.pone.0109503.

[90] Forrester SJ, Kawai T, O'Brien S, et al. Epidermal growth factor receptor transactivation: mechanisms, pathophysiology, and potential therapies in the cardiovascular system. Annu Rev Pharmacol Toxicol 2016;56:627—53. https://doi.org/10.1146/annurev-pharmtox-070115-095427.

[91] Cai H, Griendling KK, Harrison DG. The vascular NAD(P)H oxidases as therapeutic targets in cardiovascular diseases. Trends Pharmacol Sci 2003;24:471—8. https://doi.org/10.1016/S0165-6147(03)00233-5.

[92] Jurewicz M, McDermott DH, Sechler JM, et al. Human T and natural killer cells possess a functional renin-angiotensin system: further mechanisms of angiotensin II-induced inflammation. J Am Soc Nephrol 2007;18:1093—102. https://doi.org/10.1681/ASN.2006070707.

[93] Crowley SD, Song Y-S, Sprung G, et al. A role for angiotensin II type 1 receptors on bone marrow-derived cells in the pathogenesis of angiotensin II-dependent hypertension. Hypertens (Dallas, Tex 1979) 2010;55:99—108. https://doi.org/10.1161/HYPERTENSIONAHA.109.144964.

[94] Zhang J, Patel MB, Griffiths R, et al. Type 1 angiotensin receptors on macrophages ameliorate IL-1 receptor-mediated kidney fibrosis. J Clin Invest 2014;124:2198—203. https://doi.org/10.1172/JCI61368.

[95] NAVIGATOR Study Group, McMurray JJ, Holman RR, Haffner SM, et al. Effect of valsartan on the incidence of diabetes and cardiovascular events. N Engl J Med 2010;362:1477—90. https://doi.org/10.1056/NEJMoa1001121.

[96] Putnam K, Shoemaker R, Yiannikouris F, et al. The renin-angiotensin system: a target of and contributor to dyslipidemias, altered glucose homeostasis, and hypertension of the metabolic syndrome. Am J Physiol Heart Circ Physiol 2012;302:H1219—30. https://doi.org/10.1152/ajpheart.00796.2011.

[97] Nawano M, Anai M, Funaki M, et al. Imidapril, an angiotensin-converting enzyme inhibitor, improves insulin sensitivity by enhancing signal transduction via insulin receptor substrate proteins and improving vascular resistance in the Zucker fatty rat. Metabolism 1999;48:1248—55.